

MSC-R-A-64-3



POSTLAUNCH REPORT FOR
APOLLO MISSION A-102 (J)
(BP-15)

(NASA-TM-X-66757) POSTLAUNCH REPORT FOR
APOLLO MISSION A-102 (NASA) 332 p

N79-76467

00/18 Unclass
11507

CLASSIFIED DOCUMENT - TITLE ~~UNCLASSIFIED~~

NATIONAL AERONAUTICS AND SPACE ADMINISTRATION
MANNED SPACECRAFT CENTER
HOUSTON, TEXAS
October 10, 1964

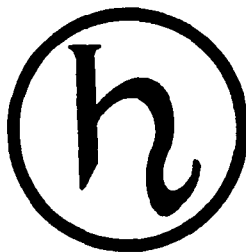
REPRODUCED BY
NATIONAL TECHNICAL
INFORMATION SERVICE
U.S. DEPARTMENT OF COMMERCE
SPRINGFIELD, VA. 22161

UNCLASSIFIED

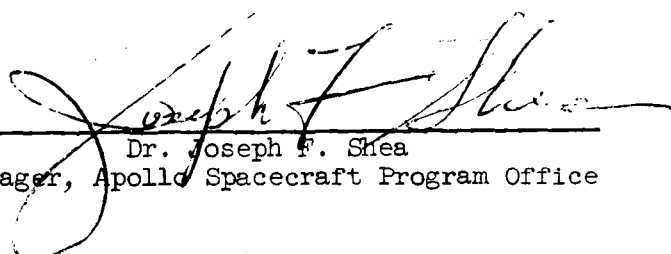
POSTLAUNCH REPORT FOR

APOLLO MISSION A-102 (C)

(BP-15)



Approved for Distribution:


Dr. Joseph F. Shea
Manager, Apollo Spacecraft Program Office

CLASSIFICATION CHANGE

UNCLASSIFIED

To
By authority of Cell-Ex 11652
Changed by Shackel Date 12/3/72
Classified Document Master Control Station, NASA
Scientific and Technical Information Facility

NATIONAL AERONAUTICS AND SPACE ADMINISTRATION

MAINED SPACECRAFT CENTER

HOUSTON, TEXAS

October 10, 1964

UNCLASSIFIED

UNCLASSIFIED

i - d

CONTENTS

	Page
ABBREVIATIONS AND SYMBOLS	iii
Abbreviations	iii
Symbols	v
TABLES	vii
FIGURES	ix
CONTRIBUTORS	xxi
1.0 SUMMARY	1-1
2.0 INTRODUCTION	2-1
3.0 FLIGHT TRAJECTORIES	3-1
4.0 SPACECRAFT DESCRIPTION AND PERFORMANCE	4-1
4.1 Spacecraft Description	4-1
4.2 Instrumentation	4-14
4.3 Electrical Power and Sequential	4-28
4.4 Communications	4-33
4.5 Pyrotechnic Devices	4-39
4.6 Launch-Escape Subsystem Propulsion	4-45
4.7 Structures	4-55
4.8 Reaction Control Subsystem	4-129
4.9 Acoustics	4-172
4.10 Heat Protection	4-178
4.11 Aerothermodynamics	4-185
4.12 Equipment Cooling	4-213
5.0 SA-7 LAUNCH-VEHICLE DESCRIPTION AND PERFORMANCE	5-1
5.1 Description	5-1
5.2 Preliminary Flight Performance	5-1
6.0 CONCLUDING REMARKS	6-1

UNCLASSIFIED

UNCLASSIFIED

		Page
7.0	APPENDIX A	
7.1	Prelaunch Operations	7-1
7.2	Launch Operations	7-10
7.3	Range Operations	7-15
7.4	Data Coverage and Availability	7-19
7.5	Telemetry Tape Selection and Verification	7-38
8.0	APPENDIX B	8-1
9.0	APPENDIX C	
9.1	C-Band Beacon Anomaly	9-1
9.2	Loss of Telemetry Measurement, SR5877T	9-5
9.3	Loss of Heat Flux Data From Calorimeter 13 (SA0553R)	9-6
10.0	REFERENCES	10-1

UNCLASSIFIED

UNCLASSIFIED

iii

ABBREVIATIONS AND SYMBOLS

Abbreviations

AI	adapter and insert
BP	boilerplate
CCW	counterclockwise
CM	command module
CW	clockwise
D.A.D.	double amplitude deflection
ECS	environmental control system
ETR	Eastern Test Range
FM	frequency modulation
FO	Florida Operations
g.e.t.	ground elapsed time
G.m.t.	Greenwich mean time
GSE	ground support equipment
IECO	inboard engine cutoff (S-I stage)
IF	intermediate frequency
IRIG	interrange instrumentation group
IU	instrument unit
KSC	John F. Kennedy Space Center
LES	launch escape subsystem
LOV	loss of vehicle
lox	liquid oxygen
MCC	Mission Control Center

UNCLASSIFIED

UNCLASSIFIED

MILA	Merritt Island Launch Area
MSC	Manned Spacecraft Center
MSFC	Marshall Space Flight Center
OECO	outboard engine cutoff (S-I stage)
OTP	Operational Test Procedure
-P	negative pitch
+P	positive pitch
PAM	pulse amplitude modulation
PIA	pre-installation acceptance
PRF	pulse repetition frequency
PLIM	postlaunch instrumentation message
R and D	Research and Development
RCS	reaction control subsystem
SA	Saturn-Apollo
SM	service module
SPL	sound pressure level
S-I	Saturn launch vehicle, first stage
S-IV	Saturn launch vehicle, second stage
T	launch time
TCV	thermal control valve
TM	telemetry
VCO	voltage controlled oscillator
VHF	very high frequency
VSWR	voltage standing wave ratio

UNCLASSIFIED

UNCLASSIFIED

v

Symbols

A_e/A_t	expansion area ratio, cross-sectional area at some point in nozzle divided by cross-sectional area at throat
D	maximum body diameter
F	thrust, lbf
g	gravitational constant
I_{XX}	moment of inertia around the X-axis, slug-ft ²
I_{YY}	moment of inertia around the Y-axis, slug-ft ²
I_{ZZ}	moment of inertia around Z-axis, slug-ft ²
L^*	characteristic length
M	Mach number
p	pressure, lb/sq in.
q	dynamic pressure, lb/sq ft
q_{max}	maximum dynamic pressure, lb/sq ft
\dot{q}	heat flux, Btu/ft ² /sec
Re_D	Reynolds number, based on maximum body diameter D
RMS	root mean square
T	launch time, sec
X	longitudinal axis of the spacecraft and launch vehicle
X_A	longitudinal location, referenced to the spacecraft, in. (fig. 4.1-3)
X_C	longitudinal location, referenced to the command module, in. (fig. 4.1-3)
X_L	longitudinal location, referenced to the launch-escape subsystem, in. (fig. 4.1-3)

UNCLASSIFIED

UNCLASSIFIED

X_{LV}	longitudinal location, referenced to the launch-vehicle S-I stage, in. (fig. 4.1-3)
X_S	longitudinal location, referenced to the service module, in. (fig. 4.1-3)
Y	plane of the Y-axis passes through the X-axis and is perpendicular to the plane of the Z-axis, in. (fig. 4.1-2)
Z	plane of the Z-axis passes through the X-axis and through the center of the CM hatch and of fins I and III of the SA-7 launch vehicle, in. (fig. 4.1-2)
α	angle of attack, deg
αq	product of angle of attack and dynamic pressure, (deg) (lb/sq ft)
ΔP	Q-ball differential pressure



Flight test symbols, Saturn-Apollo: Saturn symbol within Apollo symbol. Basic symbols: Greek and Roman.

UNCLASSIFIED

UNCLASSIFIED

vii

TABLES

Table		Page
2.0-I	APOLLO SPACECRAFT FLIGHT HISTORY	2-3
3.0-I	MISSION EVENT TIMES	3-4
3.0-II	COMPARISON OF SA-7 PLANNED AND ACTUAL TRAJECTORY PARAMETERS	3-5
4.1-I	WEIGHT COMPARISON OF BP-13 AND BP-15 SPACECRAFT. . . .	4-4
4.1-II	SPACECRAFT BP-15 MASS CHARACTERISTICS.	4-5
4.2-I	APOLLO MISSION A-102 MEASUREMENT REQUIREMENTS SUMMARY.	4-17
4.2-II	FLIGHT EQUIPMENT FOR BP-15 SPACECRAFT INSTRUMENTATION SUBSYSTEM.	4-19
4.5-I	ASSIGNMENT OF PYROTECHNIC DEVICES.	4-41
4.6-I	BP-15 SPACECRAFT LAUNCH-ESCAPE PROPULSION SUBSYSTEM MOTOR PREDICTED PERFORMANCE.	4-48
4.8-I	COMPARISON OF BP-15 SPACECRAFT INSTRUMENTED RCS CHAMBERS WITH PROTOTYPE RCS CHAMBER.	4-134
4.8-II	COMPARISON OF CALCULATED AND RECORDED MAXIMUM TEMPERATURES. SERVICE MODULE RCS QUAD A. BP-15 SPACECRAFT	4-135
4.12-I	MONITORED EQUIPMENT COOLING SUBSYSTEM PARAMETERS	4-214
4.12-II	EQUIPMENT COOLING SUBSYSTEM PARAMETERS AT UMBILICAL DISCONNECT (T-18 SEC)	4-215
7.3-I	TELEMETRY COVERAGE	7-17
7.3-II	C-BAND RADAR COVERAGE.	7-18
7.4-I	DATA AVAILABILITY.	7-21

UNCLASSIFIED

UNCLASSIFIED

Table		Page
7.4-II	ENGINEERING SEQUENTIAL CAMERA DATA	7-30
7.4-III	COMPARISON OF INSTRUMENTATION MEASUREMENTS USED ON BP-13 AND BP-15 SPACECRAFT	7-33
7.4-IV	LAUNCH-VEHICLE DATA PROCESSED FOR MSC-HOUSTON AT MSFC.	7-34
7.4-V	MSFC DATA AVAILABILITY	7-35
8.1-I	MEASUREMENT LIST FOR BOILERPLATE 15 SPACECRAFT	8-2
8.2-I	OPERATIONAL TEST PROCEDURES FOR APOLLO BP-15 SPACECRAFT AT CONTRACTOR'S MANUFACTURING FACILITY	8-11
8.2-II	OPERATIONAL TEST PROCEDURES FOR APOLLO BP-15 SPACECRAFT AT FLORIDA OPERATIONS	8-12
9.1-I	SUMMARY OF SELECTED RADAR REPORTS ON ORBITAL PASSES 1 AND 2	9-3

UNCLASSIFIED

UNCLASSIFIED

ix

FIGURES

Figure		Page
2.0-1	Saturn-Apollo space vehicle for mission A-102 at lift-off	2-4
2.0-2	Sequence of major events for Apollo mission A-102 . . .	2-5
3.0-1	Ground track for the Apollo A-102 orbital mission for the first three orbital passes	3-7
3.0-2	Altitude-longitude profile for Apollo mission A-102 for the first three orbital passes	3-8
3.0-3	Time histories of trajectory parameters for the Apollo mission A-102 launch phase	
	(a) Altitude and range	3-9
	(b) Space-fixed velocity and flight-path angle	3-10
	(c) Earth-fixed velocity and flight-path angle	3-11
	(d) Dynamic pressure and Mach number	3-12
	(e) Longitudinal acceleration along spacecraft X-axis	3-13
3.0-4	Time histories of trajectory parameters for Apollo mission A-102 for first three passes of orbital phase	
	(a) Latitude, longitude, and altitude	3-14
	(b) Space-fixed velocity and flight-path angle	3-15
4.1-1	Apollo BP-15 spacecraft	4-6
4.1-2	Y- and Z-axes and angular coordinate system used for designating locations within the BP-15 spacecraft	4-7
4.1-3	X-axis systems used for designating longitudinal locations of BP-15 spacecraft	4-8
4.1-4	Launch escape subsystem for BP-15 spacecraft	4-9
4.1-5	Command module interior equipment layout for BP-15 spacecraft (view through hatch)	4-10

UNCLASSIFIED

UNCLASSIFIED

Figure		Page
4.1-6	Command module interior equipment layout (view to right of hatch) for BP-15 spacecraft. . .	4-11
4.1-7	Command module exterior of BP-15 spacecraft	4-12
4.1-8	Cutaway view of BP-15 spacecraft service module, insert, and adapter	4-13
4.2-1	Instrumentation and communications subsystems on BP-15 spacecraft	4-20
4.2-2	Locations of linear acceleration transducers for BP-15 spacecraft	4-21
4.2-3	Strain-gage locations on BP-15 spacecraft	4-22
4.2-4	Fluctuating-pressure transducer locations on BP-15 spacecraft	4-23
4.2-5	Locations of conical surface pressure transducers on the BP-15 spacecraft	4-24
4.2-6	Locations of heat-flux calorimeter body temperature measurements on BP-15 spacecraft . . .	4-25
4.2-7	Locations of transducers on BP-15 spacecraft	4-26
4.2-8	Command module interior showing cable shielding to prevent EMI in the BP-15 spacecraft	4-27
4.3-1	Electrical power subsystem for BP-15 spacecraft	4-30
4.3-2	Electrical power subsystem components for BP-15 spacecraft	4-31
4.3-3	Launch escape sequencer subsystem for BP-15 spacecraft	4-32
4.4-1	Location of telemetry transmitters and C-band transponders on BP-15 spacecraft	4-35
4.4-2	Location of telemetry omniantenna on command module of BP-15 spacecraft	4-36

UNCLASSIFIED

UNCLASSIFIED

xi

Figure		Page
4.4-3	BP-15 spacecraft C-band beacon antenna locations on the service module	4-37
4.4-4	C-band transponder block diagram for BP-15 spacecraft	4-38
4.5-1	Location of igniter cartridges in BP-15 spacecraft	4-42
4.5-2	BP-15 launch escape tower explosive bolt installation	4-43
4.5-3	BP-15 spacecraft LES explosive bolt detail	4-44
4.6-1	BP-15 spacecraft launch escape subsystem	4-49
4.6-2	BP-15 LES launch escape motor	4-50
4.6-3	BP-15 LES launch-escape motor predicted thrust (in vacuum at 70° F)	4-51
4.6-4	BP-15 spacecraft LES pitch control motor	4-52
4.6-5	BP-15 LES pitch control motor predicted thrust (in vacuum at 70° F)	4-53
4.6-6	BP-15 spacecraft LES tower jettison motor	4-54
4.7-1	Apollo BP-15 spacecraft launch escape subsystem structure	4-67
4.7-2	Detail of command module-service module interface for BP-15 spacecraft	4-68
4.7-3	Rawinsonde atmospheric wind data at Cape Kennedy, Fla., Sept. 17-18, 1964	4-69
4.7-4	Comparison of predicted to flight measured angles of attack and α_q	4-70
4.7-5	Static pressure coefficient over the command module conical surface on BP-15 spacecraft	
	(a) Circumferential location, approximately 90° . . .	4-71
	(b) Circumferential location, 180°	4-72
	(c) Circumferential location, 357°	4-73

UNCLASSIFIED

UNCLASSIFIED

Figure		Page
4.7-6	Command module static pressure coefficients for BP-15 spacecraft flight data compared to wind tunnel data (reference 6)	4-74
4.7-7	Pressure venting scheme for BP-15 spacecraft service module, insert, and adapter compartment	4-75
4.7-8	BP-15 spacecraft service module internal pressure	4-76
4.7-9	BP-15 spacecraft service module and launch-vehicle instrument unit internal pressure (flight measured data)	4-77
4.7-10	Comparison of BP-15 to BP-13 command module instrumentation compartment internal pressures	4-78
4.7-11	Possible air leakage path caused by fracture of explosive bolt	4-79
4.7-12	Flight measured acceleration (BP-15 spacecraft)	
	(a) Launch-escape subsystem at Q-ball interface	4-80
	(b) Command module	4-82
4.7-13	Total axial force at interface of BP-15 spacecraft adapter and Saturn SA-7 instrument unit (X _A 722)	4-84
4.7-14	Power spectral distribution command module X-axis acceleration, BP-15 spacecraft	
	(a) T+48 seconds	4-85
	(b) T+73 seconds	4-86
4.7-15	Power spectral distribution, Y- and Z-axes accelerations, BP-15 spacecraft	
	(a) Tower, Y-axis, T+48 seconds, IA0011A	4-87
	(b) Tower, Z-axis, T+48 seconds, IA0012A	4-88

UNCLASSIFIED

UNCLASSIFIED

xiii

Figure		Page
	(c) Command module, Y-axis, T+48 seconds, CA0005A	4-89
	(d) Command module, Z-axis, T+48 seconds, CA0007A	4-90
4.7-16	Development view of BP-15 spacecraft service module, insert, and adapter wall showing instrument locations	4-91
4.7-17	RMS history of service module radial vibration	
	(a) Sensor SA0086D	4-92
	(b) Sensor SA0087D	4-93
	(c) Sensor SA0088D	4-94
4.7-18	RMS of fluctuating pressure over BP-15 spacecraft	
	(a) Sensor SA0162P	4-95
	(b) Sensor SA0163P	4-96
	(c) Sensor SA0164P	4-97
	(d) Sensor SA0165P	4-98
	(e) Sensor SA0166P	4-99
	(f) Sensor SA0167P	4-100
	(g) Sensor SA0168P	4-101
	(h) Sensor SA0169P	4-102
	(i) Sensor SA0170P	4-103
	(j) Sensor SA0171P	4-104
	(k) Sensor SA0172P	4-105
	(l) Sensor AA0173P	4-106
	(m) Sensor AA0174P	4-107
4.7-19	Power spectral distribution service module radial vibration, BP-15 spacecraft	
	(a) SA0086D, T+49 seconds	4-108
	(b) SA0088D, T+49 seconds	4-109
4.7-20	Power spectral distribution of BP-13 service module radial vibration at T+50 seconds	4-110
4.7-21	Power spectral distribution of BP-15 service module, strain (SA2121S)	4-111

UNCLASSIFIED

UNCLASSIFIED

Figure		Page
4.7-22	Time history of BP-15 spacecraft service module strain	
	(a) Sensor SA2120S	4-112
	(b) Sensor SA2121S	4-114
4.7-23	RMS of BP-15 service module strain	
	(a) SA2120S	4-116
	(b) SA2121S	4-117
4.7-24	Time history of BP-15 service module quasi steady state strain - SA2120S (averaged)	
	(a) SA2120S	4-118
	(b) SA2121S	4-120
4.7-25	Time history of BP-15 adapter strain	
	(a) AA0195S and AA0196S	4-122
	(b) AA0197S and AA0198S	4-123
4.7-26	BP-15 spacecraft adapter load from strain gage data at X _A 736	4-124
4.7-27	Comparison of flight noise data to design environment	
	(a) External-forward of X _A 910 to X _A 1017.75	4-125
	(b) SM RCS engine area X _A 910 to X _A 959	4-126
	(c) External X _A 838 to X _A 910	4-127
	(d) External X _A 722 to X _A 838	4-128
4.8-1	Location for service module RCS quads on BP-15 spacecraft	4-136
4.8-2	Service module RCS quad A on BP-15 spacecraft	4-137
4.8-3	Interior view of service module RCS quad A for BP-15 spacecraft	4-138
4.8-4	Spacecraft BP-15 quad A and prototype RCS chamber design	4-139

UNCLASSIFIED

UNCLASSIFIED

xv

Figure		Page
4.8-5	Method of mounting service module RCS engine to quad housing and engine supporting bracket on BP-15 spacecraft	4-140
4.8-6	Design of dummy service module RCS chambers used in quads B, C, D of BP-15 spacecraft	4-141
4.8-7	MSC coordinate axes and notation system for Apollo boilerplate and airframe, manned and unmanned spacecraft	4-142
4.8-8	Service module RCS package instrumentation locations for clockwise and counterclockwise roll engines, engine supporting bracket, and quad housing roof on BP-15 spacecraft	4-143
4.8-9	Service module RCS package instrumentation locations for +P and -P engines, engine supporting bracket, and quad housing roof on BP-15 spacecraft	4-144
4.8-10	Mounting of thermocouples on the service module RCS engines on BP-15 spacecraft	4-145
4.8-11	Service module RCS accelerometers mounted in the clockwise engine nozzle on BP-15 spacecraft	4-146
4.8-12	Temperatures measured on the positive pitch engine and housing of the service module RCS quad A of the BP-15 spacecraft	
	(a) -25 to 325 seconds	4-147
	(b) 325 to 675 seconds	4-148
	(c) 675 to 850 seconds	4-149
4.8-13	Temperatures measured on the counterclockwise roll engine and housing of the service module RCS quad A of the BP-15 spacecraft	
	(a) -25 to 325 seconds	4-150
	(b) 325 to 675 seconds	4-151
	(c) 675 to 850 seconds	4-152
4.8-14	Temperatures measured on the negative pitch engine and housing of the service module RCS quad A of the BP-15 spacecraft	
	(a) -25 to 325 seconds	4-153

UNCLASSIFIED

UNCLASSIFIED

Figure		Page
	(b) 325 to 675 seconds	4-154
	(c) 675 to 850 seconds	4-155
4.8-15	Temperature measured on the engine supporting bracket of the service module RCS quad A of the BP-15 spacecraft	
	(a) -25 to 325 seconds	4-156
	(b) 325 to 675 seconds	4-157
	(c) 675 to 850 seconds	4-158
4.8-16	Temperature measured on the underside of the quad housing roof of the service module RCS quad A of the BP-15 spacecraft	
	(a) -25 to 325 seconds	4-159
	(b) 325 to 675 seconds	4-160
	(c) 675 to 825 seconds	4-161
4.8-17	Temperatures measured on the +P, counterclockwise, and -P engine injector heads and on the engine supporting bracket of the service module RCS quad A of the BP-15 spacecraft	
	(a) 0 to 350 seconds	4-162
	(b) 350 to 700 seconds	4-163
	(c) 700 to 850 seconds	4-164
4.8-18	Temperatures measured on the +P, counterclockwise, and -P engine housings and on the quad housing roof of the service module RCS quad A of the BP-15 spacecraft	
	(a) 0 to 350 seconds	4-165
	(b) 350 to 700 seconds	4-166
	(c) 700 to 850 seconds	4-167
4.8-19	X-axis vibration measured in the clockwise roll engine nozzle of the service module RCS quad A of the BP-15 spacecraft	4-168
4.8-20	Perpendicular axis vibration measured in the clockwise roll engine nozzle of the service module RCS quad A of the BP-15 spacecraft	4-169

UNCLASSIFIED

UNCLASSIFIED

xvii

Figure		Page
4.8-21	Digital spectrum estimation of X-axis vibration over the time period T+48 to T+50 seconds measured in the clockwise roll engine nozzle of the service module RCS quad A of the BP-15 spacecraft	4-170
4.8-22	Digital spectrum estimation of the perpendicular axis vibration over the period T+48.01 to T+50.01 seconds measured in the clockwise roll engine nozzle of the service module RCS quad A of the BP-15 spacecraft	4-171
4.9-1	Overall sound pressure level time history from T-10 to T+110 seconds for BP-15 spacecraft	4-174
4.9-2	One-third octave band analysis of BP-15 spacecraft launch-vehicle sound pressure level at T+1 second	4-175
4.9-3	Comparison of BP-13 and BP-15 launch-vehicle sound pressure levels from T-2 to T+8 seconds	4-176
4.9-4	One-third octave band analysis of BP-15 aerodynamic sound pressure levels at T+53 seconds	4-177
4.10-1	Command module heat protection for BP-15 spacecraft	4-180
4.10-2	Launch-escape tower temperature transducer locations on BP-15 spacecraft	4-181
4.10-3	Bond-line LES tower temperatures measured during flight of BP-15 spacecraft	
	(a) Tower temperatures 1, 2 and 8	4-182
	(b) Tower temperatures 4, 5 and 7	4-183
	(c) Tower temperatures 3 and 6	4-184
4.11-1	Top view of BP-15 spacecraft command module showing calorimeter locations	4-189
4.11-2	Development view of BP-15 spacecraft service module, insert, and adapter compartment showing calorimeter locations	4-191

UNCLASSIFIED

UNCLASSIFIED

Figure		Page
4.11-3	Launch configuration environment in terms of Mach number (M) and Reynolds number (Re_D) for BP-15 spacecraft	4-191
4.11-4	Angle of attack history for BP-15 spacecraft (Q-ball data)	4-192
4.11-5	Heating rates measured on BP-15 spacecraft command module	
	(a) Calorimeters 1, 5, and 10	4-193
	(b) Calorimeters 6, 7, and 8	4-194
	(c) Calorimeters 2, 4, and 11	4-195
	(d) Calorimeters 3, 9, and 12	4-196
	(e) Calorimeters 1, 2, and 3	4-197
	(f) Calorimeters 4, 5, and 9	4-198
	(g) Calorimeters 10, 11, and 12	4-199
	(h) Calorimeters 1, 2, and 3	4-200
	(i) Calorimeters 11 and 12	4-200
	(j) Calorimeters 4, 5, 6 and 9	4-201
	(k) Calorimeters 3, 9 and 12	4-202
	(l) Calorimeters 2, 4 and 11	4-202
	(m) Calorimeters 1, 5 and 10	4-203
	(n) Calorimeters 6, 7 and 8	4-203
4.11-6	Comparisons of BP-13 and BP-15 spacecraft rate	
	(a) BP-13 and BP-15 calorimeter 3	4-204
	(b) BP-13 and BP-15 calorimeter 5	4-204
	(c) BP-13 and BP-15 calorimeter 10	4-205
	(d) BP-13 and BP-15 calorimeter 16	4-205
4.11-7	Heating rates measured on BP-15 spacecraft service module	
	(a) Calorimeters 14 and 16	4-206
	(b) Calorimeters 15 and 19	4-207
	(c) Calorimeters 17 and 18	4-208
	(d) Calorimeters 13 and 20	4-209
4.11-8	Comparison of calorimeter body temperatures at locations 13 and 20	4-210
4.12-1	Environmental control subsystem schematic for BP-15 spacecraft	4-216

UNCLASSIFIED

UNCLASSIFIED

xix

Figure		Page
4.12-2	Equipment cooling prelaunch data for BP-15 spacecraft	4-217
4.12-3	Sectional view of coolant-pump assembly for BP-15 spacecraft	4-218
4.12-4	Command module cabin pressure for BP-15 spacecraft	4-219
5.1-1	Apollo mission A-102 space vehicle showing cutaway views of launch vehicle	5-4
7.1-1	Spacecraft BP-15 schedule milestones at ATO Downey	7-5
7.1-2	Spacecraft BP-15 schedule milestones at MSC Florida Operations	7-6
7.1-3	BP-15 spacecraft CM SM being stacked on adapter section in Hangar AF, Cape Kennedy, Florida	7-7
7.1-4	BP-15 spacecraft being lifted to mate with the SA-7 launch vehicle at Launch Complex 37B, Cape Kennedy, Florida	7-8
7.1-5	LES being lifted for mating to the spacecraft at Launch Complex 37B, Cape Kennedy, Florida	7-9
7.2-1	Apollo mission A-102 countdown activities	
	(a) T-1 day, September 17, 1964	7-12
	(b) Launch day, September 18, 1964	7-13
	(c) Launch day, September 18, 1964	7-14
7.4-1	Engineering sequential tracking camera locations for Apollo mission A-102	7-36
7.4-2	Engineering sequential fixed camera locations for Apollo mission A-102	7-37
9.1-1	BP-15 spacecraft transponder interrogation and response	9-4
9.3-1	BP-15 spacecraft calorimeter	9-8

UNCLASSIFIED

UNCLASSIFIED

xxi

CONTRIBUTORS

Spacecraft Description: T. Dalton, W. H. Waln, D. G. Nichols,
A. L. Branscomb, A. L. Cave, V. V. Sheeley, W. F. Edson.

Instrumentation, Electrical, Sequential, and Communications:
J. F. Rutherford, J. B. Pennington, J. M. Eller, P. Katalansky,
F. M. Groark, R. Stevens, G. Manning, R. E. McCoy, R. F. Jones,
T. G. Broughton, C. P. Lassetter, A. E. Warner.

Pyrotechnics and Propulsion: W. H. Simmons, P. Davis, H. E. Heilman,
L. J. Haywood, E. A. Timmons, J. O. Payne.

Structures and Acoustics: W. M. West, B. V. Zuber, S. P. Weiss,
W. F. Rogers, B. O. French.

Reaction Control Subsystem: N. H. Chaffee

Heat Protection and Aerothermodynamics: J. E. Pavlosky,
N. W. Willis, R. M. Raper.

Equipment Cooling: D. F. Hughes, J. R. Hiers, S. P. Moody.

Trajectory and Launch Vehicle: D. J. Incerto, W. P. Beal,
J. L. Wells, M. Cassetti, R. D. Nelson, R. Teasley, G. Emanuel.

Mission Operations, Data, and Tape Selection: F. Peters,
J. M. Gerding, R. E. Reyes, K. Sorey, D. T. Jensen, D. M. Goldenbaum,
T. J. Grace, S. A. DeMars, F. B. Blanton, M. V. Britt, E. C. Wang,
R. C. Shirley, C. E. Roth, J. M. Eller, R. H. Talbert, W. T. Lauten.

Anomalies: C. J. Appelberg, E. Rangel, G. Zilling.

Editing, Summary, and Concluding Remarks: J. D. Lobb,
C. T. Stewart, F. Peters, J. M. Gerding, E. O. Zeitler, R. E. McKann,
W. J. Fitzpatrick, D. T. Jensen.

UNCLASSIFIED

1.0 SUMMARY

The Apollo spacecraft mission A-102 was successfully accomplished on September 18, 1964. The unmanned boilerplate spacecraft (BP-15) was launched at 11:22:43 a.m. e.s.t.^a into earth orbit from complex 37B of the Eastern Test Range, Cape Kennedy, Florida, by the Saturn I Block II vehicle, SA-7.

The purpose of the test was to demonstrate the compatibility of the spacecraft with the launch vehicle, to determine the launch and exit environmental parameters for design verification, and to demonstrate the alternate mode of escape-tower jettison, utilizing the launch-escape and pitch-control motors.

All mission test objectives were fulfilled by the time of orbital insertion, and additional data were obtained by telemetry through the Manned Space Flight Network until the end of effective battery life during the fourth orbital pass. Radar skin tracking was continued by the network until the spacecraft reentered over the Indian Ocean during its 59th orbital pass.

During the countdown, there were no holds caused by the spacecraft. All spacecraft subsystems fulfilled their specified functions throughout the countdown and the planned flight-test period. Engineering data were received through telemetry from all but two of the instrumented spacecraft measurements for the full flight-test period of the mission.

The actual trajectory at time of S-I stage cutoff was slightly higher than planned in velocity, altitude, and flight-path angle. At S-IV stage cutoff, altitude was slightly lower and velocity was slightly higher than planned, which resulted in a more elliptical orbit than planned.

The instrumentation subsystem was successful in determining the launch and exit environment, and telemetry reception of the data was continuous through launch and exit except for a short period during vehicle staging.

The launch-heating environment of the BP-15 spacecraft was similar to that encountered by the BP-13 spacecraft. Peak values at most points for the two flights were approximately equal; however, the influence of surface irregularities, as well as circumferential variations in heating,

^aUnless specified otherwise all times shown in this report are taken from the instant of vehicle lift-off (launch vehicle IU umbilical disconnect at 11:22:43 a.m. e.s.t.).

~~CONFIDENTIAL~~

was somewhat different for the two flights because of differences in trajectory and angle of attack. Both command and service module heating rates were within the predicted range. The heat-protection equipment on the launch-escape subsystem (LES) was subjected to temperatures much lower than the design limits which were established on the basis of an aborted mission.

The launch-escape-tower jettison by the alternate mode was successful. Positive ignition of the pitch-control motor could not be determined; however, the general trajectory indicated that it operated properly. The launch-escape motor, together with the pitch-control motor, carried the tower structure safely out of the path of the spacecraft.

All strain-gage, pressure, and accelerometer measurements indicated that the spacecraft performed satisfactorily in the launch environment. Command-module conical-surface static pressures correlated closely with wind-tunnel data, and the product of angle of attack and dynamic pressure (αq) did not exceed 1,000 (deg)(lb/sq ft). The venting system of the service module performed as expected. The command-module instrumentation compartment differential pressure reached a maximum of 13.3 psi, but vented rapidly after launch-escape subsystem separation.

A 1.8g, peak-to-peak, 10-cps vibration was noted during holddown. Other vibration modes were similar to those experienced during the BP-13 spacecraft flight. One of the simulated reaction-control-subsystem quad assemblies was instrumented for vibration on the BP-15 spacecraft flight. The measured vibration levels were above the design limit.

The strain measurements in the command module and service module indicated that all bending moments were within the design limits.

Of the 133 measurements transmitted by telemetry from the spacecraft, 131 produced continuous data.

The ground-support equipment performed satisfactorily during pre-launch and countdown operations.

~~CONFIDENTIAL~~

2.0 INTRODUCTION

Apollo mission A-102 was the second flight of an Apollo spacecraft configuration with a Saturn launch vehicle. The unmanned flight-test vehicle consisted of the boilerplate 15 (BP-15) spacecraft and the SA-7 Saturn I Block II launch vehicle. The space vehicle, shown in figure 2.0-1, was launched from Complex 37B of the Eastern Test Range, Cape Kennedy, Florida, on September 18, 1964, at 11:22:43 a.m. e.s.t.

The BP-15 spacecraft was the second of two boilerplate spacecraft (see table 2.0-I) planned to be used in demonstrating the compatibility of the Apollo spacecraft configuration with the Saturn I Block II launch vehicle in a launch and exit environment using trajectories similar to those expected for future Apollo-Saturn V orbital flights with production spacecraft. The first of this series, the BP-13 spacecraft, was successfully launched on May 28, 1964 (ref. 1).

The spacecraft flight configuration consisted of a prototype launch-escape subsystem (LES), boilerplate command module (CM), boilerplate service module (SM), and insert and adapter. Boilerplate flight-test spacecraft are developmental vehicles which simulate production spacecraft only in external size, shape, and mass characteristics.

Boilerplate flight-test spacecraft are equipped with instrumentation to obtain flight-test data for engineering analysis and evaluation. These data are used to confirm or modify the design criteria for the production spacecraft.

The flight sequence of major events during the flight of the BP-15 spacecraft into orbit is given in figure 2.0-2. Spacecraft separation from the launch vehicle was not planned for this flight; therefore, the second stage (S-IV) and instrument unit (IU) of the launch vehicle, together with the attached spacecraft (without the LES which was jettisoned), were inserted into orbit as a single unit. There were no provisions or plans for recovery of the spacecraft.

The flight test of the BP-15 spacecraft included the following features not included in the flight test of the BP-13 spacecraft:

- (1) The installation of instruments on one of the simulated reaction-control-subsystem quadrants on the SM for launch and exit temperature and vibration studies.
- (2) The demonstration of the alternate mode of LES jettison, using the launch-escape motor and pitch-control motor instead of using the tower-jettison motor, as in the normal mode of jettison.

~~CONFIDENTIAL~~

The first-order test objectives for the overall mission applied to the launch vehicle only, with the exception of verification of compatibility of the spacecraft with the launch vehicle under preflight and flight conditions.

The test objectives which applied only to the Apollo BP-15 spacecraft were as follows:

- (1) Determine the launch and exit environmental parameters to verify design criteria
- (2) Demonstrate the alternate mode of spacecraft LES jettison utilizing the launch-escape motor and pitch-control motor. These objectives were satisfactorily fulfilled.

An evaluation of the flight data has been made, and the results of the evaluation are presented in this report.

~~CONFIDENTIAL~~

UNCLASSIFIED

2-3

TABLE 2.0-I.- APOLLO SPACECRAFT FLIGHT HISTORY

Mission	Spacecraft	Description	Launch date	Launch site
A-001	BP-6	First pad abort	11-7-63	White Sands Missile Range, N. Mex.
A-002	BP-12	High q abort	5-13-64	White Sands Missile Range, N. Mex.
A-101	BP-13	Nominal launch and exit environment	5-28-64	Cape Kennedy, Florida
A-102	BP-15	Nominal launch and exit environment	9-18-64	Cape Kennedy, Florida

UNCLASSIFIED

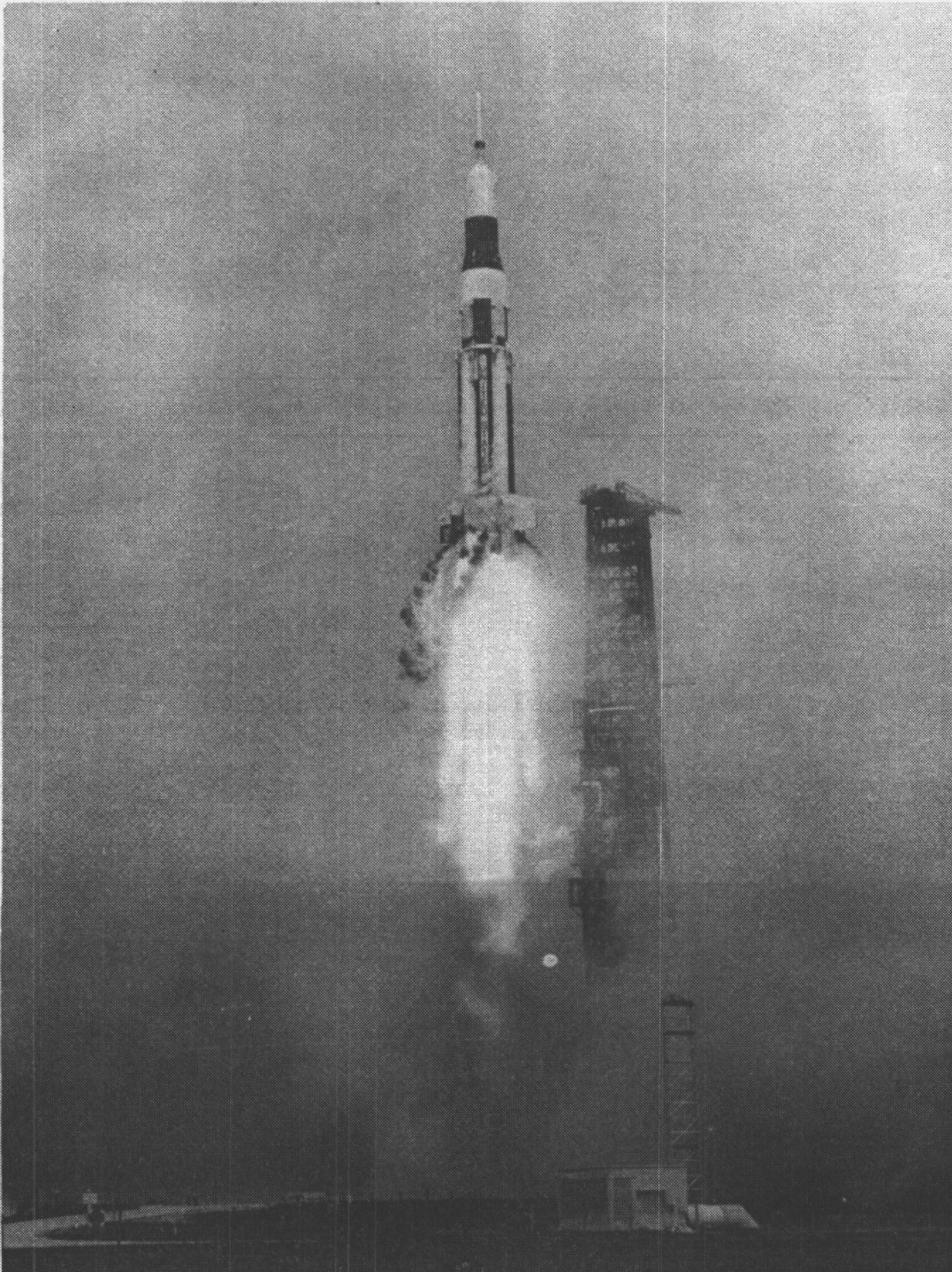
UNCLASSIFIED

Figure 2.0-1.- Saturn-Apollo space vehicle for mission A-102 at lift-off.

UNCLASSIFIED

~~CONFIDENTIAL~~

2-5

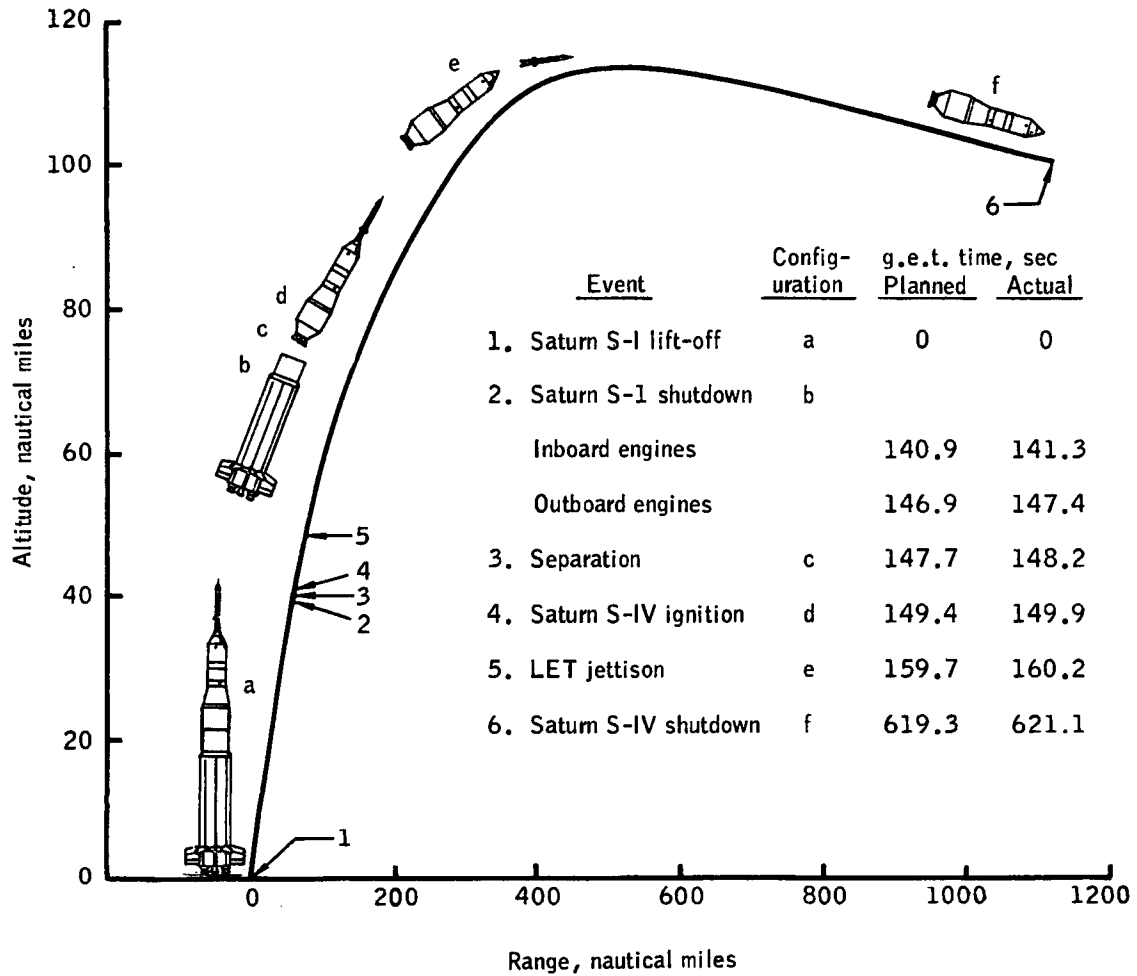


Figure 2.0-2.- Sequence of major events for Apollo mission A-102.

~~CONFIDENTIAL~~

~~CONFIDENTIAL~~

3-1

3.0 FLIGHT TRAJECTORIES

The trajectories referred to as "planned" were preflight-calculated nominal trajectories supplied by Marshall Space Flight Center (MSFC), and the trajectories referred to as "actual" were based on the Manned Space Flight Network tracking data. For both the planned and actual trajectories, the 1963 revised Patrick atmosphere was used below 25 nautical miles and the 1962 U.S. Standard Model Atmosphere was used above 25 nautical miles, except that the measured atmosphere at the time of lift-off was used for the actual trajectory up to 18.6 nautical miles. The earth model used was the Fischer Ellipsoid. The ground track for the first three orbital passes of the Apollo mission A-102 is presented in figure 3.0-1. The altitude-longitude profile for the launch and three orbital passes, presented in figure 3.0-2, shows that the actual profile was close to the nominal.

A comparison of the actual and planned mission event times for the launch phase is given in table 3.0-I. It can be seen from the table that the actual S-I cutoff sequence was approximately 0.7 second later than planned, and the actual S-IV cutoff was approximately 2.0 seconds later than planned.

The actual launch trajectory shown in figure 3.0-3 was based on the real-time data output of the Range Safety Impact Predictor Computer (IP-7094) which used FPS-16, Azusa, and the FPQ-6 radars. The data from these tracking facilities were used during the time periods listed in the following table.

Radars used	g.e.t., min:sec
FPS-16	0:00 to 0:31
^a Azusa and FPS-16	0:31 to 6:05
^a FPQ-6 and FPS-16	6:05 to 8:22
FPQ-6	8:22 to 11:04

^a Radar tracking data during these times alternated frequently between these two radars.

The actual launch trajectory is compared with the planned launch trajectory in figure 3.0-3. It can be seen from this figure that the

~~CONFIDENTIAL~~

~~CONFIDENTIAL~~

actual launch trajectory did provide the launch environment planned for this mission. At S-I stage cutoff, the actual trajectory parameters were approximately 198 feet per second high in inertial velocity, 6,400 feet high in altitude, and approximately $\frac{1}{2}^\circ$ high in flight-path angle. During the S-IV burning, the inertial velocity and flight-path angle drop below the planned at approximately T+5 minutes, and remain below until just before cutoff. At S-IV cutoff, the velocity was 3.5 feet per second greater, the flight-path angle was 0.0023° less, and the altitude was 1,704 feet less than planned, resulting in a more elliptical orbit. The perigee was approximately 0.2 nautical mile lower and the apogee was approximately 4 nautical miles higher than planned.

The orbital portion of the trajectory is shown in figure 3.0-4. The planned orbital trajectory was obtained using the nominal insertion conditions, supplied by MSFC, and integrating forward for three orbital passes. The actual orbital portion of the trajectory was derived from the orbital position and velocity vector obtained during the first pass over White Sands Missile Range (WSMR). This vector was determined from the Manned Space Flight Network tracking data using the Goddard computer. The WSMR vector was integrated backward along the flight trajectory to orbital insertion (defined as S-IV cutoff plus 10 seconds) and forward for three orbital passes. These integrated values were in good agreement with the position and velocity vectors determined by the Goddard computer for passes near Pretoria, South Africa; Carnarvon, Australia; and Point Arguello, California, during the first pass. The inertial velocities reported by these stations agreed within 5.5 ft/sec, and the flight-path angle within 0.015° . Thus the validity of the integrated orbital portion of the flight trajectory was established. It can be seen in figure 3.0-4 that the actual orbital flight trajectory was in very close agreement with the planned.

A comparison of the actual and planned trajectory parameters is given in table 3.0-II. The table shows that the actual insertion conditions and orbital parameters were in good agreement with those planned. Using the WSMR velocity vector, the estimated lifetime of the orbital configuration, consisting of the BP-15 spacecraft, the instrument unit, and the Saturn S-IV stage, was calculated to be 53 orbital passes, based on lifetime drag characteristics obtained from SA-6 data. The actual reentry of the orbital configuration into the Indian Ocean was reported during the 59th orbital pass.

A comparison of the trajectories of the BP-13 and BP-15 spacecraft indicates that SA-6 had a higher velocity through max q and that SA-7 attained the higher velocity shortly before S-I engine 8 cut-off for an overall faster trajectory than SA-6.

~~CONFIDENTIAL~~

~~CONFIDENTIAL~~

3-3

A complete detailed analysis of the flight trajectory of the launch vehicle is presented in reference 7.

~~CONFIDENTIAL~~

~~CONFIDENTIAL~~

TABLE 3.0-I.- MISSION EVENT TIMES

[Based on lift-off signal as determined by launch-vehicle
IU umbilical disconnect at 11:22:43.26 a.m. e.s.t.]

Event	Planned, sec	Actual, sec	Difference, sec
Lift-off	0	0	0
Tilt arrest	136.3	136.3	0
IECO	140.7	141.3	.6
OECO	146.7	147.4	.7
Ullage rockets ignition	147.4	148.1	.7
Separation of S-I and S-IV	147.5	148.2	.7
S-IV ignition	149.2	149.9	.7
Ullage rocket jettison	159.5	160.2	.7
Launch-escape-tower jettison	159.5	160.2	.7
S-IV cutoff	619.1	621.1	2.0

~~CONFIDENTIAL~~

~~CONFIDENTIAL~~

3-5

TABLE 3.0-II.- COMPARISON OF SA-7 PLANNED AND ACTUAL TRAJECTORY PARAMETERS

Condition	Planned	Actual	Difference
S-IV cutoff			
Time from lift-off, sec	619.1	621.1	2.0
Time from lift-off, min:sec	10:19.1	10:21.1	00:2.0
Geodetic latitude, deg North	21.9258	21.8927	-0.0331
Longitude, deg West	-61.3020	-61.1836	-0.1184
Altitude, feet	608,004	606,300	-1,704
Altitude, nautical miles	100.06	99.78	-0.28
Range, nautical miles	1,119.67	1,126.5	6.8
Space-fixed velocity, ft/sec	25,610.18	25,618.68	8.5
Space-fixed flight-path angle, deg . . .	0.0700	0.0677	-0.0023
Space-fixed heading angle, deg East of North	113.6960	113.7113	0.0153
S-IV cutoff +10 sec (insertion)			
Time from lift-off, sec	629.1	631.1	2.0
Time from lift-off, min:sec	10:29.1	10:31.1	00:2.0
Geodetic latitude, deg North	21.6491	21.6159	-0.0332
Longitude, deg West	-60.6726	-60.5549	-0.1177
Altitude, feet	608,088	606,372	-1,716
Altitude, nautical miles	100.08	99.80	-0.28
Range, nautical miles	1,158.55	1,165.36	6.9
Space-fixed velocity, ft/sec	25,615.04	25,623.54	8.5
Space-fixed flight-path angle, deg . . .	0.0716	0.0695	-0.0021
Space-fixed heading angle, deg East of North	113.9443	113.9590	0.0147

~~CONFIDENTIAL~~

~~CONFIDENTIAL~~

TABLE 3.0-II.- COMPARISON OF SA-7 PLANNED AND ACTUAL
TRAJECTORY PARAMETERS - Concluded

Condition	Planned	Actual	Difference
Orbital parameters			
Perigee altitude, statute miles	115.17	114.85	- 0.32
Perigee altitude, nautical miles	100.08	99.80	- 0.28
Apogee altitude, statute miles	136.75	140.82	4.07
Apogee altitude, nautical miles	118.83	122.37	3.54
Period, min	88.58	88.64	0.06
Inclination angle, deg	31.76	31.75	- 0.01
Maximum conditions			
Altitude, statute miles	136.75	140.82	4.07
Altitude, nautical miles	118.83	122.37	3.54
Space-fixed velocity, ft/sec	25,615.04	25,623.54	8.50
Earth-fixed velocity, ft/sec	24,287.75	24,296.21	8.46
Exit acceleration, g	5.80	5.88	0.08
Exit dynamic pressure, lb/sq ft	720.0	749.6	29.6
Lifetime, revolutions	53	59	6

~~CONFIDENTIAL~~

UNCLASSIFIED

3-7

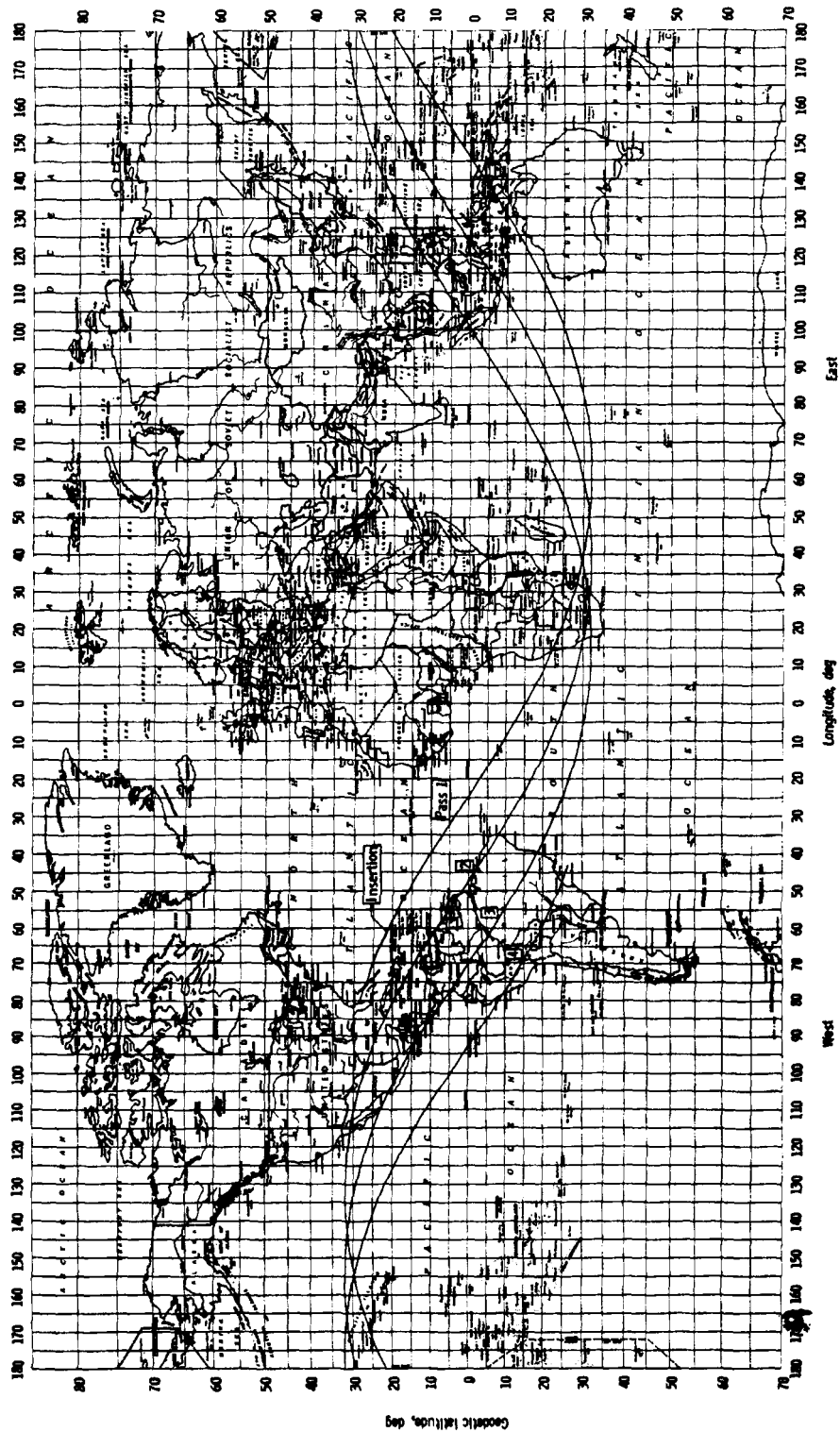


Figure 3.0-1.- Ground track for the Apollo A-102 orbital mission for the first three orbital passes.

UNCLASSIFIED

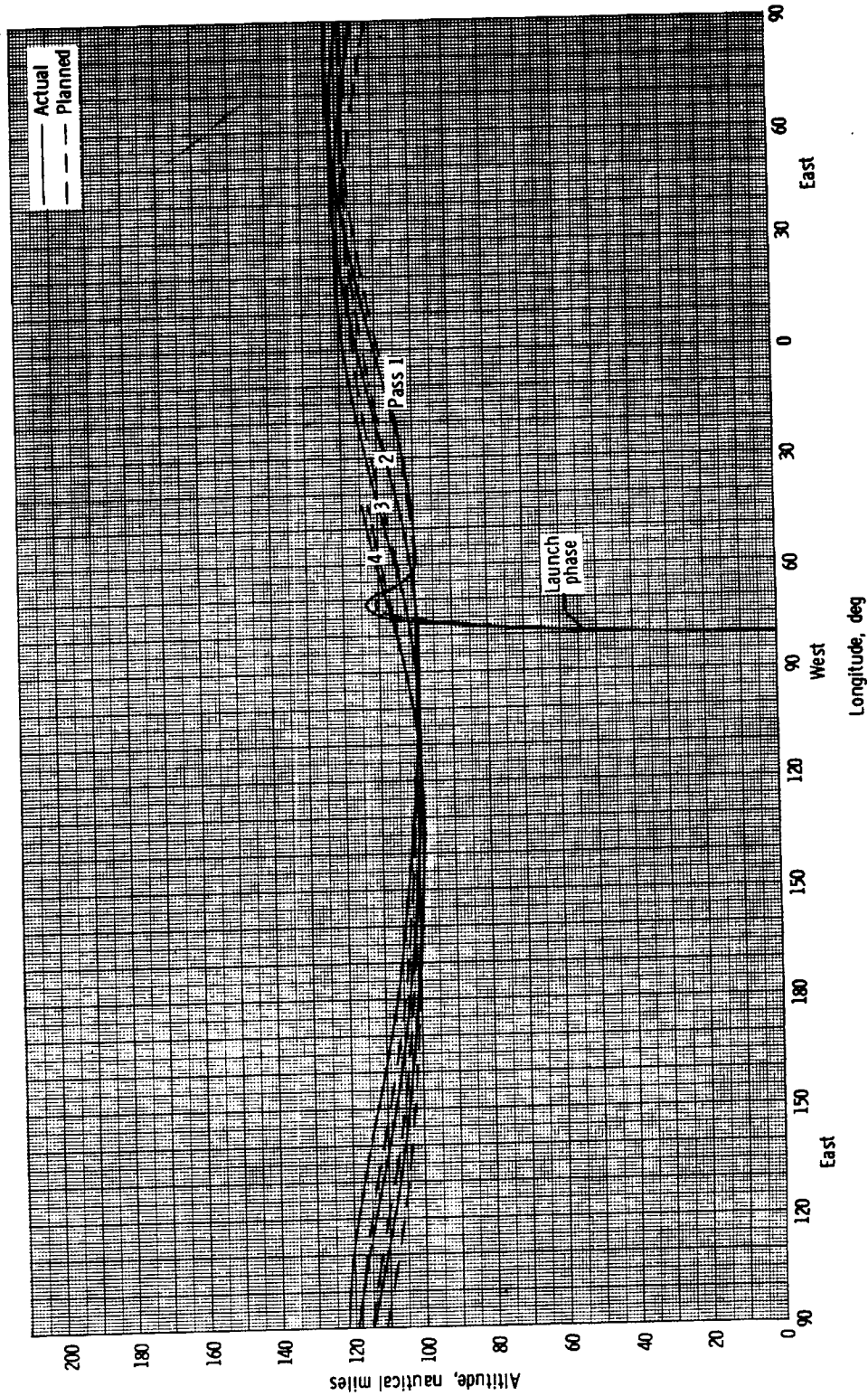
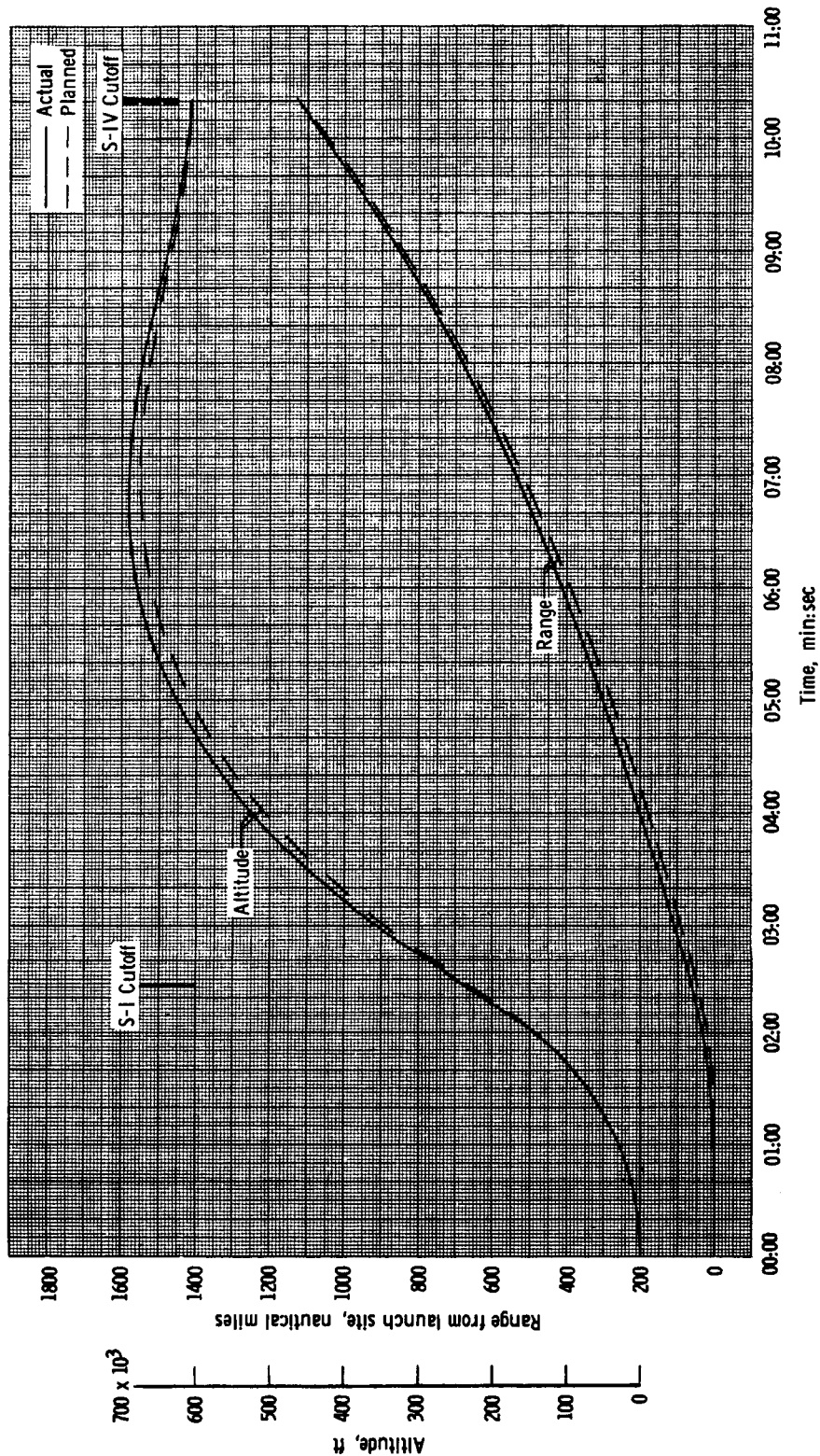
~~CONFIDENTIAL~~

Figure 3.0-2 - Altitude-longitude profile for Apollo mission A-102 for the first three orbital passes.

~~CONFIDENTIAL~~

~~CONFIDENTIAL~~

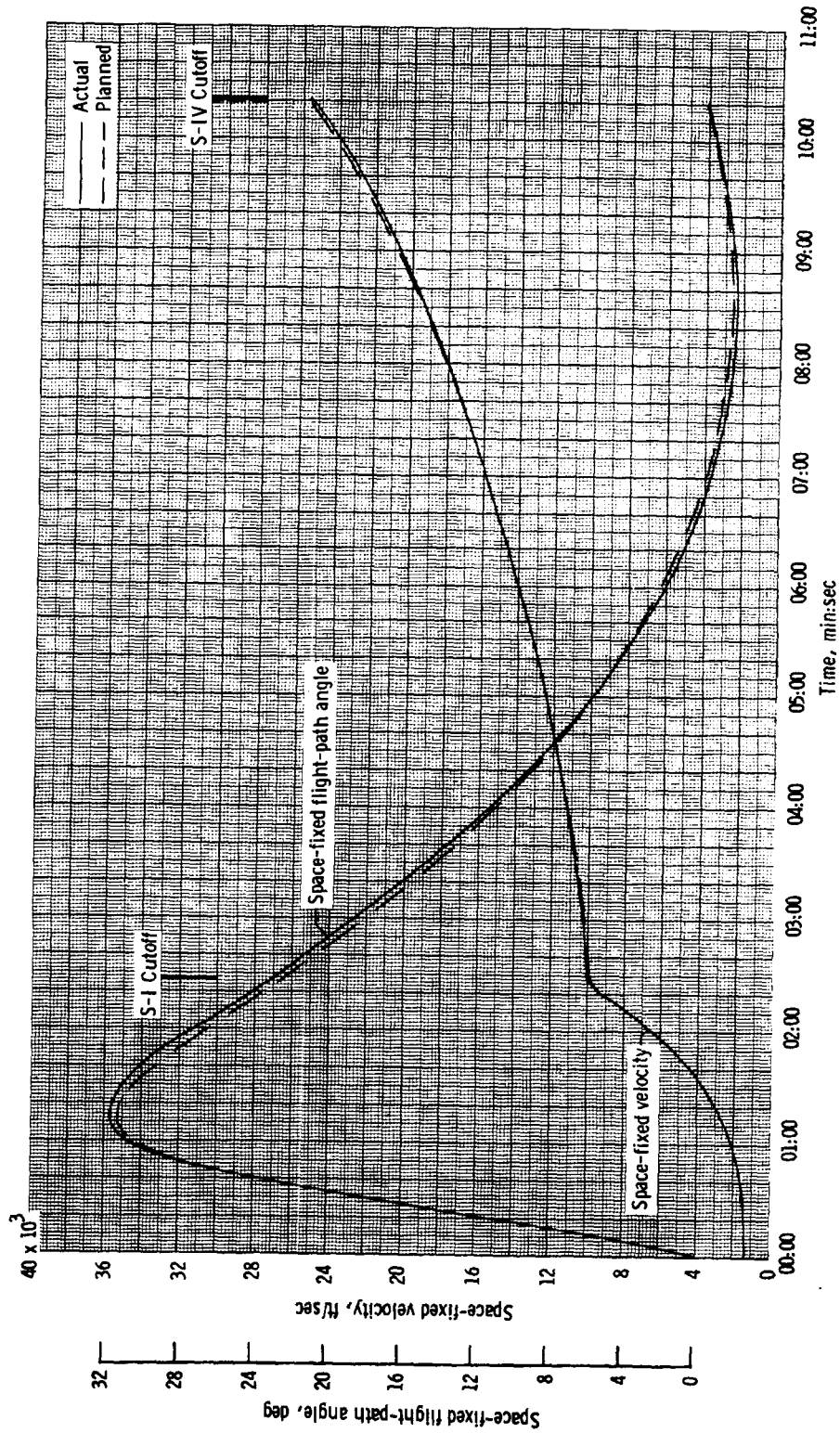
3-9



(a) Altitude and range.

Figure 3.0-3. - Time histories of trajectory parameters for the Apollo mission A-102 launch phase.

~~CONFIDENTIAL~~

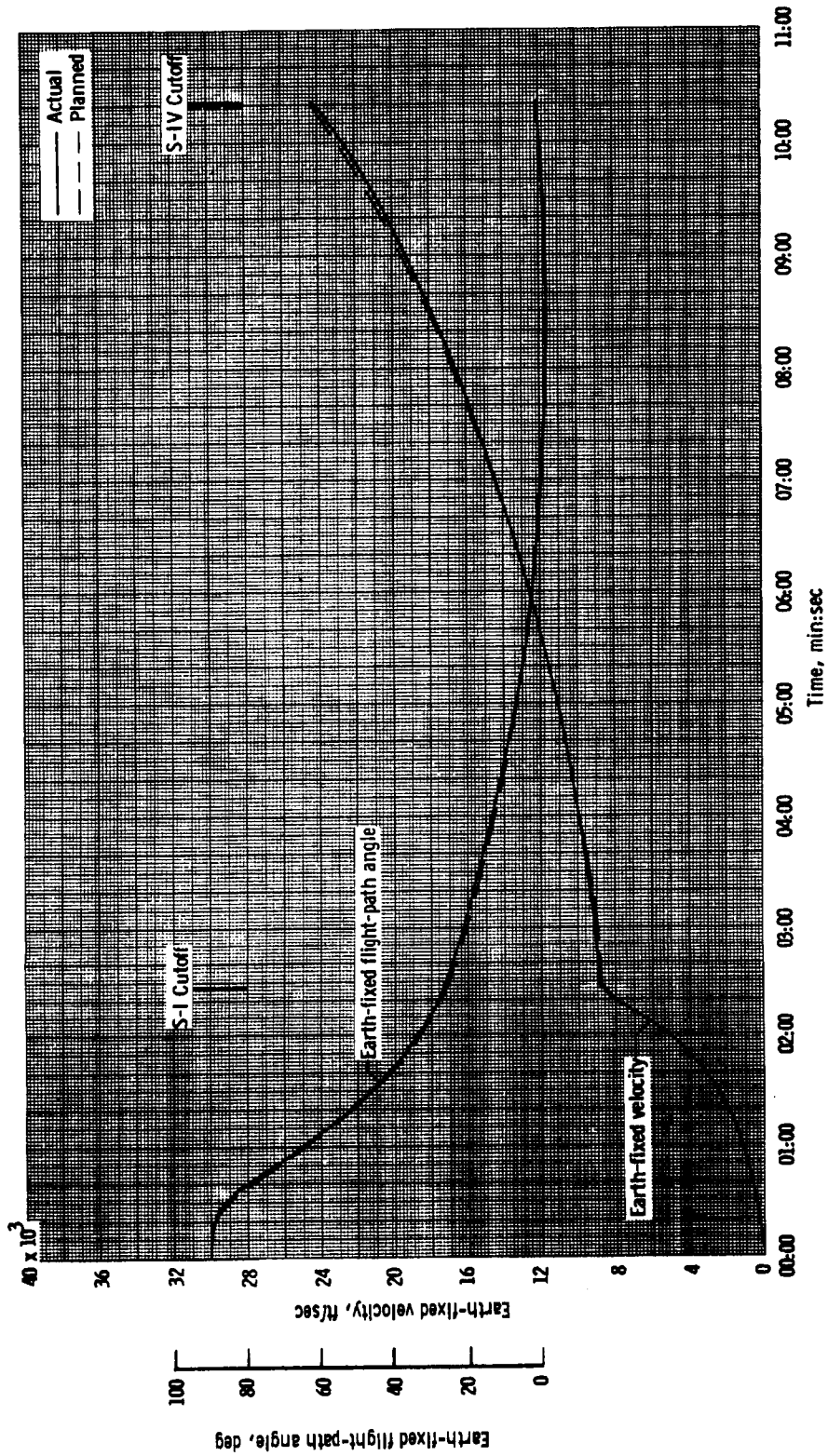
~~CONFIDENTIAL~~

(b) Space-fixed velocity and flight-path angle.

Figure 3.0-3. - Continued.

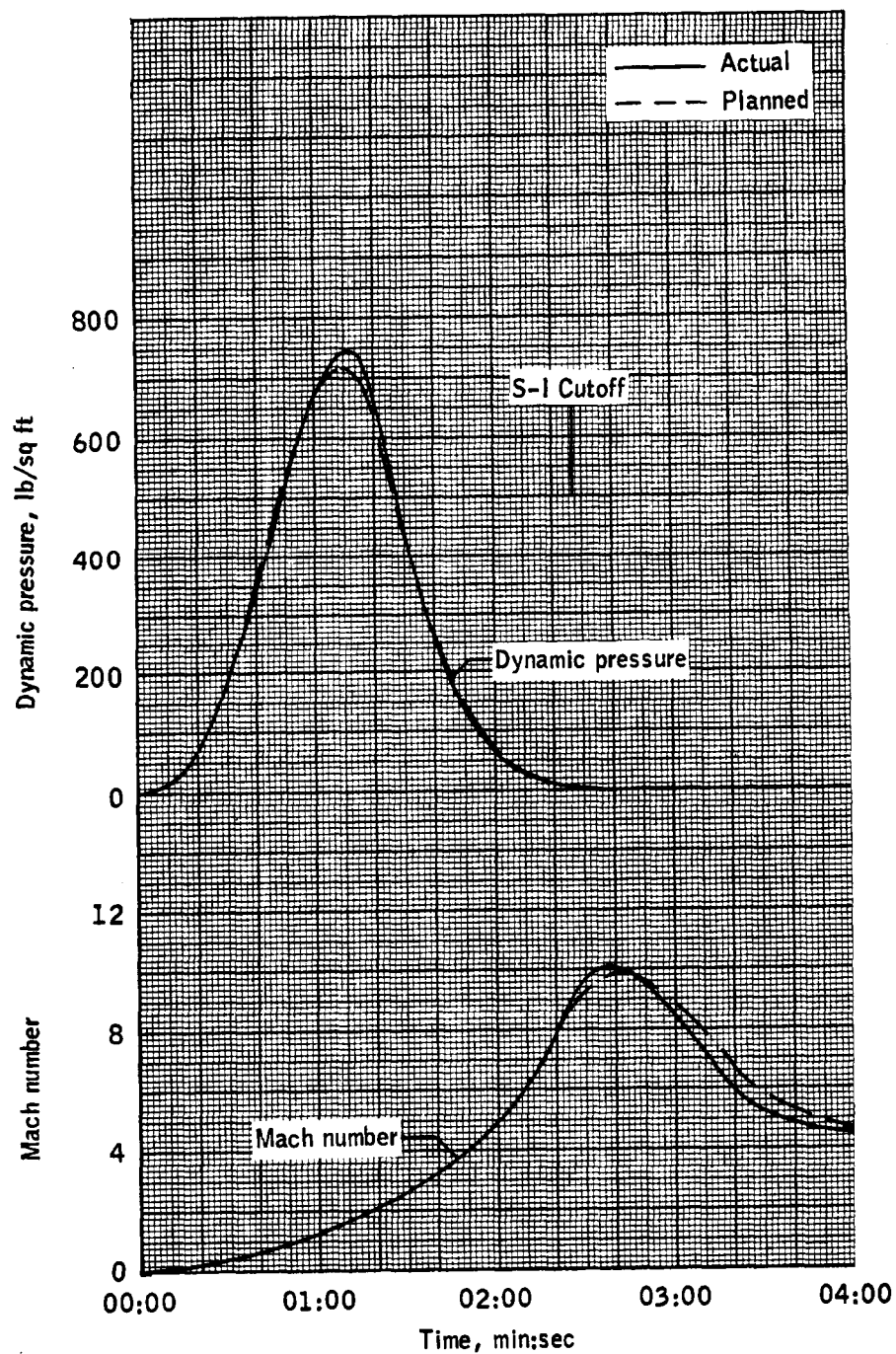
~~CONFIDENTIAL~~

~~CONFIDENTIAL~~



(c) Earth-fixed velocity and flight-path angle.

Figure 3.0-3. - Continued.

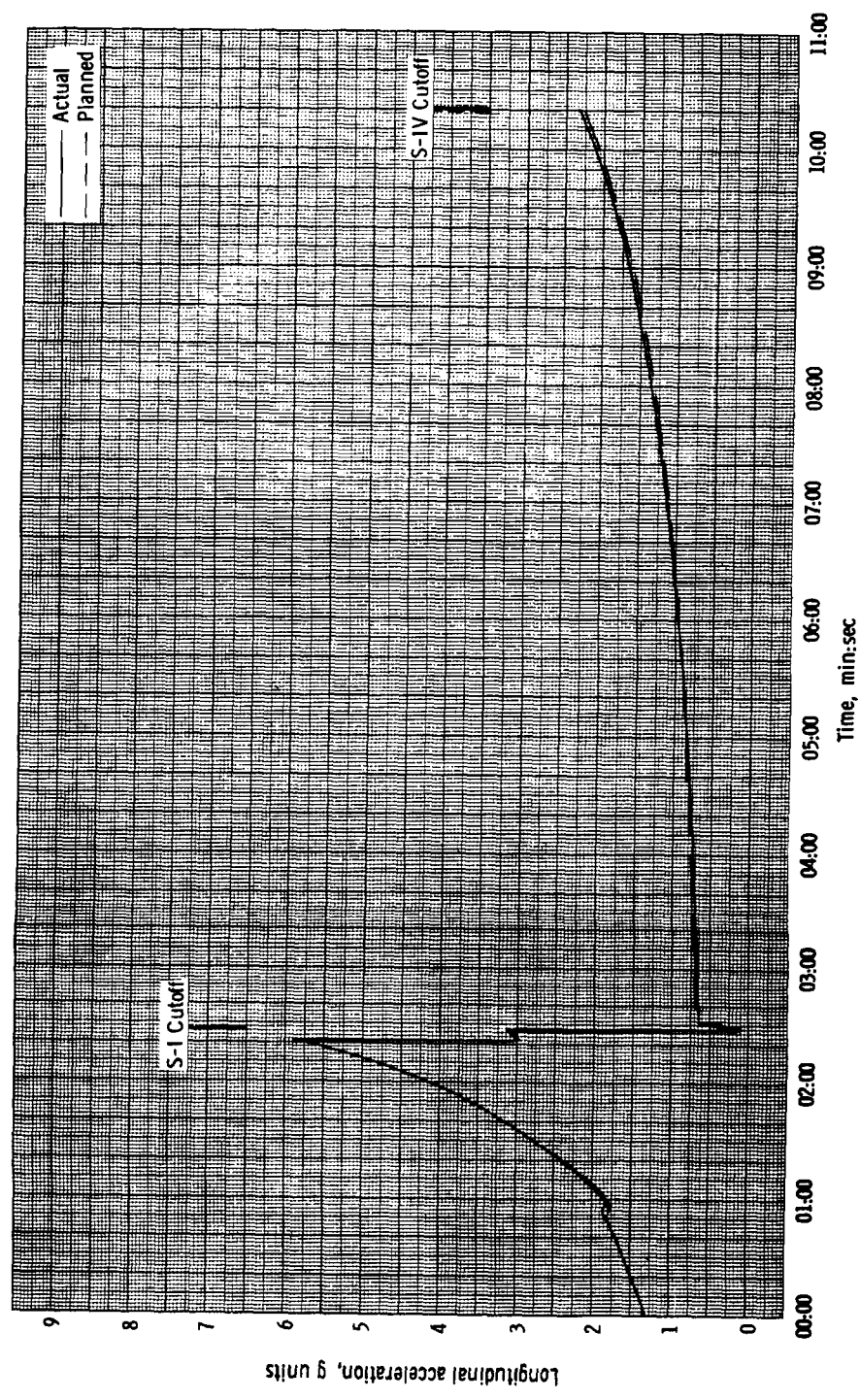
~~CONFIDENTIAL~~

(d) Dynamic pressure and Mach number.

Figure 3.0-3.- Continued.

~~CONFIDENTIAL~~

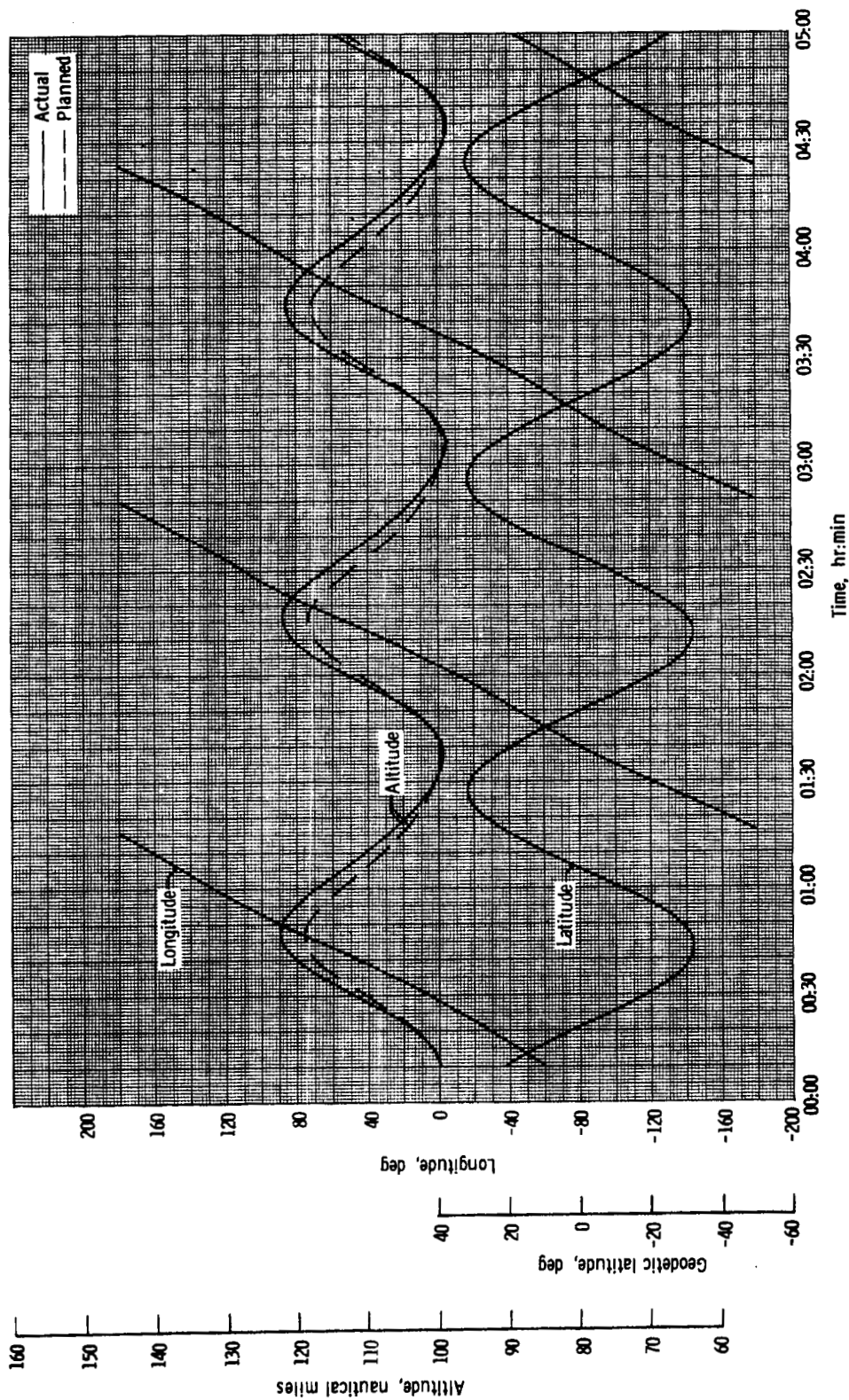
~~CONFIDENTIAL~~



(e) Longitudinal acceleration along spacecraft X-axis.

Figure 3.0-3. - Concluded.

~~CONFIDENTIAL~~

CONFIDENTIAL

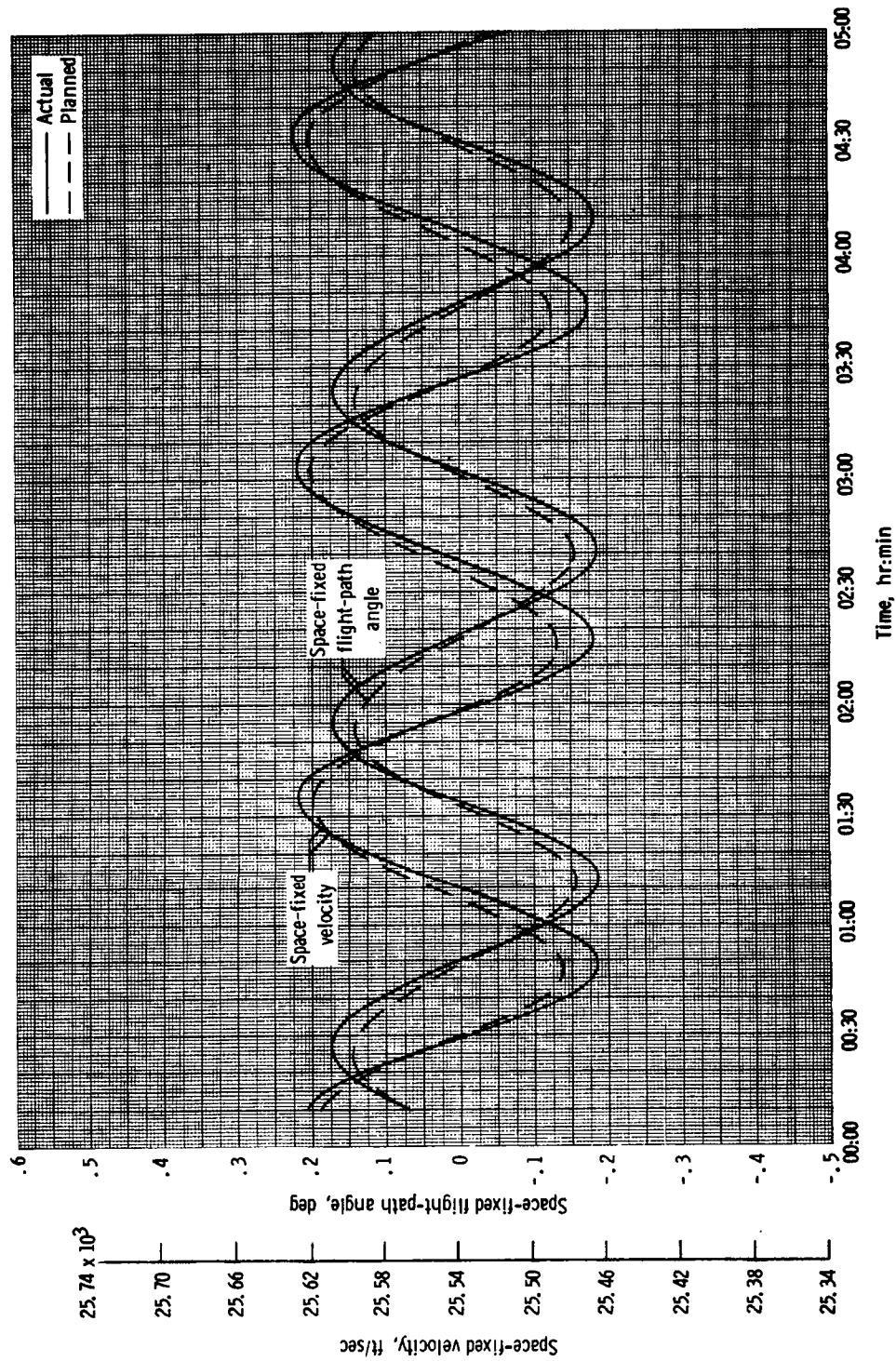
(a) Latitude, longitude, and altitude.

Figure 3.0-4 - Time histories of trajectory parameters for Apollo mission A-102 for first three passes of orbital phase.

CONFIDENTIAL

~~CONFIDENTIAL~~

3-15



6) Space-fixed velocity and flight-path angle.

Figure 3.0-4. - Concluded.

~~CONFIDENTIAL~~

4.0 SPACECRAFT DESCRIPTION AND PERFORMANCE

4.1 Spacecraft Description

The Apollo boilerplate 15 (BP-15) spacecraft was composed of four major assemblies: the launch-escape subsystem (LES), the command module (CM), the service module (SM), and the insert and adapter. These major assemblies were similar in external configuration to the production Apollo spacecraft. The major assemblies and exterior dimensions of each are shown in figure 4.1-1. The reference axes system for locations within the spacecraft is given in figures 4.1-2 and 4.1-3. The MSC axes system for orientation and motion is given in figure 4.8-7.

The launch-escape subsystem (LES) is shown in figure 4.1-4. The truss-type tower structure was a welded titanium tubular frame, and the exposed surfaces were covered with silica-filled Buna-N rubber for thermal insulation. Each of the four legs of the LES was attached to the command module by an explosive bolt. A structural skirt was mounted between the top of the tower structure and the launch-escape motor. The bolt attachments at the interface between the tower and the skirt provided LES alignment capability. Two sequencers which forwarded a firing signal to the LES pyrotechnics were attached to the underside of the skirt.

The LES motors for pitch control, tower jettison, and launch escape were live. However, there were no initiators installed in the jettison motor, and the wiring circuit from the sequencers to this motor was purposely not completed so as to simulate a jettison-motor failure. The alternate mode of tower jettison (by firing only the launch-escape and pitch-control motors) was used.

A conical section of welded Inconel sheet was mounted to the forward end of the pitch-control-motor housing. The section contained 183 pounds of sheet lead ballast to provide the proper LES mass characteristics. The ballast enclosure also provided the interface plane for mounting the Q-ball assembly. The performance of the LES is described in sections 4.5 and 4.6.

The command module was conical with a convex base and rounded apex. The apex consisted of a fiber-glass radome containing the VHF telemetry omniantenna. (See fig. 4.4-2.) The CM sides were semimonocoque aluminum structures terminating in the forward and aft heat shields. The exterior was covered with cork for protection against aerodynamic heating. Section 4.10 presents a description of the cork insulation configuration. The inner side walls and the top of the cabin were insulated with a quilted glass-fiber material. The major components of the subsystems

~~CONFIDENTIAL~~

~~CONFIDENTIAL~~

were mounted on shelves and brackets located along portions of the inner wall as shown in figures 4.1-5 and 4.1-6.

A cylindrical aluminum structure was welded to the forward bulkhead of the CM to simulate the egress tunnel of the production spacecraft. A main hatch of aluminum alloy provided access to the cabin. Prior to launch, the hatch was bolted to the CM exterior structure and sealed with epoxy.

External protuberances of the production spacecraft configuration, including the air vent, umbilical fairing, simulated SM reaction-control subsystem (RCS) quad assemblies, and two scimitar antennas, shown in figure 4.1-7, were simulated for a better definition of launch environment parameters.

The CM aft heat shield was similar in size and shape to the operational heat shield. It was composed of an inner and outer layer of laminated glass fiber over an aluminum honeycomb core and was attached to the CM by four adjustable struts. No prototype ablative material was used because the aft heat shield was not exposed to the launch environment and no recovery of the spacecraft was planned.

The boilerplate service-module assembly consisted of the CM to SM fairing, service-module structure, and insert, all of which were bolted together. The boilerplate adapter was bolted to the insert. The SM assembly and the insert, shown in figure 4.1-8, were of semimonocoque aluminum construction. For further structural details, see section 4.7.

A pneumatically actuated umbilical assembly was located approximately 18 inches below the top of the SM at 122° (fig. 4.1-2). External electrical power, ground-support-equipment (GSE) signals, and coolant fluid entered the spacecraft through the umbilical prior to launch.

Four simulated RCS quad assemblies were attached to the upper portion of the SM exterior, 90° apart. In order to duplicate the aerodynamic characteristics of the production units, the simulated units were similar in size and shape and were arranged on the SM in the same location as they would be found on the production spacecraft. The RCS quad assembly located near the -Z axis was instrumented to provide temperature and vibration measurements. For further details see section 4.8.

In addition to the transducers and associated components and wiring, the SM and adapter contained electrical wire harnesses which interfaced with the launch-vehicle instrument unit for the Q-ball, tower-jettison command, and GSE signals (fig. 4.1-8).

~~CONFIDENTIAL~~

~~CONFIDENTIAL~~

4-3

The spacecraft weight when inserted into orbit was 17,231 pounds; the spacecraft weight at lift-off was 23,838 pounds. Prior to shipment from Downey, the total weight of BP-15 spacecraft was reduced by 1,600 pounds, which made the BP-13 and BP-15 spacecraft ballast configurations almost identical. This reduction was achieved by removing ballast from the SM and adapter. The BP-15 spacecraft weight was greater than that of BP-13 spacecraft by 208 pounds at orbit insertion and 295 pounds at lift-off. This weight variation was due to known structural changes and manufacturing variations. Table 4.1-I shows major module weight differences between the BP-13 and BP-15 spacecraft. The final weight was acceptable to Marshall Space Flight Center (MSFC). Actual weights for the command module, service module, and SM insert and adapter were individually obtained at Downey. The mated SM, CM, and adapter were weighed together at the Eastern Test Range (ETR). The actual weight and the location of the longitudinal center of gravity of the launch-escape subsystem were obtained at the NASA Merritt Island Launch Area (MILA). Weight changes to the spacecraft were then monitored until launch, and the actual weight and center-of-gravity data were adjusted. The resultant mass characteristics are shown in table 4.1-II. The weights shown in this table include ballast weights of 2,014 pounds in the CM, 245 pounds in the adapter, and 183 pounds in the LES.

~~CONFIDENTIAL~~

~~CONFIDENTIAL~~

TABLE 4.1-I.- WEIGHT COMPARISON OF BP-13 and BP-15 SPACECRAFT

	Weight, lb		
	BP-13	BP-15	Difference
Command module	9,300	9,477	177
Service module	4,172	4,149	-23
SM insert and adapter	<u>3,551</u>	<u>3,605</u>	<u>54</u>
Total spacecraft in orbit	17,023	17,231	208
LES	<u>6,520</u>	<u>6,607</u>	<u>87</u>
Total spacecraft at launch	23,543	23,838	295

~~CONFIDENTIAL~~

TABLE 4.1-II.- SPACECRAFT BP-15 MASS CHARACTERISTICS

	Weight, lb	Center of gravity, in. (a)			Moment of inertia, slug-ft ² (b)		
		X _A	Y	Z	Roll, I _{XX}	Pitch, I _{YY}	Yaw, I _{ZZ}
Command module	9,477	1,041.4	2.6	5.1	5,696	4,102	4,045
Service module	4,149	950.8	0.9	0.7	4,948	4,143	4,131
SM insert and adapter	<u>3,605</u>	785.3	-2.9	-1.4	4,475	4,004	3,956
Total spacecraft in orbit	17,231	966.0	1.0	2.7	15,165	49,513	49,385
Launch escape subsystem	<u>6,607</u>	1,294.4	^b 0.0	^b -0.2	257	9,158	9,187
Total spacecraft at launch	23,838	1,057.0	0.7	1.9	15,432	169,821	169,687

^aCenter of gravity is shown in the spacecraft coordinate system. For spacecraft coordinates see figures 4.1-2 and 4.1-3.

^bMoments of inertia are calculated, as are the Y and Z centers of gravity for the launch escape subsystem.

UNCLASSIFIED

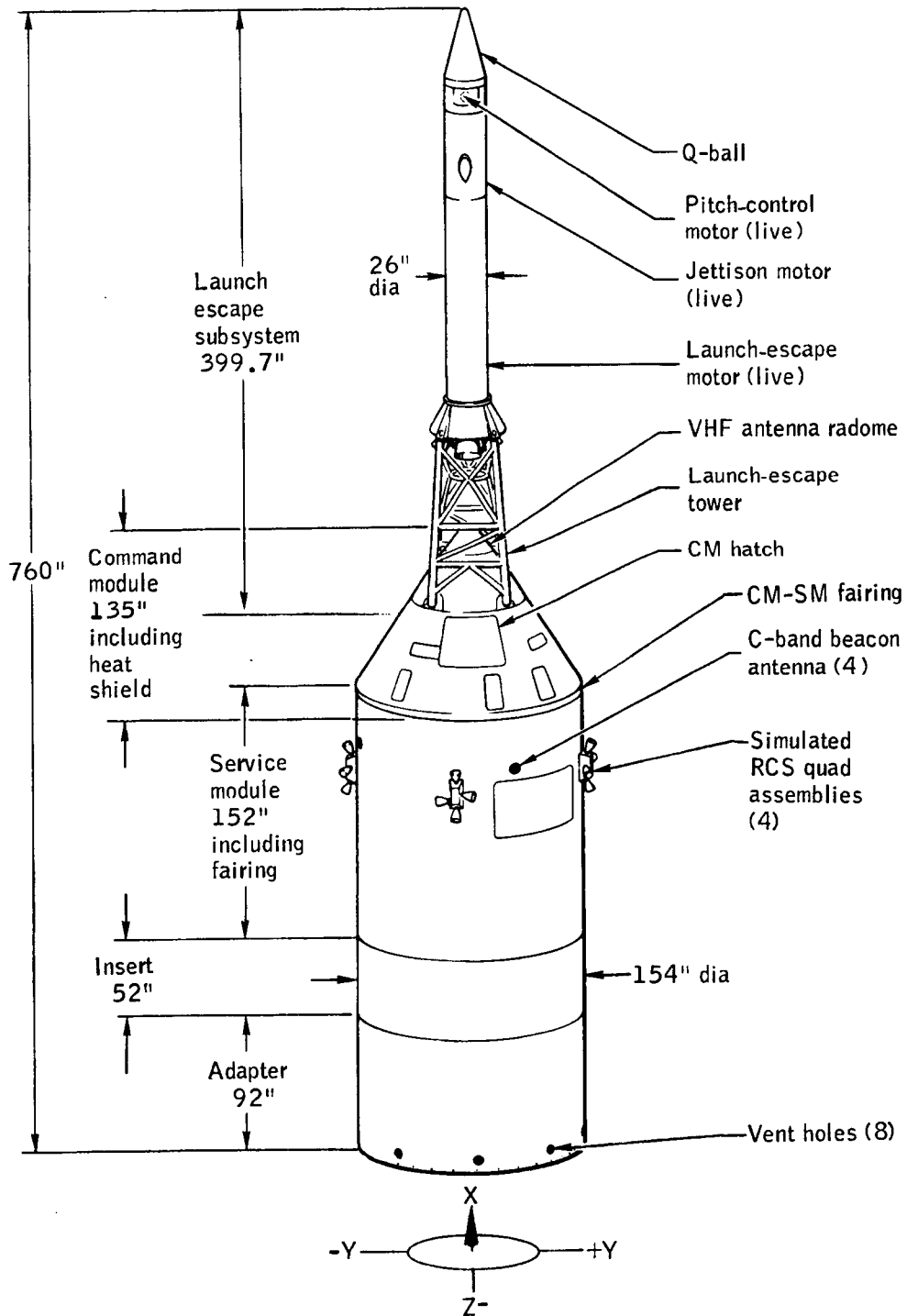


Figure 4.1-1.- Apollo BP-15 spacecraft.

UNCLASSIFIED

UNCLASSIFIED

4-7

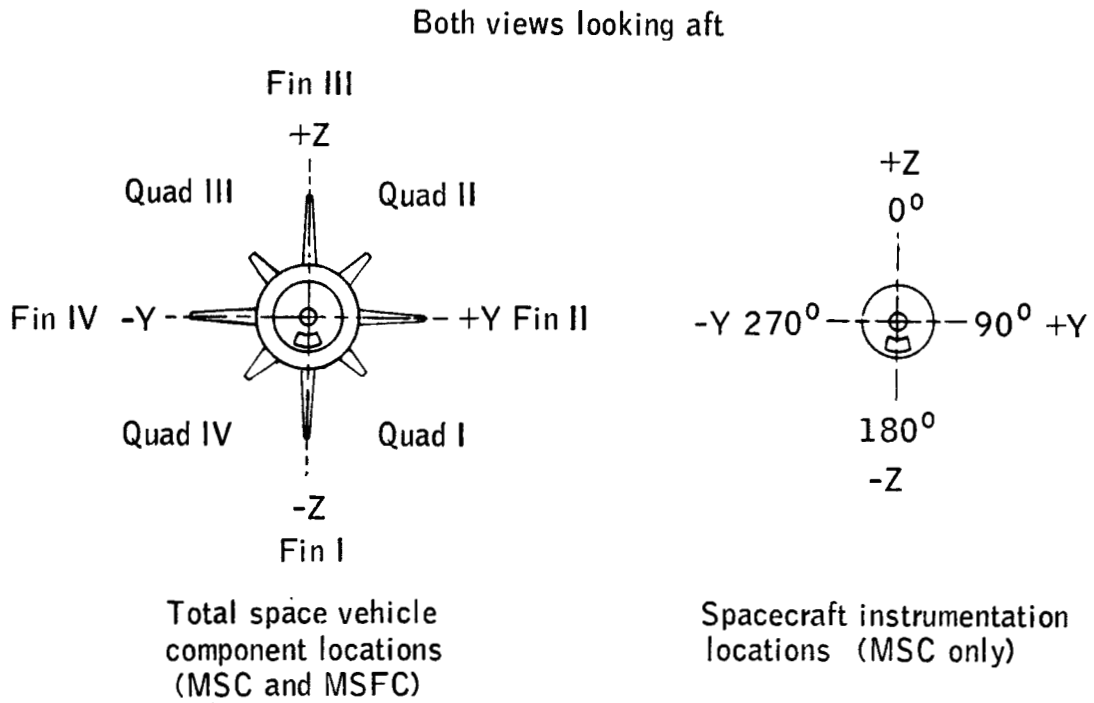


Figure 4.1-2.- Y- and Z-axes and angular coordinate system used for designating locations within the BP-15 spacecraft.

UNCLASSIFIED

UNCLASSIFIED

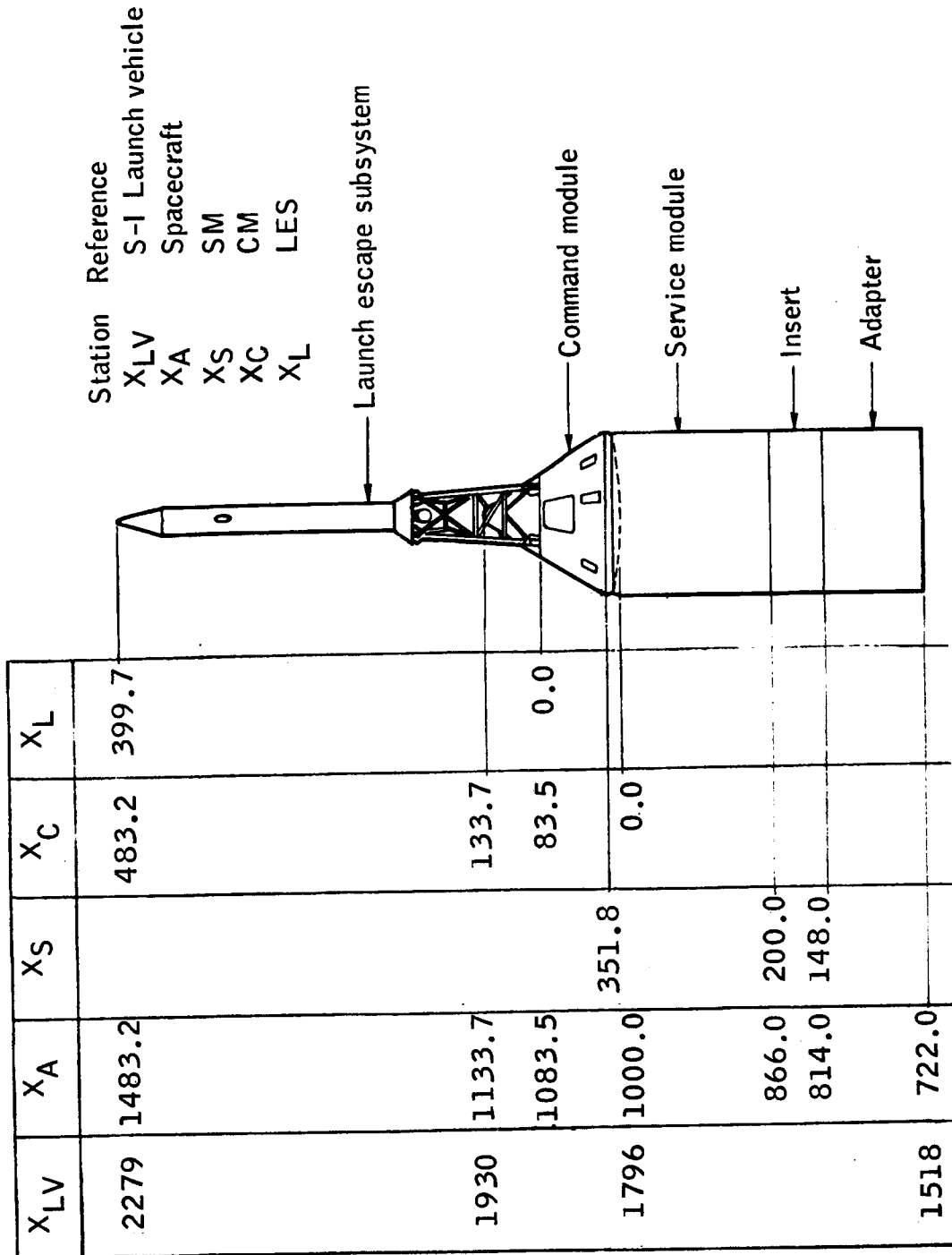


Figure 4.1-3.- X-axis systems used for designating longitudinal locations within BP-15 spacecraft.

UNCLASSIFIED

UNCLASSIFIED

4-9

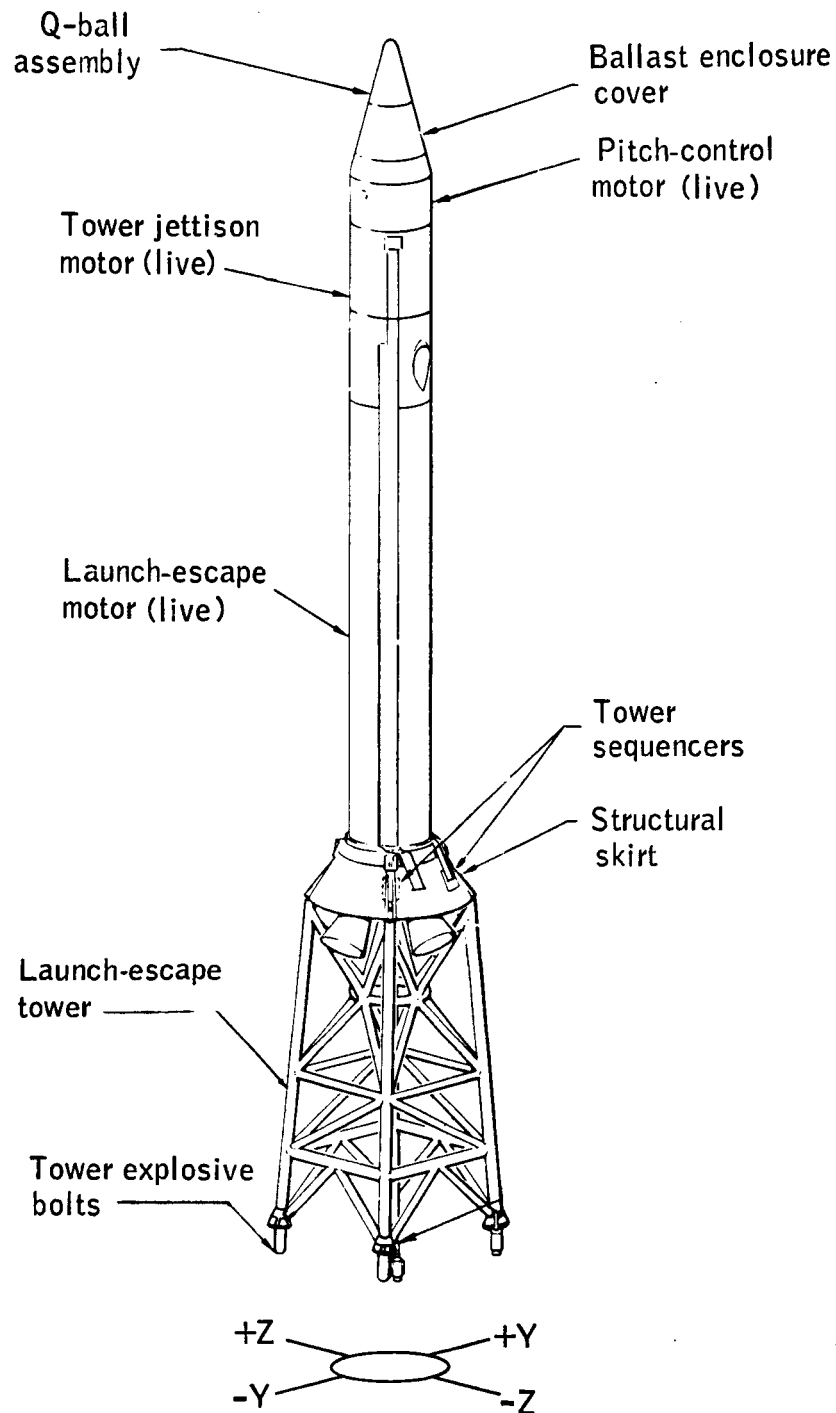


Figure 4.1-4.- Launch escape subsystem for BP-15 spacecraft.

UNCLASSIFIED

UNCLASSIFIED

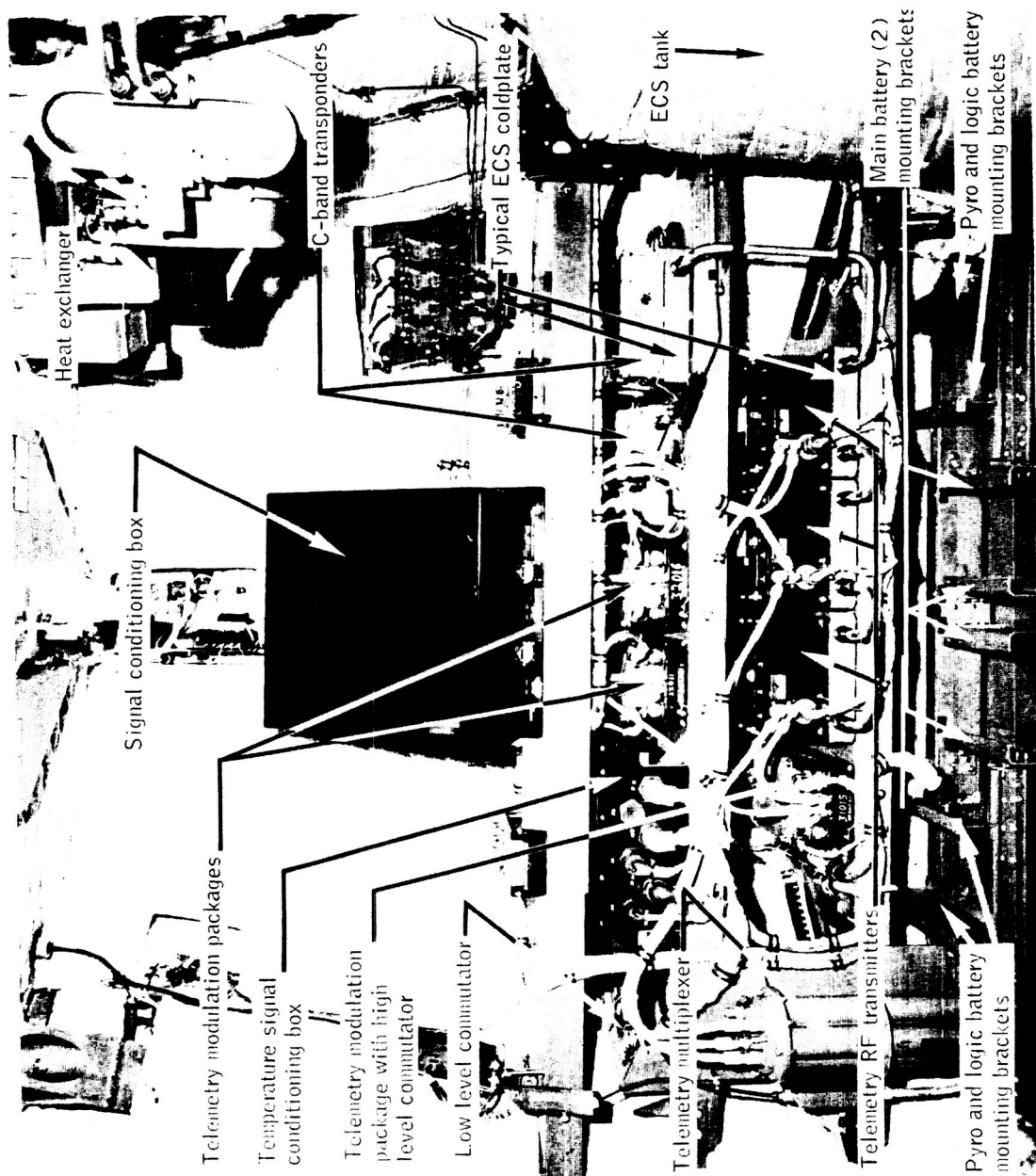


Figure 4.1-5.- Command module interior equipment layout for BP-15 spacecraft (view through hatch).

UNCLASSIFIED

UNCLASSIFIED

4-11

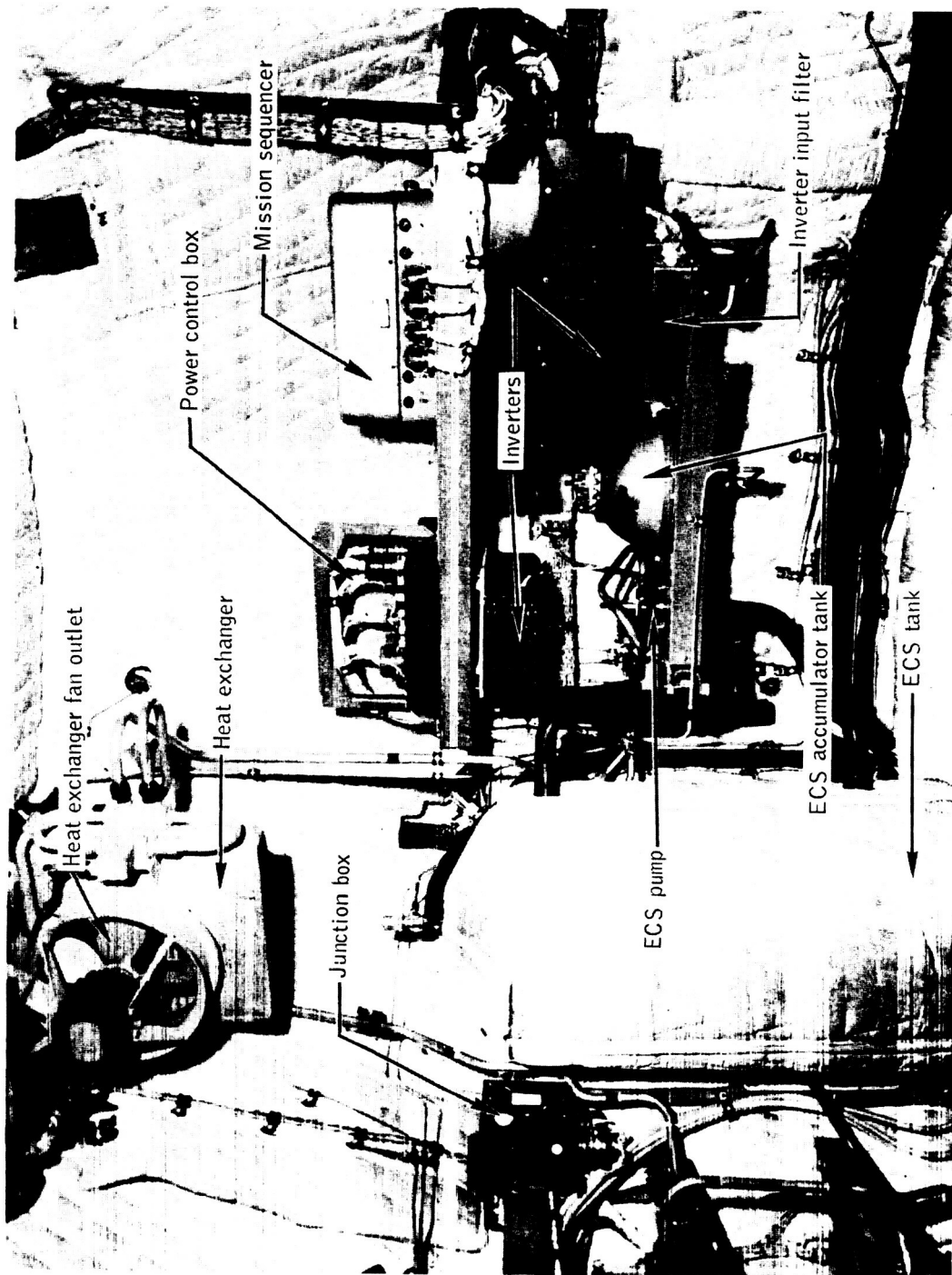


Figure 4.1-6.-Command module interior equipment layout for BP-15 spacecraft (view to right of hatch).

UNCLASSIFIED

UNCLASSIFIED

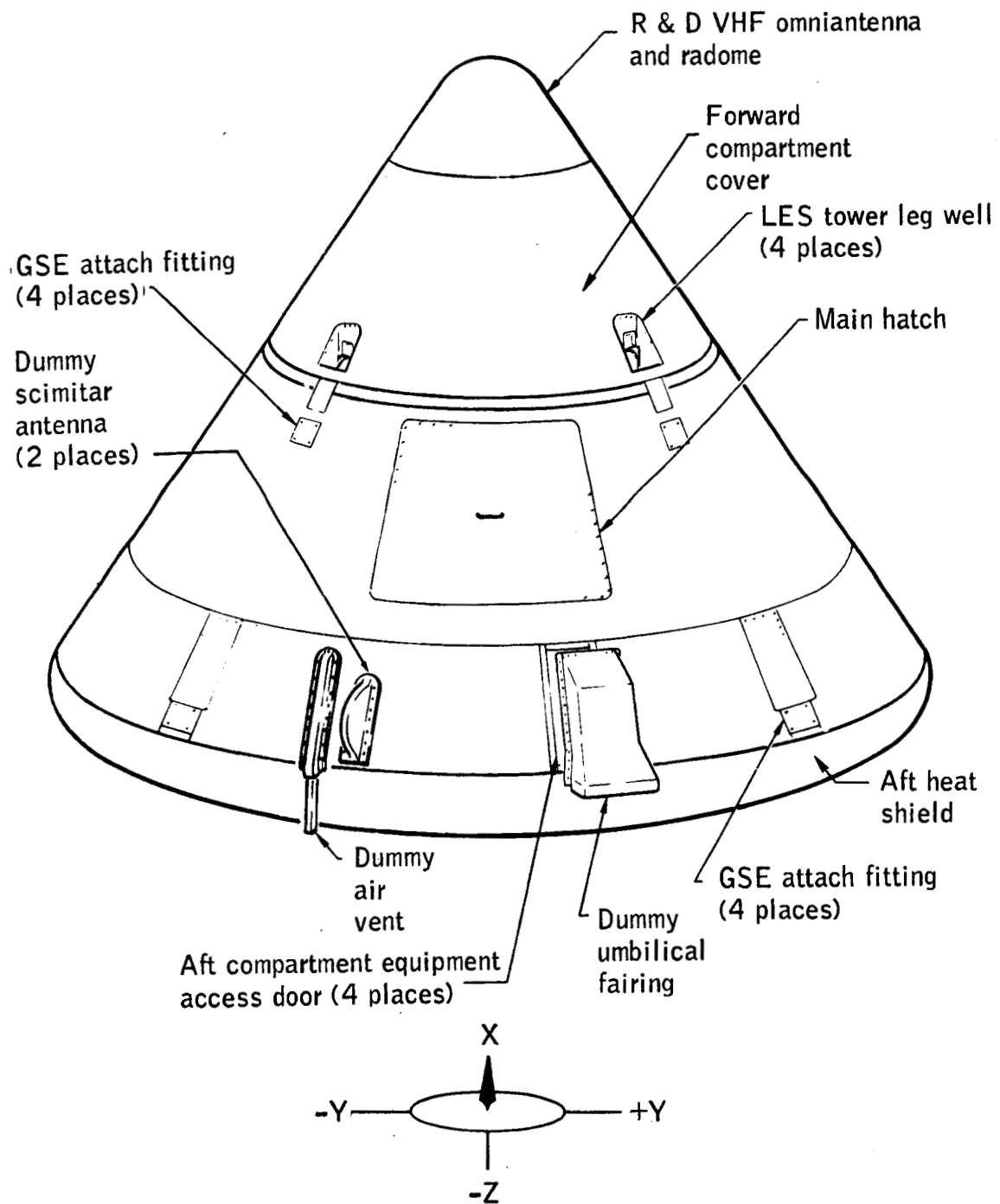


Figure 4.1-7.- Command module exterior of BP-15 spacecraft.

UNCLASSIFIED

~~CONFIDENTIAL~~

4-13

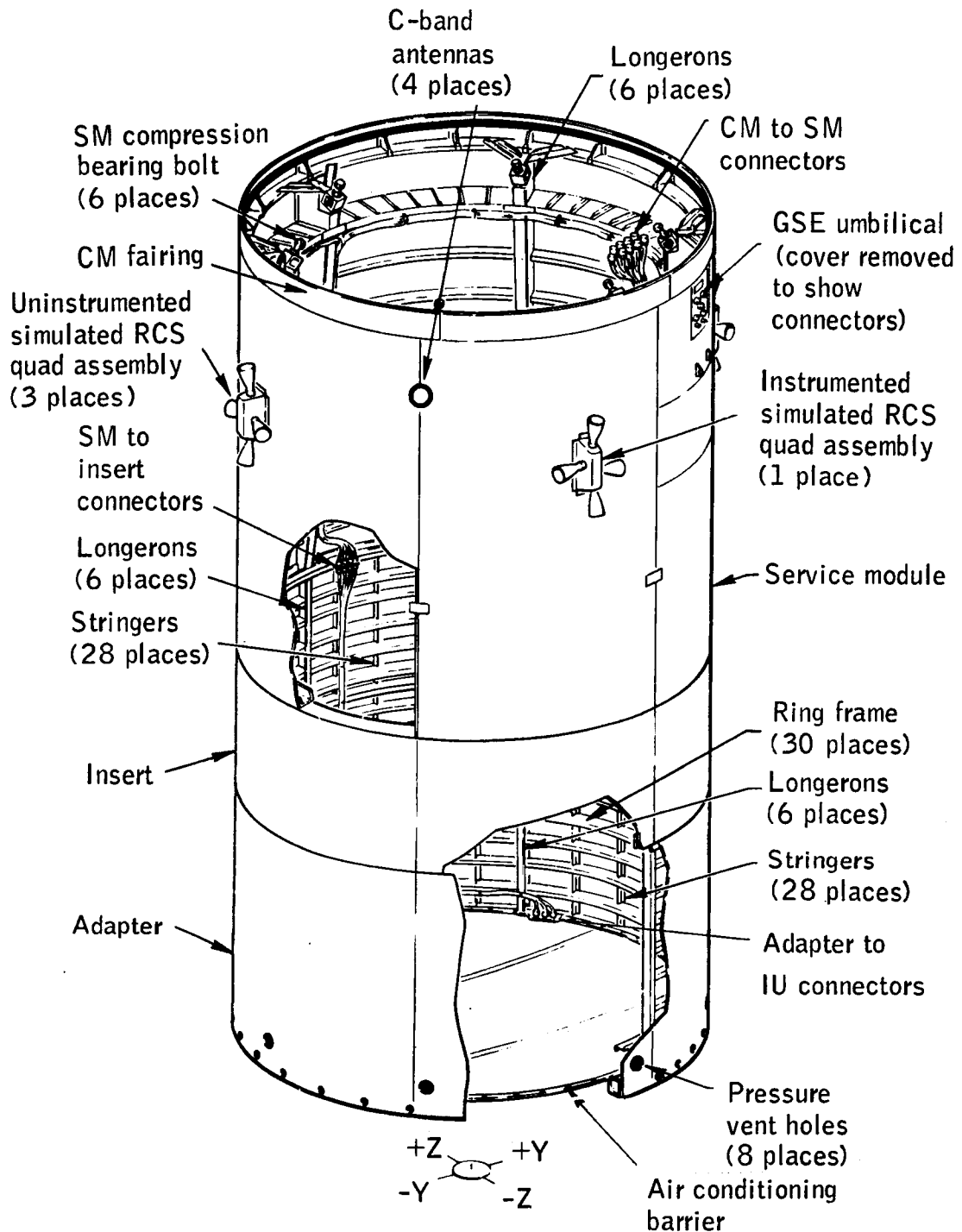


Figure 4.1-8.- Cutaway view of BP-15 spacecraft service module, insert, and adapter.

~~CONFIDENTIAL~~

UNCLASSIFIED

4.2 Instrumentation

Description.- The instrumentation subsystem provided conditioned analog signals which indicated the launch and exit environment of the BP-15 spacecraft to the communications subsystem. Specific instrumentation was supplied to satisfy measurement requirements in the following areas: acceleration, acoustics, vibration, pressure, temperature, heat flux, strain, frequency, voltage, current, and discrete events.

The block diagram in figure 4.2-1 shows both the instrumentation subsystem and the communications subsystem. Table 4.2-I presents a summary of the measurement requirements for the Apollo mission A-102. Table 4.2-II lists the flight equipment used to obtain the required measurements, and table 8.1-I is a detailed list of the individual measurements on board the spacecraft. The location of the major instrumentation components within the command module are shown in figures 4.1-5 and 4.1-6. The locations of most of the transducers are shown in figures 4.2-2 to 4.2-7.

Also included in table 8.1-I are the ground-support-equipment (GSE) measurements and the transducer outputs which monitored angle of attack, angle of sideslip, and dynamic ram pressure from the Q-ball system furnished by the NASA-MSFC. The six Q-ball outputs, two radial vibration measurements, and one acoustic microphone output were routed to the launch-vehicle instrumentation unit and conditioned for launch-vehicle telemetry.

All of the measurements monitored on the BP-15 spacecraft required some type of conditioning before they reached the modulation section. The instrumentation subsystem included two signal conditioning boxes, one low-level (0 to 10 mv) and one high-level (0 to 5 v).

The heat flux and temperature low-level signals were conditioned in the temperature signal conditioning box. These signals were routed to the low-level $90 \times 1\frac{1}{4}$ commutator and were sequentially sampled at 1.25 times per second. The signal conditioning box also provided 0, 5 mv, and 10 mv d-c reference voltages to the $90 \times 1\frac{1}{4}$ commutator to enable accurate data reduction of the low-level system.

Amplification of the low-level signals was provided in order to give an output PAM wavetrain varying between 0 and 5 v d-c.

The high-level signals requiring conditioning were fed to the main conditioning box. This box distributed the high-level signals to the 90×10 commutator and to the modulation packages. It also supplied

~~UNCLASSIFIED~~

~~CONFIDENTIAL~~

4-15

the commutator with 0 and 5 v d-c reference voltages for data reduction purposes. The 90×10 commutator sequentially sampled each of its inputs 10 times per second and provided a PAM wavetrain varying between 0 and 5 v d-c.

Both the PAM wavetrains and the continuous signals were fed to the modulation section where they frequency modulated their respective voltage controlled oscillators (VCO). The modulation section consisted of three modulation packages designated as A, B, and C. Package A contained VCO for IRIG channels 6, 9 to 16, and channel E. Packages B and C each contained VCO for IRIG channels 6 to 8 and 10 to 18. The outputs of the VCO in each modulation package were mixed into two separate video composite signals by two mixer amplifiers. One amplifier supplied a composite output to the GSE for test purposes, and the other supplied a composite signal to its associated transmitter in the RF package.

Configuration changes from BP-13 spacecraft.- Shielding, as shown in figure 4.2-8, was added to the cabling between the low-level commutator and the low-level temperature conditioning box input to eliminate the electromagnetic interference (EMI) experienced on the BP-13 spacecraft. This interference was present only when the BP-13 spacecraft had the CM hatch removed and was adjacent to the service structure on the launch pad.

Strain-gage ranges were changed from 1,000 and 4,000 $\mu\text{in./in.}$ used on BP-13 spacecraft to 500 $\mu\text{in./in.}$ because of the low magnitude of measurements experienced during BP-13 spacecraft flight.

Sixteen temperature measurements and two vibration measurements were added to instrument the RCS quad. The addition of the vibration measurements necessitated the deletion of two fluctuating pressure measurements so that the high-response channels could be used for the vibration measurements.

Performance.- The flight performance of the BP-15 spacecraft instrumentation subsystem was satisfactory. Of the 133 measurements instrumented on the BP-15 spacecraft, only 2 failed to provide continuous data. Calibration of the thermocouple system used in the RCS is to be verified.

Data were lost for approximately 4 seconds during launch-vehicle staging due to flame attenuation from the S-I stage retrorockets. No interruption of RF transmission due to launch-escape-motor flame attenuation was noted. Evaluation of the telemetry data received during the first orbital pass of the spacecraft indicated that instrumentation was operating properly.

~~CONFIDENTIAL~~

~~CONFIDENTIAL~~

Temperature measurement SR5877T, located on the +pitch nozzle of the instrumented RCS quad (fig. 4.8-9) failed to show the expected rise in temperature. A constant output of approximately 4-percent information bandwidth was indicated during countdown and launch. This information level seen prior to launch appeared to be normal for ambient conditions. During the flight, the reading was inconsistent with the actual environment determined by other thermocouple measurements in the immediate area. This measurement was satisfactorily calibrated electrically prior to launch, but this was not a positive indication that the entire thermocouple circuitry was flightworthy since the thermocouple was not included in the calibration circuit. For additional details regarding this measurement see sections 4.8 and 9.2.

Heat-flux measurement SA0553R located on the SM under the +pitch nozzle of the instrumented RCS quad (fig. 4.2-6) provided questionable data. Response was normal when the unit was calibrated approximately 2 minutes prior to launch which indicated circuit continuity. Analysis of the data indicated the transducer responded to excitation at main-stage ignition. There was no further response from this circuit, while the corresponding body-temperature measurement SA0563T increased normally with aerodynamic heating during the flight. The exact time or mode of malfunction was not apparent from the flight data. For additional details regarding this measurement see sections 4.11 and 9.3.

~~CONFIDENTIAL~~

UNCLASSIFIED

4-17

TABLE 4.2-I.- APOLLO MISSION A-102 MEASUREMENT REQUIREMENTS SUMMARY

Measurement	Quantity	Location	Requirement
Acceleration	2 3 2	LES CM SM	Determine structural body bending mode responses under flight loads.
Vibration	1 3 ^a 2 2	CM SM Adapter SM-RCS	Determine structural vibration mode responses under flight loads.
Pressure	9	CM	Determine static aerodynamic loading on outside conical surface.
	1 1	CM SM	Determine flight pressure venting characteristics.
Fluctuating pressure	2 11	Adapter SM	Determine aerodynamic loading on exterior surfaces and acoustical environment.
Acoustic	^a 1	SM	Determine exterior acoustic level under flight environment.
Strain	2 4	SM Adapter	Determine structural stresses and flight loads.
Heat flux	12 7 1	CM SM Adapter	Determine aerodynamic heating rates on exterior surfaces.
Temperature	12 7 1	CM SM Adapter	Determine calorimeter body temperature for accurate data reduction of heat flux.
	8	LES	Determine tower temperature caused by aerodynamic heating.
	1 1	CM SM	Determine interior temperature within SM and crew compartment.
	6	CM	Verify proper heat transfer from RF packages.
	16	SM-RCS	Determine RCS temperatures during flight.

^aTransmitted on launch-vehicle telemetry.

UNCLASSIFIED

UNCLASSIFIED

TABLE 4.2-I.- APOLLO MISSION A-102 MEASUREMENT REQUIREMENTS SUMMARY - Concluded.

Measurement	Quantity	Location	Requirement
Voltage	2 4	LES CM	Verify proper electrical operation of power subsystem.
Current	1	CM	Verify proper electrical operation of main power subsystem.
Frequency	2	CM	Verify proper interrogation rate of transponders.
Discrete event	2	LES	Verify tower jettison sequence command.
	1	CM	Indication of system R and Z calibration mode.
	2	Launch vehicle	Verify tower jettison command from launch-vehicle separation timer.
	1	Launch vehicle	Provide data time reference at vehicle lift-off.

UNCLASSIFIED

UNCLASSIFIED

4-19

TABLE 4.2-II.- FLIGHT EQUIPMENT FOR BP-15 SPACECRAFT INSTRUMENTATION SUBSYSTEM

Component	Vendor	Model	Quantity
TM modulation package	Bendix	TATP-316	3
90 x 10 commutator	Applied Electronics	340-23-5	1
90 x $1\frac{1}{4}$ commutator	Fifth Dimension	LDA12N-432	1
Main signal conditioning box	Brown	CH-150	1
Temperature signal conditioning box	Microdot	401-0110-1	1
Amplifier rack	NASA-MSFC	1-A	11
d-c amplifier	Engineered Magnetics	2000D-1	7
Vibration system: Accelerometer a-c amplifier	Endevco	28153	1
	Endevco	2242M5A	1
	Endevco	2633M10	1
Vibration system: Accelerometer a-c amplifier	Endevco	28191	2
	Endevco	2633M13	2
	Endevco	2242M5A	2
Vibration system: Accelerometer a-c amplifier	Endevco	28191	3
	Endevco	242M5A	3
	Endevco	2633M10A	3
Pressure system: Transducer d-c amplifier	Statham	PA-288TC-15-350	13
	Engineered Magnetics	2000D-1	13
Pressure transducer	Wiancko	P2-3236-1	11
Accelerometer	Donner	4310	7
Strain gage	Baldwin-Lima-Hamilton	EBF-13D	48
Resistance thermometer	Trans-Sonics	2168A	9
		2168A-2	8
		2168A-2-12	1
		T 408-2A-2	2
Thermocouple	Continental Sensing	TC-6	9
		TC-6A	3
Calorimeter	Hy-Cal	C-1123-A-5-012	8
	Hy-Cal	C-1123-A-25-0	12
Zone box	Microdot	401-0138-1	20
	Rugge de Forrest	3878-2	12
Acoustic system: Microphone Emitter-follower a-c amplifier }	NASA MSFC		
	Gulton	50M10401	1
	Glennite	FCT-601V	1
Q-ball assembly	Nortronics	F-16	1

UNCLASSIFIED

UNCLASSIFIED

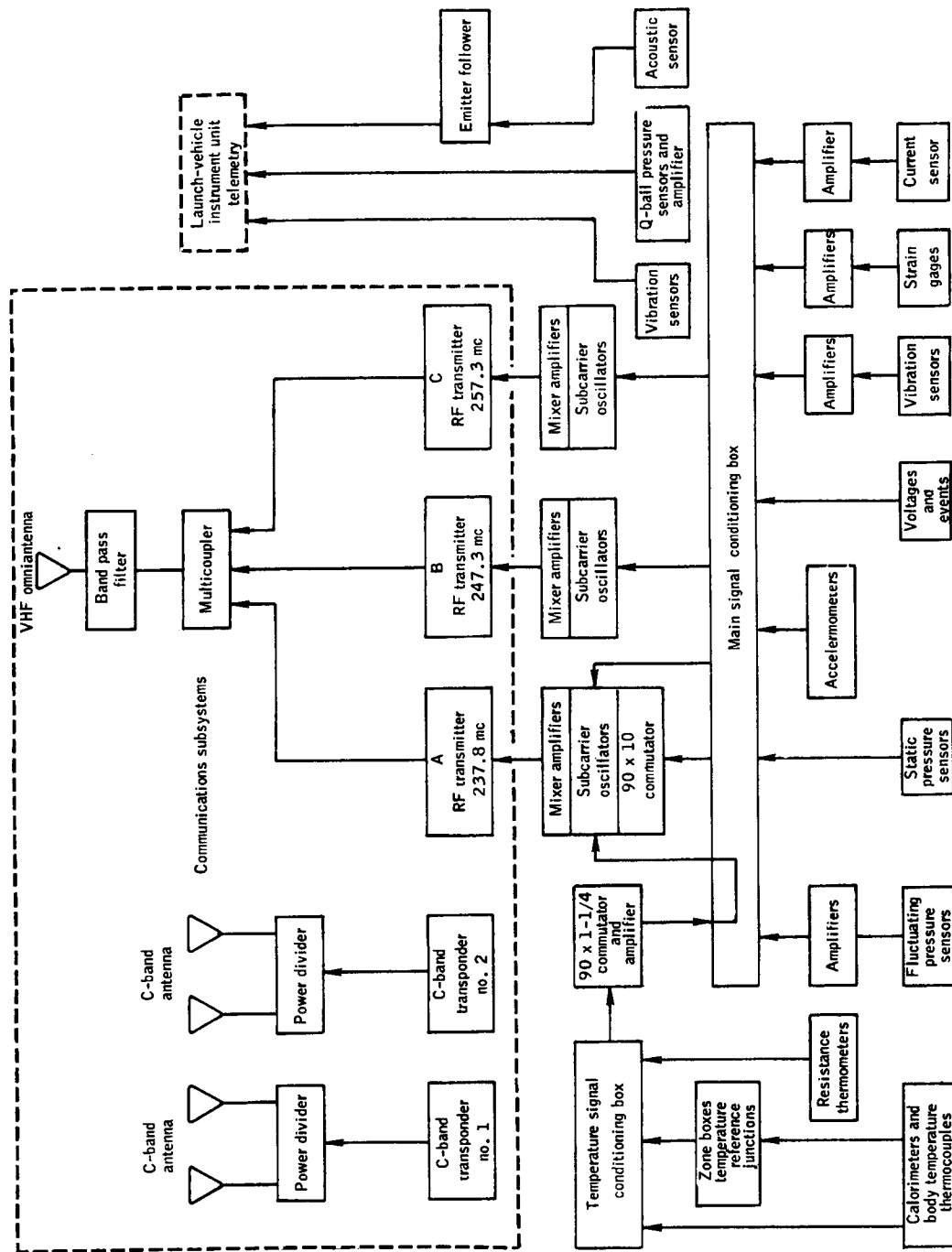
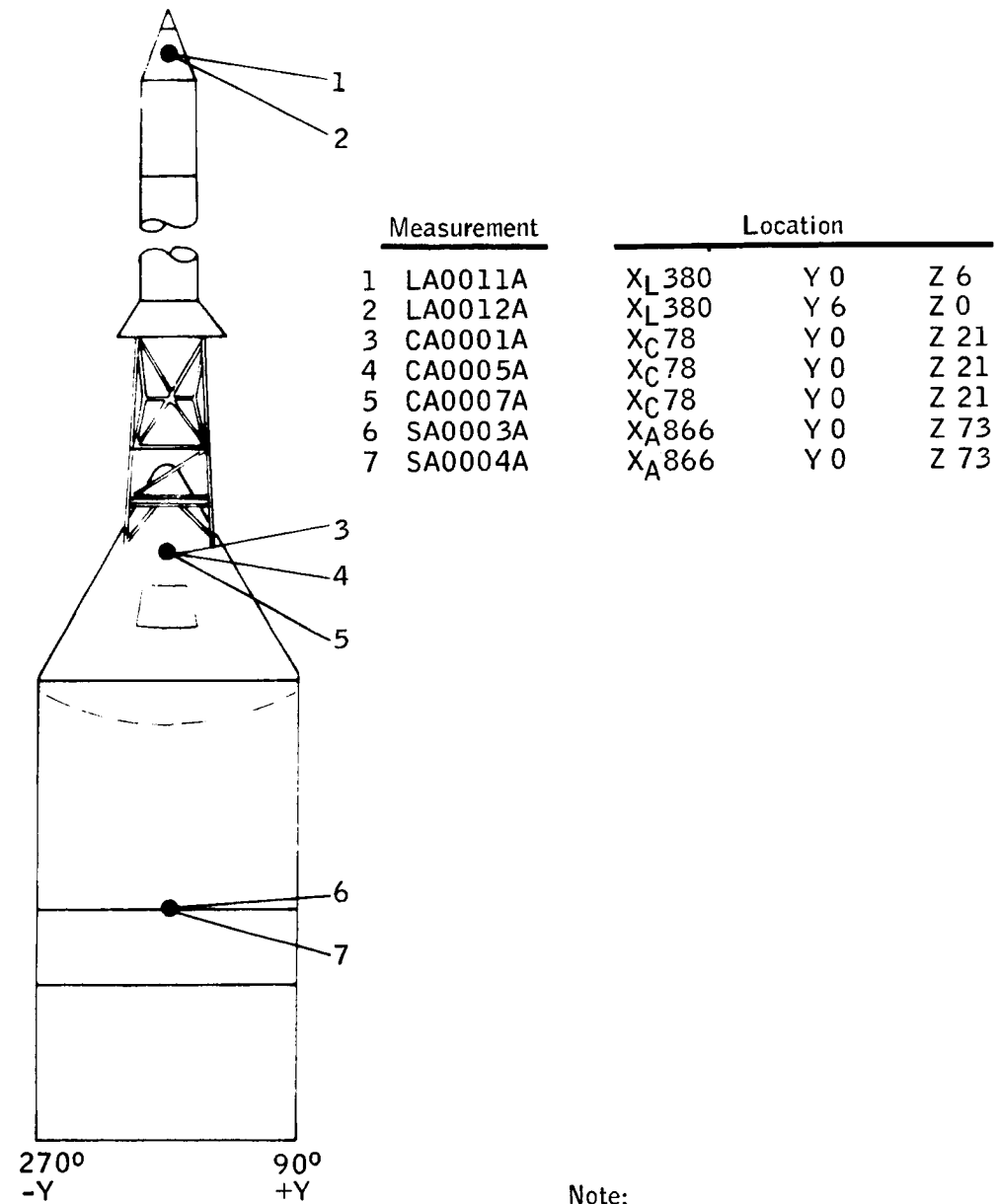


Figure 4-2-1. - Instrumentation and communications subsystems on BP-15 spacecraft.

UNCLASSIFIED



Note:

Measurement numbers refer to listing in table 8.1-I.

○ Far side
● Near side

Figure 4.2-2.- Locations of linear acceleration transducers for BP-15 spacecraft.

UNCLASSIFIED

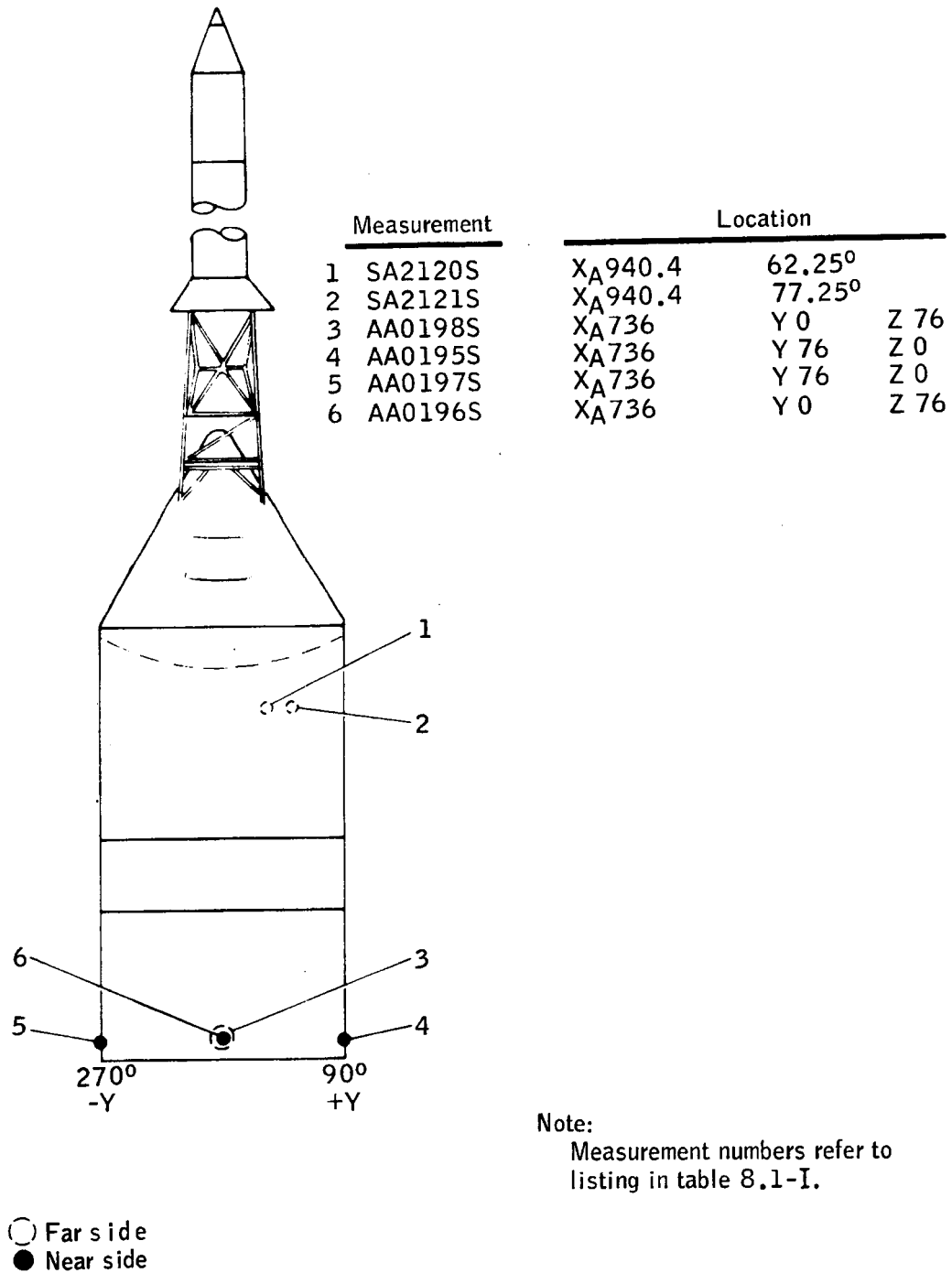


Figure 4.2-3.- Strain-gage locations on BP-15 spacecraft.

UNCLASSIFIED

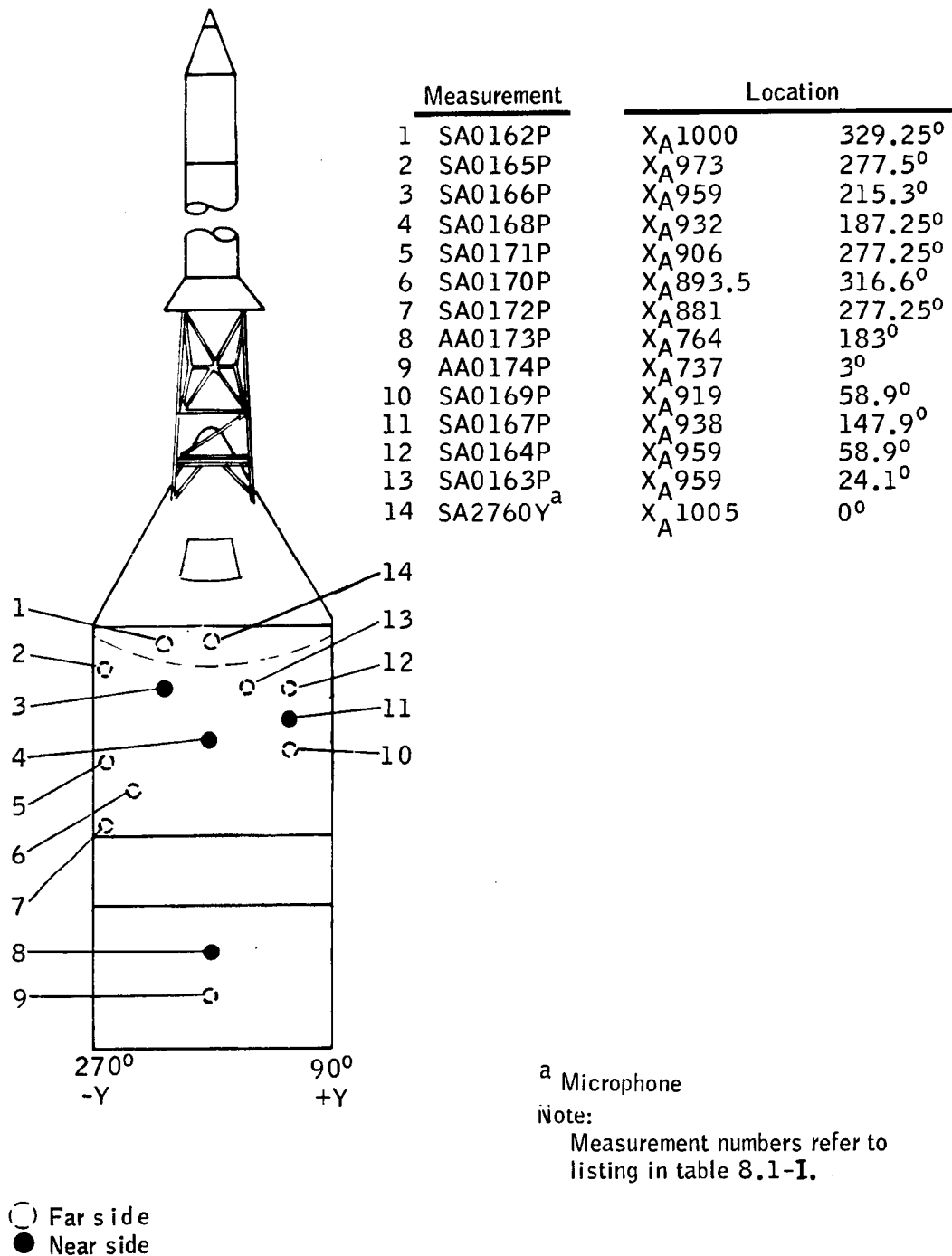
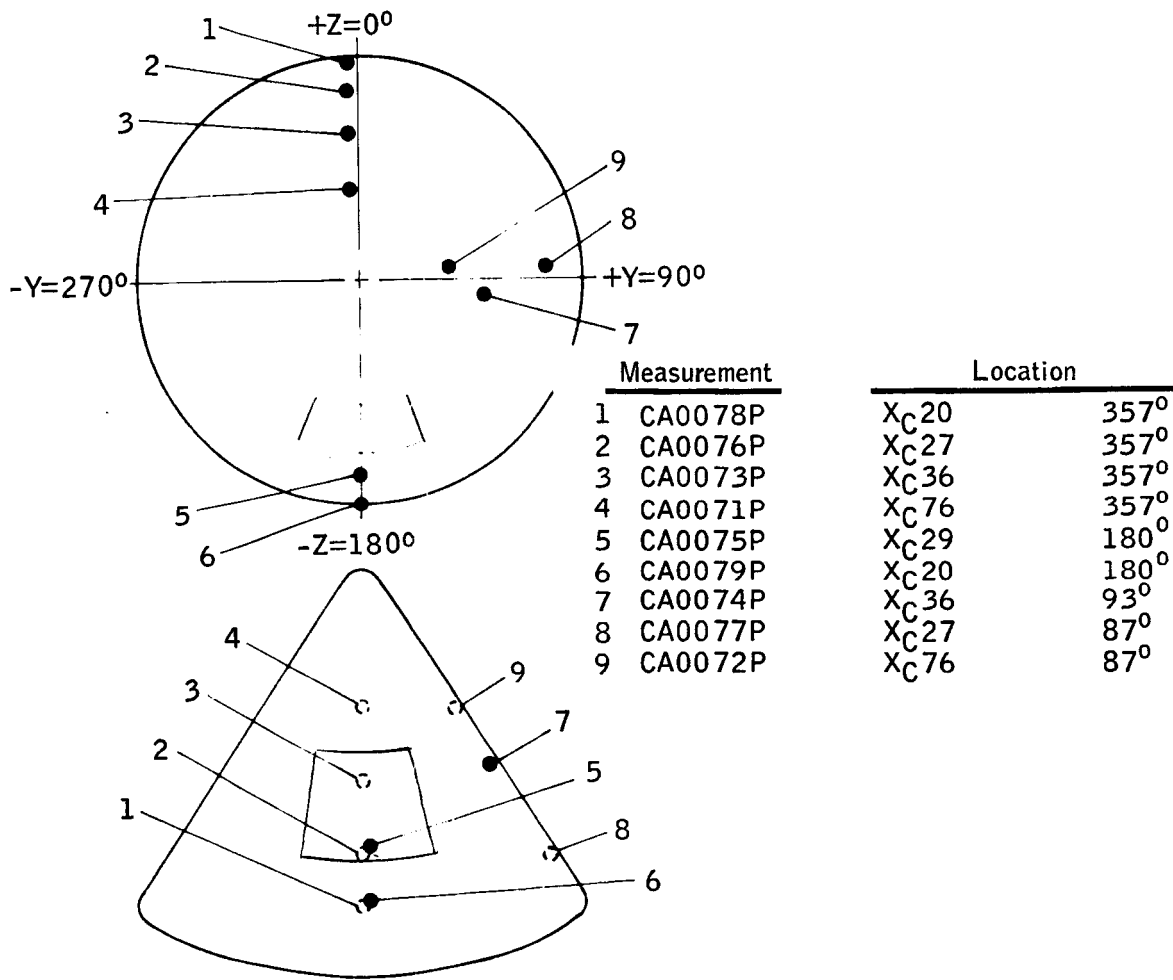


Figure 4.2-4.- Fluctuating-pressure transducer locations on BP-15 spacecraft.

UNCLASSIFIED



Note:
Measurement numbers refer to
listing in table 8.1-I.

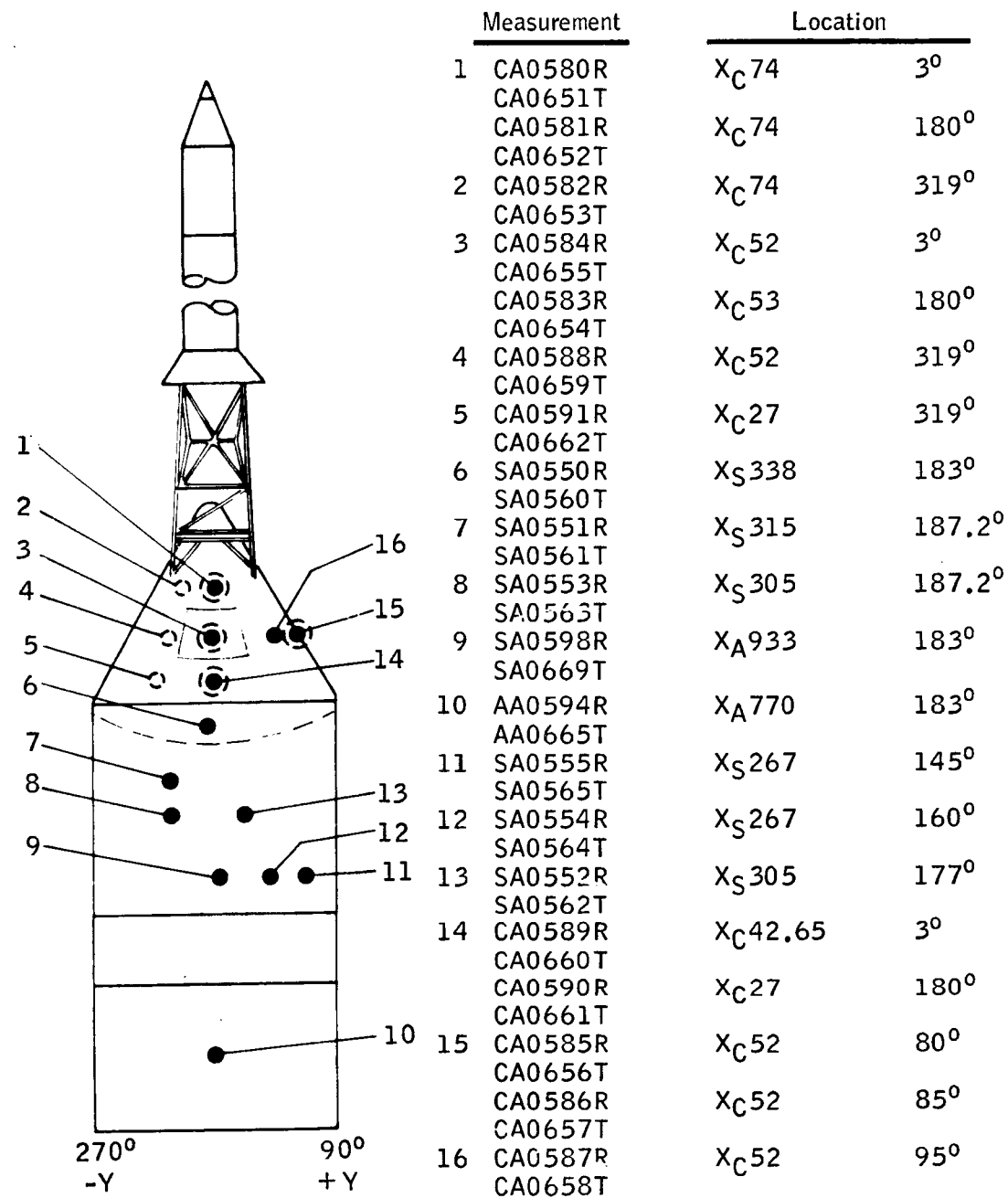
○ Far side
● Near side

Figure 4.2-5.- Locations of conical-surface pressure transducers
on the BP-15 spacecraft.

UNCLASSIFIED

UNCLASSIFIED

4-25



Note:

Measurement numbers refer to listing in table 8.1-I.

○ Far side
● Near side

Figure 4.2-6.- Locations of heat-flux calorimeter body temperature measurement on BP-15 spacecraft.

UNCLASSIFIED

UNCLASSIFIED

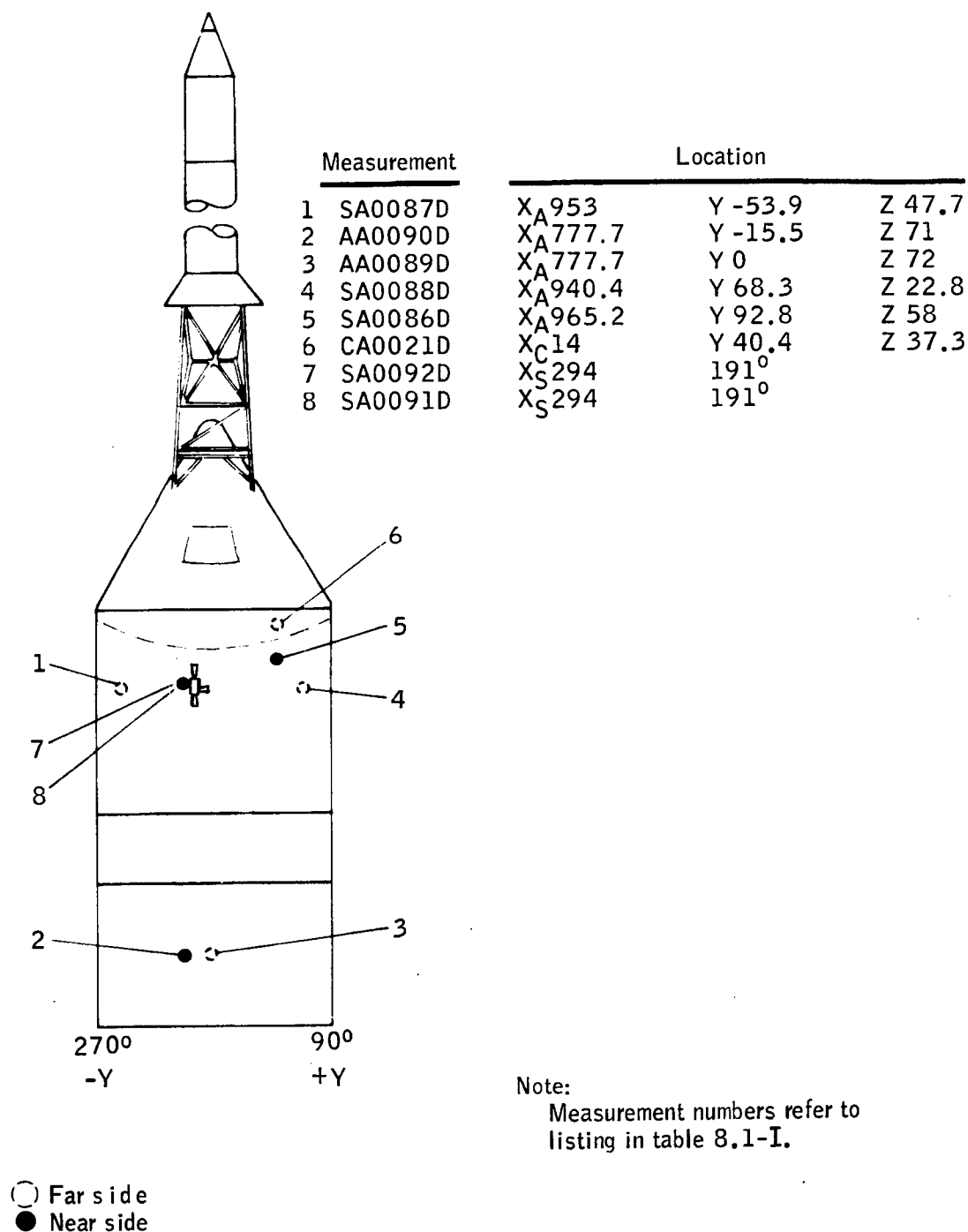


Figure 4.2-7.- Locations of vibration transducers on BP-15 spacecraft.

UNCLASSIFIED

UNCLASSIFIED

4-27

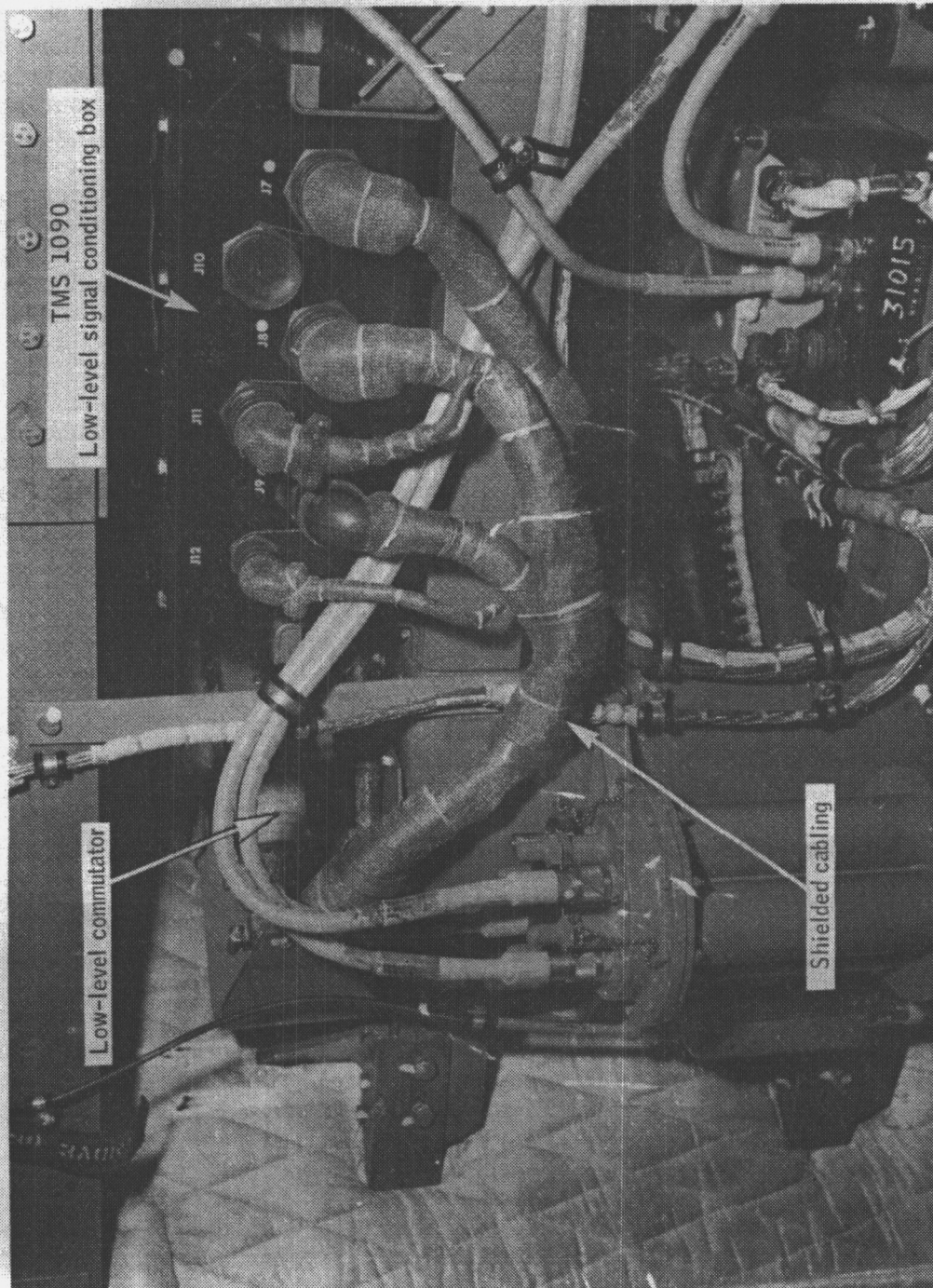


Figure 4.2-8.- Command module interior showing cable shielding to prevent EMI in the BP-15 spacecraft.

UNCLASSIFIED

~~CONFIDENTIAL~~

4.3 Electrical Power and Sequential

Electrical subsystem. - The electrical subsystem provided the power and circuitry for the communications, environmental control, instrumentation, and sequencing subsystems. A block diagram of the electrical circuitry and components is shown in figure 4.3-1, with a layout showing the location of the components within the command module in figure 4.3-2.

Spacecraft power was provided by an external ground-support equipment (GSE) power supply until T-12 minutes, at which time the power loads were transferred to the internal spacecraft batteries. The battery power for the instrumentation, environmental control, and communication subsystems came from two silver-zinc main batteries A and B, which were rated at 120 amp-hr at a 12-amp discharge rate.

The main batteries successfully met all power requirements for the mission including the first orbital pass and exceeded the planned battery life. Main battery A, which had a current drain of approximately 17 amps, supplied 7 hours and 38 minutes of useful power. This was verified by the reception of transmitter A at the Hawaii Radar Station on the fifth orbital pass.

Main battery B supplied useful power for 5 hours and 20 minutes. The current drain on battery B was approximately 25 amps from T-12 minutes to T+5.6 minutes. At T+5.6 minutes the ECS fan operation was terminated, dropping the current drain on battery B to approximately 17 amps. The useful life of battery B was verified by the reception of transmitter C at the Pretoria, South Africa, range station on the fourth orbital pass.

The electrical subsystem for the BP-15 spacecraft was identical to that flown on the BP-13 spacecraft, with the exception of the prelaunch conditioning of the main batteries and of the sequencer pyro and logic batteries. The BP-15 main batteries were activated using 135 cc of electrolyte per cell as compared with 133 cc used on the BP-13 spacecraft. The logic and pyro batteries flown on the BP-15 spacecraft were used on the second discharge cycle, while those flown on the BP-13 spacecraft were used on the first. These changes in prelaunch conditioning were based on the results of battery performance improvement tests completed since the BP-13 spacecraft flight.

Sequential subsystem. - The sequential components consisted of a mission sequencer having two independent circuits (A and B) for reliability and two tower sequencers. As shown in figure 4.3-3, each tower sequencer was controlled by one of the two mission sequencer circuits. The sequential subsystem included no built-in time delay between receipt of the signal and initiation of the pyrotechnics in the explosive bolts, launch-escape motor, and pitch-control motor.

~~CONFIDENTIAL~~

UNCLASSIFIED

4-29

Using GSE power, the mission-sequencer logic and pyro circuits were armed at T-7 minutes. Each circuit had one pyro battery and one logic battery, which were rated at 6 amp-hr at a 1-amp discharge rate. After arming, the voltages on the logic and pyro batteries were between 33.25 and 33.7 volts. Telemetry data indicated that the logic and pyro buses remained armed and the batteries functioned satisfactorily through tower jettison as required.

Twelve seconds after separation of the S-I and S-IV stages, a signal was sent from the S-IV instrument unit to the sequencer logic circuitry. The signal closed the firing circuits, and ignited the LES explosive bolts, launch-escape motor, and pitch-control motor. Tower-separation command was confirmed by telemetry data which indicated relay closures in circuits A and B. Physical separation of the tower from the spacecraft was verified by the termination of the electrical measurements on the tower. Optical data confirmed ignition of the launch-escape motor and separation of the LES tower.

The sequential subsystem flown on the BP-15 spacecraft was identical to that used on the BP-13 spacecraft and performed satisfactorily.

UNCLASSIFIED

UNCLASSIFIED

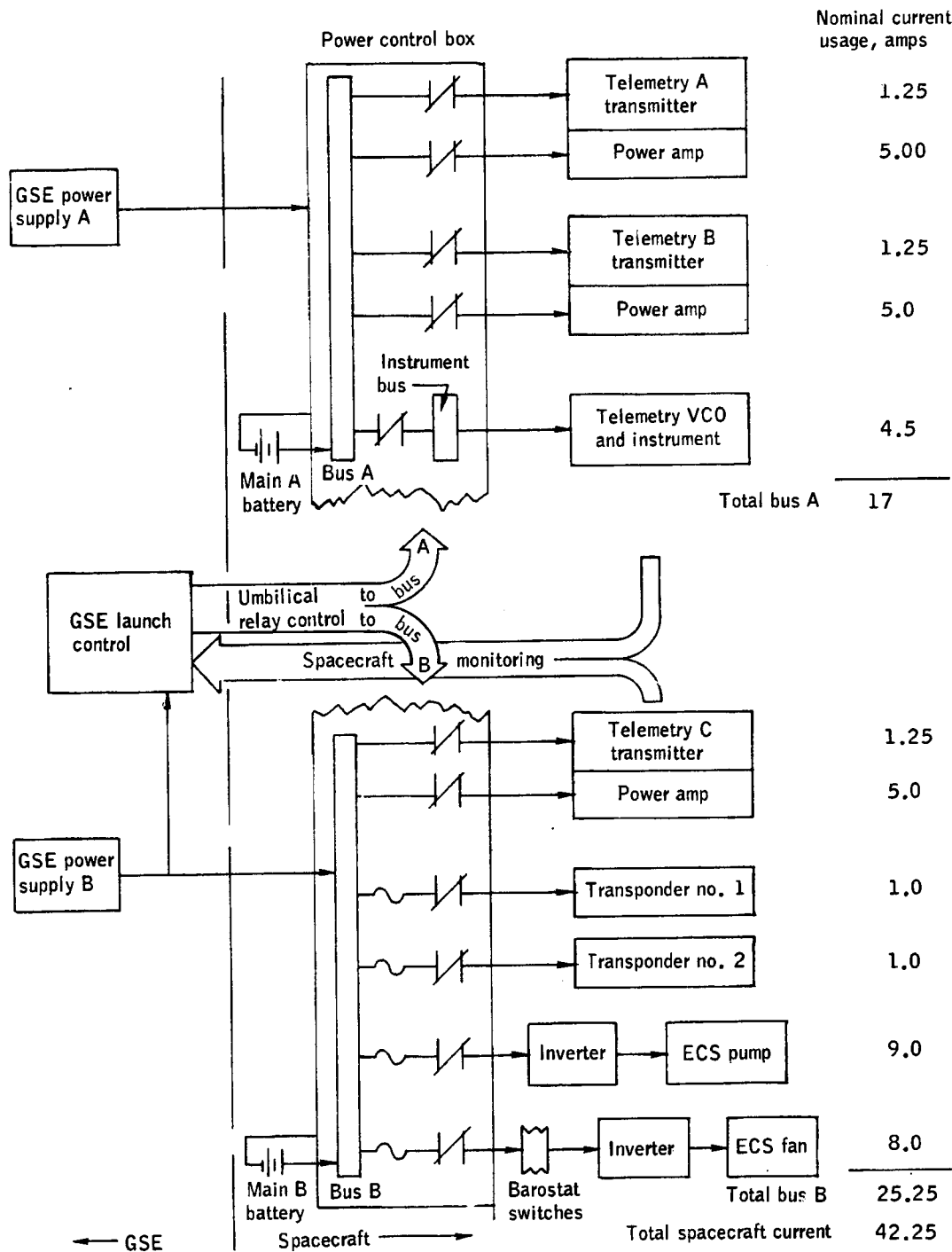


Figure 4.3-1. - Electrical power subsystem for BP-15 spacecraft.

UNCLASSIFIED

UNCLASSIFIED

4-31

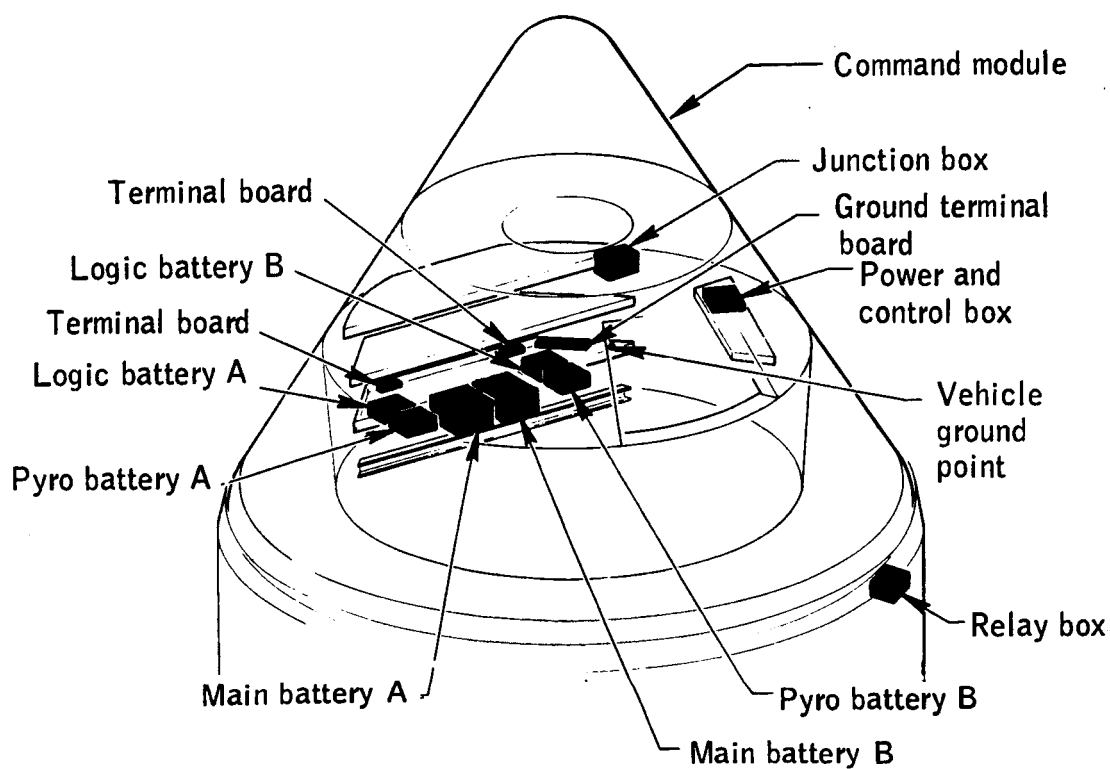


Figure 4.3-2. - Electrical power subsystem components for BP-15 spacecraft.

UNCLASSIFIED

UNCLASSIFIED

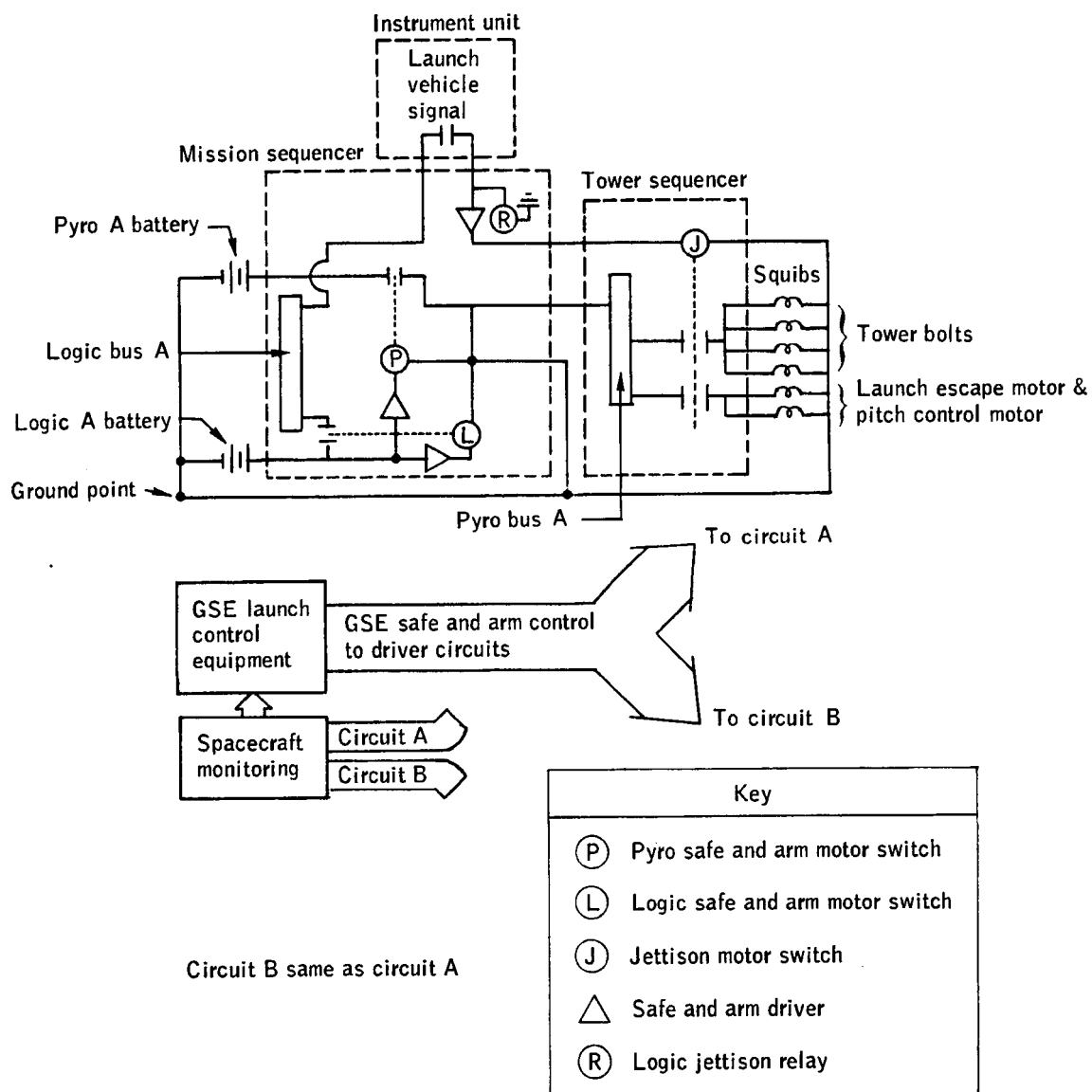


Figure 4.3-3.- Launch escape sequencer subsystem for BP-15 spacecraft.

UNCLASSIFIED

UNCLASSIFIED

4-33

4.4 Communications

Description. - The communications subsystem of the BP-15 spacecraft consisted of three VHF telemetry transmitter packages and two C-band transponders (fig. 4.2-1).

Each of the transmitter packages shown in figure 4.4-1 consisted of a d-c to d-c converter, a 2-watt FM transmitter, a 10-watt RF amplifier, an RF bandpass filter, and a power-line filter. The RF carrier frequencies were 237.8 mc, 247.3 mc, and 257.3 mc, and were designated as telemetry links A, B, and C, respectively. The RF carrier deviation of each transmitter was set for ± 125 kc.

The RF outputs of the three transmitter packages were fed into a multiplexer which combined the individual outputs into one RF composite signal. This signal was fed by way of a bandpass filter unit to a VHF omni-antenna located beneath the radome at the apex of the command module (fig. 4.4-2).

The power for the A and B transmitter packages was supplied by the main bus A of the spacecraft power system, and the power for package C was supplied by the main bus B of the spacecraft power system. Power required for nominal transmitter performance was 6.5 amp at 28 ± 4 v d-c per unit.

Two redundant C-band transponders, shown in figures 4.2-1 and 4.4-1, were used for tracking the spacecraft during launch, exit, and the initial orbital phases of the mission. Each transponder received and transmitted through a power divider which, in turn, fed or received from two helical antennas (figs. 4.4-3 and 4.4-4), which were flush-mounted, 180° apart, on the surface of the service module. Power for each of the transponders was supplied by the main bus B of the spacecraft power system.

The transponders were interrogated with an RF signal consisting of two 1-microsecond pulses spaced 3.5 microseconds apart. The transponder decoder (fig. 4.4-4) received the signal and triggered the transponder transmitters. Each of the two transponder transmitters generated a 0.75 microsecond pulse in reply. These pulses were transmitted at a minimum peak power output of 500 watts.

Performance. - During the launch phase of the BP-15 spacecraft, the three telemetry transmitter systems performed satisfactorily and provided good quality data. The only interruption of RF transmission during the launch phase occurred for a period of 3 seconds on all links at the time of S-I staging ($T+148.2$ sec). Telemetry reception was maintained at Cape Kennedy until $T+570$ seconds. A complete list of

UNCLASSIFIED

UNCLASSIFIED

telemetry acquisition and loss-of-signal times for all range stations is recorded in table 7.3-I.

During the launch phase, the measured temperature extremes in the transmitting system were 43° F and 50° F. These values were well within the maximum allowable limit of 150° F, and they compare favorably with the 40° F and 55° F extremes measured during the launch phase of the BP-13 spacecraft (ref. 1). During the first pass over Cape Kennedy, the measured temperature extremes were 49° F and 56° F as compared with 89° F and 120° F measured on the first pass of the BP-13 spacecraft, indicating improved performance of the equipment cooling subsystem.

The two C-band transponders, carried on the BP-15 spacecraft for tracking, were interrogated during launch by the Patrick Air Force Base radar. The only loss of transponder signal during the launch phase lasted for a period of 2 seconds at the time of launch-vehicle staging.

Throughout the launch and orbital phases of the BP-15 spacecraft, the performance of the C-band transponders was good. The pulse repetition frequency (PRF), measured by way of telemetry link A, of the two beacons was normal.

The last range station to report acquisition of the transponders was Hawaii on the third orbital pass. The C-band radar coverage times from acquisition to loss of signal for each of the participating range stations is shown in table 7.3-II.

In conclusion, the communications subsystem successfully fulfilled the specified mission requirements, and performance was not degraded by either anomalies or malfunctions.

UNCLASSIFIED

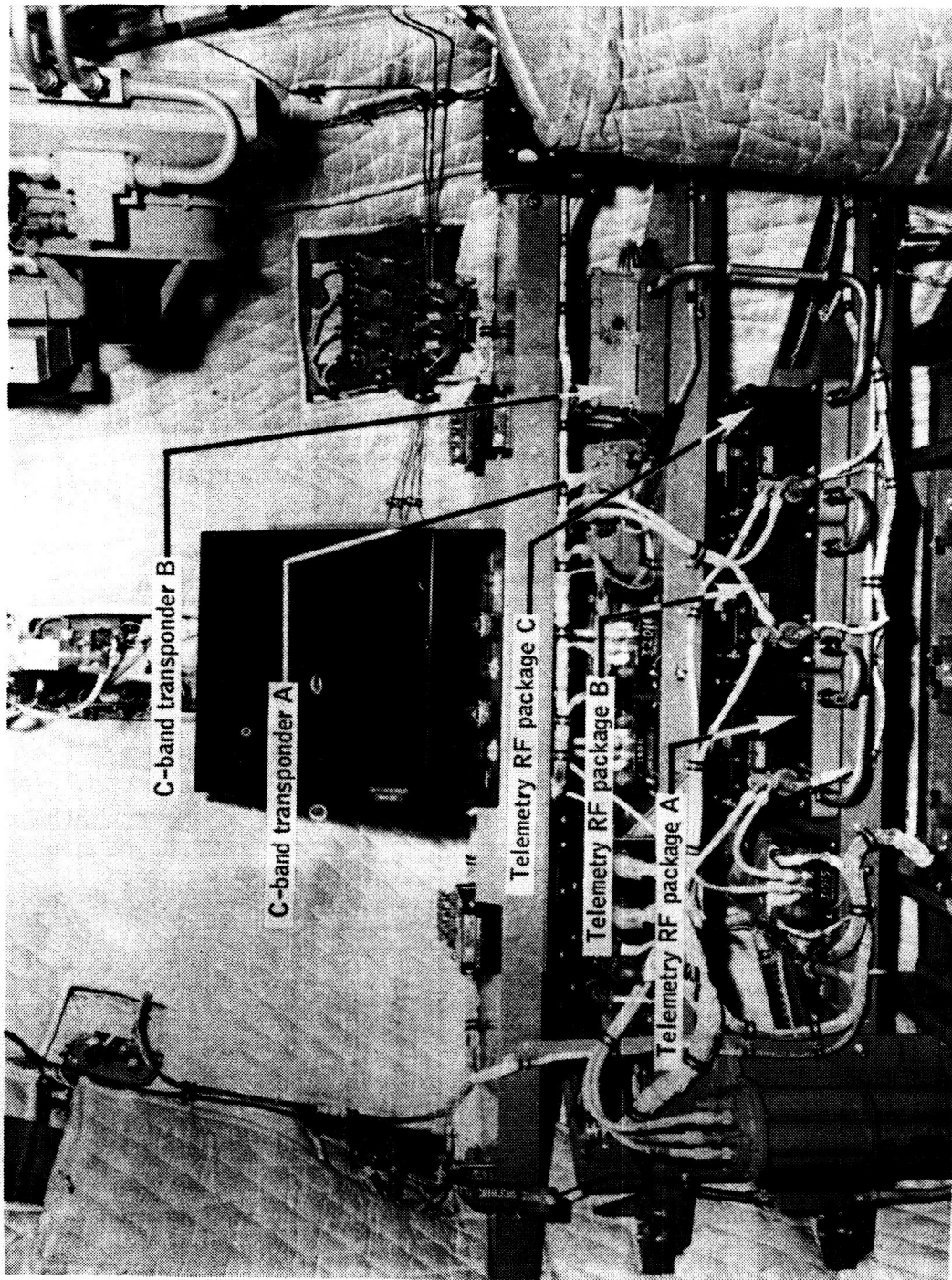


Figure 4.4-1.- Location of telemetry transmitters and C-band transponders on BP-15 spacecraft.

UNCLASSIFIED

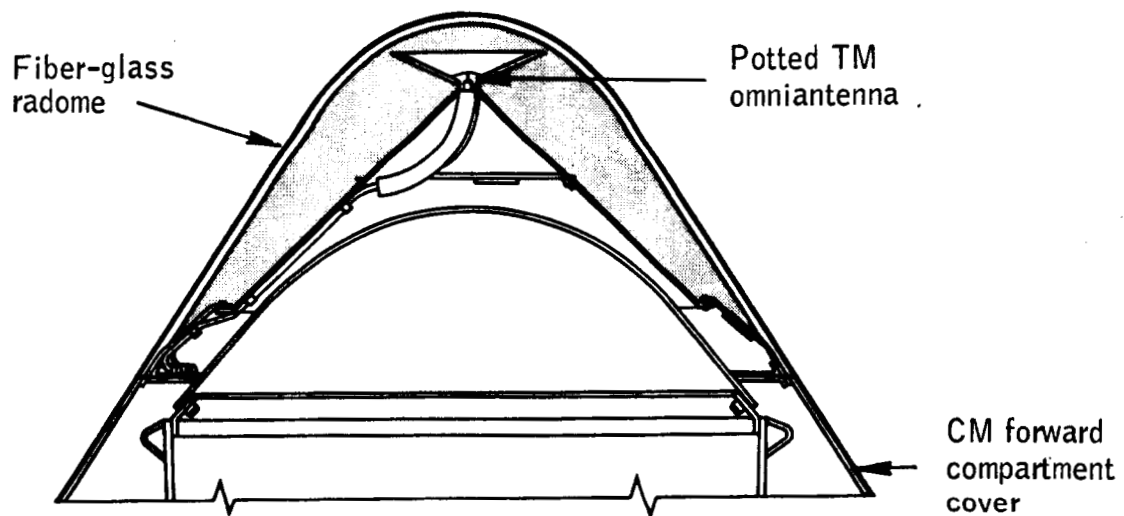


Figure 4.4-2. - Location of telemetry omniantenna on command module of BP-15 spacecraft.

UNCLASSIFIED

~~CONFIDENTIAL~~

4-37

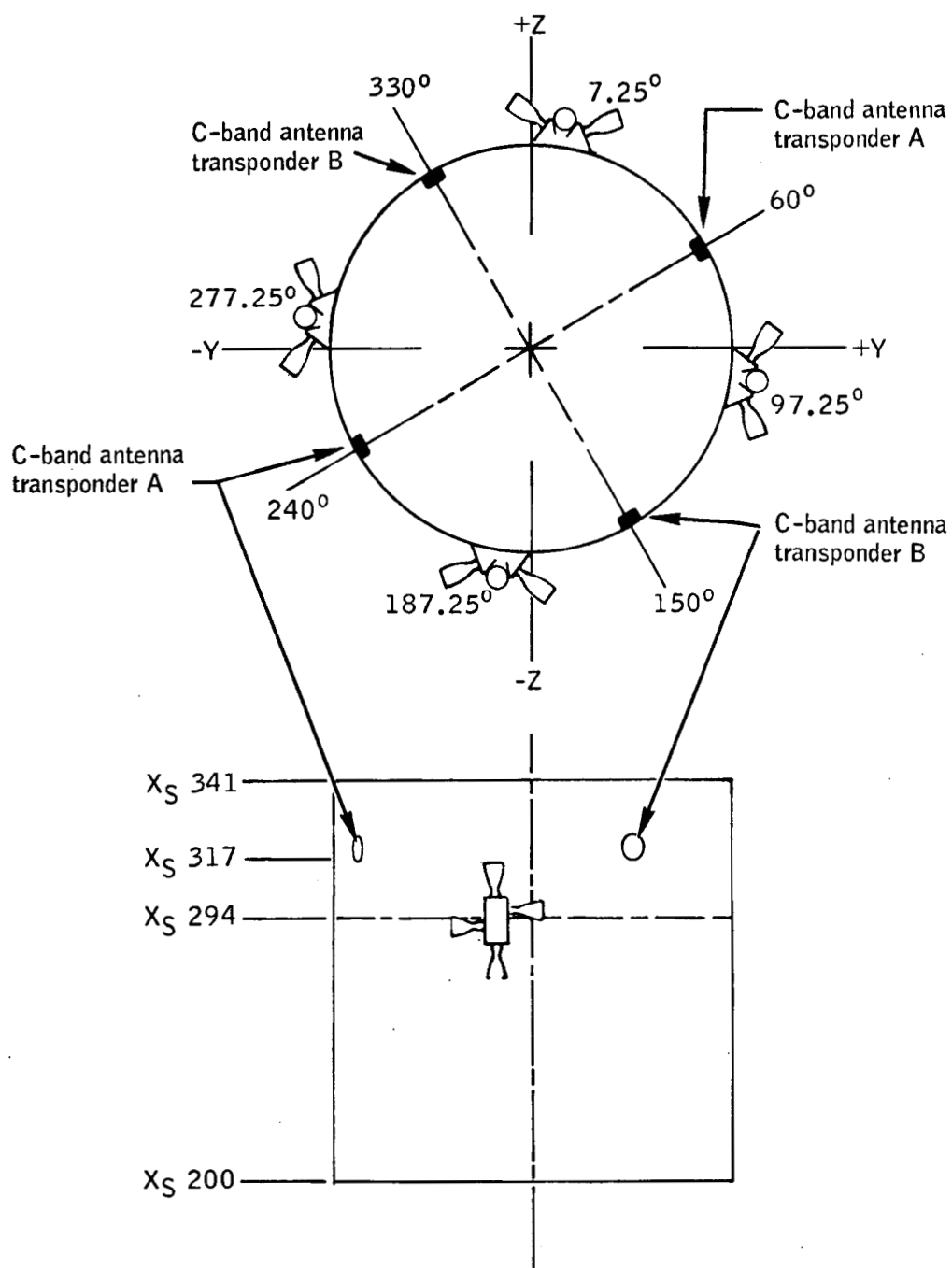


Figure 4.4-3.- BP-15 spacecraft C-band beacon antenna locations on the service module.

~~CONFIDENTIAL~~

UNCLASSIFIED

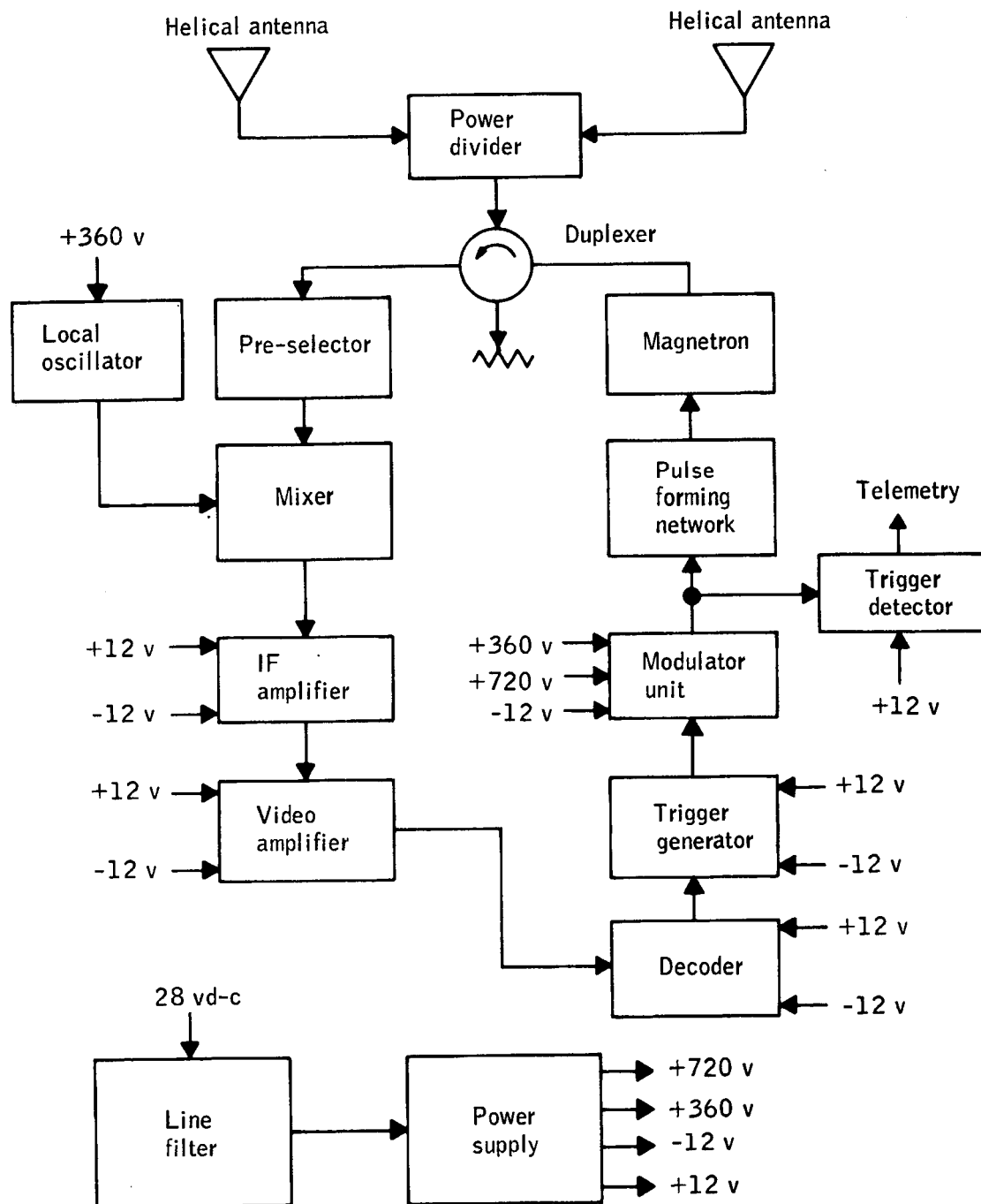


Figure 4.4-4.- C-band transponder block diagram for BP-15 spacecraft.

UNCLASSIFIED

~~CONFIDENTIAL~~

4-39

4.5 Pyrotechnic Devices

Pyrotechnic devices were used on the BP-15 spacecraft to ignite the launch-escape and pitch-control motors and to release the launch-escape tower from the attachment to the command module. The assignments of the pyrotechnic devices are shown in table 4.5-I.

The spacecraft prototype igniter cartridges (ME 453-0014-0081) were installed in the launch-escape and pitch-control motors as shown in figure 4.5-1. Redundant cartridges were employed to enhance the reliability for ignition. Each cartridge contained the Apollo standard hot bridgewire initiator (ME 453-0009-0004) designed to ignite the propellant within 10 milliseconds when a current of 3.5 amps is applied to the bridgewire.

The ME453-0014-0081 prototype cartridge performed satisfactorily on the BP-6 and BP-12 spacecraft (refs. 2 and 3), and photographic data indicated satisfactory performance on the BP-15 spacecraft.

The same cartridge configuration except for a different thread size (ME 453-0014-0082) ignited the tower-jettison motors satisfactorily on the BP-6, BP-12, and BP-13 spacecraft (refs. 1 to 3).

The launch-escape tower was secured to the command module by an explosive bolt assembly in each tower leg as shown in figure 4.5-2. The bolt assemblies were of an interim configuration, pending completion of the development of the production spacecraft dual-mode bolts. The bolts were identical to those which were used successfully on the BP-6, BP-12, and BP-13 spacecraft with the exception that the bolt body threads on the BP-15 configuration were precision rolled to reduce stress concentration at the thread root, instead of being machine cut.

Each bolt assembly contained an ME 111-0001-0015 cartridge (see fig. 4.5-3) with dual initiators which ignited the single propellant charge. The propellant gas pressure, operating against the actuating piston (area ratio, approximately 20 to 1) compressed the silicone plugs. The silicone plugs, under high pressure, served as a hydraulic fluid, which loaded and broke the bolt in tension. The initiators were not the Apollo standard initiators, but had the same response-time characteristics and were of similar configuration. The only exceptions were a slightly higher bridgewire resistance (1.35 ± 0.1 ohm) and a larger thread size to accommodate the interim explosive bolt. The Apollo standard initiators (1.00 ohm bridgewire resistance) are planned to be used with the production spacecraft dual-mode bolts.

The firing current was applied simultaneously to the explosive bolts and igniter cartridges of the launch-escape and pitch-control motors.

~~CONFIDENTIAL~~

~~CONFIDENTIAL~~

The bolts released the tower, and the rocket motors propelled the tower out of the path of the spacecraft.

The primary purpose of the pyrotechnic devices was to ignite the rocket motors and to release the launch-escape tower. Optical and telemetry data indicated that separation occurred at T+160.2 seconds.

~~CONFIDENTIAL~~

TABLE 4.5-I.- ASSIGNMENT OF PYROTECHNIC DEVICES

Nomenclature	Part number	Location	Initiator cartridge		Hotwire initiator serial number	Connector number	Bridgewire resistance, ohms (a)
			Lot number	Serial number			
Explosive bolt cartridge	ME 111-0001-0015	X _C 83.5, 220°	5	b ₁₁₀₆	1118 1114	E 18 P11 E 18 P12	1.31 1.39
Explosive bolt cartridge	ME 111-0001-0015	X _C 83.5, 320°	LAC-4989	b ₁₀₂₉	1043 1059	E 18 P17 E 18 P18	1.39 1.31
Explosive bolt cartridge	ME 111-0001-0015	X _C 83.5, 40°	LAC-4989	b ₁₀₃₅	0200 0213	E 18 P15 E 18 P16	1.32 1.34
Explosive bolt cartridge	ME 111-0001-0015	X _C 83.5, 140°	6	b ₁₁₃₂	1171 1178	E 18 P13 E 18 P14	1.39 1.40
Igniter cartridge	ME 453-0014-0081	Pitch-control motor	1	c ₁₂₈₀	4562	E 18 P3	1.01
			1	c ₁₂₈₁	4448	E 18 P4	1.07
Igniter cartridge	ME 453-0014-0081	Launch-escape motor	1	c ₁₀₉₂	4498	E 18 P1	1.01
			1	c ₁₀₉₈	4518	E 18 P2	1.07

^aMeasured during OTP POD-C-4058 prior to transporting the spacecraft to Complex 37B, Cape Kennedy, Fla. Measurements which were taken when first received at MSC-FO, and after torquing-in on the launch pad, were within 0.001-ohm of these values.

^bThe two initiators were permanently secured within the explosive-bolt initiator cartridge.

^cThe initiator was a separate unit which was inserted into each initiator cartridge.

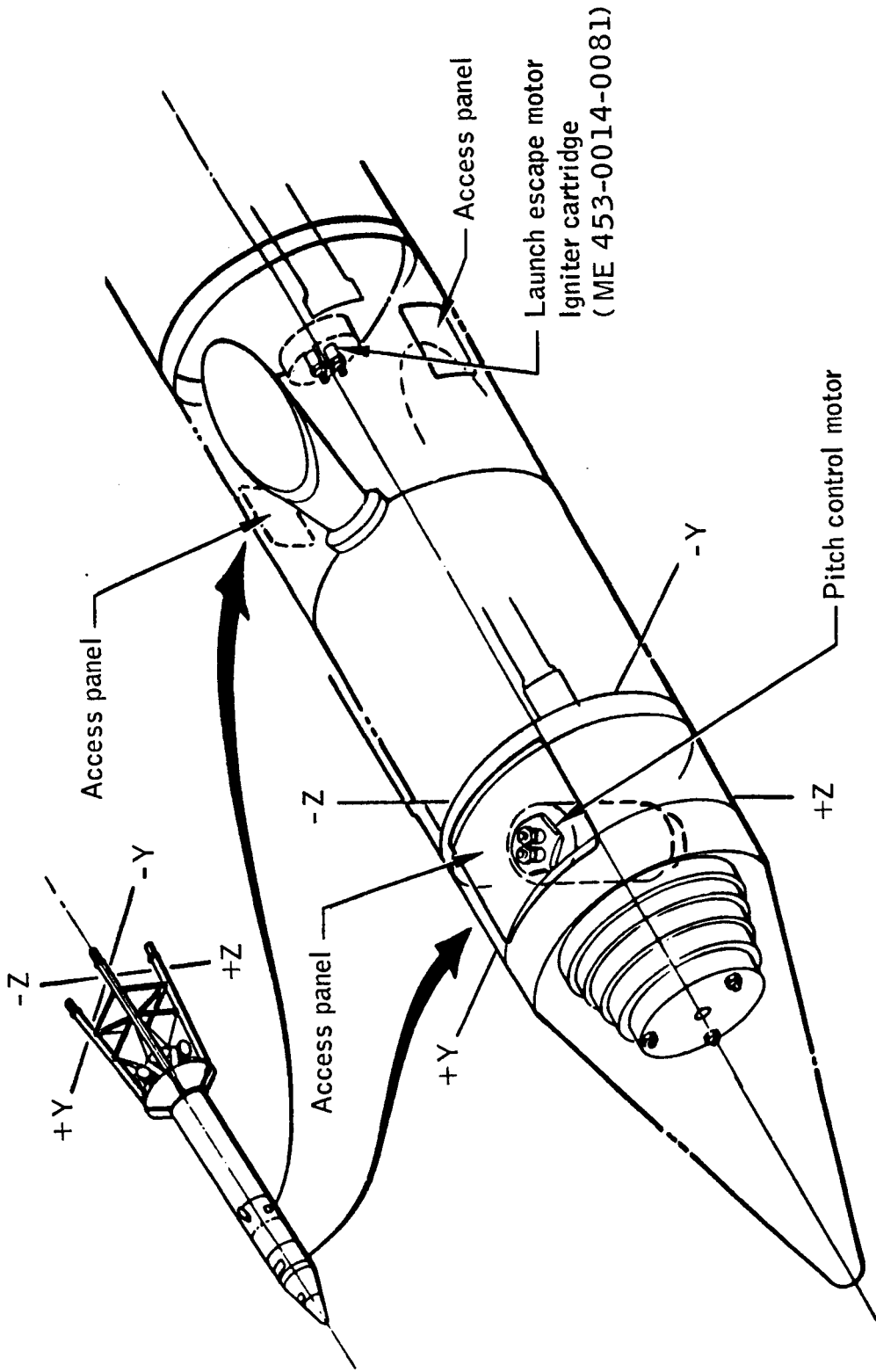
~~CONFIDENTIAL~~~~CONFIDENTIAL~~

Figure 4.5-1.- Location of igniter cartridges in BP-15 spacecraft.

~~CONFIDENTIAL~~

4-43

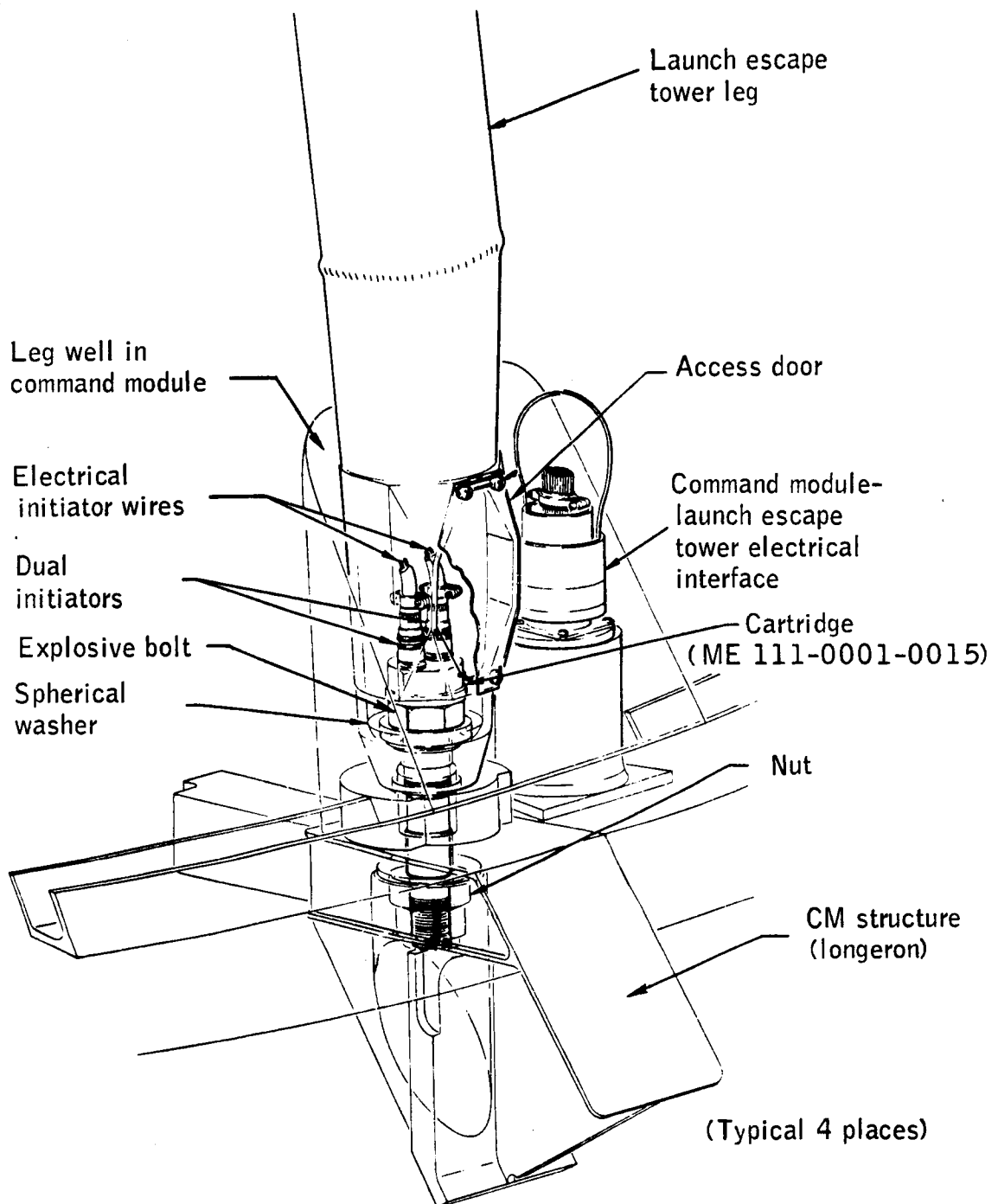


Figure 4.5-2.- BP-15 launch escape tower explosive bolt installation.

~~CONFIDENTIAL~~

UNCLASSIFIED

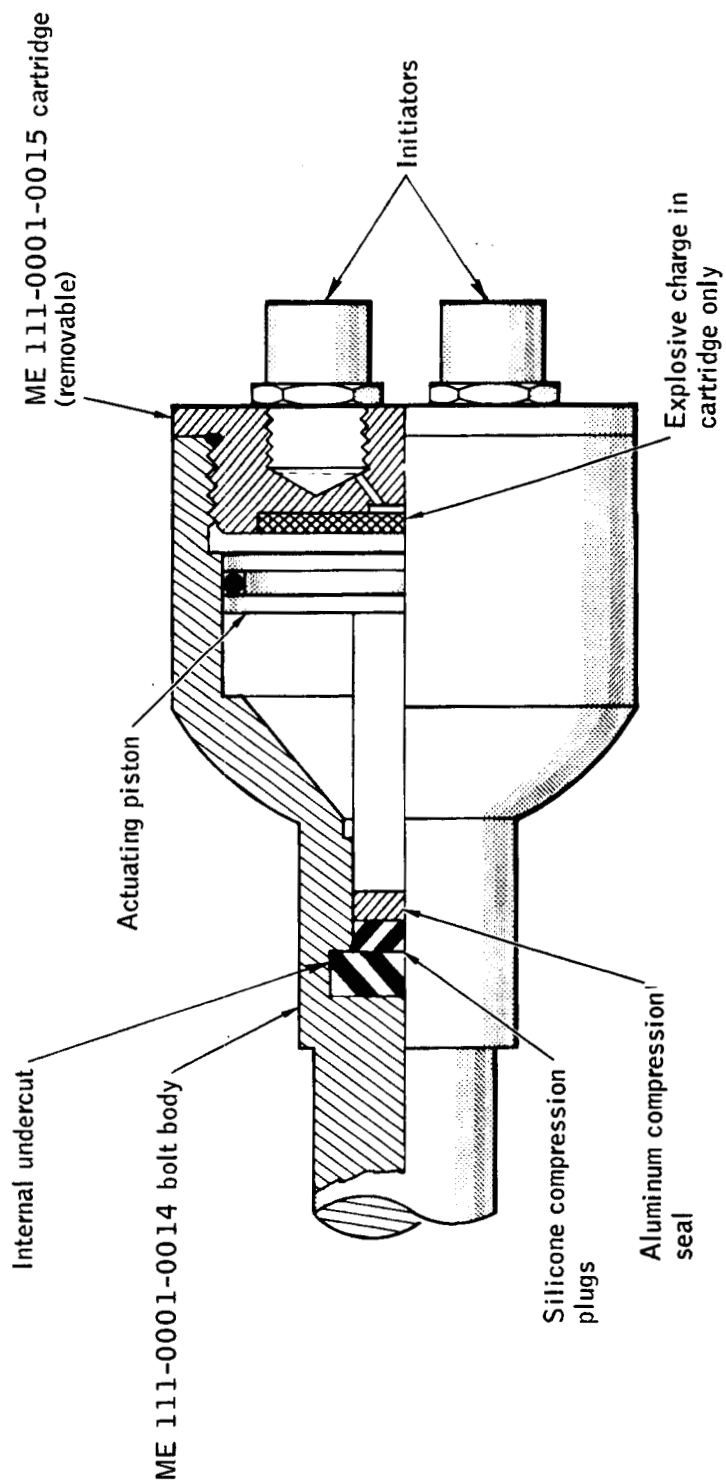


Figure 4.5-3. - BP-15 spacecraft LES explosive bolt detail.

UNCLASSIFIED

~~CONFIDENTIAL~~

4-45

4.6 Launch-Escape Subsystem Propulsion

The launch-escape, pitch-control, and tower-jettison motors used in the BP-15 spacecraft launch-escape subsystem were of the same configuration as the respective motors used in the qualification test program for Apollo Block I and Block II.

To demonstrate alternate mode of tower jettison, the launch-escape and pitch-control motors were utilized, and the tower-jettison motor contained no initiators.

During a normal Apollo mission, the alternate mode of tower jettison is planned for use in the event that the normal mode, using only the tower-jettison motor, fails.

Launch-escape motor.- The launch-escape motor is designed to provide the propulsive force required to remove the command module from the launch vehicle in the event the mission is aborted during the count-down or launch phase through approximately 35 seconds of Saturn V second-stage burning (at an altitude of approximately 295,000 ft). In addition, the launch-escape motor may be used in the alternate mode of tower jettison.

The location of the motor with respect to the command and service module is shown in figure 4.1-1, and the location with respect to the launch escape subsystem is shown in figure 4.6-1. A motor configuration diagram is shown in figure 4.6-2.

The launch-escape motor used a case-bonded solid propellant of polysulfide fuel binder and ammonium perchlorate oxidizer cast into an eight-point, internal-burning, star configuration. The motor had four nozzles spaced 90° apart and canted 35° outward from the longitudinal axis of the motor. The four nozzles had graphite throat inserts and fiber-glass phenolic exit cones. A nominal thrust vector off-set of 2.75° from the motor centerline was provided by the use of one oversize and one undersize nozzle in the pitch plane. The thrust-vector offset was provided so that the negative pitch thrust vector passed more nearly through the center of gravity of the launch escape vehicle. Polyurethane blowout closures were glued into each nozzle throat to provide a sealed environment inside the motor during handling and storage.

The motor was ignited by a head-end mounted igniter, which incorporated redundant hot-bridgewire initiators. The igniter was mounted in the forward end of the motor, concentric with the longitudinal axis. The igniter propellant was of the same formulation as the propellant used in the motor. The initiators were used to ignite boron-potassium nitrate pellets, which, in turn, ignited the igniter propellant.

~~CONFIDENTIAL~~

~~CONFIDENTIAL~~

The predicted performance parameters for the motor are presented in table 4.6-I. A predicted thrust as a function of time is presented in figure 4.6-3.

Pitch-control motor.- The pitch-control motor is designed to provide a positive pitching moment to change the initial attitude of the command module in order to remove the command module from the launch area during a pad abort and from the flight path of the launch vehicle during a flight abort. For the alternate mode of tower jettison the pitch-control motor provides the pitching moment required to assure proper clearance of the launch escape tower from the launch vehicle and command module. The positive pitch thrust counteracts the negative thrust vector angle of the launch escape motor for approximately 0.6 second to provide greater lateral displacement of the LES away from the spacecraft prior to LES tumbling.

The pitch-control motor used the same propellant formulation as the launch-escape motor. The propellant was cast into a 14-point, internal-burning, star configuration.

The motor had one nozzle containing a graphite throat insert housed in a steel structural shell. A polyurethane blowout closure was glued into the nozzle to provide a sealed environment inside the motor during handling and storage.

The motor was ignited by a pellet-type igniter which was mounted in the head end of the motor, concentric with the longitudinal axis. Redundant hot-bridgewire pyrotechnic initiators were used to ignite boron-potassium nitrate pellets, which ignited the motor propellant.

Location of the motor with respect to the command and service modules is shown in figure 4.1-1, and the location with respect to the launch-escape subsystem is shown in figure 4.6-1. A motor configuration diagram is shown in figure 4.6-4.

Predicted performance parameters are presented in table 4.6-I. The predicted thrust as a function of time is presented in figure 4.6-5.

Tower-jettison motor.- The tower-jettison motor is designed to provide the propulsive force for removing the launch-escape subsystem from the flight vehicle for a normal mission after approximately 35 seconds of Saturn V second-stage burning, and from the command module during an aborted mission, when the abort occurs before approximately 35 seconds of Saturn V second-stage burning.

The tower-jettison motor had no function in the secondary mode of tower jettison, and on BP-15 spacecraft the motor was not connected electrically to the sequencing circuit.

~~CONFIDENTIAL~~

~~CONFIDENTIAL~~

4-47

The motor configuration for this flight was basically of the qualification design. The only change was the addition of approximately forty $\frac{1}{4}$ -inch-diameter high-shear bolts on 2-inch centers around the circumference at each end of the interstage adapter to reinforce the spot-welded flanges. These bolts were added following an interstage failure during the tower-jettison motor static test (see fig. 4.6-1).

The location of the motor with respect to the command and service modules is shown in figure 4.1-1, and the location with respect to the launch-escape subsystem is presented in figure 4.6-1. A motor configuration diagram is shown in figure 4.6-6.

Flight performance. - No motor instrumentation was used for the BP-15 spacecraft launch-escape subsystem; therefore, actual motor performance is unavailable. See figure 4.6-3 and 4.6-5 for predicted performance of the individual motors.

The ignition signal for the launch-escape and pitch-control motors was relayed from the sequencer at T+160.2 seconds. A review of photographic coverage of the flight revealed that the first noticeable flame from the launch-escape motor occurred at approximately T+160.2 seconds. Positive ignition of the pitch-control motor could not be determined from the photographic coverage. However, the general trajectory and tumbling rate of the jettisoned portion of the LES indicated that the performance of the pitch-control motor, as well as the launch-escape motor, was satisfactory.

Recovery of the LES was not attempted; therefore, no postflight analysis was possible.

~~CONFIDENTIAL~~

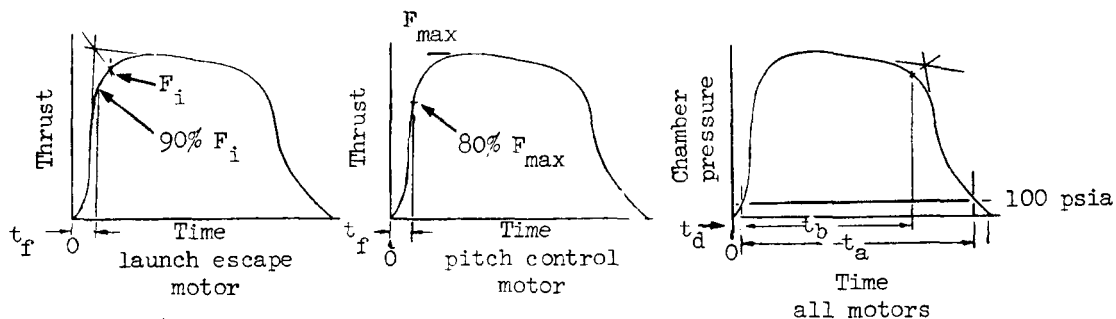
~~CONFIDENTIAL~~

TABLE 4.6-I.- BP-15 SPACECRAFT LAUNCH-ESCAPE PROPULSION
SUBSYSTEM MOTOR PREDICTED PERFORMANCE¹

[At 70° F grain conditioning temperature and vacuum atmospheric pressure]

Parameter	Launch escape	Pitch control
Ignition delay, t_d , sec	0.045	0.015
Thrust rise time, t_r , sec	0.090	0.090
Burning time, t_b , sec	3.230	0.625
Action time, t_a , sec	6.200	1.005
Total time, t_t , sec	9.900	1.250
Maximum chamber pressure, p_{max} , psia	1,480	1.635
Average chamber pressure during burning time, p_b , psia	1,296	1,403
Maximum thrust, F_{max} , lbf	161,700	2,800
Average thrust during burning time, F_b , lbf	147,500	2,390
Total impulse, I_t , lbf-sec	615,300	1,770

¹Based upon historical static test data, propellant burning rate, and motor geometric configuration.



F_i Ignition thrust

0 Firing current application time

~~CONFIDENTIAL~~

~~CONFIDENTIAL~~

4-49

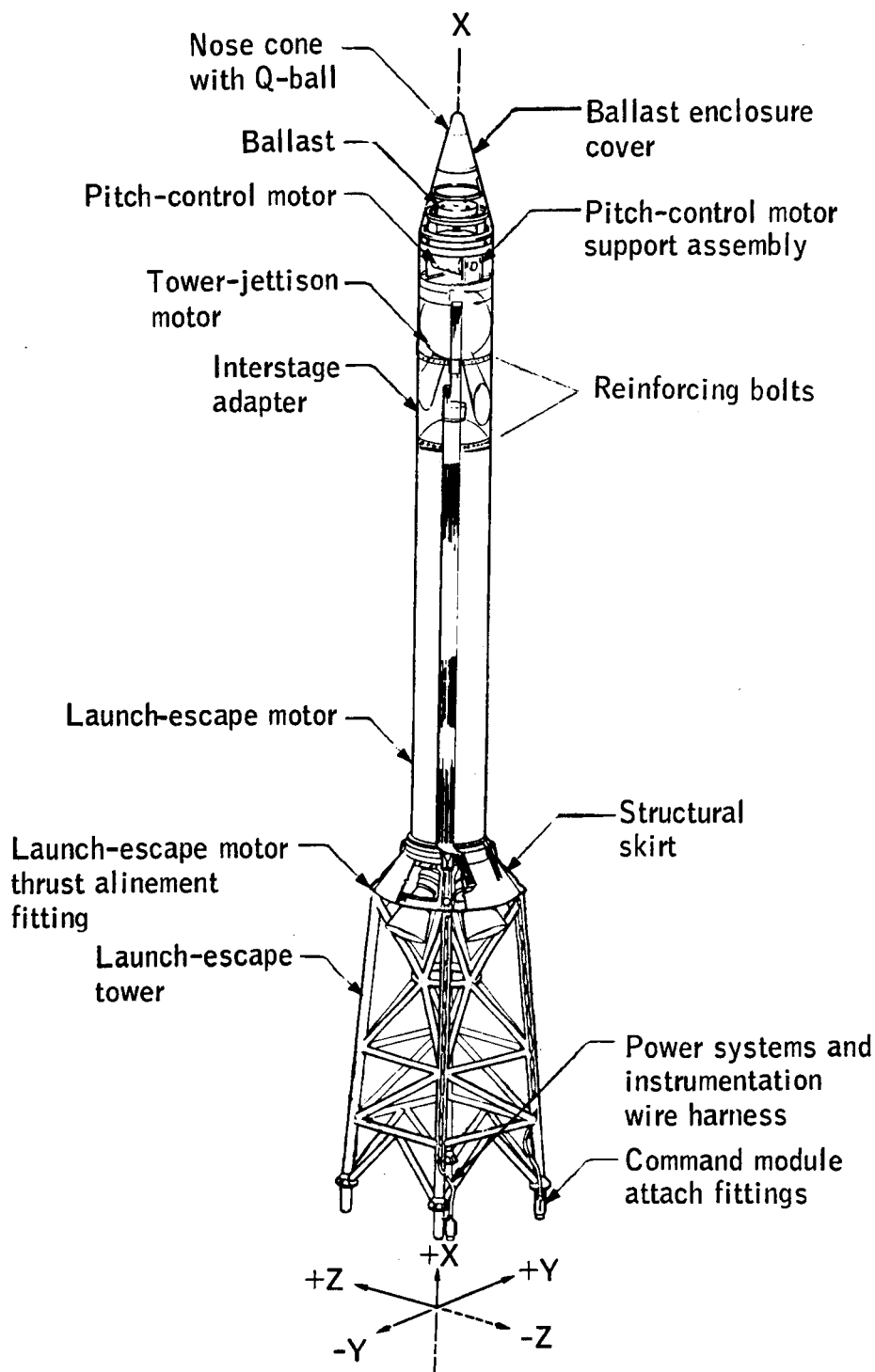


Figure 4.6-1.- BP-15 spacecraft launch escape subsystem.

~~CONFIDENTIAL~~

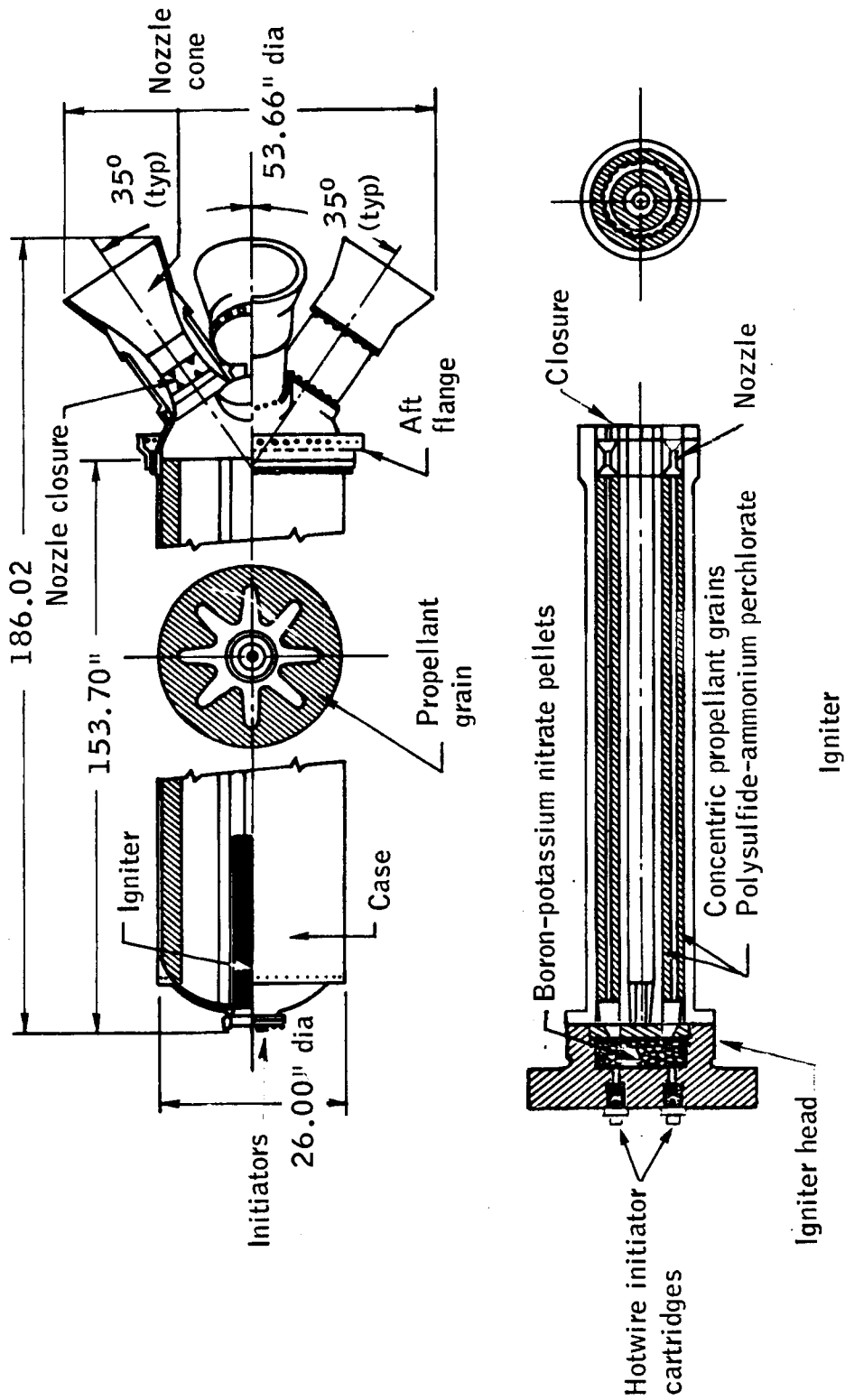
~~CONFIDENTIAL~~

Figure 4.6-2.- BP-15 LES launch-escape motor.

~~CONFIDENTIAL~~

~~CONFIDENTIAL~~

4-51

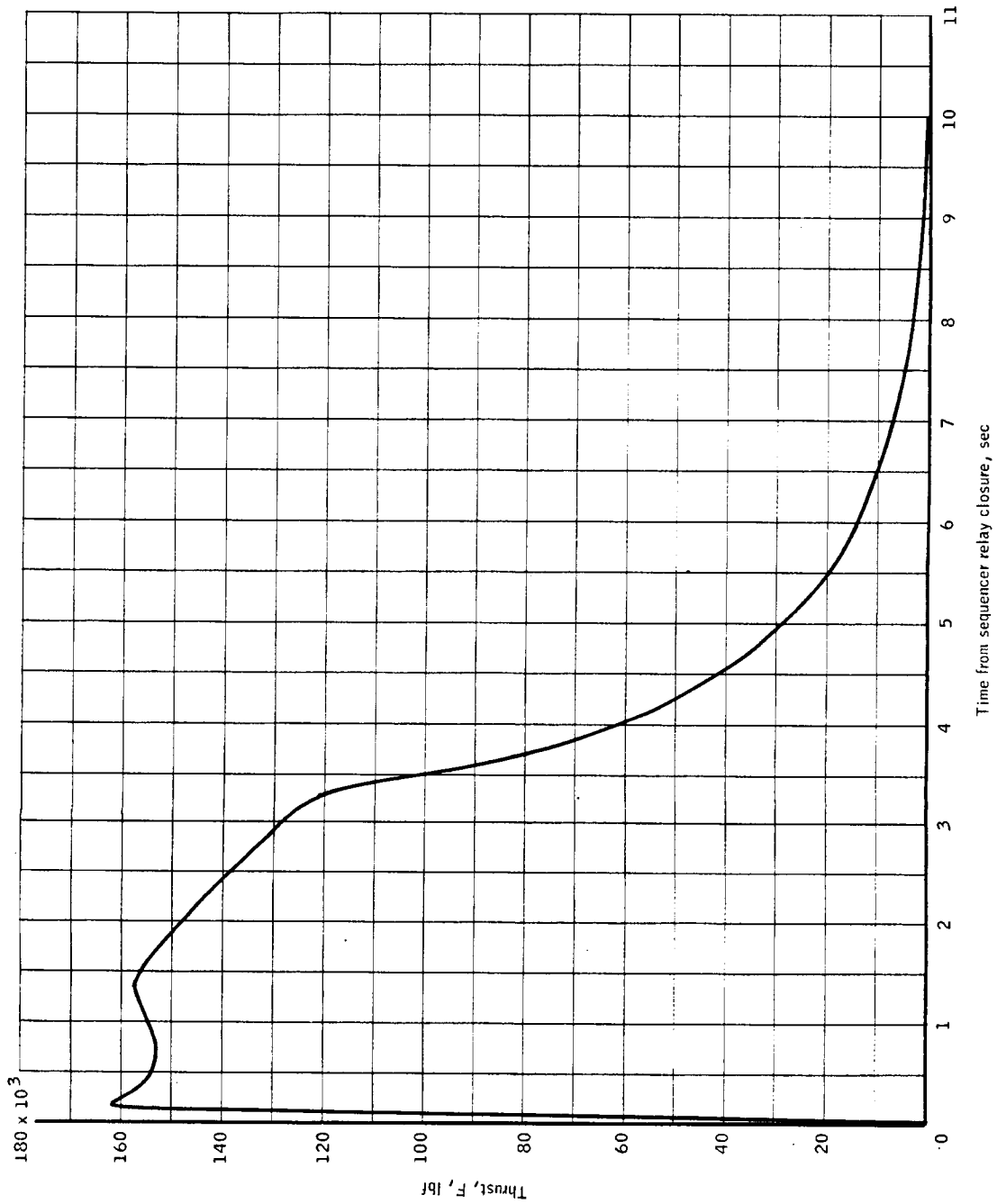


Figure 4.6-3.- BP-15 LES launch-escape motor predicted thrust (in vacuum at 70°F).

~~CONFIDENTIAL~~

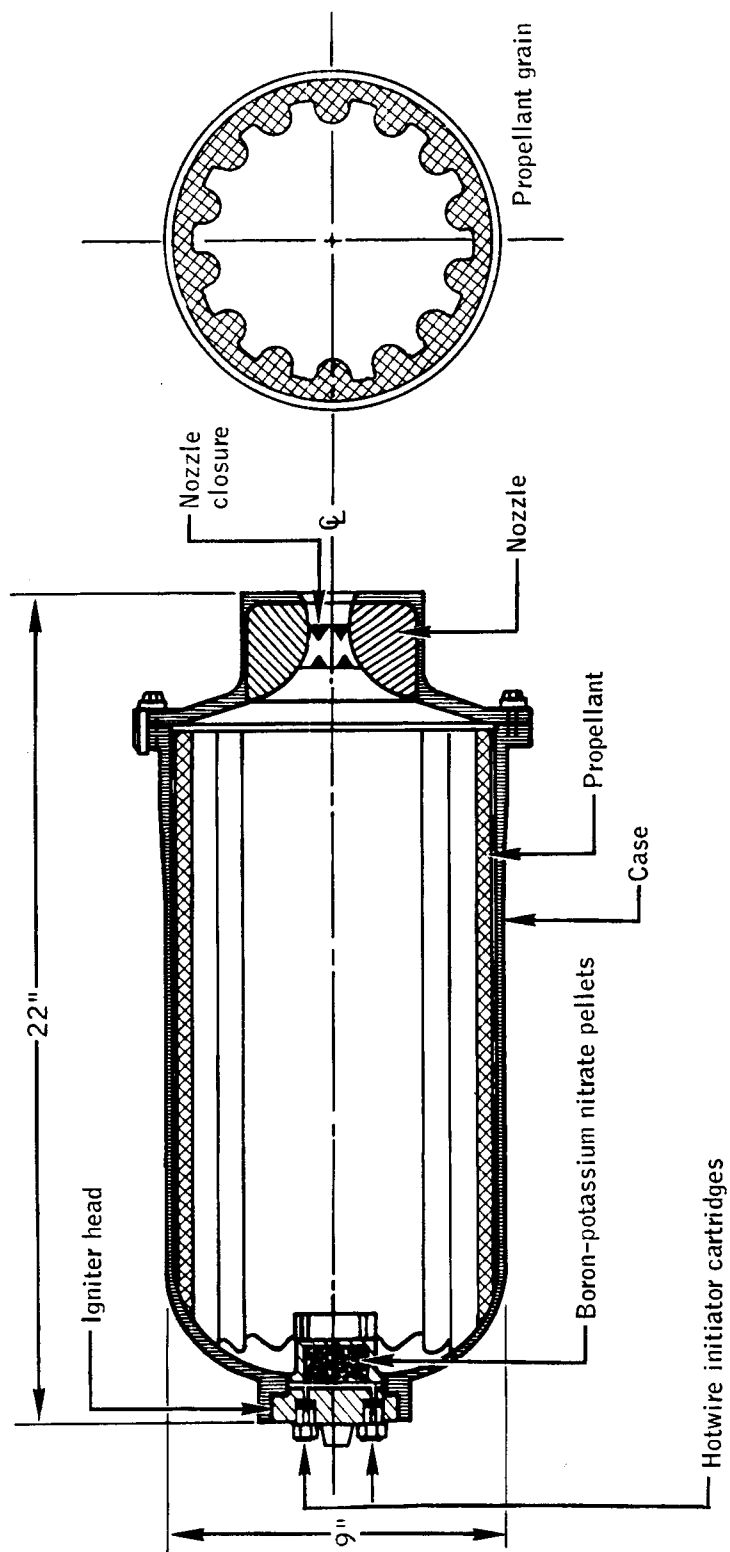
~~CONFIDENTIAL~~

Figure 4.6-4.- BP-15 spacecraft LES pitch control motor.

~~CONFIDENTIAL~~

~~CONFIDENTIAL~~

4-53

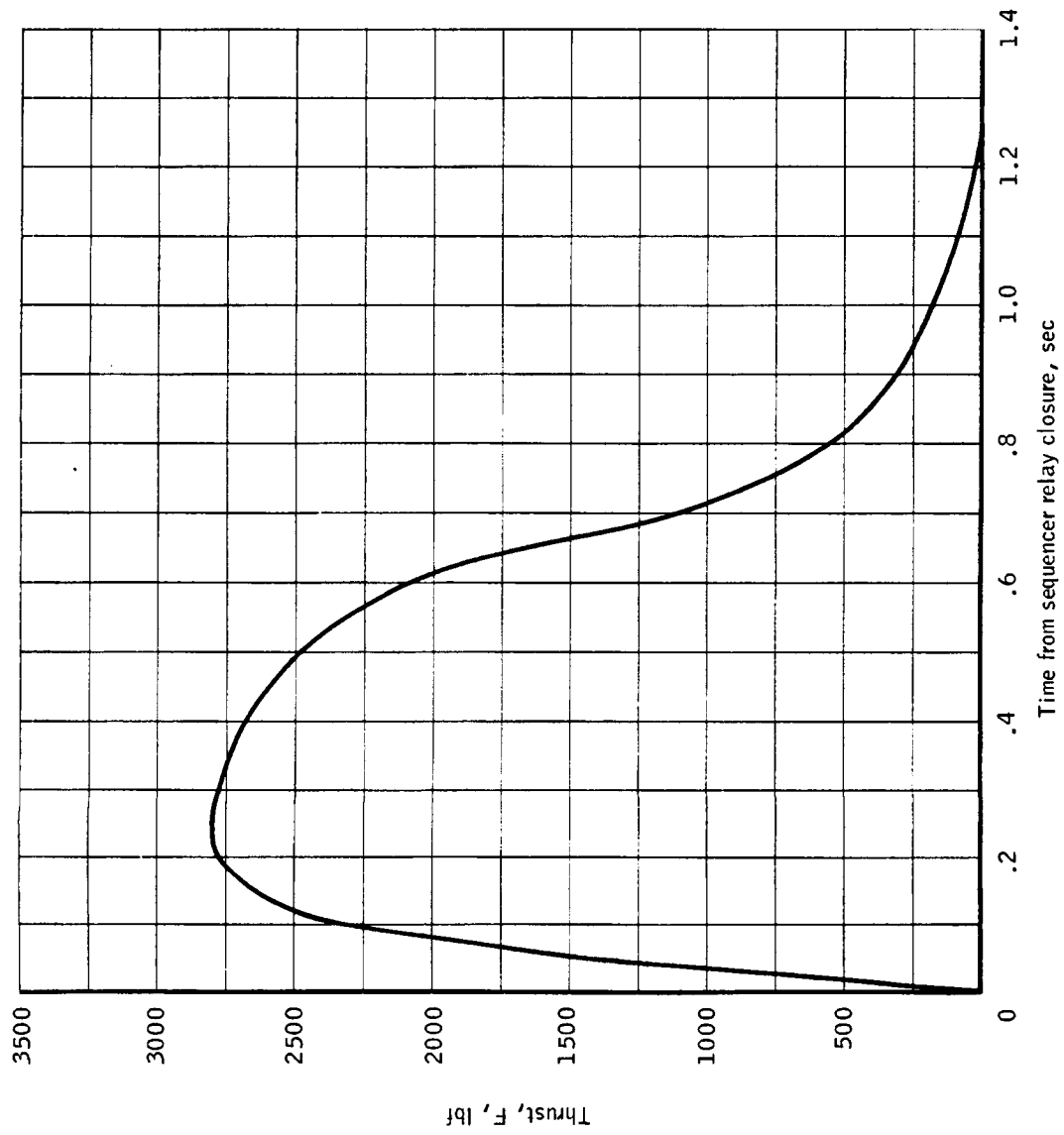


Figure 4.6-5.- BP-15 LES pitch control motor predicted thrust (in vacuum at 70°F).

~~CONFIDENTIAL~~

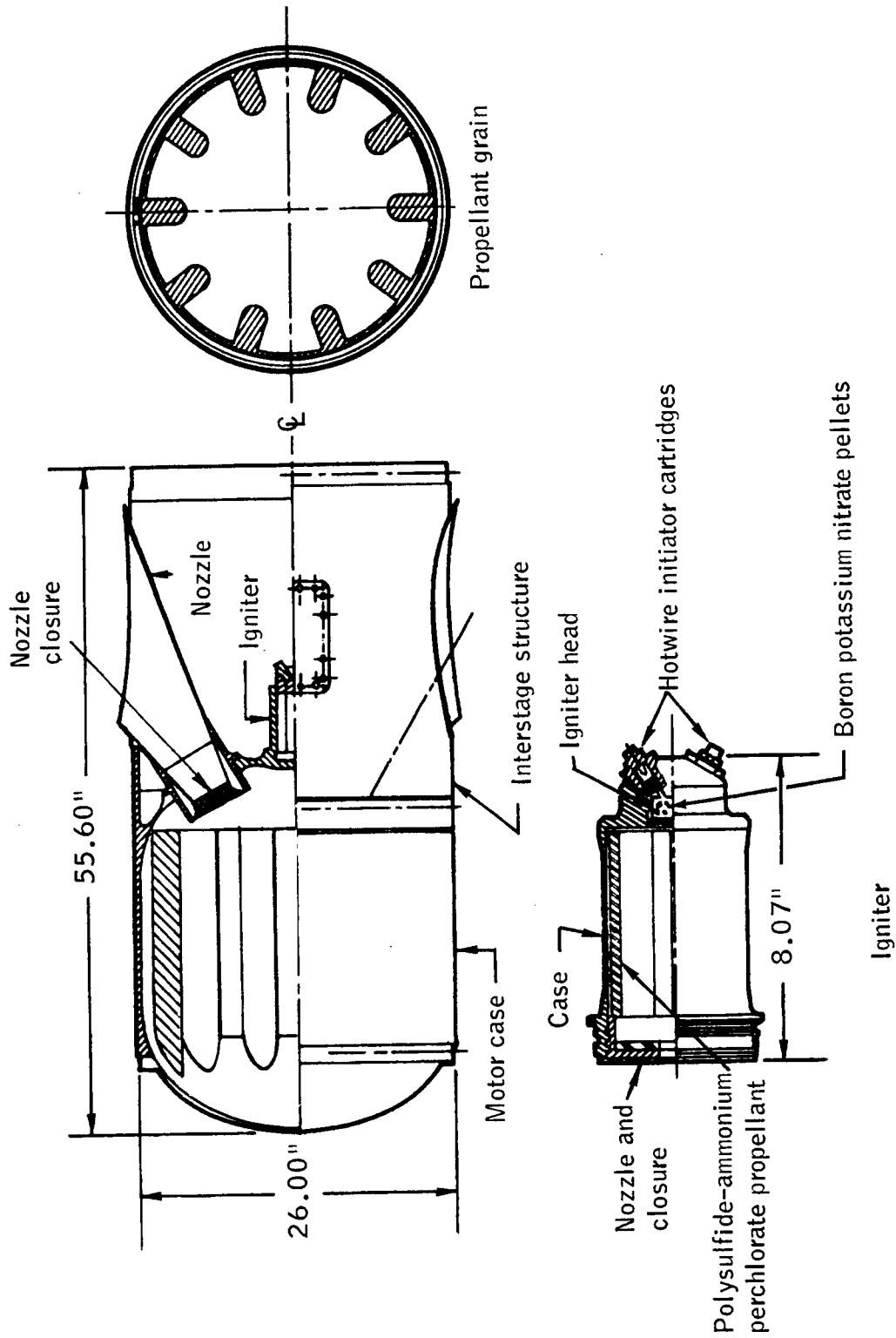
~~CONFIDENTIAL~~~~CONFIDENTIAL~~

Figure 4.6-6.- BP-15 spacecraft LES tower jettison motor.

~~CONFIDENTIAL~~

4-55

4.7 Structures

Summary. - Examination of all spacecraft strain gage, pressure, and acceleration data indicates that the spacecraft performed adequately in the launch environment. Maximum values of α_q did not exceed 1,000 (deg)(lb/sq ft) (minimum allowable $\alpha_q = 5,800$ (deg)(lb/sq ft)). Static pressures measured on the CM conical surface were in agreement with BP-13 spacecraft flight and wind-tunnel data. The spacecraft SM venting system performed as expected. The CM instrumentation compartment differential pressure differed radically from that of BP-13 spacecraft and reached a maximum value of 13.3 psi ($P_{\text{external}} < P_{\text{internal}}$) at tower jettison. X-axis oscillatory accelerations of 1.8g peak-to-peak were measured in the CM during the hold-down period prior to lift-off. These oscillations had a frequency of approximately 10 cps and damped out rapidly at lift-off. Adapter strain-gage data show low amplitude oscillatory strains during the same time period.

Power spectral analysis of Y- and Z-axis accelerations show pre-dominant frequencies of 16 and 40 cps during the boost phase. The 16 cps oscillation was also observed on the CM X-axis acceleration records and was noted during the flight of the BP-13 spacecraft. Adapter strain-gage data do not show that significant oscillatory bending moments were produced in the adapter.

Service-module vibration records showed the expected response to fluctuating pressure. Amplitudes and frequency distribution were similar to those observed during the flight of the BP-13 spacecraft. The SM strain-gage data show low-level strain resulting from the shell mode response with a maximum overall RMS value of 33 $\mu\text{in./in.}$

Strain-gage data from the SM and adapter indicate that both static and dynamic loads were of an acceptable magnitude.

Acceleration data from instrumentation in an RCS engine nozzle show levels of acceleration which were above the design values. An examination of nozzle vibration and SM vibration records indicated no structural failure of the RCS assembly.

Fluctuating pressures on the SM and adapter surfaces were recorded and, in general, verify the design specifications.

Structural description. - The structural assembly for BP-15 spacecraft consisted of the following components: launch-escape subsystem (LES), command module (CM), service module (SM), insert, and adapter. (See fig. 4.1-1.)

~~CONFIDENTIAL~~

~~CONFIDENTIAL~~

The launch-escape subsystem consisted of a motor package and tower truss structure, as shown in figure 4.7-1. The launch-escape tower consisted of a 6AL-4V titanium welded truss structure with four main longitudinal members of 3.6-inch-diameter by 0.125-inch tubing, and connecting members of 2.5-inch-diameter by 0.050-inch tubing. The tower truss structure was 118 inches long and approximately 36 by 36 inches wide at the nozzle skirt attachment and 47 by 51 inches at the CM attachment. The interface between the launch-escape motor and the truss structure was a skirt which was a semimonocoque structure in the form of a truncated cone. The skin was 0.140-inch-thick 6AL-4V titanium sheet which was attached to four titanium longerons. The skirt was attached to the tower at the upper ends of the longitudinal members by four bolts. Separation housings were bolted to the lower ends of the longitudinal members and attached to the CM by means of four pyrotechnic bolts. The launch-escape subsystem structural configuration was identical to that which is planned to be used on the production Apollo spacecraft.

The boilerplate command module was a semimonocoque-type aluminum structure which consisted of skin, stringers, longerons, and frames. The outer skin was 5456 aluminum with a thickness of 0.190 inch.

An inner compartment containing instrumentation, an electrical power system, and ballast required to provide proper weight and center-of-gravity location was provided in the command module. The command module was attached to the SM longerons by three tension tie rods. Compressive loads were carried by six pads, three of which were also capable of taking shear loads. The CM-SM interface connections were similar to production connections. See figure 4.7-2 for a typical connection.

The boilerplate structural assembly shown in figure 4.1-8 consisted of the service module, 141 inches long; the SM insert, 52 inches long; and the adapter, 92 inches long; making an overall length of 285 inches. In addition, a fairing 10.75 inches long was attached to the top of the service module. The outside diameter of the assembly was 154.0 inches. The types of construction of the three components were similar.

The semimonocoque structure of the service module consisted of an aluminum skin which was reinforced with ring frames and longerons. The insert and adapter had stringers in addition to the longerons. The longerons were riveted to the skin and extended the entire length of each section. The longerons were made up to two steel tees joined by an aluminum web and were of constant depth in the insert and adapter. The depth of the longerons in the service module varied linearly from a maximum of 17.2 inches at the top end, where it mated with the command module, to 5.50 inches at the bottom end. The skin of all three components was made of 2024-T3 aluminum alloy and was of a constant

~~CONFIDENTIAL~~

~~CONFIDENTIAL~~

4-57

thickness of 0.16 inch over the entire boilerplate. The skin was reinforced with a total of 30 ring frames. The ring frames in the three components were all made from 2024-T4 aluminum with the exception of the bottom frame of the adapter, which was made of steel. The ring frames in the service module were evenly spaced at approximately 12-inch intervals, whereas the ring frames in the insert and adapter were spaced at varying intervals of approximately 7 to 10 inches. In addition to the six heavy longerons, there were a total of 28 tee-shaped stringers made of 7075-T6 aluminum in the insert and adapter sections.

The service module-to-insert and insert-to-adapter interfaces were bolted connections consisting of 24 bolts each (4 bolts at each longeron). The interface connection between the adapter and instrument unit consisted of 32 bolts, evenly spaced around the circumference.

The parachute compartment of the command module was vented to the space between the instrumentation compartment and the aft heat shield by a connecting tube which passed through the instrumentation compartment. This space was vented to the service module through the clearance in the tension ties holes. (See fig. 4.7-2.) The service module was vented to the atmosphere by eight holes, 4.9 inches in diameter, in the skin of the adapter at X_A 735. An air-conditioning barrier made from a coated nylon cloth was installed at the interface of the adapter and the launch-vehicle instrument unit (IU). Thus, the venting of the service module and instrument unit were independent of each other.

Launch winds and preflight α predictions.- Preflight α predictions were based on the planned trajectory and upper atmospheric winds obtained from rawinsonde soundings made at Cape Kennedy, Florida, at T-14 hours. The launch (T-0) and the T-14 hour wind profiles are shown in figure 4.7-3. The wind velocities were fairly low and the variations from T-14 to T-0 were small as shown in figure 4.7-3. The predicted angles of attack based on the preflight trajectory and the T-0 wind profile are compared in figure 4.7-4 to angles of attack from a preliminary evaluation of Q-ball data by MSFC. A comparison of α profiles using these angles of attack is also shown in figure 4.7-4. As can be seen, α did not exceed 1,000 (deg)(lb/sq ft) during this flight. This was a comparatively low value since the minimum allowable, which occurs at maximum dynamic pressures, was 5,800 (deg)(lb/sq ft).

Command module static pressures.- Static pressures were measured throughout the flight at nine points on the surface of the command module. The locations of the static pressure instrumentation are shown in figure 4.2-5. Static pressure coefficients from T+20 seconds to T+90 seconds are shown in figure 4.7-5. A typical comparison of the flight-data coefficients with wind-tunnel data (ref. 6) at T+70 seconds (M = 1.55) is shown in figure 4.7-6. The correlation between the

~~CONFIDENTIAL~~

~~CONFIDENTIAL~~

flight-measured data and wind-tunnel data is good, and consequently pressure loads obtained by the integration of these distributions agreed well with the predicted pressure loads.

Spacecraft venting. - The pressure inside the compartment made up by the service module, insert, and adapter, and the pressure in the command module instrumentation compartment were measured and transmitted throughout the flight.

The pressure inside the compartment made up by the service module, insert, and adapter was measured in order to verify the adequacy of the venting scheme used. This compartment was the only part of the spacecraft with planned venting. The venting consisted of eight equally spaced 4.9-inch-diameter holes located 13 inches forward of the interface between the adapter and the instrument unit (fig. 4.7-7). The purpose of the SM compartment venting is the following:

- (1) To maintain the differential pressures ($p_{\text{internal}} - p_{\text{external}}$) within the bursting and crushing limits of the structure.
- (2) To keep axial force relief provided by SM internal pressure at a minimum.
- (3) To maintain the differential pressure across the air-conditioning barrier at less than 0.7 psi.

As shown in figure 4.7-8, the flight-measured pressure inside the service module, insert, and adapter compartment was slightly lower than that predicted, except for the period from approximately T+67 to T+80 seconds. Recorded SM internal pressure histories from the BP-13 spacecraft and the BP-15 spacecraft show close agreement. The comparison of the SM, insert, and adapter compartment pressure with that in the instrument unit, as shown in figure 4.7-9, verifies that the differential pressure across the air-conditioning barrier did not exceed the 0.7-psi limit. The data verify that the venting scheme used was adequate.

The command-module instrumentation compartment pressure was not required for verification of the venting scheme for the compartment made up by the service module, insert, and adapter. The command-module instrumentation compartment was not deliberately vented nor was it deliberately sealed. Figure 4.7-10 shows the pressure time history of this compartment for both BP-15 spacecraft and BP-13 spacecraft. It can be seen from this figure that these pressure histories differ quite radically. A maximum differential pressure of 13.3 psi ($p_{\text{external}} < p_{\text{internal}}$) was recorded prior to tower jettison. It is apparent that the BP-15 spacecraft instrumentation compartment was of much tighter construction than the BP-13 spacecraft. It can be seen in figure 4.7-10 that at the

~~CONFIDENTIAL~~

~~CONFIDENTIAL~~

4-59

approximate time of LES jettison ($T+160.2$ sec) there was a marked increase in the leak rate of BP-15 spacecraft command-module instrumentation compartment.

The results of a venting analysis indicate that the observed decrease in pressure could have resulted from venting through a leak area of approximately 0.75 square inch. This leak area could have been obtained by one tower bolt clearing its hole completely (fig. 4.7-11) or by the loosening of the washers around each bolt, allowing venting through the clearance around the $\frac{7}{8}$ -inch-diameter bolt in the 1-inch-diameter hole. However, a rigorous explanation of the increased leak rate at tower separation cannot be offered with the available information.

It should be noted that the tower bolt, attachment scheme, and cabin construction used in BP-15 spacecraft are not of production spacecraft configuration.

Quasi-steady flight loads.- Since the SA-7 trajectory was approximately a zero-lift trajectory, the quasi-steady lateral loads were low. The maximum α_q experienced by the BP-15 spacecraft was 990 (deg)(lb/sq ft) compared with 4,600 (deg)(lb/sq ft) for the BP-13 spacecraft. Inertial loads at the interface of the adapter and IU have been calculated at the maximum α_q flight condition ($\alpha_q = 990$ (deg)(lb/sq ft) at $T+75$ sec). Time histories of vehicle longitudinal and lateral accelerations are presented in figure 4.7-12. Bending moments resulting from air loads at maximum α_q were also determined. The net bending moment on the adapter-IU, including air and inertial loads, was 1.31×10^6 in-lb for the maximum α_q flight condition. Maximum net load was small, approximately 25 percent of that experienced by the BP-13 spacecraft.

The axial forces at $X_A 722$ (adapter-IU interface) were very similar for the BP-13 and BP-15 spacecraft. The BP-15 spacecraft experienced slightly lower axial loads than the BP-13 spacecraft because of smaller angles of attack and dynamic pressures. Predicted axial force at $X_A 722$ (adapter-IU interface) for the BP-15 spacecraft is compared with that calculated from flight data for both the BP-15 and BP-13 spacecraft in figure 4.7-13. The predicted axial force for the BP-15 spacecraft is lower than the actual force, due mainly to the lower q of the preflight trajectory and to the small difference in predicted and actual SM internal pressures.

~~CONFIDENTIAL~~

~~CONFIDENTIAL~~

LES pitch rates.- LES jettison and the resulting LES motions were determined from engineering film taken at Cocoa Beach and Melbourne, Florida. The initial LES motion was forward and translational in the negative Z-axis direction. During pitch-control-motor thrust decay, the LES pitch rate began to increase. Between 3 and 4 seconds after initiation of the LES jettison sequence, the pitch rate had built up to a steady-state value of 675 deg/sec. Predicted LES steady-state pitch rates were 793 deg/sec. Stress analysis, with loads produced by the observed pitch rate, shows that the tumbling rate was sufficient to cause yielding in the LES ballast support plate. The analysis shows that the tumbling rate was not sufficient to cause separation of the LES components from the main LES assembly. The quality of the best films available was not good enough to verify that no components of the LES separated from the assembly.

X-axis vibrations.- An accelerometer system designed to measure X-axis acceleration was located in the CM at the position shown in figure 4.2-2. The system was ranged for amplitudes from -2.0g to +10.0g and for a frequency response from 0 to 30 cps.

The X-axis acceleration records, from the measurement identified as CA001A, show a 10-cps oscillation having a peak-to-peak amplitude of about 1.8g which damped out rapidly at lift-off. The 1.8g value occurred after S-I engine ignition but before vehicle release. Data obtained from the adapter strain-gage system show maximum oscillatory strains during hold-down with peak-to-peak values of 80 μ in./in.

The maximum oscillatory X-axis acceleration recorded after lift-off was about 0.5g peak-to-peak and occurred at maximum dynamic pressure (T+73 sec). The majority of the X-axis vibration energy after lift-off is shown by power-spectral-density analysis to be concentrated at a frequency of approximately 16 cps (fig. 4.7-14). The 16-cps oscillation was also observed in the Y- and Z-axis acceleration records from the BP-15 and BP-13 spacecraft. Further analysis will be required to determine the nature of this oscillation.

Y- and Z-axis accelerations.- The Apollo BP-15 spacecraft was instrumented with six accelerometers to measure accelerations along the Y- and Z-axes of the vehicle. Biaxial measurements were provided in the forward extremity of the LES, in the command module, and in the service module. The LES or tower accelerometers were ranged for $\pm 2.0g$, and CM and SM accelerometers for $\pm 0.5g$.

Tower Y- and Z-axis acceleration measurements at the limit of the instrument range, $\pm 2.0g$, occurred periodically from 41 to 70 seconds after lift-off. Examination of oscillograph records and narrow-band

~~CONFIDENTIAL~~

~~CONFIDENTIAL~~

4-61

analyses of the tower-accelerometer data show that the majority of the response energy was concentrated at frequencies of approximately 16 and 42 cps.

The command module Y- and Z-axis accelerations exhibited similar waveforms at corresponding times. Both command-module and tower accelerations show energy at 16 and 43 cps which indicates excitation of free-free body bending modes having frequencies of 16 and 43 cps. Examination of the power-spectral-density plots presented in figure 4.7-15 showed the majority of energy to have been concentrated at frequencies well above that of the first few body-bending modes (first bending mode frequency ≈ 1.9 cps). The measured response would not be expected to contribute significantly to the overall structural loads, and no evidence of any significant oscillatory bending moment is shown on the oscillograph records of adapter strain or RMS histories of adapter strain.

As during the flight of the BP-13 spacecraft, the only excitation of the first free-free vehicle lateral body-bending mode, observed on the oscillograph records, occurred at S-IV engine ignition. Maximum tower-acceleration values during staging were below 0.8g peak-to-peak. Estimated inertial loads produced by this oscillation would produce less than 5 percent of the design allowable bending moment (based on adapter-IU interface allowable loads). The Y- and Z-axis accelerations of the command and service modules verified all conclusions drawn from the tower Y- and Z-axis acceleration measurements since they exhibited the same frequencies at smaller amplitudes.

SM radial vibrations.- The service module was instrumented with three accelerometers with a range of $\pm 50g$. The frequency response range of the accelerometer identified as SA0086D was from 20 to 1,000 cps. Accelerometers identified as SA0087D and SA0088D had frequency-response ranges from 20 to 790 cps. Two similar instruments were installed in the SM adapter. All radial vibration accelerometers were installed on the flanges of the frames adjacent to the skin to measure radial vibration of the SM and adapter shells at the positions shown in figure 4.7-16.

Inspection of the SM radial vibration records showed random response as during flight of the BP-13 spacecraft. Random vibration response, RMS values of 11 to 15g, were determined from lift-off data. These vibrations died out rapidly as the vehicle rose, and the noise environment became less severe. The vibration response began to increase at T+40 seconds and continued to build up as free-stream dynamic pressure increased and the vehicle approached transonic Mach numbers. Root mean square (RMS) accelerations from SA0086D reached a maximum of 21g RMS at T+50 seconds and decreased sharply to 7.5g RMS at T+55 seconds. From T+55 seconds to T+74 seconds, the RMS value remained

~~CONFIDENTIAL~~

~~CONFIDENTIAL~~

fairly constant. After maximum dynamic pressure at T+73 seconds, the RMS value gradually decreased as Mach number increased and dynamic pressure decreased.

The vibration data recorded from SA0087D and SA0088D exhibited the same general trend as SA0086D with smaller RMS values. Maximum RMS acceleration values from SA0087D and SA0088D were 18g and 15g, respectively. A cursory examination of the adapter radial vibration data recorded through MSFC telemetry show the same general trends as data from SA0086D, SA0087D, and SA0088D, but with smaller RMS values in the comparable frequency range. RMS histories of the SM radial vibration are presented in figure 4.7-17.

The rapid decrease in radial vibration amplitudes noted in the preceding paragraph may be attributed to the decrease in fluctuating pressure which occurred at the same time as the decrease in vibration amplitude (T+50 sec, $M = 0.81$). The decrease in fluctuating pressure amplitudes was expected and can be associated with changes in the aerodynamic flow at this Mach number and angle of attack. Fluctuating pressure and radial vibration records from the BP-15 spacecraft show the same trends as BP-13 spacecraft, and the trend of fluctuating pressure history in this Mach number range has been verified in wind-tunnel tests (ref. 6).

The recorded vibration response of the SM can be attributed to the excitation of shell modes of the SM insert and adapter structure by the fluctuating pressures acting on the SM walls. Evidence supporting this conclusion is presented in the RMS histories of radial vibration and fluctuating pressures of figures 4.7-17 and 4.7-18. A comparison of these two plots shows very good time correlation between the RMS histories of radial vibration and fluctuating pressure.

Power spectral analysis of vibrations recorded from SA0086D and SA0088D shows vibration energy concentrated at 330 cps (fig. 4.7-19). Spectral analysis of data from SA0087D shows similar concentrations. All radial vibration data from the BP-15 spacecraft show good agreement with BP-13 spacecraft data (figs. 4.7-19 and 4.7-20). The narrow-band analysis shown in figure 4.7-19 shows energy concentrated at resonant frequencies which were determined in ground vibration testing of the BP-9 spacecraft (a similar boilerplate vehicle) verifying the conclusion that the observed response was that of shell mode-response.

The low level of SM strain data (33 $\mu\text{in./in. RMS}$) recorded during this flight indicates the observed shell-mode excitation did not produce stress levels which would damage the BP-15 spacecraft structure. Strain-gage power spectral densities are presented in figure 4.7-21

~~CONFIDENTIAL~~

~~CONFIDENTIAL~~

4-63

and show a low level of strain energy. The SM strain and acceleration power spectral densities show energy concentrations at the same frequencies.

RCS engine nozzle vibration. - The BP-15 spacecraft was provided with an instrumented simulated RCS quad assembly. A detailed description of the RCS assemblies is given in section 4.8. Two accelerometers were mounted in the CW engine nozzle. The instruments were located as shown in figure 4.8-5 with both accelerometers ranged at $\pm 200g$. The nozzle X-axis accelerometer SA0091D had a frequency response range of 20 to 1,000 cps, and the accelerometer SA0092D had a frequency response range of 20 to 450 cps.

The RMS histories of nozzle vibrations are presented in figures 4.8-19 and 4.8-20. The RMS histories of SM radial vibration presented in figure 4.7-17 show excellent time correlation with the RMS histories of nozzle vibration which indicates that both SM and nozzle vibrations are excited by the same forcing functions. Dynamic design-load factors for these nozzles were 135g, 0-to-peak, at the center of gravity of the nozzle. The load factors were applied parallel to the vehicle X-axis and perpendicular to the nozzle centerline in the vehicle Y-Z plane.

Maximum acceleration value recorded from the nozzle X-axis measurement (SA0091D) was 174g, 0-to-peak, (T+73.7 sec). Maximum acceleration value in the radial direction (SA0092D) was 160g, 0-to-peak, (T+48 sec). Correcting these maximum values to the design load condition (G levels at nozzle center of gravity) yields a maximum of 151g parallel to the X-axis, and 139g in the radial direction. The recorded values of acceleration in both directions were above the RCS-mount-assembly design values. Resultant accelerations significantly higher than design values can be determined by vectorial summation of the X-axis and radial nozzle accelerations.

Power-spectral-density analysis of the nozzle X-axis and radial vibrations are presented in figures 4.8-21 and 4.8-22 and show the majority of the energy to be concentrated at frequencies which can be associated with nozzle cantilever modes of vibration.

Vibration records from the nozzle and SM accelerometers do not give any indication of a structural failure of the RCS assembly. Further analysis is required to determine the significance of these vibrations.

Strain gages. - There were six strain gages mounted on the spacecraft structure. Two strain gages were mounted in the SM and four in the adapter. The SM strain gages were located to measure the circumferential tensile and compressive strains in the frames. The adapter

~~CONFIDENTIAL~~

~~CONFIDENTIAL~~

strain gages were located to measure longitudinal tensile and compressive strain in the stringers.

The strain gages in the SM were located on the inner flange of the frame at X_A 940.4 and circumferentially at 62.25° and 77.25° from the +Z-axis. The adapter strain gages were located on the inner flange of the tee-section stringers on the Y- and Z-axis at X_A 736 at a radius of 76 inches. Locations of SM and adapter strain gages are shown in figure 4.7-16. Strain-gage ranges and frequency response are shown in table 8.1-I.

Data validity from the strain gages is questionable after T+85 seconds due to the presence of thermal strain. No accurate method of analyzing the amount of thermal strain present in the structure is available.

The SM strain-gage system was ranged for $\pm 500 \mu\text{in./in.}$ A time history of the SM strain recorded by instrument numbers SA2121S and SA2120S is shown in figure 4.7-22. The strain gage identified as SA2121S began to measure dynamic strain at approximately 0.1 second after S-I ignition with a peak-to-peak value of $110 \mu\text{in./in.}$ at T+0 seconds. The strain decreased from T+0 until approximately T+6 seconds at which time the strains were too low to be read. Beginning at T+41 seconds, the dynamic strain increased to a maximum value of $130 \mu\text{in./in.}$ peak-to-peak, at T+49 seconds, and then tapered off to zero at approximately T+90 seconds. A power-spectral analysis of the strain data recorded from SA2121S at a time slice from T+48 to T+50 seconds showed that the maximum energy was concentrated around 330 cps, as shown in figure 4.7-21. The oscillatory strain recorded from instrument SA2120S showed generally the same trends as SA2121S except the magnitude was somewhat smaller. This can be seen in the RMS time histories of the strain data recorded from the two gages shown in figure 4.7-23.

The quasi-steady state level of the strain data from the two SM strain gages was determined by utilizing a 21-point averaging data processing routine (see section 7.4). From this analysis, it was determined that the quasi-steady state strain indicated by SA2120S was small until T+52 seconds at which time the quasi-steady state strain increased to approximately $+40 \mu\text{in./in.}$ and then gradually decreased to zero at approximately T+73 seconds. Instrument SA2121S indicated zero quasi-steady state strain until T+54 seconds, at which time it decreased to approximately $-20 \mu\text{in./in.}$ and then gradually increased to zero at approximately T+67 seconds. This change in quasi-steady state strain is shown in figure 4.7-24. The variation of quasi-steady state strain in the service module frames may be attributed to the influence of the change in the circumferential static pressure distribution resulting from the change in Mach number and altitude with time.

~~CONFIDENTIAL~~

~~CONFIDENTIAL~~

4-65

The adapter strain-gage system was ranged from ± 500 $\mu\text{in./in.}$ The time histories of the strain measured by the four adapter gages are shown in figure 4.7-25. The data given in this figure do not include the static strain (due to lg axial load) of -18.4 $\mu\text{in./in.}$ at that location. The maximum compressive strain measured was -120 $\mu\text{in./in.}$ at approximately T+67 seconds from instrument AA0197S. From the adapter strain data, the quasi-steady state flight loads, axial force, and bending moment at station X_A 736 were determined. A time history of these loads are presented in figure 4.7-26. In referring to these loads, it should be realized that the accuracy of the loads determined from strain-gage data is questionable because of the low magnitude of loads and strains experienced during the flight.

Overall dynamic loads through the launch phase of the flight at the adapter section were shown to be very small, having a maximum RMS value of 5 $\mu\text{in./in.}$ During holddown, however, the adapter experienced strains of 80 $\mu\text{in./in.}$ peak-to-peak, with a maximum RMS value of 10 $\mu\text{in./in.}$ A comparison of steady-state adapter strain levels (determined from a 21-point averaging routine) with real-time total strain plots was made. This comparison shows very small differences between steady-state and total strains, verifying the conclusion that no significant oscillatory bending moments were produced in the adapter.

Examination of all strain-gage data indicates that the structure performed adequately in the flight environment encountered.

Fluctuating pressure. - The fluctuating pressures generated by the turbulent flow over the spacecraft SM were measured by means of 13 pressure transducers. The pressure range of all transducers was 0 to 15 psia with the frequency response of each shown in table 8.1-I. The transducers were mounted so as to sense pressures on the SM external surface. Locations of the transducers are shown in figure 4.7-16.

Recorded pressures at lift-off were invalid since the ambient static pressure was at the upper limit of the transducer range. As dynamic pressure increased during the flight, there was a gradual increase in fluctuating pressure amplitude until T+50 seconds, when a sudden decrease occurred (fig. 4.7-18). The trend of the data around T+50 seconds is associated with changes in the character of the local flow at this free-stream Mach number (0.9) and has been verified by wind-tunnel tests. After T+50 seconds, the levels again gradually increased through maximum dynamic pressure (T+73 sec). As the free-stream dynamic pressure decreased, the fluctuating pressure levels decreased.

The highest noise level measured was in the vicinity of an RCS nozzle. The fluctuating pressure history in the area around this nozzle did not show the drop off at T+50 seconds (fig. 4.7-18(d)) exhibited by

~~CONFIDENTIAL~~

~~CONFIDENTIAL~~

the data obtained from all other transducers. This is attributed to the unique location of this transducer which was directly beneath a forward-facing RCS nozzle as shown in figure 4.7-16 (measurement SA0165P).

RMS pressure histories from all fluctuating pressure transducers are shown in figure 4.7-18. A comparison of flight-measured noise environment with Apollo design environment for several spacecraft zones is given in figure 4.7-27.

~~CONFIDENTIAL~~

UNCLASSIFIED

4-67

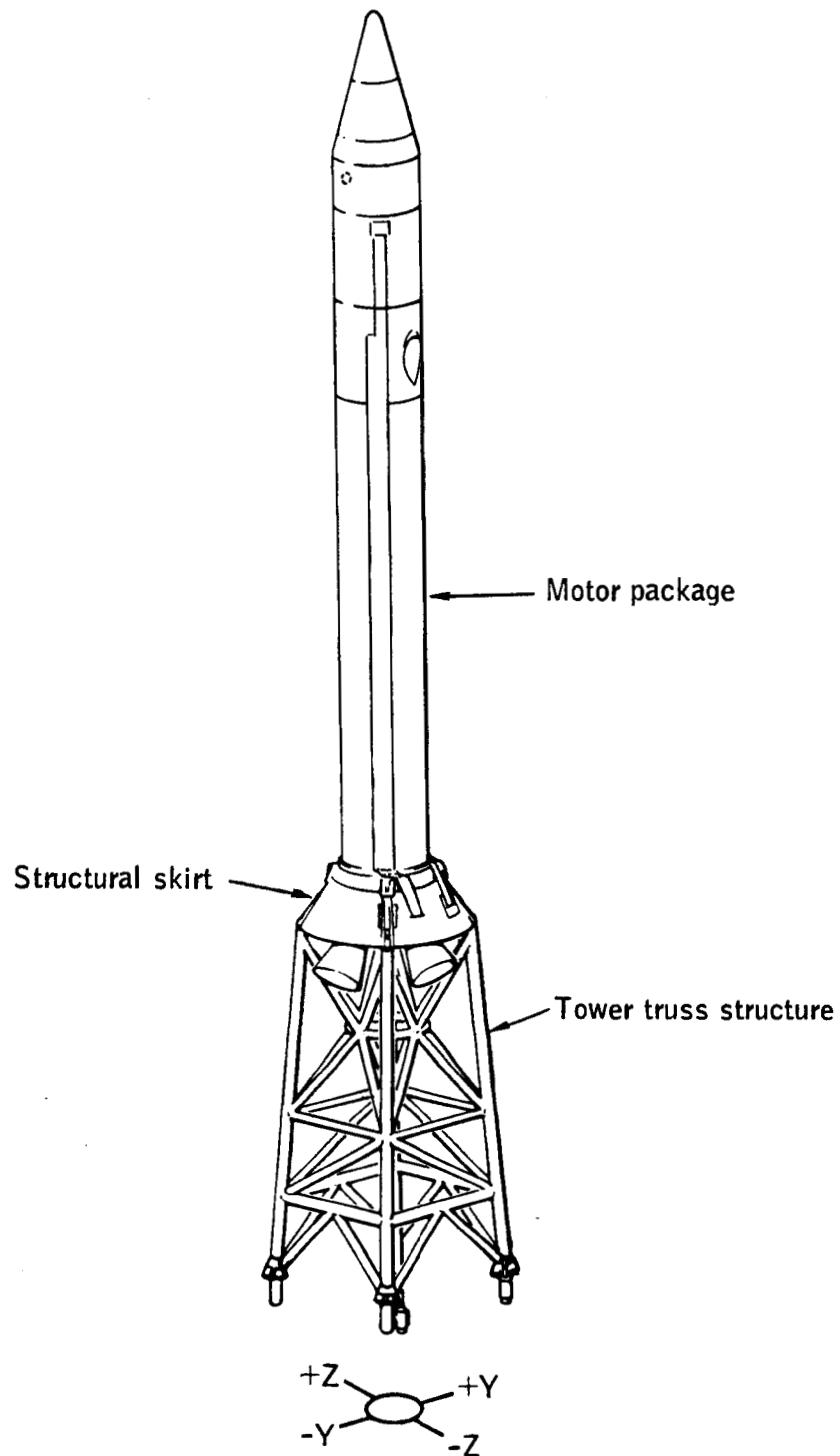


Figure 4.7-1. - Apollo BP-15 spacecraft launch escape subsystem structure.

UNCLASSIFIED

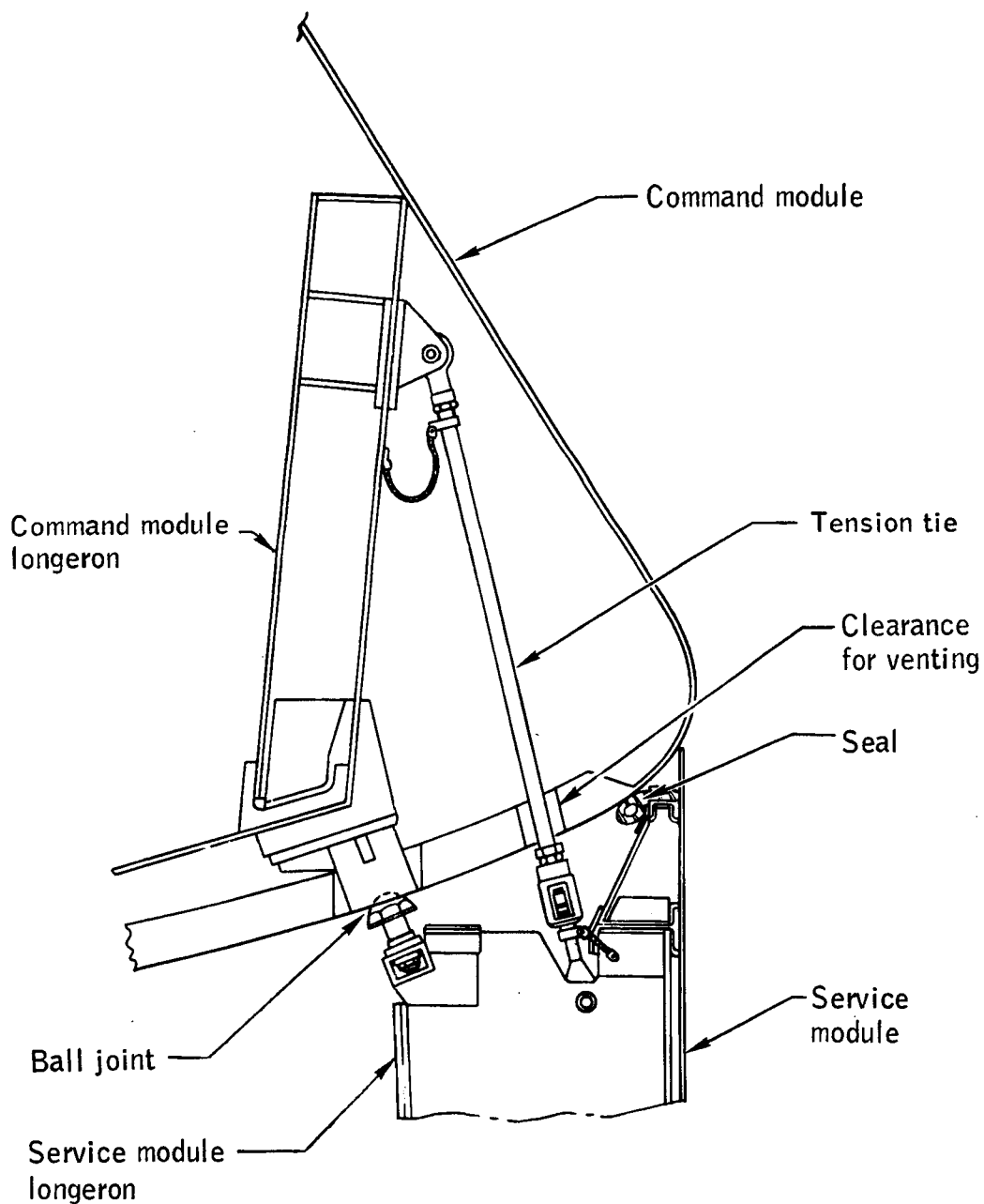
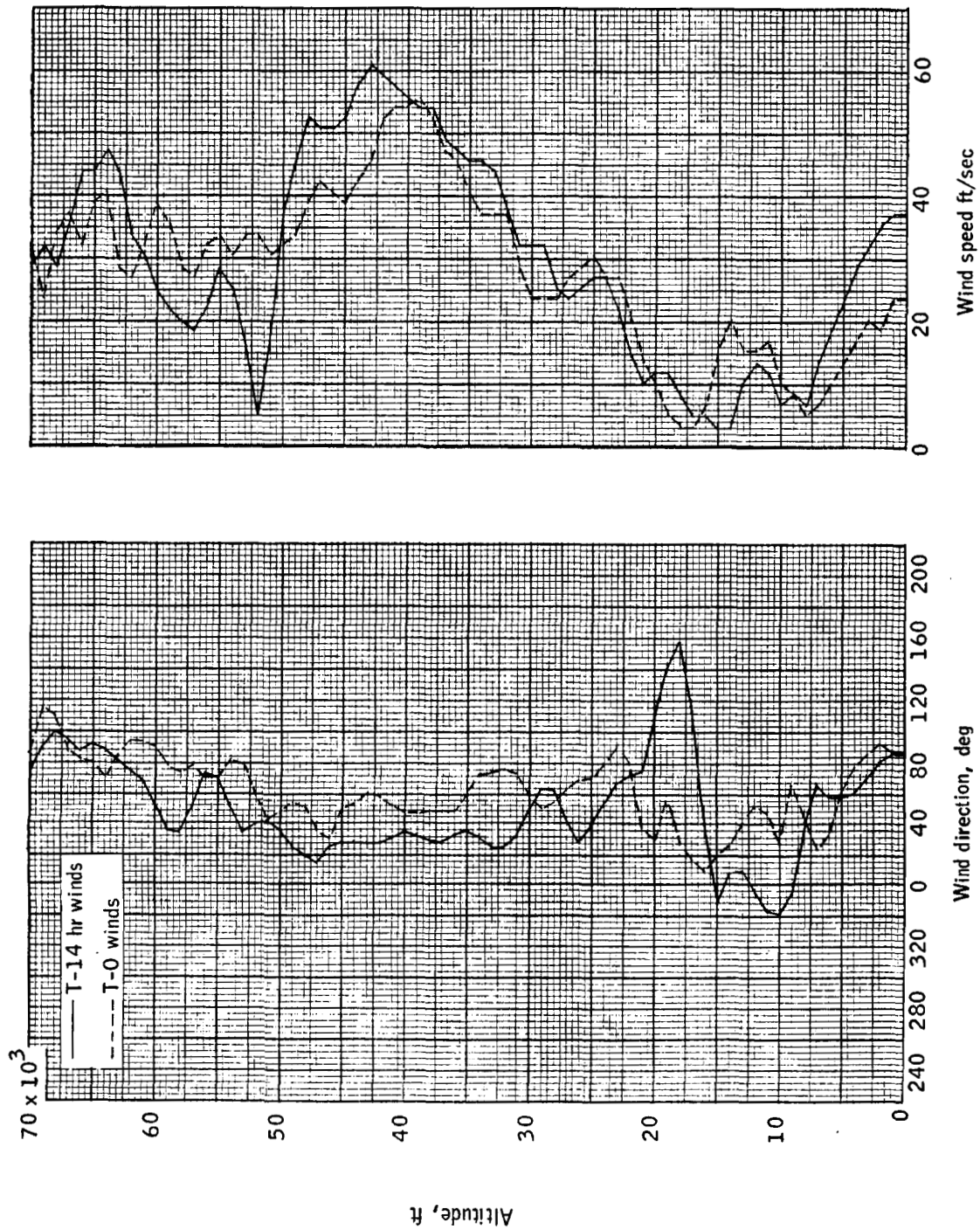
~~CONFIDENTIAL~~

Figure 4.7-2.- Detail of command module-service module interface for BP-15 spacecraft.

~~CONFIDENTIAL~~

4-69



UNCLASSIFIED

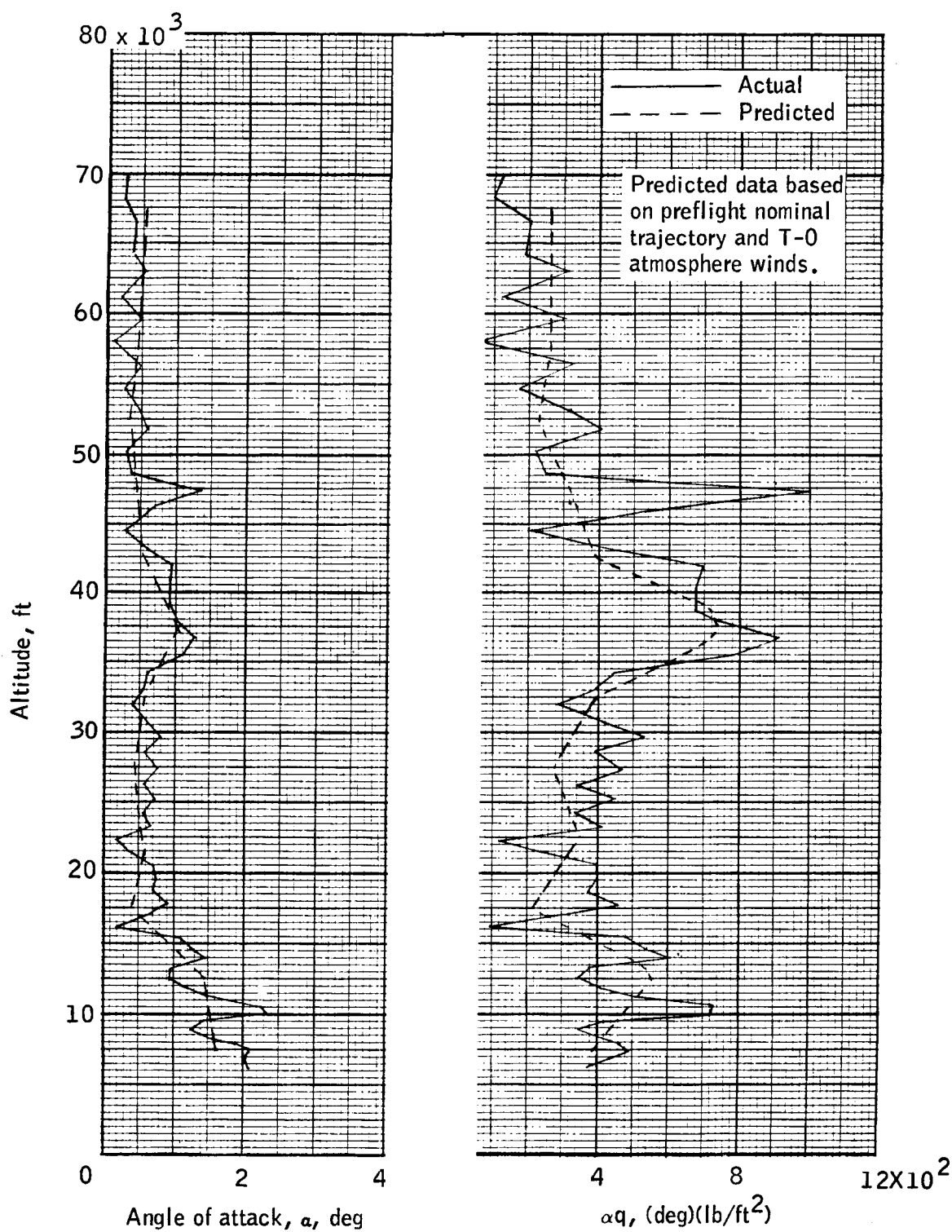
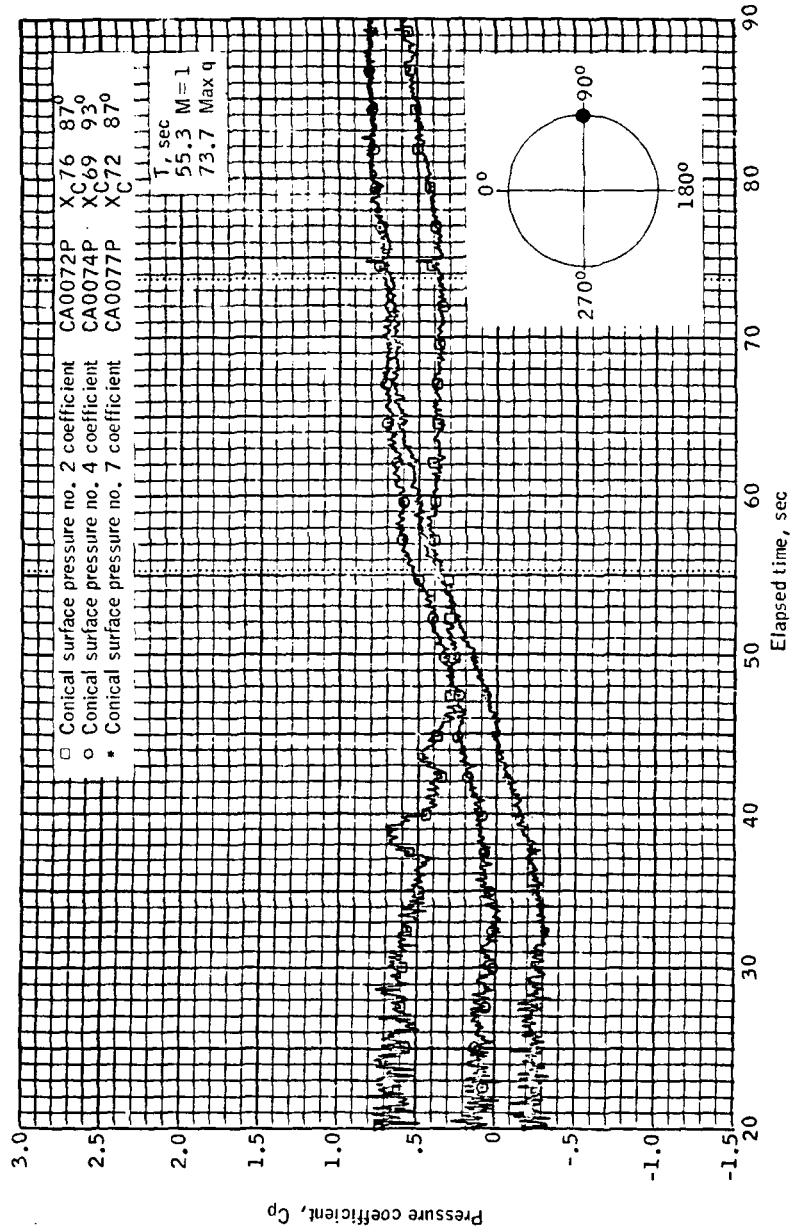
~~CONFIDENTIAL~~

Figure 4.7-4.- Comparison of predicted to flight measured angles of attack and αq .

~~CONFIDENTIAL~~

~~CONFIDENTIAL~~

4-71



(a) Circumferential location, approximately 90° .

Figure 4.7-5.- Static pressure coefficient over the command module conical surface on BP-15 spacecraft.

~~CONFIDENTIAL~~

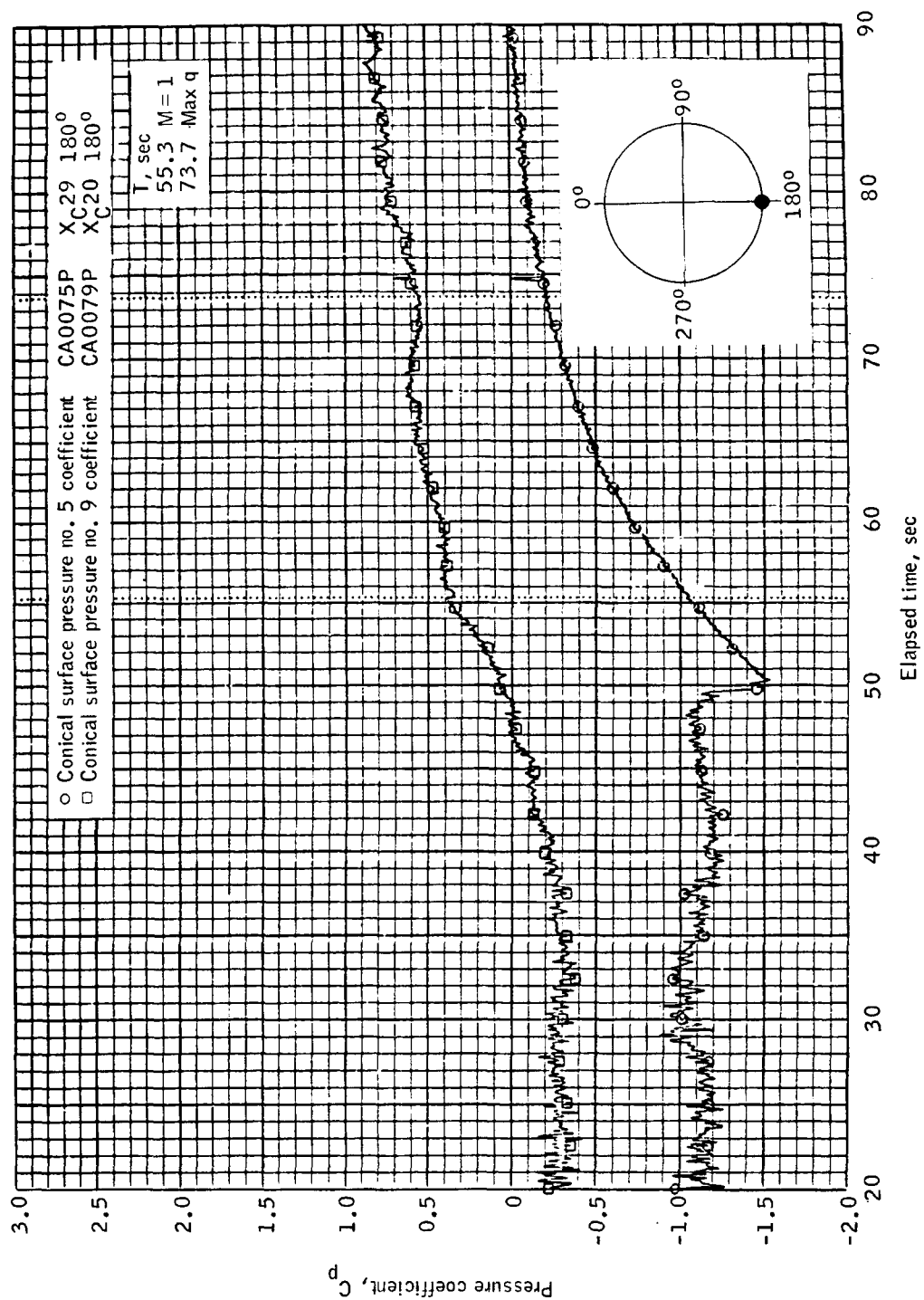
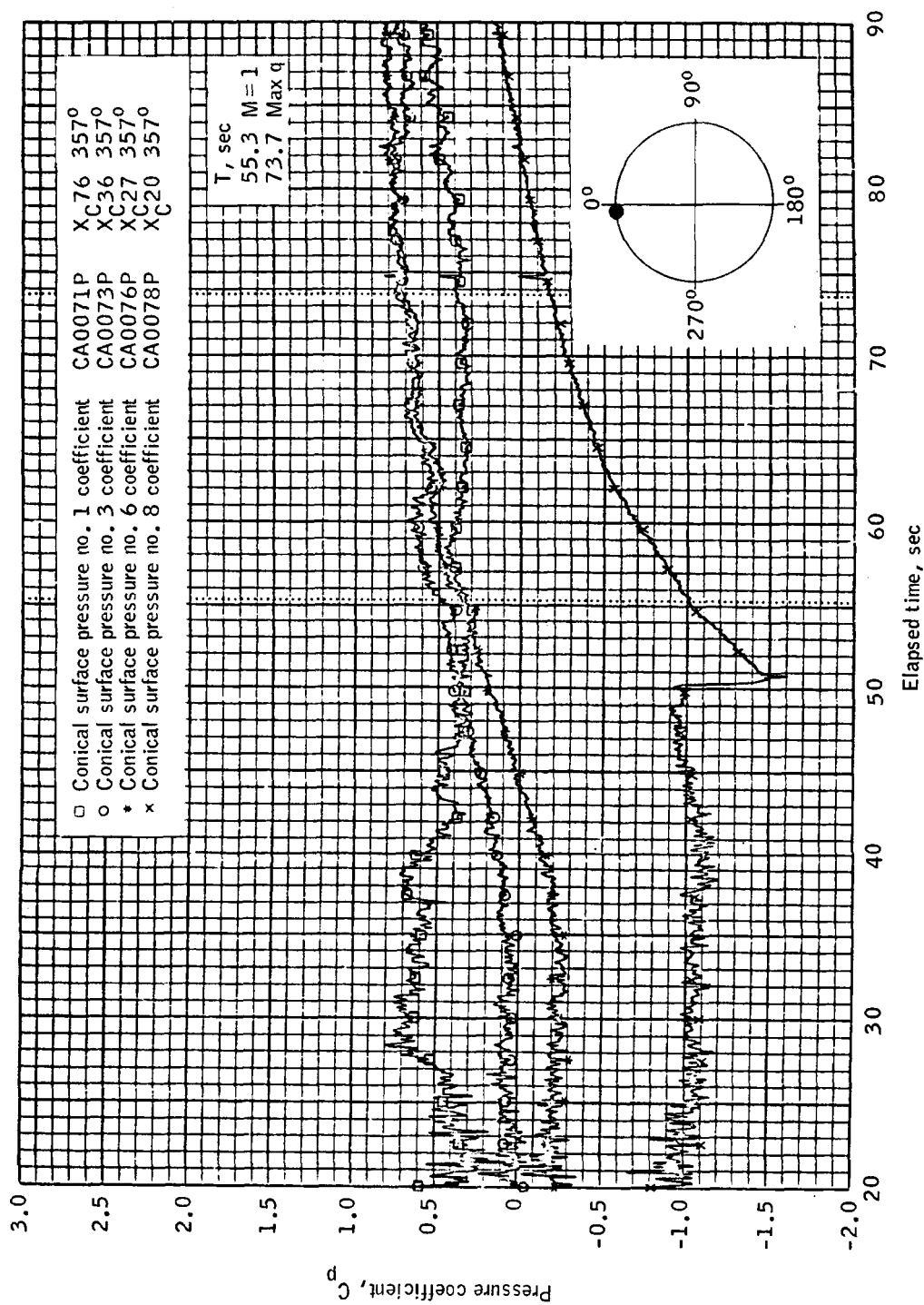
~~CONFIDENTIAL~~(b) Circumferential location, 180° .

Figure 4.7-5.- Continued.

~~CONFIDENTIAL~~

~~CONFIDENTIAL~~

4-73



(c) Circumferential location, 357°.

Figure 4.7-5.- Concluded.

~~CONFIDENTIAL~~

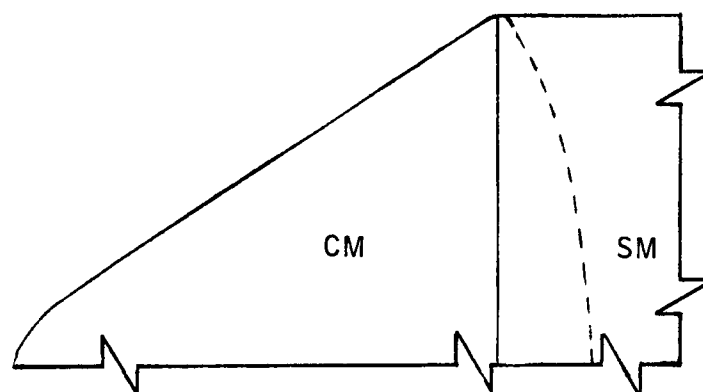
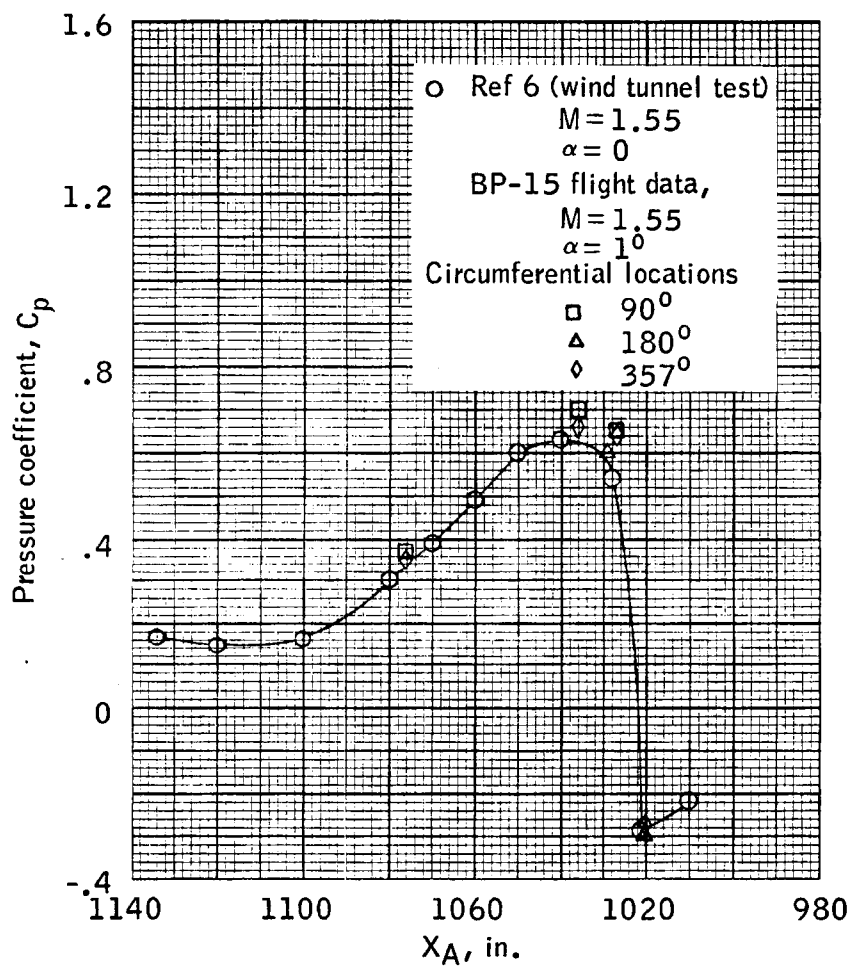
~~CONFIDENTIAL~~

Figure 4.7-6.- Command module static pressure coefficients for BP-15 spacecraft flight data compared to wind tunnel data (reference 6).

~~CONFIDENTIAL~~

~~CONFIDENTIAL~~

4-75

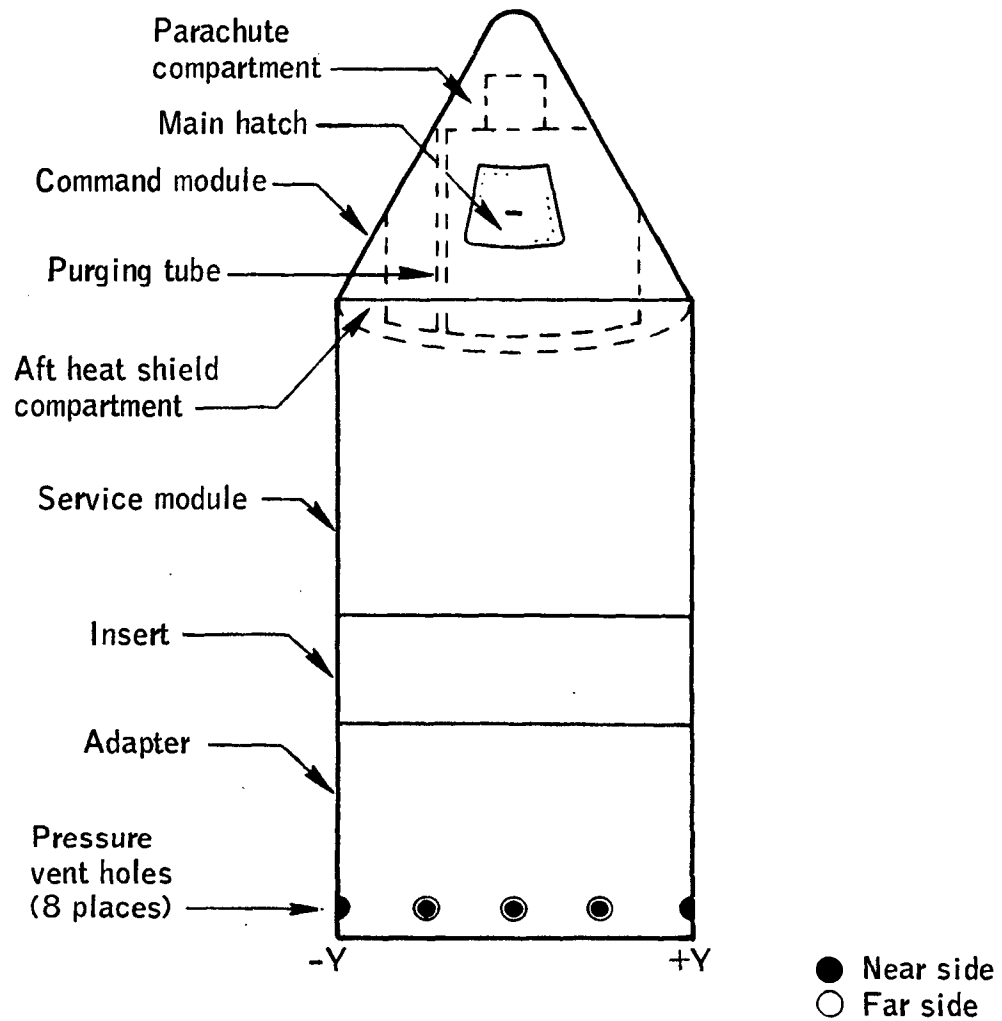


Figure 4.7-7.- Pressure venting scheme for BP-15 service module, insert, and adapter compartment.

~~CONFIDENTIAL~~

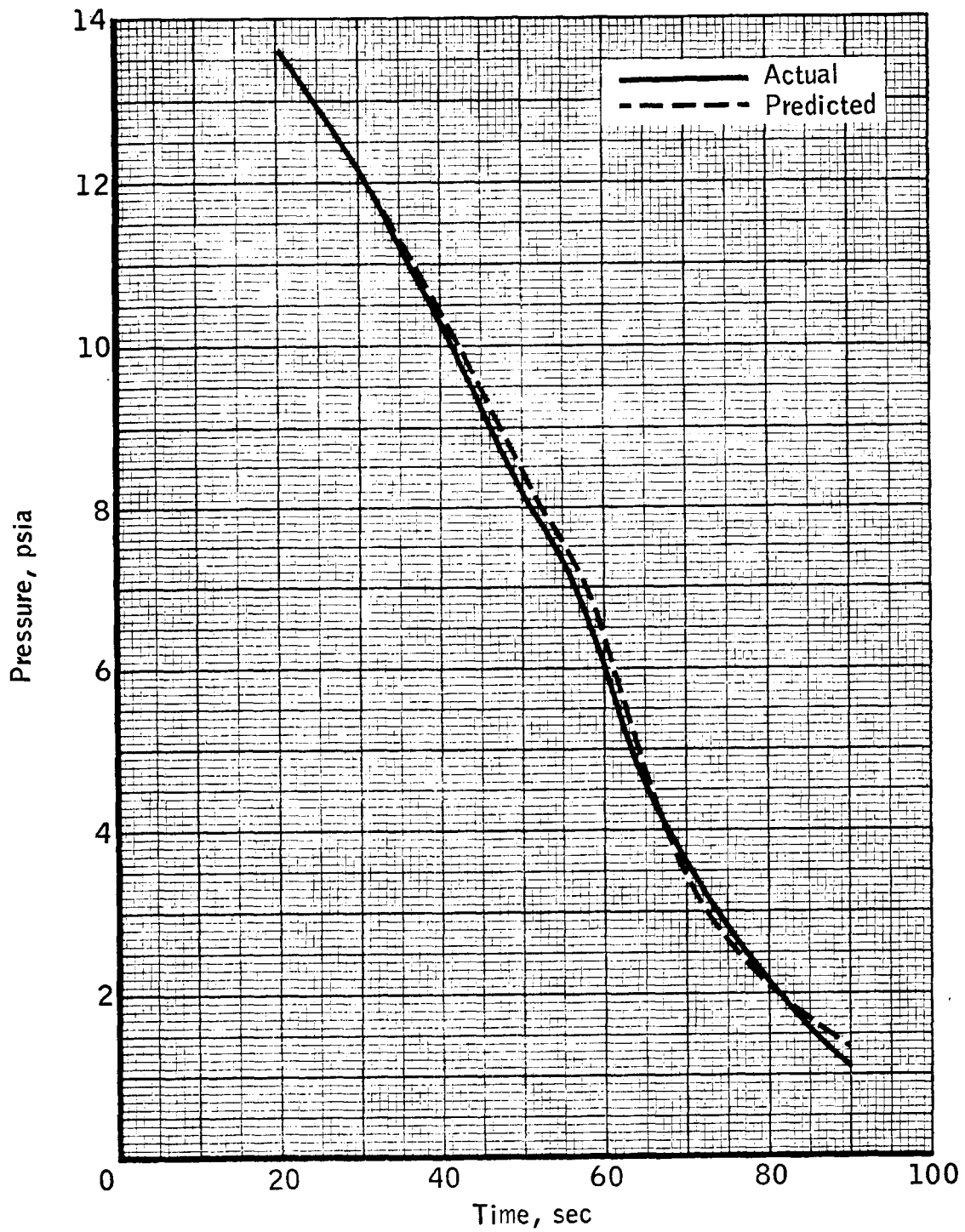
~~CONFIDENTIAL~~

Figure 4.7-8.- Service module internal pressure in BP-15 spacecraft.

~~CONFIDENTIAL~~

~~CONFIDENTIAL~~

4-77

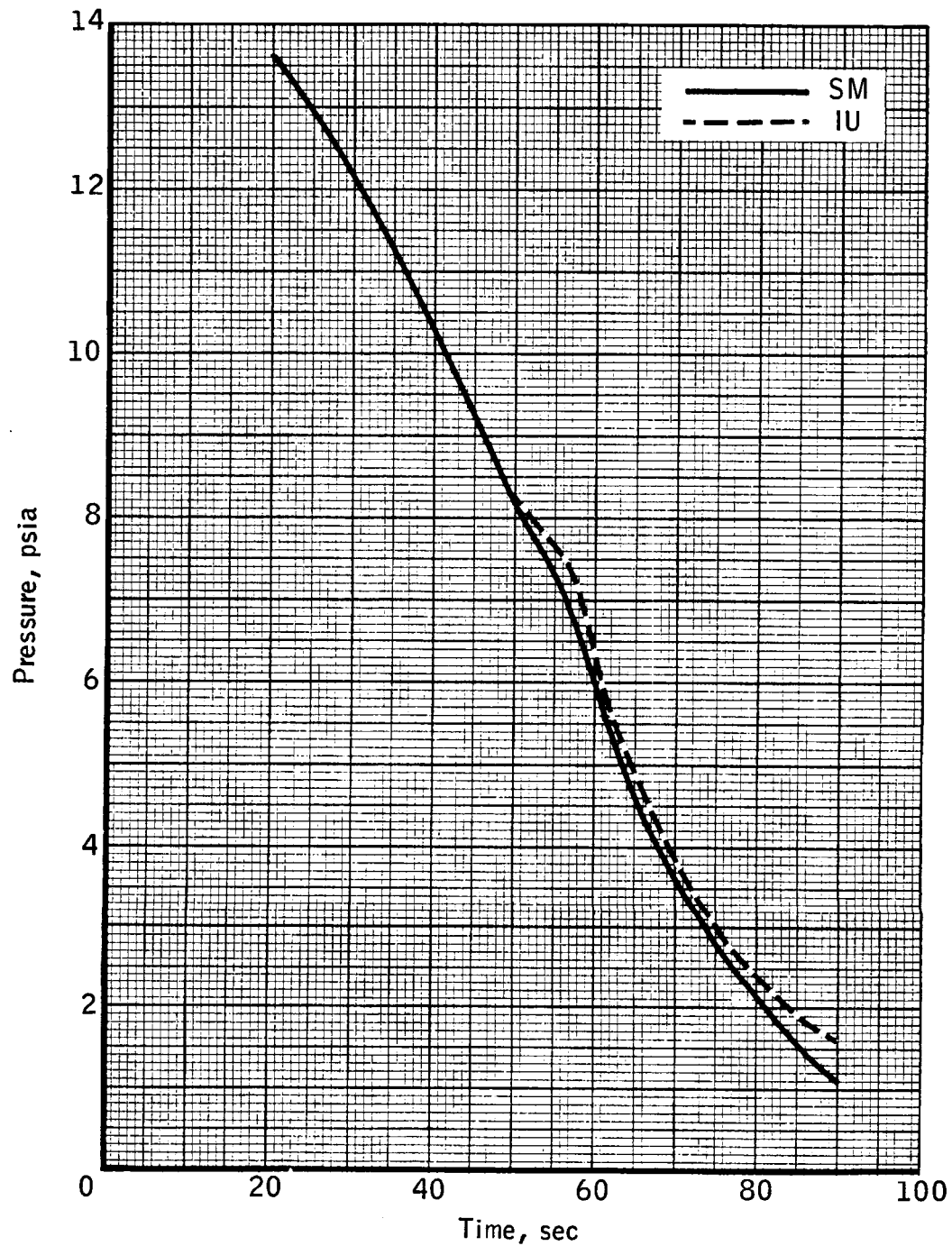


Figure 4.7-9.- BP-15 spacecraft service module and launch-vehicle instrument unit internal pressure (flight measured data).

~~CONFIDENTIAL~~

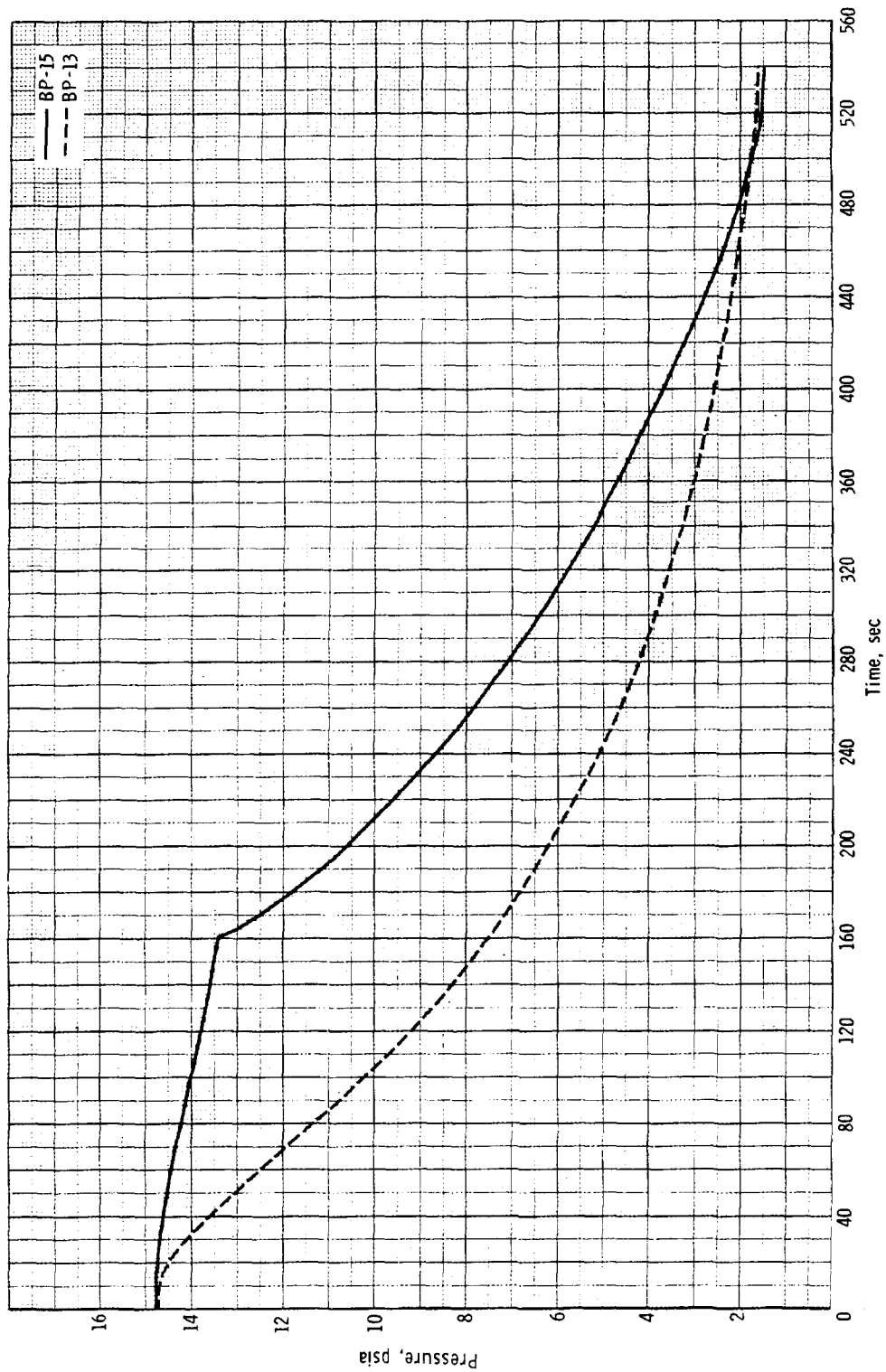
~~CONFIDENTIAL~~

Figure 4.7-10. - Comparison of BP-15 to BP-13 command module instrumentation compartment internal pressures.

~~CONFIDENTIAL~~

~~CONFIDENTIAL~~

4-79

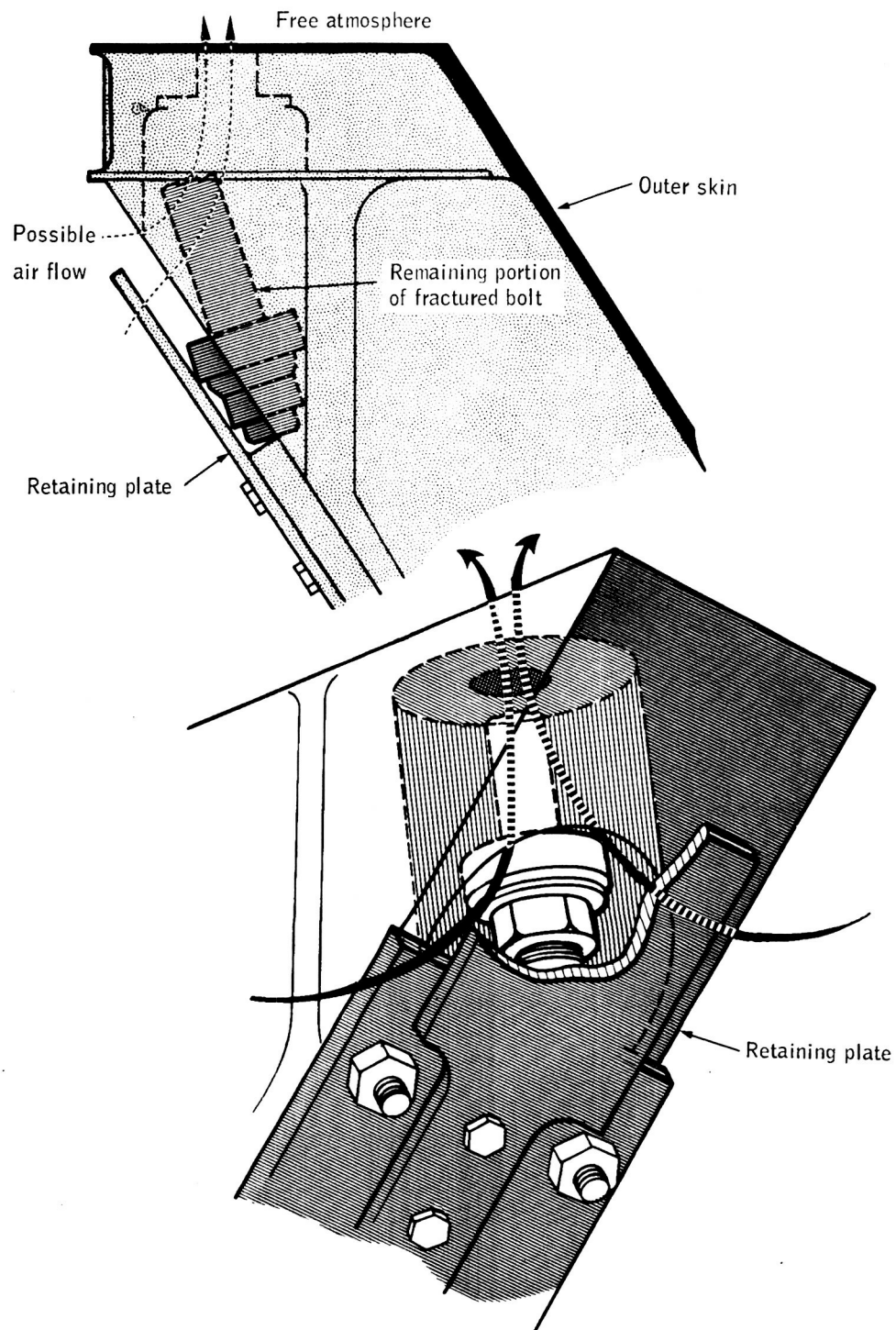
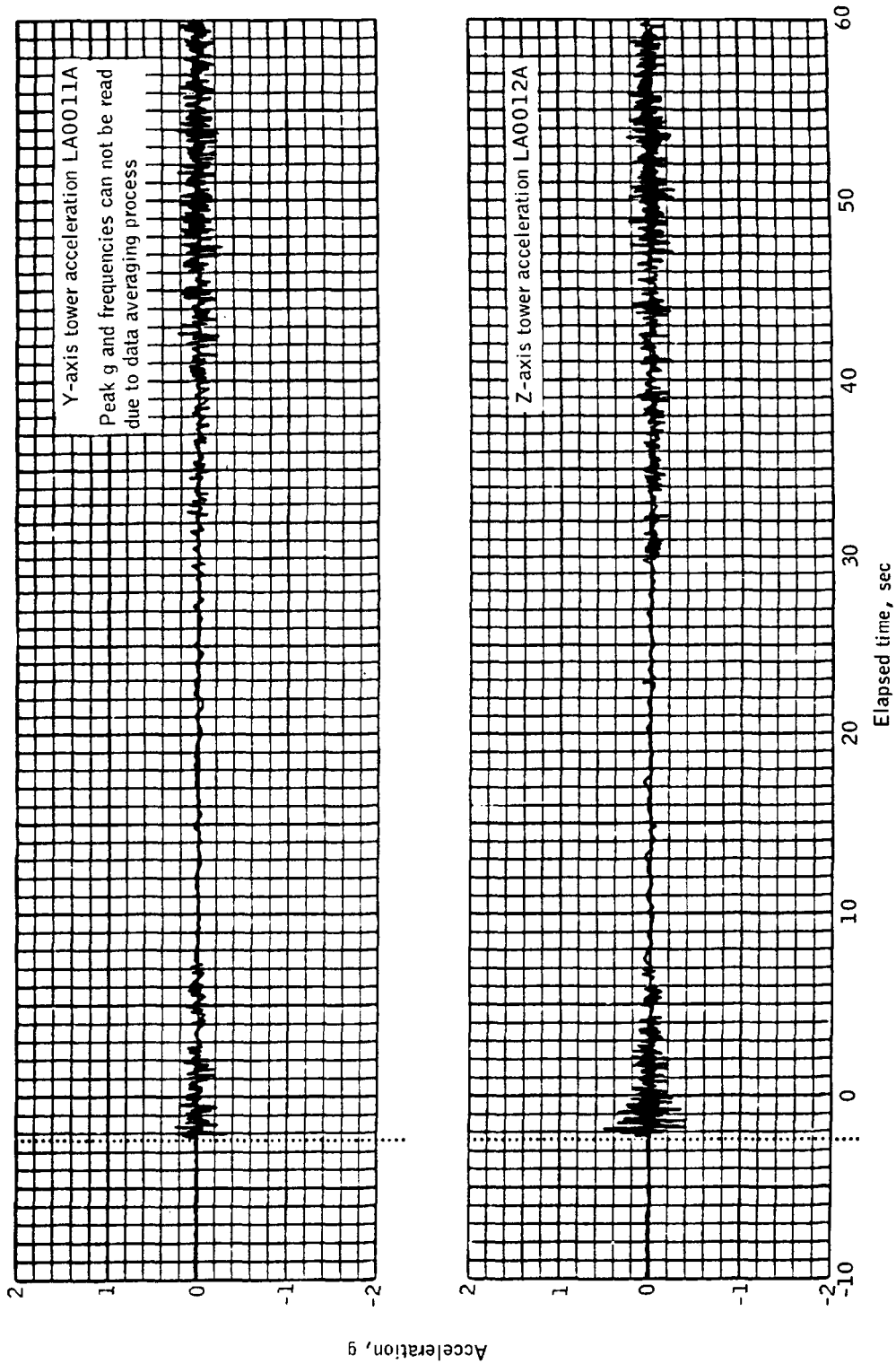


Figure 4.7-11.- Possible air leakage path caused by fracture of explosive bolt.

~~CONFIDENTIAL~~

~~CONFIDENTIAL~~

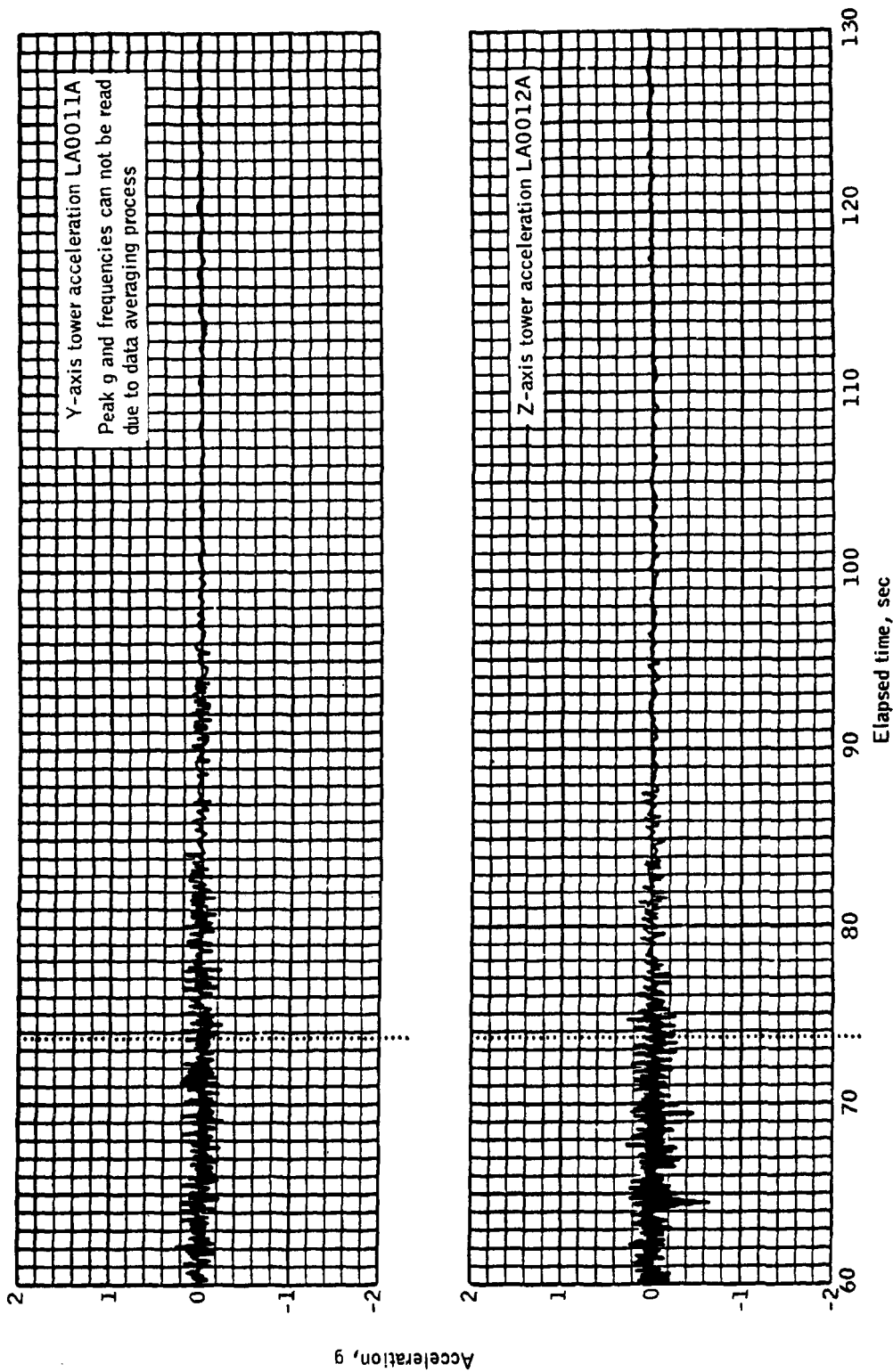
(a) Launch-escape subsystem at Q-ball interface

Figure 4.7-12.- Flight measured acceleration (BP-15 spacecraft).

~~CONFIDENTIAL~~

~~CONFIDENTIAL~~

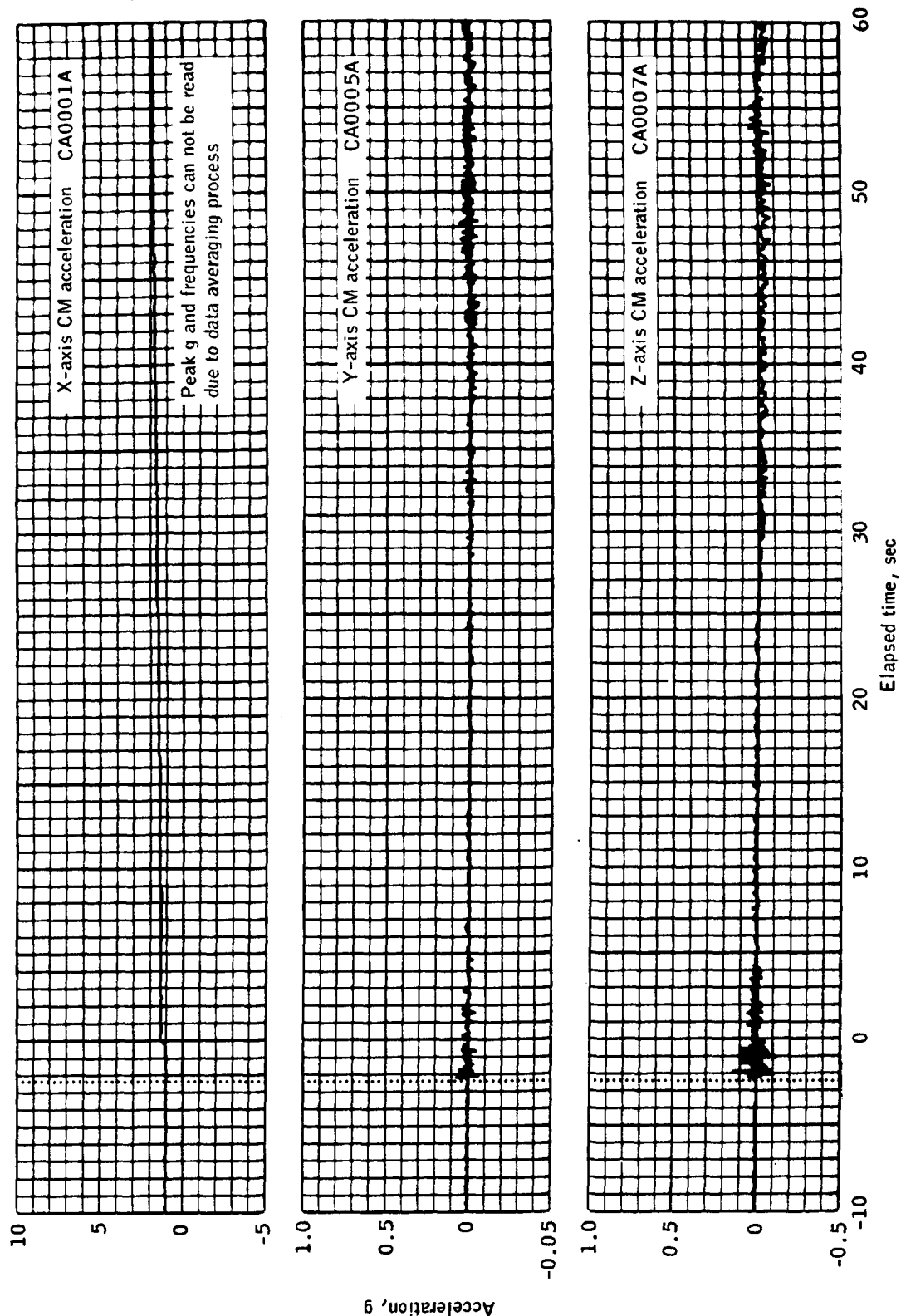
4-81



~~CONFIDENTIAL~~

(a) Launch-escape subsystem at Q-ball interface, concluded.

Figure 4.7-12.- Continued.

~~CONFIDENTIAL~~

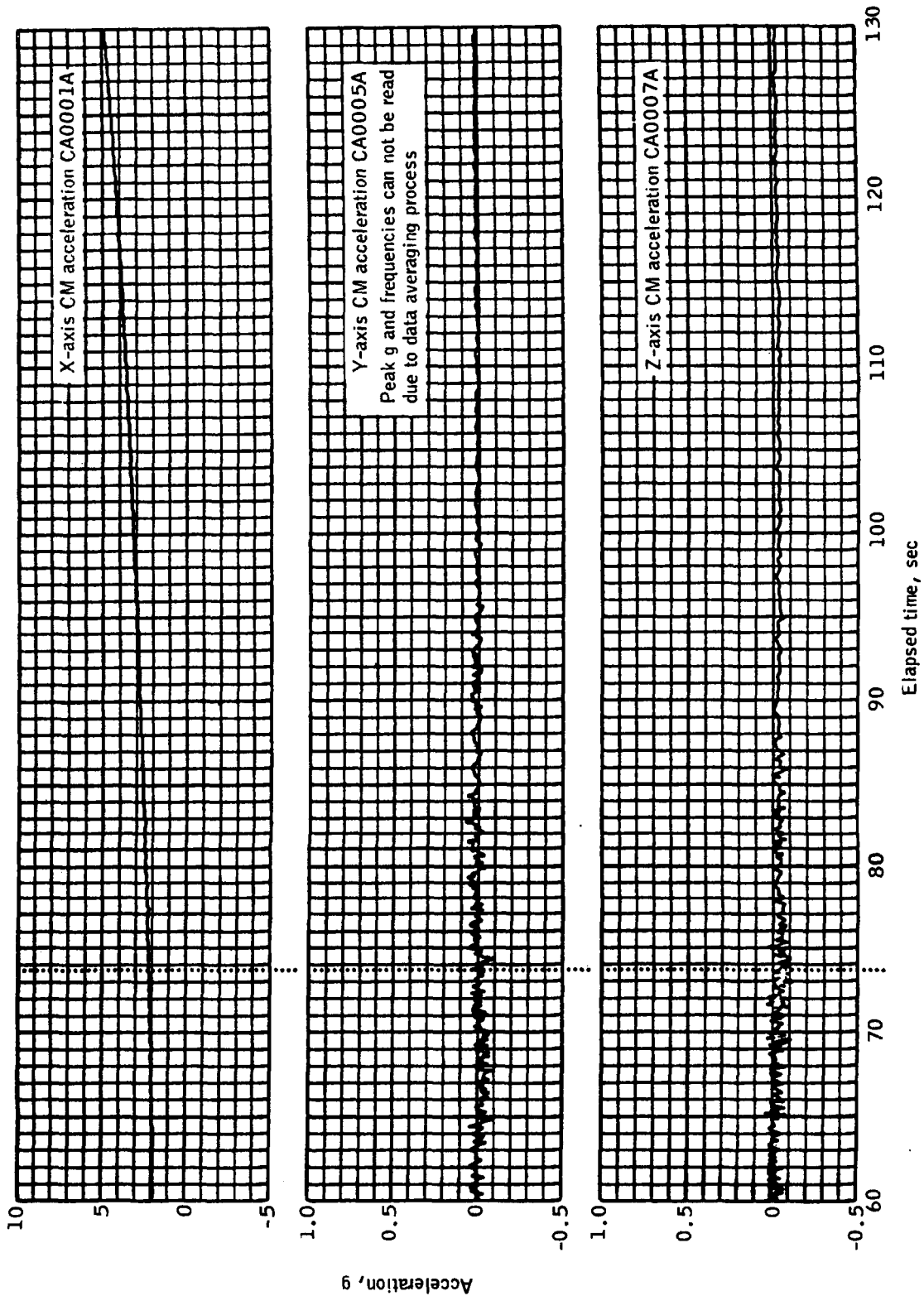
(b) Command module.

Figure 4.7-12.- Continued.

~~CONFIDENTIAL~~

~~CONFIDENTIAL~~

4-82A

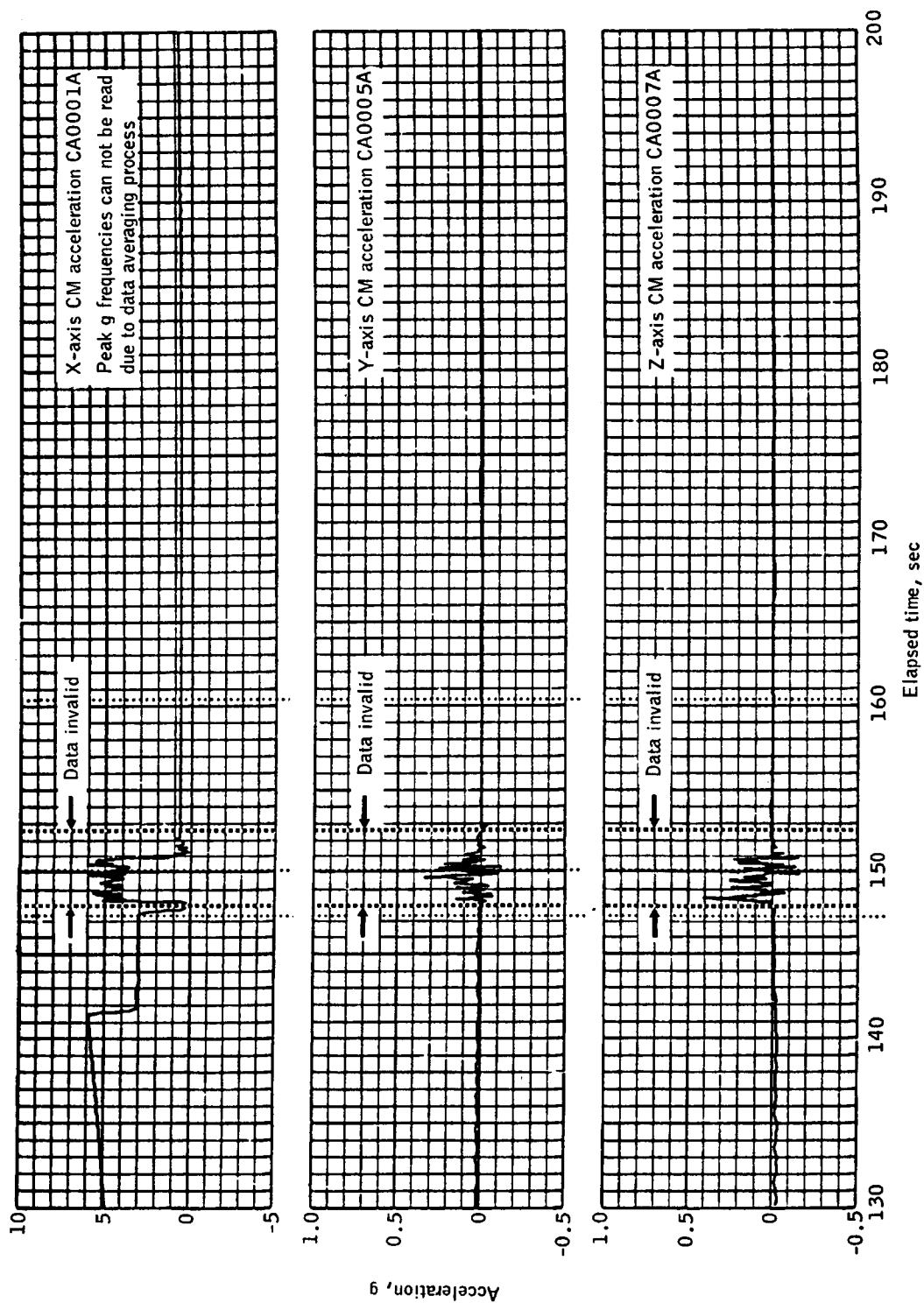


~~CONFIDENTIAL~~

(b) Command module, continued.

Figure 4.7-12.- Continued.

~~CONFIDENTIAL~~



~~CONFIDENTIAL~~

(b) Command module, concluded.

Figure 4.7-12.- Concluded.

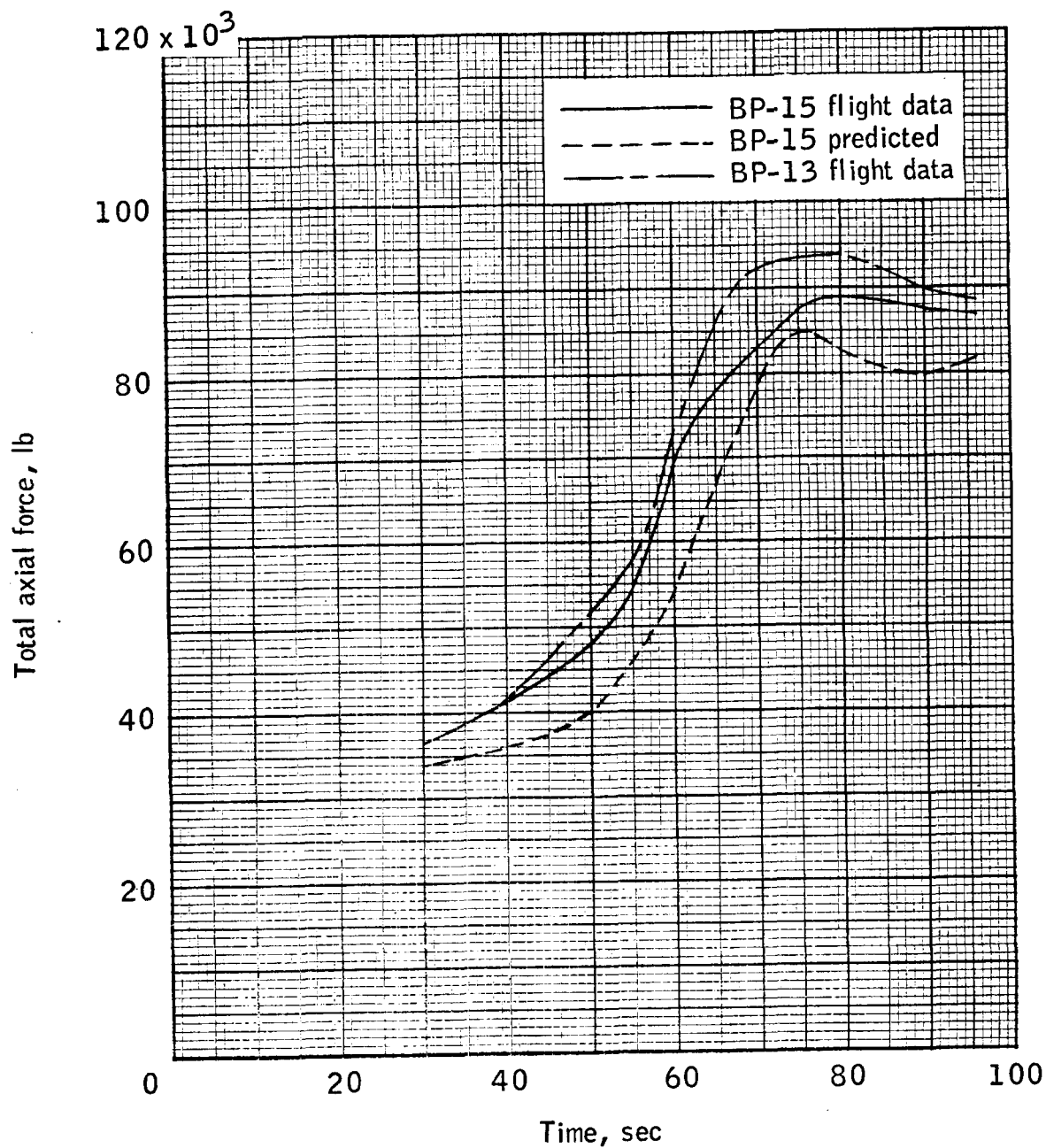
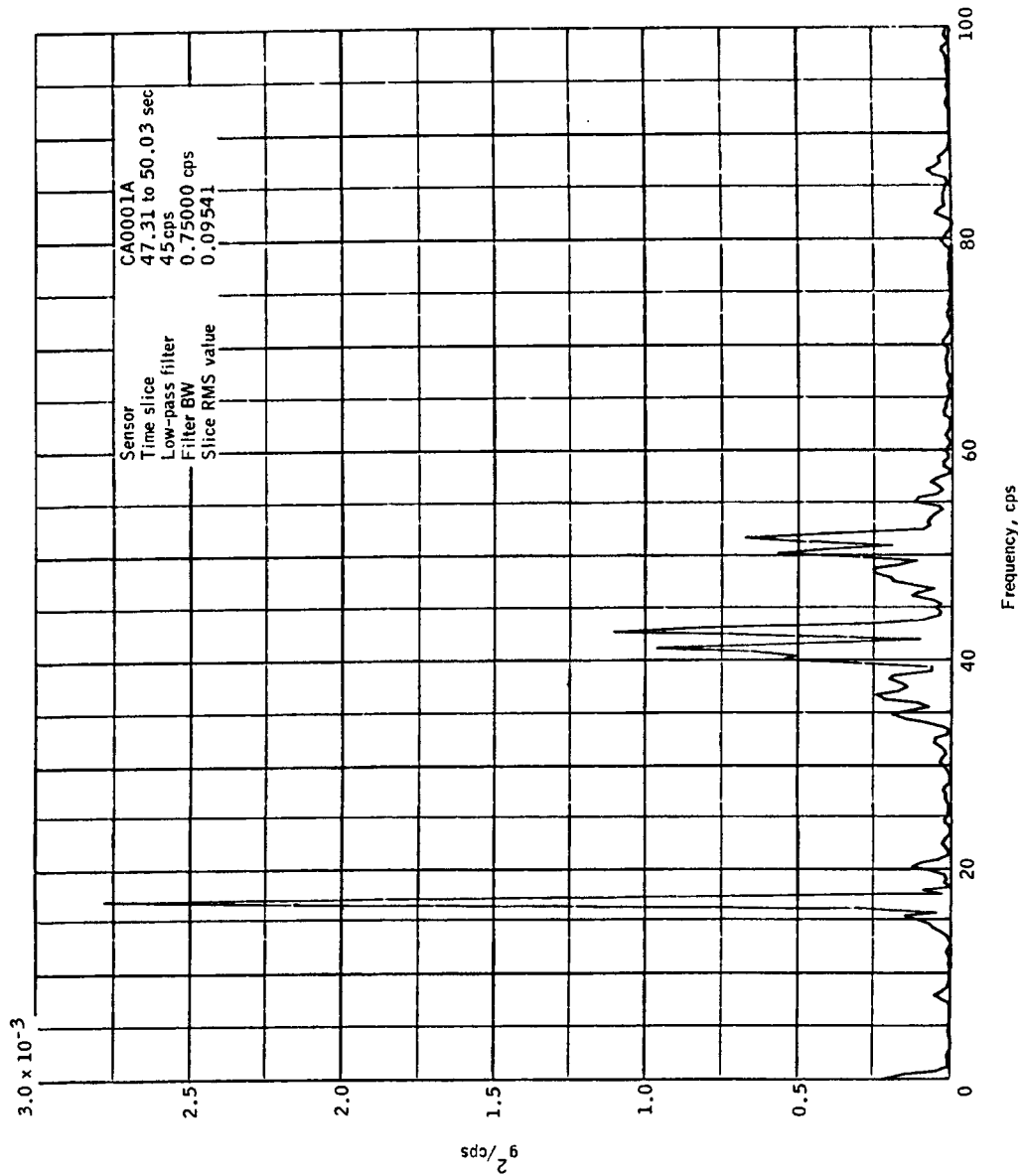
~~CONFIDENTIAL~~

Figure 4.7-13.- Total axial force at interface of BP-15 spacecraft adapter and Saturn SA-7 instrument unit ($X_A 722$).

~~CONFIDENTIAL~~

~~CONFIDENTIAL~~

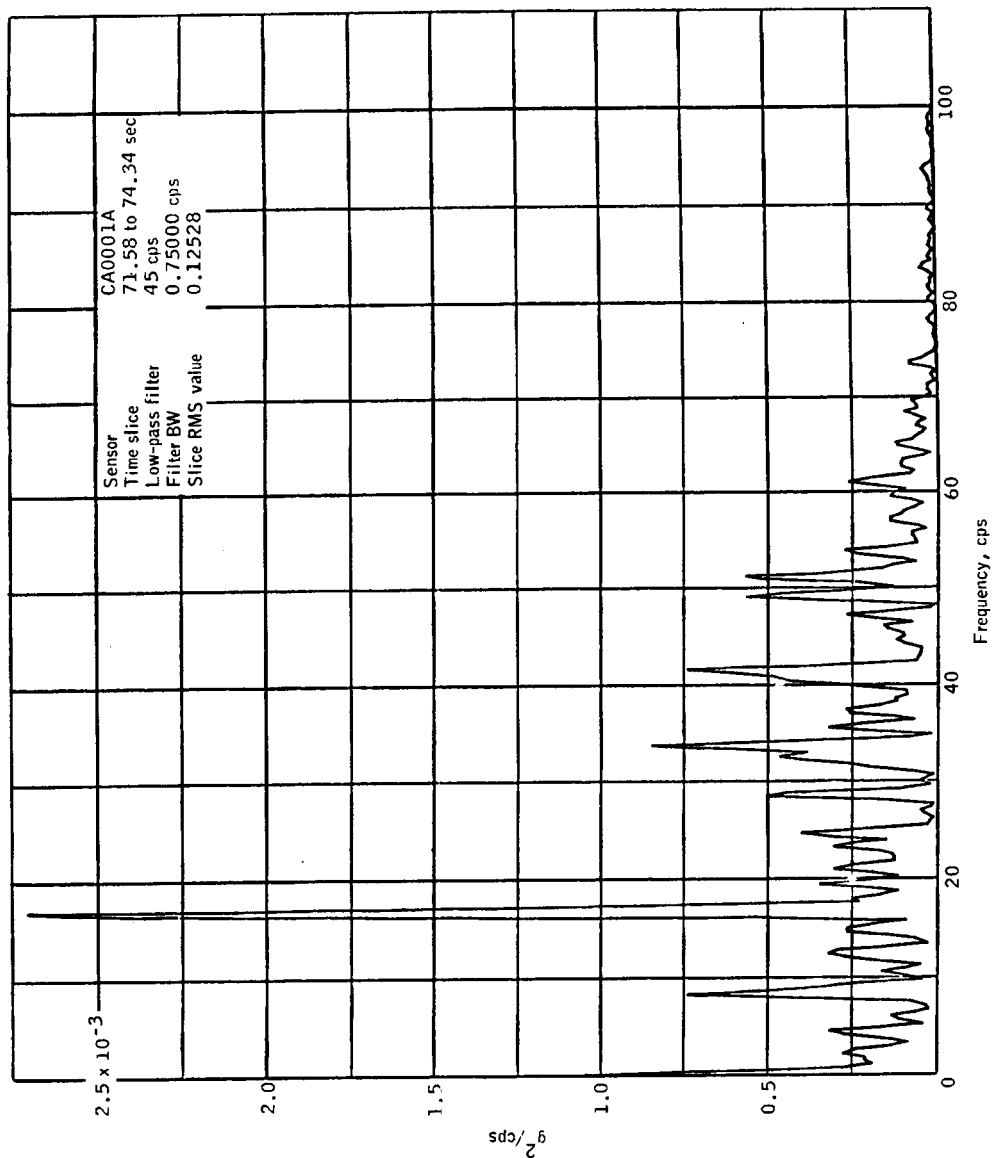
4-85



(a) T + 48 second.

Figure 4.7-14.- Power spectral distribution command module X-axis acceleration, BP-15 spacecraft.

~~CONFIDENTIAL~~

~~CONFIDENTIAL~~

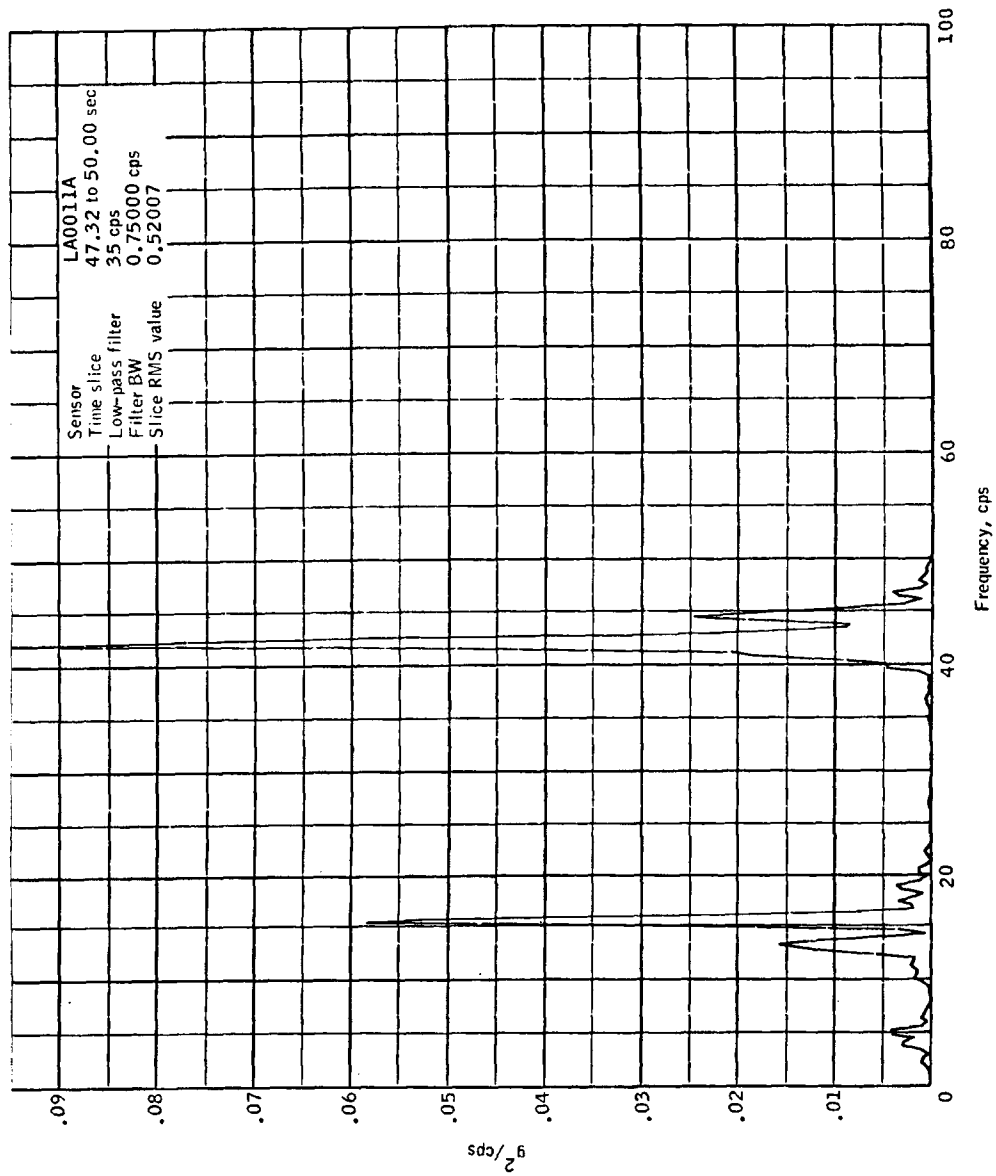
(b) T + 7.3 second.

Figure 4.7-14.- Concluded.

~~CONFIDENTIAL~~

~~CONFIDENTIAL~~

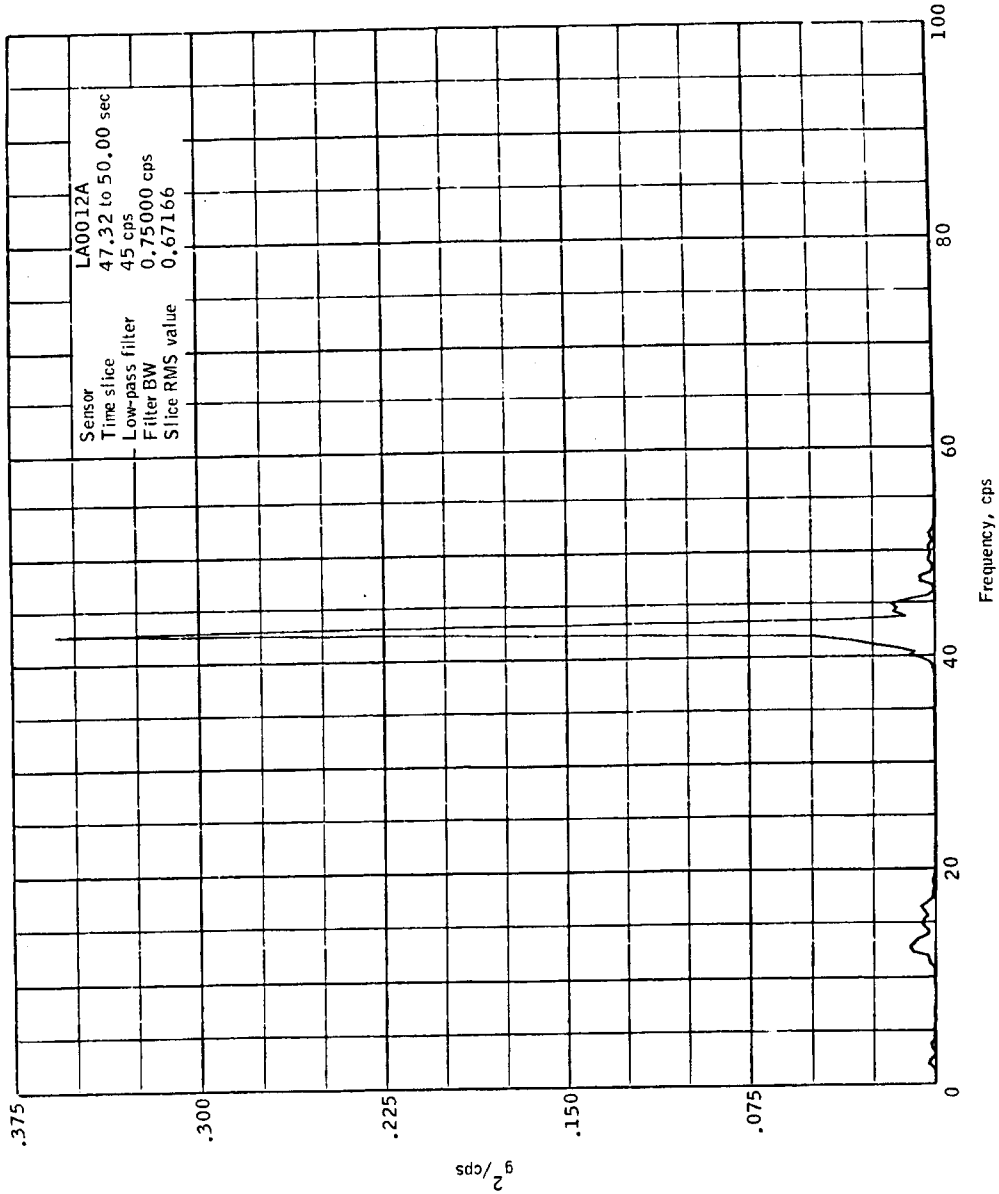
4-87



(a) Tower, Y-axis, T + 48 second, LA0011A.

Figure 4.7-15.- Power spectral distribution, Y and Z axes accelerations, BP-15 spacecraft.

~~CONFIDENTIAL~~

~~CONFIDENTIAL~~

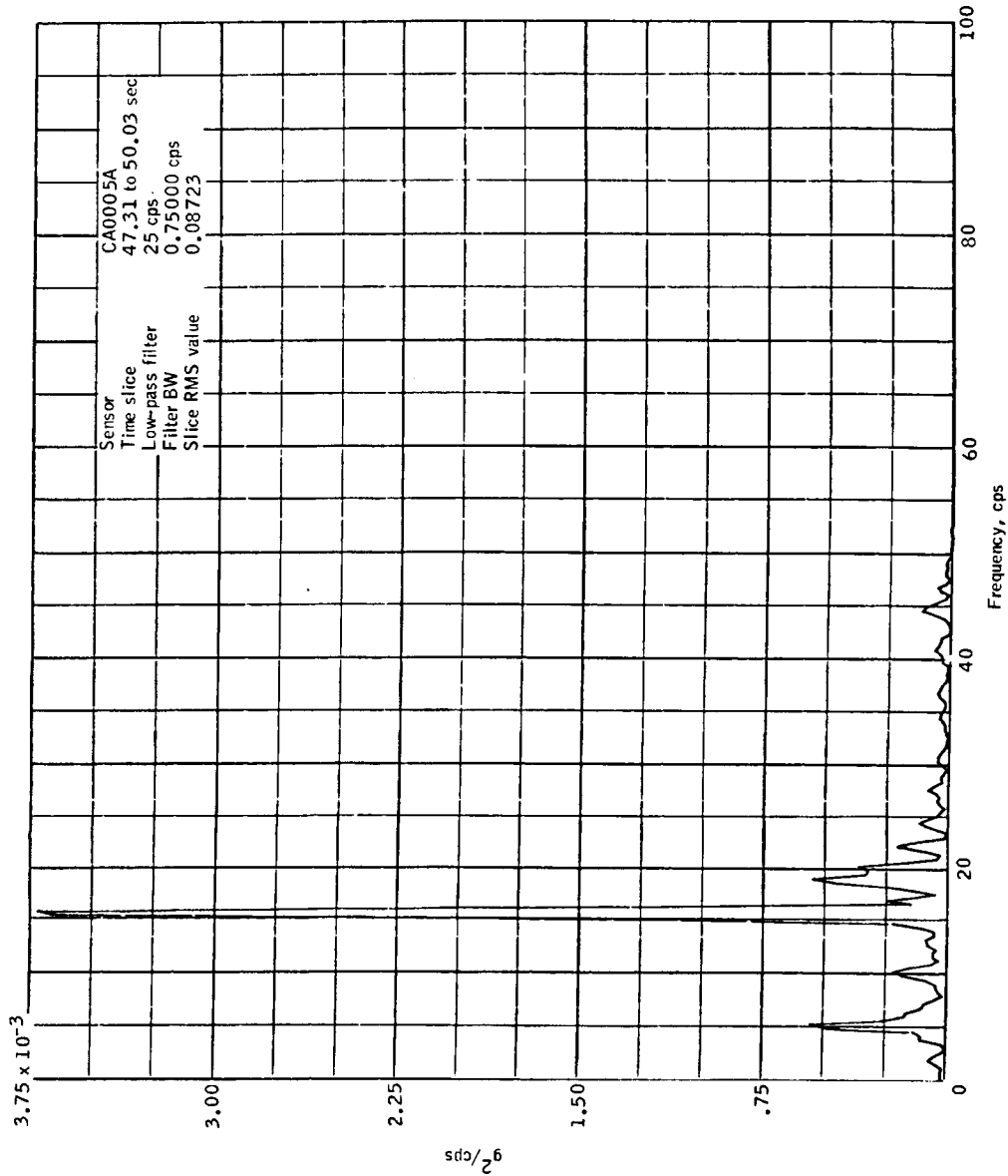
(b) Tower, Z-axis, T + 48 second, LA0012A.

Figure 4.7-15.- Continued.

~~CONFIDENTIAL~~

~~CONFIDENTIAL~~

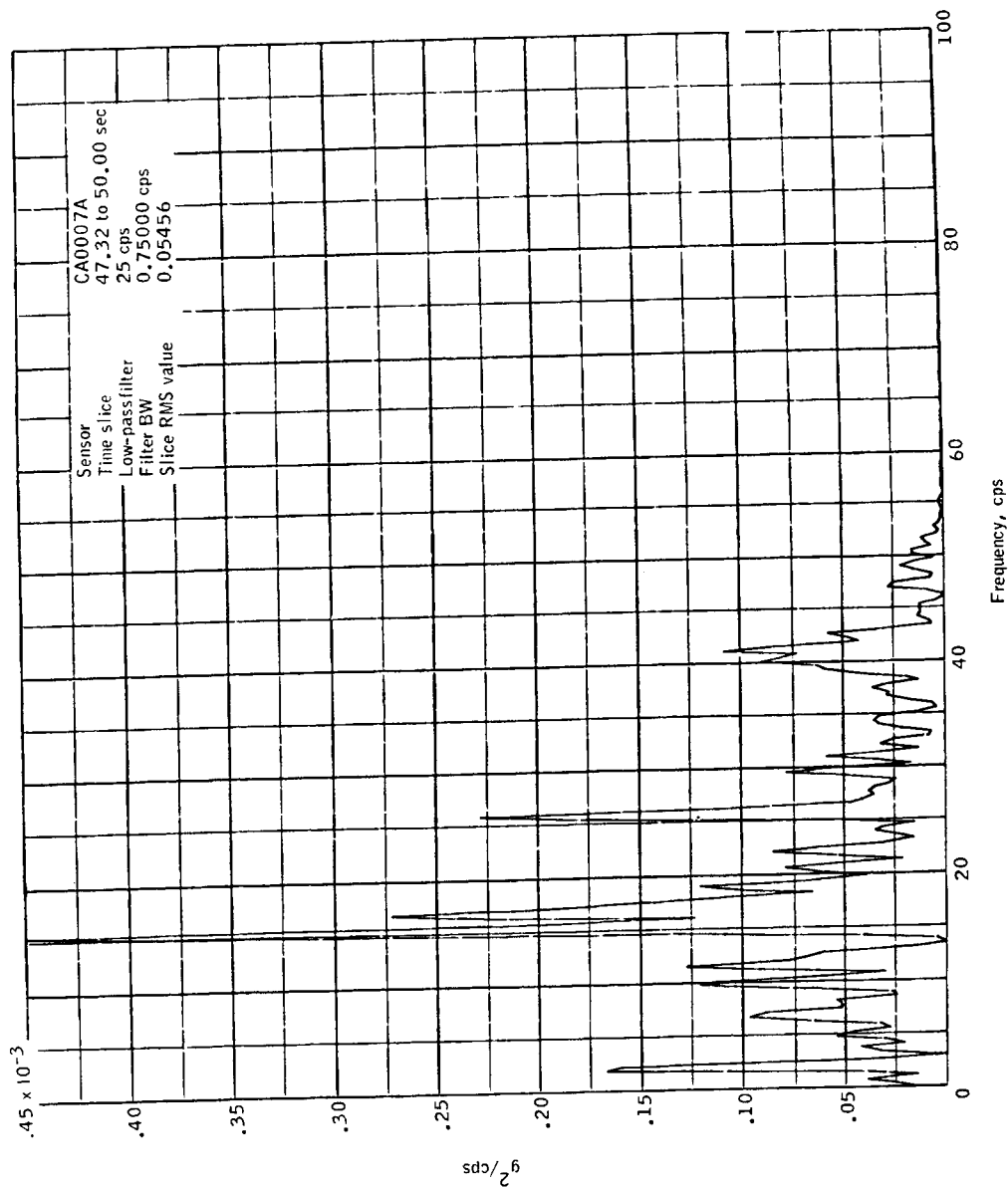
4-89



(c) Command module, Y-axis, T + 48 second, CA0005A.

Figure 4.7-15.- Continued.

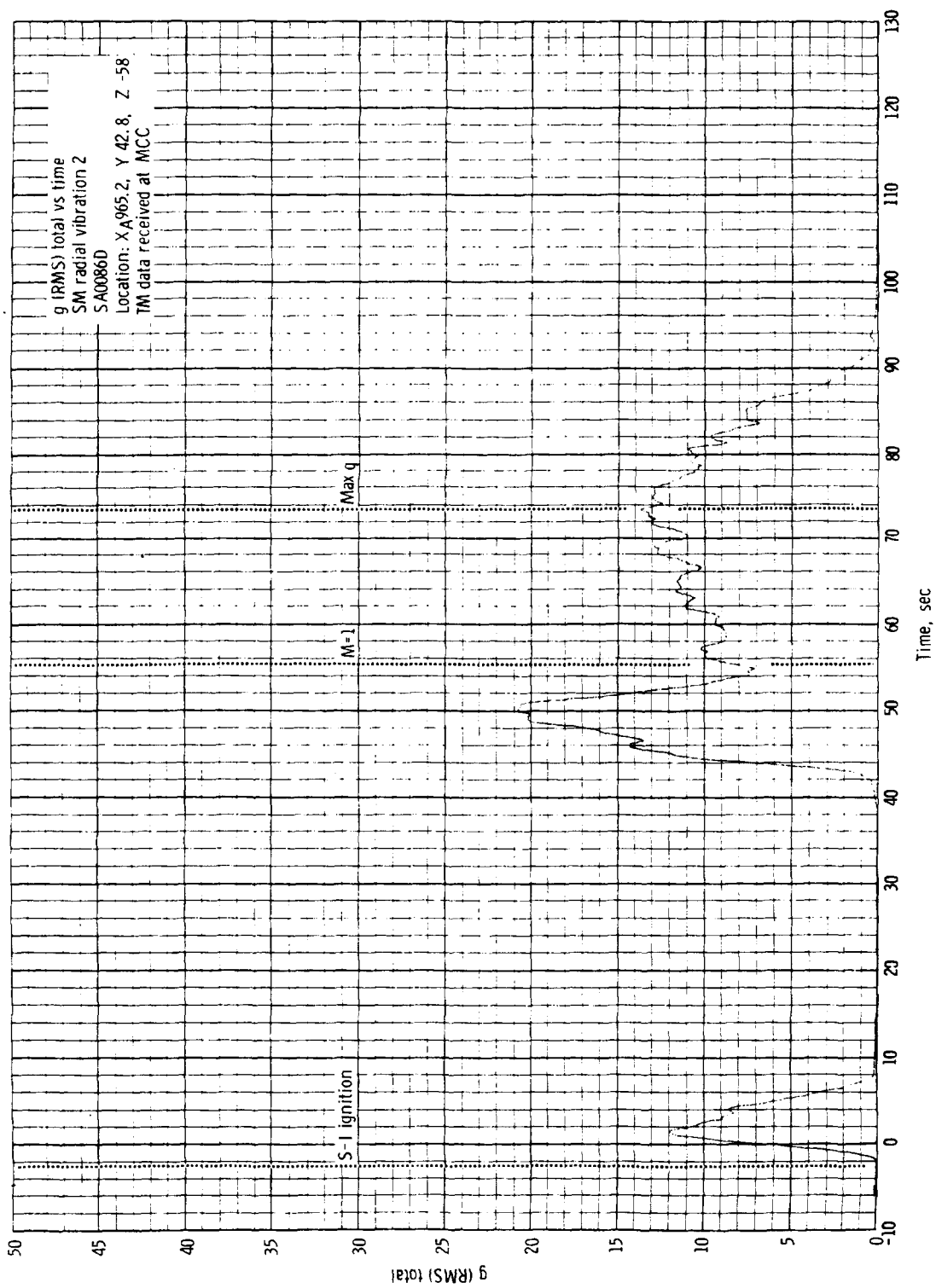
~~CONFIDENTIAL~~

~~CONFIDENTIAL~~

(d) Command module, Z-axis, T + 48 second, CA0007A.

Figure 4.7-15.- Concluded.

~~CONFIDENTIAL~~

~~CONFIDENTIAL~~

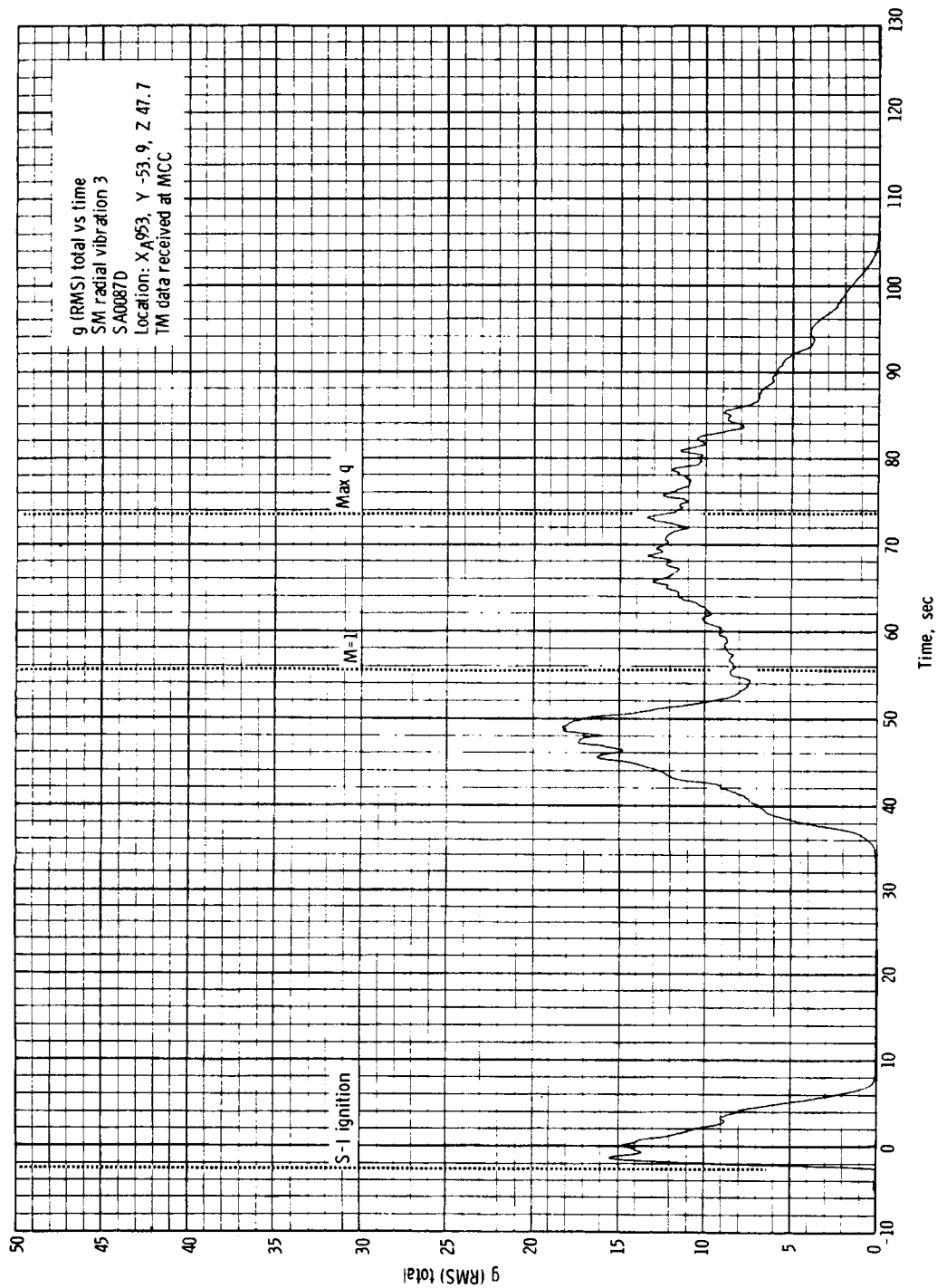
(a) Sensor SA00860

Figure 4.7-17. - RMS history of service module radial vibration.

~~CONFIDENTIAL~~

~~CONFIDENTIAL~~

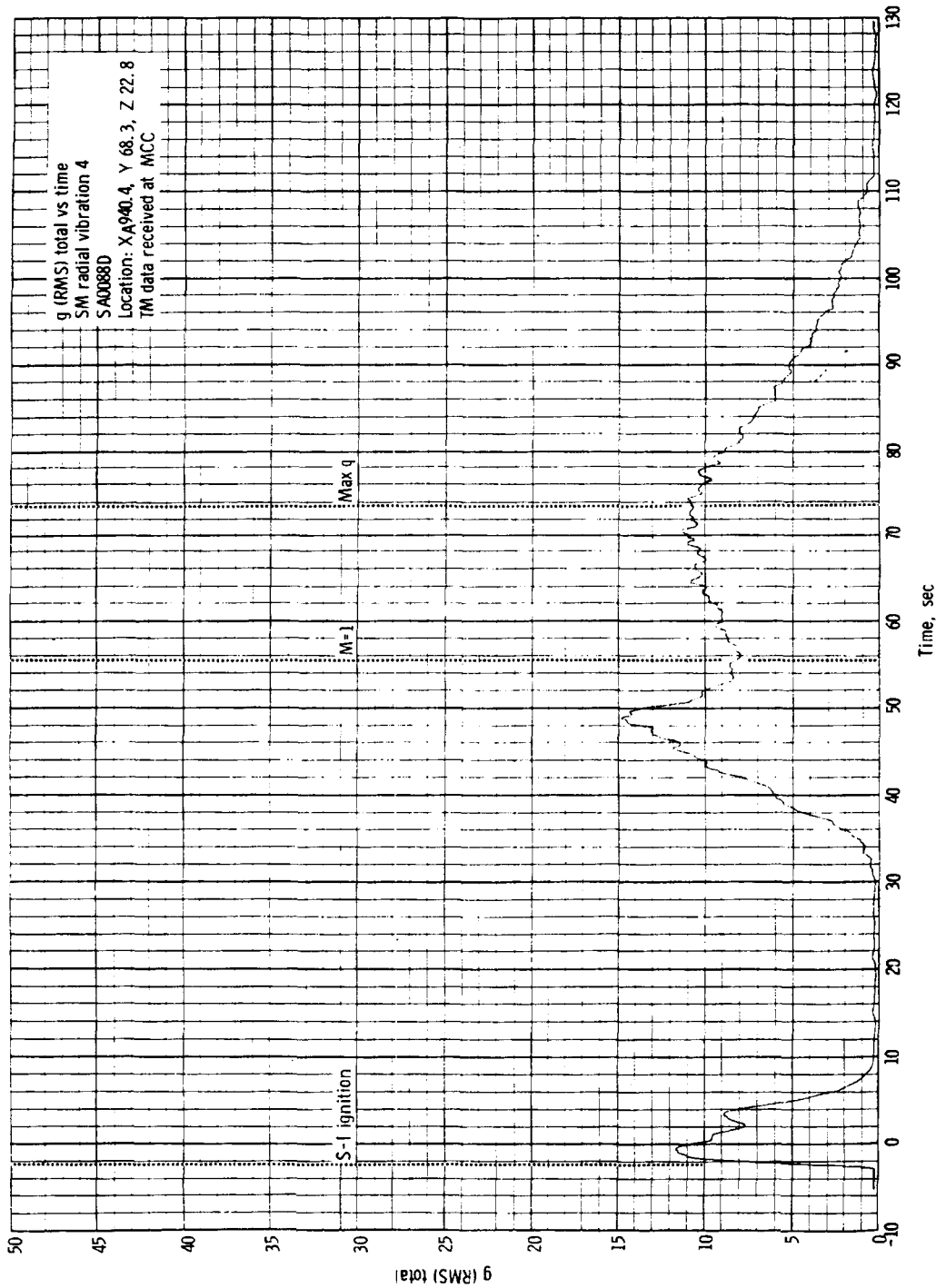
4-93



(b) Sensor SA0087D.

Figure 4.7-17. - Continued.

~~CONFIDENTIAL~~

~~CONFIDENTIAL~~

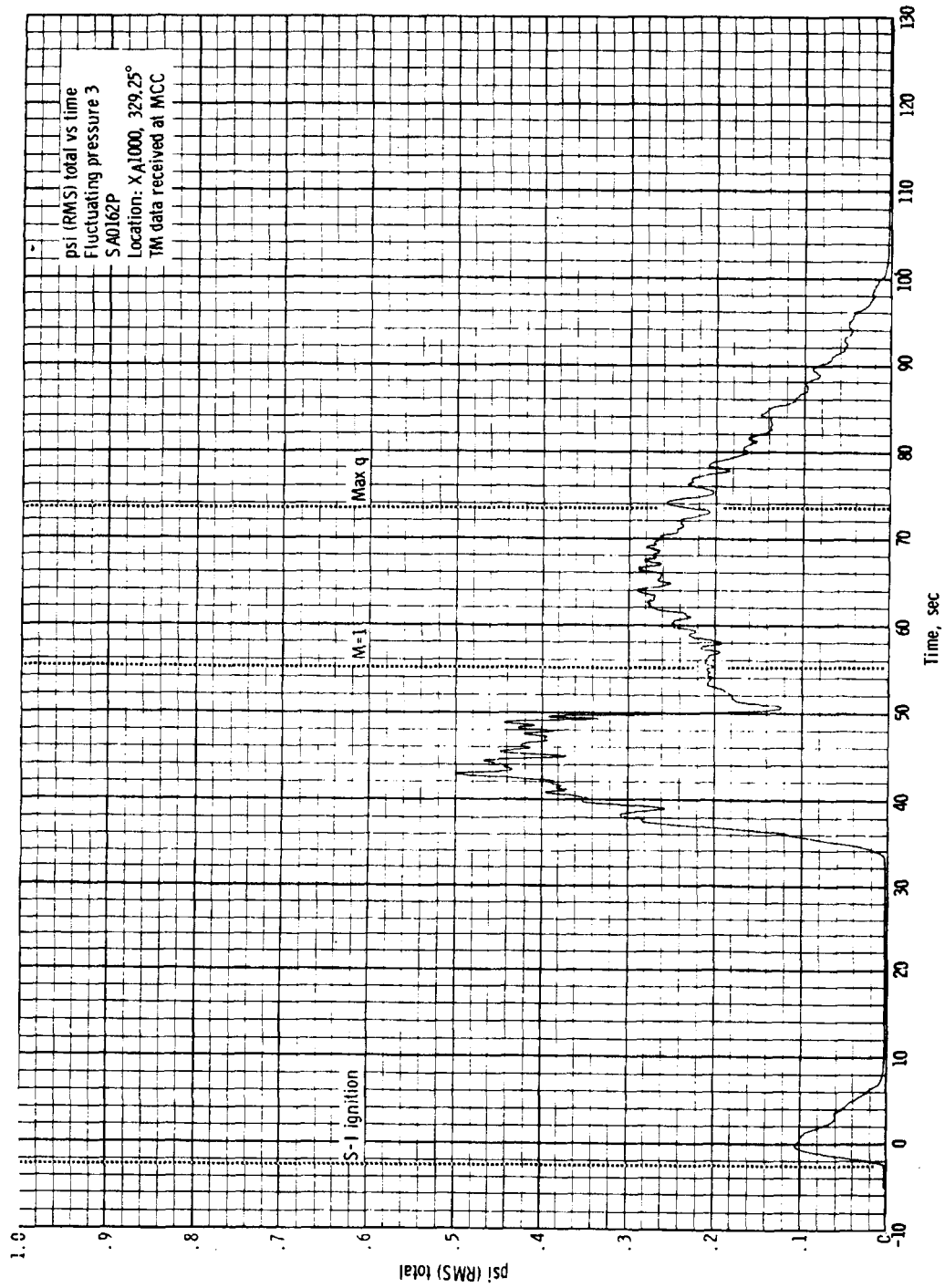
(c) Sensor SA0088D.

Figure 4.7-17. - Concluded.

~~CONFIDENTIAL~~

~~CONFIDENTIAL~~

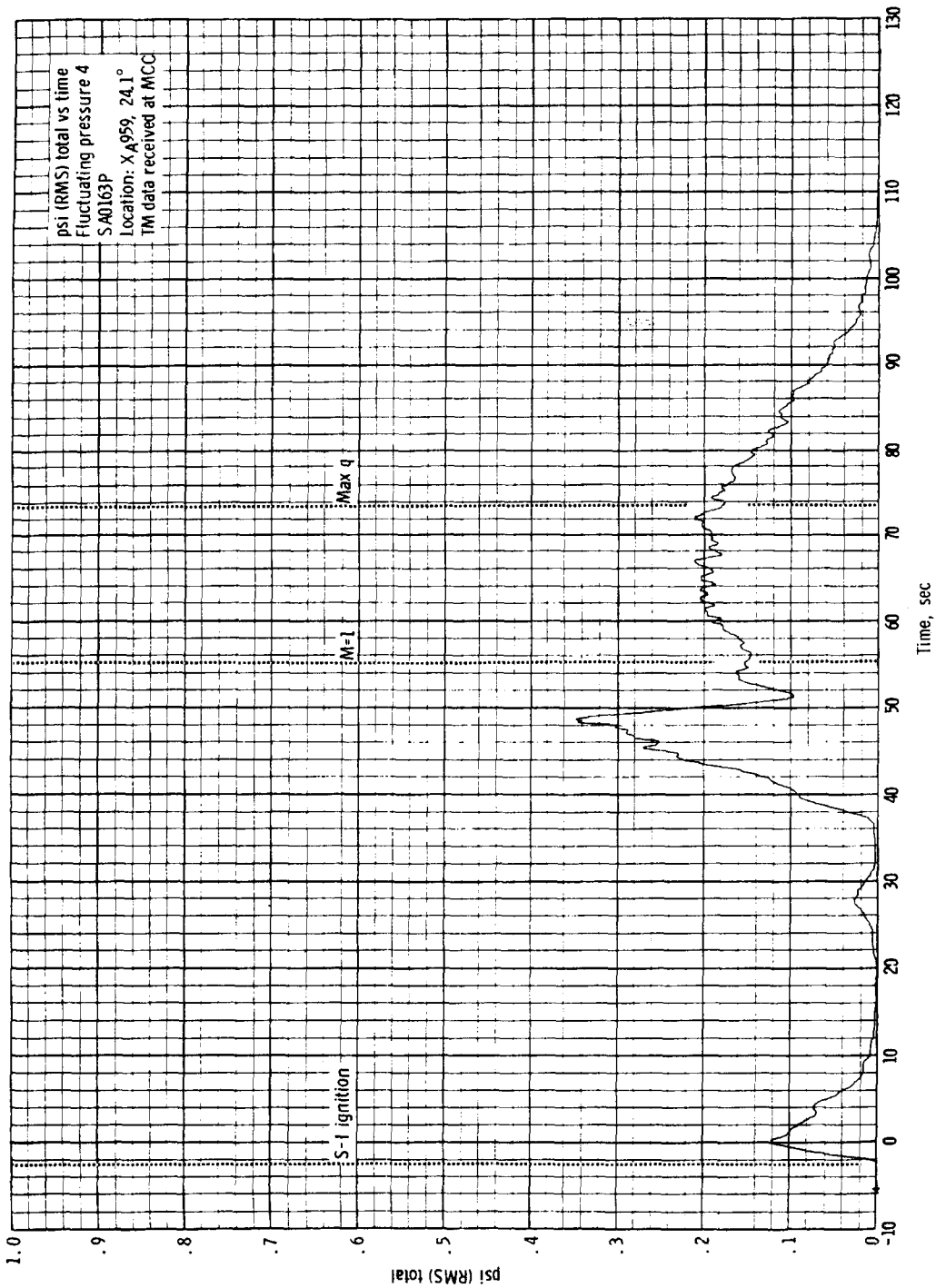
4-95



(a) Sensor SA0162P.

Figure 4.7-18. - RMS of fluctuating pressure over BP-15 spacecraft.

~~CONFIDENTIAL~~

~~CONFIDENTIAL~~

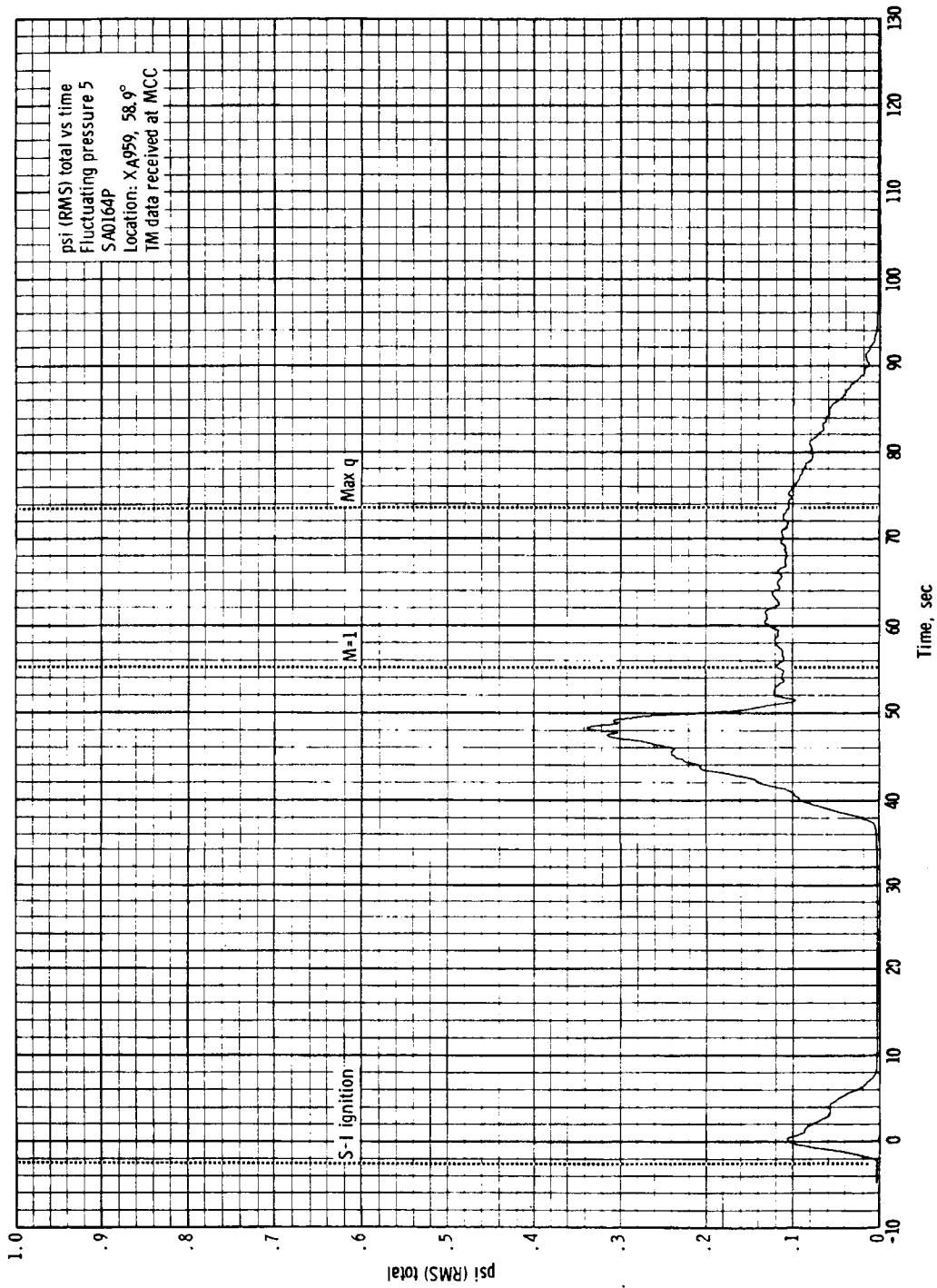
(b) Sensor SA0163P.

Figure 4.7-18. - Continued.

~~CONFIDENTIAL~~

~~CONFIDENTIAL~~

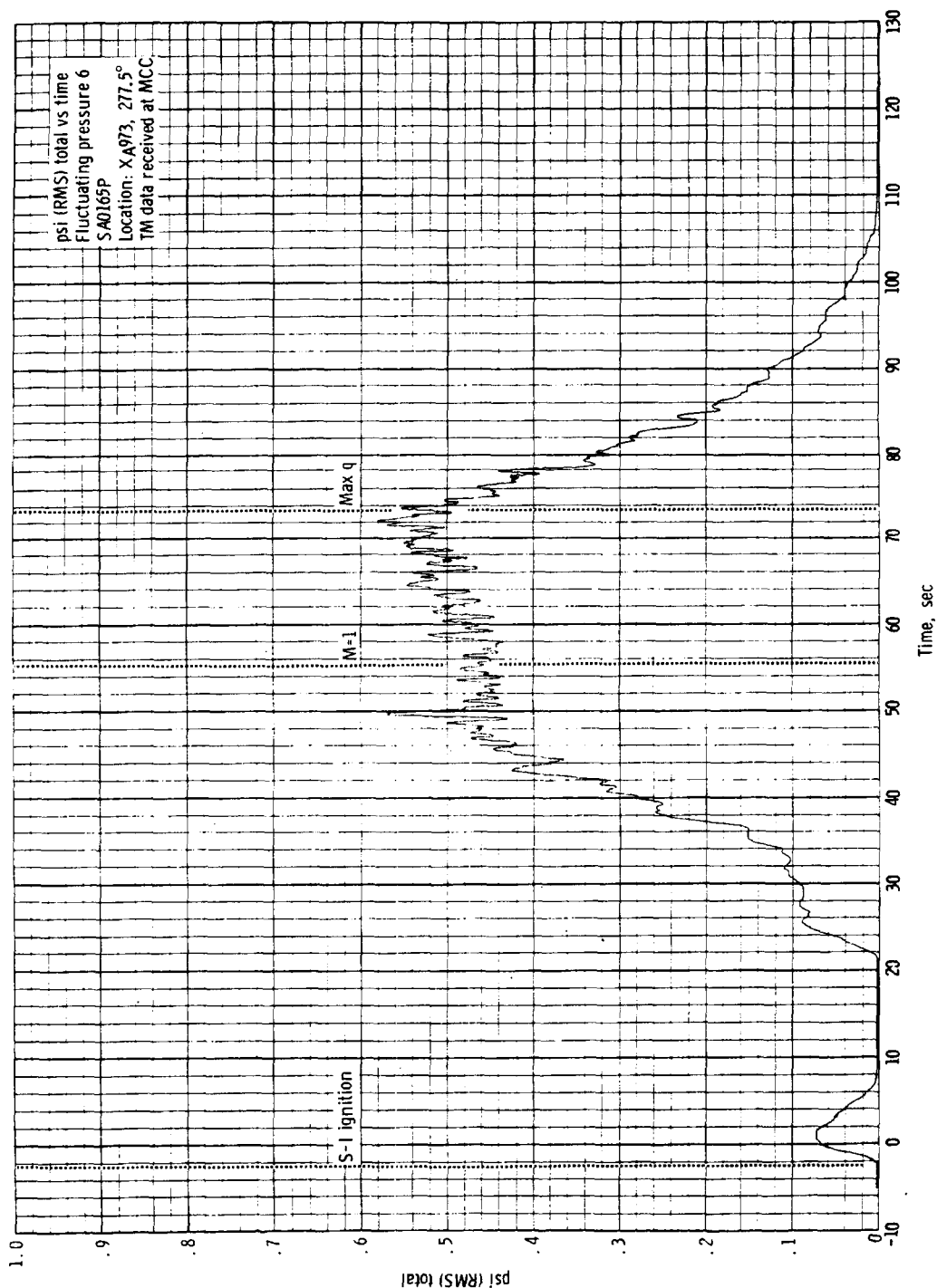
4-97



(c) Sensor SA0164P.

Figure 4.7-18. - Continued.

~~CONFIDENTIAL~~

~~CONFIDENTIAL~~

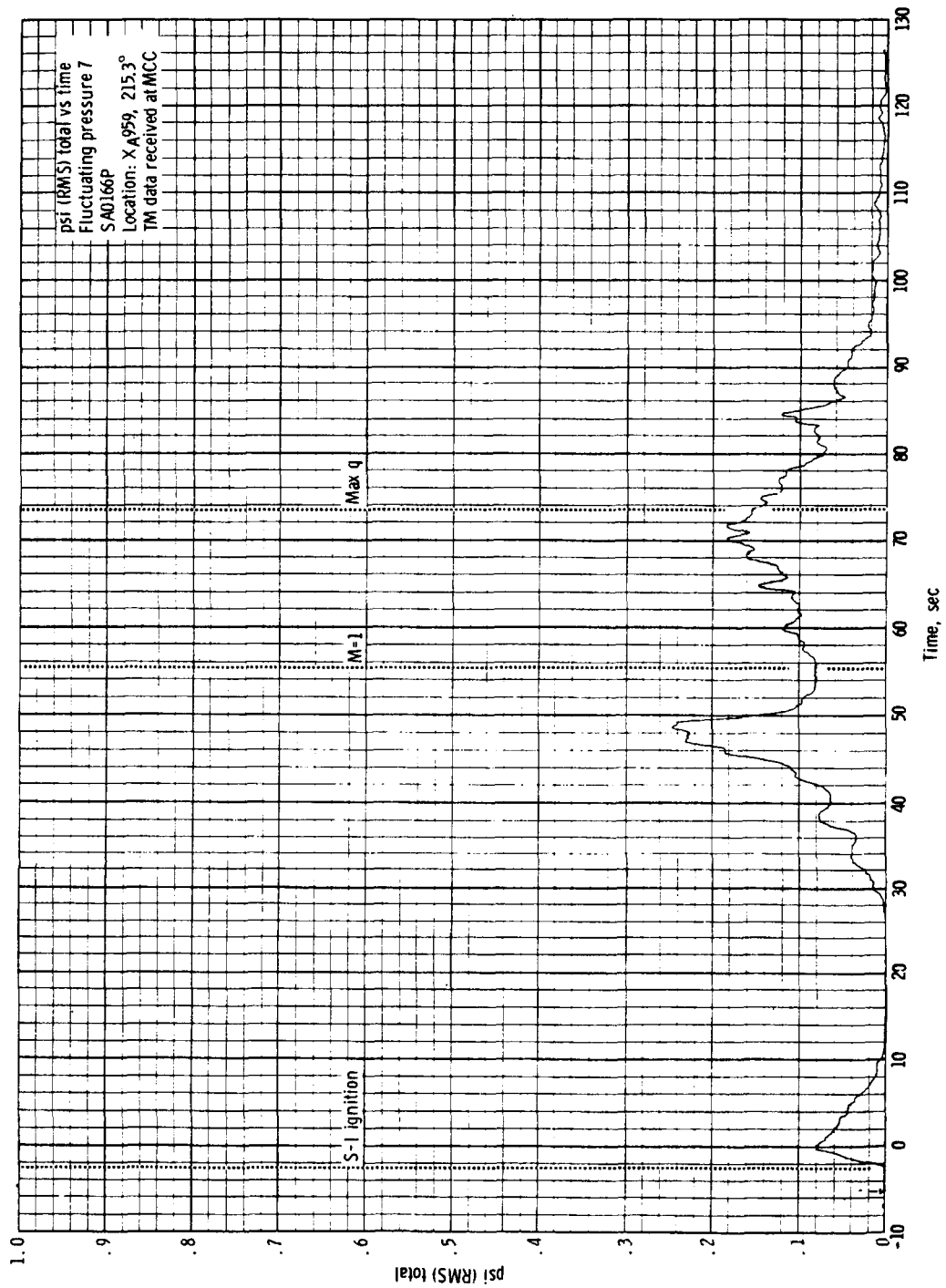
(d) Sensor SA0165P.

Figure 4.7-18. - Continued.

~~CONFIDENTIAL~~

~~CONFIDENTIAL~~

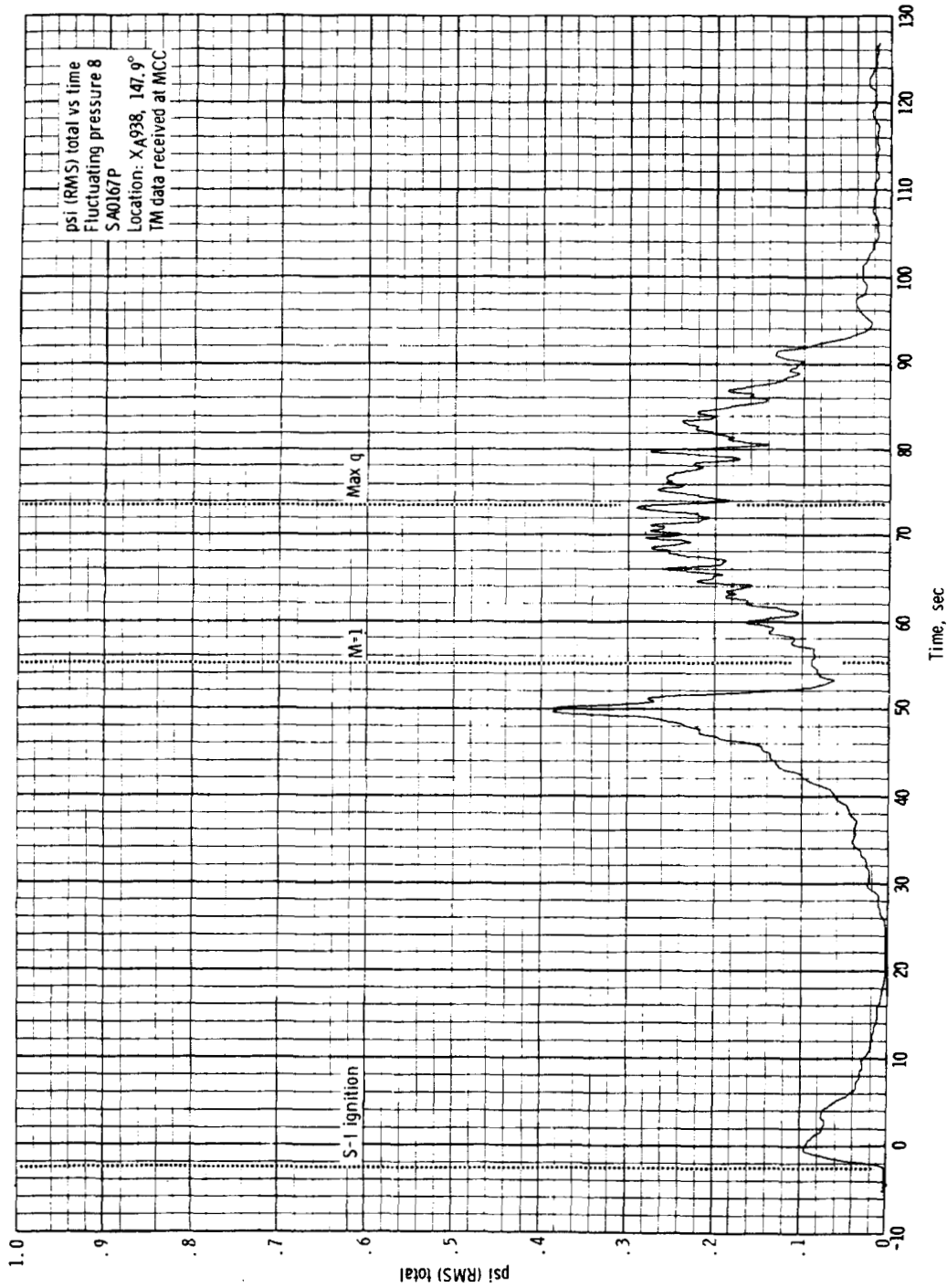
4-99



(e) Sensor SA0166P.

Figure 4.7-18. - Continued.

~~CONFIDENTIAL~~

~~CONFIDENTIAL~~

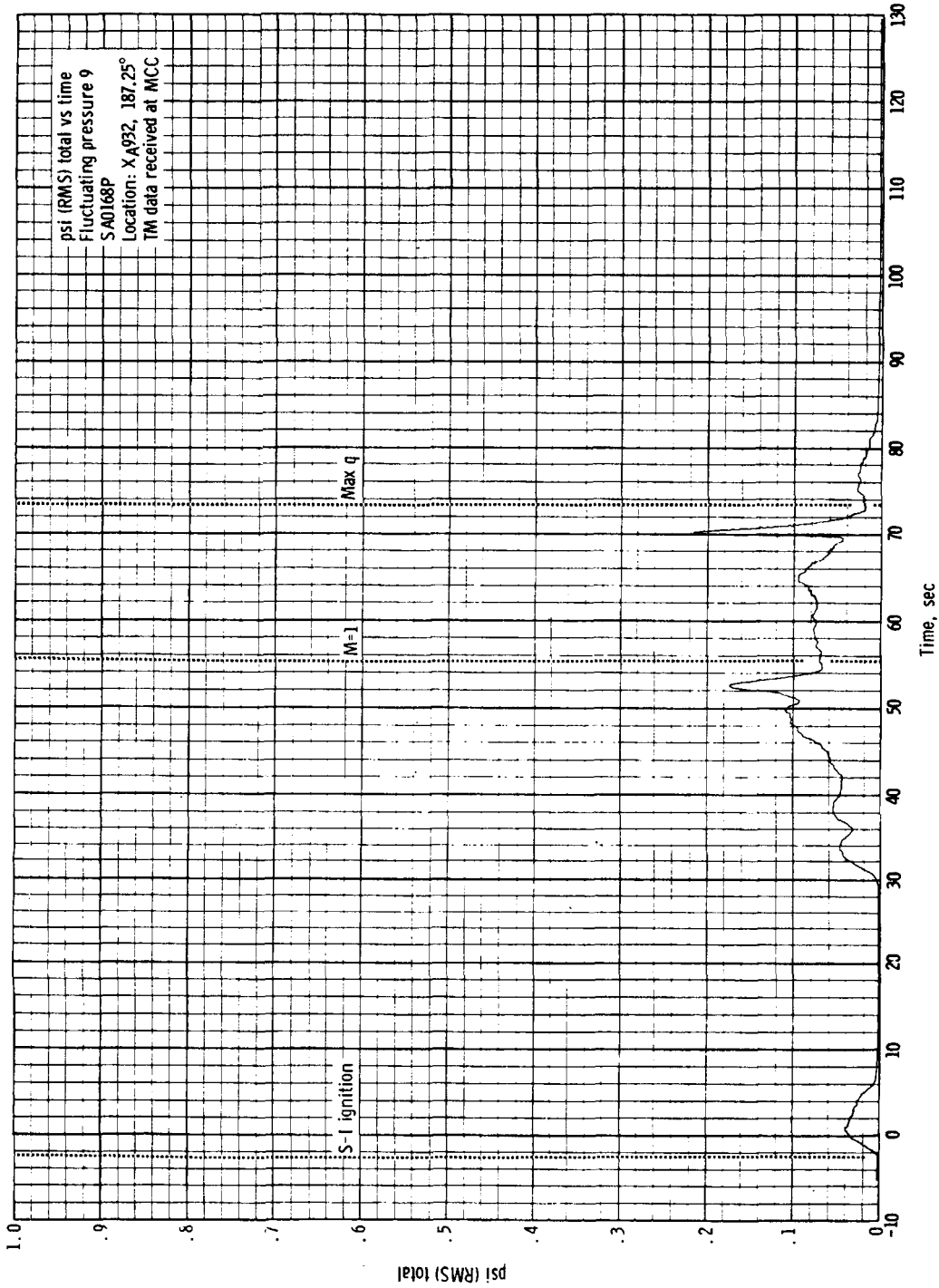
(f) Sensor SA0167P.

Figure 4.7-18. - Continued.

~~CONFIDENTIAL~~

~~CONFIDENTIAL~~

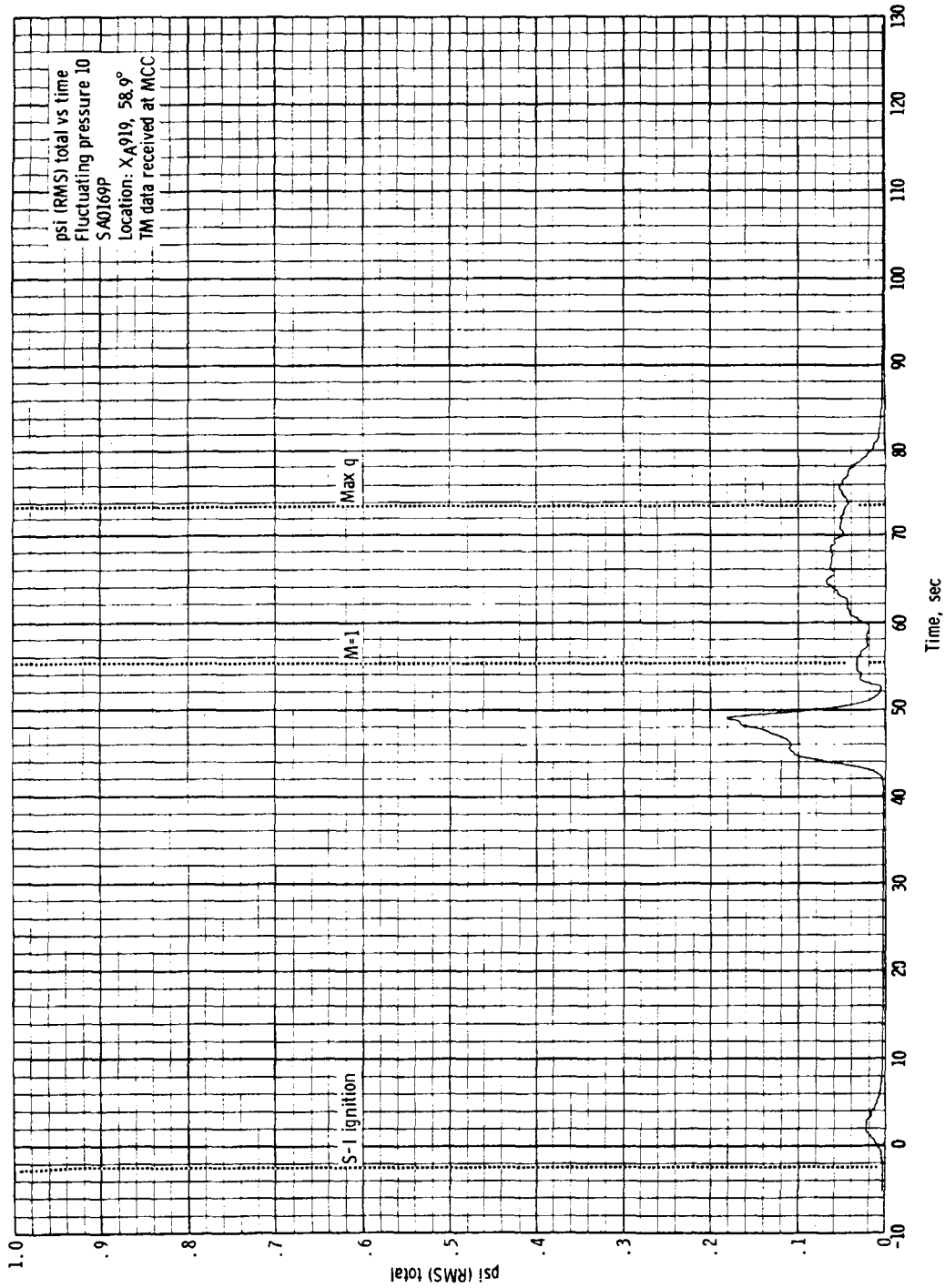
4-101



(g) Sensor SA0168P.

Figure 4.7-18. - Continued.

~~CONFIDENTIAL~~

~~CONFIDENTIAL~~

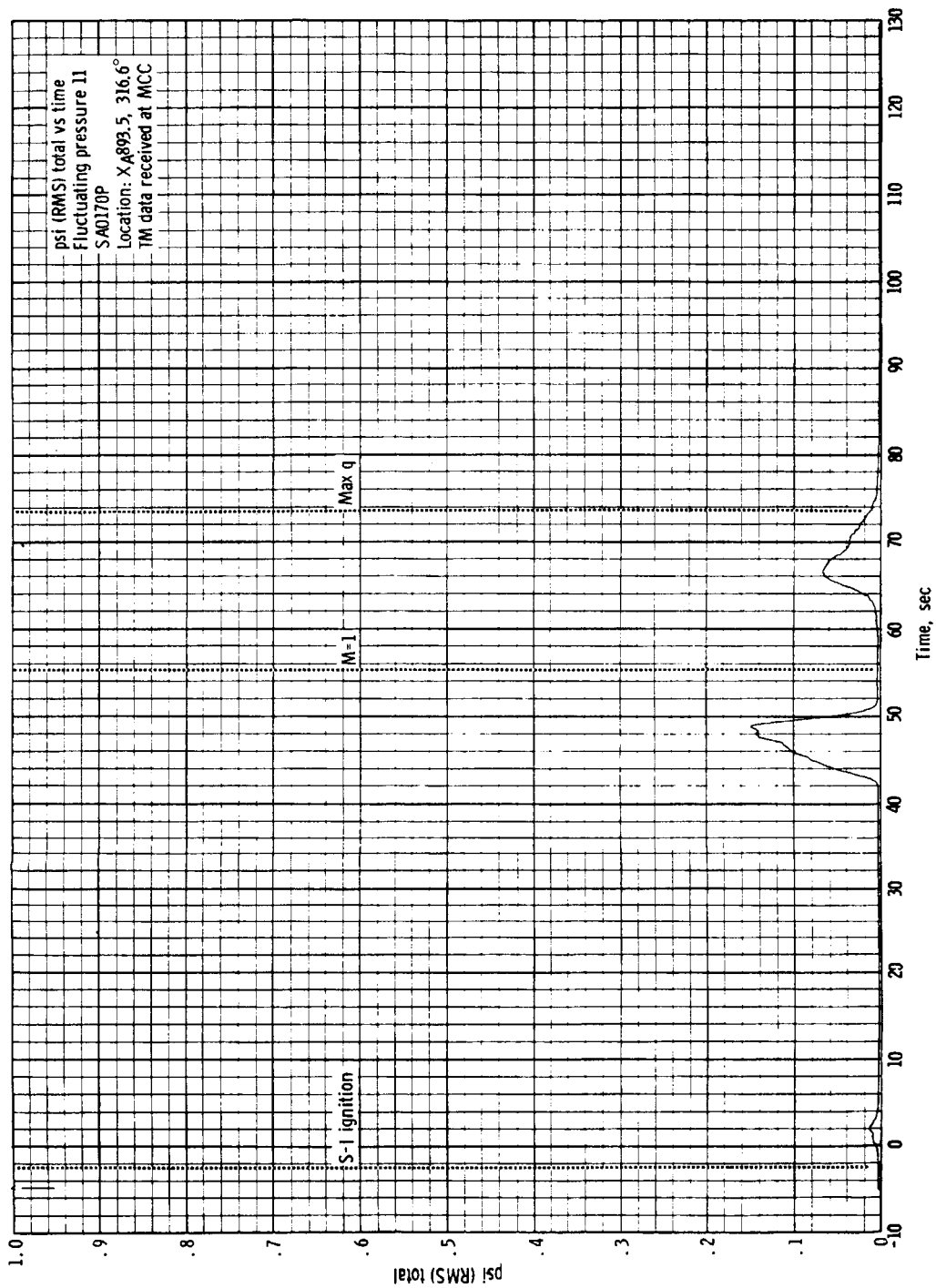
(h) Sensor SA0169P.

Figure 4.7-18. - Continued.

~~CONFIDENTIAL~~

~~CONFIDENTIAL~~

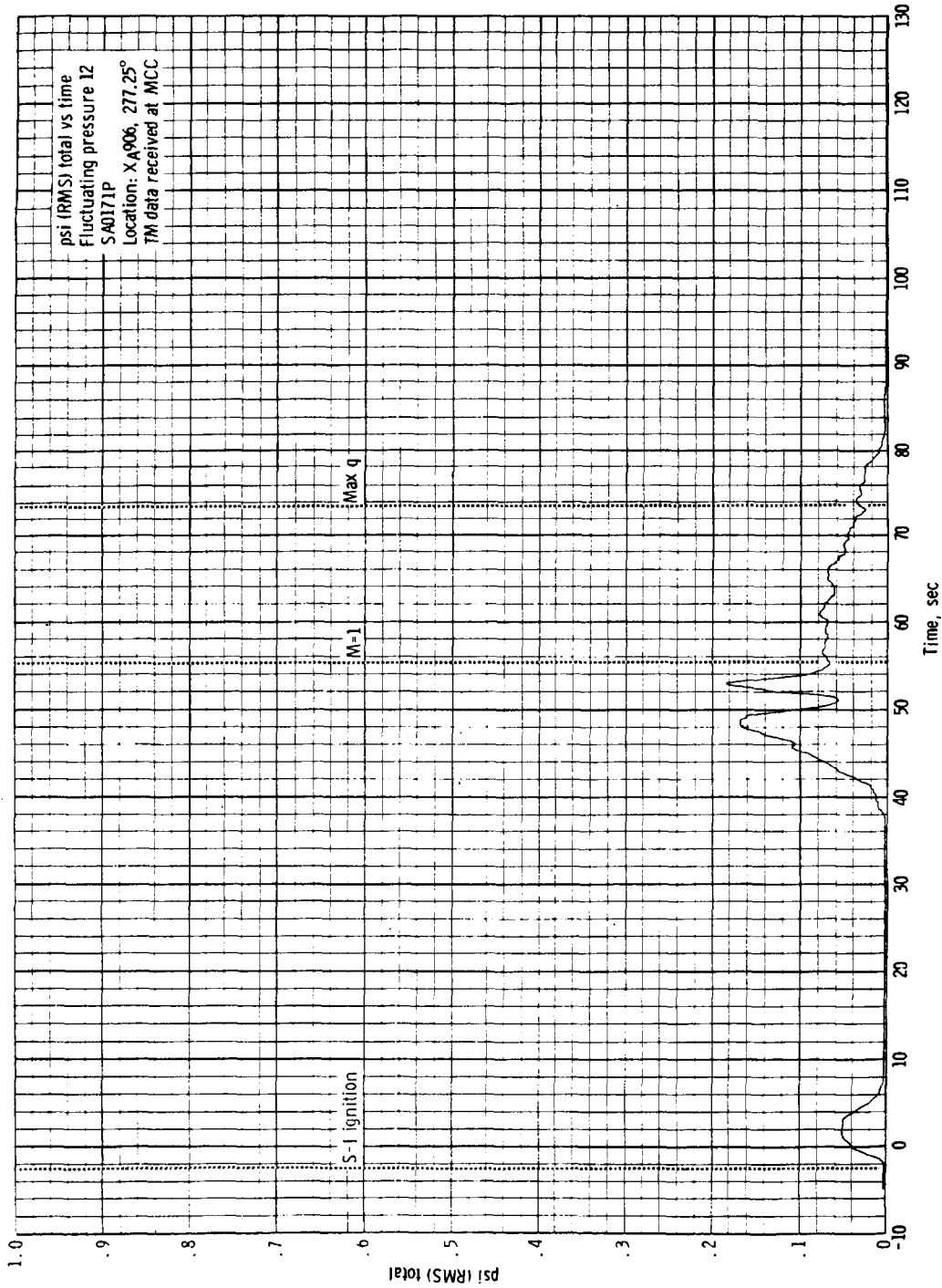
4-103



(i) Sensor SA0170P.

Figure 4.7-18. - Continued.

~~CONFIDENTIAL~~

~~CONFIDENTIAL~~

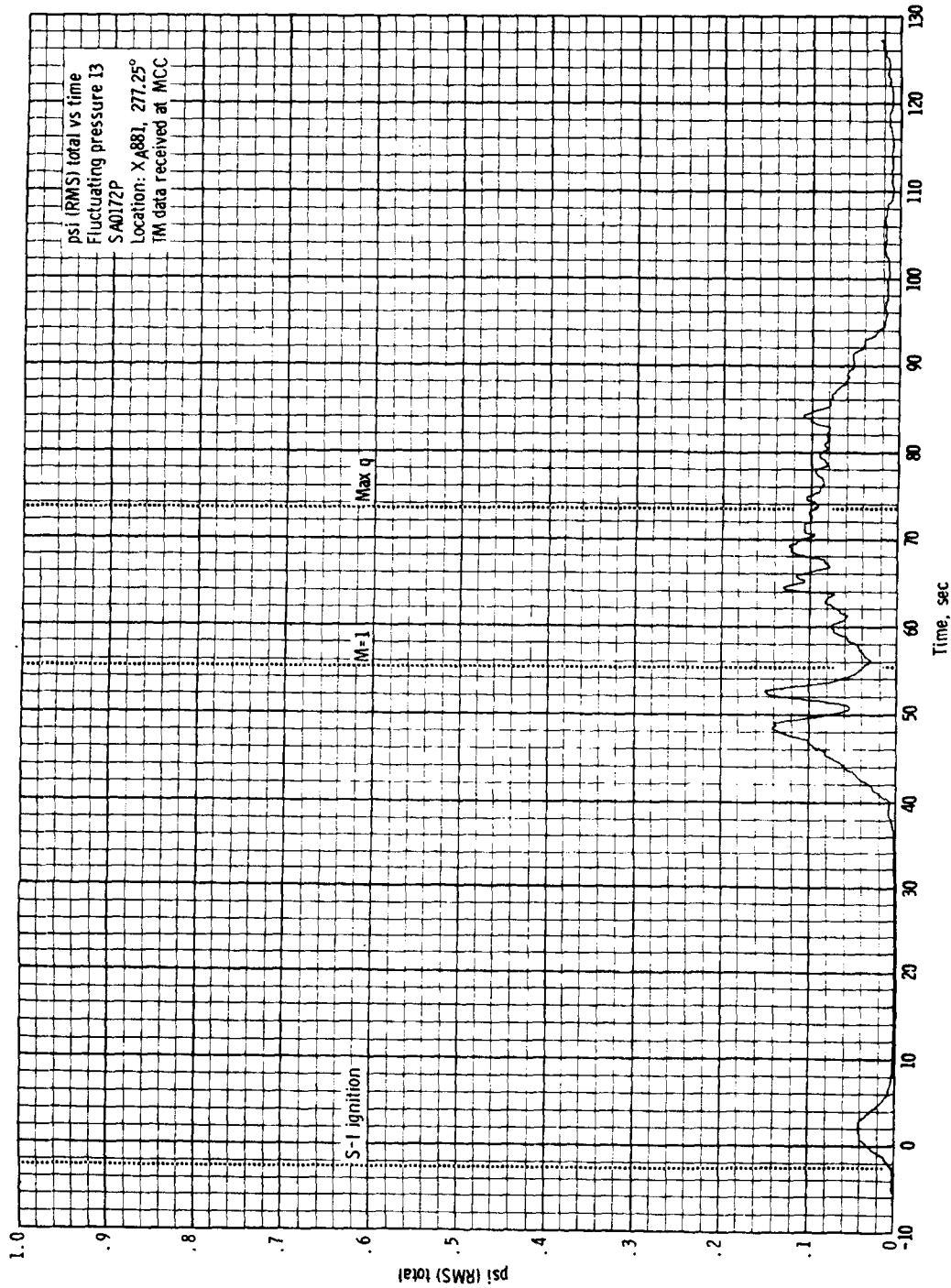
(j) Sensor SA0171P.

Figure 4.7-18. - Continued.

~~CONFIDENTIAL~~

~~CONFIDENTIAL~~

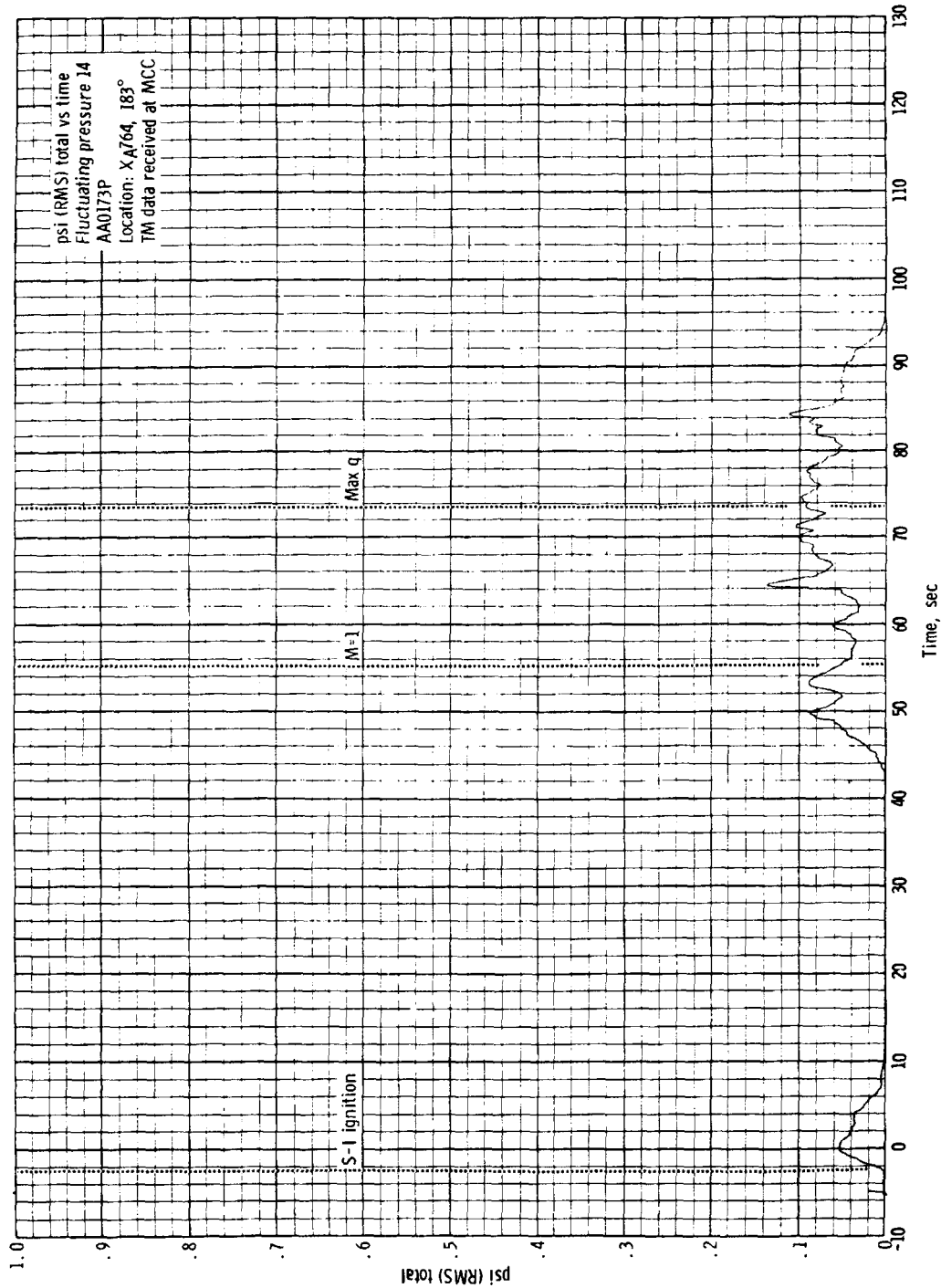
4-105



(k) Sensor SA0172P.

Figure 4.7-18. - Continued.

~~CONFIDENTIAL~~

~~CONFIDENTIAL~~

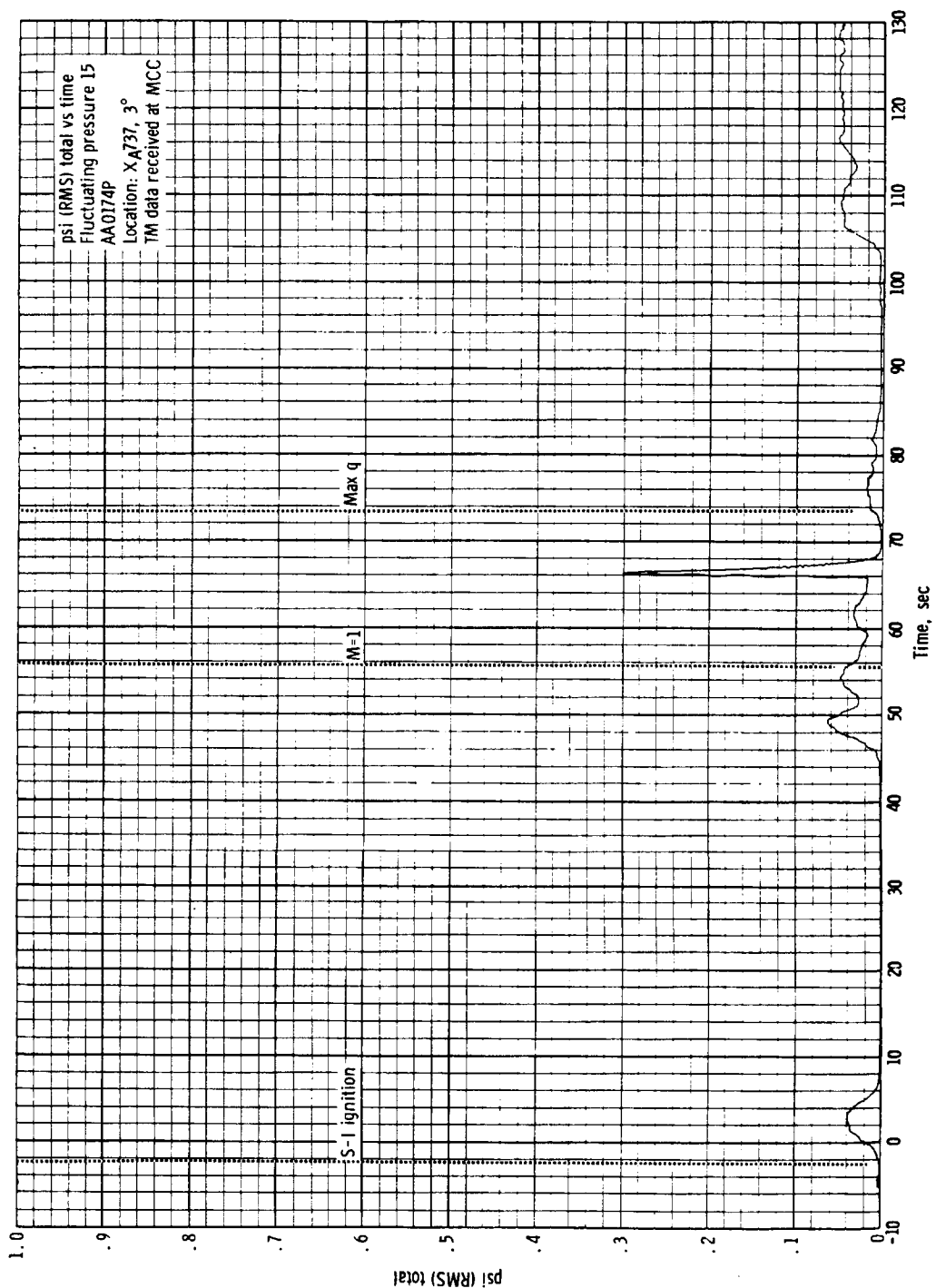
(I) Sensor AA0173P.

Figure 4. 7-18. - Continued.

~~CONFIDENTIAL~~

~~CONFIDENTIAL~~

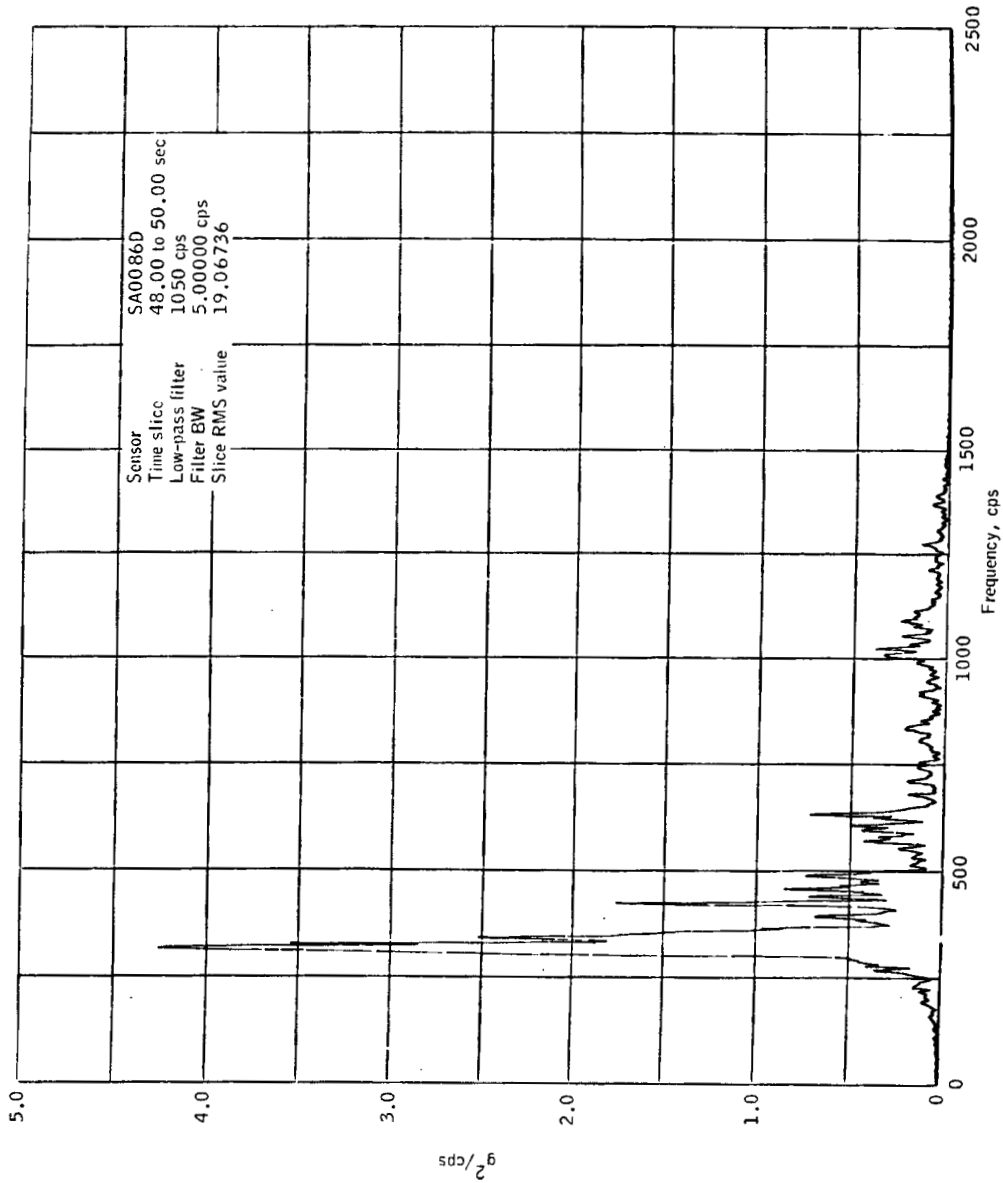
4-107



(m) Sensor AA0174P.

Figure 4.7-18. - Concluded.

~~CONFIDENTIAL~~

~~CONFIDENTIAL~~

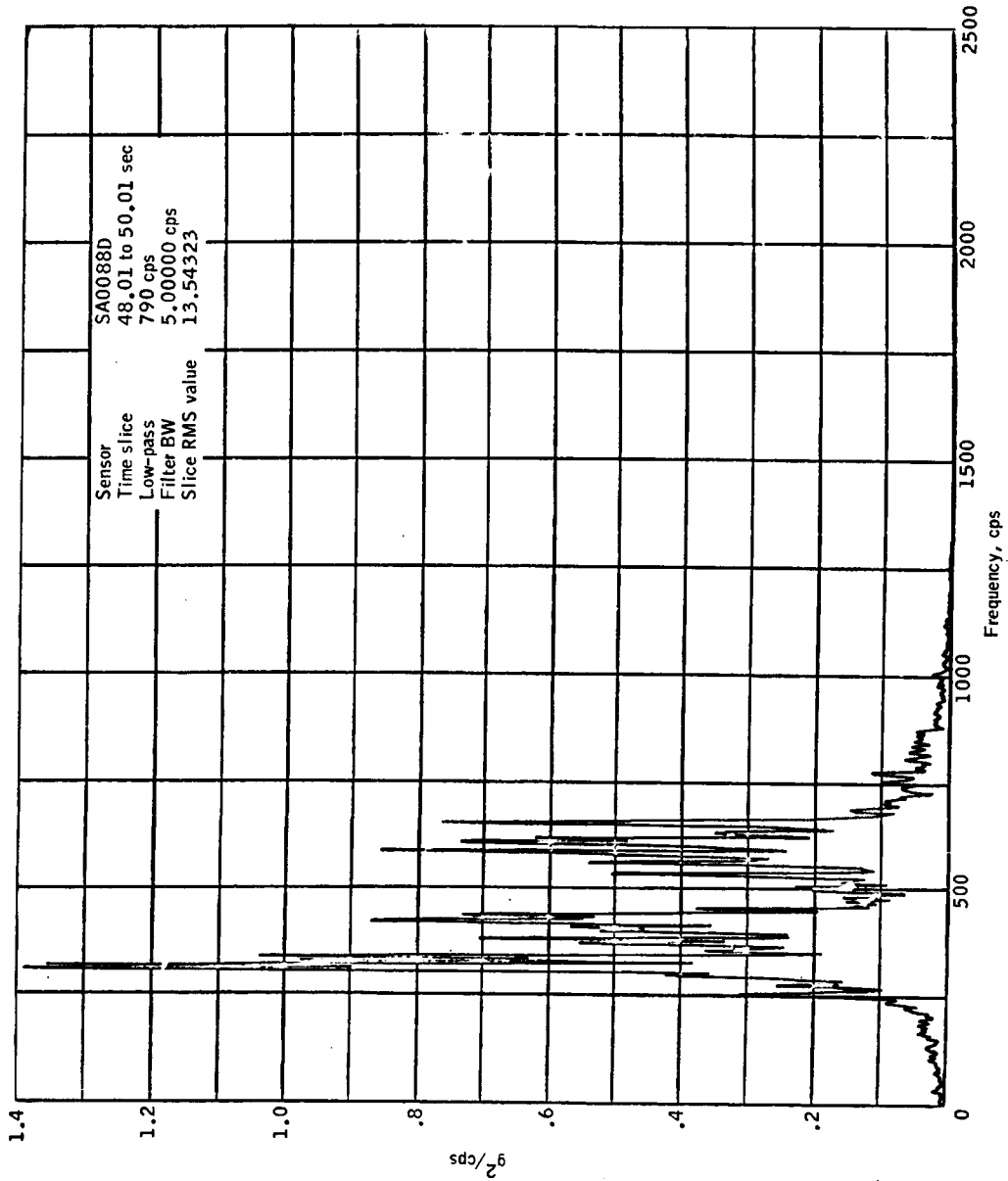
(a) SA0086D, T + 49 seconds.

Figure 4.7-19.- Power spectral distribution of service module radial vibration, BP-15 spacecraft.

~~CONFIDENTIAL~~

~~CONFIDENTIAL~~

4-109



(b) SA0088D, T + 49 second.

Figure 4.7-19.- Concluded.

~~CONFIDENTIAL~~

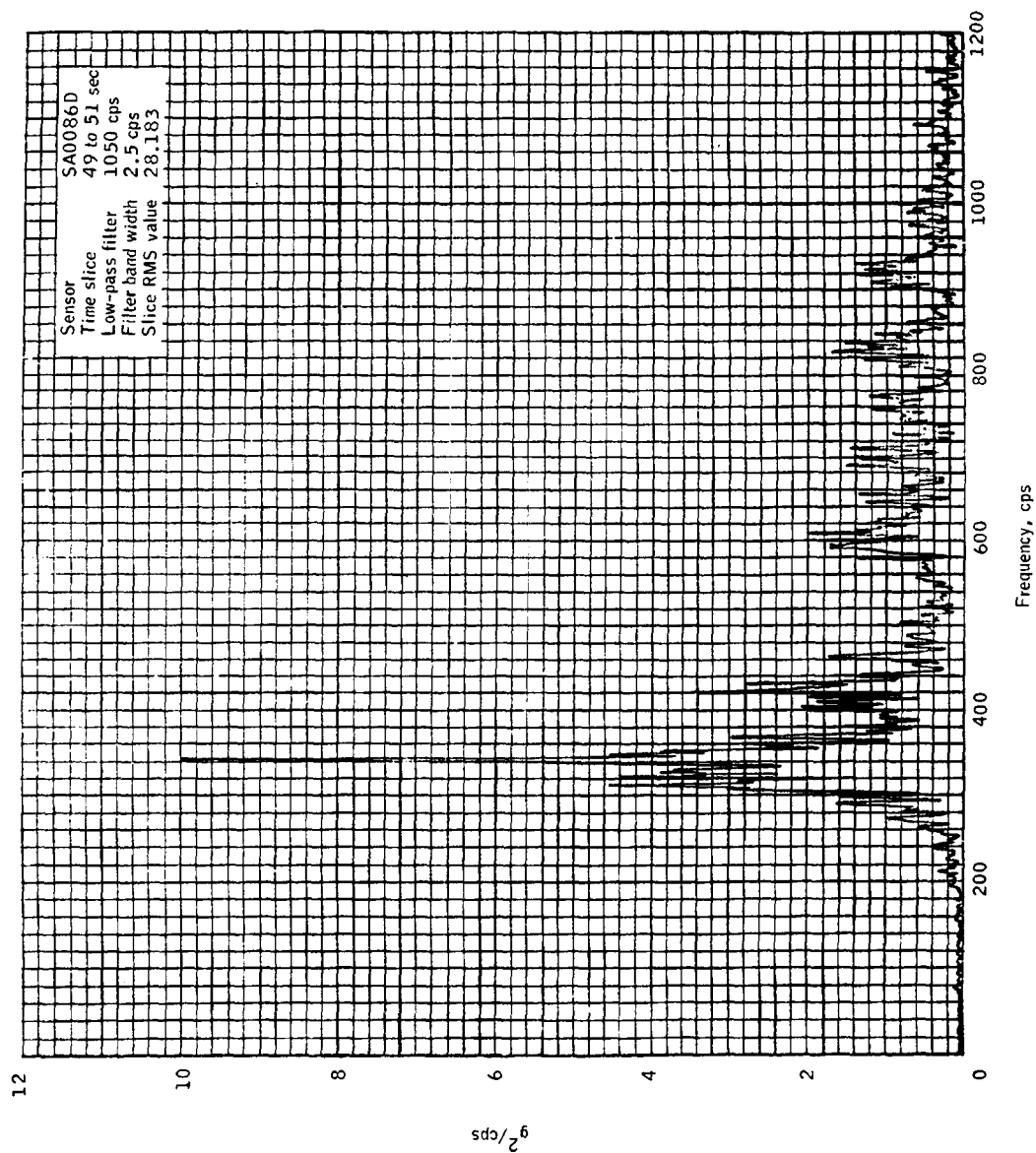
~~CONFIDENTIAL~~

Figure 4.7-20.- Power spectral distribution of BP-13 service module radial vibration at T+50 sec.

~~CONFIDENTIAL~~

~~CONFIDENTIAL~~

4-111

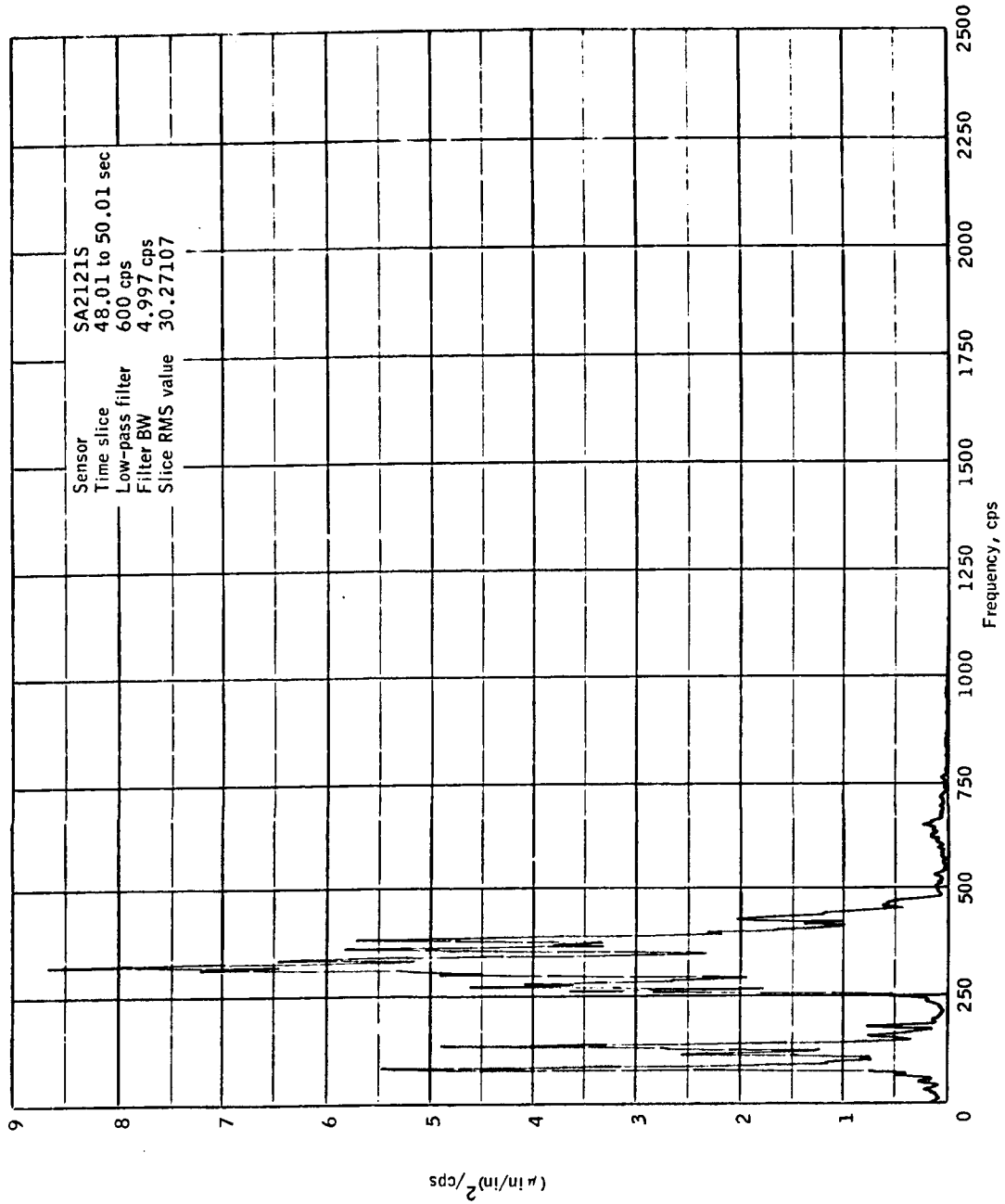
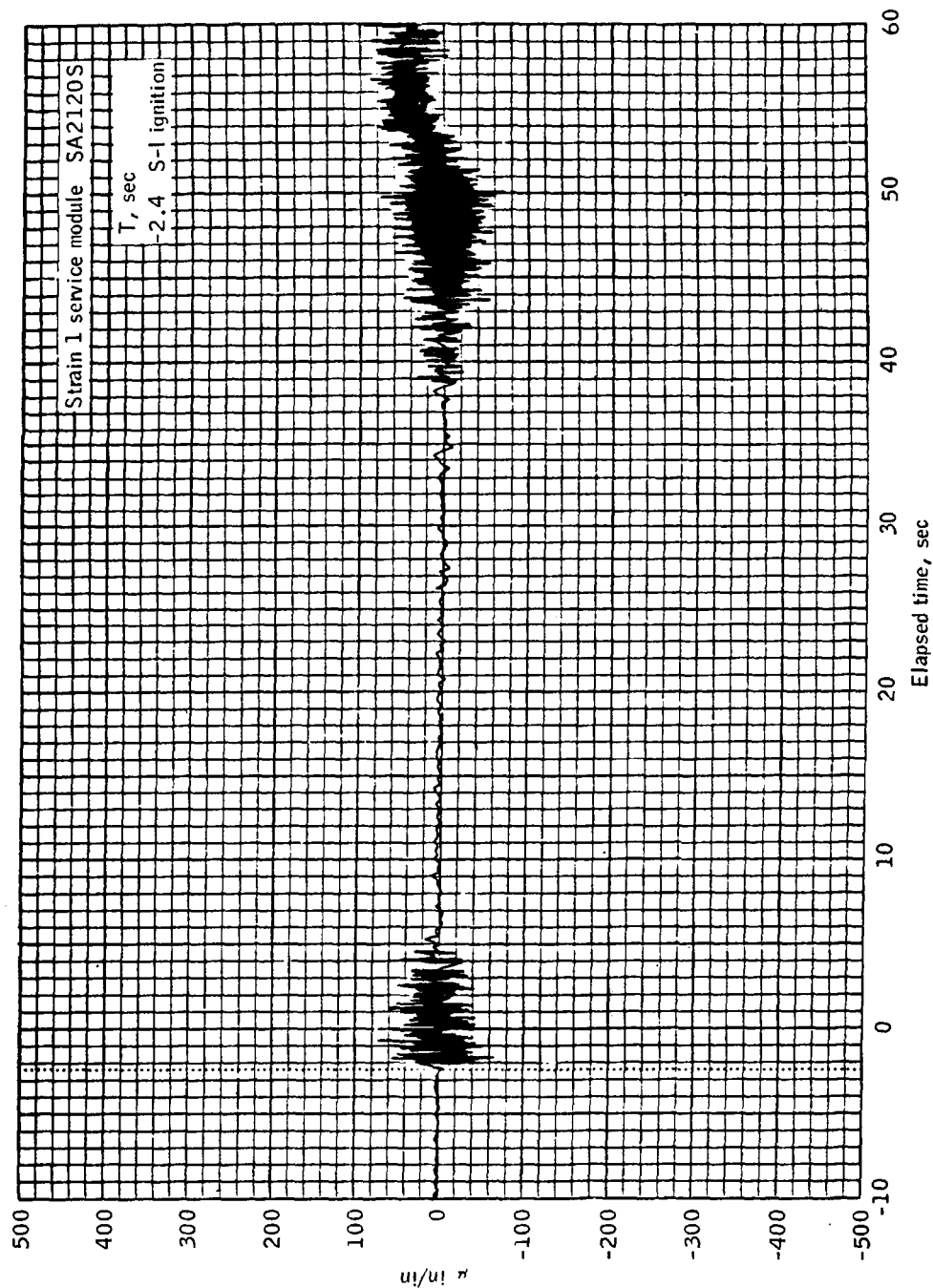


Figure 4.7-21.- Power spectral distribution of BP-15 spacecraft service module strain (SA2121S).

~~CONFIDENTIAL~~

~~CONFIDENTIAL~~

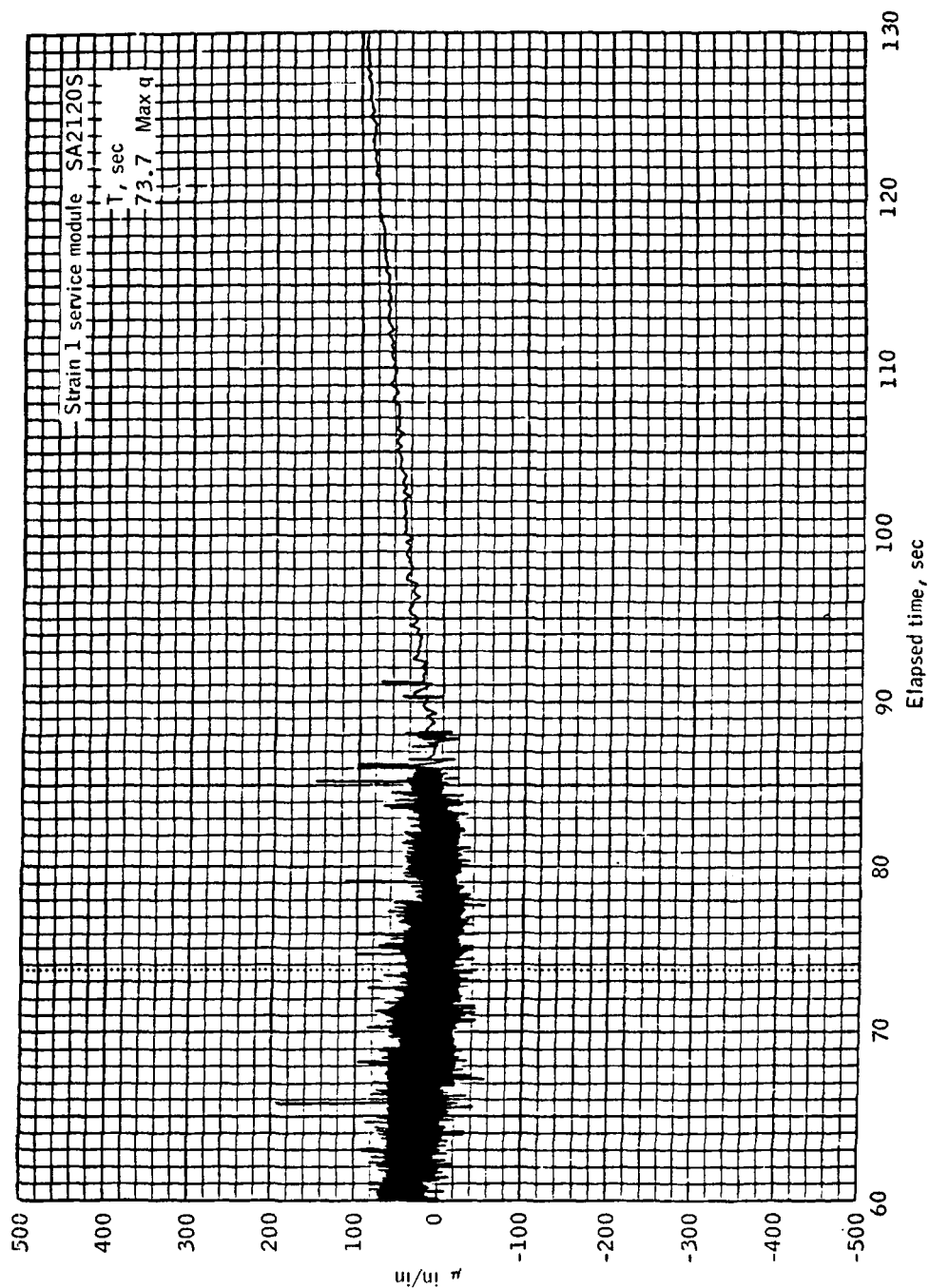
(a) Sensor SA2120S.

Figure 4.7-22.- Time history of BP-15 spacecraft service module strain.

~~CONFIDENTIAL~~

~~CONFIDENTIAL~~

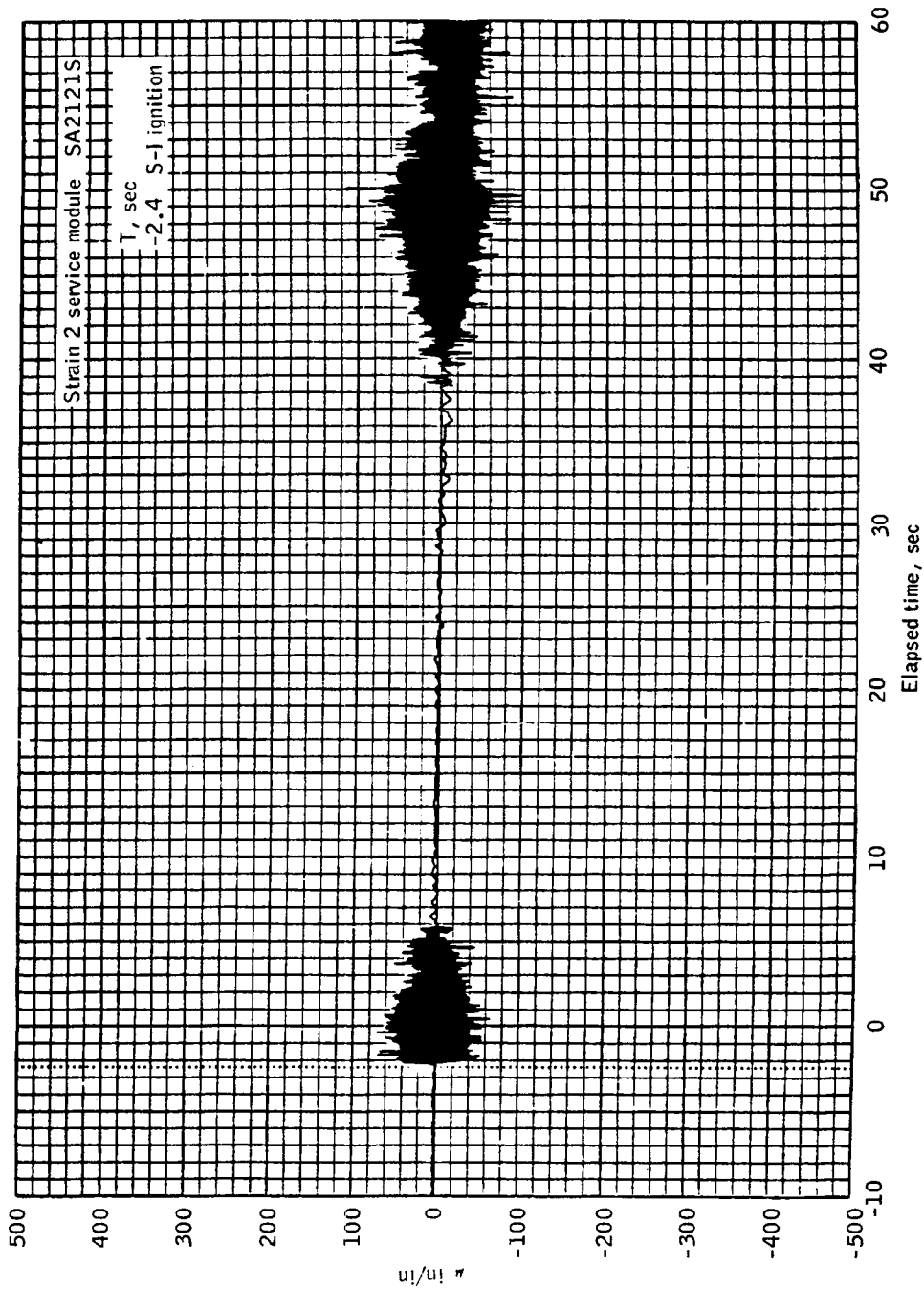
4-113



(a) Sensor SA2120S, concluded.

Figure 4.7-22.- Continued.

~~CONFIDENTIAL~~

~~CONFIDENTIAL~~

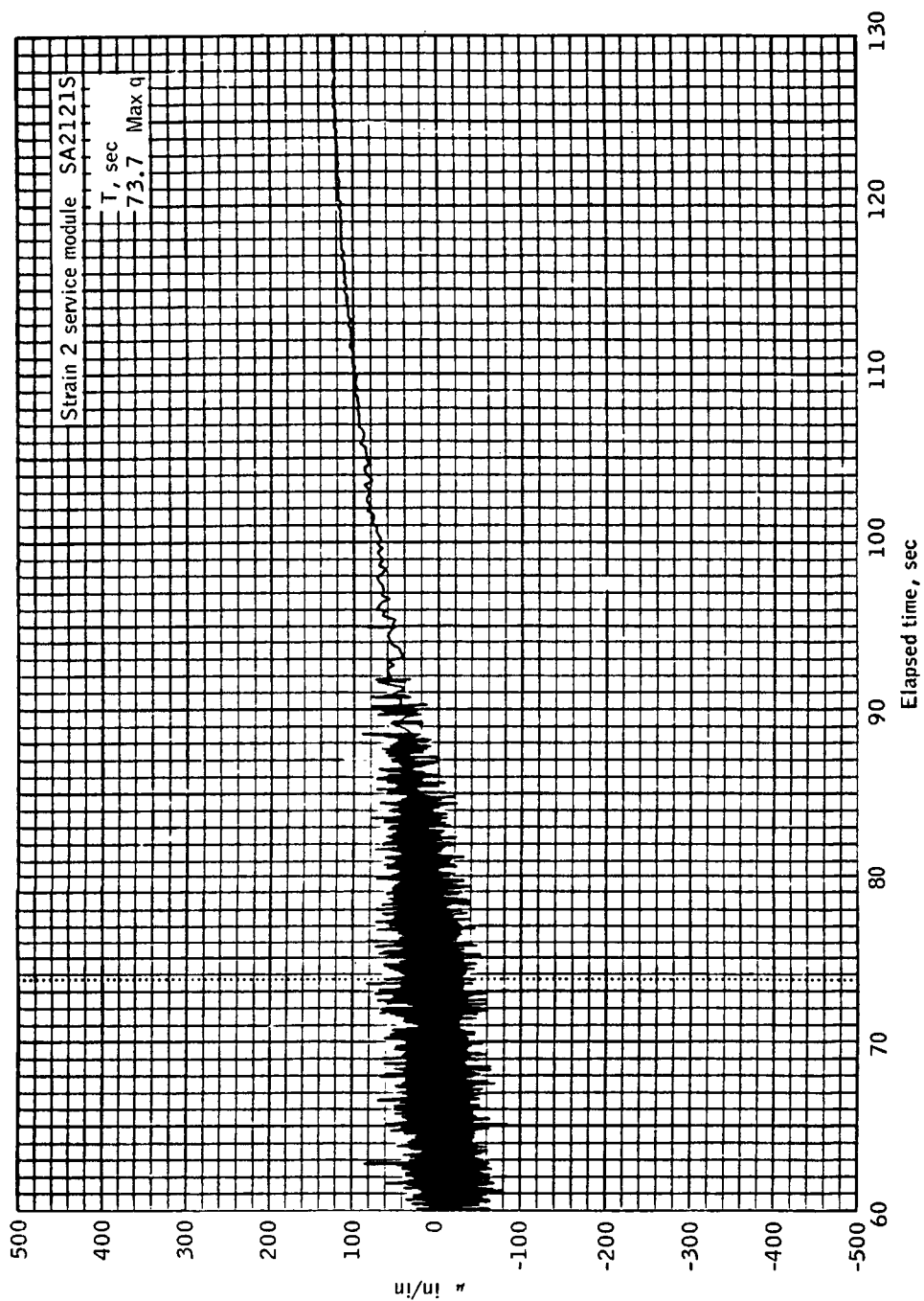
(b) Sensor SA2121S.

Figure 4.7-22.- Continued.

~~CONFIDENTIAL~~

~~CONFIDENTIAL~~

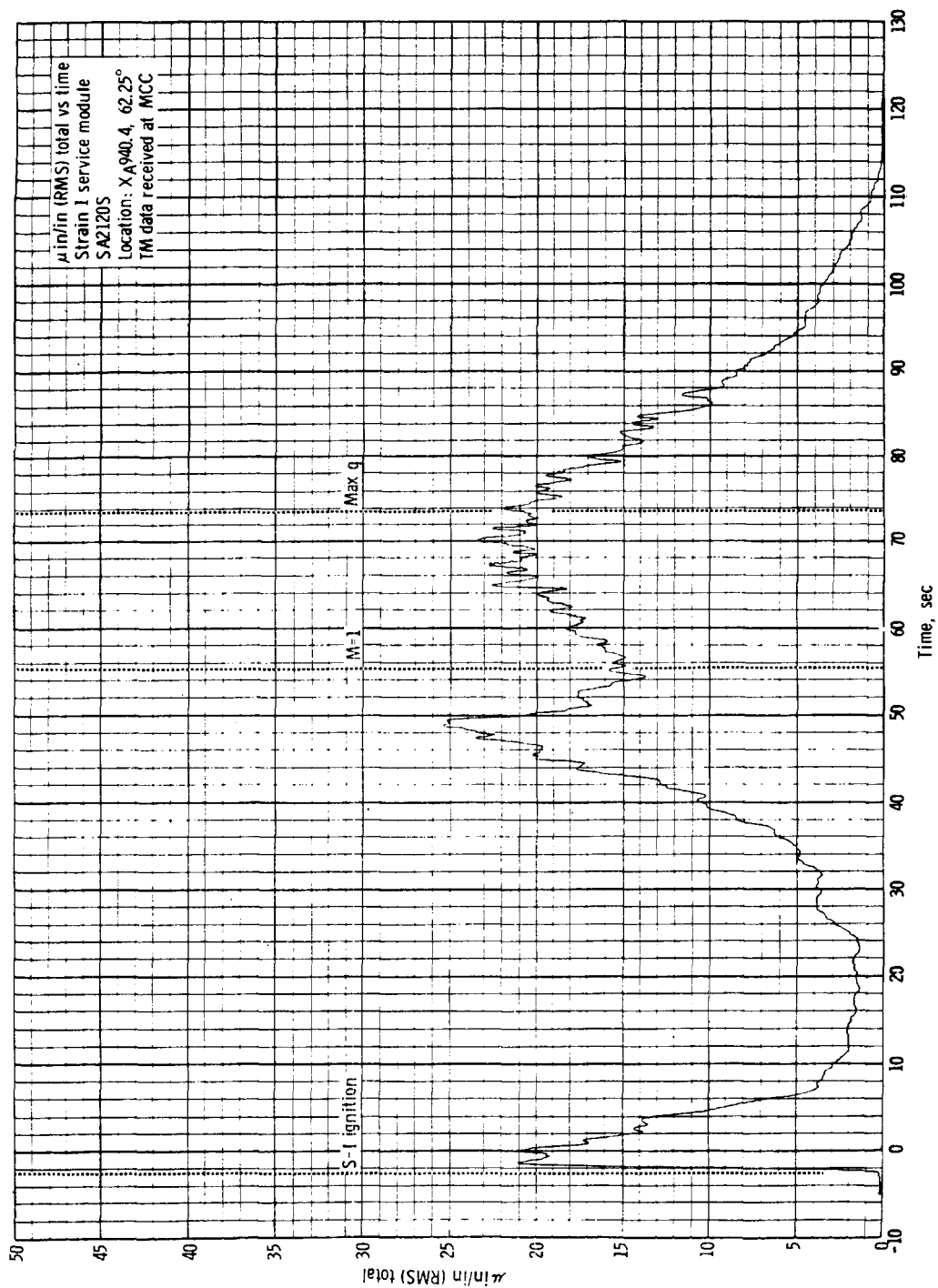
4-115



(b) Sensor SA2121S, concluded.

Figure 4.7-22.- Concluded.

~~CONFIDENTIAL~~

~~CONFIDENTIAL~~

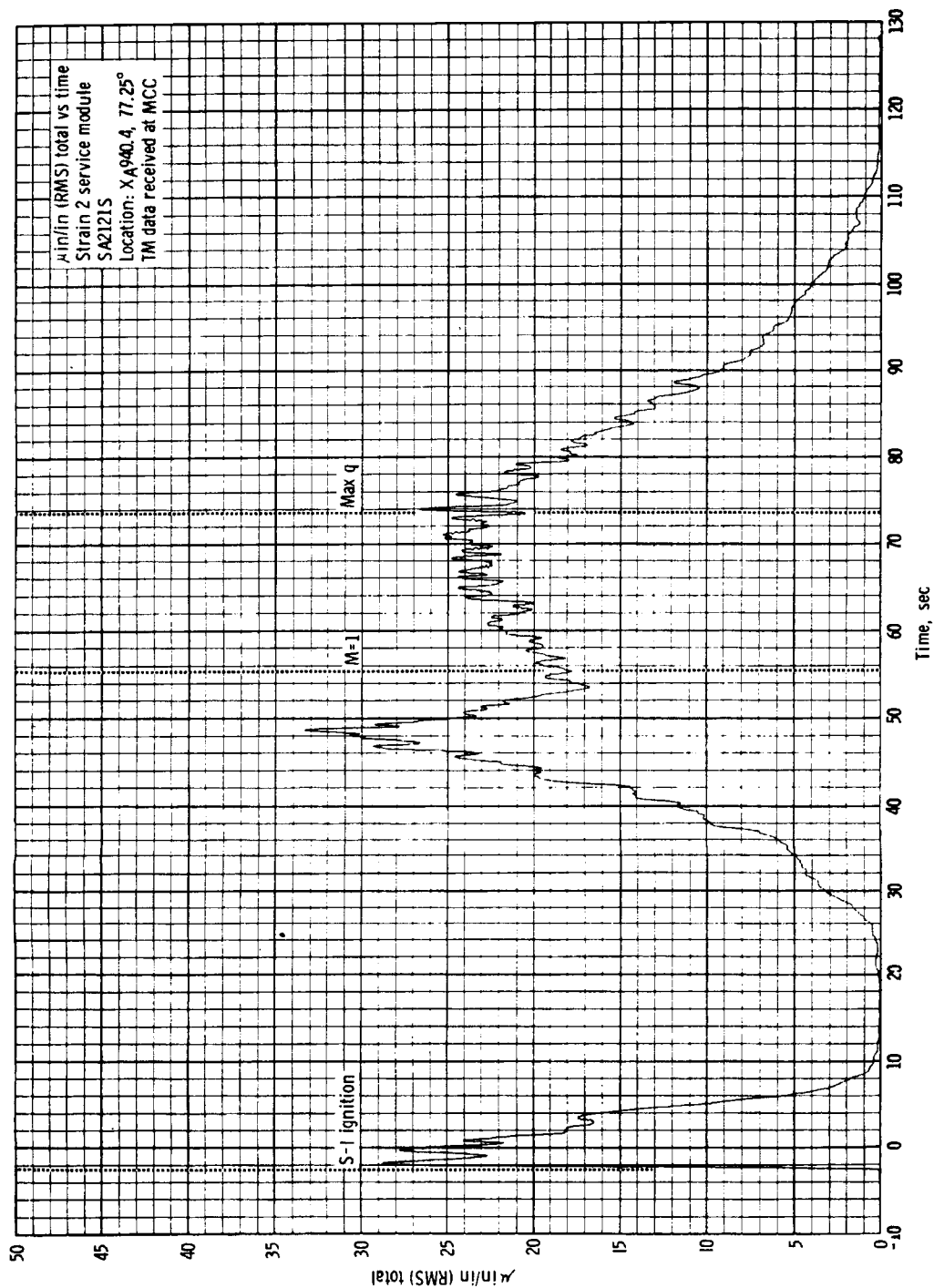
(a) SA2120S.

Figure 4.7-23. - RMS of BP-15 service module strain.

~~CONFIDENTIAL~~

~~CONFIDENTIAL~~

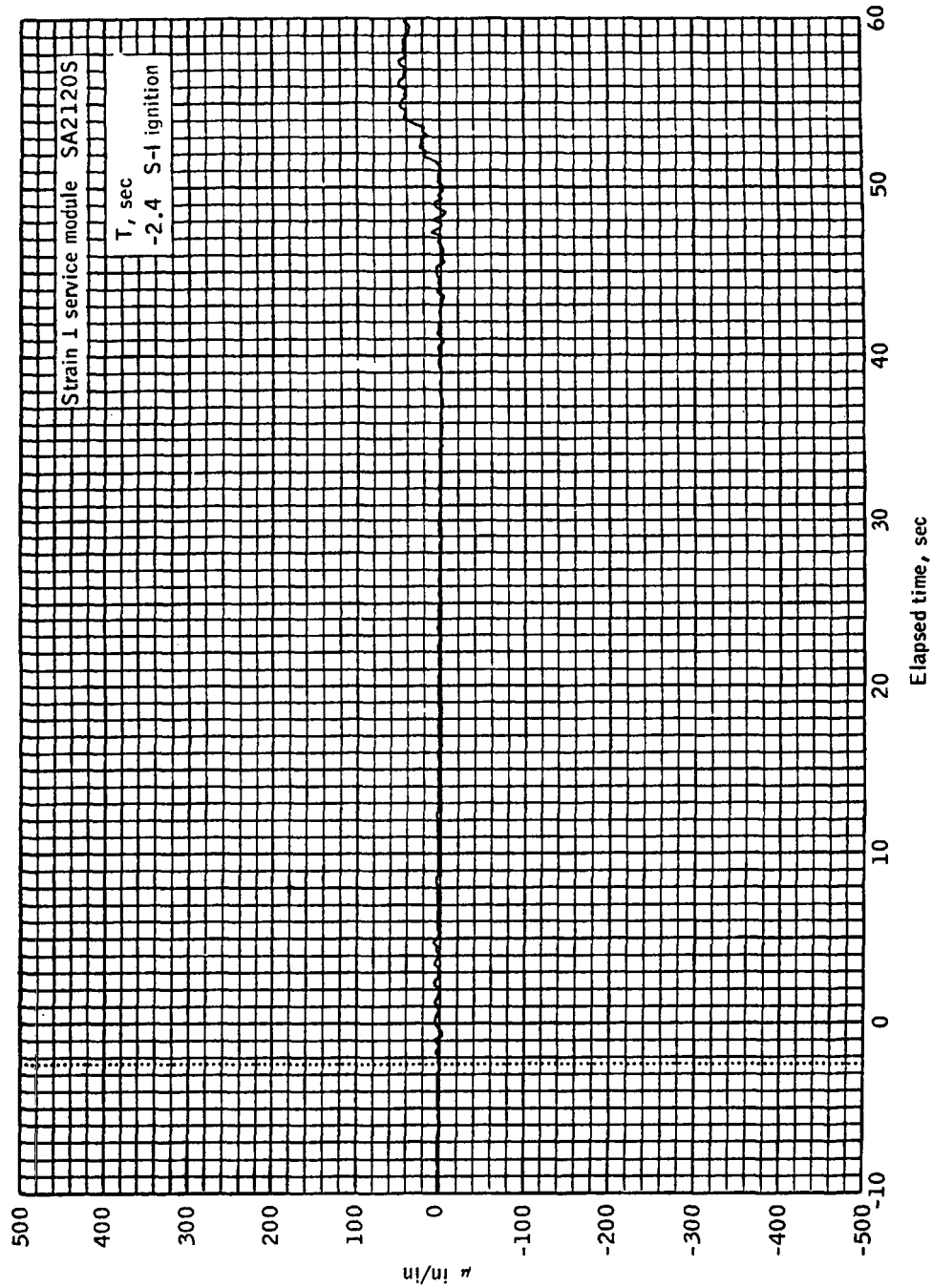
4-117



(b) SA2121S.

Figure 4. 7-23. - Concluded.

~~CONFIDENTIAL~~

~~CONFIDENTIAL~~

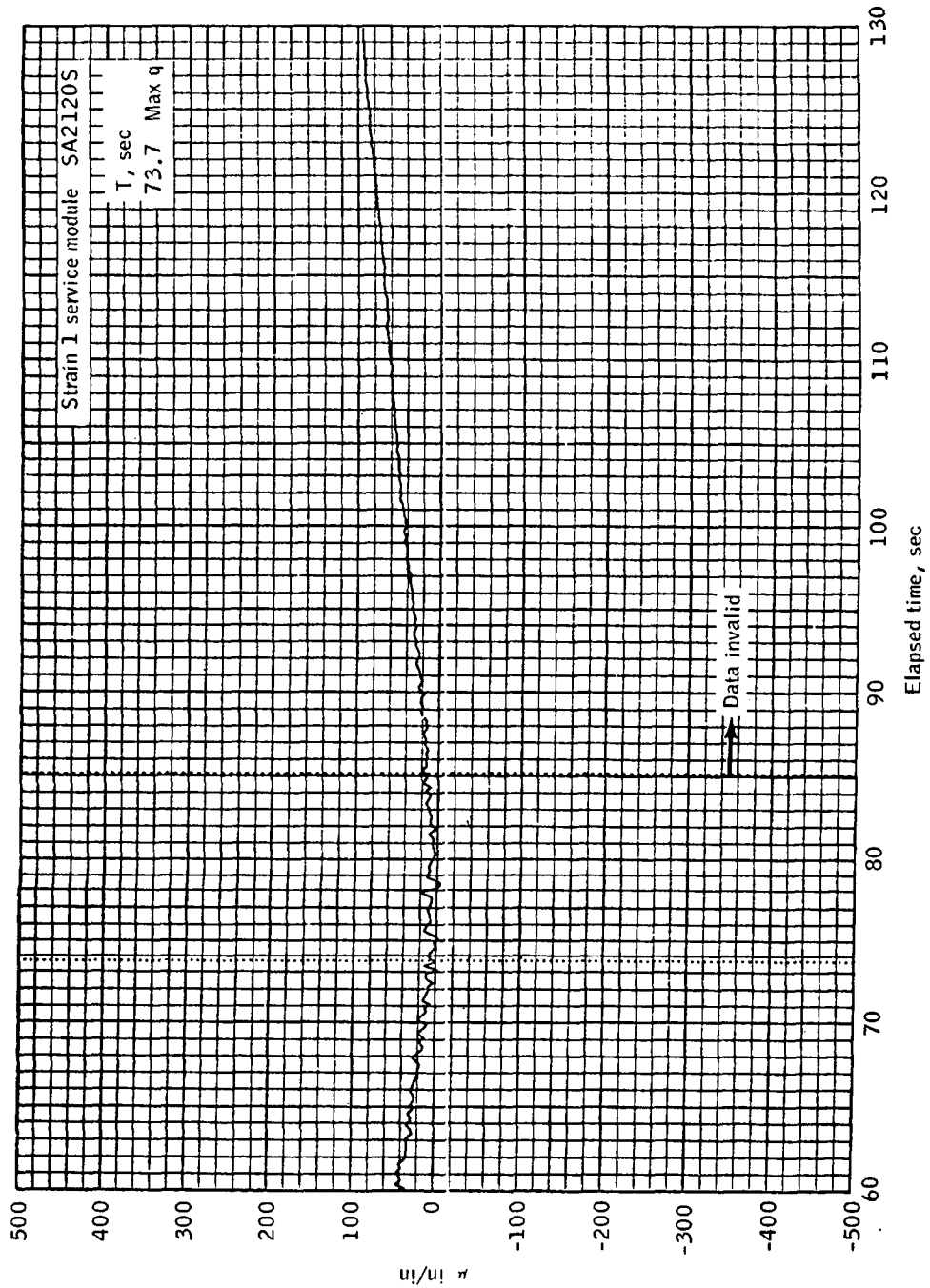
(a) Sensor SA2120S.

Figure 4.7-24.- Time history of BP-15 service module quasi-steady state strain SA2120S (averaged).

~~CONFIDENTIAL~~

~~CONFIDENTIAL~~

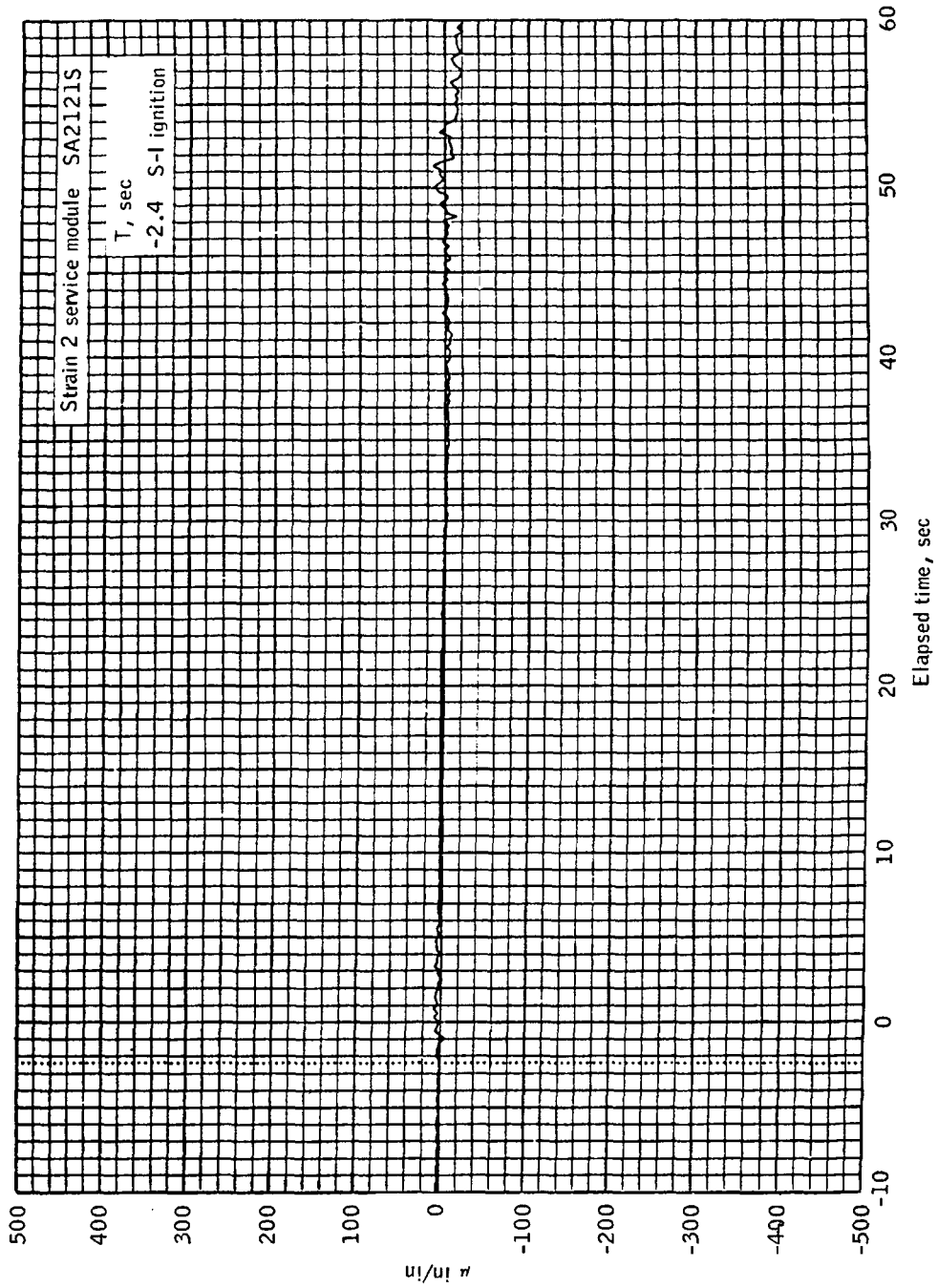
4-119



(a) Sensor SA2120S, concluded.

Figure 4.7-24. - Continued.

~~CONFIDENTIAL~~

~~CONFIDENTIAL~~

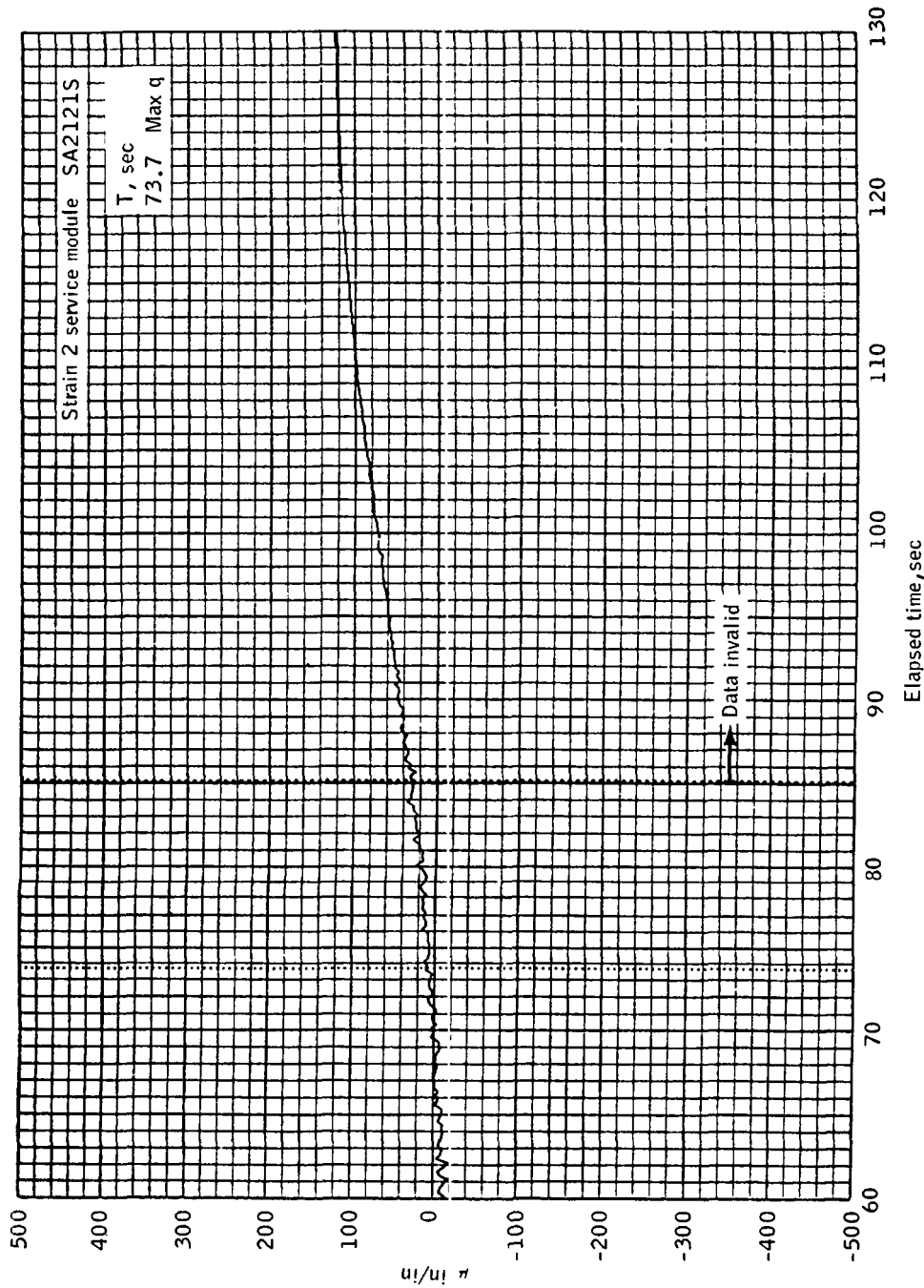
(b) Sensor SA2121S.

Figure 4.7-24.- Continued.

~~CONFIDENTIAL~~

~~CONFIDENTIAL~~

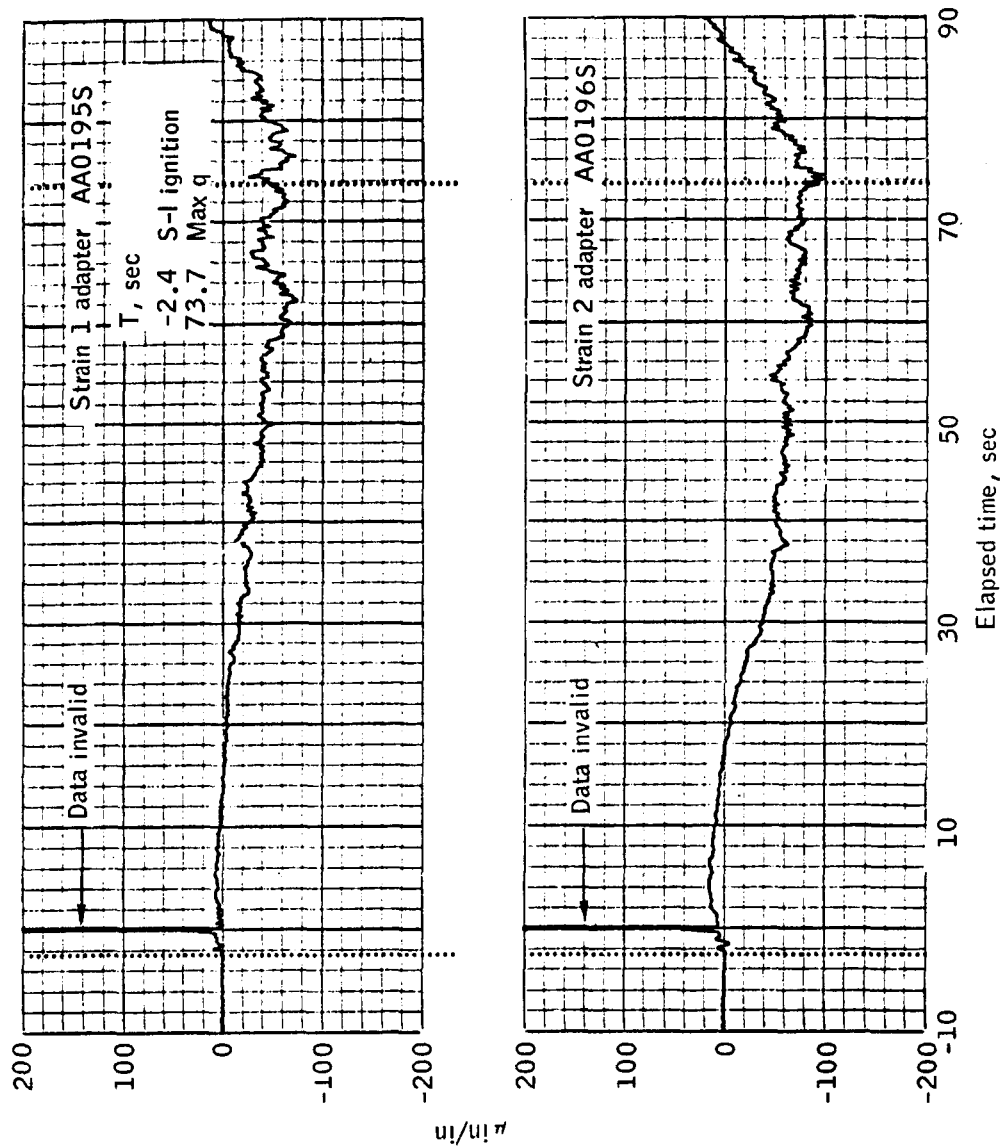
4-121



(b) Sensor SA2121S, concluded.

Figure 4.7-24.- Concluded.

~~CONFIDENTIAL~~

~~CONFIDENTIAL~~

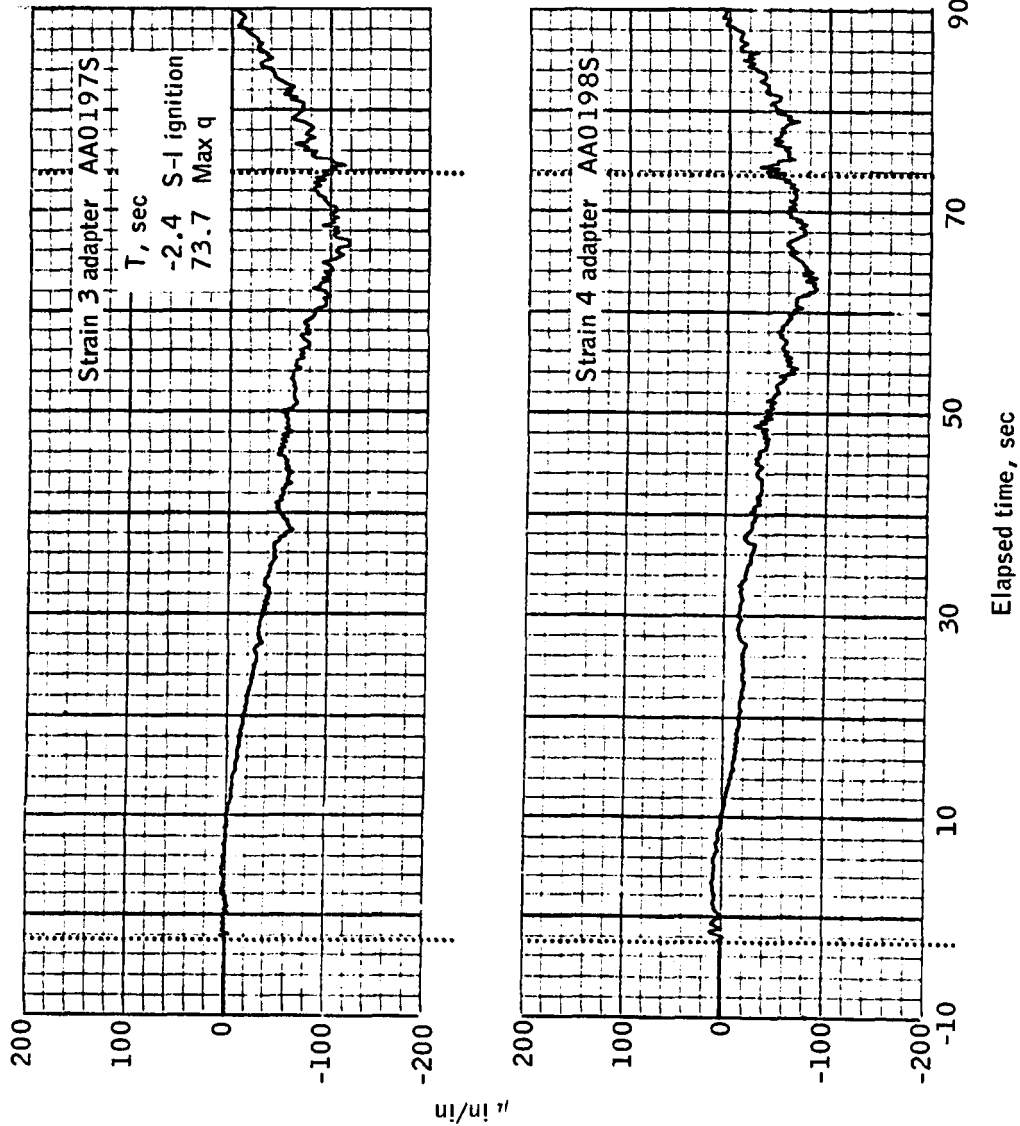
(a) AA0195S and AA0196S.

Figure 4.7-25.- Time history of BP-15 adapter strain.

~~CONFIDENTIAL~~

~~CONFIDENTIAL~~

4-123



(b) AA0197S and AA0198S.

Figure 4.7-25.- Concluded.

~~CONFIDENTIAL~~

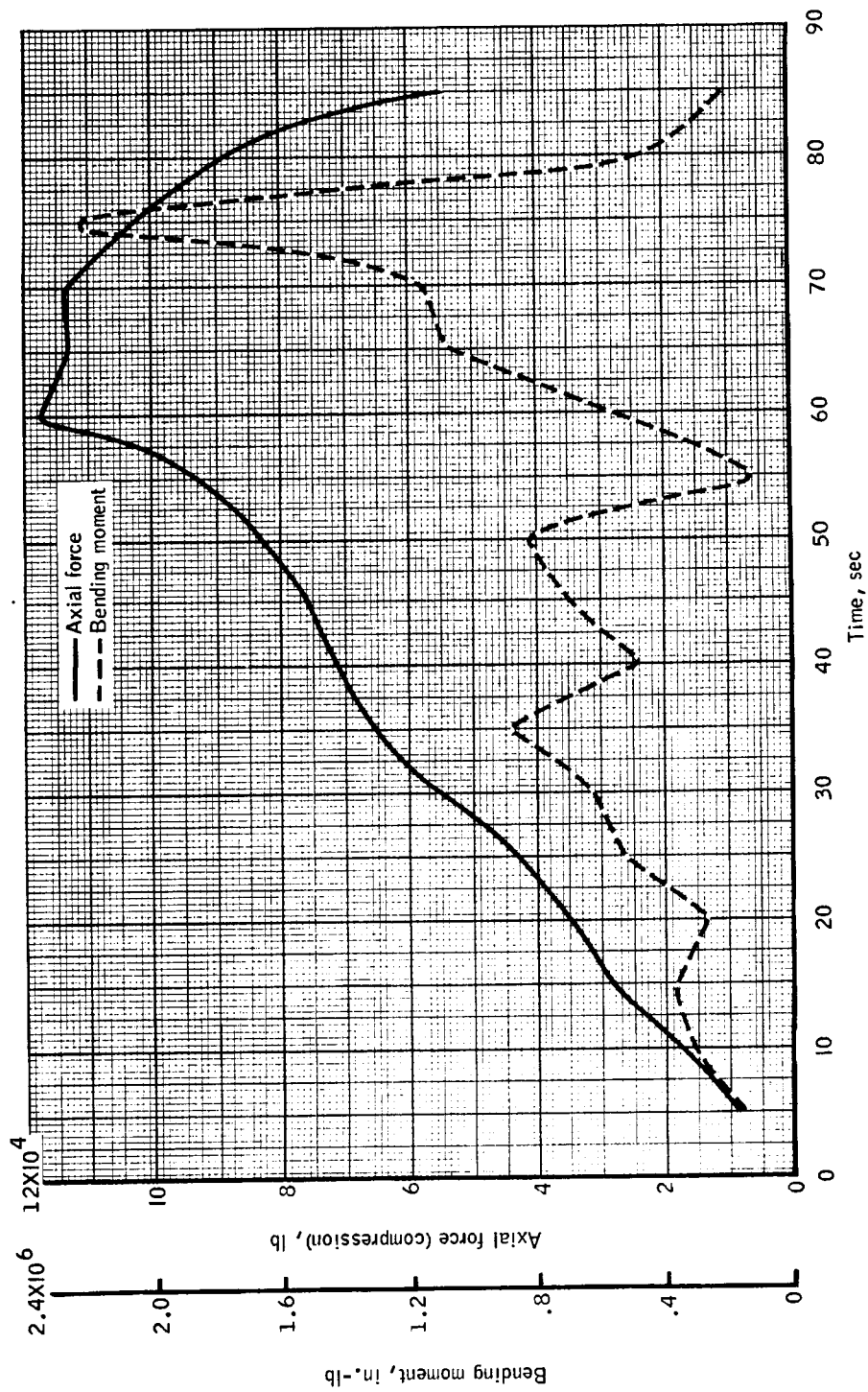
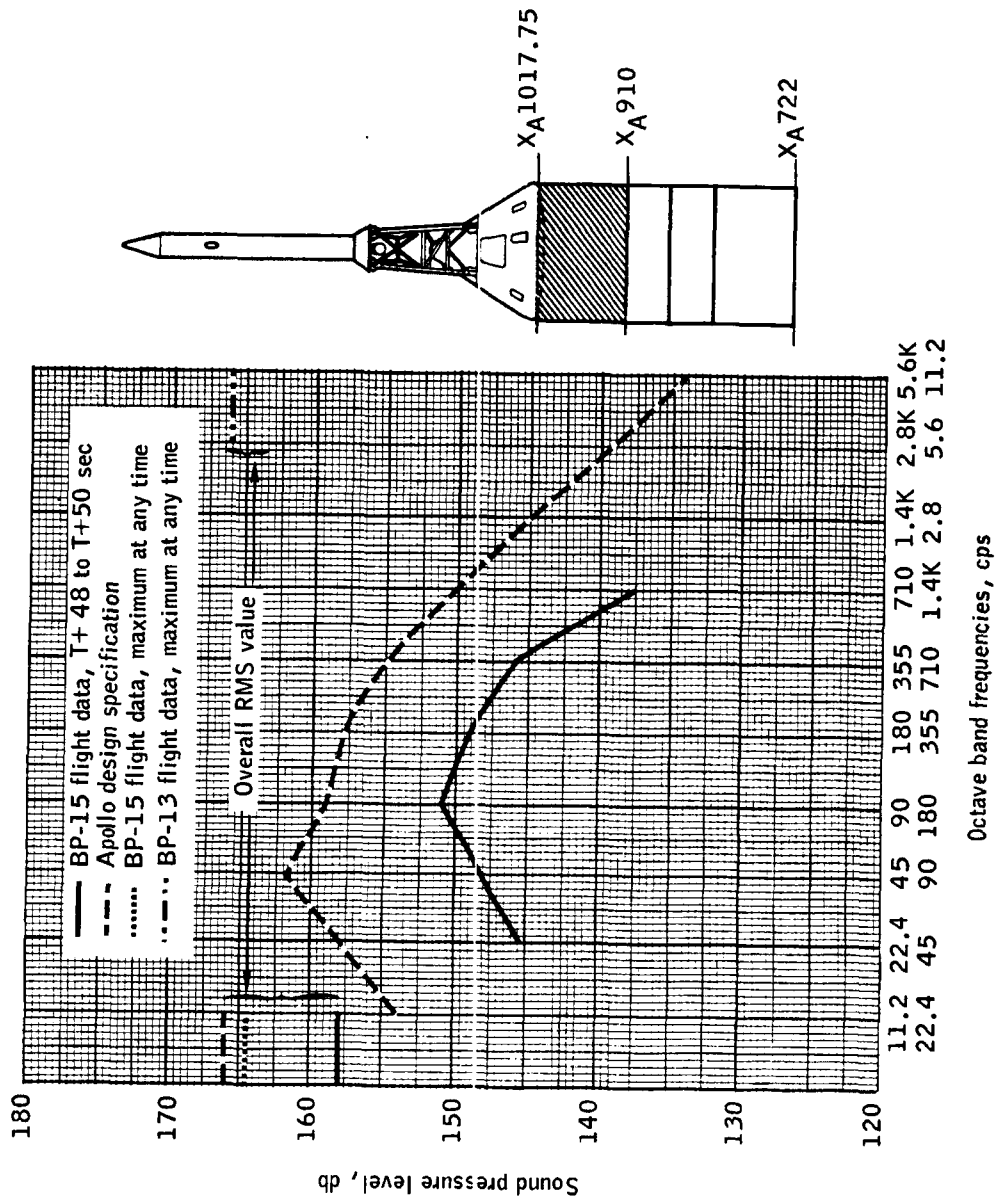
~~CONFIDENTIAL~~

Figure 4.7-26.- BP-15 spacecraft adapter load from strain gage data at XA 736.

~~CONFIDENTIAL~~

~~CONFIDENTIAL~~

4-125

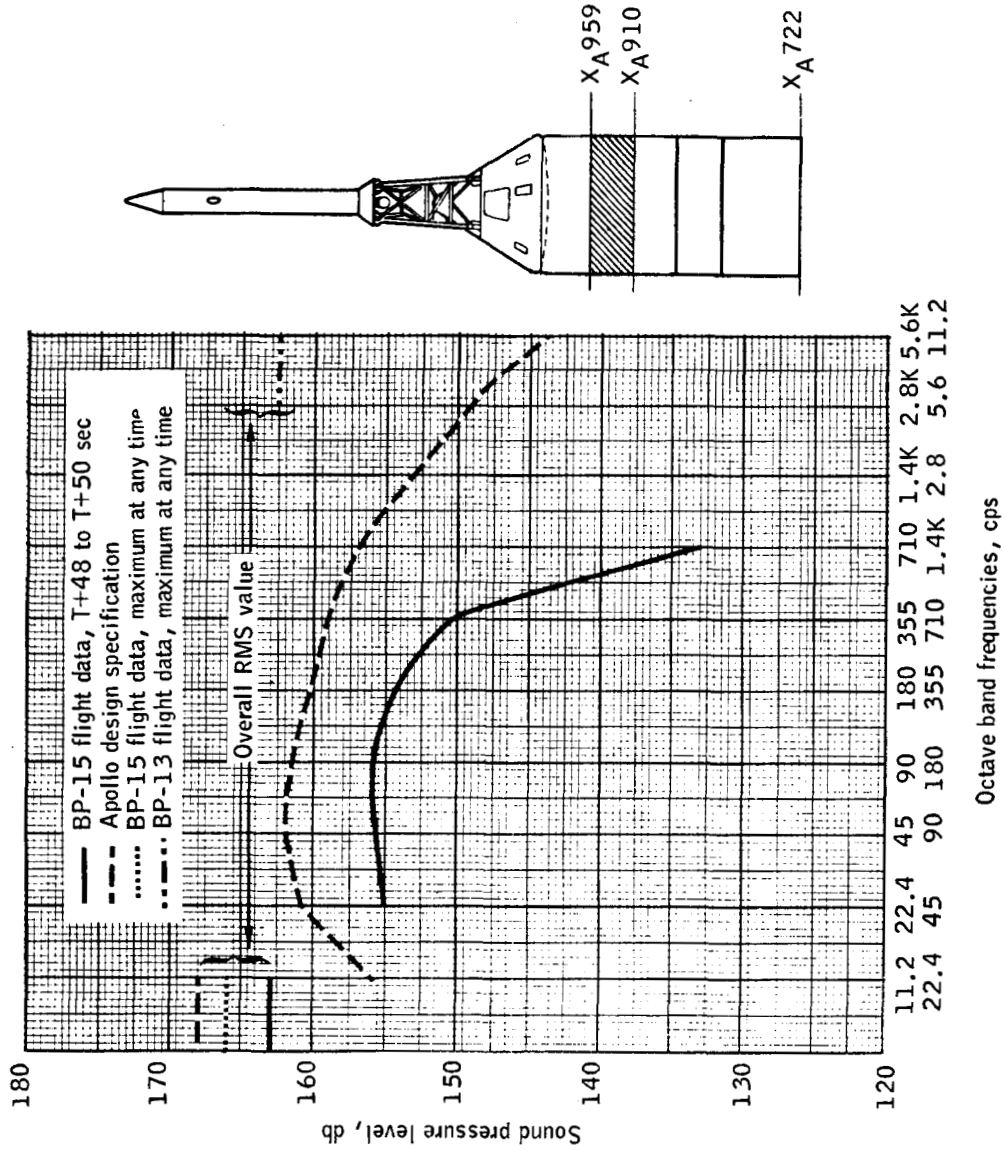


(a) External-forward of $X_A 910$ to $X_A 1017.75$.

Figure 4.7-27.- Comparison of flight noise data to design environment.

~~CONFIDENTIAL~~

~~CONFIDENTIAL~~



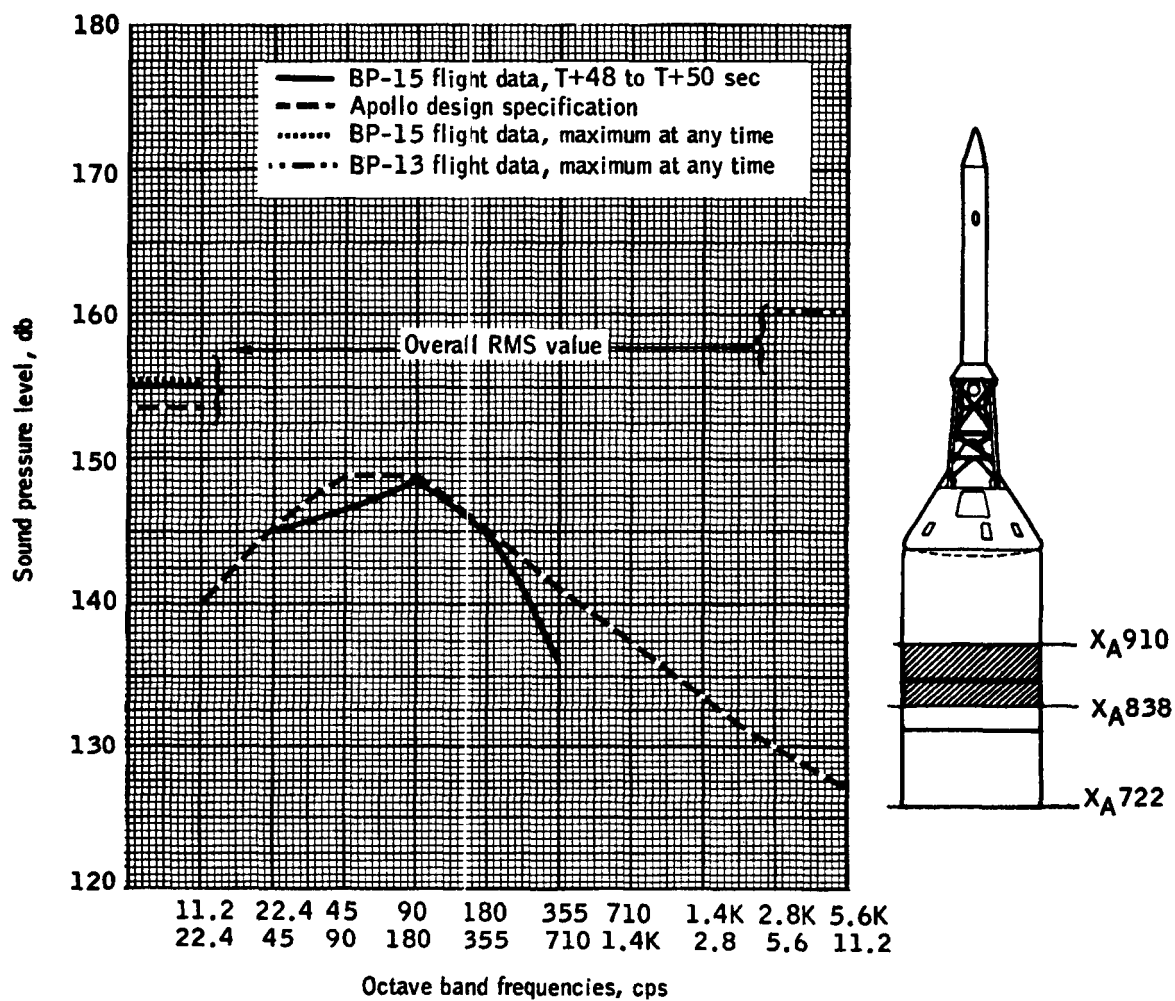
(b) SM RCS engine area XA910 to XA959.

Figure 4.7-27.- Continued.

~~CONFIDENTIAL~~

~~CONFIDENTIAL~~

4-127



(c) External X_A 838 to X_A 910.

Figure 4.7-27.- Continued.

~~CONFIDENTIAL~~

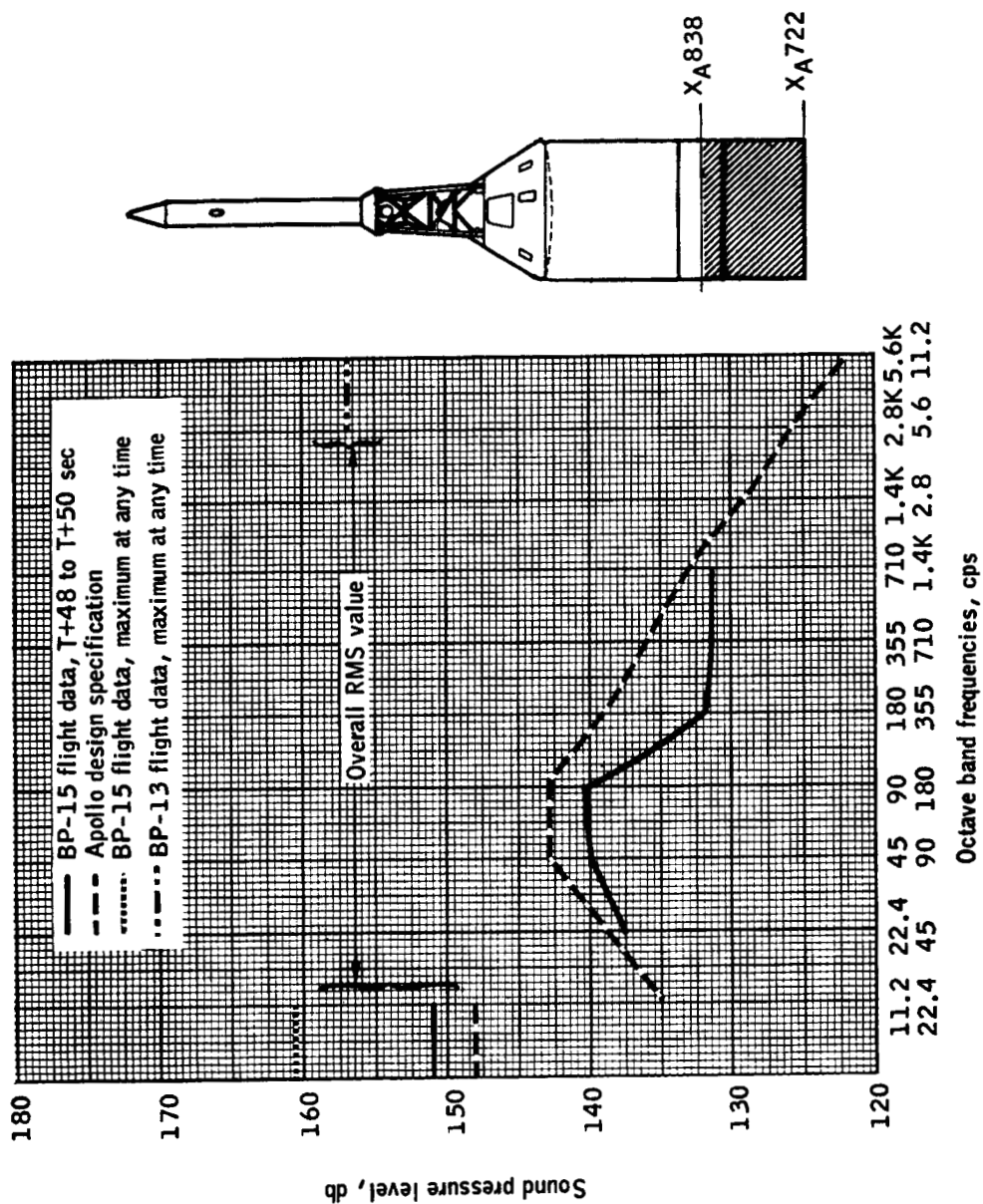
~~CONFIDENTIAL~~(d) External X_A 722 to X_A 838.

Figure 4.7-27.- Concluded.

~~CONFIDENTIAL~~

~~CONFIDENTIAL~~

4-129

4.8 Reaction Control Subsystem

An instrumented reaction control subsystem (RCS) package was carried on the BP-15 spacecraft in order to define the aerodynamic heating and vibration levels to be experienced by the RCS package during launch. This information was not available from any previous flights, wind-tunnel tests, or hardware-development tests.

Description. - The RCS for the BP-15 spacecraft consisted of one instrumented, simulated RCS quad assembly and three uninstrumented, simulated quad assemblies, all located at X_g 294 on the service module (SM).

The instrumented unit, quad A, was located near the -Z axis at 187.25° as shown in figure 4.8-1. The uninstrumented units, quads B, C, and D, were located at successive 90° intervals from quad A.

Quad A, shown in figures 4.8-2 and 4.8-3, consisted of four simulated RCS engines, the insulated quad housing, and the engine-supporting bracket. The quad housing was fabricated from 2024T3 aluminum. The discovery of a housing fabrication error necessitated the addition of a 4.50-inch by 5.50-inch by 0.25 inch aluminum plate under the clockwise (CW) roll and counterclockwise (CCW) roll engines for structural purposes (fig. 4.8-2). These aluminum plates will not be on prototype hardware. In all other respects, the housing was prototype hardware. A one-quarter inch thickness of cork insulation was bonded to the outer surface of the housing for thermal protection. The engine-supporting bracket was fabricated from 6061T6 aluminum and was a prototype item. The chambers¹ were fabricated from L-605 cobalt base stellite superalloy and consisted of a cylindrical combustion chamber and a nozzle which were welded together at an expansion area ratio (A_e/A_t) of approximately 7.7. The combustion chambers had a characteristic length (L^*) of 8.5 inches. All four engines were identical. The chamber differed from the prototype chamber in several respects as listed in table 4.8-I. The two chambers are compared visually in figure 4.8-4. The injector heads were fabricated from aluminum. The design of the BP-15 spacecraft engine injector head differed substantially from that of a prototype injector head because of the necessity for passing the instrumentation leads through it. Although the design was "boilerplate", the thermal capacitance and the heat-transmission characteristics of the BP-15 spacecraft injector heads

¹The chamber is defined as that portion of the engine in which the propellants react and high-temperature gas flow occurs. The chamber consists of a combustion chamber, throat, and nozzle (fig. 4.8-2). An engine consists of the chamber and its associated injector head and valves.

~~CONFIDENTIAL~~

~~CONFIDENTIAL~~

were essentially the same as for a prototype injector head. Propellant valves and lines were not installed for this flight. The engine was mounted to the quad housing at the injector head so that there was no direct contact between the chamber and the housing. A 0.060-inch-thick phenolic-fiberglass laminate insulating washer reduced thermal conduction between the injector head and the housing. The method of mounting, shown schematically in figure 4.8-5, is identical for prototype hardware.

Quads B, C, and D were dummy assemblies. The engines consisted of solid 4140 stainless steel combustion chambers and throats which were overwrapped with a phenolic-fiberglass laminate. The laminate extended to form the nozzle as shown in figure 4.8-6. These dummy engines were heavier than the Quad A engines, but were similar in aerodynamic configuration and were of the same configuration as those flown on the BP-13 spacecraft. The quad housings were fabricated from 0.160-inch-thick 4130 stainless steel.

Instrumentation.- The RCS instrumentation for the BP-15 spacecraft consisted of 16 temperature sensors mounted on the positive pitch (+P), CCW roll, and negative pitch (-P) engines, and on the housing structure, as shown in figures 4.8-7 to 4.8-9. Two accelerometers were mounted in the CW roll engine nozzle (fig. 4.8-8). The +P, CCW, and -P engines had temperature sensors located on the nozzle, engine flange, injector head, and on the housing immediately below the engine. The +P and CCW engines also have temperature sensors mounted in the combustion chamber just upstream of the throat. A temperature sensor was mounted on the underside of the quad housing roof and on the engine-supporting bracket. The temperature sensors on the injector heads and on the engine supporting bracket were resistance thermometers. The other temperature sensors were Chromel-Alumel thermocouples contained in a $\frac{1}{8}$ -inch-thick columbium sheathed case with internal insulation of magnesium oxide. The thermocouples were mechanically clamped to the chambers and housing. There was no direct contact of the Chromel-Alumel thermocouple wires with the surface of the chambers or housings. The thermocouple mounting arrangement and details of the thermocouple design are shown in figure 4.8-10.

The two accelerometers were mounted in the CW engine nozzle perpendicular to the engine axis, as shown in figure 4.8-11. Vibration was measured both in the direction of spacecraft X-axis and in the direction of an axis approximately perpendicular to the spacecraft X-axis. Epoxy potting compound was added to secure the accelerometer cables to the CW engine nozzle.

RCS temperature.- Since no RCS temperature data from the BP-13 spacecraft mission or from wind-tunnel tests were available for comparison with BP-15 spacecraft data, a theoretical analysis was performed to

~~CONFIDENTIAL~~

~~CONFIDENTIAL~~

4-131

predict the maximum temperatures which would be attained on the BP-15 spacecraft RCS package. This analysis predicted maximum temperatures at the nozzle exit planes of the +P, CCW and -P engines of 2,180° F, 2,000° F, and 1,800° F, respectively, which occurred at T+154 seconds. The predicted values at the various sensor locations are listed and compared with measured values in table 4.8-II. The large discrepancies evident between predicted and actual values indicate either significant errors in the analytical approach used for the temperature predictions or invalid temperature data.

Examination of the temperature data indicates that 15 of the 16 temperature sensors functioned during the mission. The thermocouple located 1 inch from the exit plane of the +P engine nozzle (measurement SR5877T) did not function, and no data were obtained for that location.

The time-temperature data from the 15 functioning sensors are shown in figures 4.8-12 to 4.8-14, grouped by engine. The thermocouple data from the engine-supporting bracket and the underside of the quad-housing roof are shown individually in figures 4.8-15 and 4.8-16. The data are plotted as a 5-point average of the individual data points.

After an initial temperature drop resulting from aerodynamic cooling, the temperature of the +P engine began to increase at T+40 seconds. Maximum temperatures of 603° F and 745° F, as shown in figure 4.8-12, were reached at the +P engine throat and flange, respectively, at approximately T+132 seconds. Maximum temperatures of approximately 1,080° F and 830° F, occurring at T+154 seconds, were predicted for the throat and flange. The +P engine injector head, which was the hottest of the three injector heads monitored, reached a maximum temperature of 159° F at T+850 seconds. This is well below the predicted value of 360° F.

The CCW engine temperature data, figure 4.8-13, also show an initial drop, with temperature rise beginning at T+40 seconds, similar to that of the positive P engine. A maximum temperature of 775° F was reached 1.3 inches from the nozzle exit plane of the CCW engine at T+150 seconds. This was the highest temperature recorded by any of the sensors during the flight, but is considerably less than the predicted value of 1,865° F. The CCW engine throat temperature reached a maximum value of approximately 360° F at T+160 seconds, as compared with a predicted value of 1,300° F occurring at T+154 seconds. The CCW engine injector head reached a maximum temperature of 142° F at T+525 seconds and stabilized at that point, well below the predicted value of 382° F.

The temperatures attained on the -P engine were far below predicted values (see table 4.8-II), the highest temperature recorded for this engine being 205° F on the nozzle occurring at T+200 seconds. The -P engine injector head reached a temperature of approximately 116° F at T+850 seconds and was still increasing slowly at that point.

~~CONFIDENTIAL~~

CONFIDENTIAL

The capability of the quad housing and supporting bracket to modulate the injector head temperatures by permitting the heat to diffuse throughout the structure is illustrated by the relative insensitivity of injector head temperature to engine flange temperature. Although flange temperatures varied from a maximum of 745° F on the +P engine to a maximum of 122° F on the -P engine, the three injector head temperatures remained within 50° F of one another through T+850 seconds. Data from the three injector heads and the engine-supporting bracket are shown in figure 4.8-17. These data indicate that by T+850 seconds, the +P and CCW engine injector heads had attained an equilibrium condition in which heat input from the chamber was equal to heat output to the housing and engine-supporting bracket. The engine-supporting bracket temperature was still increasing at T+850 seconds but was starting to peak at that point. The -P engine injector head was still increasing in a linear manner at T+850 seconds resulting from heat input from both the engine-supporting bracket and the -P chamber. The temperatures of the +P, CCW, and -P engine housings, and of the quad-housing roof are shown in figure 4.8-18. The maximum temperature difference between these four sensors was 55° F during the high-heating period of launch; and at T+850 seconds, the four sensors were within 25° F of one another, indicating the capability of the structure to distribute the heat input from the chambers.

Because of the discrepancies between predicted and measured temperatures, a substantial amount of additional analysis will be required to evaluate further the instrumentation and the analytical approach in order to relate the data from the BP-15 spacecraft flight to temperatures which will occur on later flights with prototype and qualified hardware. The results of the additional analysis will be given in a supplemental report. Substitution of prototype hardware is expected to result in increased nozzle temperatures since the thinner L-605 nozzle wall of the prototype engine will have a lower thermal capacitance and an increased thermal resistance to heat conduction down and circumferentially around the nozzle. The aluminum injector head temperatures will also be higher on prototype engines since the thermal conductivity of the molybdenum combustion chamber is approximately nine times greater than that of the L-605 combustion chamber of BP-15 spacecraft, thus facilitating greater heat conduction into the injector head from the chamber. The resultant prototype injector head temperature increase will be tempered by the addition of the propellant valves to the injector, which adds thermal capacitance to the injector. The magnitude of these temperature increases has not been established at this time.

RCS vibration.- The RMS time histories from the two accelerometers mounted in the CW engine nozzle are shown in figure 4.8-19 for the X-axis and in figure 4.8-20 for the perpendicular axis. Vibration response began to increase at T+20 seconds, reaching 40g RMS at T+44 seconds in the

CONFIDENTIAL

~~CONFIDENTIAL~~

X-axis, and reaching 51g RMS at T+49 seconds in the perpendicular axis. A sudden decrease in g levels was experienced during the period of T+49 to T+54 seconds. The RMS vibration level then increased to a maximum of 47g in the X-axis at T+70 seconds, approximately 45g in the perpendicular axis at T+63 and T+68 seconds. The vibration level decreased following maximum dynamic pressure, and neither sensor indicated an output beyond T+120 seconds. The vibration data obtained were above the design limit. Power-spectral-density plots for a 2-second time period between T+48 and T+50 seconds for the X-axis and perpendicular axis are shown in figures 4.8-21 and 4.8-22. Most of the power in both axes was concentrated around 190 cps, at which frequency peaks of 100 to 115 g^2/cps occurred. Further analysis is required to relate these data to values which can be expected with prototype hardware. For additional analysis in the report refer to section 4.7.

~~CONFIDENTIAL~~

~~CONFIDENTIAL~~

TABLE 4.8-I.- COMPARISON OF BP-15 SPACECRAFT INSTRUMENTED
RCS CHAMBER WITH PROTOTYPE RCS CHAMBER

	BP-15 spacecraft RCS chamber	Prototype RCS chamber
Material	L-605 superalloy	Molybdenum and L-605 superalloy (see fig. 4.8-4)
Overall length, in.	9.359	9.984
Combustion chamber length, in.	2.375	3.000
Characteristic length, L^* , in.	8.5	11.5
Combustion chamber wall thickness, in.	uniform 0.090	Varies between 0.064 minimum and 0.187 maximum (see fig. 4.8-4)
Throat wall thickness, in.	0.130	0.161
Nozzle wall thickness beyond $A_e/A_t = 15$, in.	Varies from 0.041 to 0.030	0.012

~~CONFIDENTIAL~~

~~CONFIDENTIAL~~

4-135

TABLE 4.8-II.- COMPARISON OF CALCULATED AND RECORDED MAXIMUM TEMPERATURES.
SERVICE MODULE RCS QUAD A. BP-15 SPACECRAFT.

Measurement (a)	Maximum preflight calculated temperature, °F	Maximum mission A-102 (BP-15) measured temperature, °F
+P engine nozzle exit plane	2,180	(b)
+P engine nozzle	2,020	(c)
+P engine throat	1,080	603
+P engine flange	830	745
+P engine injector head	360	159
+P engine housing	(d)	143
Counterclockwise engine nozzle exit plane	2,000	(b)
Counterclockwise engine nozzle	1,865	775
Counterclockwise engine throat	1,300	360
Counterclockwise engine flange	1,060	230
Counterclockwise engine injector head	382	142
Counterclockwise engine housing	(d)	126
-P engine nozzle exit plane	1,800	(b)
-P engine nozzle	1,840	205
-P engine throat	1,180	(b)
-P engine flange	(d)	122
-P engine injector head	350	116
-P engine housing	(d)	107
Engine supporting bracket	(d)	142
Quad housing roof	(d)	122

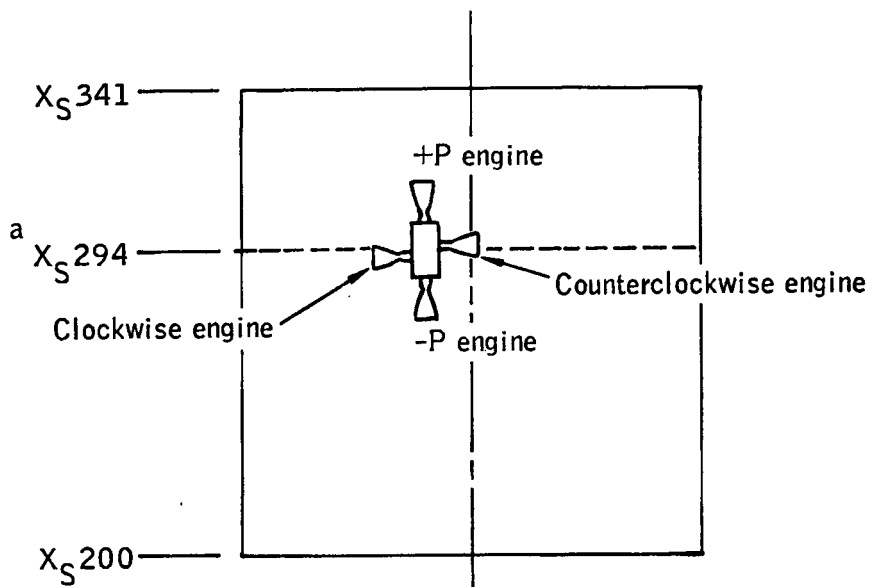
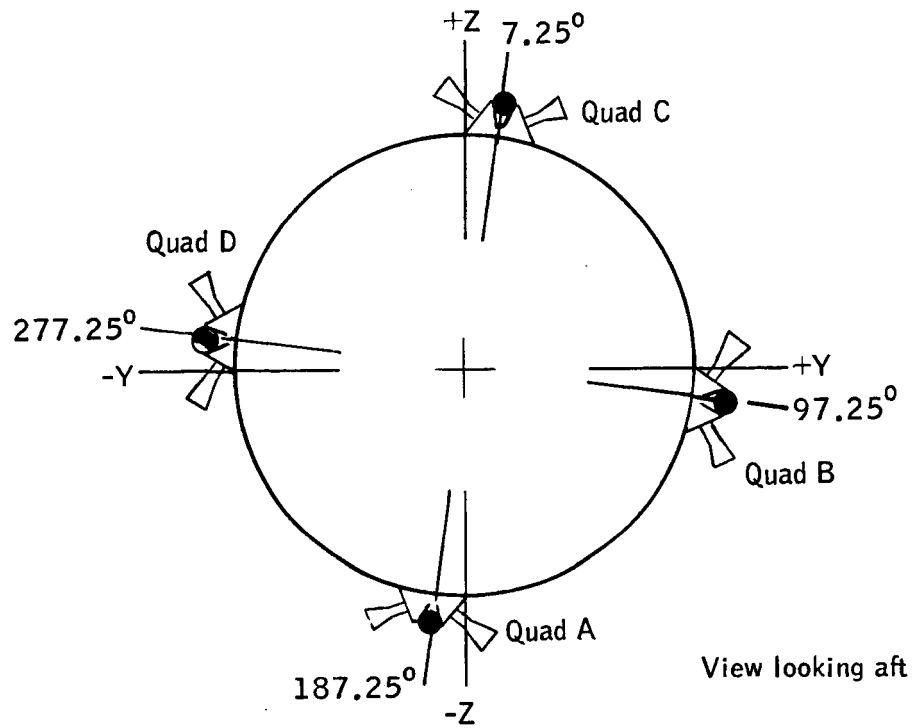
^a See figures 4.8-8 and 4.8-9 for measurement location

^b Not instrumented

^c Sensor inoperative

^d Not calculated

~~CONFIDENTIAL~~

~~CONFIDENTIAL~~

^a Centerline of RCS quads B, C, & D is at $X_S 292.9$

Figure 4.8-1.- Location for service module RCS quads on BP-15 spacecraft.

~~CONFIDENTIAL~~

~~CONFIDENTIAL~~

4-137

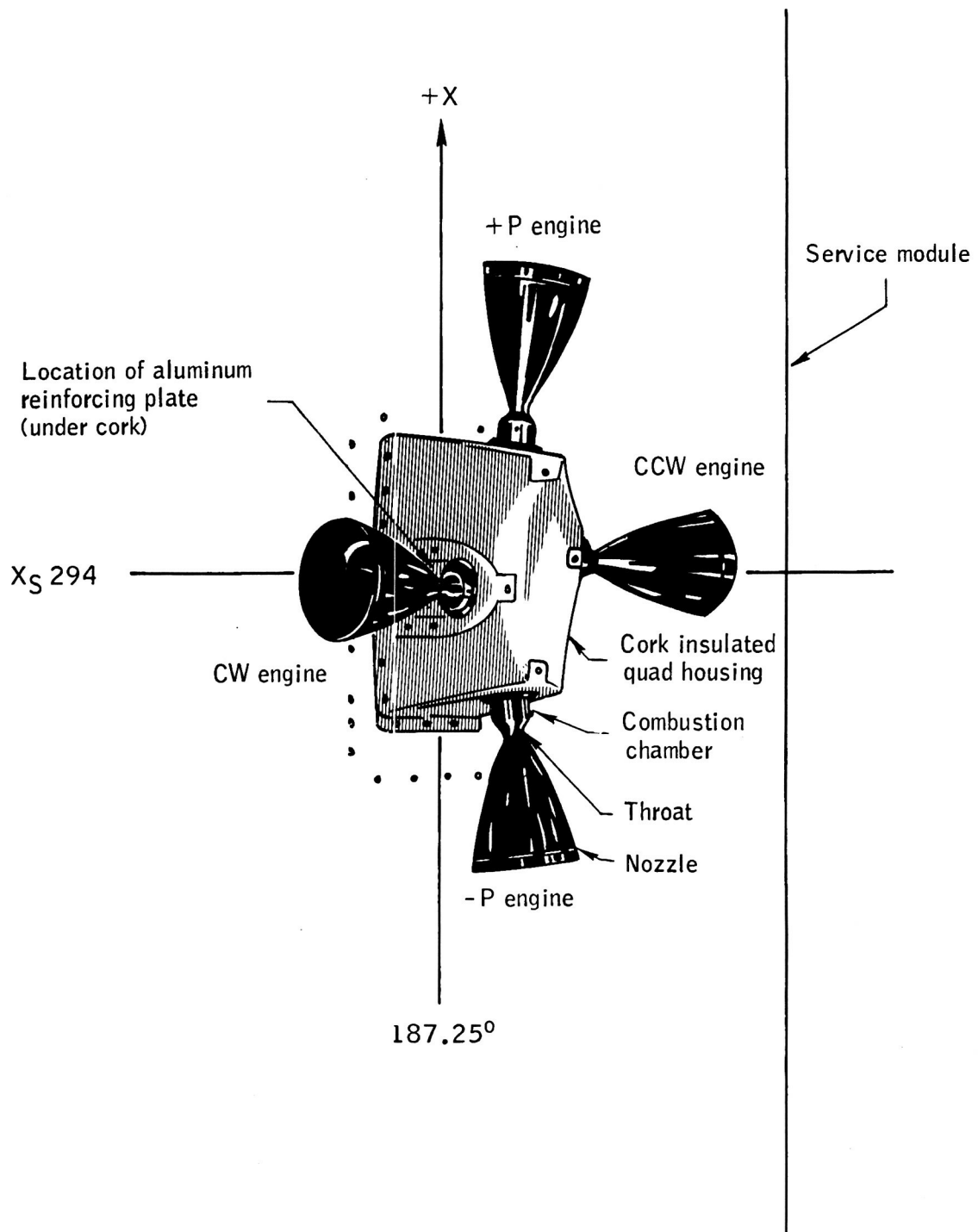


Figure 4.8-2.- Service module RCS quad A on BP-15 spacecraft.

~~CONFIDENTIAL~~

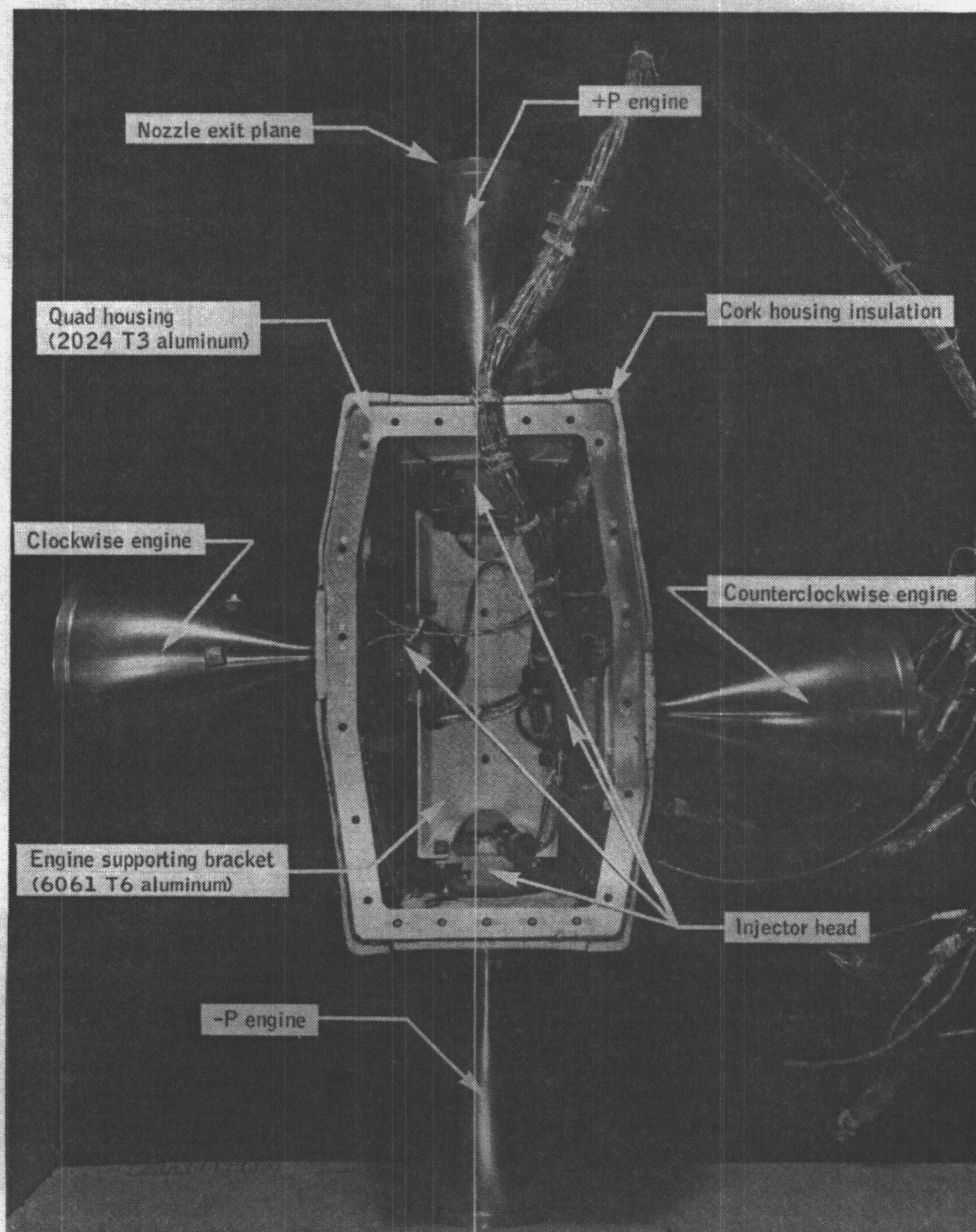
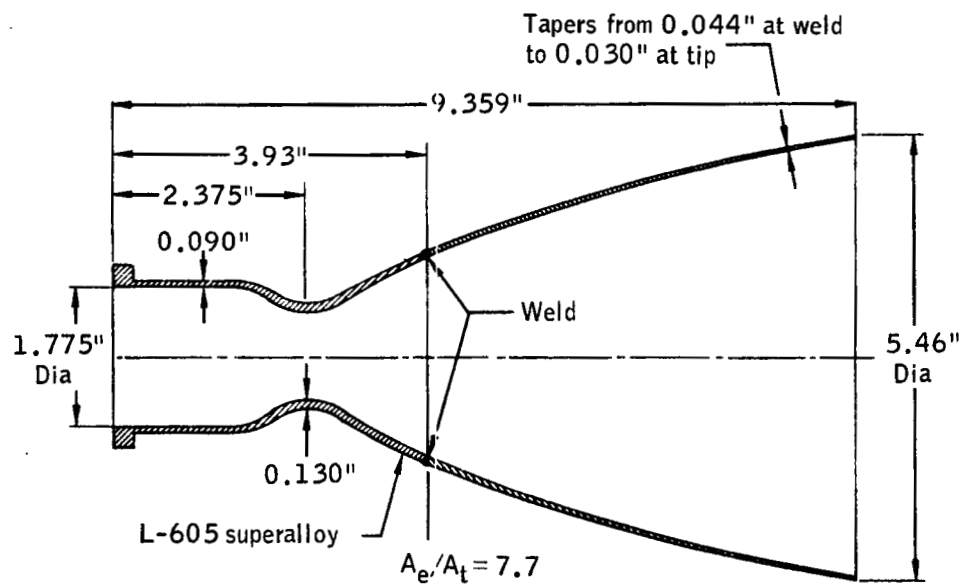
~~CONFIDENTIAL~~

Figure 4.8-3.- Interior view of service module RCS quad A for BP-15 spacecraft.

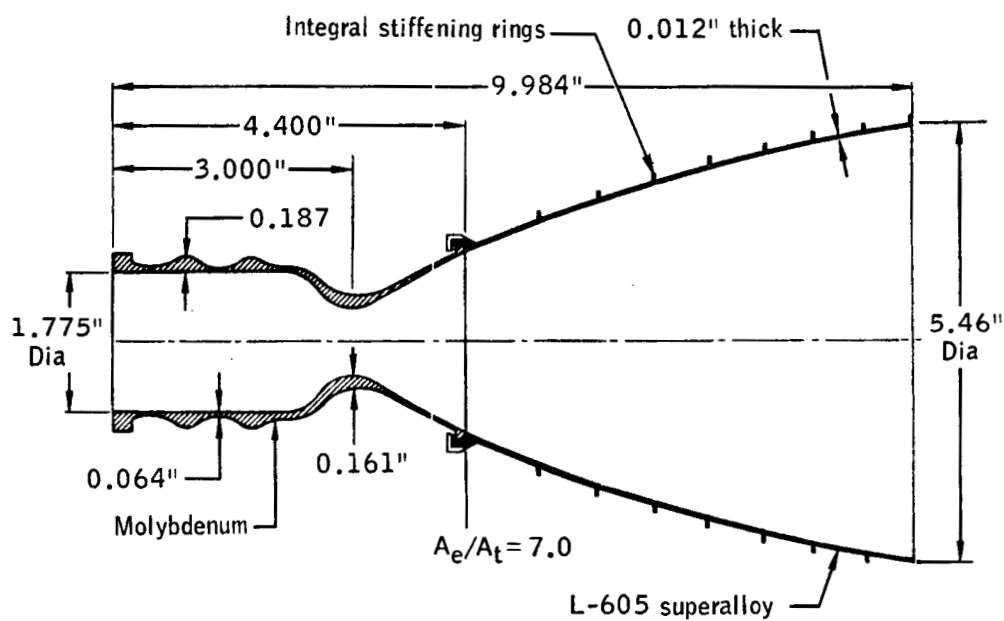
~~CONFIDENTIAL~~

~~CONFIDENTIAL~~

4-139



BP-15 RCS engine



Prototype RCS engine

Figure 4.8-4.- Spacecraft BP-15 quad A and prototype RCS chamber design.

~~CONFIDENTIAL~~

~~CONFIDENTIAL~~

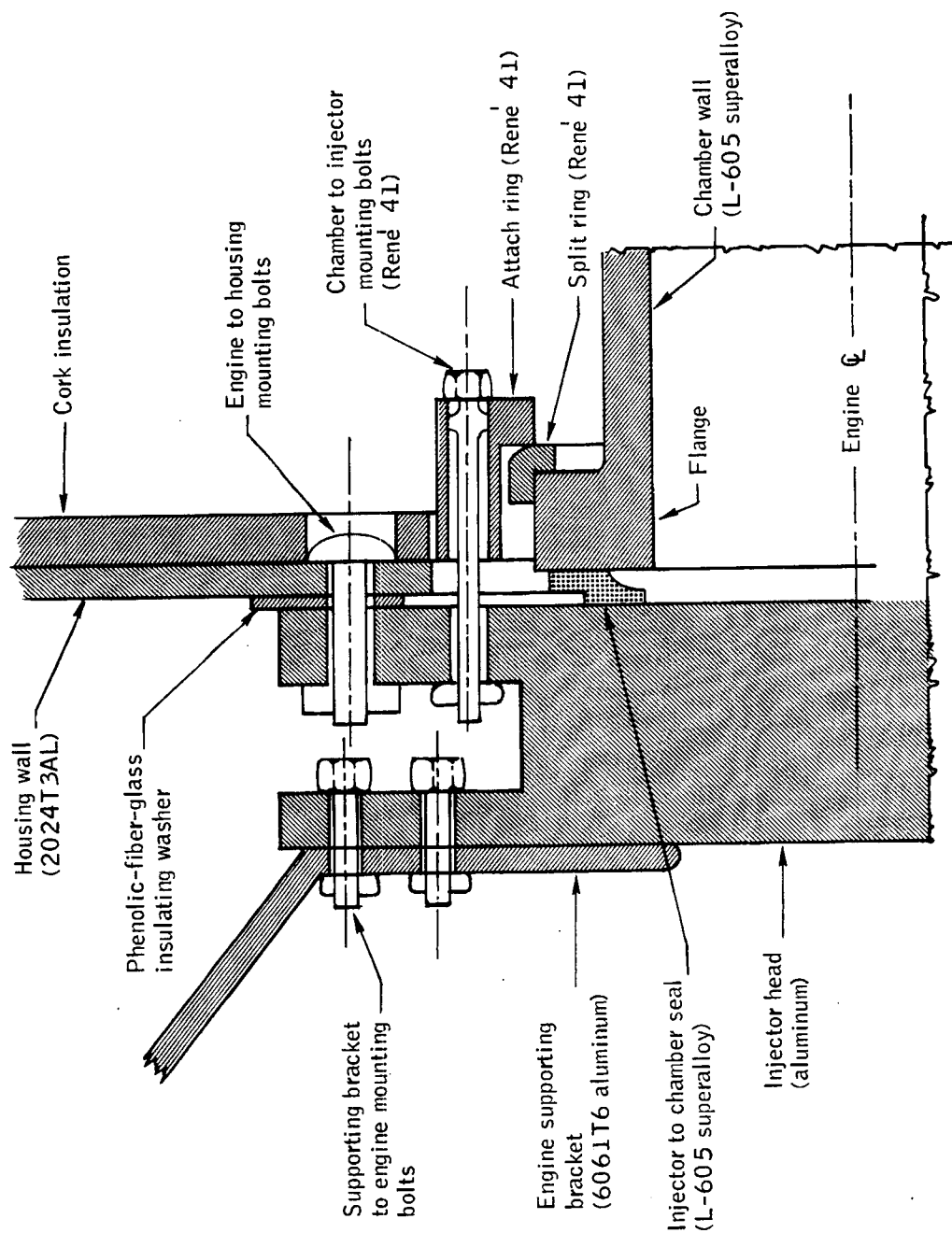
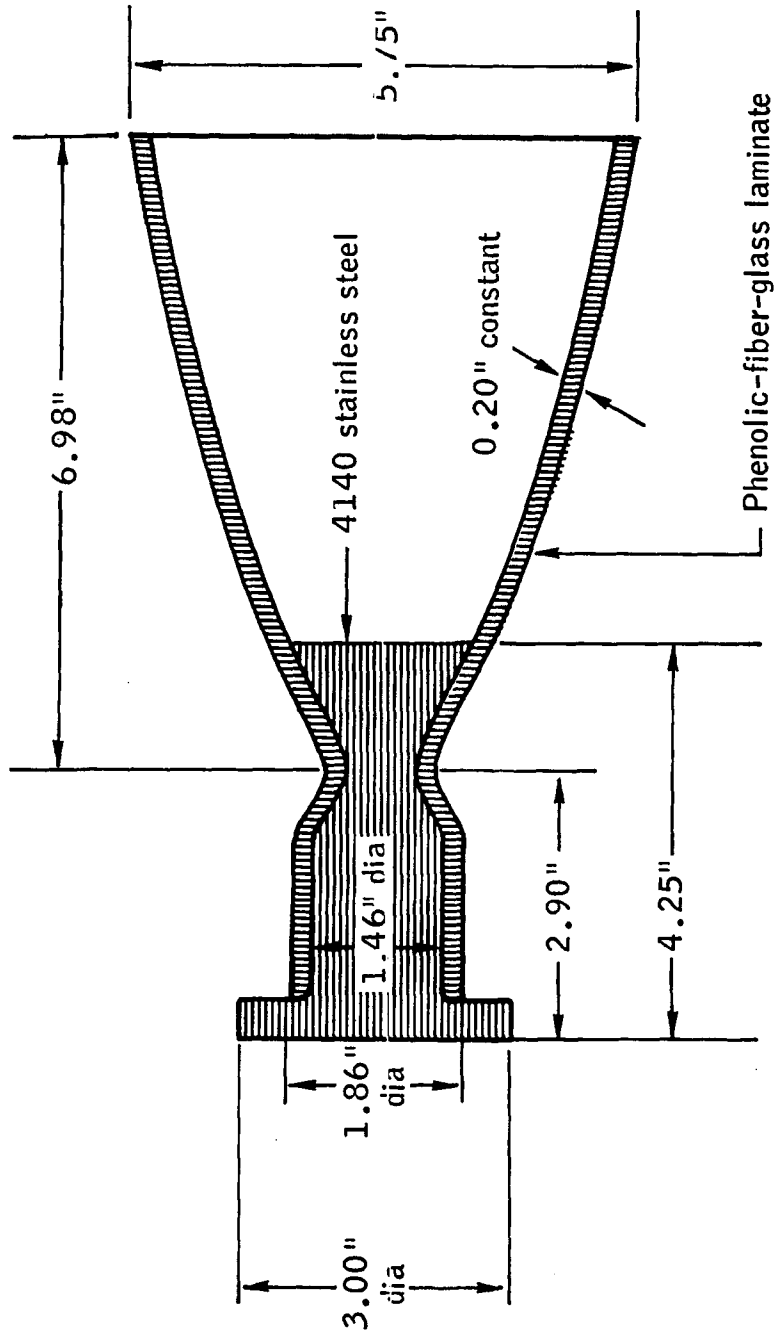


Figure 4.8-5.- Method of mounting service module RCS engine to quad housing and engine supporting bracket on BP-15 spacecraft.

~~CONFIDENTIAL~~

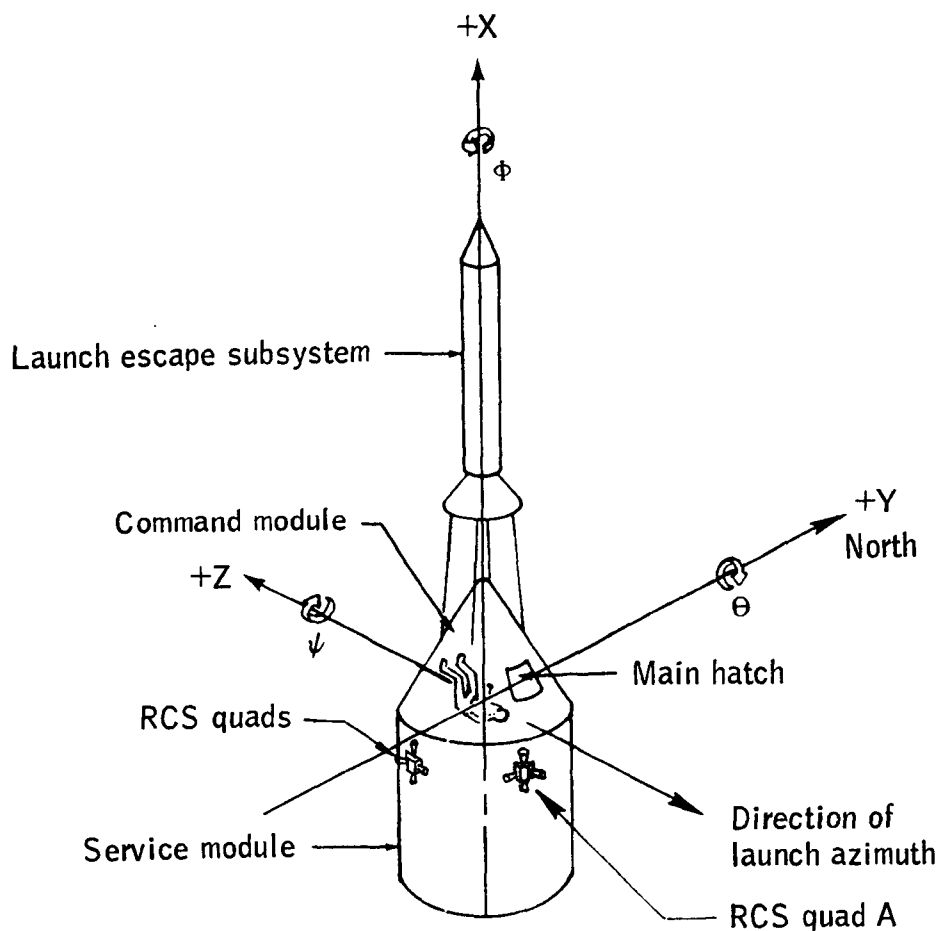
~~CONFIDENTIAL~~

4-141



~~CONFIDENTIAL~~

Figure 4.8-6.- Design of dummy service module RCS chambers used in quads B, C, D of BP-15 spacecraft.

~~UNCLASSIFIED~~

Direction	Axis	Moment	Positive direction	Spacecraft maneuver & symbol	Linear velocity	Angular velocity
Longitudinal	X	L	Y to Z	Roll ϕ	u	p
Lateral	Y	M	Z to X	Pitch θ	v	q
Vertical	Z	N	X to Y	Yaw ψ	w	r

Figure 4.8-7.- MSC coordinate axes and notation system for Apollo boilerplate and airframe, manned and unmanned spacecraft.

~~UNCLASSIFIED~~

~~CONFIDENTIAL~~

4-143

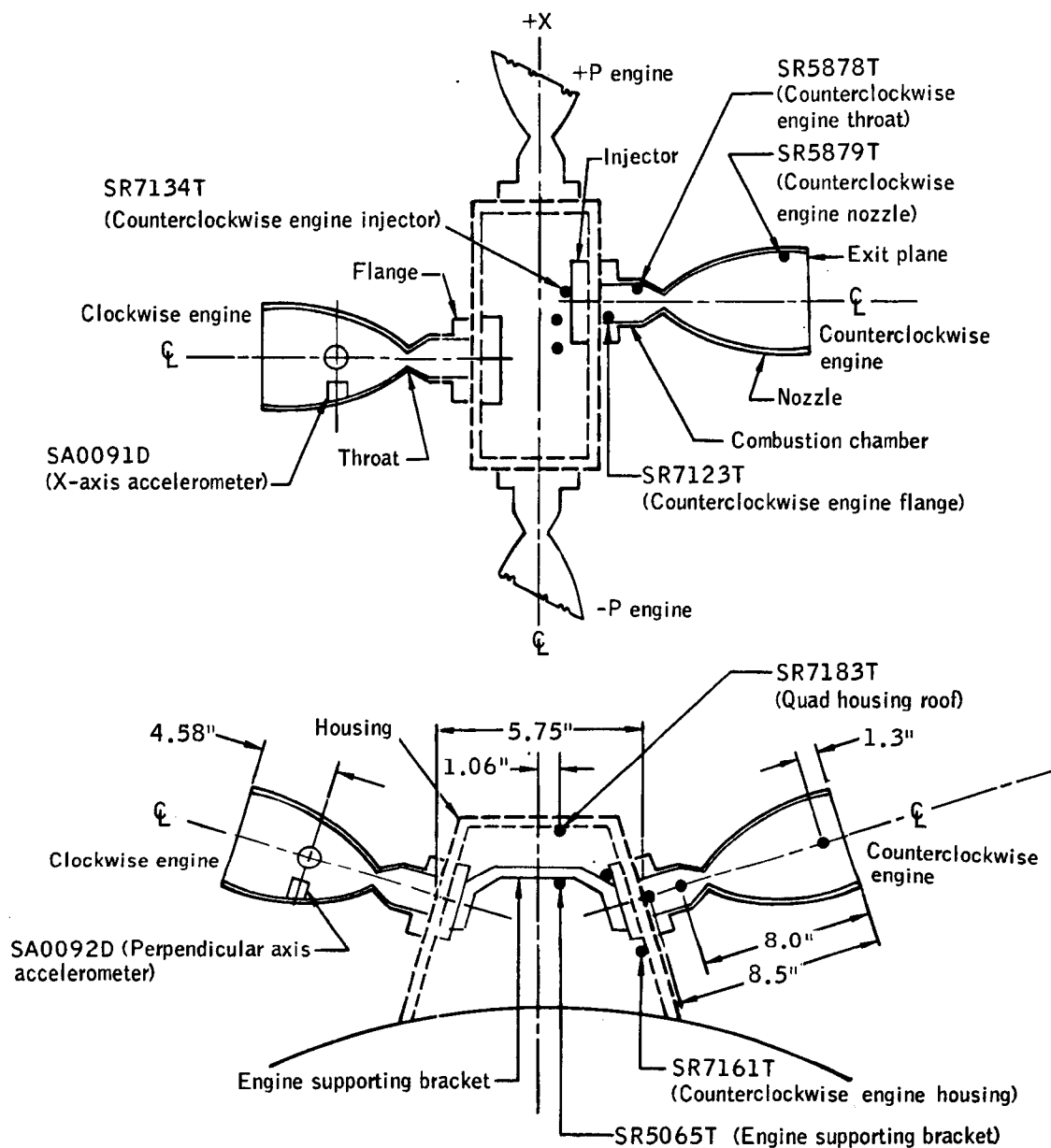


Figure 4.8-8.- Service module RCS package instrumentation locations for clockwise and counterclockwise roll engines, engine supporting bracket, and quad housing roof on BP-15 spacecraft.

~~CONFIDENTIAL~~

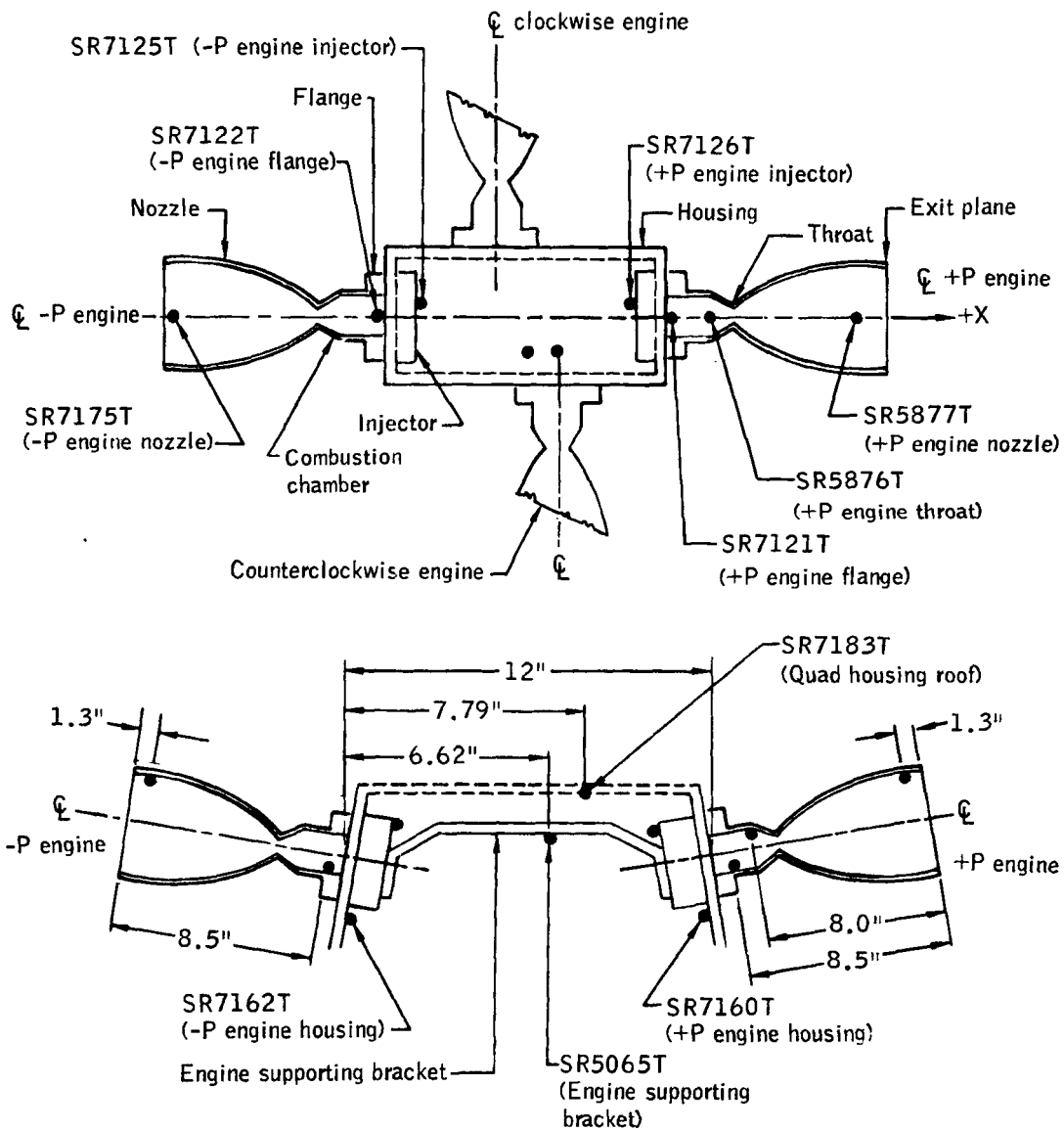
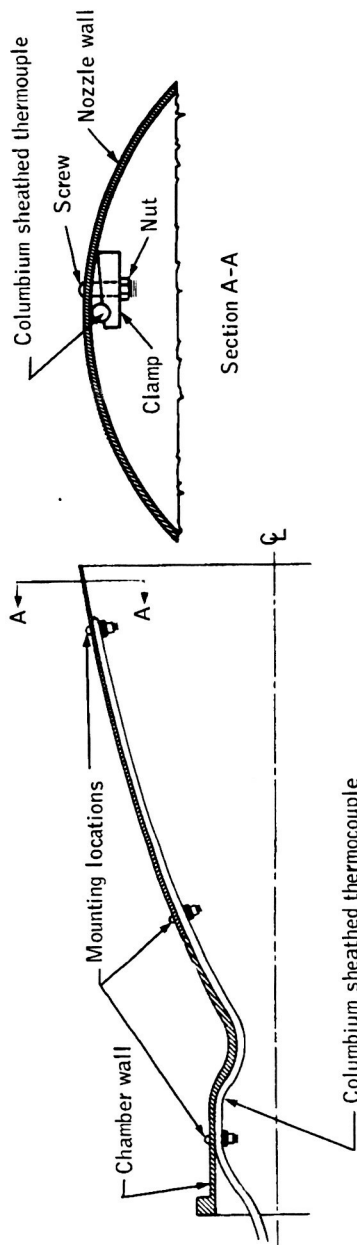
~~CONFIDENTIAL~~

Figure 4.8-9.- Service module RCS package instrumentation locations for +P and -P engines, engine supporting bracket, and quad housing roof on BP-15 spacecraft.

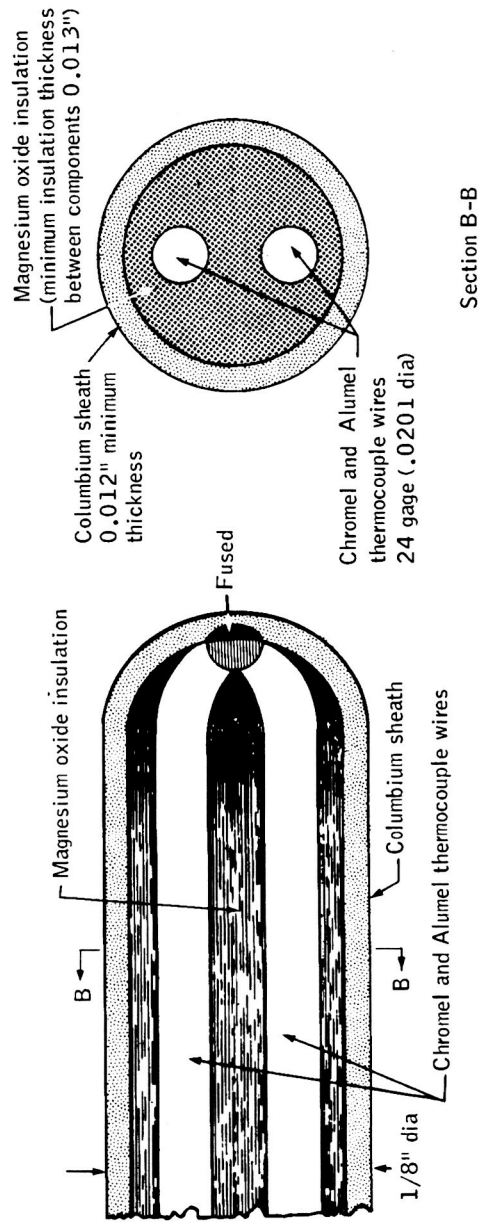
~~CONFIDENTIAL~~

~~CONFIDENTIAL~~

4-145



(a) Typical installation.



(b) Thermocouple design detail.

Figure 4.8-10.- Mounting of thermocouples on the service module RCS engines on BP-15 spacecraft.

~~CONFIDENTIAL~~

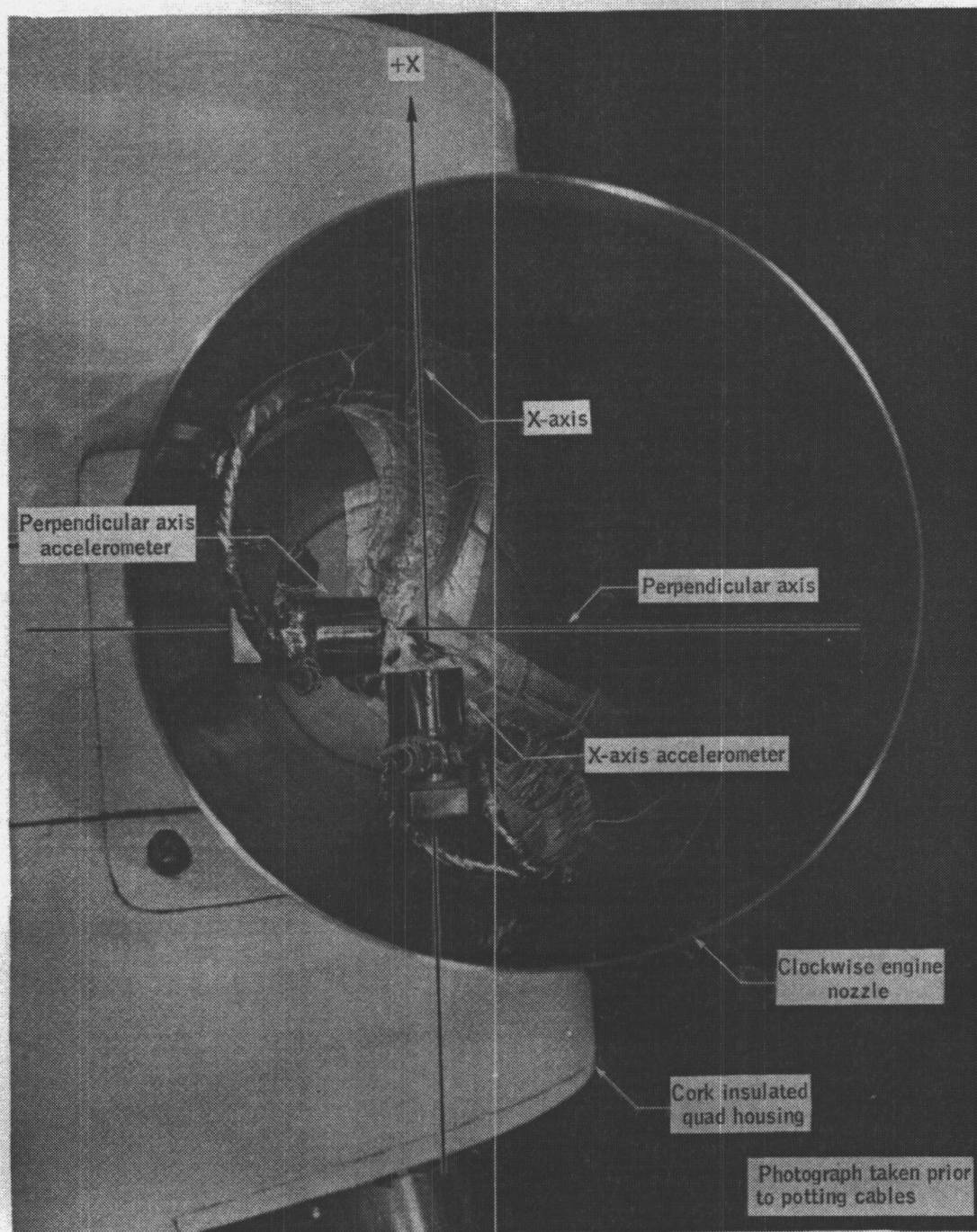
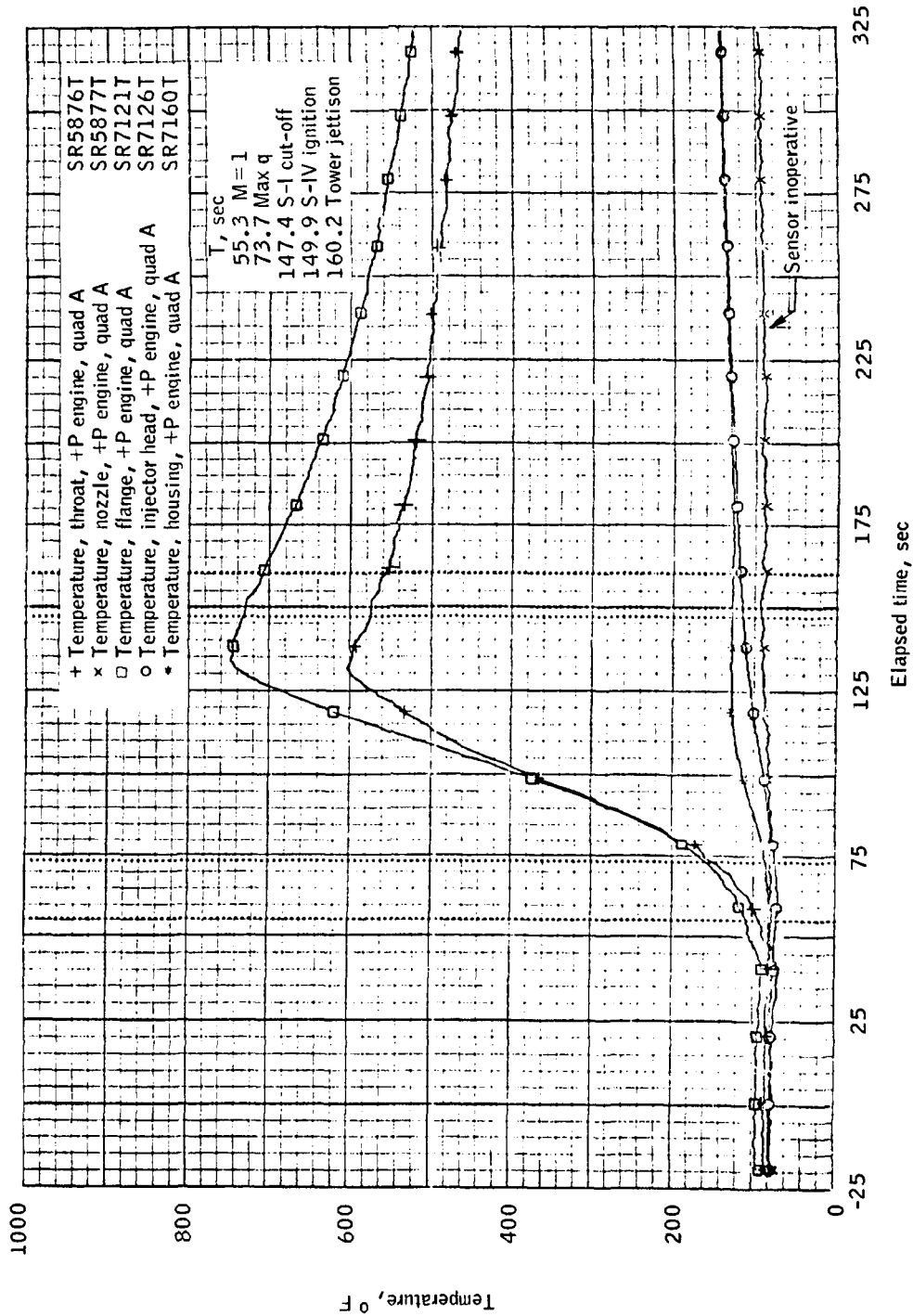
~~CONFIDENTIAL~~

Figure 4.8-11.- Service module RCS accelerometers mounted in the clockwise engine nozzle on BP-15 spacecraft.

~~CONFIDENTIAL~~

~~CONFIDENTIAL~~

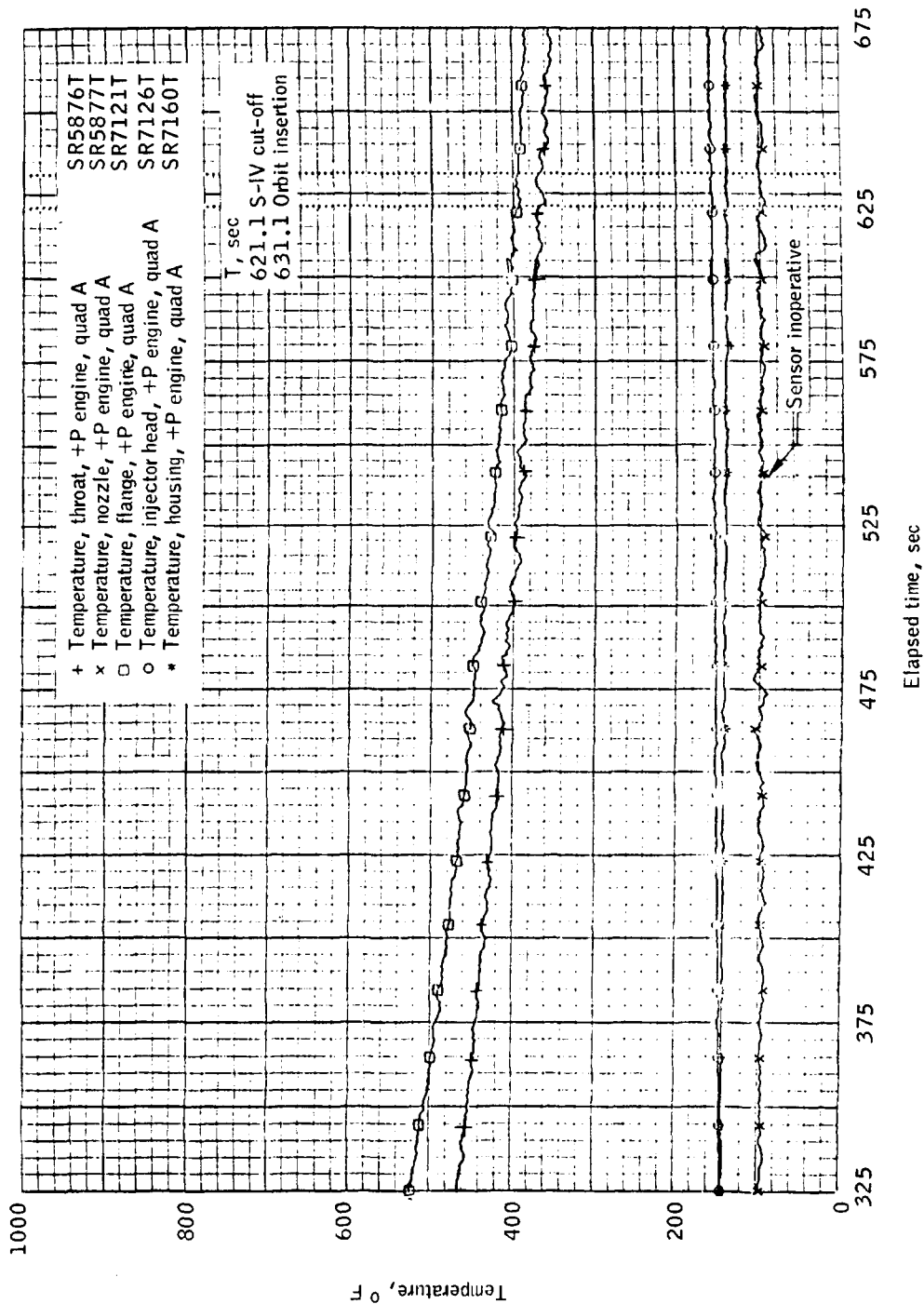
4-147



(a) -25 to 325 seconds.

Figure 4.8-12. - Temperatures measured on the positive pitch engine and housing of the service module RCS quad A of the BP-15 spacecraft.

~~CONFIDENTIAL~~

~~CONFIDENTIAL~~

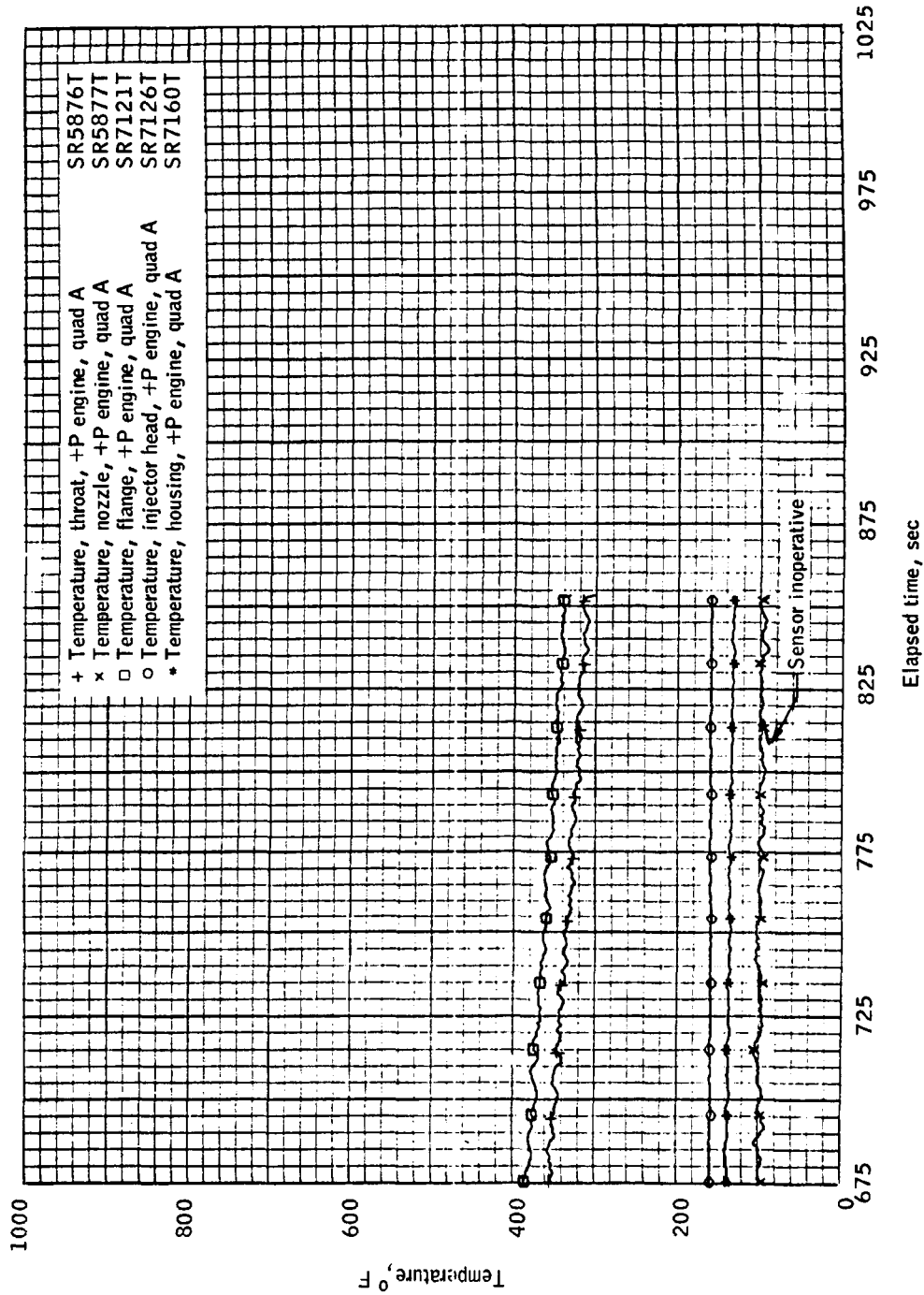
(b) 325 to 675 seconds.

Figure 4.8 12.- Continued.

~~CONFIDENTIAL~~

~~CONFIDENTIAL~~

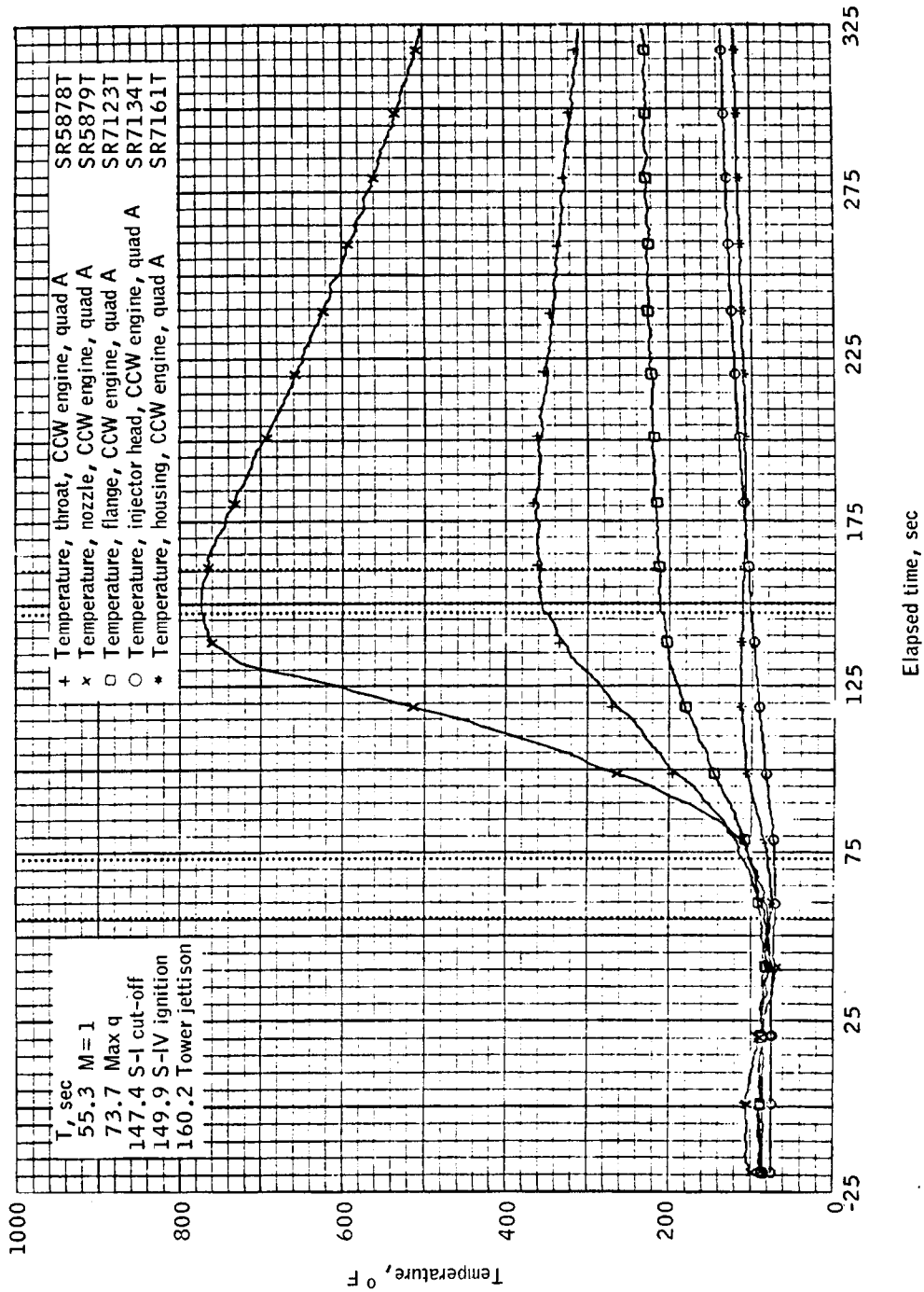
4-149



(c) 675 to 850 seconds.

Figure 4.8-12.- Concluded.

~~CONFIDENTIAL~~

~~CONFIDENTIAL~~

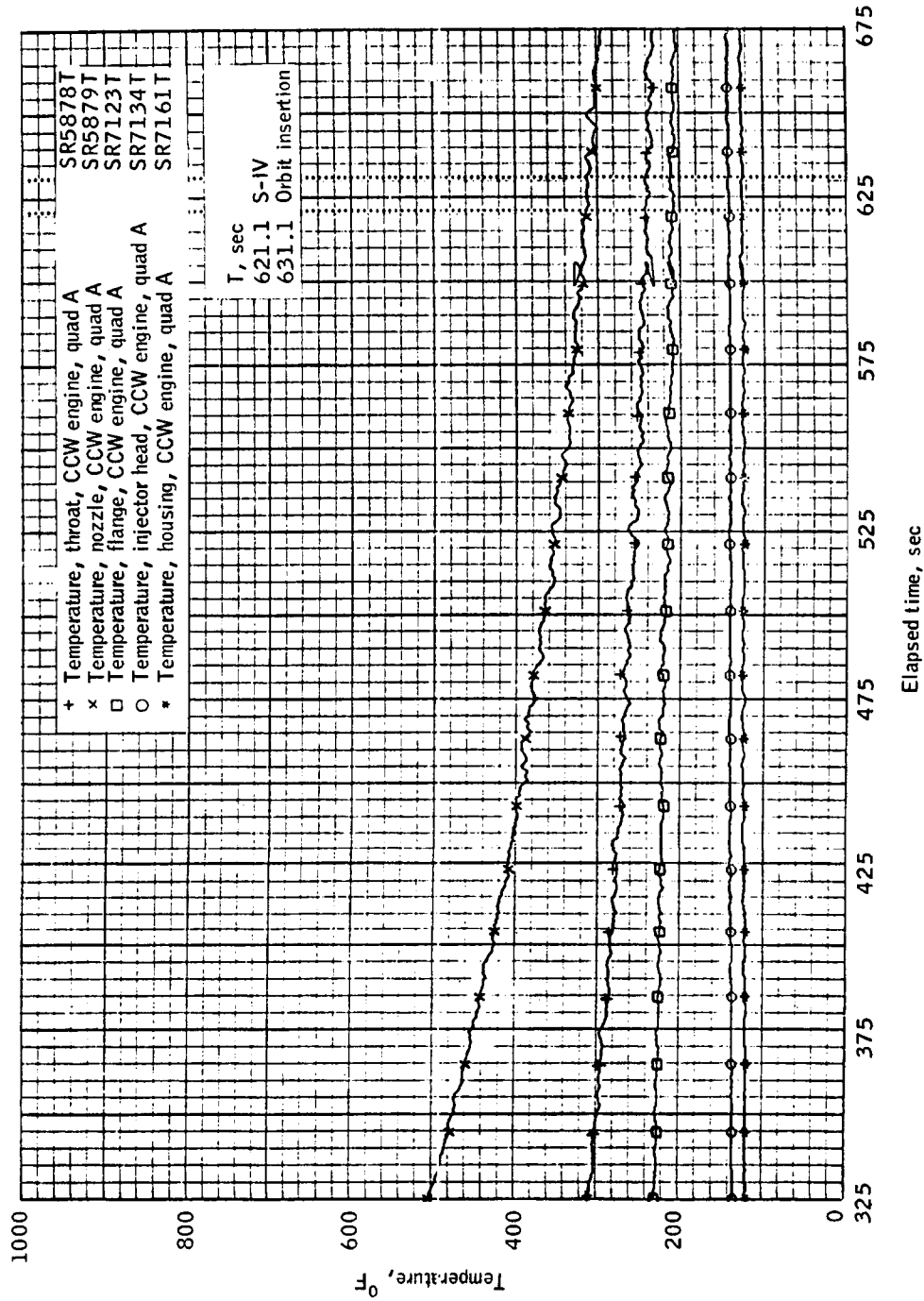
(a) -25 to 325 seconds.

Figure 4.8-13.- Temperatures measured on the counterclockwise roll engine and housing of the service module RCS quad A of the BP-15 spacecraft.

~~CONFIDENTIAL~~

~~CONFIDENTIAL~~

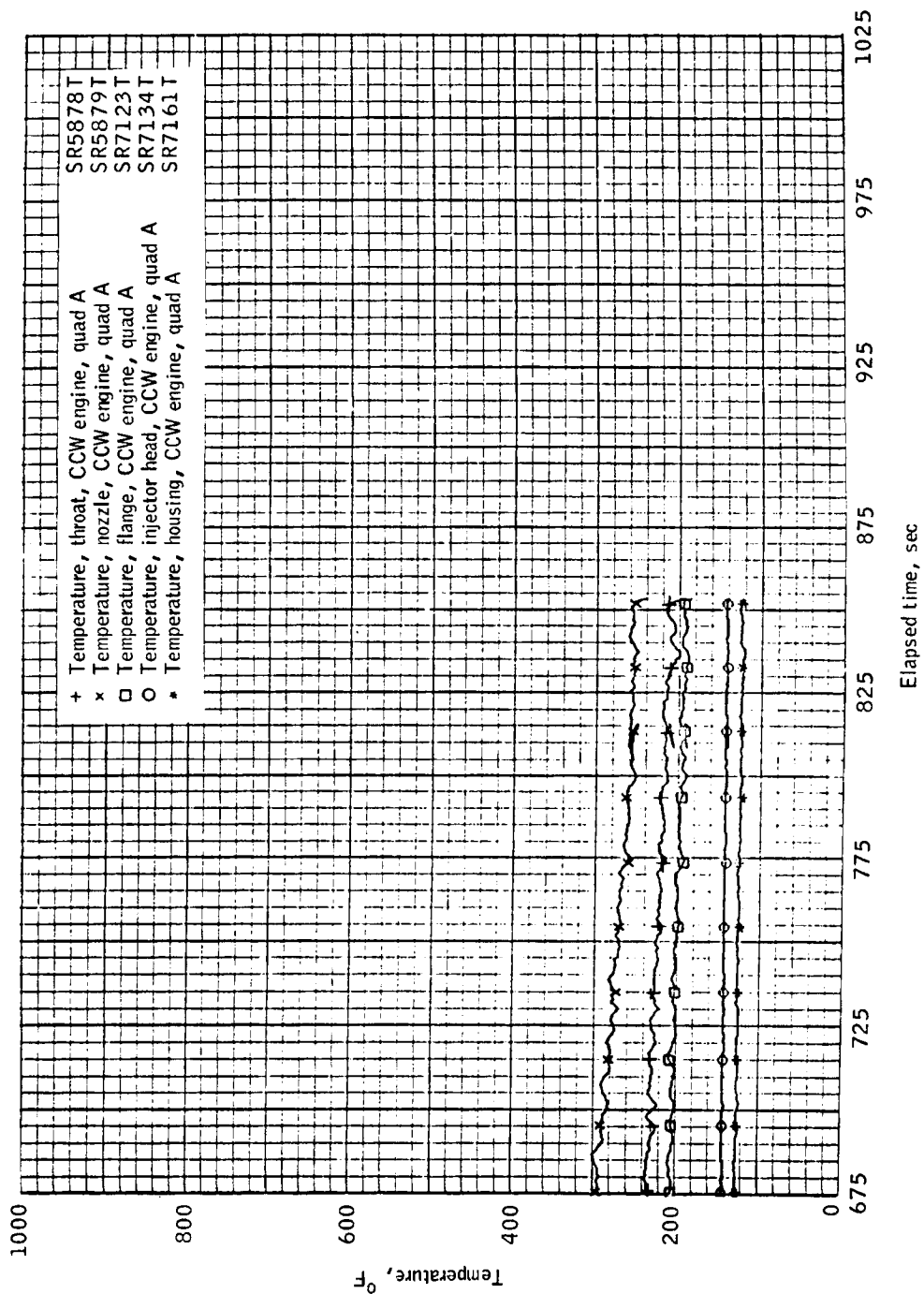
4-151



(b) 325 to 675 seconds.

Figure 4.8-13.- Continued.

~~CONFIDENTIAL~~

~~CONFIDENTIAL~~

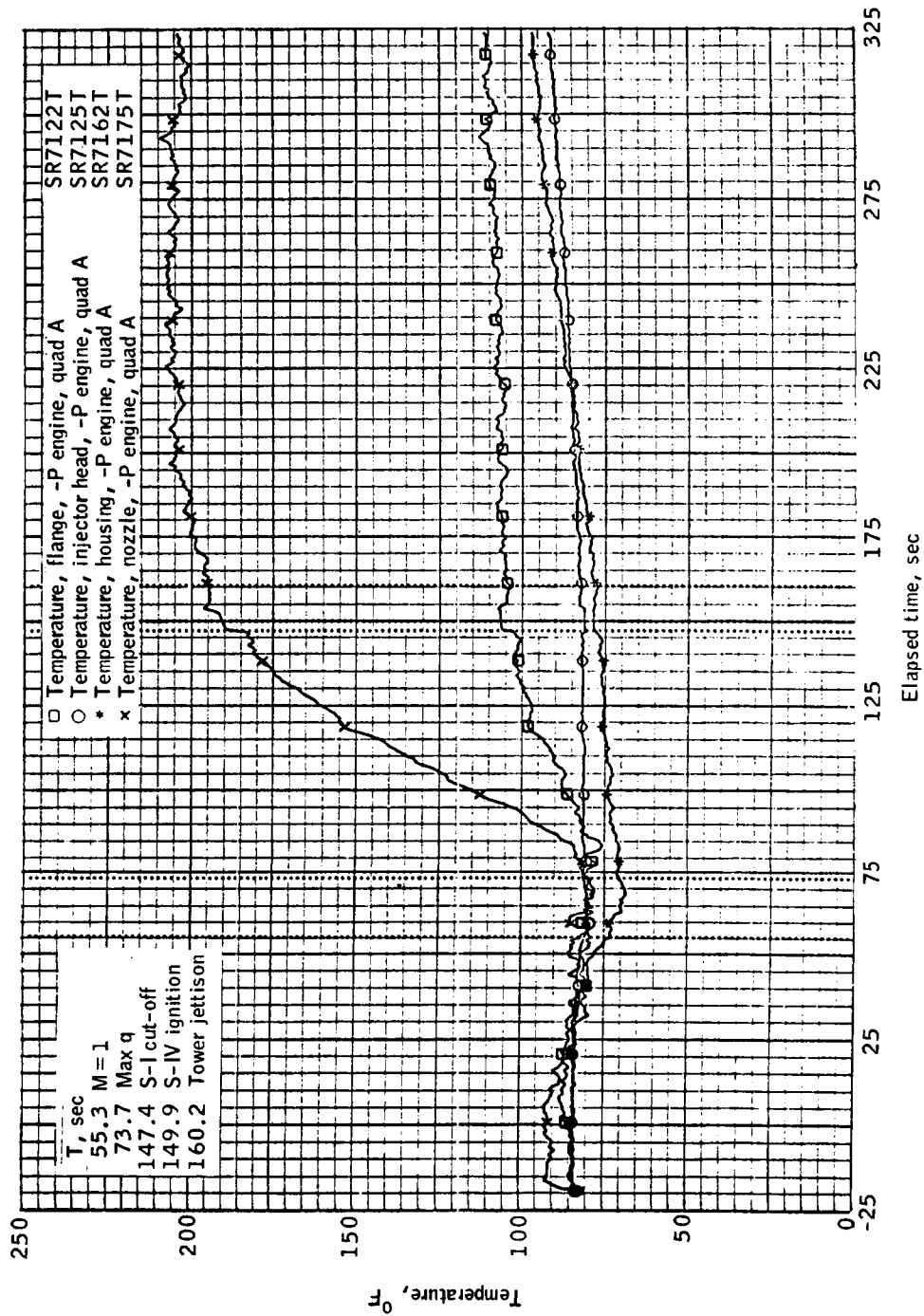
(c) 675 to 850 seconds.

Figure 4.8-13.- Concluded.

~~CONFIDENTIAL~~

~~CONFIDENTIAL~~

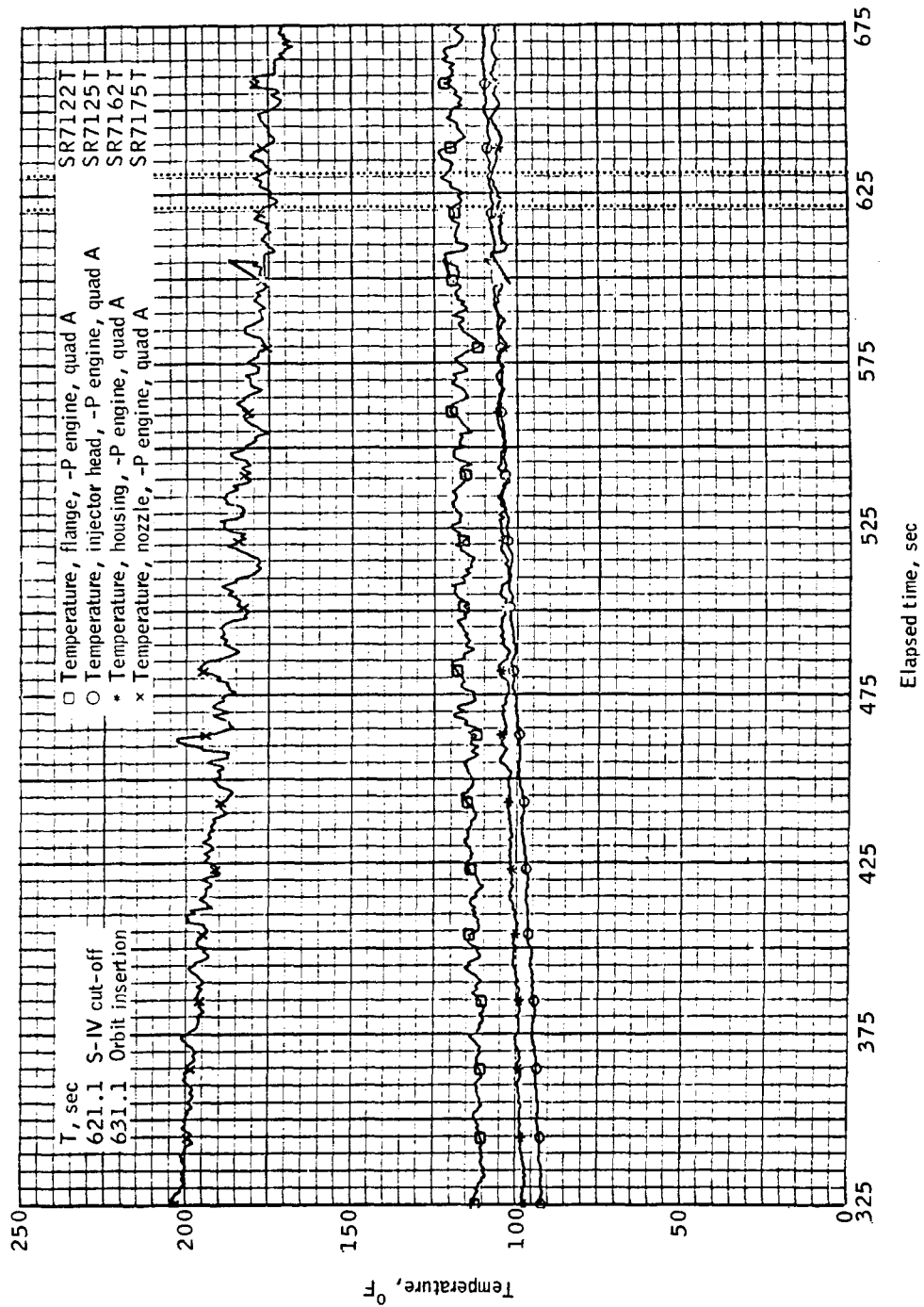
4-153



(a) -25 to 325 seconds.

Figure 4.8-14.- Temperatures measured on the negative pitch engine and housing of the service module RCS quad A of the BP-15 spacecraft.

~~CONFIDENTIAL~~

~~CONFIDENTIAL~~

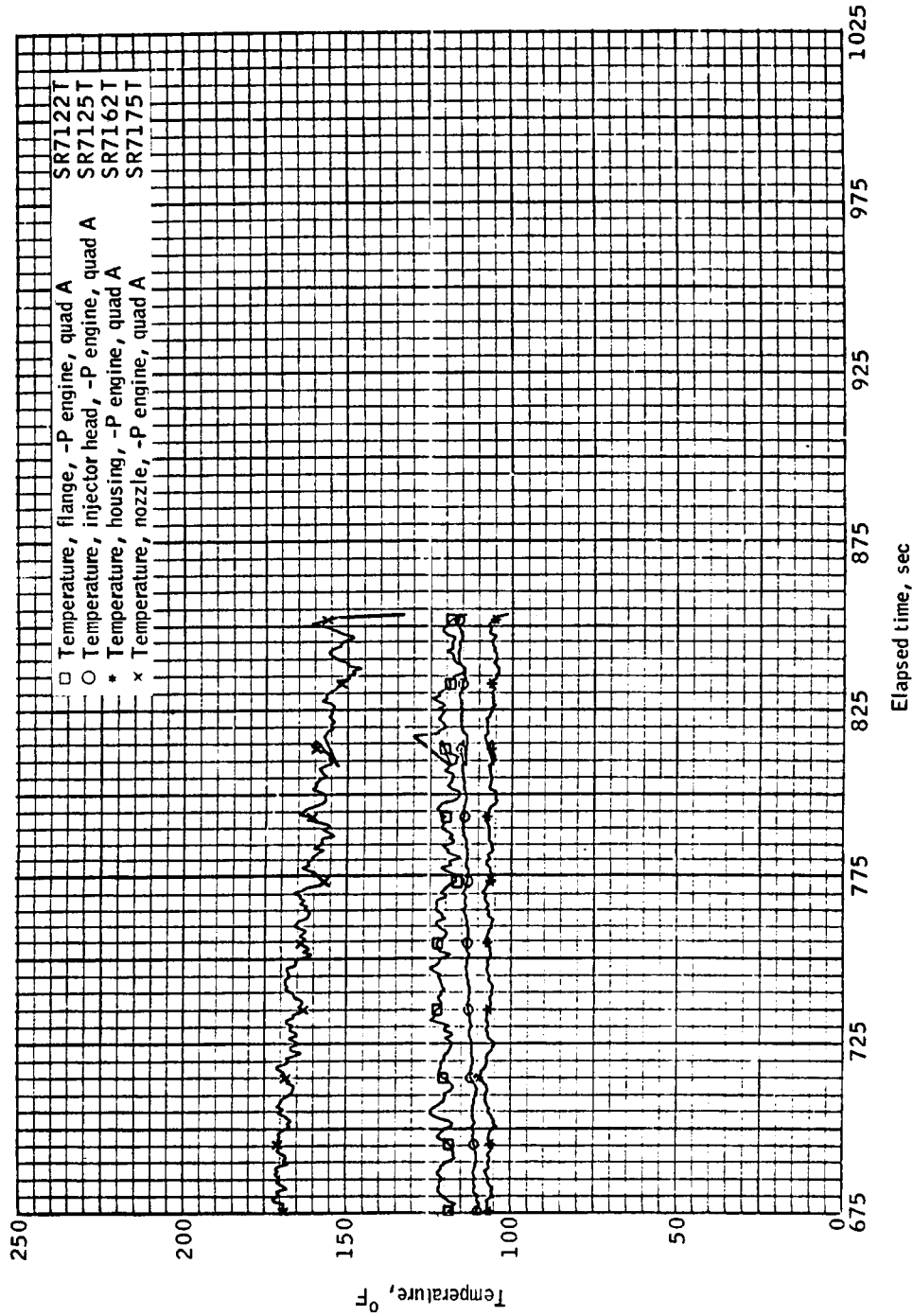
(b) 325 to 675 seconds.

Figure 4.8-14. - Continued.

~~CONFIDENTIAL~~

~~CONFIDENTIAL~~

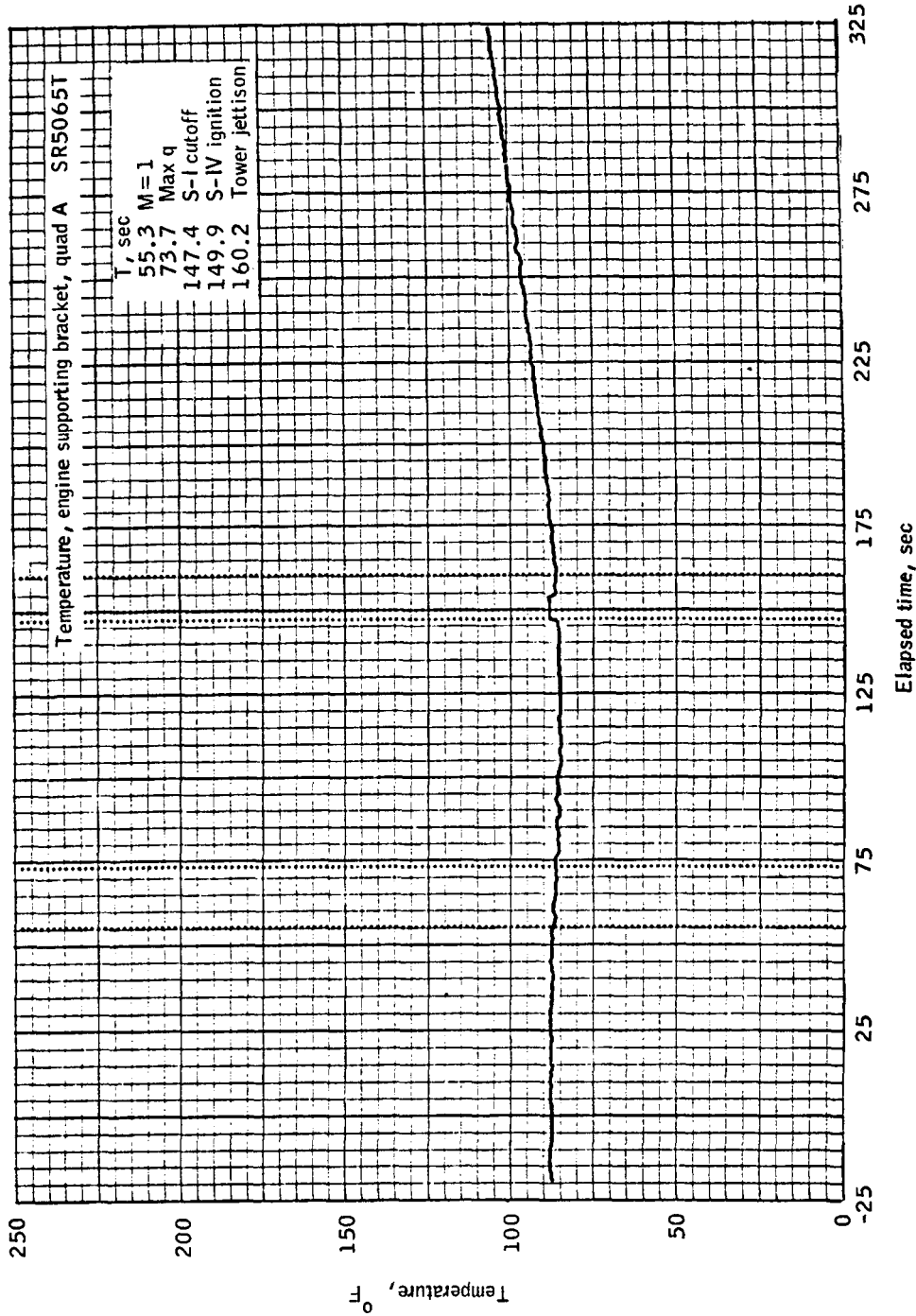
4-155



(c) 675 to 850 seconds.

Figure 4.8-14.- Concluded.

~~CONFIDENTIAL~~

~~CONFIDENTIAL~~

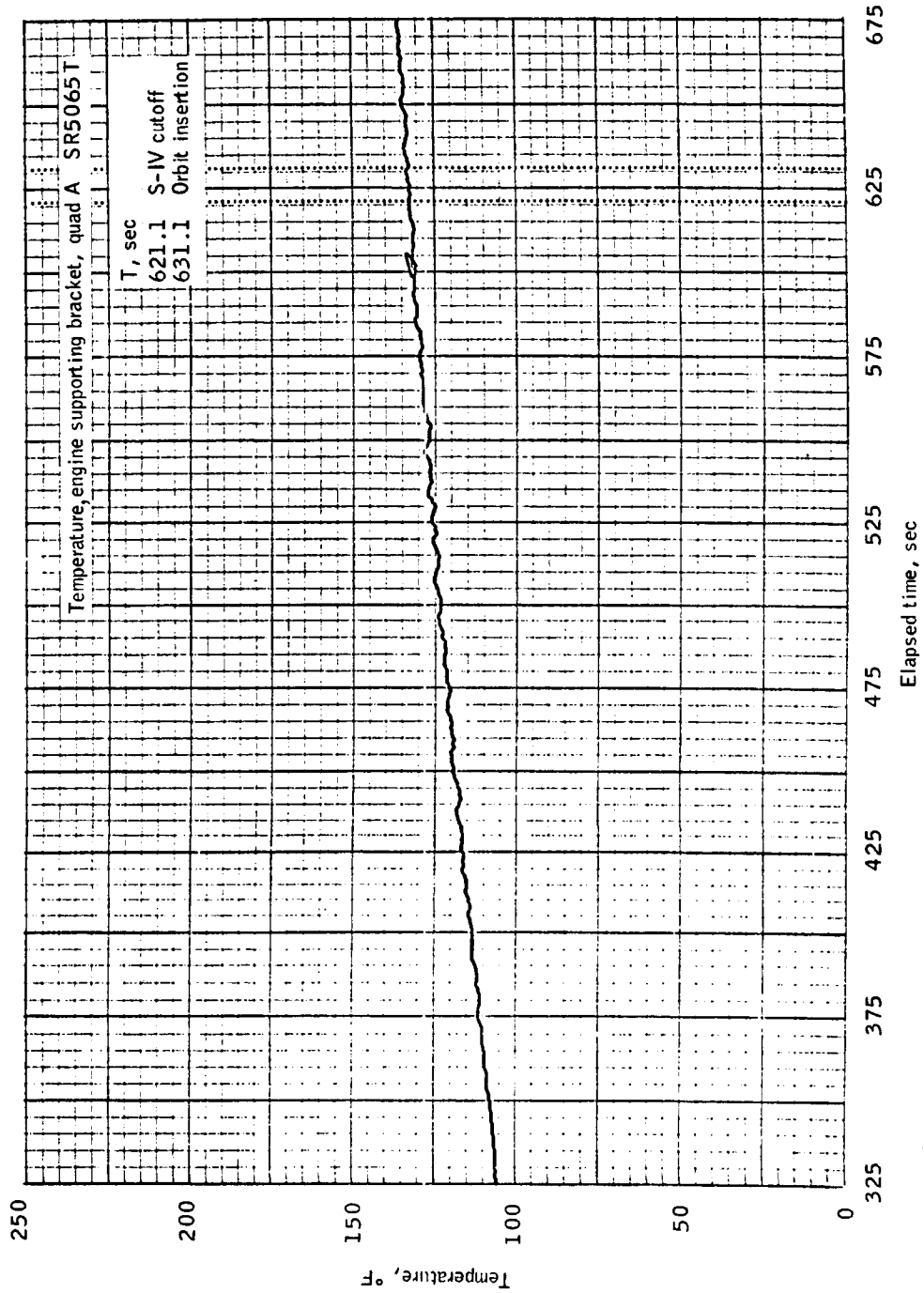
(a) -25 to 325 seconds.

Figure 4.8.15.- Temperature measured on the engine supporting bracket of the service module RCS quad A of the BP-15 spacecraft.

~~CONFIDENTIAL~~

~~CONFIDENTIAL~~

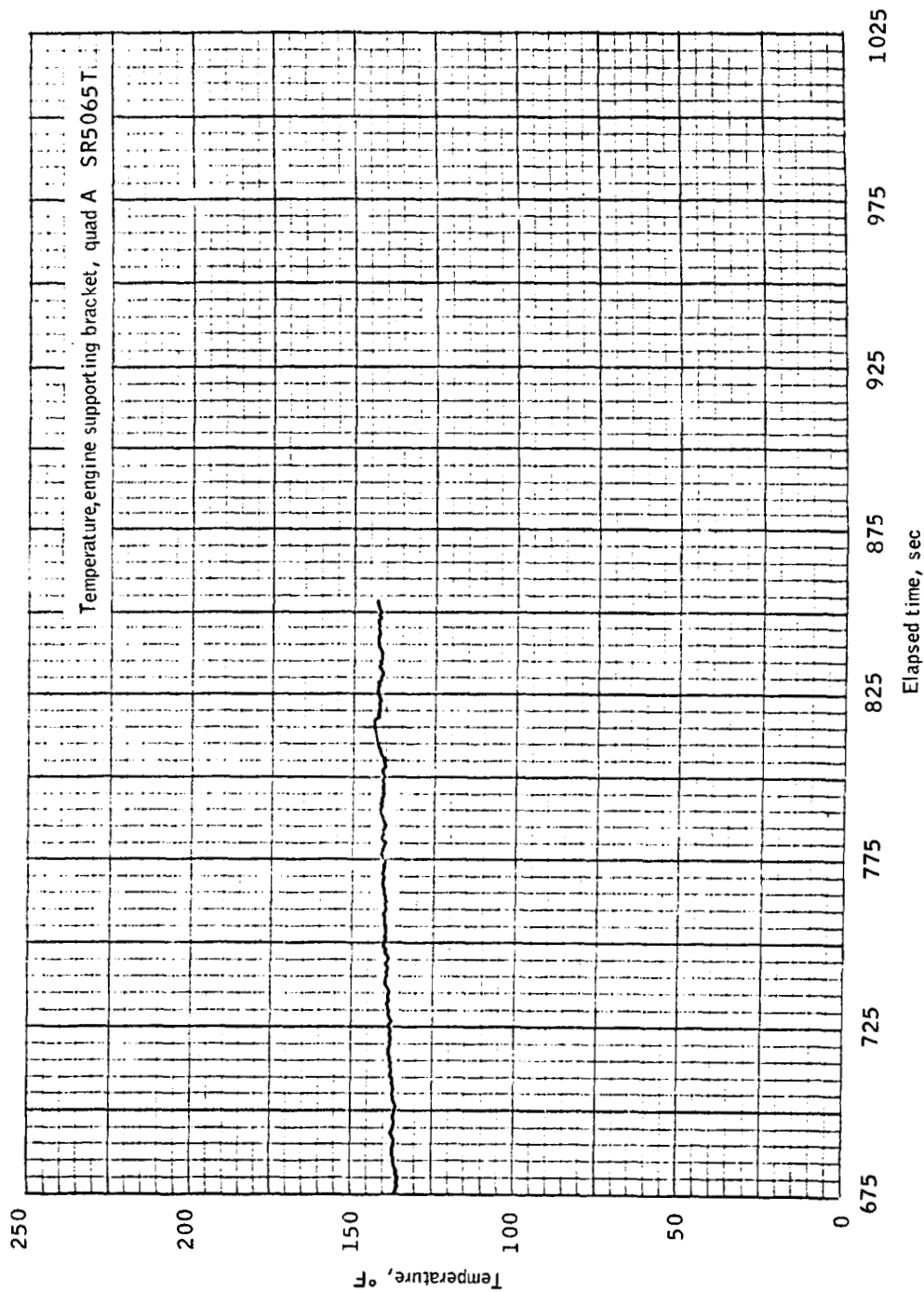
4-157



(b) 325 to 675 seconds.

Figure 4.8-15.- Continued.

~~CONFIDENTIAL~~

~~CONFIDENTIAL~~

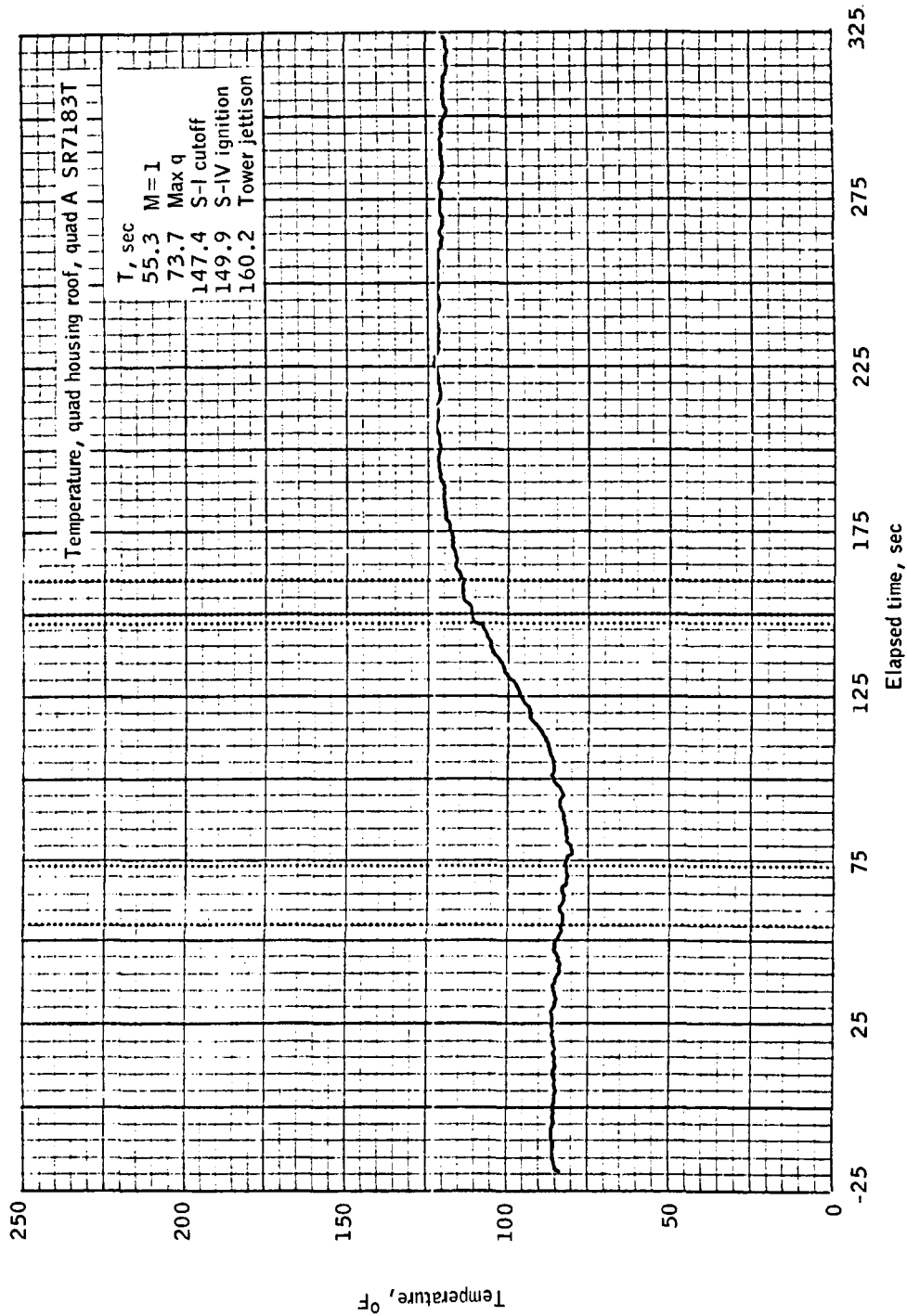
(c) 675 to 850 seconds.

Figure 4.8-15.- Concluded.

~~CONFIDENTIAL~~

~~CONFIDENTIAL~~

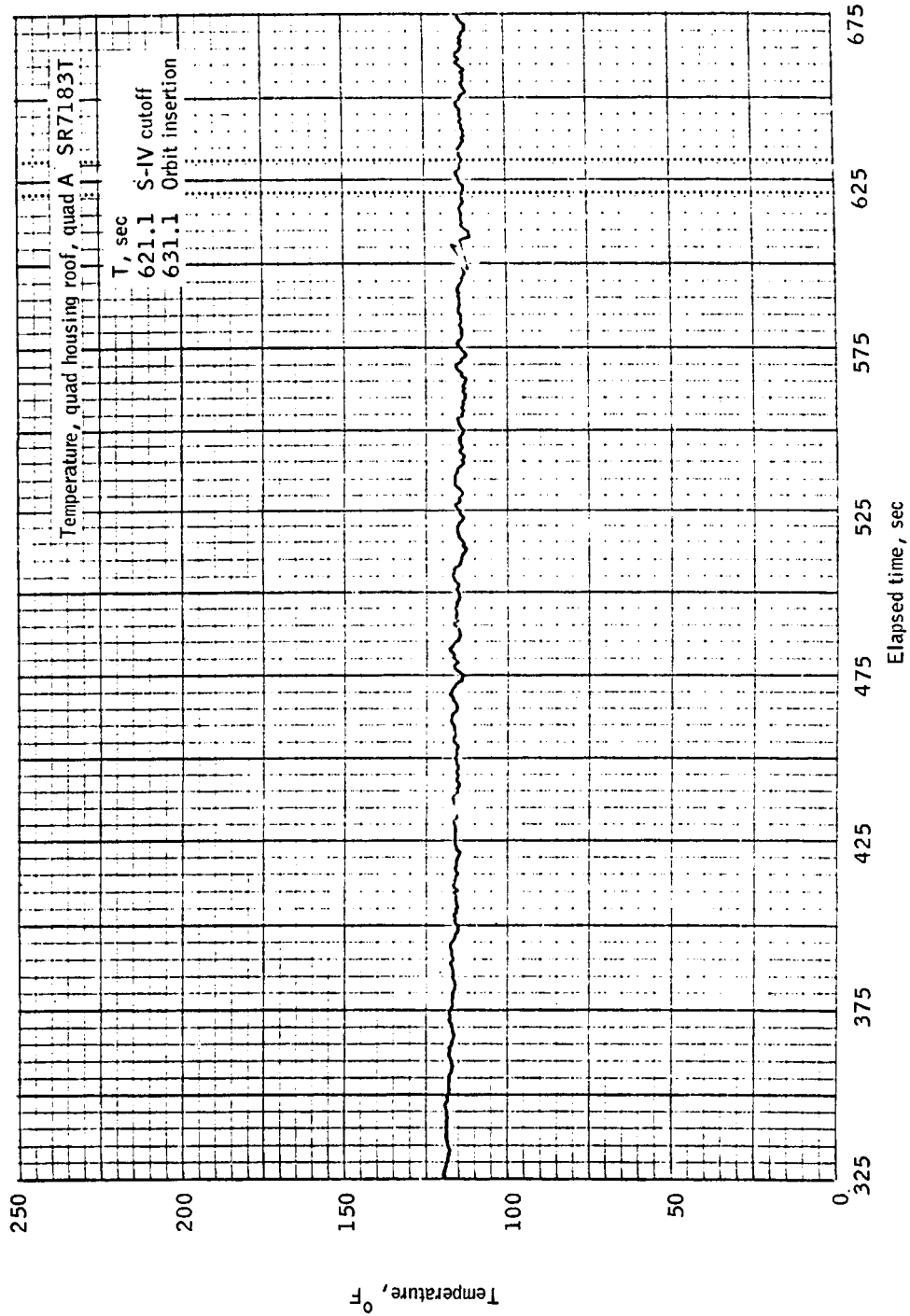
4-159



(a) -25 to 325 seconds.

Figure 4.8-16.- Temperature measured on the underside of the quad housing roof of the service module RCS quad A of the BP-15 spacecraft.

~~CONFIDENTIAL~~

~~CONFIDENTIAL~~

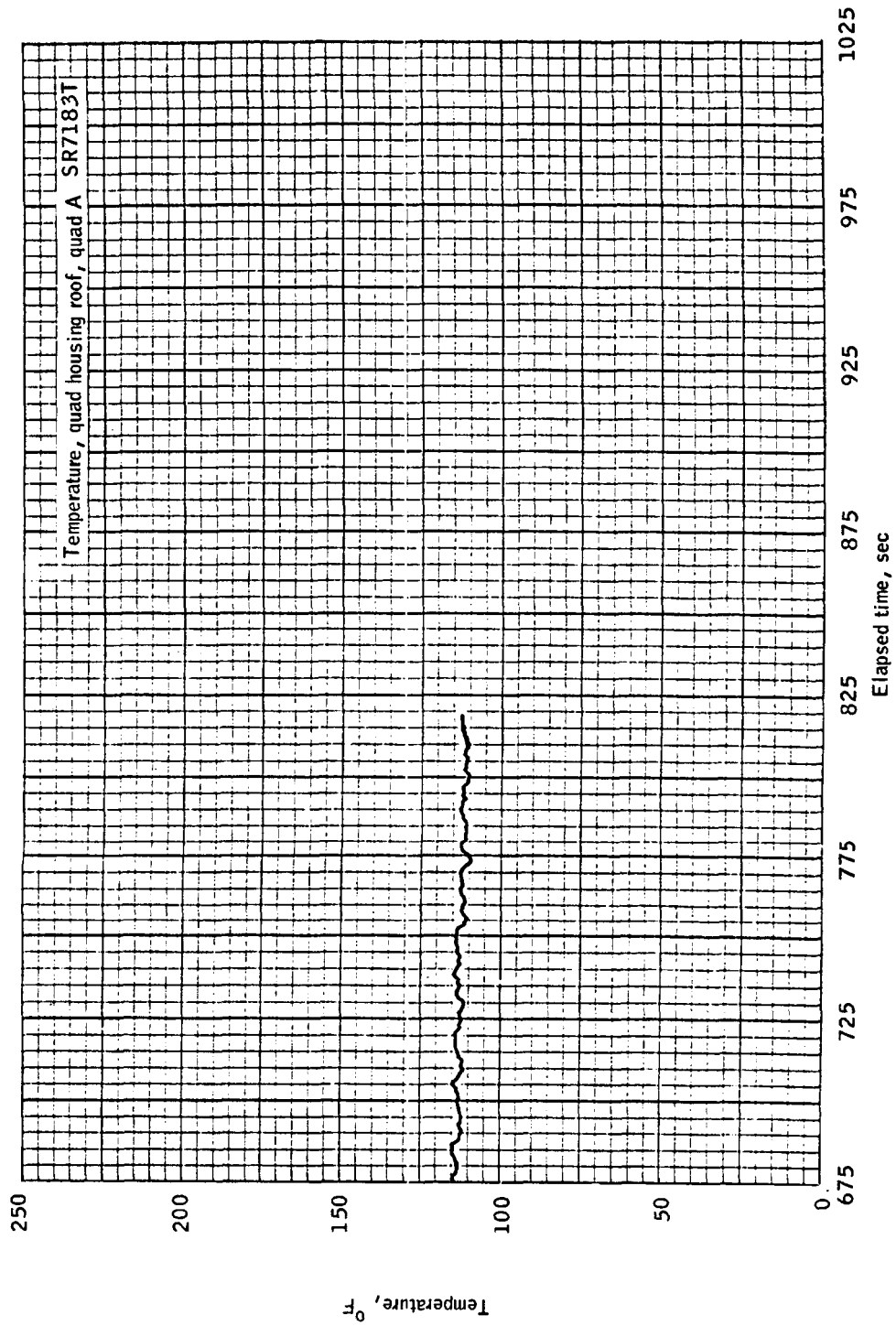
(b) 325 to 675 seconds.

Figure 4.8-16.- Continued.

~~CONFIDENTIAL~~

~~CONFIDENTIAL~~

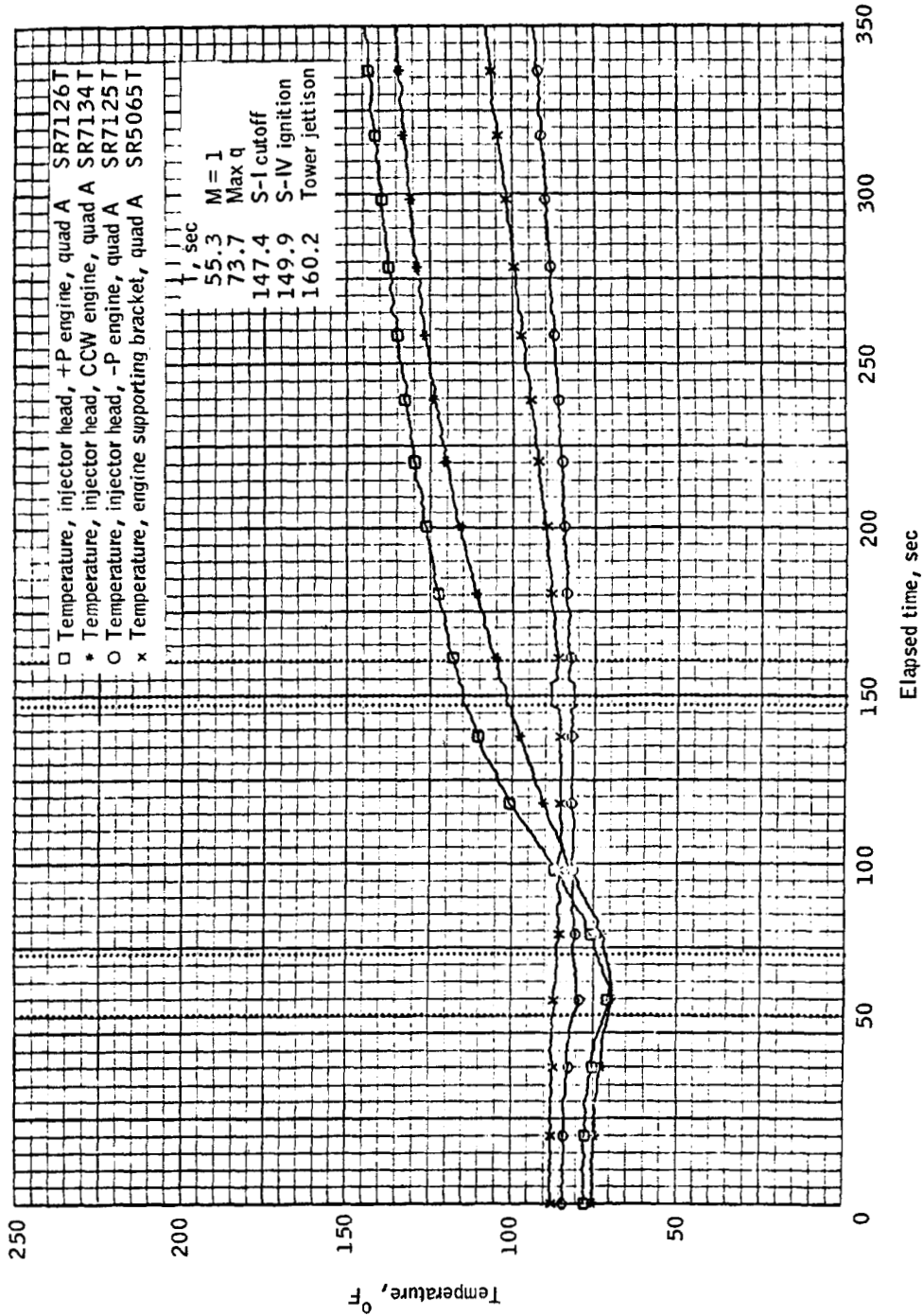
4-161



(c) 675 to 825 seconds.

Figure 4.8 16.- Concluded.

~~CONFIDENTIAL~~

~~CONFIDENTIAL~~

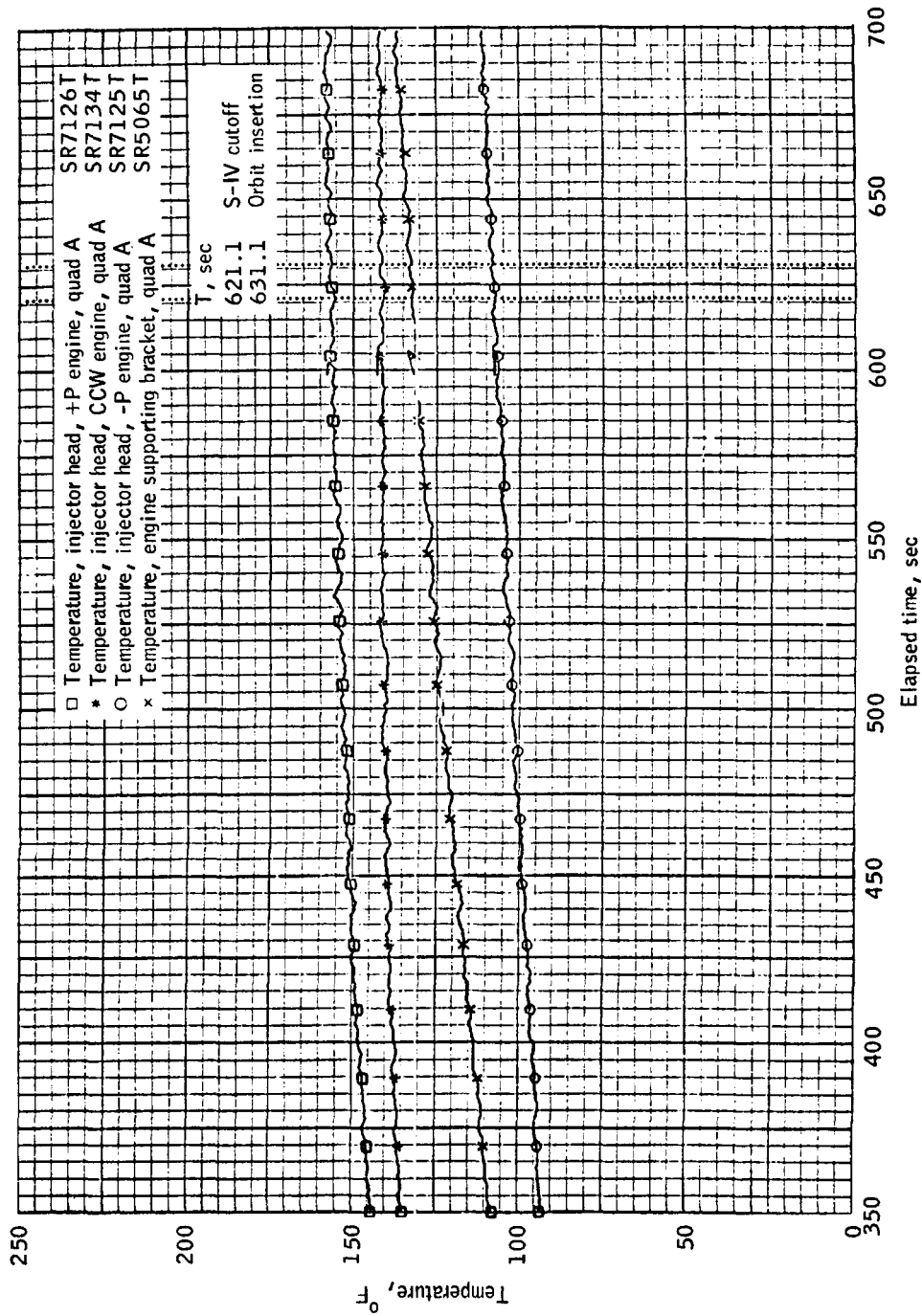
(a) 0 to 350 seconds.

Figure 4.8-17.- Temperatures measured on the +P, counterclockwise, and -P engine injector heads and on the engine supporting bracket of the service module RCS quad A of the BP-15 spacecraft.

~~CONFIDENTIAL~~

~~CONFIDENTIAL~~

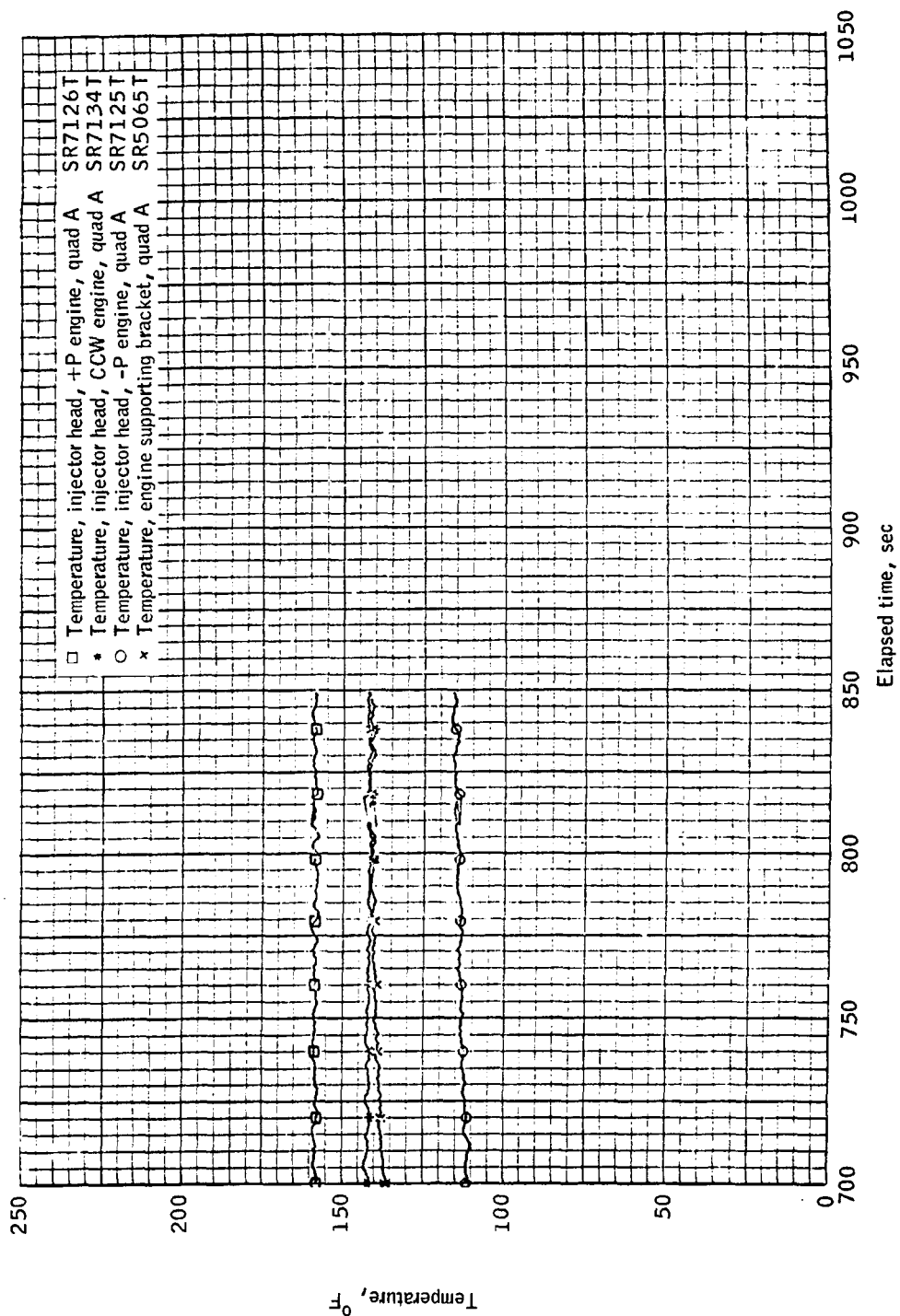
4-163



(b) 350 to 700 seconds.

Figure 4.8-17.- Continued.

~~CONFIDENTIAL~~

~~CONFIDENTIAL~~

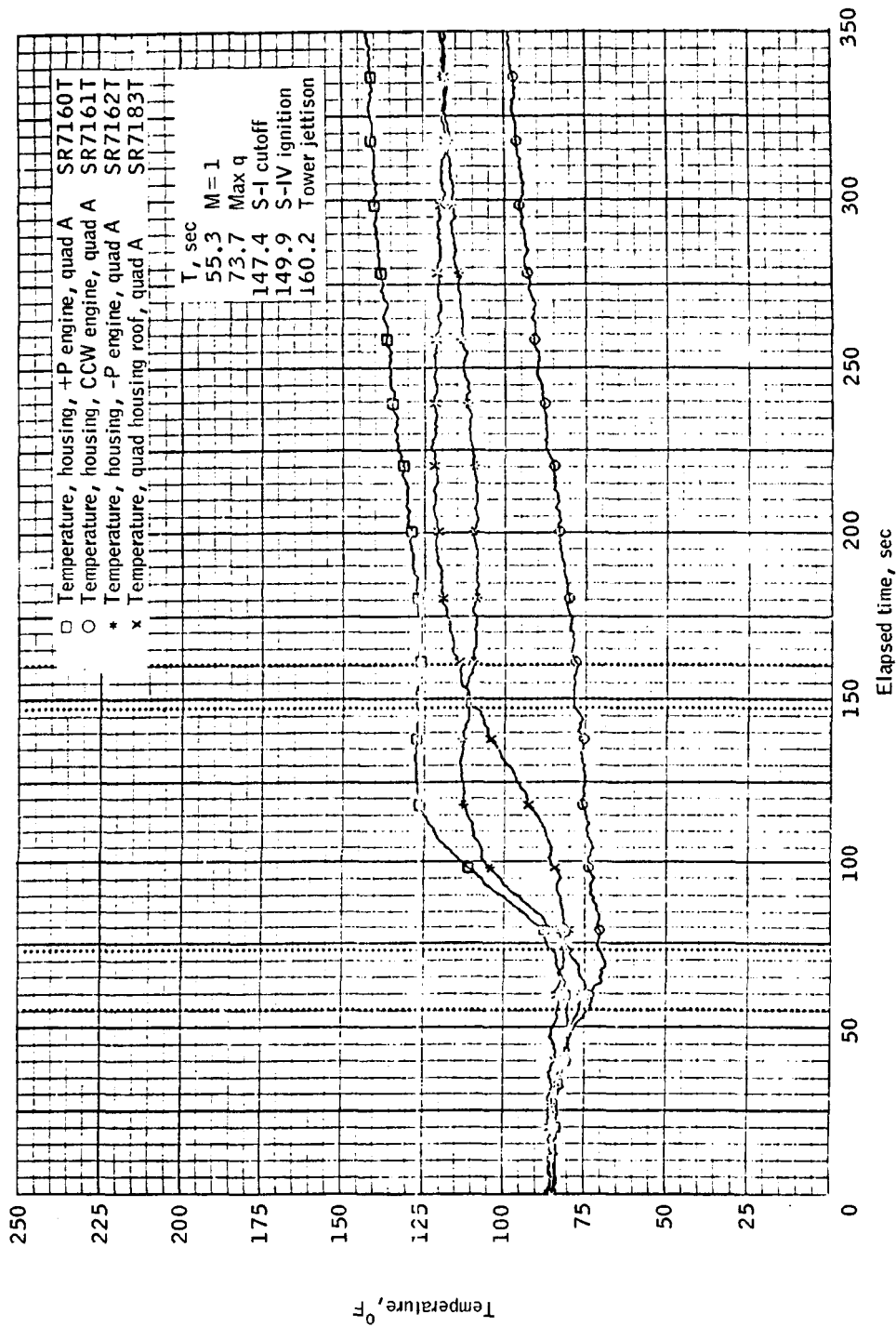
(c) 700 to 850 seconds.

Figure 4.8-17.- Concluded.

~~CONFIDENTIAL~~

~~CONFIDENTIAL~~

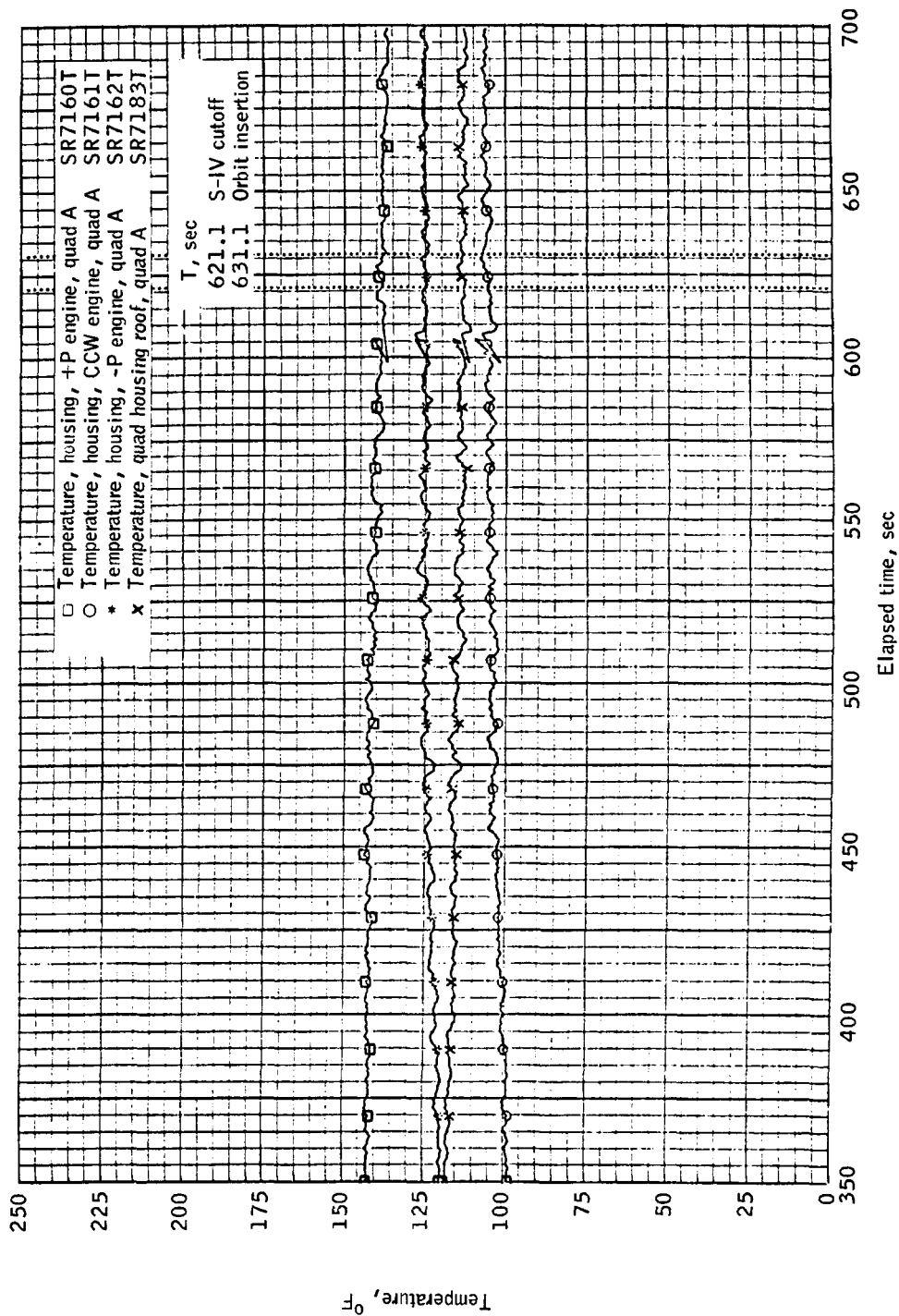
4-165



(a) 0 to 350 seconds.

Figure 4.8-18.- Temperatures measured on the +P, counterclockwise, and -P engine housings and on the quad housing roof of the service module RCS quad A of the BP-15 spacecraft.

~~CONFIDENTIAL~~

~~CONFIDENTIAL~~

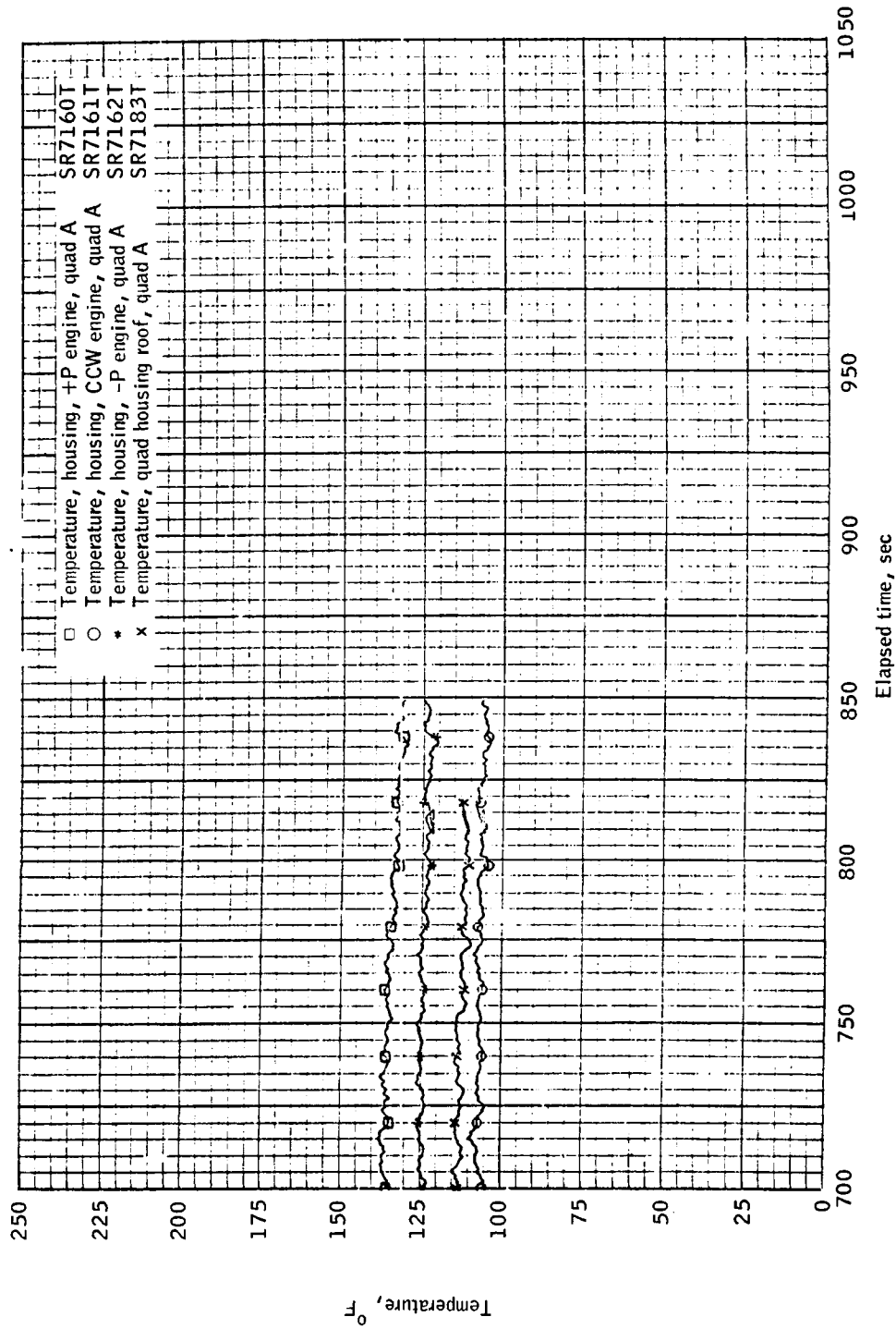
(b) 350 to 700 seconds.

Figure 4.8-18.- Continued.

~~CONFIDENTIAL~~

~~CONFIDENTIAL~~

4-167



(c) 700 to 850 seconds.

Figure 4.8-18.- Concluded.

~~CONFIDENTIAL~~

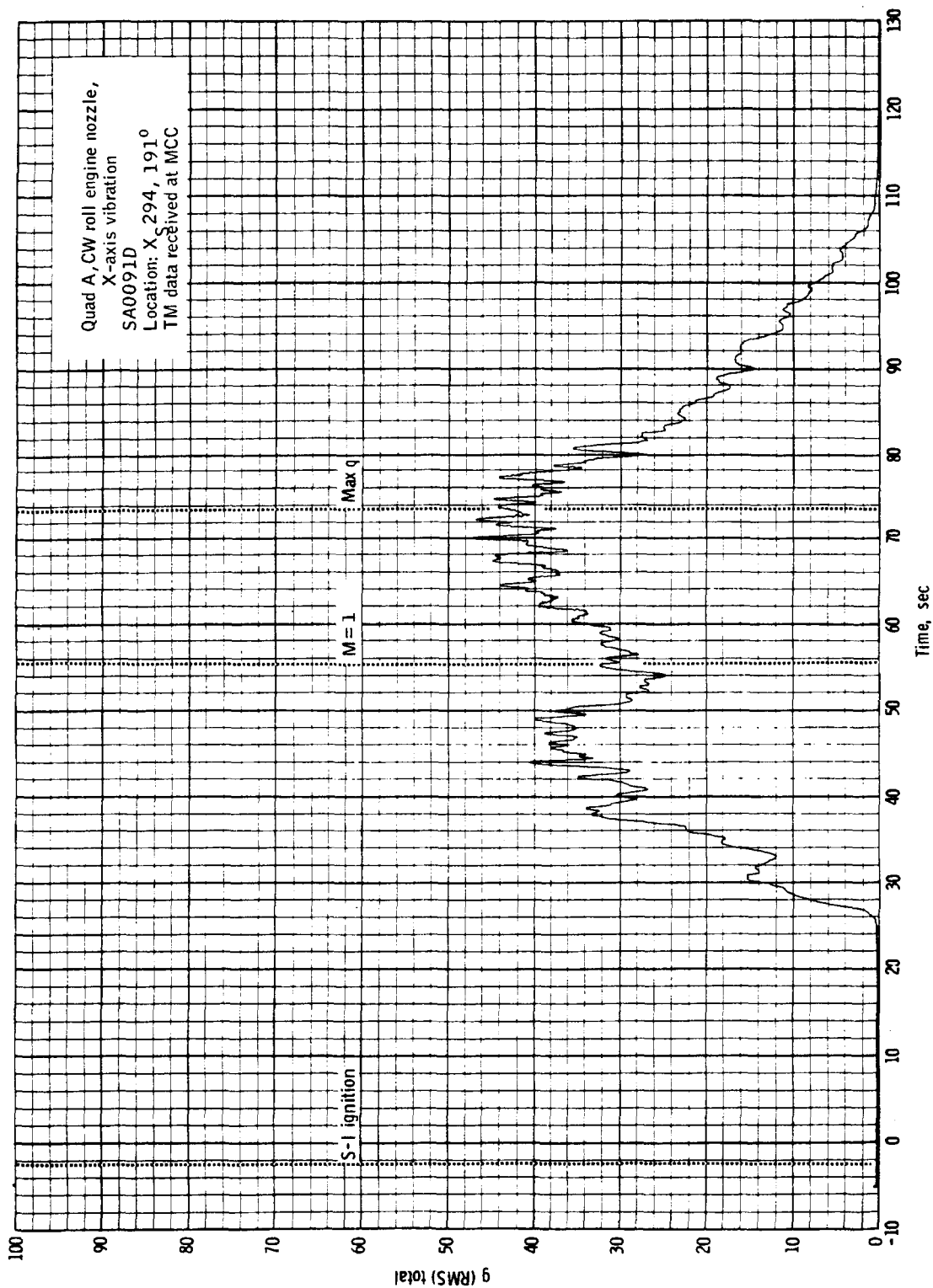
~~CONFIDENTIAL~~

Figure 4.8-19.- X-axis vibration measured in the clockwise roll engine nozzle of the service module RCS quad A of the BP-15 spacecraft.

~~CONFIDENTIAL~~

~~CONFIDENTIAL~~

4-169

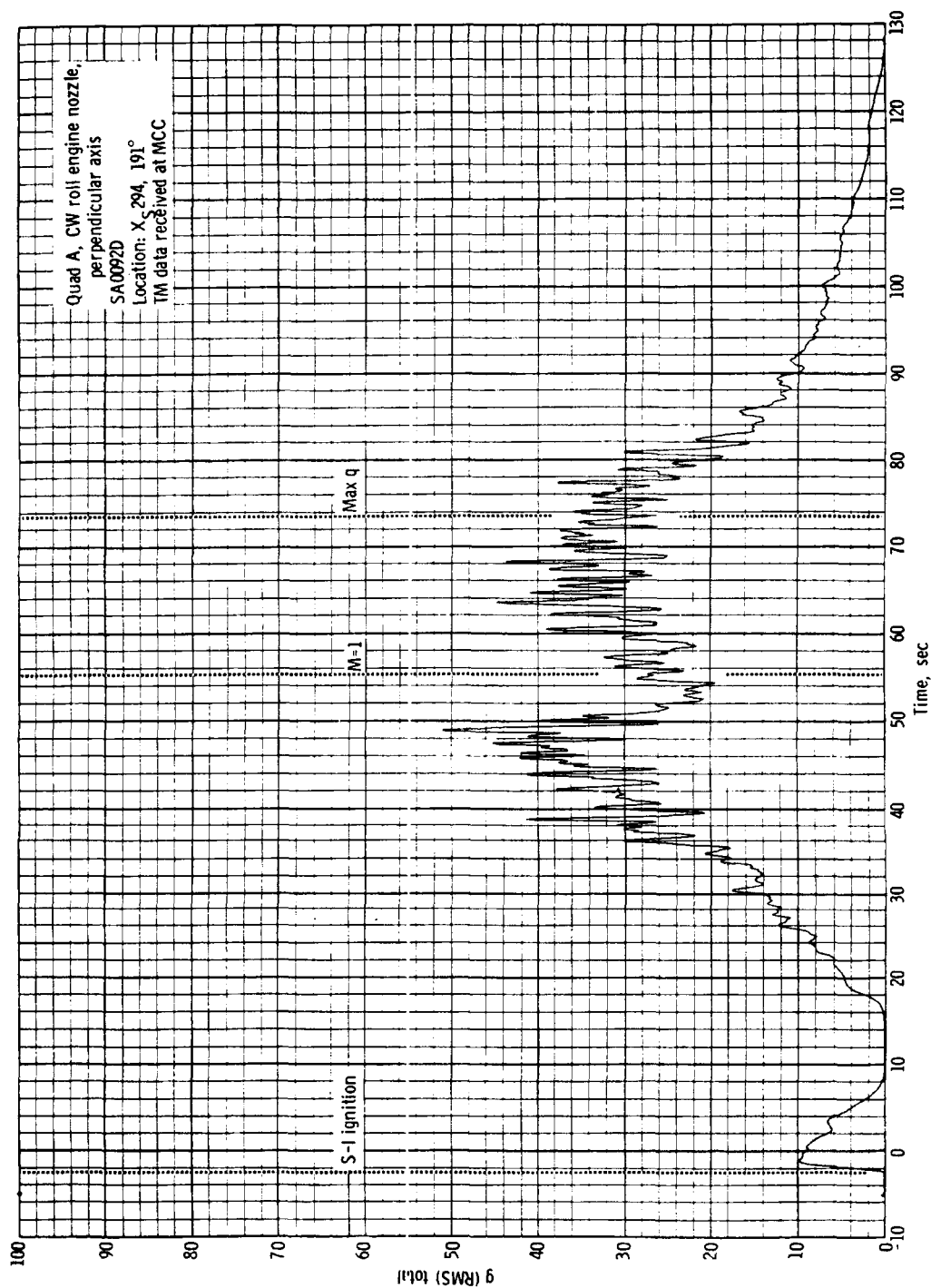


Figure 4.8-20. - Perpendicular axis vibration measured in the clockwise roll engine nozzle of the service module RCS quad A of the BP-15 spacecraft.

~~CONFIDENTIAL~~

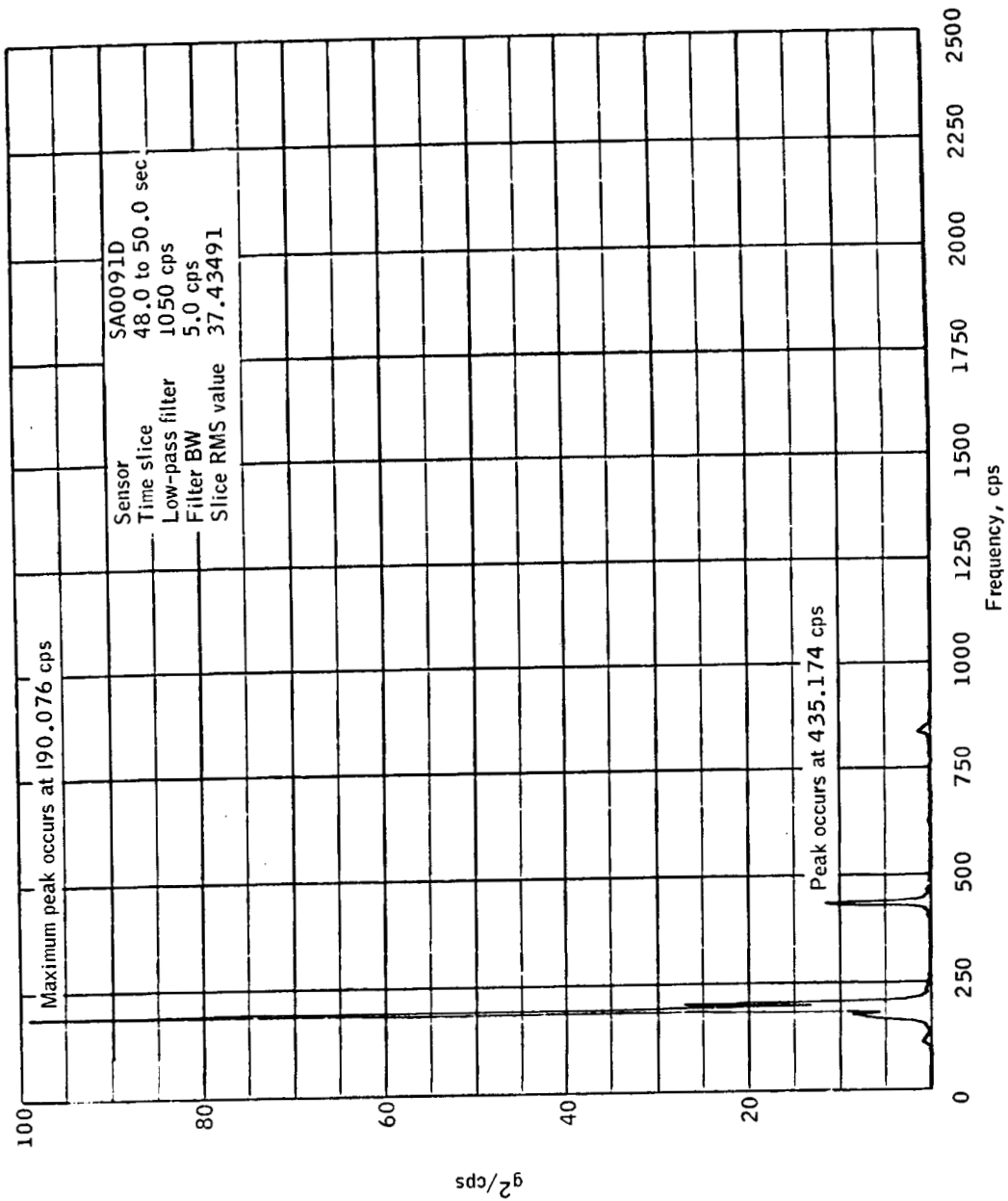
~~CONFIDENTIAL~~

Figure 4.8 21.- Digital spectrum estimation of X-axis vibration over the time period T+48 to T+50 seconds measured in the clockwise roll engine nozzle of the service module RCS quad A of the BP-15 spacecraft.

~~CONFIDENTIAL~~

~~CONFIDENTIAL~~

4-171

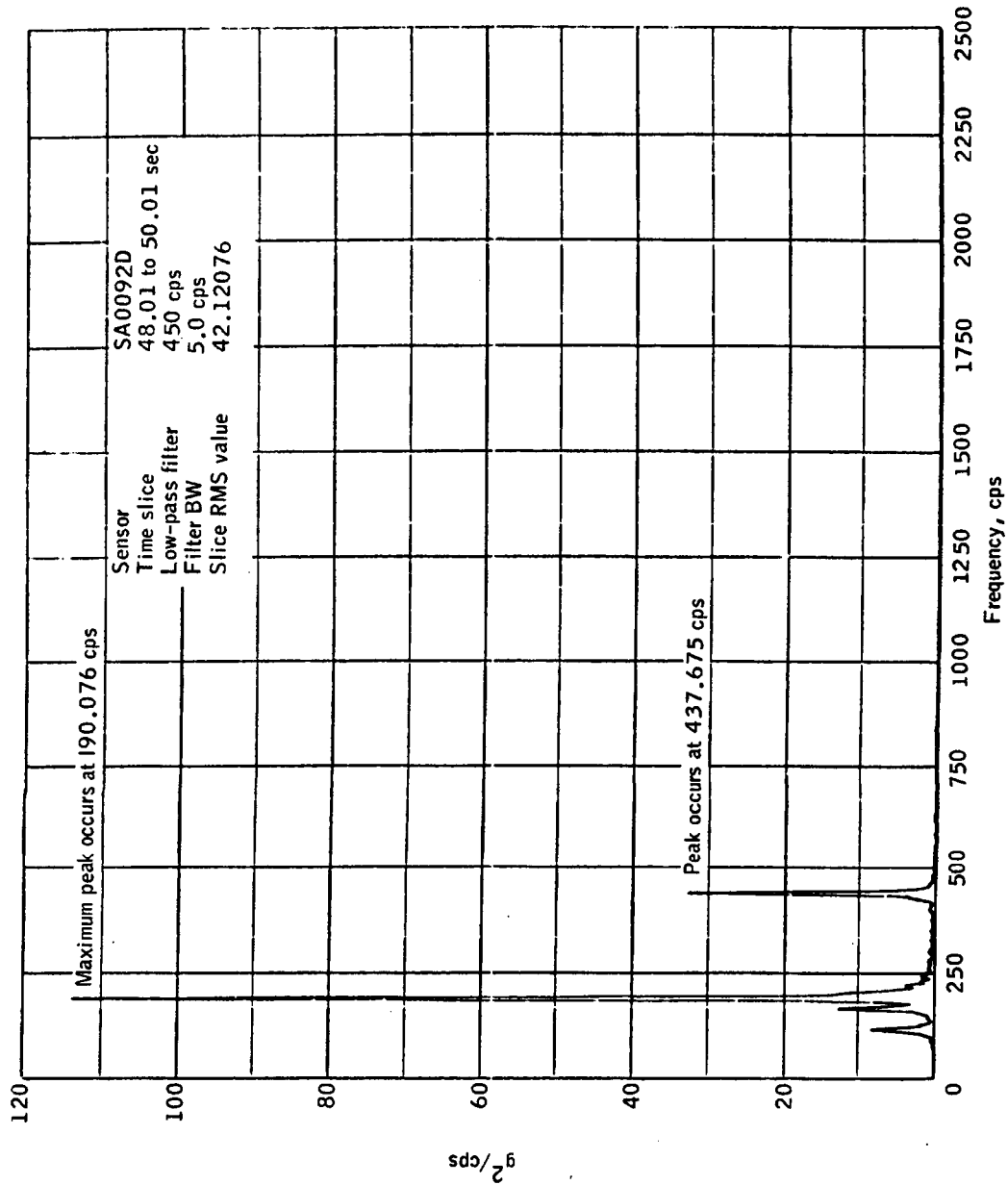


Figure 4.8-22.- Digital spectrum estimation of the perpendicular axis vibration over the period T+48.01 to T+50.01 seconds measured in the clockwise roll engine nozzle of the service module RCS quad A of the BP-15 spacecraft.

~~CONFIDENTIAL~~

~~CONFIDENTIAL~~

4.9 Acoustics

The Apollo BP-15 spacecraft was instrumented to measure the exterior acoustic environment during flight. This environment consisted of noise generated by the launch vehicle and noise generated aerodynamically. Available wind-tunnel data (ref. 6) on the Apollo spacecraft configuration indicated that the aerodynamic noise environment could, for a nominal Saturn trajectory, reach a maximum sound pressure level (SPL) of 168 decibels (db) (ref: $0.0002 \text{ dynes/cm}^2$) at the CM-SM interface. This location was instrumented on the BP-13 spacecraft (ref. 10), and an SPL of 166 db (ref. $0.0002 \text{ dynes/cm}^2$) was measured. It was anticipated that this sound pressure level would also be measured on the BP-15 spacecraft.

Therefore, the BP-15 spacecraft was instrumented with thirteen fluctuating pressures and one microphone to verify the wind-tunnel predictions. Eleven of the fluctuating pressures and the microphone were installed on the service module and two fluctuating pressures on the adapter. The transducers are listed and the specific locations are indicated in figure 4.2-4 and table 8.1-I.

The piezoelectric microphone sensed the applied differential pressure, i.e., pressure variations, and converted the pressure to a linear voltage that was proportional to SPL.

The fluctuating pressure transducers, however, were absolute pressure gages. The instrument sensed the static pressure and the static pressure variations. The pressures were converted to a linear voltage. Since the pressure transducer had to accommodate atmospheric pressure at lift-off, an instrument with a 0 to 15 psia range was used. This range determined a lower limit for useable fluctuating pressure data.

A B&K spectrum analyzer was used to make overall and one-third octave band SPL time histories for the frequency capabilities shown in table 8.1-I. A time discrepancy was apparent in the reduced microphone data. By correlating an oscillograph recording with the reduced data, this discrepancy was reduced to a systematic error of 0.4 second.

The overall SPL level time history for the microphone is presented in figure 4.9-1. The launch vehicle noise began when the launch vehicle was ignited at T-2.4 seconds and reached a maximum of 14 db (ref. $0.0004 \text{ dynes/cm}^2$) at T+1 second. As the vehicle accelerated, the sound pressure level decreased until it dropped below the instrumentation capabilities at T+10 seconds.

~~CONFIDENTIAL~~

~~CONFIDENTIAL~~

4-173

A one-third octave band analysis of the launch vehicle noise at T+1 second is presented in figure 4.9-2. This analysis shows that the maximum SPL had a broad band spectrum and is relatively flat from 125 to 600 cps.

Figure 4.9-3 is a comparison of the overall launch vehicle noise time histories for BP-15 and BP-13 spacecraft, and depicts the similarity between BP-15 and BP-13 launch vehicle SPL. There is very little difference between the two curves.

The aerodynamic noise measured on the BP-15 spacecraft was less severe than the noise levels measured on BP-13. The SPL exceeded the ambient instrumentation noise at T+32.5 seconds (fig. 4.9-1) and continued to increase to a 149 decibels peak at T+43 seconds. The SPL then decreased to 140 db at T+47.5 seconds. An 18 db increase occurred from T+47.5 to T+49.5 seconds; therefore, a one-third octave band analysis was made at T+49.5 and is presented in figure 4.9-4. This rapid increase has been experienced during wind tunnel testing of the Apollo vehicle (ref. 6) and has been related to local sonic flow conditions at the vehicle shoulder.

During supersonic flow, the BP-15 spacecraft SPL remained at approximately 150 db through the maximum dynamic pressure range. At T+100 seconds, the aerodynamic SPL dropped to 140 db, which is considered insignificant.

A rigorous explanation for the lower aerodynamic levels indicated has not been resolved. The vehicle configurations were similar for BP-15 and BP-13 spacecraft, but the trajectories produced a different angle of attack and dynamic pressure time history. In addition, the fluctuating pressures were relocated to aid in structural analysis. Because of these differences, including the instrumentation lower limit capabilities described above, additional investigation and study will be required before a solution is obtained.

Fluctuating pressure 3 at X_A 1000 and 329.25° and fluctuating pressure at X_A 973 and 277.5° were very active during transonic flight and the high dynamic pressure range. See section 4.7.

In summary, the launch vehicle noise for BP-15 was similar to that for BP-13 spacecraft. Both reached a maximum of 148 db. (See fig. 4.9-3.) The aerodynamic noise measured on the BP-15 microphone reached a maximum of 158 db (fig. 4.9-1) which is less severe than the BP-13 microphone measurement which was 164 db at the same time in flight. This difference may be related to the different trajectories.

~~CONFIDENTIAL~~

UNCLASSIFIED

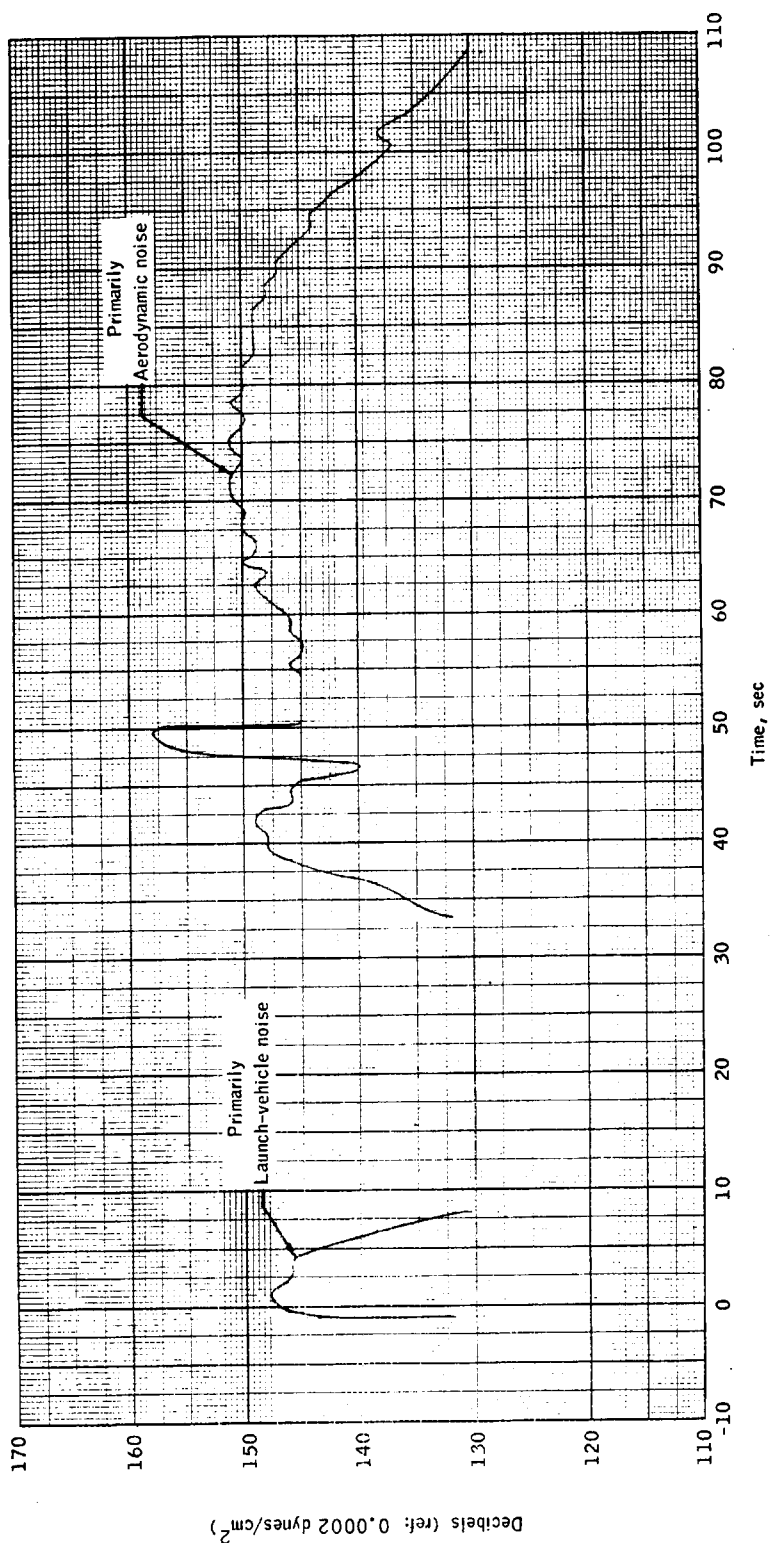


Figure 4.9-1.1.- Overall sound pressure level time history from T-10 to T+110 seconds for BP-15 spacecraft

UNCLASSIFIED

UNCLASSIFIED

4-175

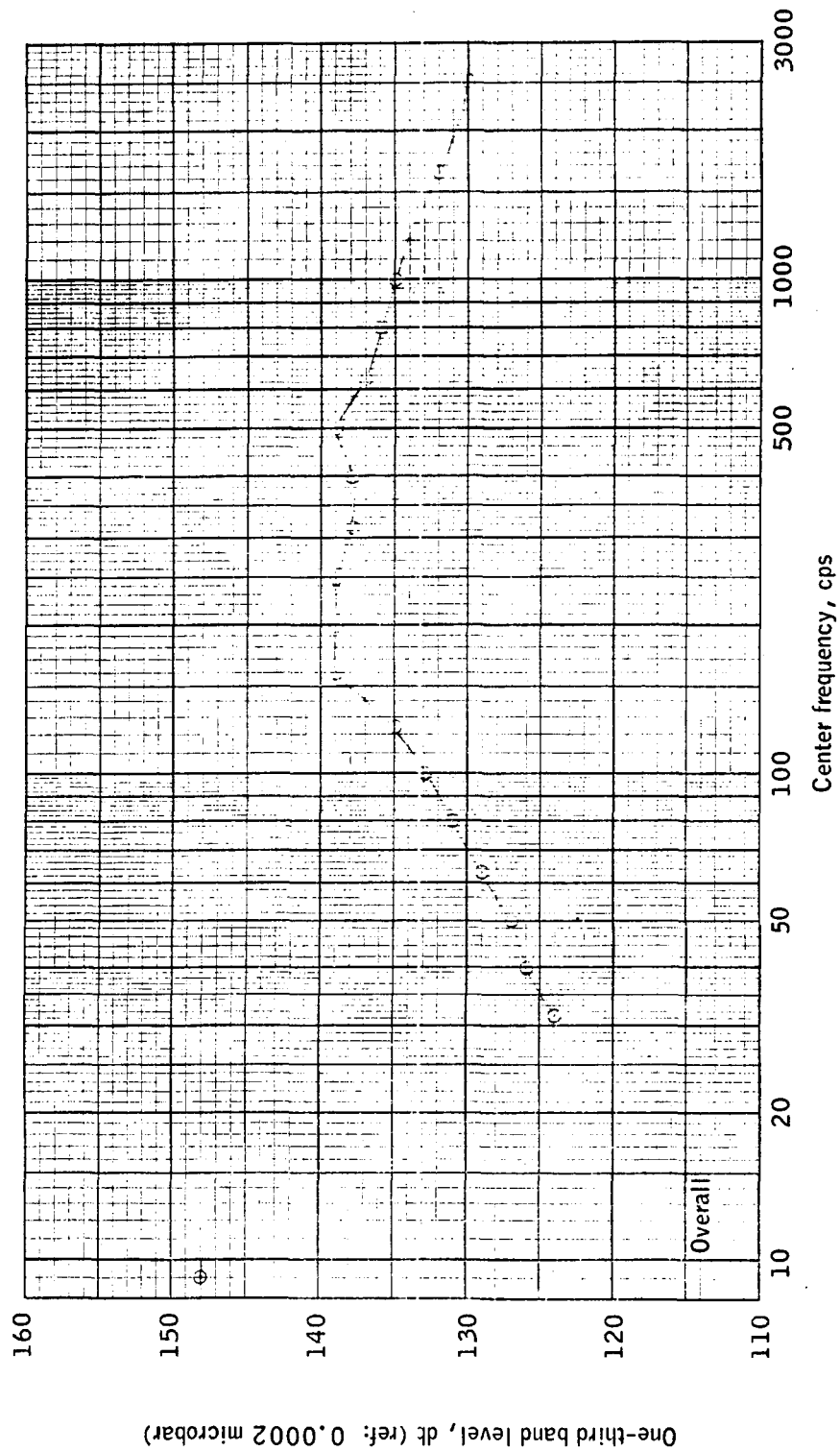


Figure 4.9-2.- One-third octave band analysis of BP-15 spacecraft launch-vehicle sound pressure levels at T+1 second.

UNCLASSIFIED

UNCLASSIFIED

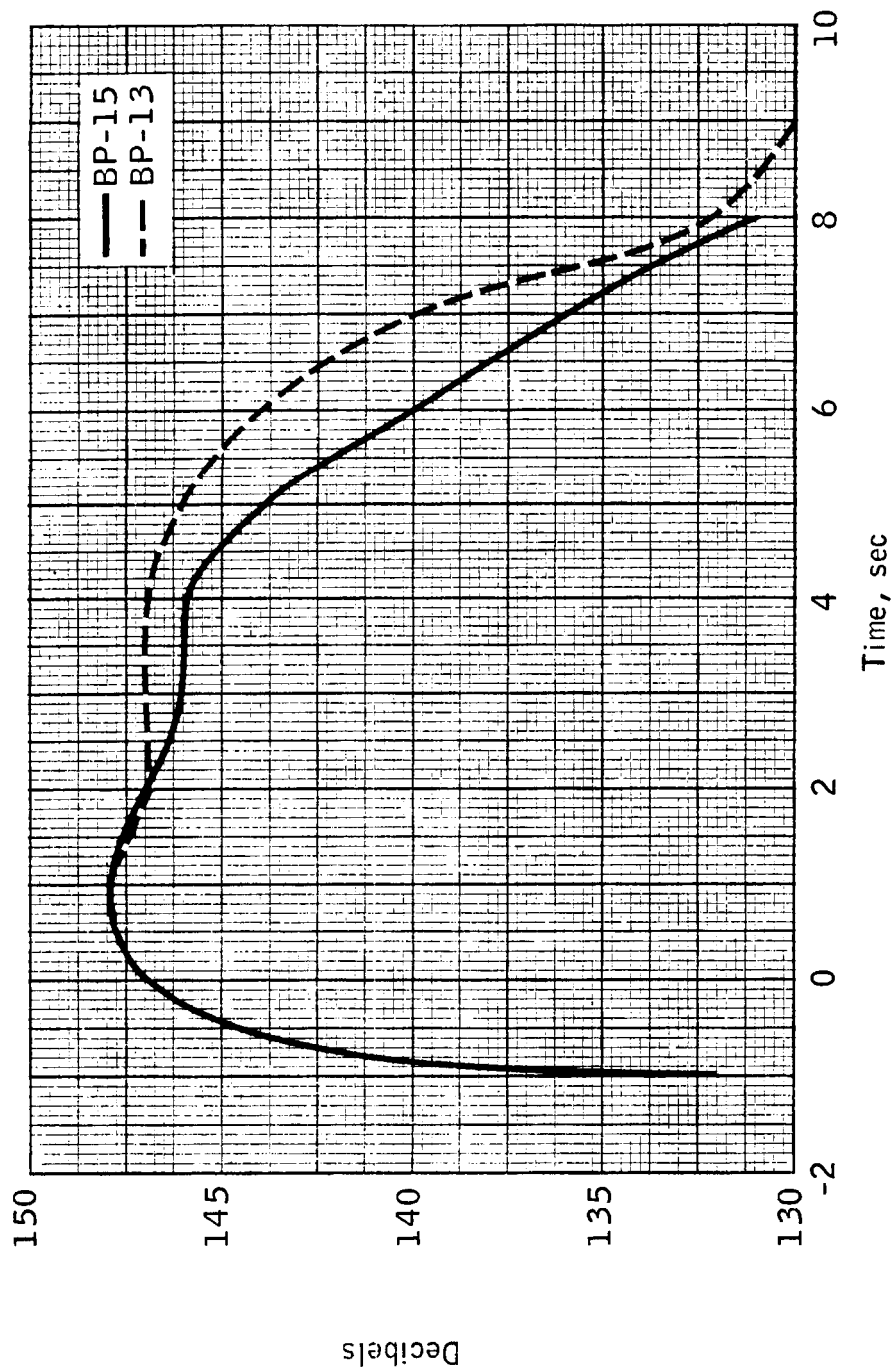


Figure 4.9-3.- Comparison of BP-15 with BP-13 spacecraft launch-vehicle sound pressure levels from T-2 to T+8 seconds.

UNCLASSIFIED

UNCLASSIFIED

4-177

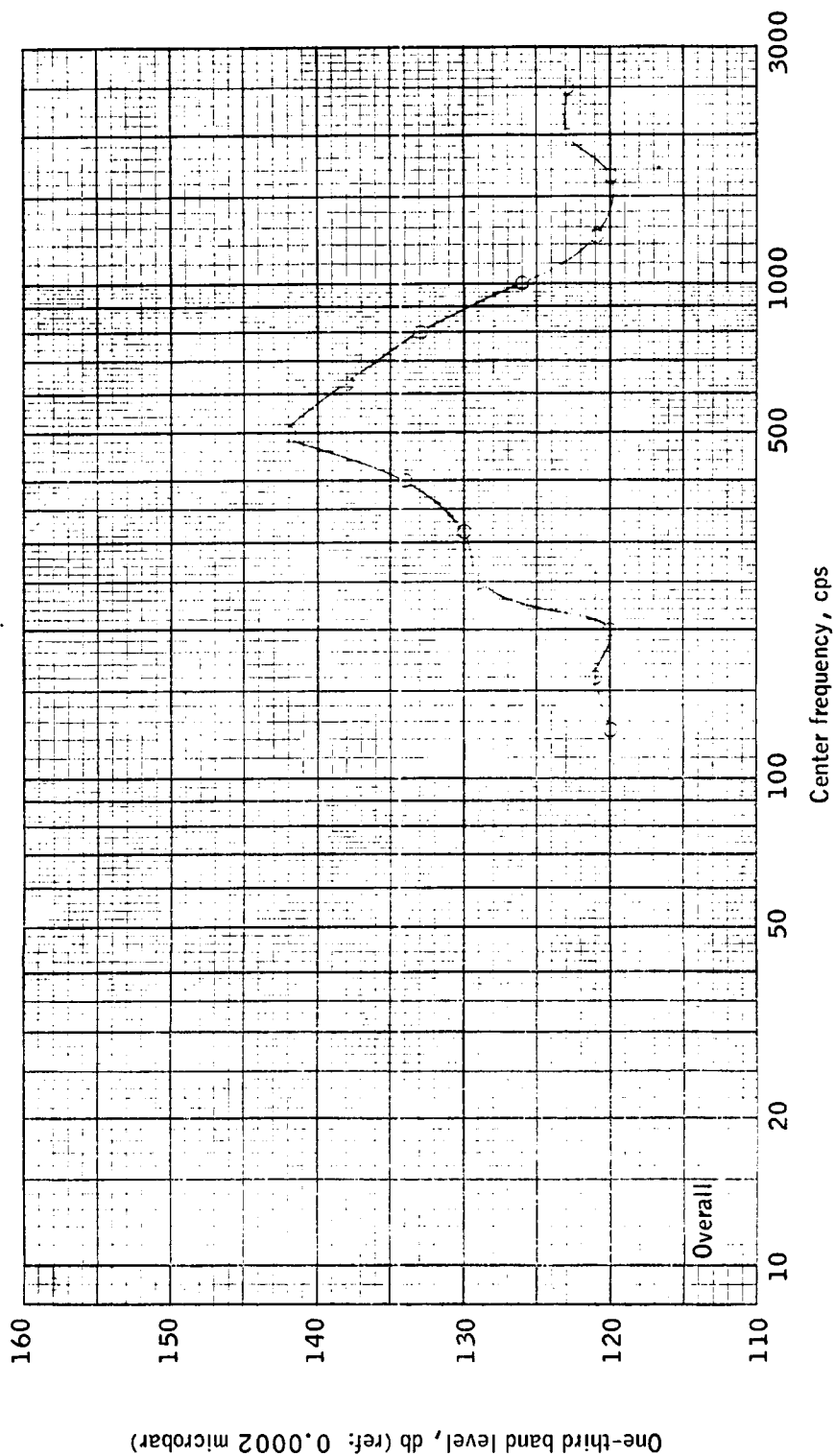


Figure 4.9-4.- One-third octave band analysis of BP-15 spacecraft aerodynamic sound pressure levels at T+49.5 seconds.

UNCLASSIFIED

~~CONFIDENTIAL~~

4.10 Heat Protection

The heat protection on the BP-15 spacecraft consisted of epoxy-impregnated cork covering the forward section of the command module and the RCS housing and silica-filled Buna-N rubber covering the truss members of the launch-escape subsystem.

The forward section of the boilerplate command module was covered with varying thicknesses (fig. 4.10-1) of cork-based thermal insulation. This was to prevent the aluminum skin of the command module from exceeding the design temperature of 250° F during the powered flight phase of the mission. No thermal insulation was required between $X_{C115.94}$ and $X_{C133.72}$ because of the ablative qualities of the fiber-glass radome. The aft heat-shield area was not exposed to the launch environment, and thus no heat protection was required.

The command module (CM), service module (SM), insert and adapter were not instrumented for skin temperatures.

Calorimeters mounted flush with the exterior wall of the CM and SM were used to measure launch-heating rates. A description of the launch-heating environment is covered in section 4.11, Aerothermodynamics.

The heat protection for the launch-escape tower consisted of Buna-N rubber (60 percent silica filled) covering the truss members. Several plies of rubber were built up eccentric to the structural tube with the maximum thickness in the region of highest heating. Truss members perpendicular to the flow were protected by a maximum thickness of 0.375 inch of rubber. Legs and diagonal members were protected by a maximum of 0.3 inch of rubber. Figure 4.10-2 shows the launch-escape tower truss members and the location of the temperature sensors. Sensors were mounted on the metal surfaces and covered with the Buna-N insulation.

Figure 4.10-3 shows the measured temperatures at the interface of the rubber and the metal surface (bond line) during powered flight. The figure indicates that at the time of tower jettison the maximum bond-line temperature on the diagonal member was 101° F. Both instrumented truss members which were perpendicular to the air flow indicated a maximum temperature of 89° F. The bond-line temperatures of the members parallel to the air flow did not exceed 90° F. The temperature of the truss member nearest the LES motor nozzle did not exceed 90° F at the time of tower jettison. Temperatures measured during Apollo mission A-101 (BP-13 spacecraft) were within 10° F of the above temperatures.

~~CONFIDENTIAL~~

~~CONFIDENTIAL~~

4-179

Aerodynamic heating produced a maximum truss-member bond-line temperature which was less than 20 percent of the design limit (550° F). The thickness of the ablative material necessary to withstand the design limit temperature was calculated for the most severe thermal condition that the launch escape subsystem might experience. This design condition would occur not only if the tower were exposed to aerodynamic heating during the powered flight phase but also if it were enveloped by the launch-escape rocket plume, with its heating and erosion, during an abort. There was no abort during the A-102 mission, and at the time the LES separated from the command module by the alternate mode of tower jettison, the truss members had reached maximum temperatures appreciably below the structural design limit.

~~CONFIDENTIAL~~

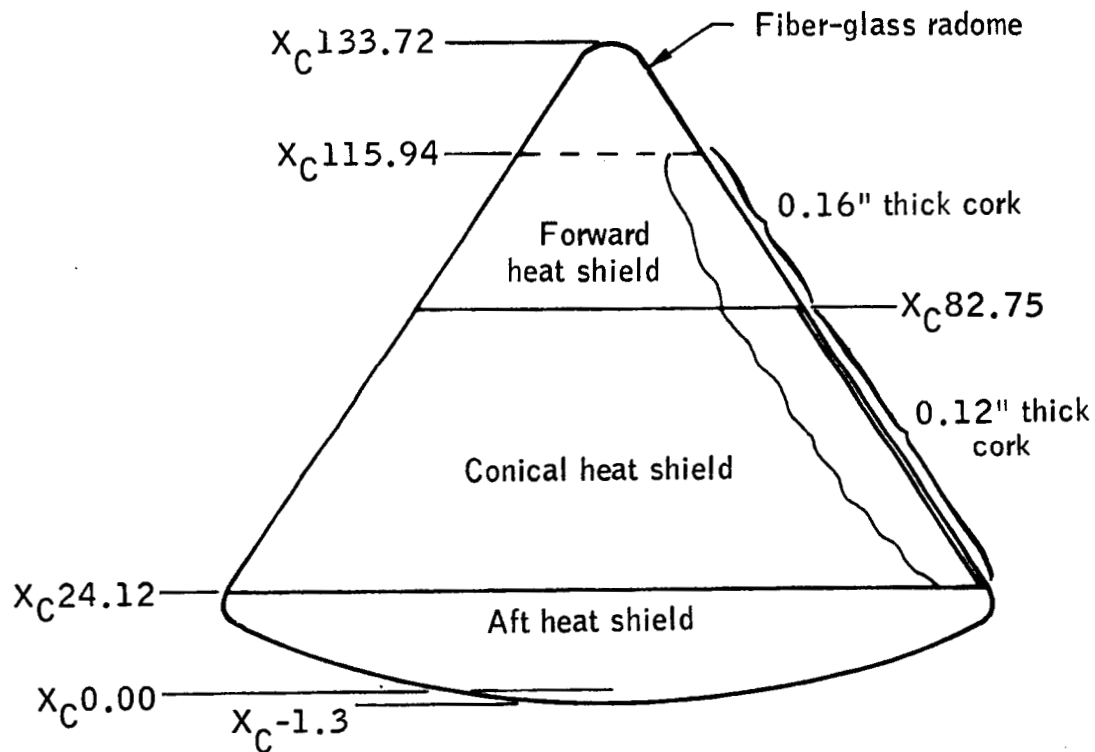
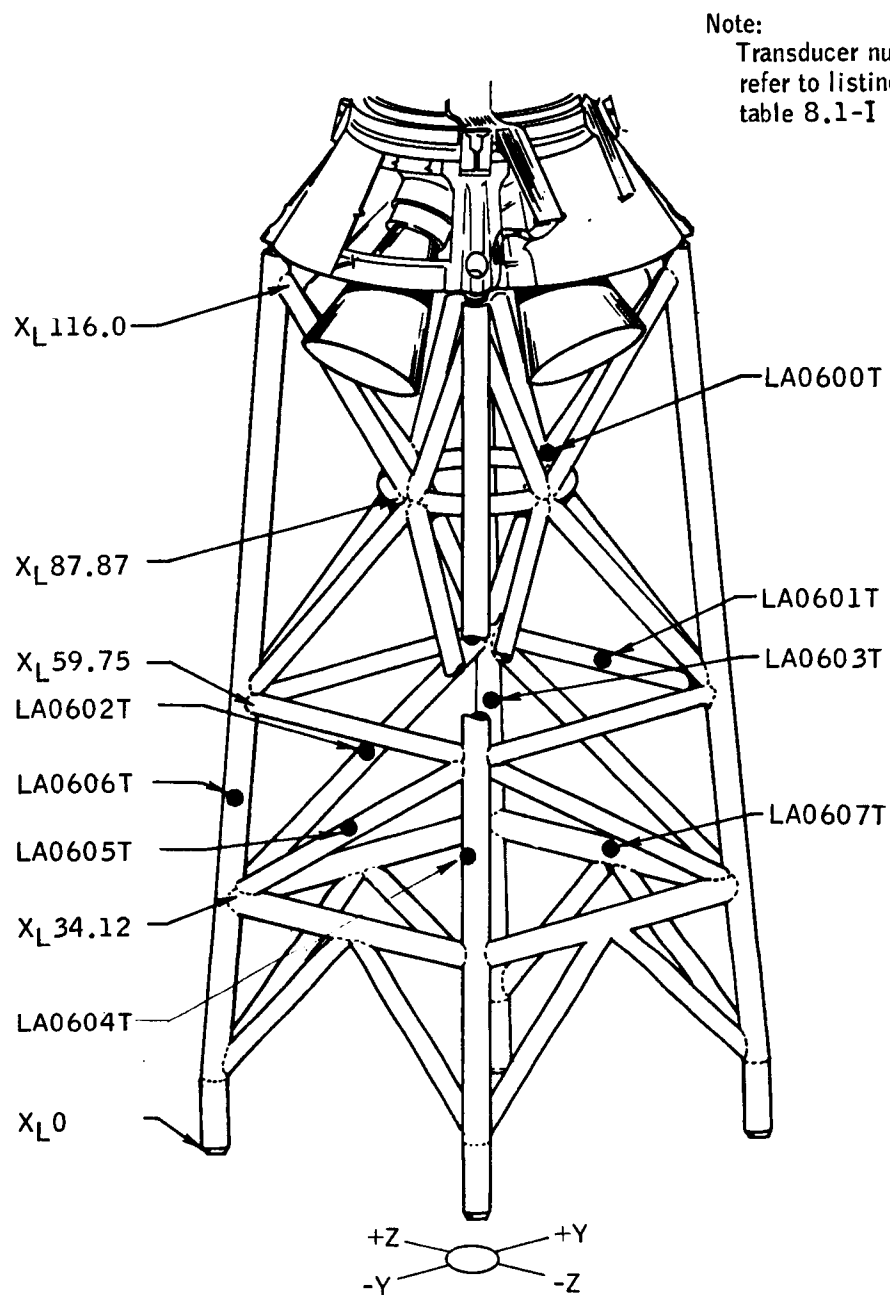
~~CONFIDENTIAL~~

Figure 4.10-1. - Command module heat protection for BP-15 spacecraft.

~~CONFIDENTIAL~~

~~UN~~CLASSIFIED

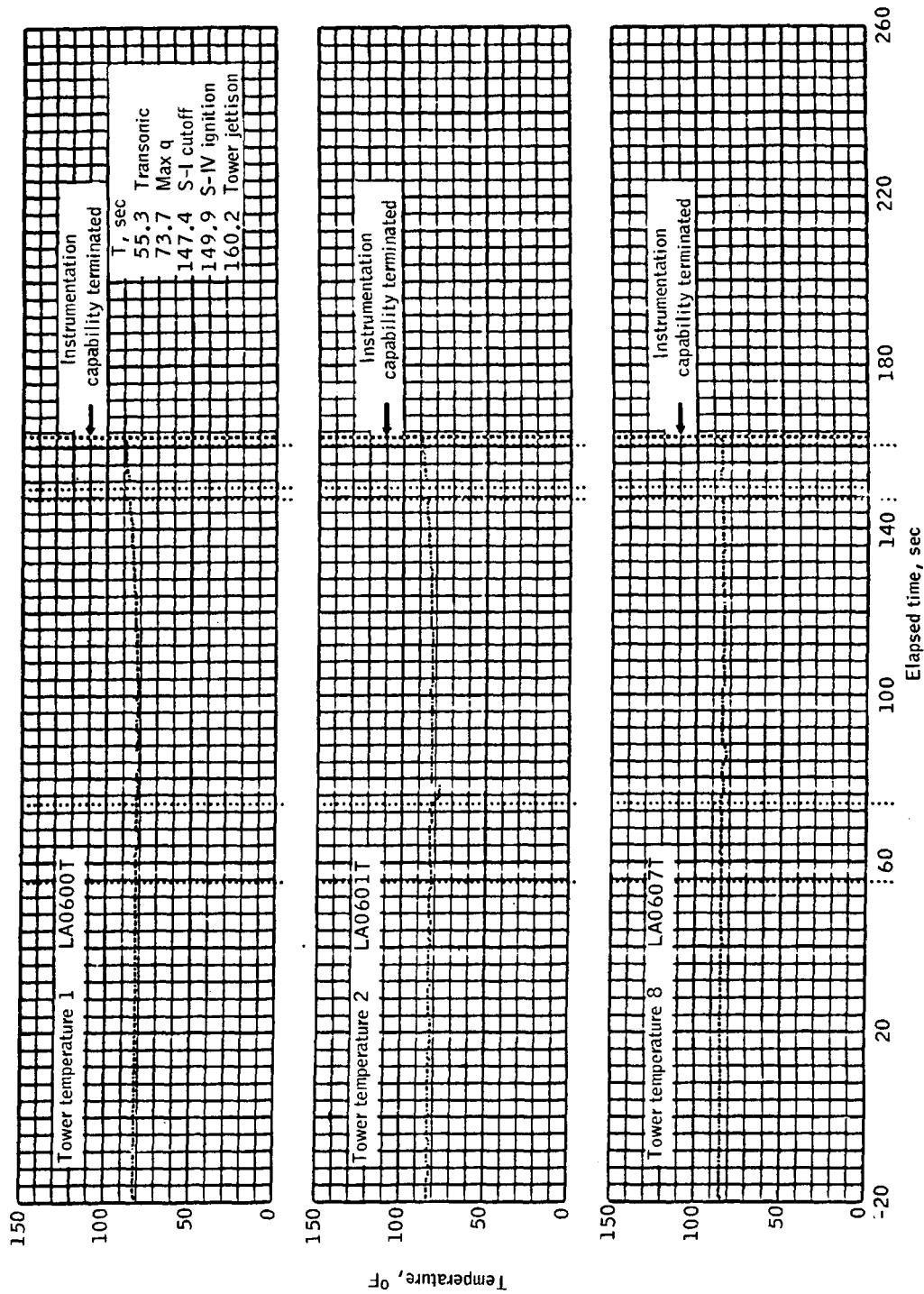
4-181



Eight temperature sensors bonded to structure

Figure 4.10-2. - Launch-escape tower temperature transducer locations on BP-15 spacecraft.

UNCLASSIFIED

~~CONFIDENTIAL~~

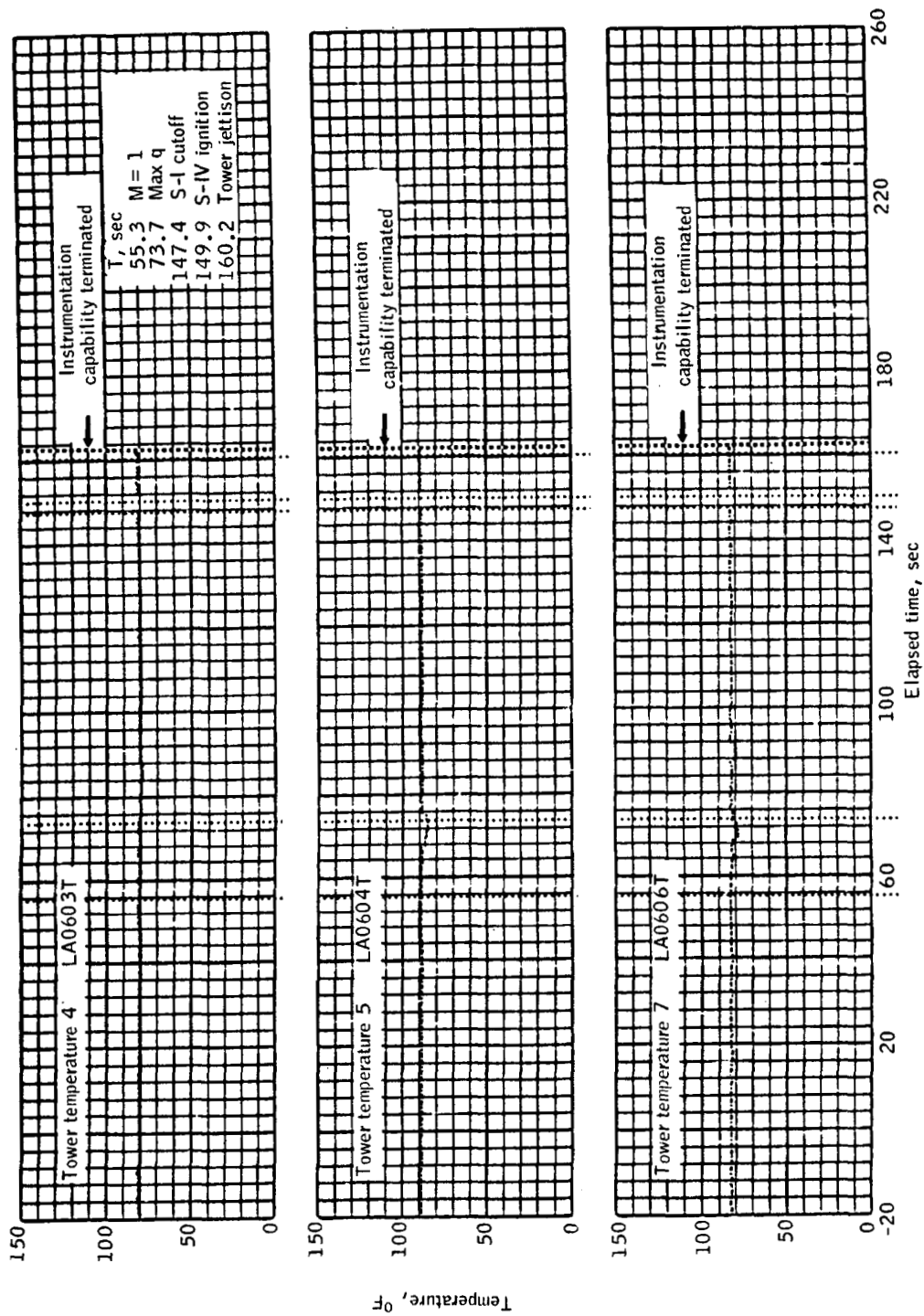
(a) Tower temperatures 1, 2 and 8.

Figure 4.10-3.- Bond-line LES tower temperatures measured during flight of BP-15 spacecraft.

~~CONFIDENTIAL~~

CONFIDENTIAL

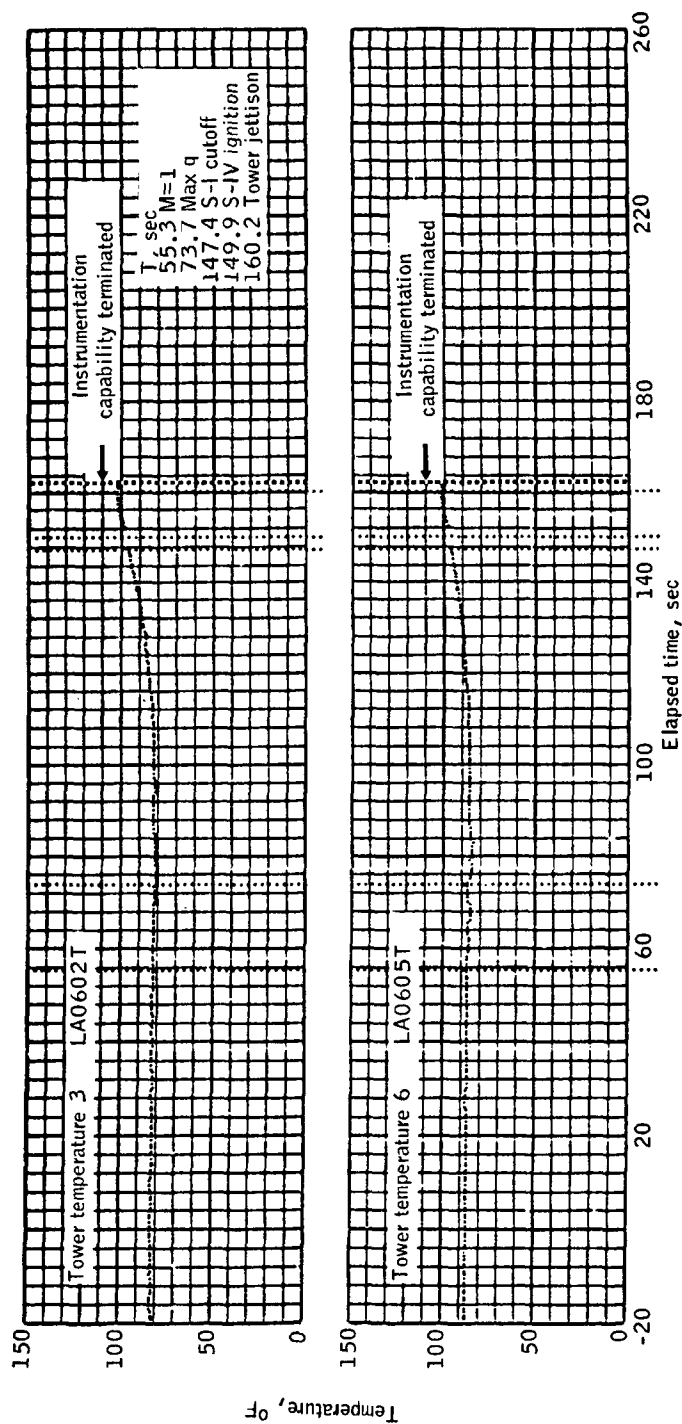
4-183



(b) Tower temperatures 4, 5 and 7.

Figure 4.10-3.- Continued.

CONFIDENTIAL

~~CONFIDENTIAL~~

(c) Tower temperatures 3 and 6.

Figure 4.10-3.- Concluded.

~~CONFIDENTIAL~~

~~CONFIDENTIAL~~

4-185

4.11 Aerothermodynamics

In order to define the launch heating environment, 20 asymptotic calorimeters were installed on the spacecraft: 12 on the command module, 7 on the service module, and 1 on the adapter section (figs. 4.11-1 and 4.11-2). Instrumentation locations were selected to determine heating rates both in clean areas and in the vicinity of various surface irregularities. The maximum measured heating rates of $7.2 \text{ Btu/ft}^2/\text{sec}$ on the command module and $0.9 \text{ Btu/ft}^2/\text{sec}$ on the service module are similar to those obtained on the BP-13 spacecraft (ref. 1) and are in agreement with predicted values (ref. 4).

All calorimeters appeared to function normally through lift-off; however, the calorimeter located on the service module behind the forward RCS nozzle did not respond to the main heat pulse at $T+60$ seconds. The calorimeter in the same position also failed during the flight of the BP-13 spacecraft.

The flight environment for the BP-15 spacecraft is shown in figure 4.11-3 and is very similar to that of the BP-13 spacecraft. The Reynolds number based on the maximum body diameter exceeded 10^7 and had decreased to 5×10^4 at staging. Hence, turbulent flow was expected throughout that portion of the trajectory during which heating occurred. A Mach number of 9.5 was reached at the time of staging. The peak heating rates were generally attained at a Mach number of 3.7 and a Reynolds number of 4×10^6 .

The angle of attack began a gradual increase at about $T+80$ seconds and continued to increase throughout the heating period (fig. 4.11-4). A more severe increase occurred between $T+130$ and $T+135$ seconds. Although Q -ball data during this portion of the flight are not very accurate, the data indicate the above trends. These trends in angle of attack are also indicated by the calorimeter data.

Command module heating. - The heating rate histories recorded by the command module calorimeters are presented in figure 4.11-5 and are grouped to show circumferential variations, variations along conical elements, and the influence of various surface irregularities.

At all locations, the major heat pulse was experienced from $T+60$ to $T+145$ seconds with peak values occurring between $T+100$ and $T+112$ seconds. Peak heating values varied from $7.2 \text{ Btu/ft}^2/\text{sec}$ at the location of calorimeters 7 and 12 to $3.3 \text{ Btu/ft}^2/\text{sec}$ at the location of

~~CONFIDENTIAL~~

~~CONFIDENTIAL~~

calorimeter 2. All calorimeters except those along the 180° conical element (2, 4, and 11) experienced a second peak at approximately $T+135$ seconds. The heating recorded by calorimeters 2, 4, and 11 dropped sharply as the heating at the locations of the other calorimeters approached this second peak. At $T+135$ seconds the Mach number was about 7 and the Reynolds number was about 2×10^5 .

An examination of circumferential variations and variations along conical elements indicates an angle-of-attack effect on local heating which is consistent with the trends of the Q-ball data. This effect is illustrated in figure 4.11-5(h) which shows the circumferential variation in heating at X_{C74} . Calorimeters 1 and 3 located on the windward side received the highest heat load, while calorimeter 2 on the leeward side received the lowest. This same effect can be seen on calorimeters 11 and 12 at X_{C27} (fig. 4.11-5(i)) and on calorimeters 4, 5, 6, and 9 at X_{C54} (fig. 4.11-5(j)). The extended heating at calorimeter 5 after $T+100$ seconds is attributed to the influence of the scimitar antenna. The angle-of-attack increase began to influence heating at approximately $T+90$ seconds. The second peak on the windward calorimeters and the corresponding rapid decrease on the leeward calorimeters (2, 4, and 11) occurred at the same time ($T+130$ to $T+135$ seconds) as the rapid increase in angle of attack (fig. 4.11-4). In the period from $T+90$ to $T+123$ seconds, the location of the windward conical element varied between 360° and 345° , and between 345° and 310° during the period from $T+125$ seconds to $T+135$ seconds. This movement of the effective wind vector caused the second peak at the location of calorimeter 3 to be higher than that at the location of calorimeter 1.

The magnitude of the heating at these second peaks is consistent with predictions based on wind-tunnel data for an angle of attack of 5° (ref. 5).

Calorimeters 3, 9, and 12 located downstream of the tower leg well indicated no significant influence of this surface irregularity on local heating (fig. 4.11-5(k)). No sharp dropoff in heating at the location of calorimeter 3, similar to that experienced by the BP-13 spacecraft, was experienced during the flight of BP-15 spacecraft. (See fig. 4.11-7(a).) It appears that at the location of calorimeter 3, the flow was separated after approximately 95 seconds on the BP-13 spacecraft, whereas it was attached throughout the heating period on the BP-15 spacecraft.

Calorimeters 2, 4, and 11 (fig. 4.11-5(l)) indicate no significant effect of the hatch cover on local heating; however, examination of this figure substantiates the conclusions concerning angle of attack.

~~CONFIDENTIAL~~

~~CONFIDENTIAL~~

4-187

The calorimeter nearest the apex on the leeward side (calorimeter 2) would be the first to respond to angle-of-attack effects as evidenced by reduced heating. This effect can be noted during the gradual increase in angle of attack from T+90 to T+125 seconds, as well as during the rapid increase shortly thereafter.

A comparison of the data obtained at calorimeters 5 and 10 on the BP-13 and BP-15 spacecraft (figs. 4.11-6(b) and 4.11-6(c)) indicates that the upstream influence of the scimitar antenna was greater during the flight of the BP-15 spacecraft. The heating at location 10 is approximately the same on both vehicles; however, the location of calorimeter 5 experienced a lower heat pulse on the BP-13 spacecraft. During the flight of the BP-15 spacecraft the heating at calorimeter 5 was approximately equal to that of the heating at calorimeter 10. (See fig. 4.11-5(m).)

The heating in the vicinity of the strake stub is illustrated in figure 4.11-5(n). As on the BP-13 spacecraft, calorimeter 8 registered heating rates lower than did calorimeters 6 and 7, which were approximately equal. Further analysis is required to determine the reason for this difference.

The heating caused by the LES motor during tower jettison is evident at all locations at approximately T+160 seconds.

Service module and adapter heating.- The heating-rate histories for the service module and adapter calorimeters, presented in figure 4.11-7, were similar to those obtained on the BP-13 spacecraft. Figure 4.11-6(d) compares the heating in a "clean" area during the two flights.

All service module calorimeters recorded decrease in heating at about T+135 seconds, again reflecting the effect of a sudden increase in angle of attack.

As during the flight of the BP-13 spacecraft, calorimeter 13 located on the surface of the service module behind the forward RCS nozzle did not respond to the main heat pulse at T+60 seconds. However, the calorimeter body-temperature history indicated that this area experienced higher heating than any other region on the service module, an observation which is consistent with predictions based on wind-tunnel measurements (ref. 4).

With the exception of calorimeter 13, the service module calorimeter body temperatures remained within 6 percent of each other. Body temperature for calorimeter 13 was about 30 percent higher than the body temperature for nearby calorimeters 18 and 20. The maximum heating rates

~~CONFIDENTIAL~~

~~CONFIDENTIAL~~

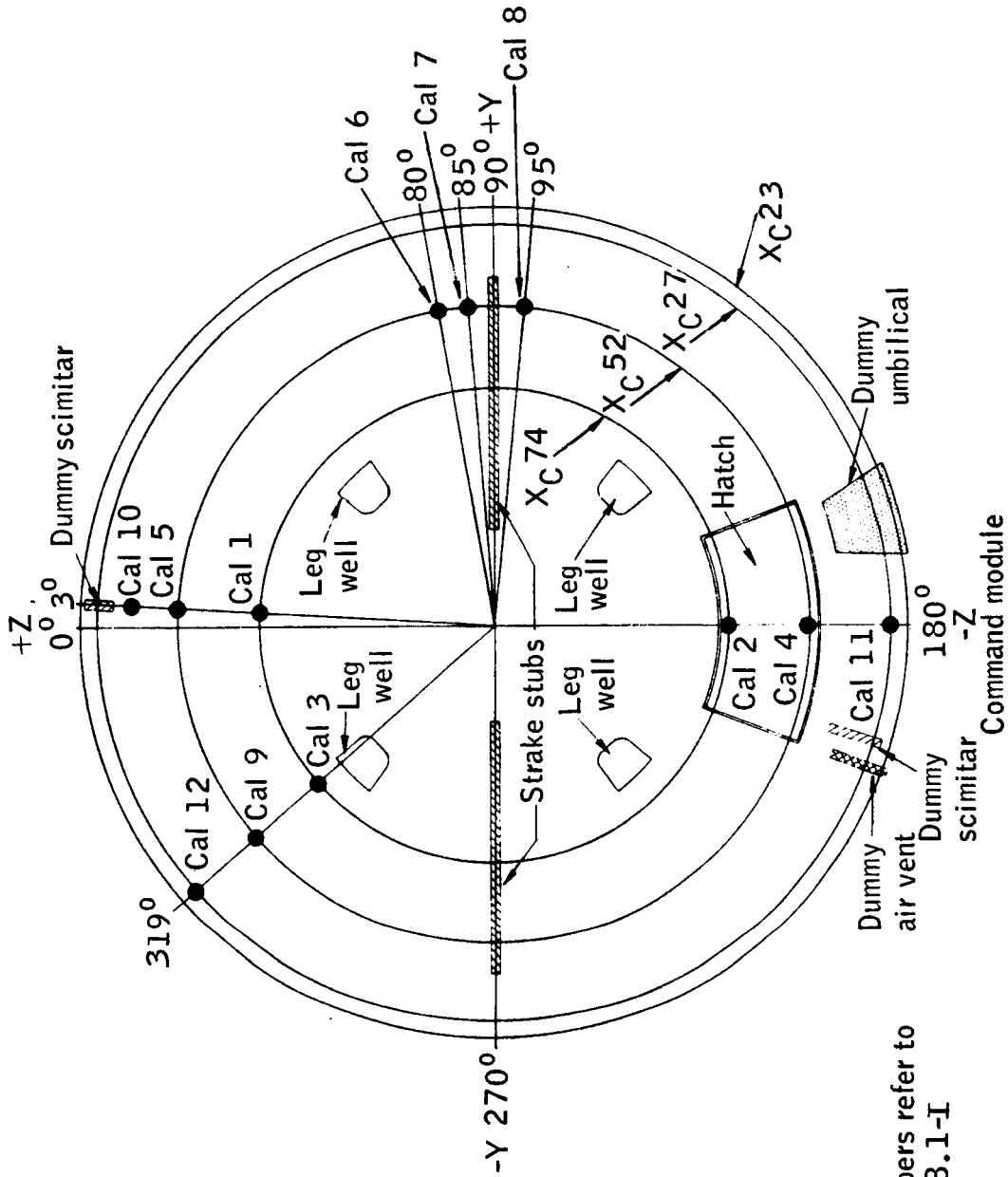
for calorimeters 18 and 20 were about 30 percent higher than the rates for "clean" area calorimeters such as calorimeter 16. See figures 4.11-8, and 4.11-7(a) to 4.11-7(d).

Summary.- The launch heating environment of the BP-15 spacecraft was similar to that of the BP-13 spacecraft. Peak values at most locations were approximately equal; however, the influence of surface irregularities as well as circumferential variations in heating were somewhat different during the two missions. Heating rates on both the command and service modules were within predicted values.

~~CONFIDENTIAL~~

UNCLASSIFIED

4-189



Note:
Calorimeter numbers refer to
listing in table 8.1-I

Figure 4.11-1. - Top view of BP-15 spacecraft command module showing calorimeter locations.

UNCLASSIFIED

~~CONFIDENTIAL~~

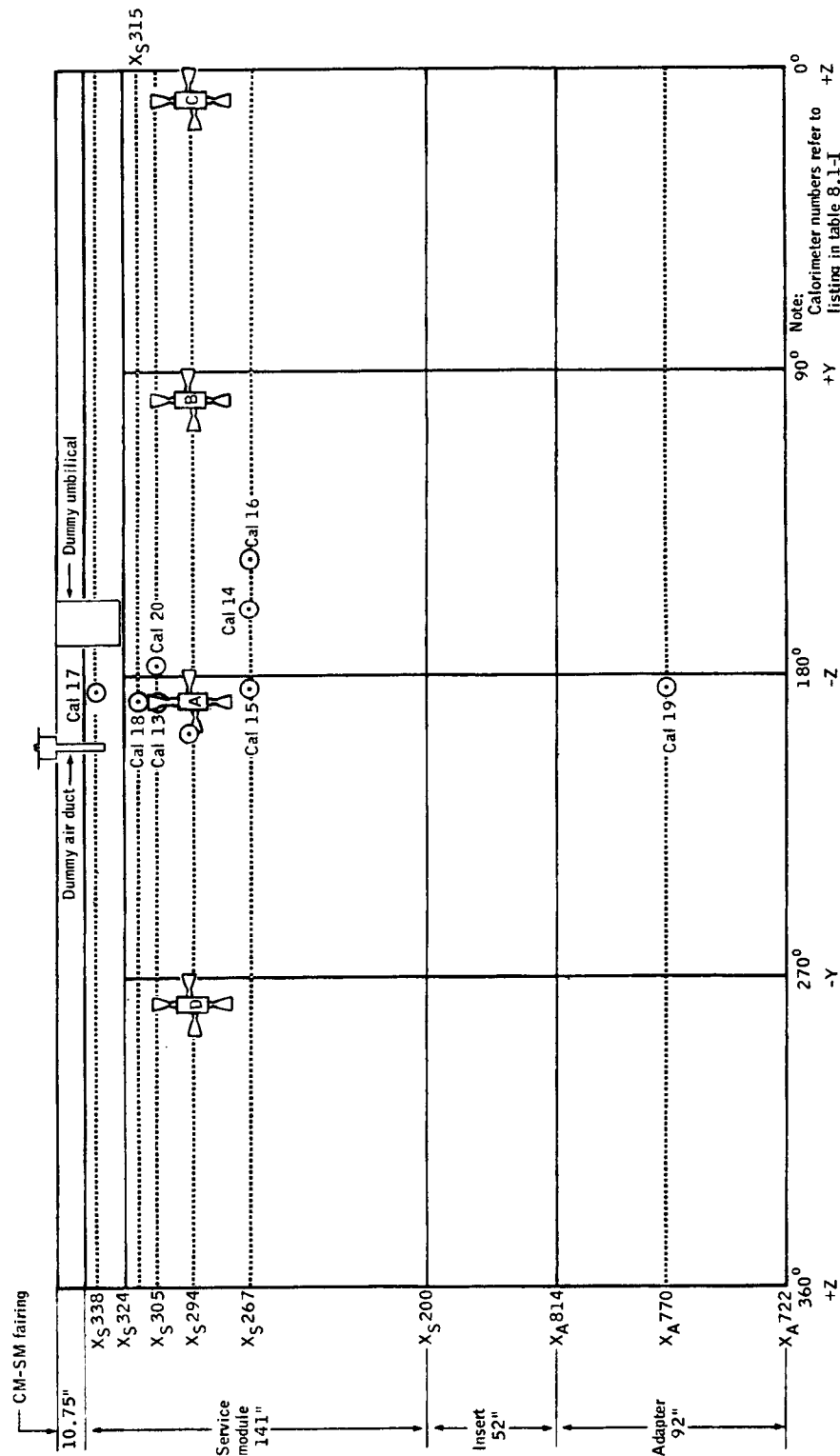


Figure 4.11-2. - Development view of BP-15 spacecraft service module, insert, and adapter compartment showing calorimeter locations.

~~CONFIDENTIAL~~

~~CONFIDENTIAL~~

4-191

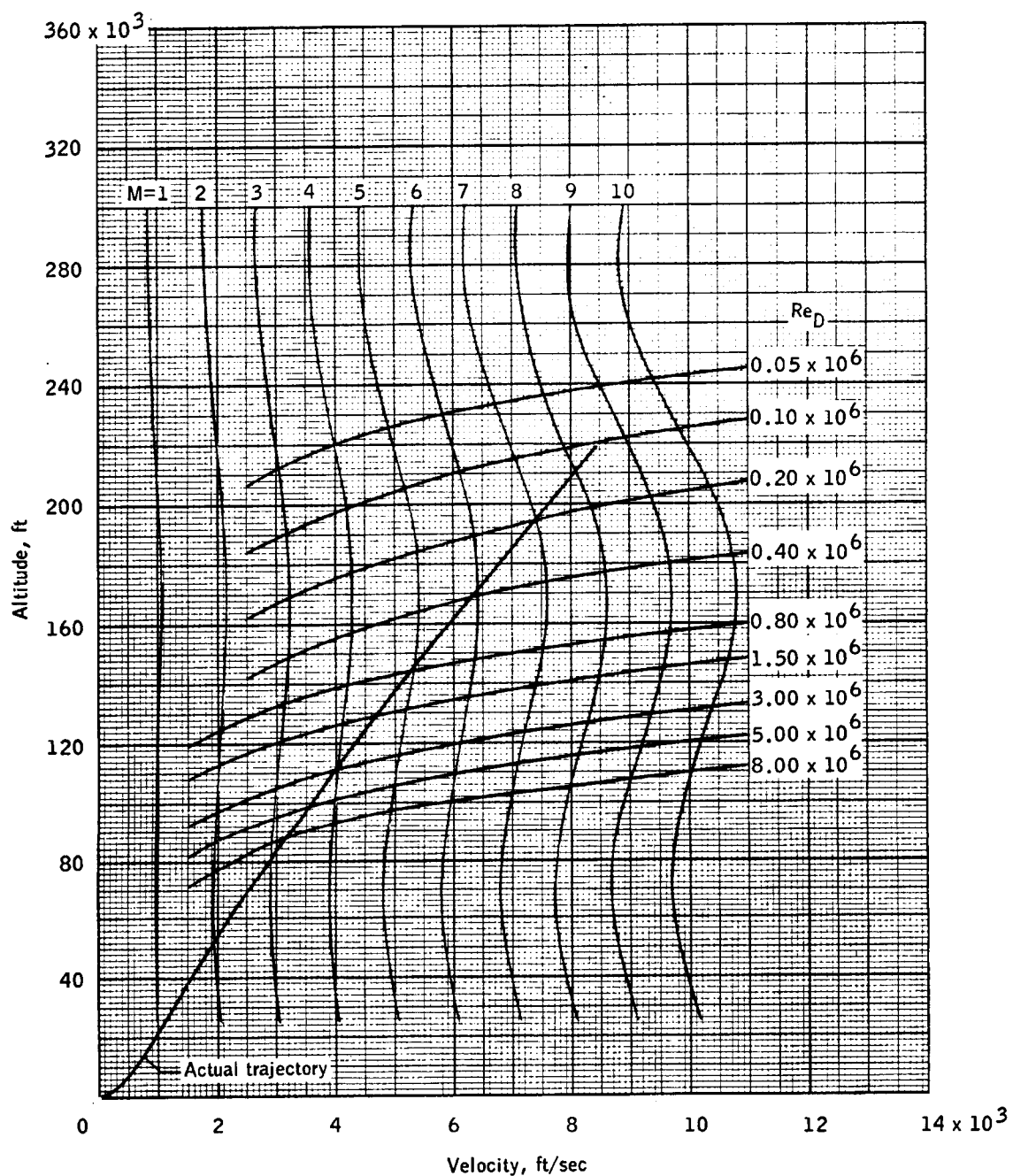


Figure 4.11-3.- Launch configuration environment in terms of Mach number (M) and Reynolds number (Re_D) for BP-15 spacecraft.

~~CONFIDENTIAL~~

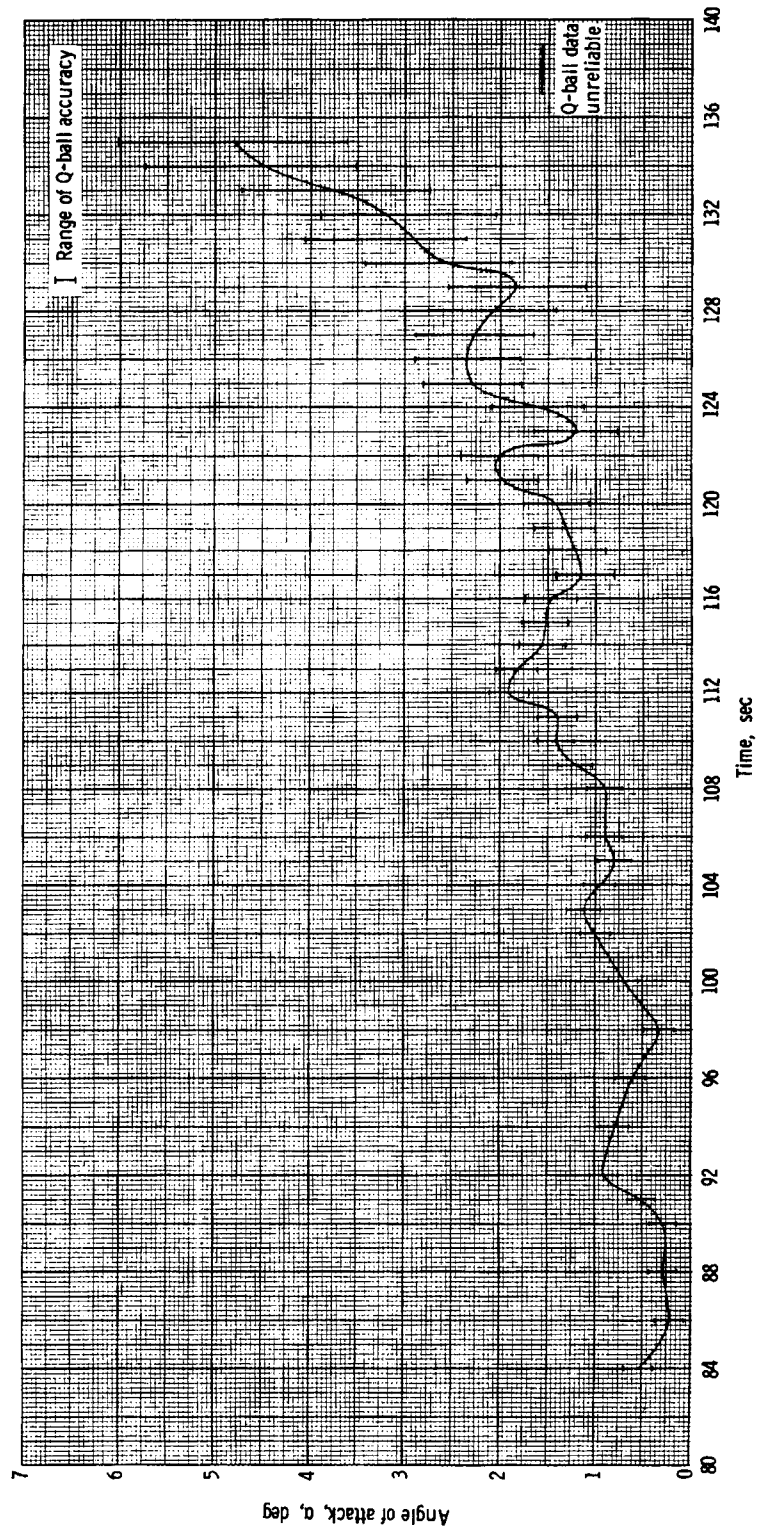
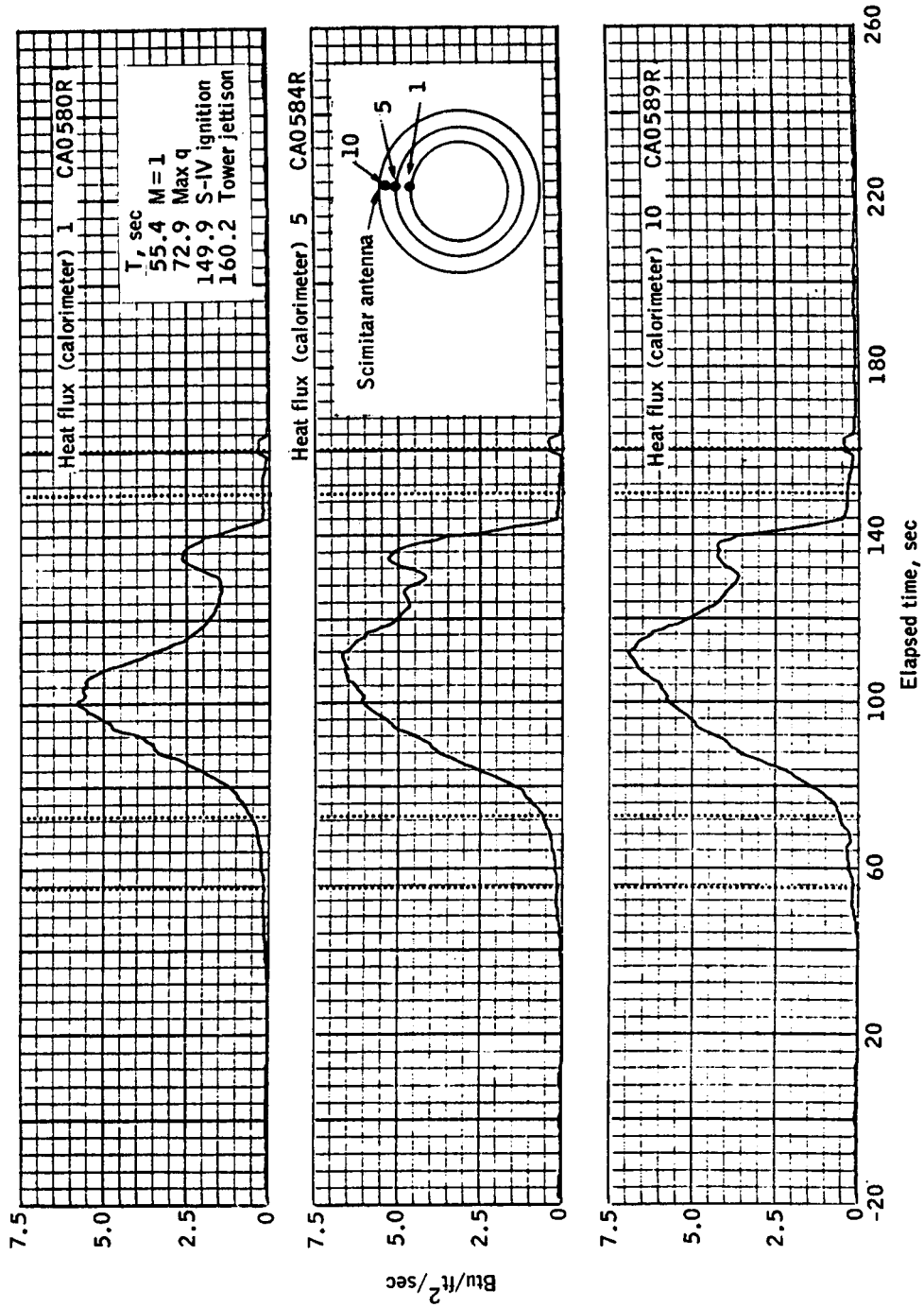
~~CONFIDENTIAL~~

Figure 4.11-4. - Angle of attack history for BP-15 spacecraft (Q-ball data).

~~CONFIDENTIAL~~

~~CONFIDENTIAL~~

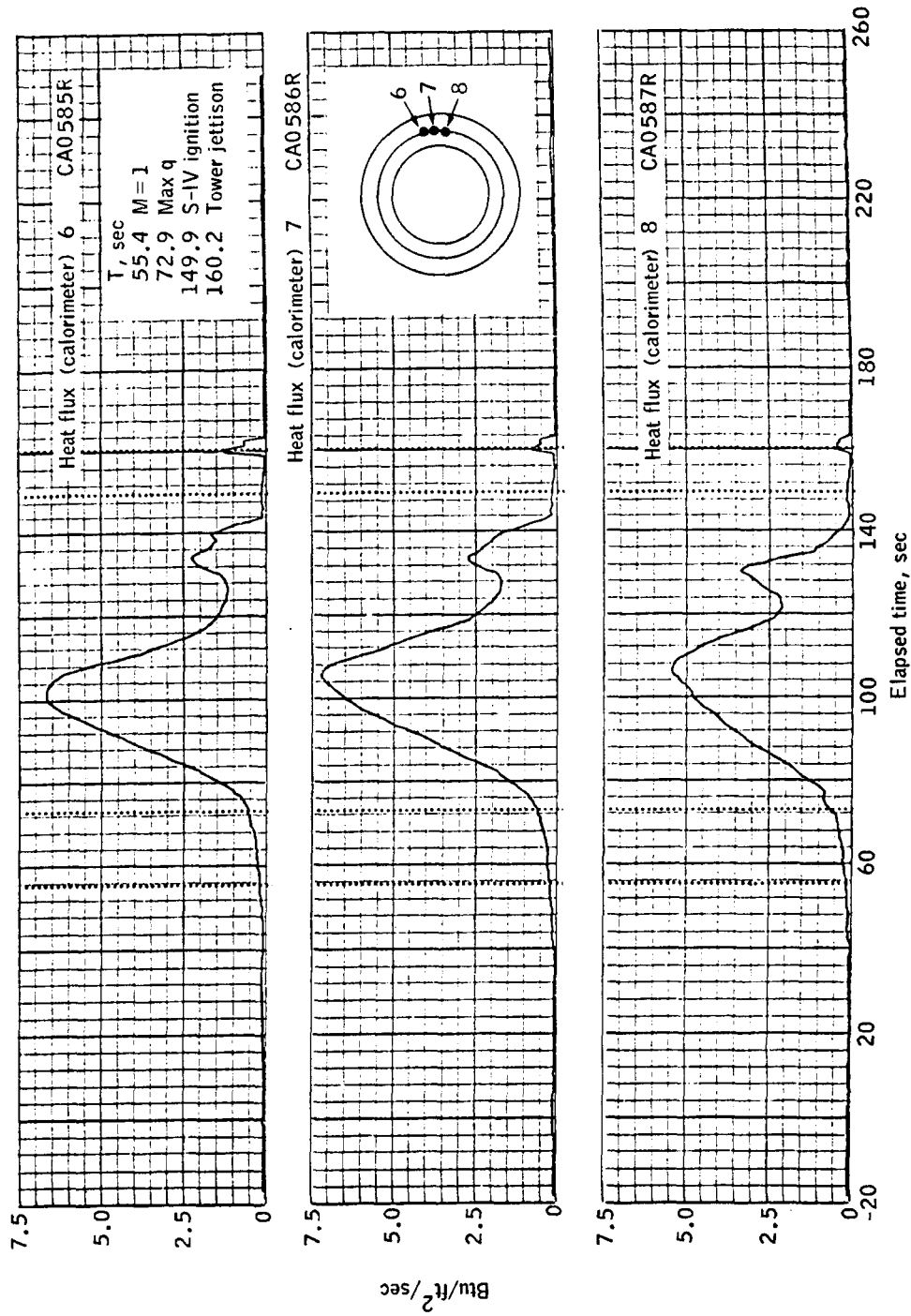
4-193



(a) Calorimeters 1, 5, 10.

Figure 4.11-5.- Heating rates measured on BP-15 spacecraft command module.

~~CONFIDENTIAL~~

~~CONFIDENTIAL~~

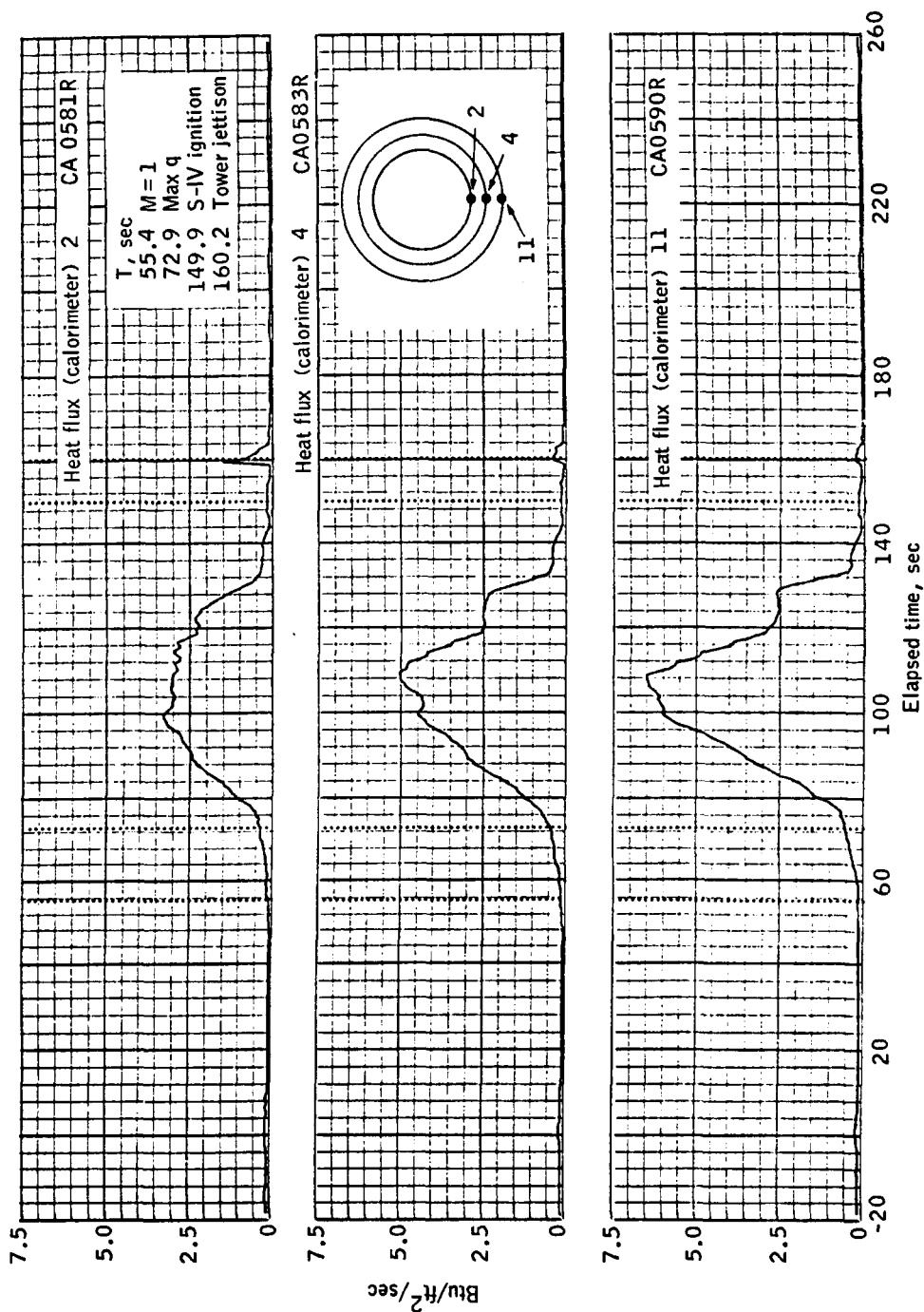
(b) Calorimeters 6, 7, 8.

Figure 4.11-5.- Continued.

~~CONFIDENTIAL~~

~~CONFIDENTIAL~~

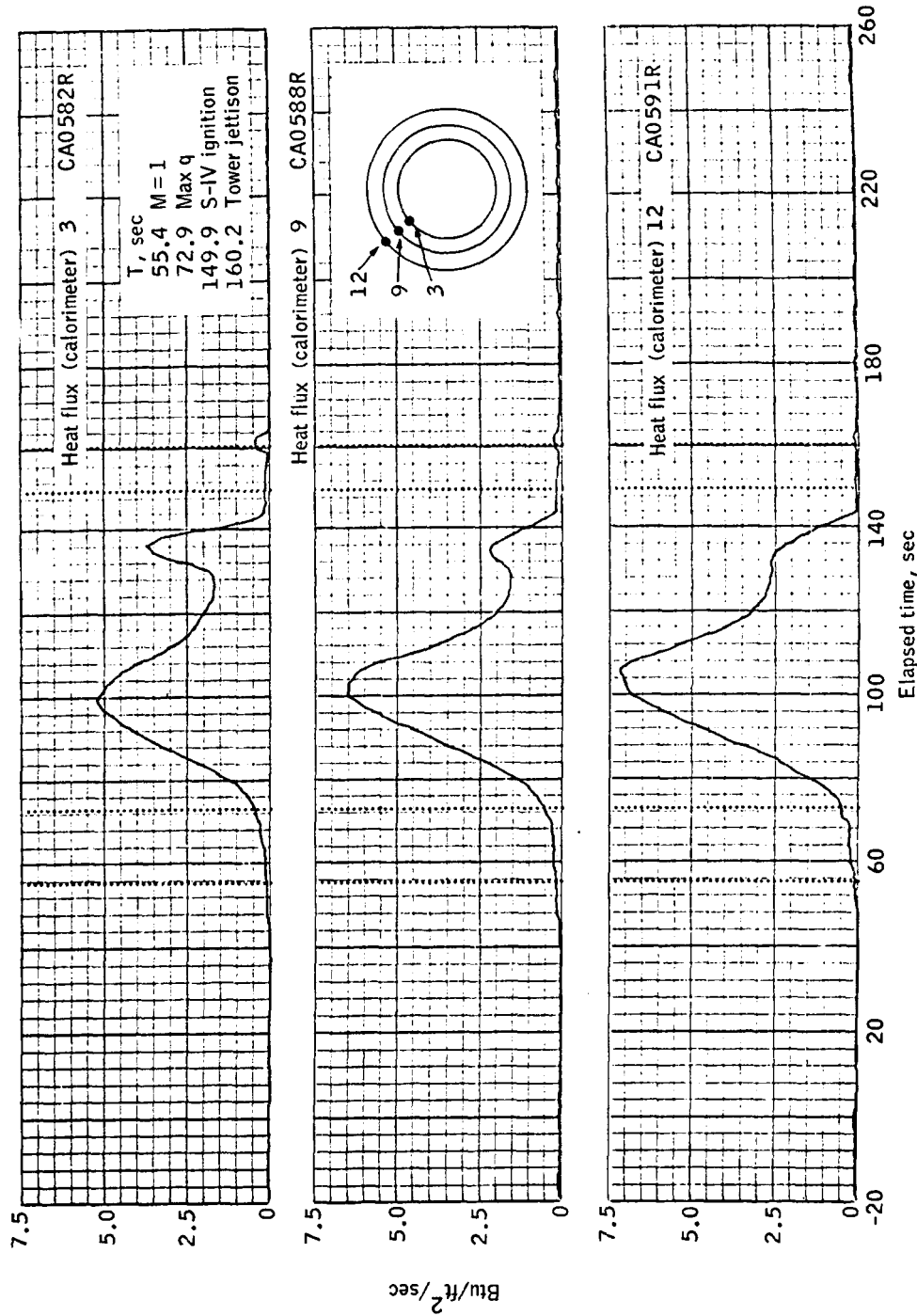
4-195



(c) Calorimeters 2, 4, 11.

Figure 4.11-5.- Continued.

~~CONFIDENTIAL~~

~~CONFIDENTIAL~~

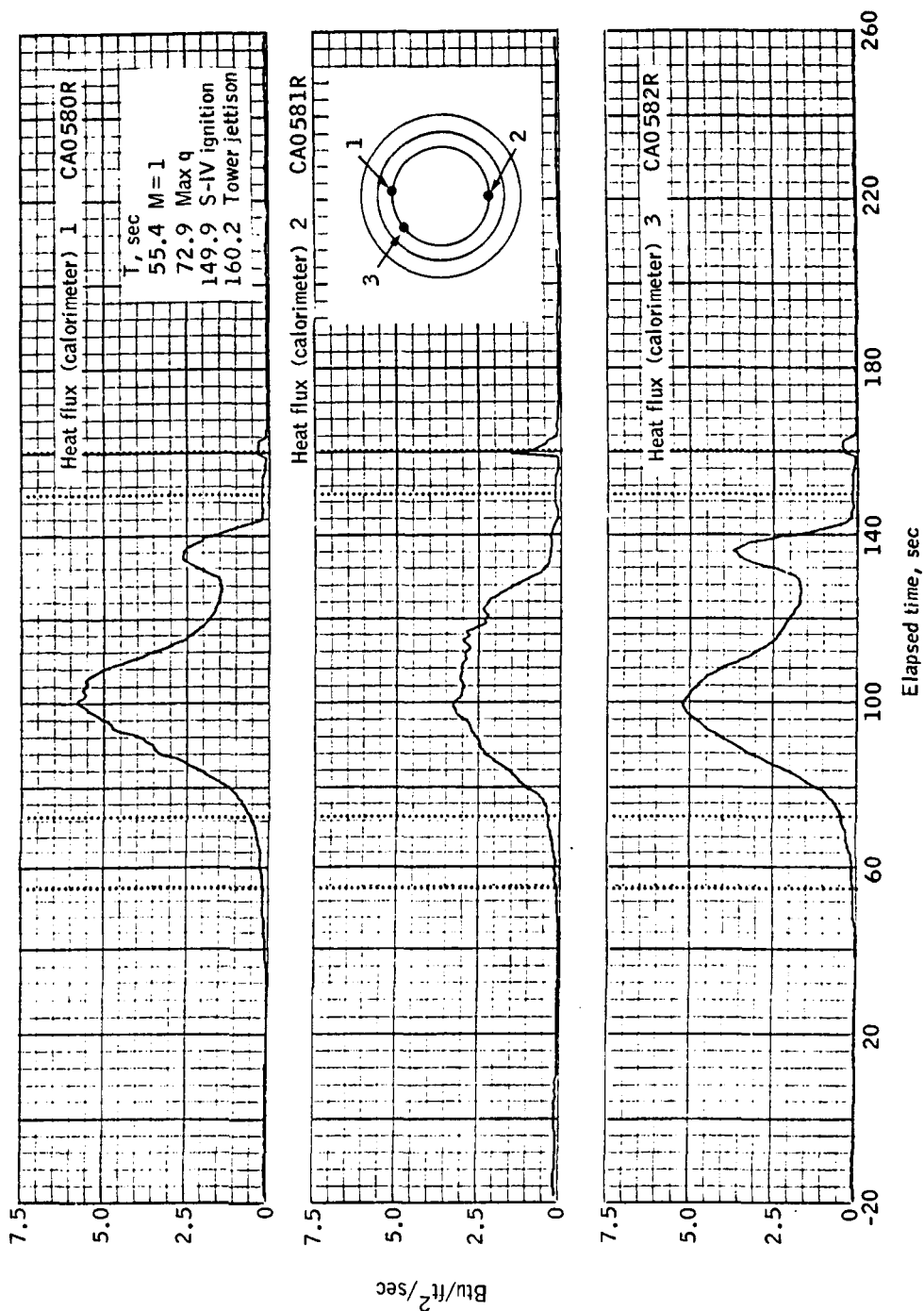
(d) Calorimeters 3, 9, 12.

Figure 4.11-5.- Continued.

~~CONFIDENTIAL~~

~~CONFIDENTIAL~~

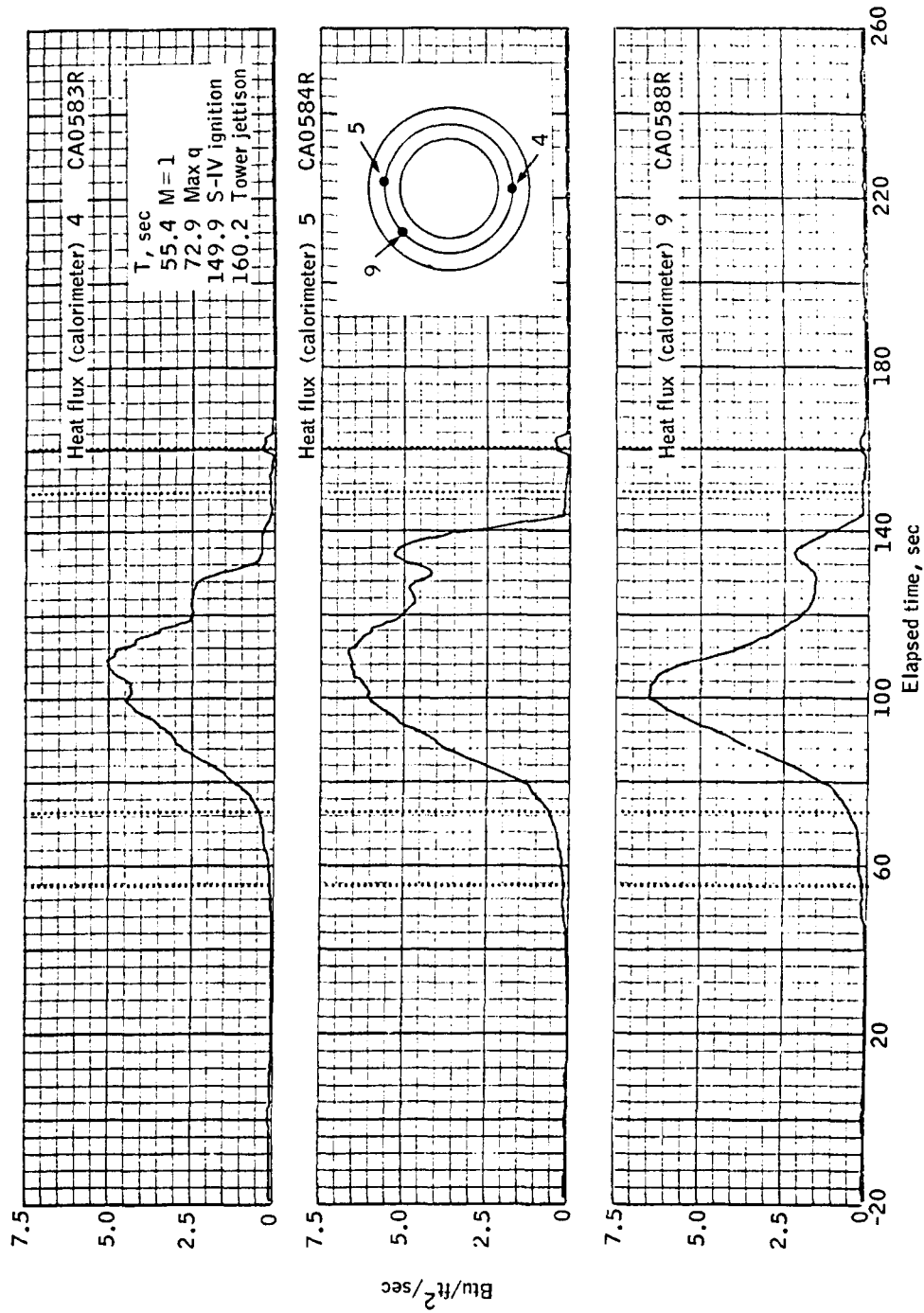
4-197



(e) Calorimeters 1, 2, 3.

Figure 4.11-5.- Continued.

~~CONFIDENTIAL~~

~~CONFIDENTIAL~~

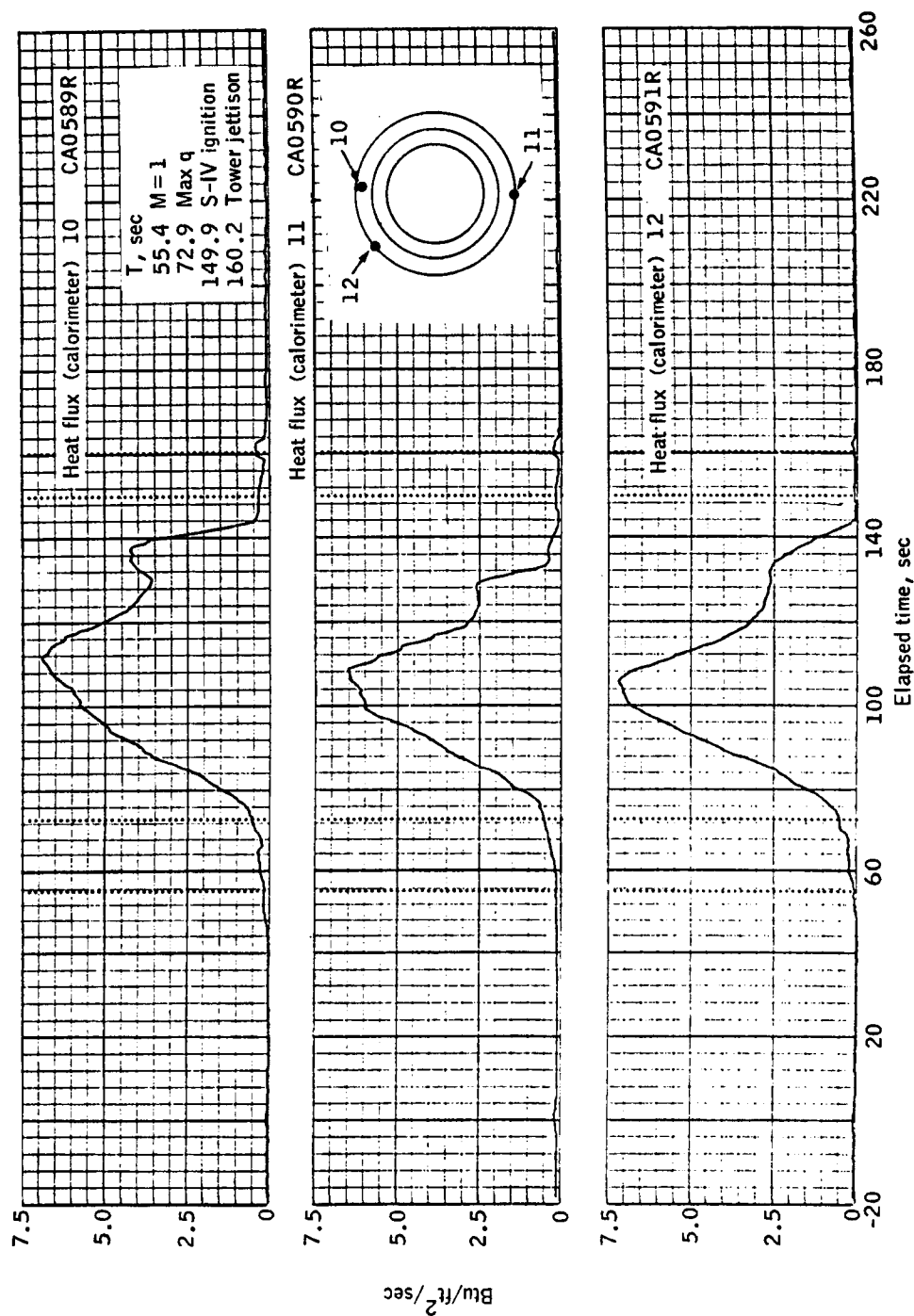
(f) Calorimeters 4, 5, 9.

Figure 4.11-5.- Continued.

~~CONFIDENTIAL~~

~~CONFIDENTIAL~~

4-199



(g) Calorimeters 10, 11, 12.

Figure 4.11-5.- Concluded.

~~CONFIDENTIAL~~

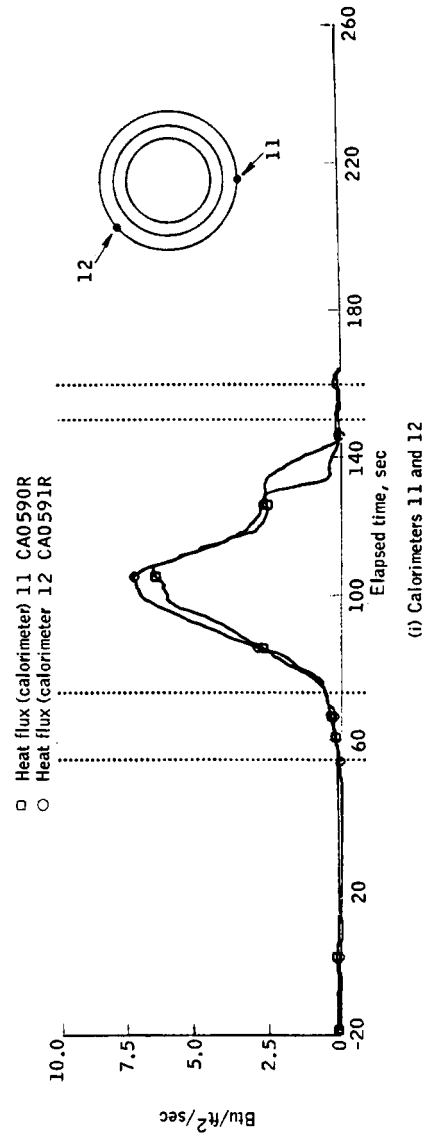
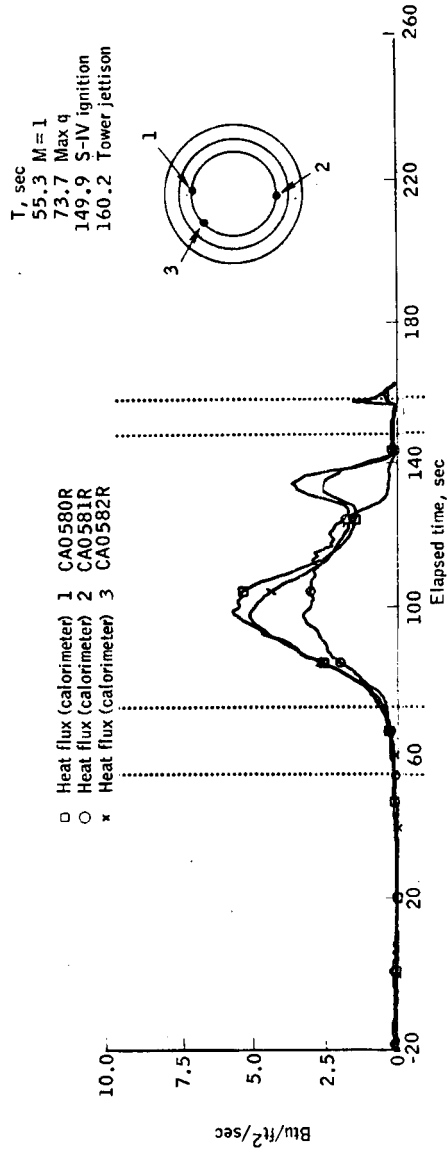
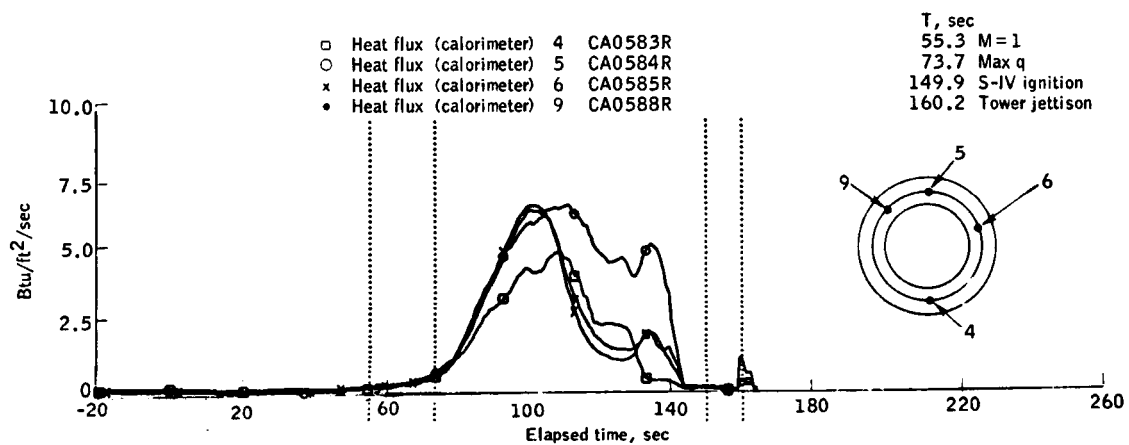
~~CONFIDENTIAL~~

Figure 4.11-5. - Continued.

~~CONFIDENTIAL~~

~~CONFIDENTIAL~~

4-201



(j) Calorimeters 4,5,6 and 9

Figure 4.11-5. - Continued.

~~CONFIDENTIAL~~

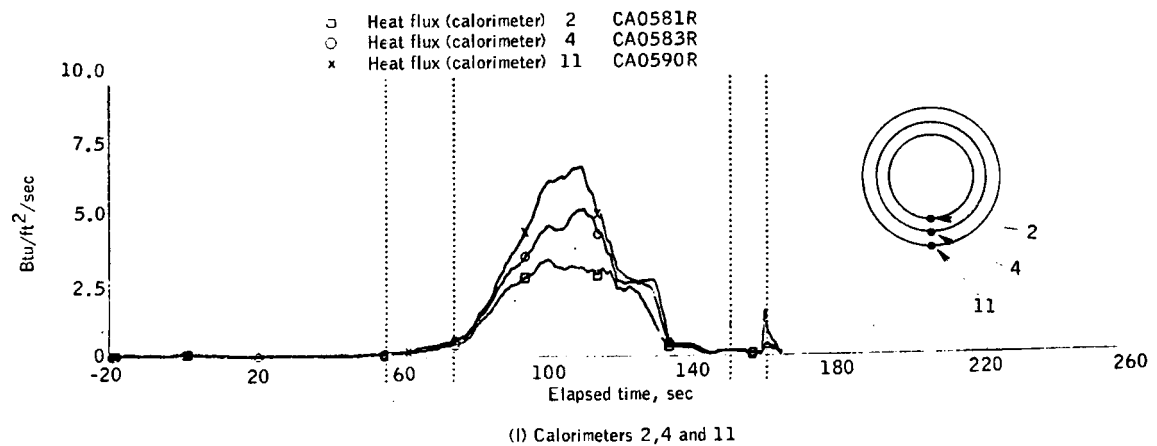
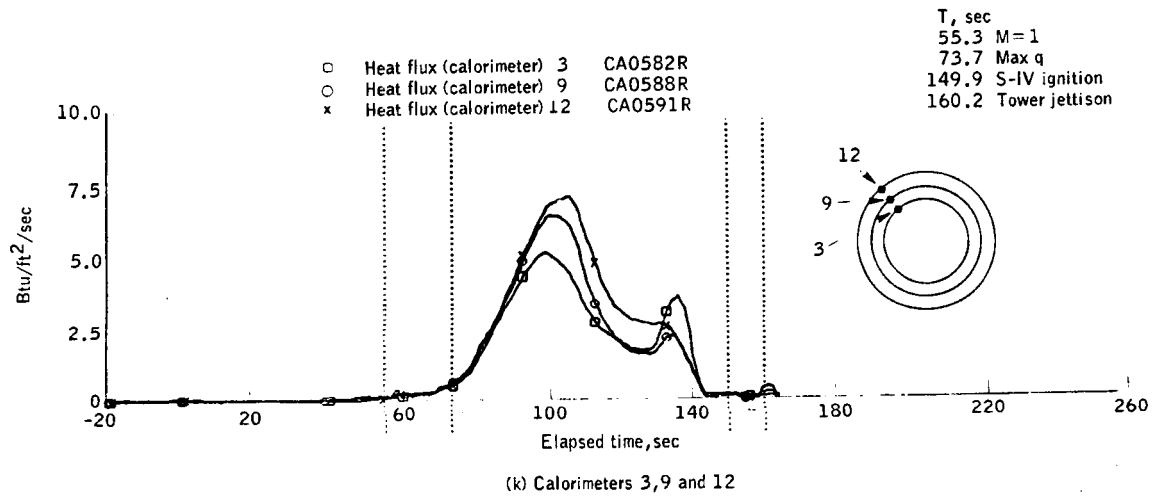
~~CONFIDENTIAL~~

Figure 4.11-5. - Continued.

~~CONFIDENTIAL~~

~~CONFIDENTIAL~~

4-203

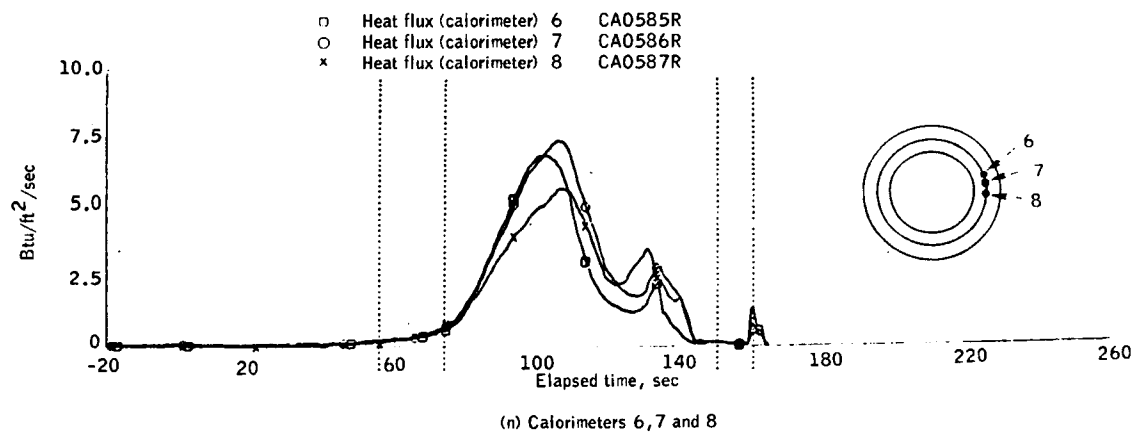
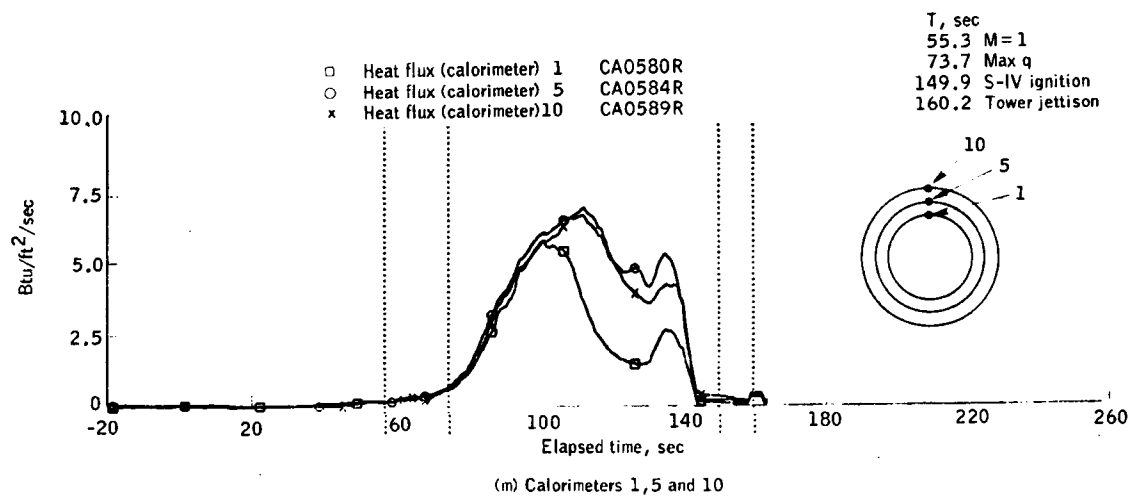
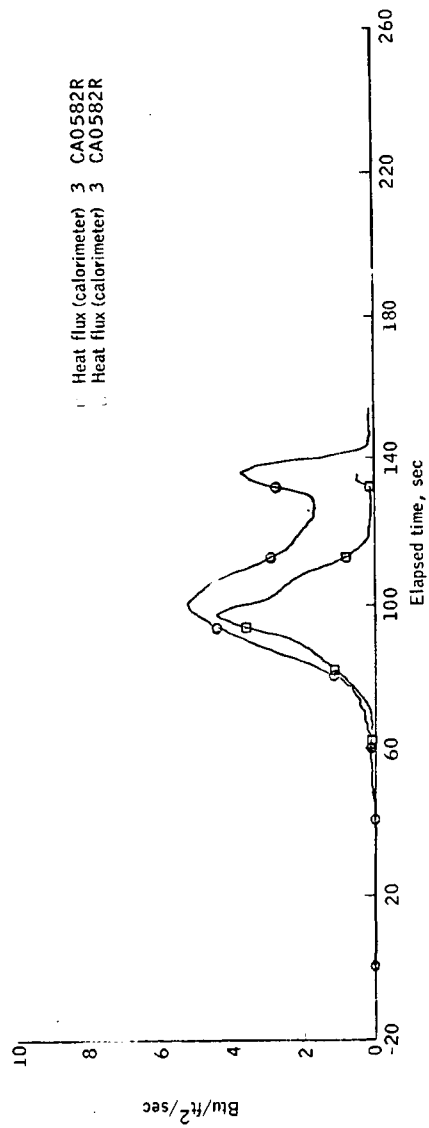
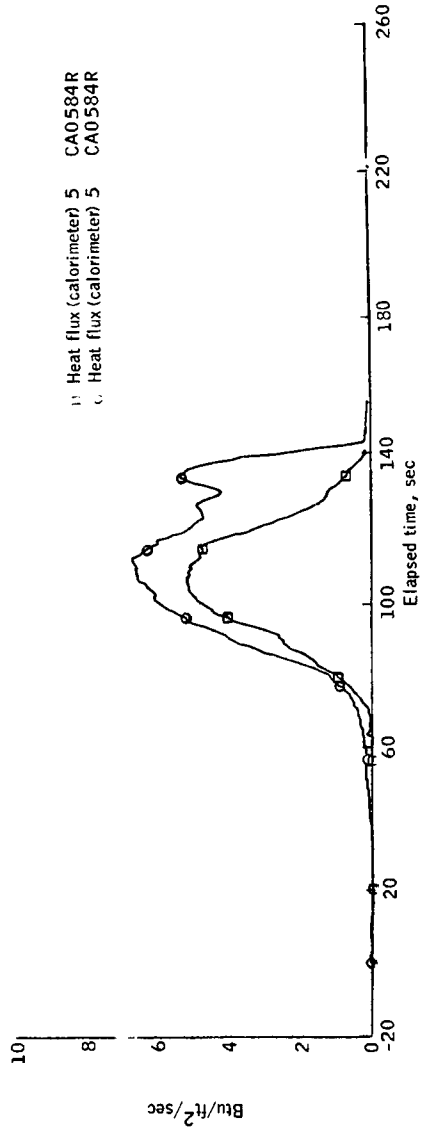


Figure 4.11-5. - Concluded.

~~CONFIDENTIAL~~



(a) BP-13 and BP-15 calorimeter 3.

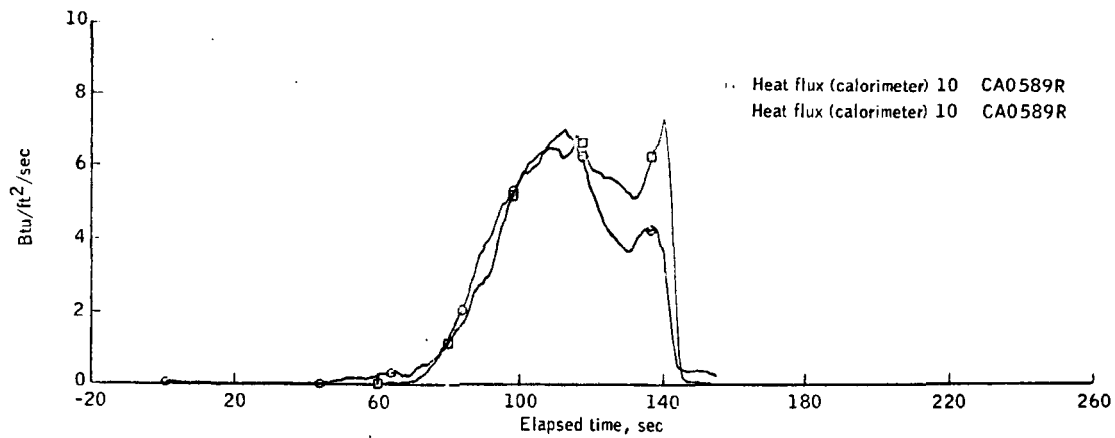


(b) BP-13 and BP-15 calorimeter 5.

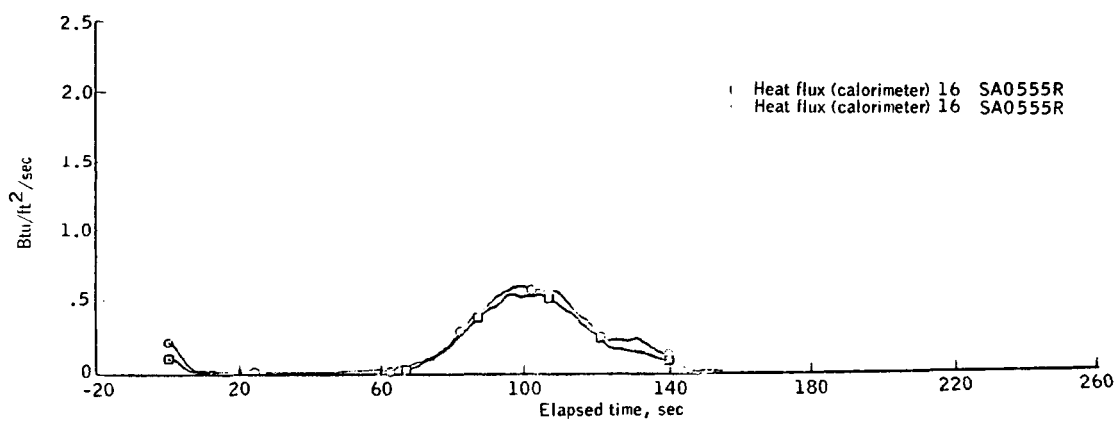
Figure 4.11-6.- Comparisons of BP-13 and BP-15 spacecraft rate.

~~CONFIDENTIAL~~

4-205



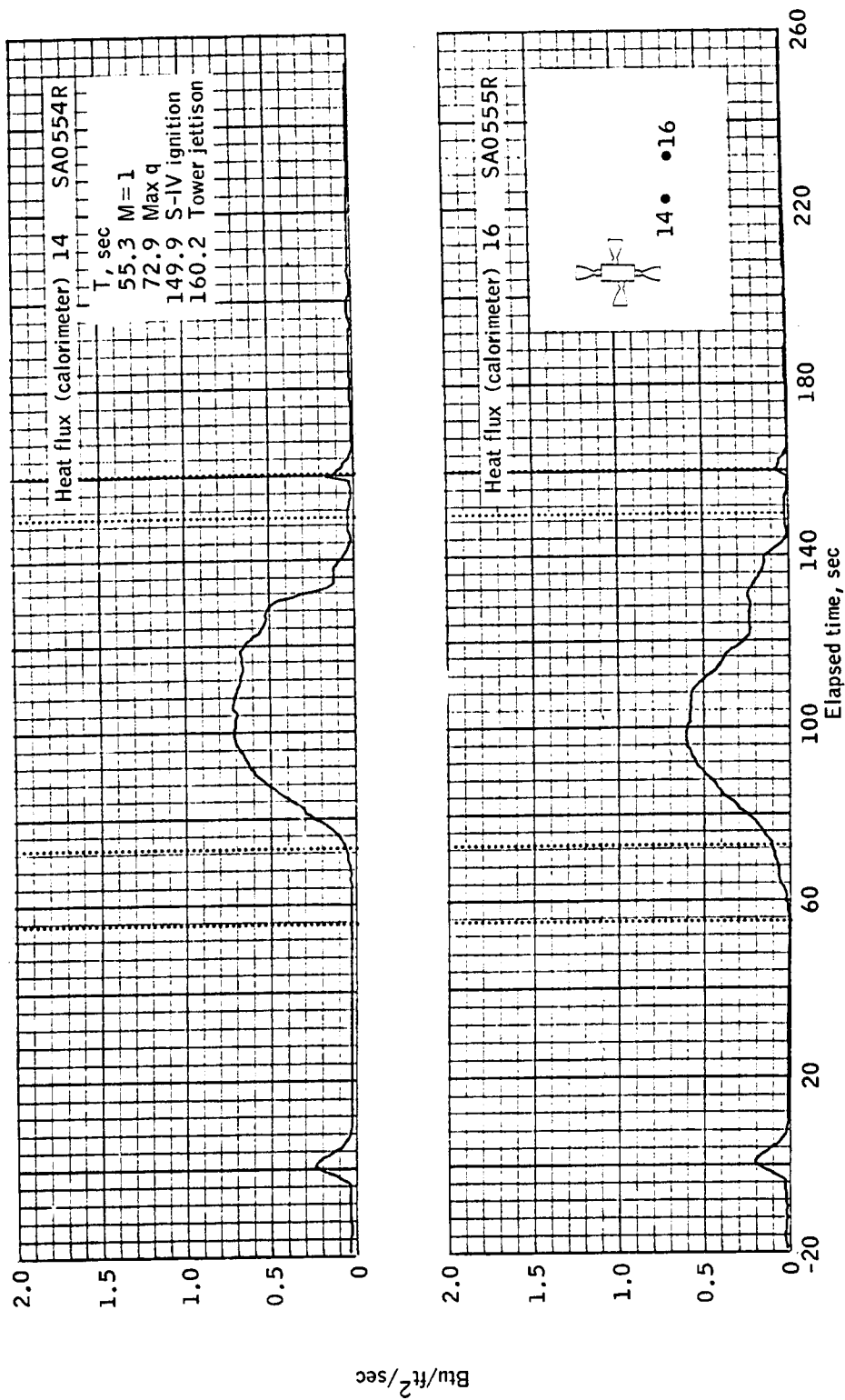
(c) BP-13 and BP-15 calorimeter 10.



(d) BP-13 and BP-15 calorimeter 16.

Figure 4.11-6.- Concluded.

~~CONFIDENTIAL~~

~~CONFIDENTIAL~~

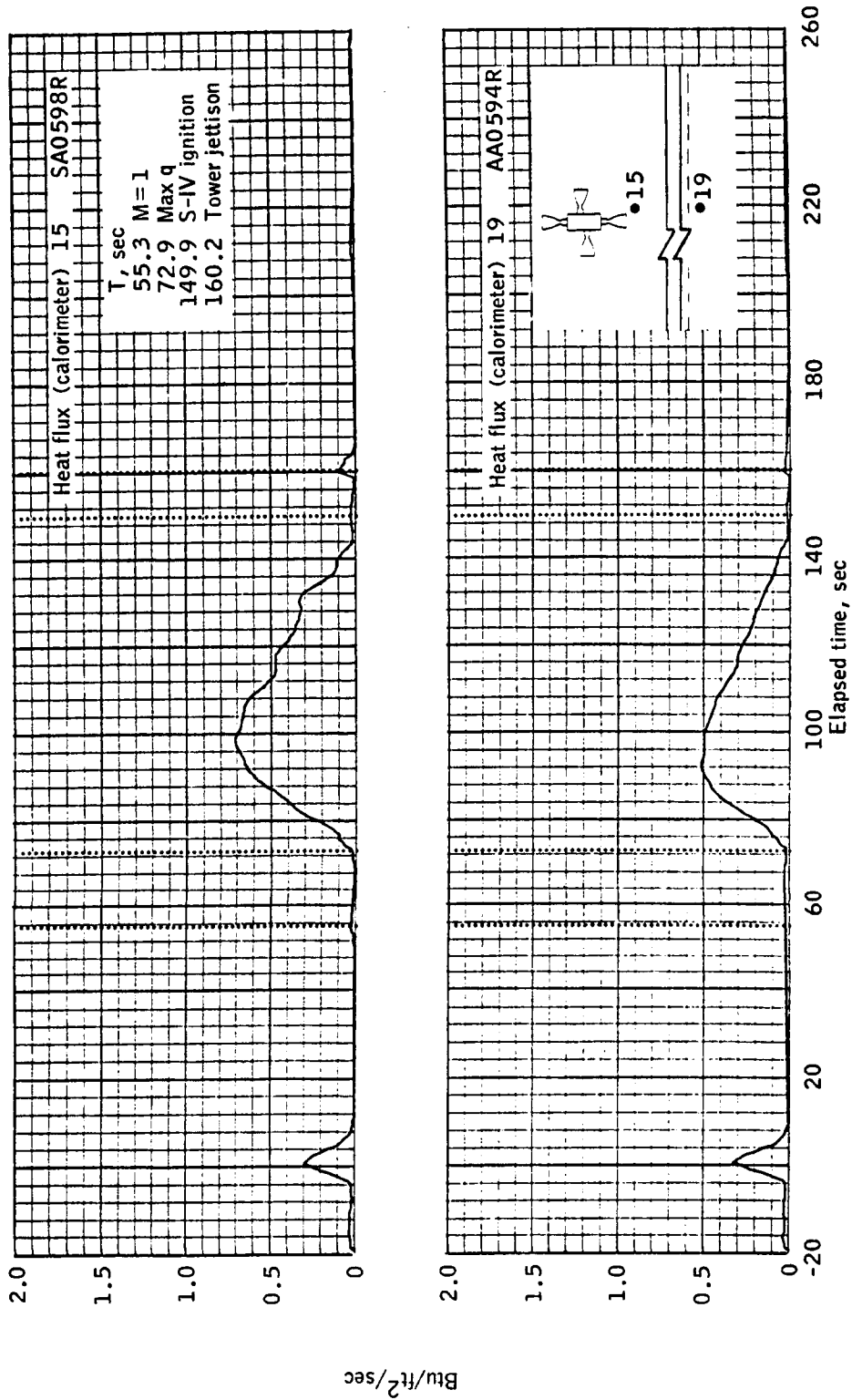
(a) Calorimeters 14 and 16.

Figure 4.11-7.- Heating rates measured on BP-15 spacecraft service module.

~~CONFIDENTIAL~~

~~CONFIDENTIAL~~

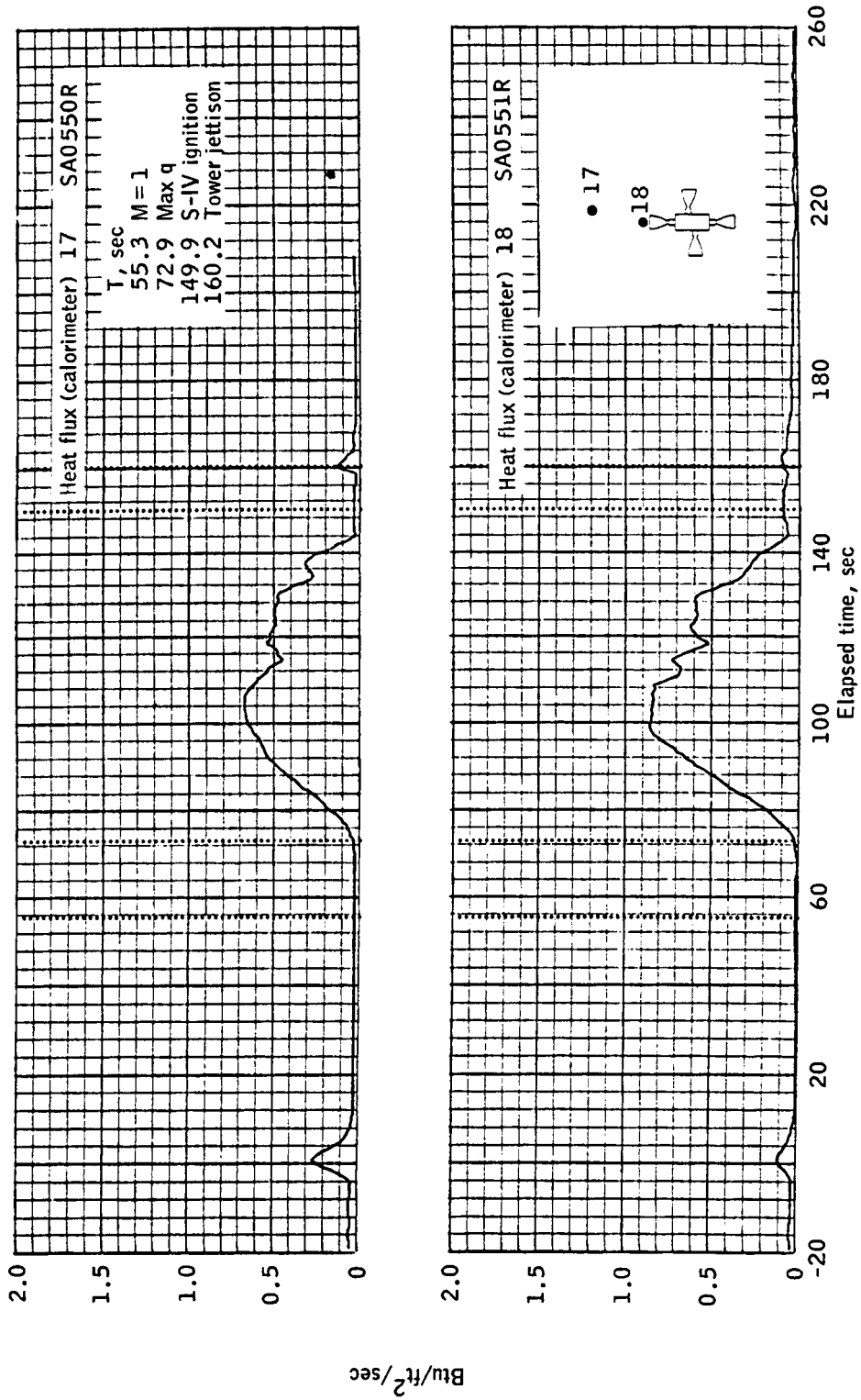
4-207



(b) Calorimeters 15 and 19.

Figure 4.11-7.- Continued.

~~CONFIDENTIAL~~

~~CONFIDENTIAL~~

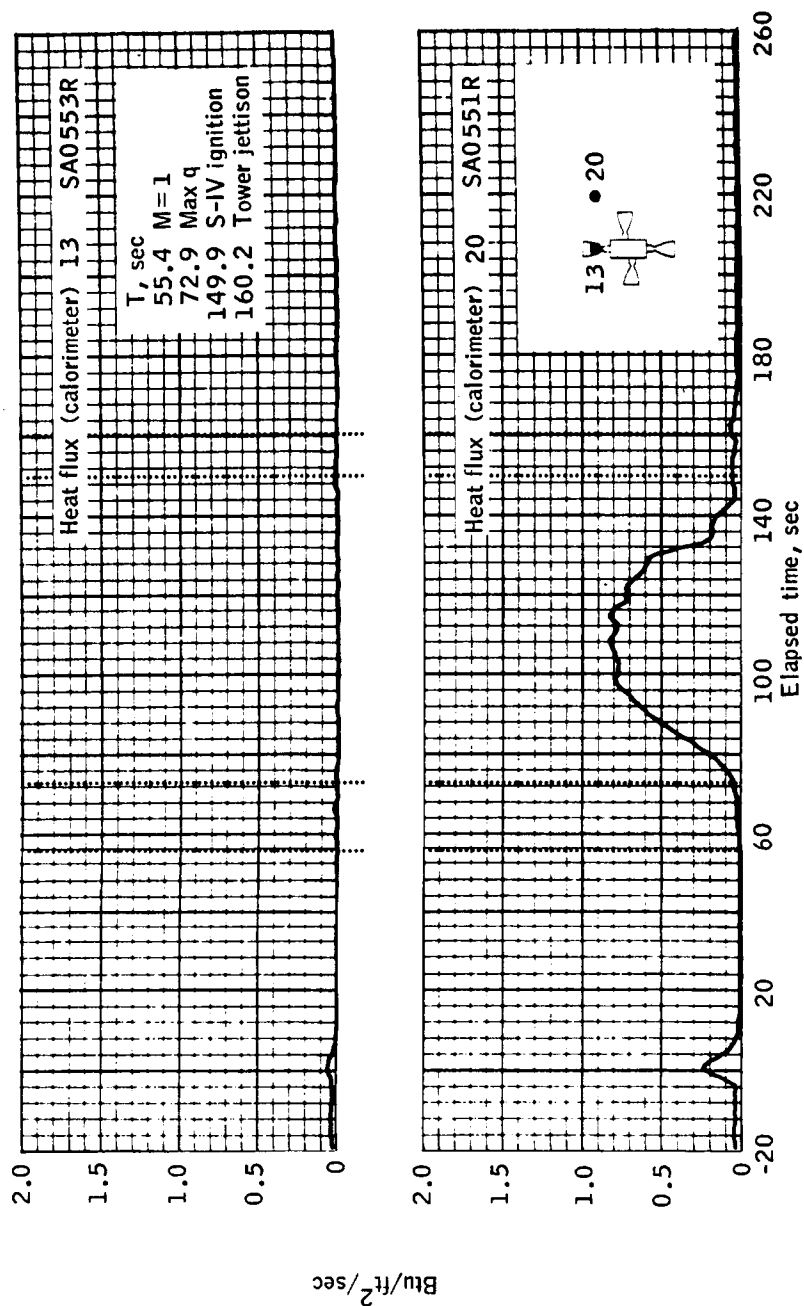
(c) Calorimeters 17 and 18.

Figure 4.11-7.- Continued.

~~CONFIDENTIAL~~

~~CONFIDENTIAL~~

4-209



(d) Calorimeters 13 and 20

Figure 4.11-7.- Concluded.

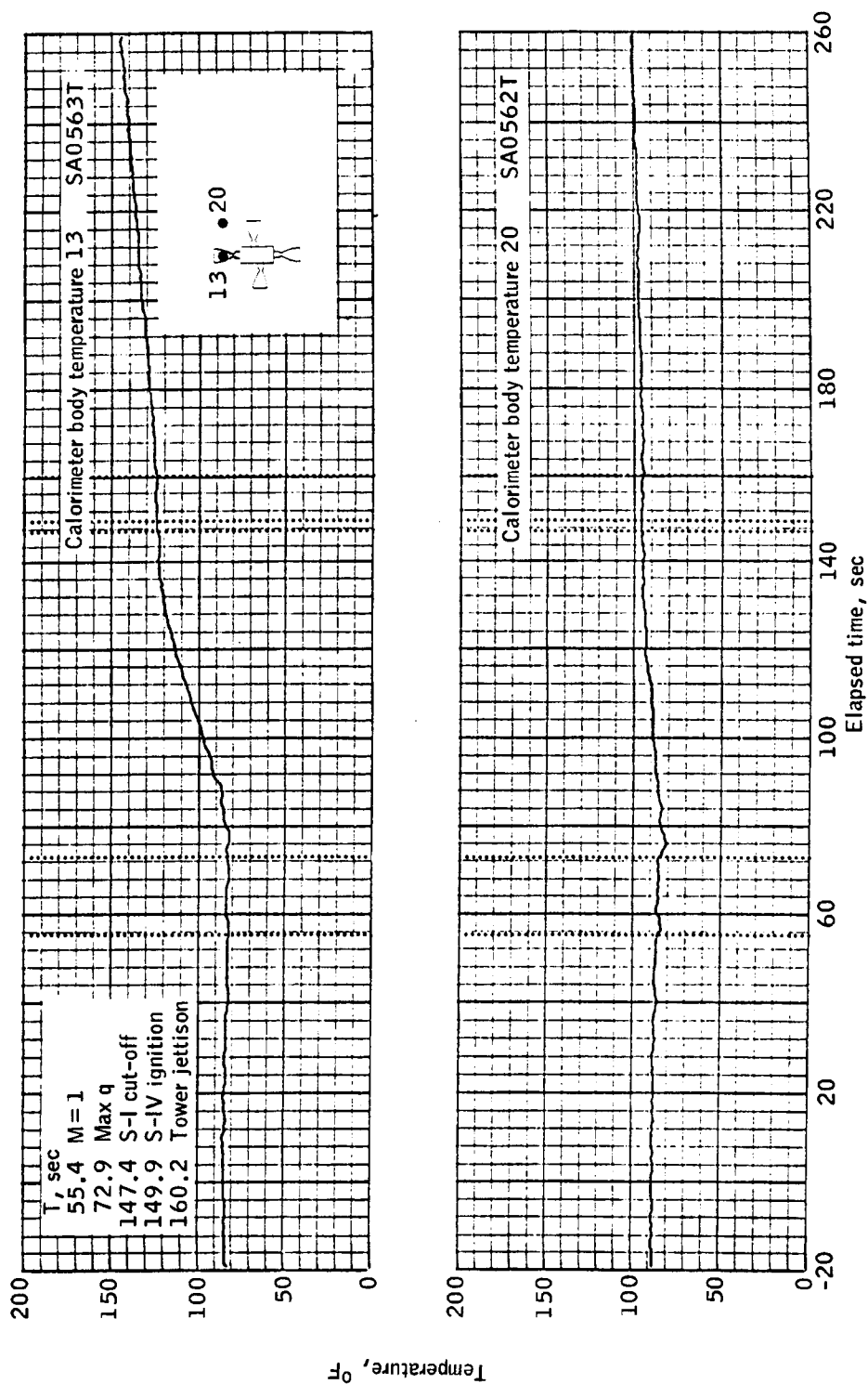
~~CONFIDENTIAL~~

Figure 4.11-8.- Comparison of calorimeter body temperatures at locations 13 and 20.

~~CONFIDENTIAL~~

UNCLASSIFIED

4-211

4.12 Equipment Cooling

Description.- The equipment cooling subsystem for the BP-15 spacecraft consisted of the equipment required to protect critical electrical components from over-heating. Thermal control of these components was provided by cabin-air convective cooling and by coldplate conductive cooling. There was no similarity between this subsystem and the environmental control subsystem for the Apollo production spacecraft.

The equipment cooling subsystem was a passive, closed-loop heat-transport system. The subsystem included five coldplates, a cabin-air heat-exchanger and fan, a coolant storage tank, an accumulator, and a coolant pump. The electronic equipment which was mounted on the coldplates consisted of three telemetry RF amplifier and transmitter packages and two radar beacon transponders. The coolant fluid was a mixture of 40-percent water and 60-percent ethylene glycol (specification MIL-E-9500). The water was distilled and deionized, and the mixture contained no inhibitors. The water-glycol mixture was recirculated through a 35-micron absolute filter located in the ground support equipment. The subsystem schematic is shown in figure 4.12-1.

During the prelaunch activities, the equipment cooling subsystem was serviced with, and subsequently cooled by, the ground support equipment (GSE) model S14-052, water-glycol cooling unit. The GSE circulated cold water-glycol through the spacecraft coolant storage tank and maintained the stored coolant temperature below 20° F. During this same period, the onboard coolant pump circulated the cold water-glycol from the coolant storage tank through the coldplates and the cabin heat exchanger coils. The warmed coolant then returned to the pump and passed through the thermal control valve (TCV). When the coolant temperature at the pump outlet was less than 40° ±5° F, the TCV routed the coolant directly to the coldplates. When the pump outlet coolant temperature exceeded 40° ±5° F, the TCV routed coolant fluid by way of the storage tank to the coldplates. Thus, in effect, a volume of cold fluid was withdrawn from the storage tank to replace the volume of warm coolant. The temperature of the recirculated coolant to the coldplates was maintained below 40° ±5° F, by the use of the TCV, until the temperature of the coolant in the storage tank reached 45° F, at which time, the TCV was maintained in the open position to allow all coolant to flow from the pump through the tank and to the coldplates.

Cooling of the water-glycol by GSE ceased at T-18 seconds when the spacecraft umbilical was disconnected. Monitoring of some of the parameters which measured the subsystem performance was also discontinued at this time. Table 4.12-I shows the parameters monitored before and after imbilical disconnect.

UNCLASSIFIED

UNCLASSIFIED

The equipment cooling subsystem was designed to maintain the cabin-air temperature below 100° F through launch and to maintain the communications equipment below 150° F for one orbital pass, provided the coolant stored in the tank was below 20° F at umbilical disconnect. These criteria included a 60-minute hold after umbilical disconnect.

After umbilical disconnect, the spacecraft system continued to circulate the water-glycol. At a cabin pressure of 5.45 ± 0.5 psia, two baroswitches turned off the power to the single-phase inverter, which powered the cabin fan. When the fan turned off, convective cooling of the cabin ceased.

The configuration of the equipment cooling subsystem of the BP-15 spacecraft was similar to that of BP-13 spacecraft. The only configuration change was that the BP-15 spacecraft cabin temperature probe was relocated to sense the inlet gas-stream temperature in the cabin heat exchanger rather than the outlet gas-stream temperature. The probe was relocated to enable the sensing of a more representative gas temperature.

Several hardware changes were made to the system as a result of the experience obtained from the BP-13 spacecraft ground and flight tests and BP-15 spacecraft ground tests. The cabin heat-exchanger bypass valve on BP-15 spacecraft was permanently positioned to bypass 50 percent of the coolant around the heat-exchanger core. On the BP-13 spacecraft this valve operated to deliver cold water-glycol to the heat exchanger core when the cabin temperature was greater than 70° F. Below a cabin-air temperature of 70° F, 50 percent of the water-glycol was bypassed around the core. During the BP-13 spacecraft checkout, the cabin-air temperature taken at the heat-exchanger outlet, was found to be 45° to 55° F. This temperature was judged to be too cold for sustained operation of the batteries. As a result, operation time for the cabin fan and coolant pump was manually programed during the BP-15 spacecraft launch countdown to maintain the cabin air temperature at approximately 75° F and the coldplate-outlet temperature below 100° F (fig. 4.12-2).

The problems encountered during the BP-13 spacecraft checkout, and the anomaly in the operation of the pump during the countdown and flight led to several changes in the coolant pump for the BP-15 spacecraft. The stainless-steel ball bearings were individually inspected and selected for conformance to the ABEC type 7 bearing code to maintain the impeller shaft alinement. The motor stator was sprayed with epoxy resin and baked under vacuum to prevent oxidation or corrosion of the stator. In addition, the motor and pumps were assembled in a dry nitrogen atmosphere, hermetically sealed, and shipped and stored in a dry nitrogen-filled sealed container to prevent oxidation (fig. 4.12-3).

UNCLASSIFIED

UNCLASSIFIED

4-213

Performance.- The equipment cooling subsystem was operated as planned during the launch countdown. The GSE circulated 16° F coolant at a rate of 2.8 gallons per minute to the coolant storage tank. The onboard coolant pump and cabin fan operated with no apparent malfunction. The coolant pump-outlet pressure was 31 psig, indicating normal pump operation. The low pump-outlet pressure and the high total current measured during the BP-13 spacecraft countdown were not evident for the BP-15 spacecraft. During the countdown for the BP-15 spacecraft, manual programming of the operation of the fan and pump was used to maintain the cabin-air and coldplate outlet temperatures within the range desired (fig. 4.12-2). The values of the equipment-cooling subsystem parameters taken immediately prior to umbilical disconnect are shown in table 4.12-II.

The telemetry data indicated that the cabin fan was turned off by the barowsitches at T+33¹/₄ seconds, as shown by the drop in the electrical system total current from 42 to 35 amperes. The cabin pressure at this time was 5.3 psia, which is within the specified range and in agreement with prelaunch testing.

The cabin pressure rate of decay increased at T+161 seconds at the time when the launch-escape subsystem (LES) explosive bolts were fired (fig. 4.12-4).

The BP-15 spacecraft did not include gas-pressure-relief or control valves, and during launch, pressure was relieved by leakage through the pressure shell. Cabin leakage was to be equivalent to the flow from a $\frac{1}{4}$ - to $\frac{1}{2}$ -inch diameter hole. See section 4.7 for additional detail regarding this change in cabin pressure decay rate. There was no structural configuration similarity between the boilerplate cabin and the production spacecraft cabin pressure shell.

The telemetry data indicated that the coolant pump continued to operate during the launch and orbital phases of the mission until power depletion with no apparent malfunction. The electrical equipment chassis temperatures ranged from 43° to 50° F at launch and from 50° to 55° F at the end of the first orbital pass.

The equipment cooling subsystem satisfactorily fulfilled the function required of the subsystem during the mission.

UNCLASSIFIED

UNCLASSIFIED

TABLE 4.12-I. - MONITORED EQUIPMENT COOLING SUBSYSTEM PARAMETERS

Ground support equipment	Telemetry
Cabin air temperature	Cabin air temperature
Coldplate inlet coolant temperature	Cabin interior pressure
Coldplate outlet coolant temperature	TM RF transmitter A temperature
Tank outlet coolant temperature	TM RF transmitter B temperature
Tank inlet pressure	TM RF transmitter C temperature
Pump outlet pressure	TM RF amplifier A temperature
GSE (S14-052) delivery temperature	TM RF amplifier B temperature
GSE (S14-052) delivery rate	TM RF amplifier C temperature

UNCLASSIFIED

UNCLASSIFIED

4-215

TABLE 4.12-II.- EQUIPMENT COOLING SUBSYSTEM PARAMETERS
AT UMBILICAL DISCONNECT (T-18 SEC)

Parameter	Planned	Measured
Cabin air temperature, °F	55 to 100 ^a	64
Coldplate inlet coolant temperature, °F . . .	40 ± 5	40
Coldplate outlet coolant temperature, °F . .	45 to 50 ^b	45
Tank outlet coolant temperature, °F	70 (max)	30
Tank inlet pressure, psig	20	20
Pump outlet pressure, psig	32 ± 2	31
GSE (S14-052) delivery temperature, °F . . .	As required	16
GSE (S14-052) delivery rate, gallons per min	As required	2.8

^a75° F, optimum

^b100° F, maximum

UNCLASSIFIED

UNCLASSIFIED

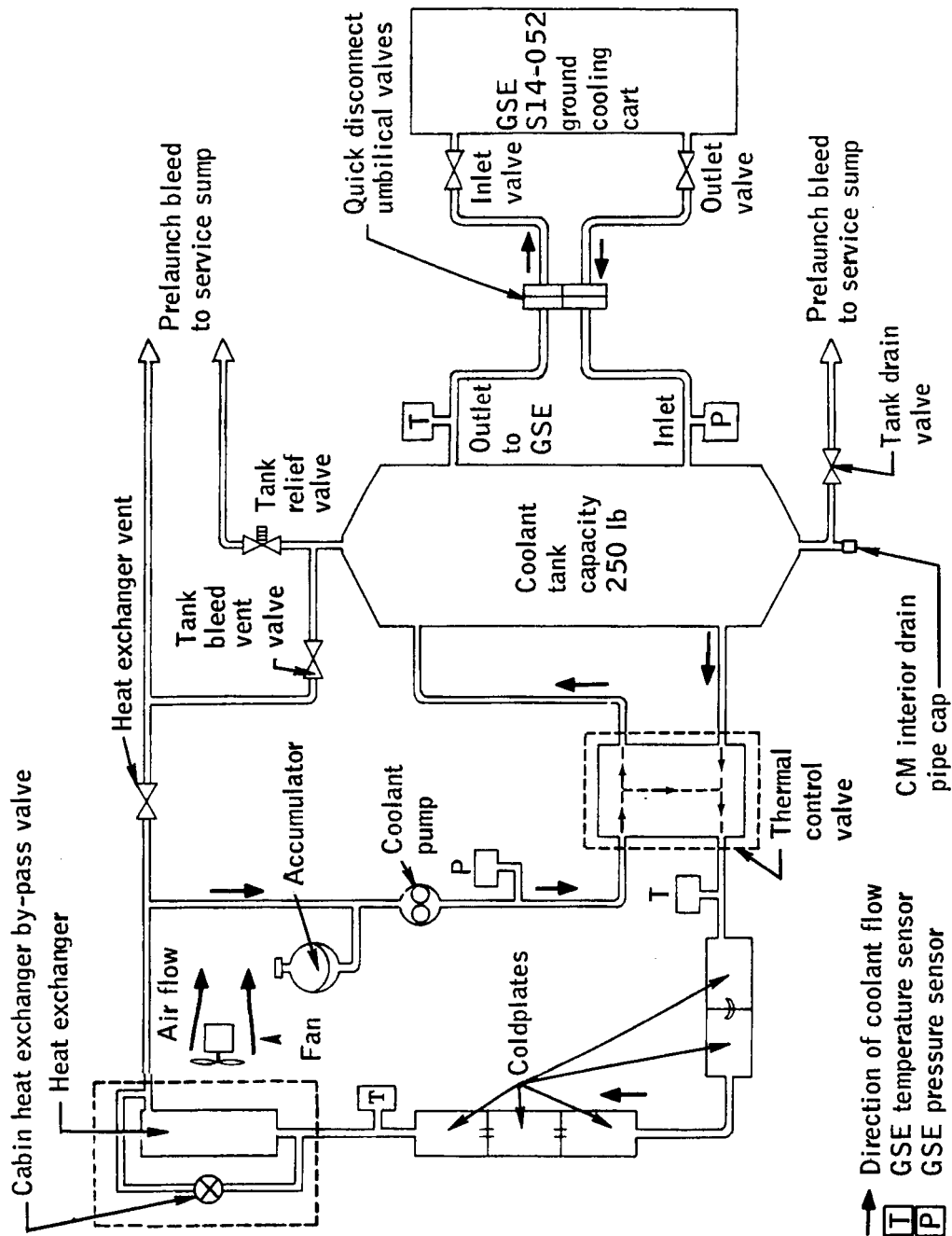


Figure 4.12-1. - Environmental control subsystem schematic for BP-15 spacecraft.

UNCLASSIFIED

UNCLASSIFIED

4-217

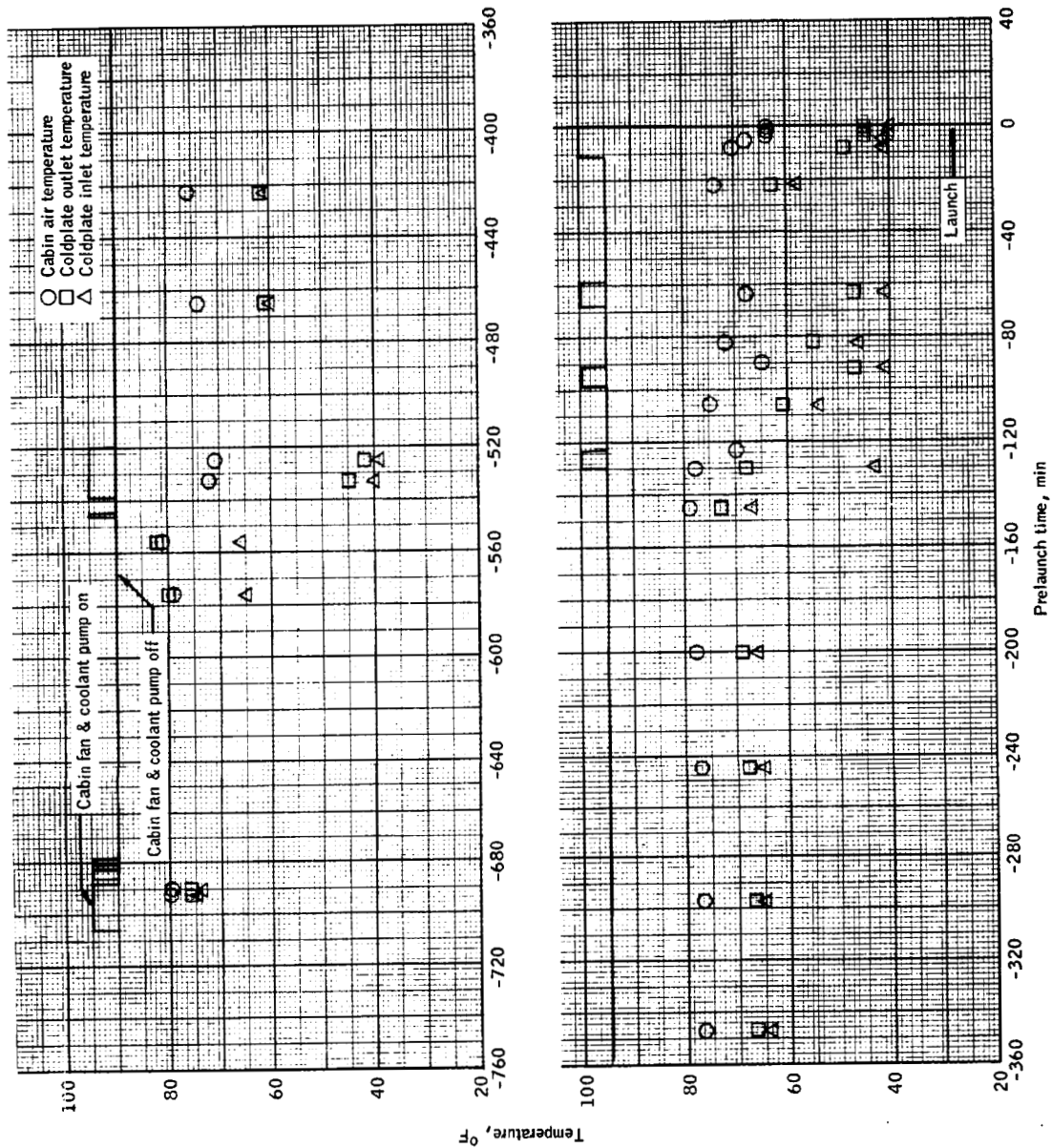


Figure 4.12-2.- Equipment cooling prelaunch data for BP-15 spacecraft.

UNCLASSIFIED

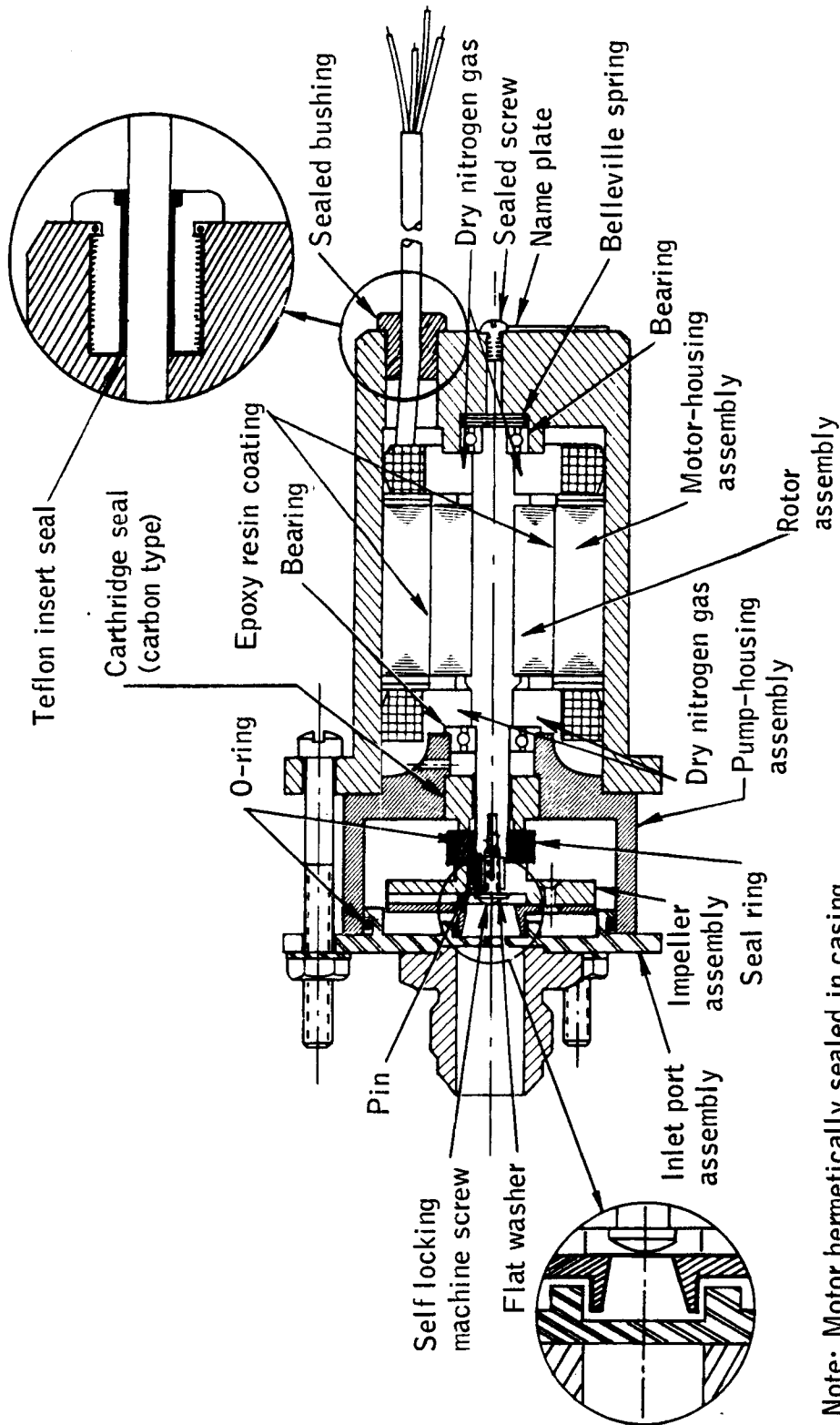
~~CONFIDENTIAL~~~~CONFIDENTIAL~~

Figure 4.12-3.- Sectional view of coolant-pump assembly for BP-15 spacecraft.

~~CONFIDENTIAL~~

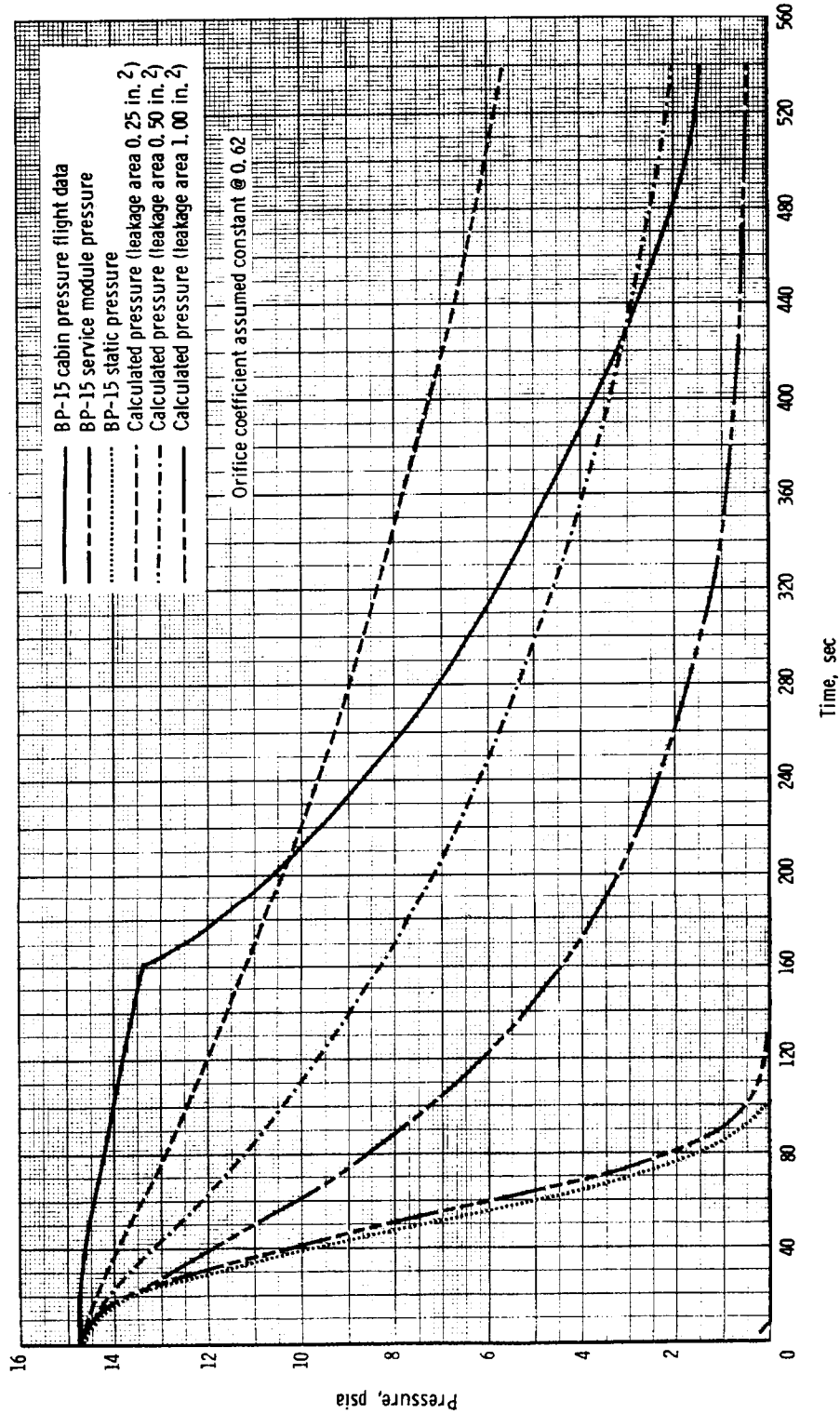


Figure 4.12-4. - Command module cabin pressure for BP-15 spacecraft.

~~CONFIDENTIAL~~

~~CONFIDENTIAL~~

5-1

5.0 SA-7 LAUNCH-VEHICLE DESCRIPTION AND PERFORMANCE

5.1 Description

The Saturn I is a two-stage launch vehicle consisting of stages S-I and S-IV, an instrument unit (IU), and various fairings and adapters. The total vehicle length is approximately 190 feet, consisting of an 80.3-foot-long by 257-inch-diameter S-I stage, a 41-foot-long by 220-inch-diameter S-IV stage, a 4.8-foot-long by 154-inch-diameter instrument unit, and a 64.1-foot-long by 154-inch-maximum-diameter boilerplate spacecraft and launch escape subsystem (LES). Vehicle details and dimensions are presented in figure 5.1-1.

The S-I stage dry weight is 107,170 pounds with a propellant capacity of 850,000 pounds (lox and RP-1). Eight H-1 engines mounted in two clusters, four inboard and four outboard, produce a total sea-level thrust of 1.5 million pounds.

The S-IV stage dry weight is 13,857 pounds with a propellant capacity of 100,335 pounds (LH₂ and lox). The six RL10A-3 engines of the S-IV stage produce a combined thrust of 90,000 pounds.

The instrument unit contains most of the flight control equipment, including the vehicle inertial guidance and control system and the airborne hardware of six tracking and four telemetry systems. The IU also has an integral power supply and distribution system, cooling systems, and a gaseous nitrogen supply system. The IU begins to function prior to lift-off to command S-I start sequencing and to maintain programing, sequencing, and flight control through S-I and S-IV stage operation.

Vehicle telemetry systems are provided for each stage and the IU. These systems include six airborne systems and one digital data acquisition system for preflight checkout in the S-I stage, three systems in the S-IV stage, and four systems in the IU.

5.2 Preliminary Flight Performance

After 11 seconds of vertical flight, the launch vehicle began to roll to the proper flight azimuth of 105° east of north and completed the maneuver at T+25.7 seconds. At T+12.6 seconds, the preprogramed pitch-attitude profile was initiated and continued until T+136.3 seconds, at which time an essentially constant pitch attitude was maintained until the initiation of active guidance at 17.3 seconds after separation of the S-I and S-IV stages. The shutdown of the S-I stage occurred at T+147.4 seconds which was only 0.7 second later than nominal.

~~CONFIDENTIAL~~

~~CONFIDENTIAL~~

The actual trajectory parameters as compared with nominal were at that time about 122.0 ft/sec (37.2 m/sec) high in space-fixed velocity, 1.19 nautical miles (2.2 km) high in altitude, and 0.55 nautical mile (1.02 km) greater in range.

Separation of the S-I and S-IV stages occurred at T+148.2 seconds, followed by ignition of the S-IV stage 1.7 seconds later. All ullage rockets functioned as expected and were successfully jettisoned. Following the initiation of closed-loop guidance, the vehicle was steered into a nearly nominal orbit after S-IV shutdown, which occurred about 2 seconds later than had been predicted.

The overall performance of both the S-I and S-IV propulsion systems was highly satisfactory, with all engine parameters being near predicted values. All four of the S-I retrorockets performed as expected. The total S-IV burn time was 1.3 seconds longer than predicted, as compared with the expected 2σ dispersion of ± 1.1 seconds. The S-IV common bulkhead pressure was steady at approximately 0.8 psia with no indication of leakage.

Stability of the total vehicle during S-I stage flight was maintained through utilization of the ST-124 stabilized platform and associated hardware. This was the first test of the ST-124 and control rate gyros in closed loop during this phase of flight. In addition, the ASC-15 guidance computer was used for the first time to generate the roll and pitch program for S-I stage flight. A preliminary analysis of flight parameters indicated that all guidance and control hardware functioned in a satisfactory manner. Lateral load torques caused by wind were very small, and, consequently, the stabilizing torques from the gimballed engines were small (0.50° deflection or less). The maximum wind component, which occurred in the yaw plane, was only 49.2 ft/sec (15 m/sec). Since the pitch program was designed for zero winds, the angles of attack were very small (1° or less during maximum dynamic pressure). A small aerodynamic roll moment (approximately 3° roll attitude) was experienced during S-I stage flight which was similar to what had occurred on earlier flights. Pitch and yaw disturbances during separation were very small, but at the start of separation a disturbing torque caused the roll rate to build up to a maximum of 2.3 deg/sec with a corresponding roll attitude of 5° about 3 seconds after separation. Upon S-IV ignition, the corrective action of the engine actuators caused a maximum rate overshoot to 6 deg/sec with very adequate damping. The roll rate observed would correspond to a 1.1° misalignment of one ullage rocket.

At guidance activation, the S-IV vehicle attitude was changed from 67° to 75° nose down within 21 seconds in response to adaptive steering commands. The lateral deviations accumulated during S-I burn required

~~CONFIDENTIAL~~

~~CONFIDENTIAL~~

5-3

maximum transients of 1.5° and 6° in the X and Y commanded angles, respectively. Such transients are not considered severe.

A preliminary analysis of orbital insertion conditions (S-IV cut-off plus 10 seconds) has indicated that the difference between the guidance computer value of space-fixed velocity and the value obtained from orbital tracking was 6.2 ft/sec (1.9 m/sec). The lateral velocity difference obtained was 14.8 ft/sec (4.5 m/sec). Such comparisons are preliminary, and the uncertainty in these values is from 3 to 6 ft/sec.

Very low bending moments (about one-fourth of the magnitude experienced during mission A-101) were observed during the flight. The low magnitude can be attributed to the low angles of attack experienced. No significant disturbances were noted during launch-escape subsystem (LES) jettison, but some first mode bending was observed after jettisoning.

Base thermal and pressure environments for the S-I stage were similar to those experienced during mission A-101. Skin temperatures of the S-IV and S-I stages indicated slightly higher values than had occurred during mission A-101. These higher values were probably due to the faster trajectory flown on mission A-102.

Overall performance of the launch-vehicle telemetry instrumentation system was good with only 8 of 1,235 measurements having failed completely.

A complete detailed evaluation of the performance of the launch vehicle is given in reference 7.

~~CONFIDENTIAL~~

UNCLASSIFIED

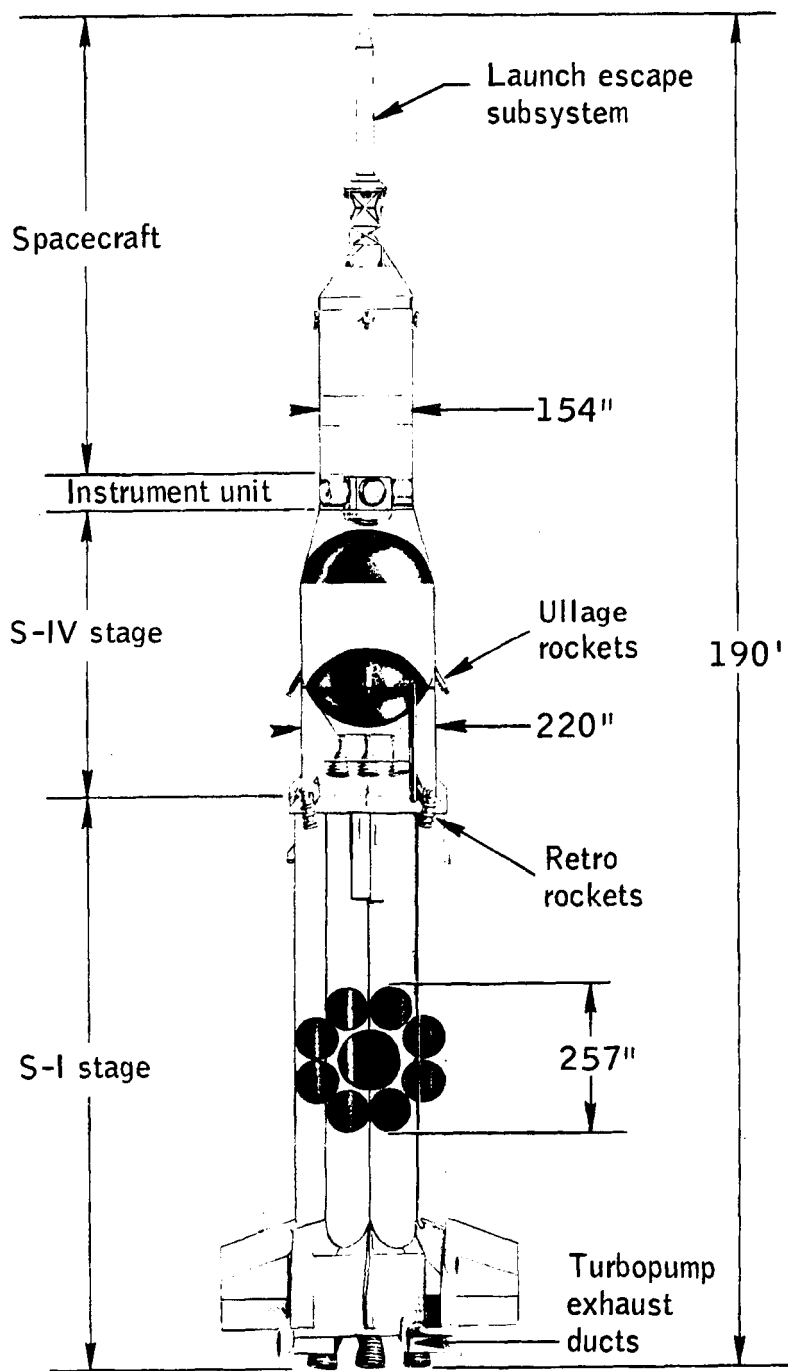


Figure 5.1-1.- Apollo mission A-102 space vehicle showing cutaway views of launch vehicle.

UNCLASSIFIED

~~CONFIDENTIAL~~

6-1

6.0 CONCLUDING REMARKS

All of the spacecraft test objectives for the Apollo mission A-102 were fulfilled.

The compatibility of the spacecraft with the launch vehicle was further confirmed under launch and exit condition.

Satisfactory engineering data, covering designated parameters of spacecraft environment for a Saturn V type launch trajectory, were obtained for use in verifying launch and exit design criteria.

The launch-escape motor together with the pitch-control motor propelled the launch-escape subsystem safely out of the path of the spacecraft in a demonstration of the alternate mode of launch-escape tower jettison.

Flight data from the instrumented simulated RCS quad assembly differed from the values assumed for design criteria for the RCS. Additional investigation and analysis will be necessary to complete the flight data and design criteria.

Flight data on spacecraft launch environment near the RCS quad A was insufficient for verifying criteria. Additional investigation and analysis will be required.

The flight trajectory of the mission provided the launch environment planned for the mission.

All spacecraft subsystems performed the functions required for a satisfactory mission.

~~CONFIDENTIAL~~

~~UNCLASSIFIED~~

7-1

7.0 APPENDIX A

7.1 Prelaunch Operations

Initial checkout of the BP-15 spacecraft was accomplished in the Apollo test and operations (ATO) area at the contractor's facility at Downey, California. Final checkout terminated at Cape Kennedy, Florida, with the launch operation.

The major tests and operations performed on the spacecraft, or in conjunction with spacecraft operations, were conducted in accordance with the detailed Operational Test Procedures (OTP). (See appendix B, section 8.2.) These procedures define the step-by-step test operations to be performed and the response or values required for approval, where applicable. The OTP's were used throughout the checkout operations at Downey, California, (ATO) and at Hangar AF and Launch Complex 37B facilities at Cape Kennedy, Florida. (See section 8.2.)

On March 6, 1964, the command module, service module, insert, adapter, and launch-escape tower were transferred to ATO from the manufacturing facilities. The schedule of milestone events for the BP-15 spacecraft during the ATO period is given in figure 7.1-1.

The schedule of ground support equipment (GSE) modifications and validation at Downey, California, is indicated in figure 7.1-1. BP-13 spacecraft GSE electronics equipment was used at Cape Kennedy rather than shipping additional GSE electronics from Downey.

Individual subsystems tests were performed from April 29, 1964, to May 11, 1964. Subsystems were programed for individual checkout during this period in coordination with modification work on the vehicle and associated GSE. BP-15 spacecraft subsystems tests differed from those of BP-13 spacecraft in that no special measuring devices (SMD) or special adaptive devices (SAD) were used during this phase of the BP-15 spacecraft operations.

Stacking, alinement, and hookup took place between May 11, 1964, and May 18, 1964. The spacecraft assemblies were mated and alined in the Navajo tower and all GSE was connected in preparation for the integrated subsystems test. Prior to the start of this phase of operations, the mass characteristics were determined for each spacecraft module. A complete quality control inspection by the spacecraft contractor's and NASA personnel was also accomplished.

The integrated subsystems test was started on May 19, 1964, and was completed with the exception of the last 10 steps (electromagnetic

~~UNCLASSIFIED~~

~~CONFIDENTIAL~~

interference (EMI) tests) of the procedure. The spacecraft equipment was operating normally, but the pyro-substitute unit had grounding problems similar to those encountered during BP-13 spacecraft checkout at Cape Kennedy. The integrated subsystems test was continued on May 25, 1964, utilizing fused, 1-ohm resistor circuits to measure firing and/or transient signals. CEC recorders were used to read the firing indications. The identical technique was utilized previously at Cape Kennedy with the BP-13 spacecraft. The EMI portion of the integrated subsystem test was then completed.

Spacecraft removal from the Navajo tower was performed following debriefing and acceptance of the integrated subsystems test. The service module, insert, adapter, and assorted GSE were shipped on June 3, 1964, by the B-377 PG aircraft. The command module and launch-escape tower were shipped on June 19, 1964. The B-377 PG was also utilized for this shipment, because of the non-availability of an Air Force C-133B. The spacecraft and associated GSE were transported to Cape Kennedy without damage to the equipment.

The BP-15 spacecraft operations at Cape Kennedy, Florida, began with the receiving inspection of the GSE and spacecraft assemblies in Hangar AF. Prior to arrival of the spacecraft, the decision was made that no hangar testing would be performed. This alleviated the need for removal and return of the BP-13 spacecraft GSE from Complex 37B. Figure 7.1-2 presents the scheduled milestones for the BP-15 spacecraft prelaunch operations.

The command and service modules were mated in Hangar AF on June 22, 1964. Final installation of the adapter air-conditioning barrier was completed, and the command and service module assembly was mated to the adapter. (See figure 7.1-3.) The entire stack was then single-point weighed and loaded on the vertical transport. The spacecraft was then transported (in the stacked configuration) to Complex 37B for mating with the launch vehicle (SA-7) on June 26, 1964. Figure 7.1-4 shows the spacecraft being hoisted.

The instrumented RCS quad assembly was received from Downey, California, and it was installed and checked out immediately following the mating of the spacecraft with the launch vehicle. This task was completed on June 29, 1964.

BP-15 spacecraft prelaunch operations were extended approximately 2 weeks because of a stress-corrosion problem in the liquid oxygen dome of the S-I engines. The eight engines were removed, reworked by the contractor, static fired, and reinstalled in the S-I stage. During this time, a special test was performed at the request of MIT, for the

~~CONFIDENTIAL~~

~~CONFIDENTIAL~~

7-3

purpose of gathering data which could be used to verify current design criteria for GSE used in the alinement of the stable platform of the guidance and navigation subsystem while the spacecraft was on the pad.

Upon arrival, the launch-escape tower was transported to the Merritt Island launch area (MILA) where the assembly of the launch-escape subsystem (LES) was completed in the ordnance storage building. All LES motors arrived at Cape Kennedy prior to receipt of the launch-escape tower. A launch-escape motor grain inspection using a boroscope was also performed at MILA. Upon completion of the LES assembly, the LES was weighed and balanced, and the assembly was transported to the GE-Mark VI storage building on Cape Kennedy, where it remained until it was mated to the command module at Complex 37B on August 16, 1964. Figure 7.1-5 shows the LES being lifted for mating.

The spacecraft-launch vehicle integrated tests began with the electrical mating and interface checks on August 7, 1964, and they were successfully completed on September 15, 1964, with the countdown demonstration test. Testing consisted of overall test 1 (plugs in), overall test 2 (plugs out and live ordnance in), the RFI test, and the simulated flight test.

Following completion of the simulated flight test, while removing test hardware, a broken tower separation bolt was discovered in the LES. The LES was demated from the spacecraft, and all tower bolts were replaced with the improved bolts which had precision-rolled threads to minimize stress concentration. The resultant electrical disconnection was of particular concern since it invalidated the simulated flight test, which is the final spacecraft readiness test prior to launch. The LES was remated to the spacecraft on September 4, 1964, and all electrical connections were reverified by initiating a tower jettison signal from the launch vehicle instead of rerunning the simulated flight test.

One of the major differences in the BP-15 spacecraft prelaunch operations from those of BP-13 spacecraft was the countdown demonstration test. This test was programed into the SA-7 schedule by John F. Kennedy Space Center (KSC) for the purpose of increasing the proficiency of the launch personnel and to insure an on-time launch.

The BP-15 spacecraft prelaunch operations were completely suspended for a total of 3 days because of severe weather conditions caused by hurricanes Cleo and Dora. The space vehicle remained on the launch pad within the service structure with clam-shell doors closed during the hurricane periods, and no damage was sustained.

A flight-readiness review, conducted on September 11, 1964, established that the BP-15 spacecraft was acceptable for launch.

~~CONFIDENTIAL~~

UNCLASSIFIED

The overall BP-15 spacecraft prelaunch operation, both at Downey and Cape Kennedy, progressed smoothly. It was evident throughout the operation that experience gained during the prelaunch operations of the BP-13 spacecraft was being utilized and the methods were being improved.

UNCLASSIFIED

UNCLASSIFIED

7-5

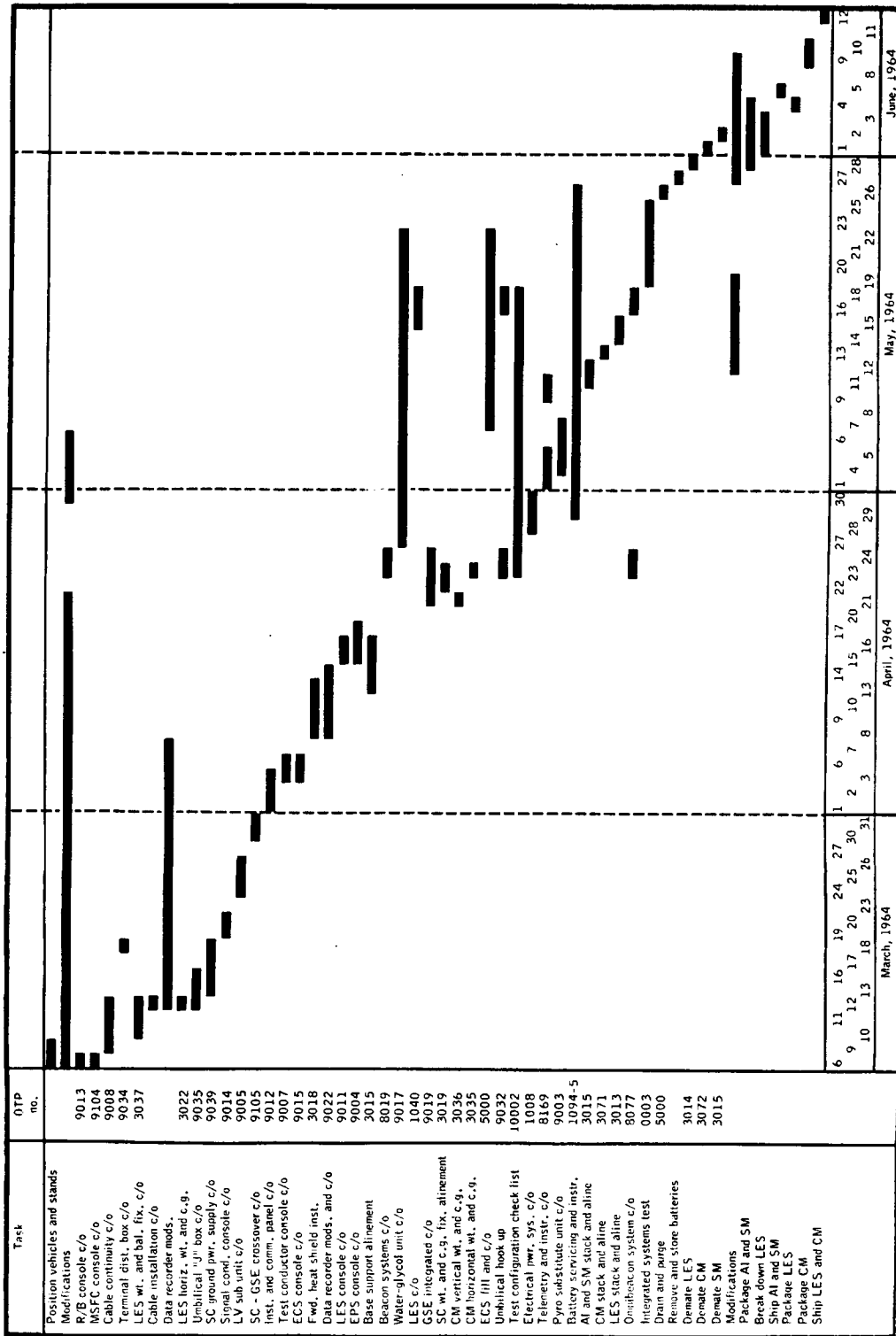


Figure 7.1-1. - Spacecraft BP-15 schedule milestones at ATO Downey.

UNCLASSIFIED

UNCLASSIFIED

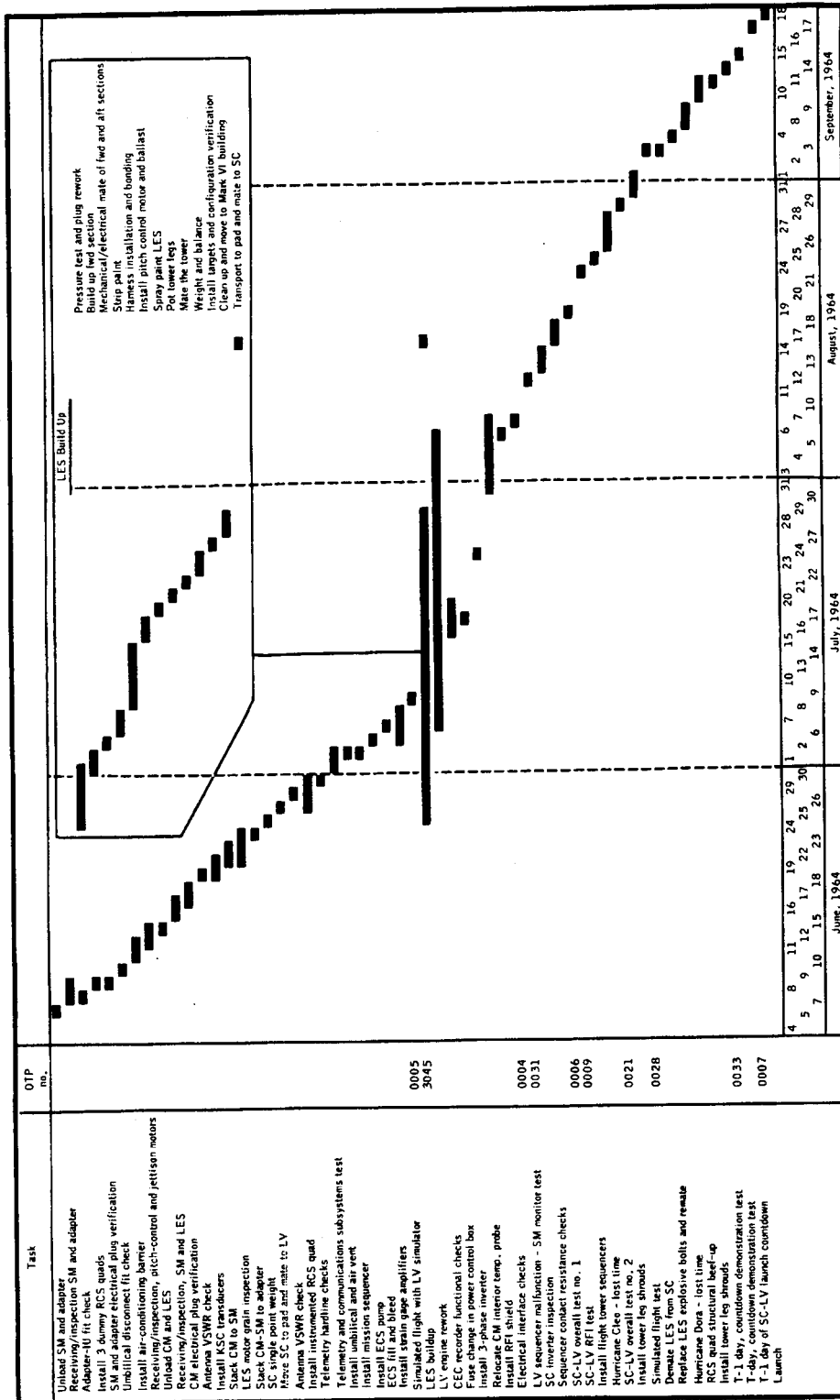


Figure 7.1-2 - Spacecraft BP-15 schedule milestones at MSC Florida Operations.

UNCLASSIFIED

UNCLASSIFIED

7-7

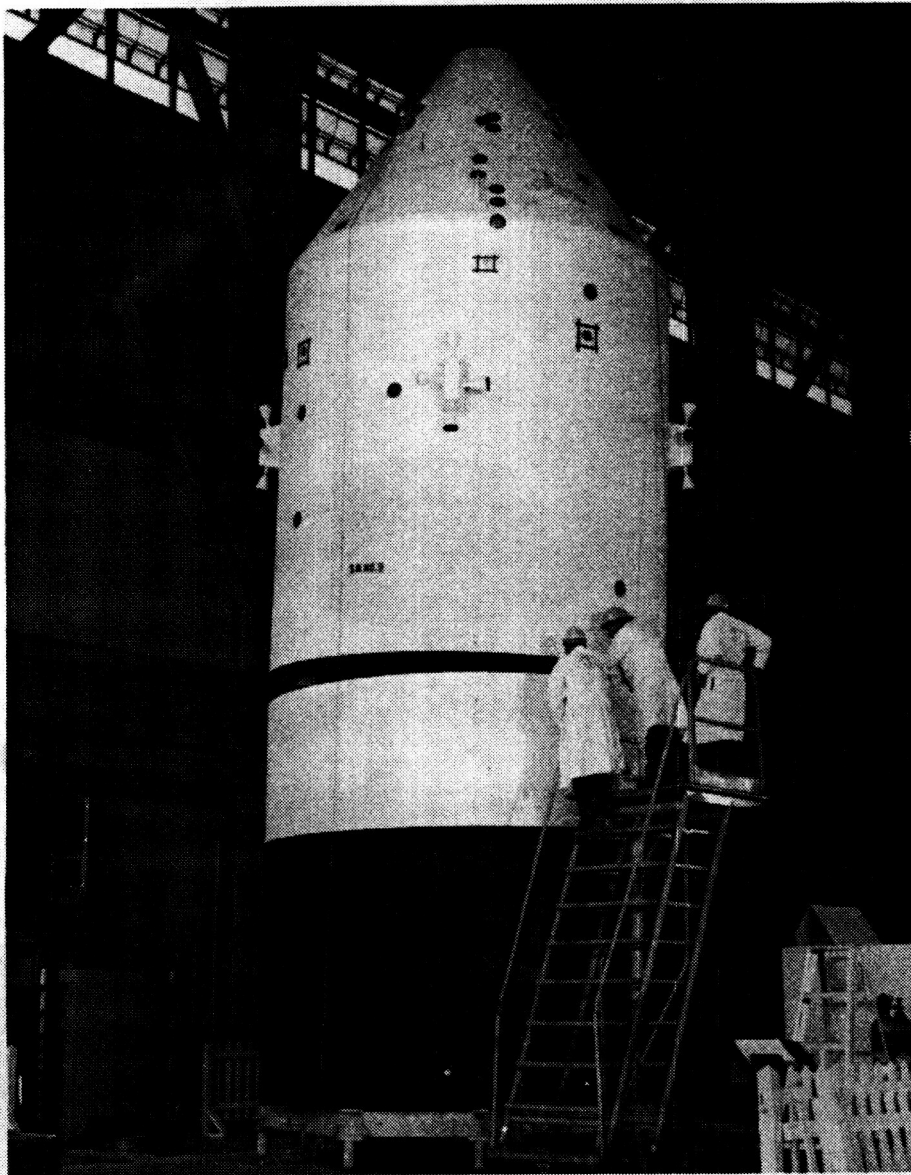


Figure 7.1-3.- BP-15 spacecraft CM-SM being stacked on adapter section in Hanger AF, Cape Kennedy, Florida.

UNCLASSIFIED

UNCLASSIFIED

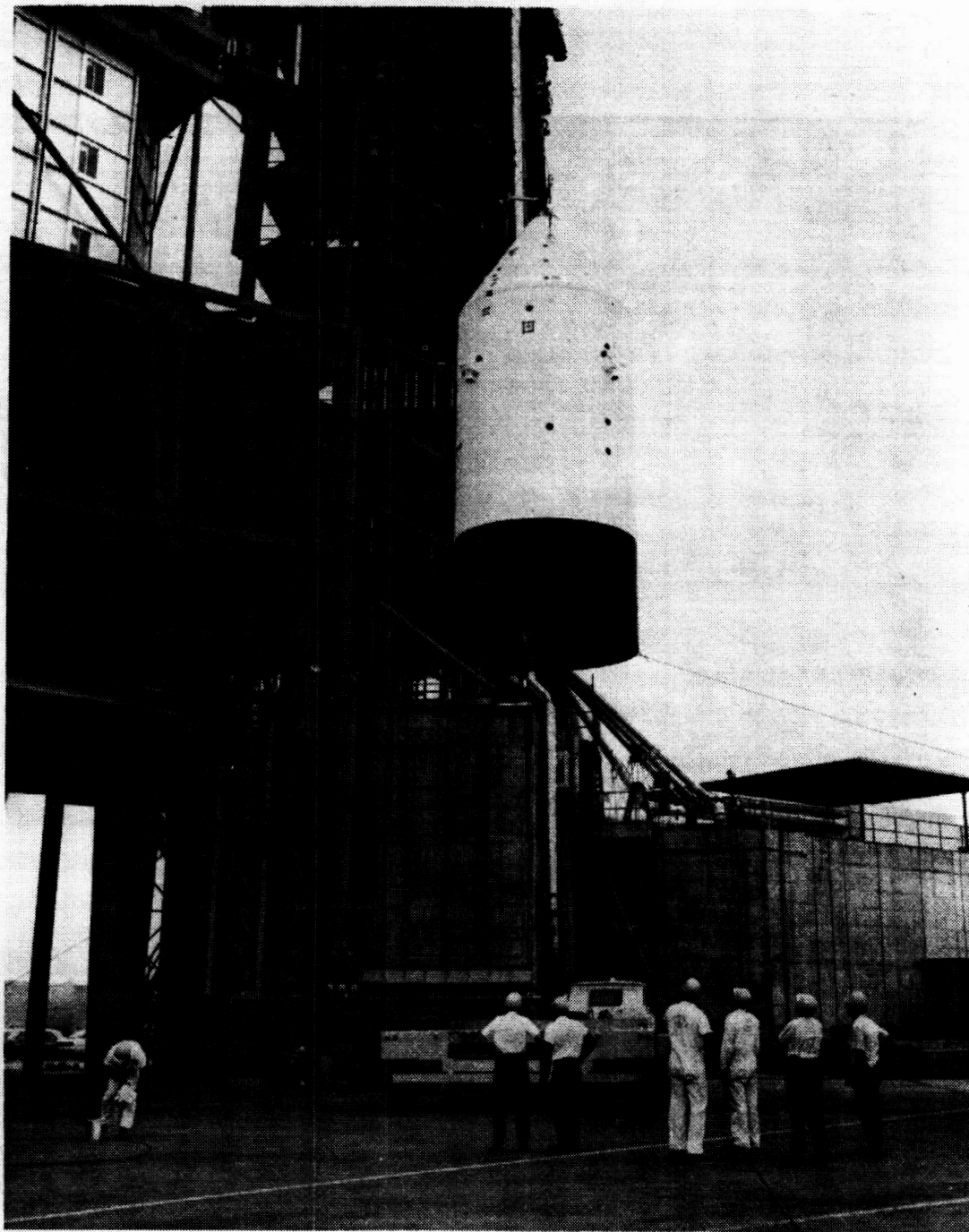


Figure 7.1-4.- BP-15 spacecraft being lifted to mate with the SA-7 launch vehicle at Launch Complex 37B, Cape Kennedy, Florida.

UNCLASSIFIED

UNCLASSIFIED

7-9



Figure 7.1-5.- LES being lifted for mating to the spacecraft at Launch Complex 37B, Cape Kennedy, Florida.

UNCLASSIFIED

UNCLASSIFIED

7.2 Launch Operations

The T-1 day countdown began at 7:30 a.m. e.s.t. on September 17, 1964, at T-875 minutes. The spacecraft portion of the countdown, however, did not begin until 9:40 a.m. e.s.t. and consisted of tower-bolt ordnance electrical connection closeout and electrical verification.

The usual T-1 day activities performed on the BP-15 spacecraft were conducted on T-1 day of the countdown demonstration test on September 14, 1964, thus eliminating the need to repeat these tasks.

The final countdown began at 11:25 a.m. e.s.t. on September 17, 1964, at T-545 minutes, with a planned T-0 time of 10:00 a.m. e.s.t. Figure 7.2-1 shows the schedule of actual and planned time for the tasks performed during the launch count. The spacecraft testing proceeded normally without any holds or equipment malfunctions. Only two events of major significance occurred during the count: one was the difficulty encountered by the Range and Hangar S ground station in distinguishing the C-band beacons responses because of multipath interference from the Patrick Air Force Base radar, and the other was an inadvertent actuation at T-360 minutes of the service structure adjustable 4-level Firex system during removal of an air conditioning duct. Approximately 50 percent of the service module exterior was wetted.

The count was continued until T-245 minutes when a hold was called because of the wet umbilicals. The water had entered one S-IV umbilical connector which, in turn, produced erroneous indications of S-IV engine exciter firing. Power was removed from the S-IV stage, and the moisture was dried from the connector. The count was resumed 69 minutes later.

The count continued until T-30 minutes when a scheduled hold began. During this scheduled 21-minute hold, the S-IV liquid oxygen (lox) prepressurizing regulator indicated a malfunction. Analysis of the problem indicated that the regulator was operating satisfactorily; however, the hold had been extended 4 minutes longer than scheduled. The count progressed to T-12 minutes when it was again interrupted because of a malfunctioning S-I hydraulic-pump temperature interlock, which prevented the S-I hydraulic pumps from being started. Since measurements indicated normal temperatures, the interlock was jumpered out in the blockhouse distributor. The total hold time was 20 minutes.

The count was resumed at T-12 minutes and progressed to T-5 minutes when a Range safety hold was called because of intermittent operation of the Grand Turk Island radar. Because of S-IV lox bubbling and spacecraft battery lifetime constraints, the count was recycled to T-13 minutes, and the spacecraft was transferred to external power. During the hold, difficulty was encountered with the swing arm hydraulic test. This problem

UNCLASSIFIED

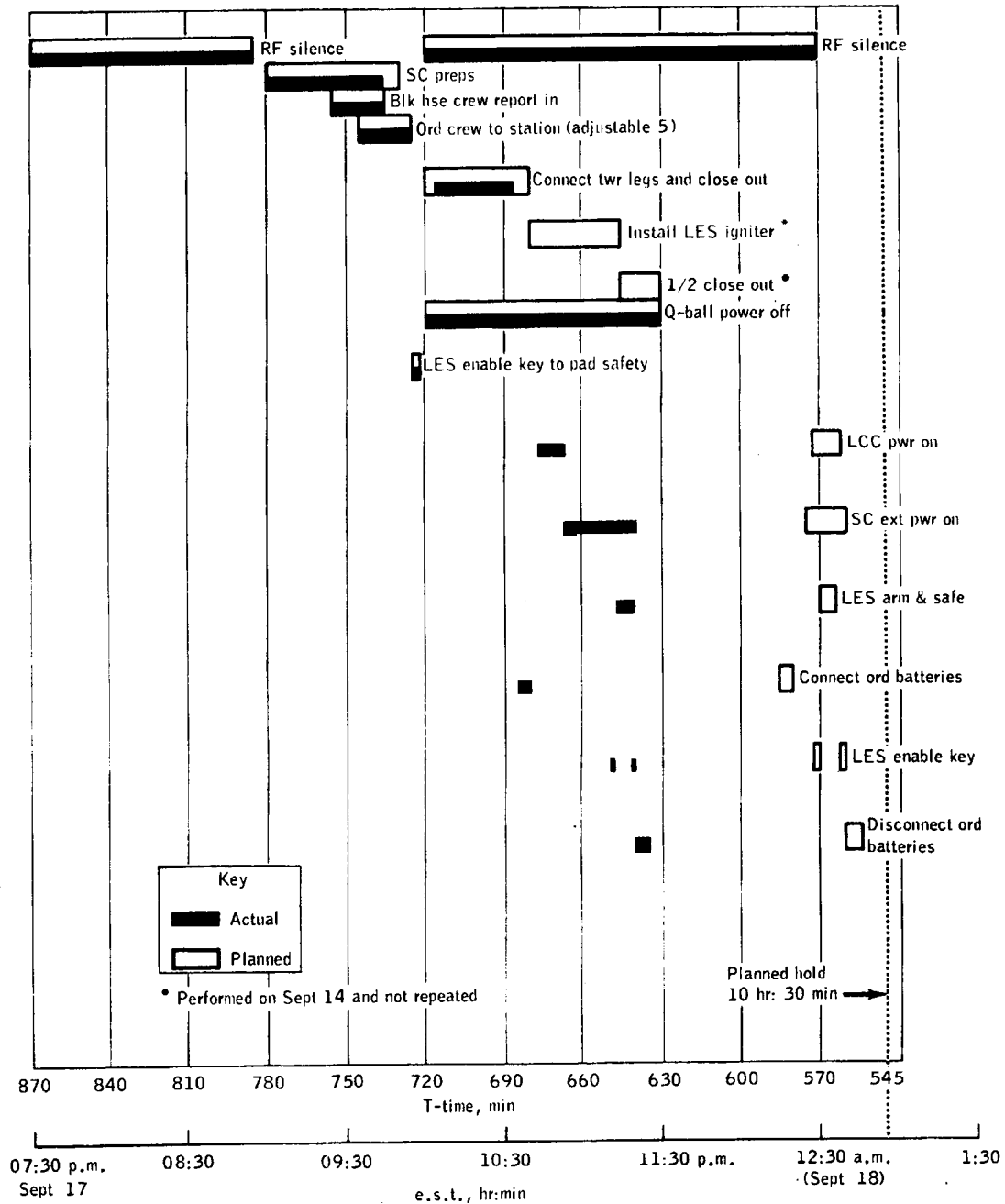
UNCLASSIFIED

7-11

was corrected by a jumper in a blockhouse distributor without adding to the Range hold. After 50 minutes, the radar problem was corrected, and the count resumed and was continuous through lift-off which occurred at 11:22:43 a.m. e.s.t. on September 18, 1964.

UNCLASSIFIED

UNCLASSIFIED



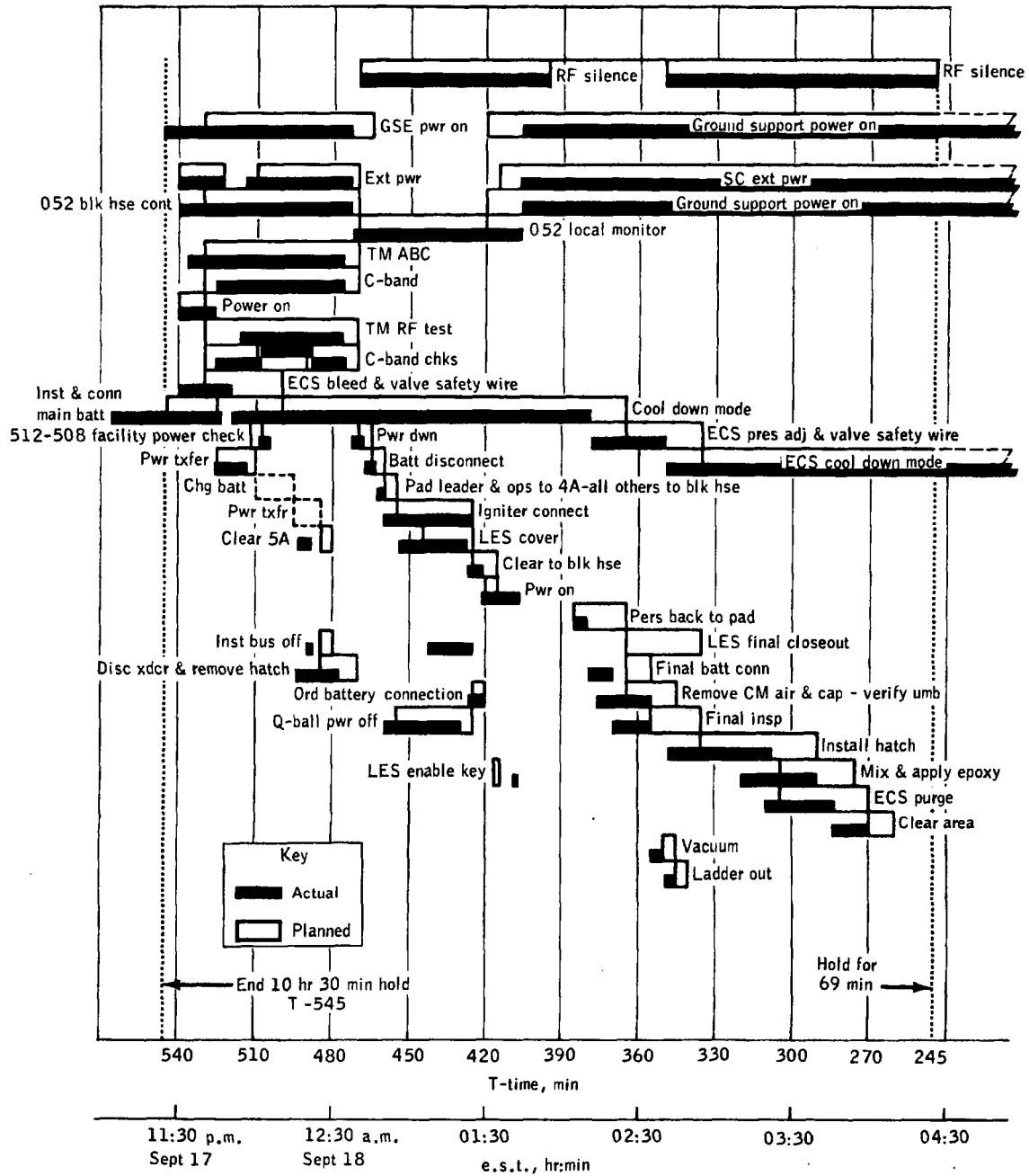
(a) T -1 day, September 17, 1964.

Figure 7.2-1.- Apollo mission A-102 countdown activities.

UNCLASSIFIED

UNCLASSIFIED

7-13

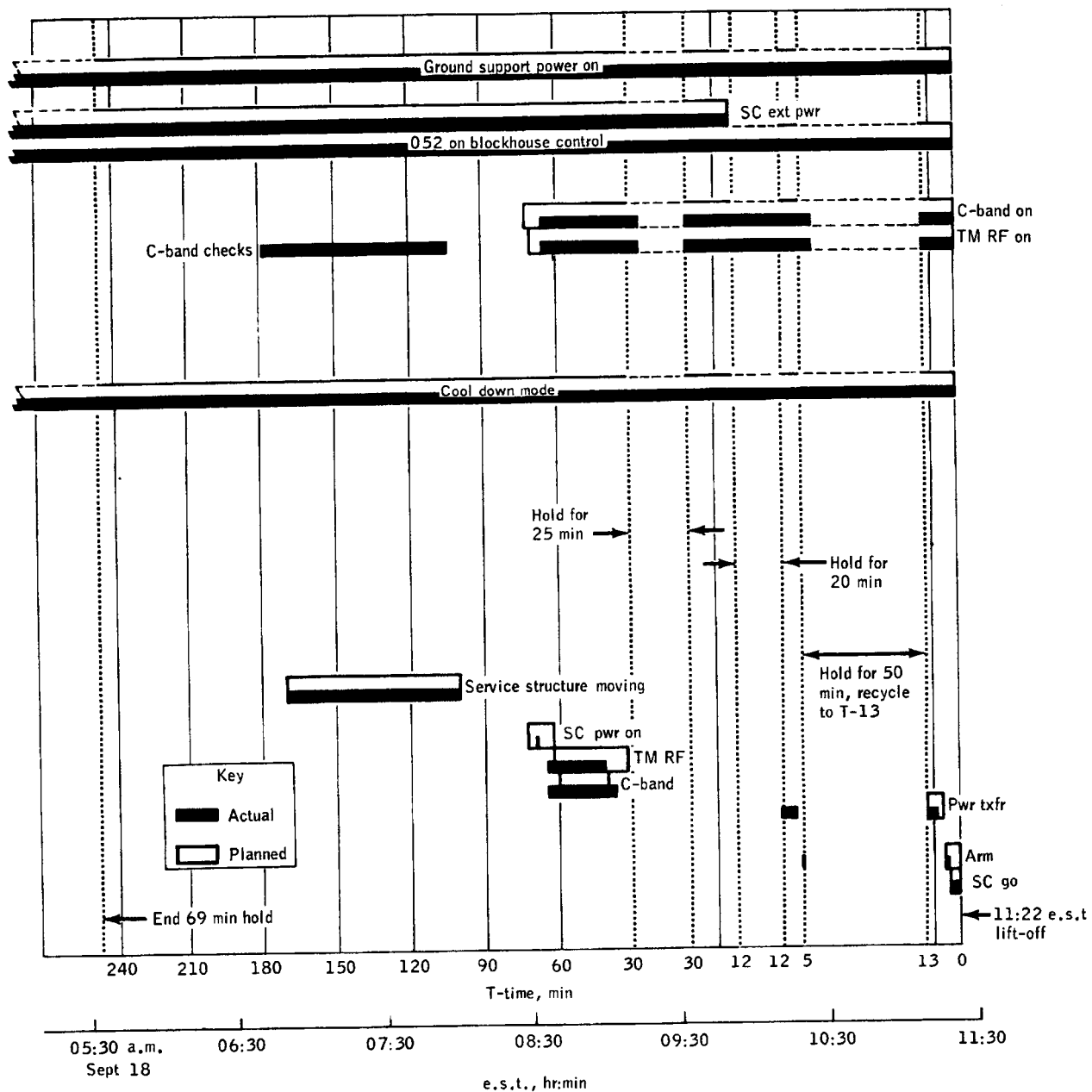


(b) Launch day, September 18, 1964.

Figure 7.2-1.- Continued.

UNCLASSIFIED

UNCLASSIFIED



(c) Launch day, September 18, 1964.

Figure 7.2-1.- Concluded.

UNCLASSIFIED

UNCLASSIFIED

7-15

7.3 Range Operations

The Network which provided telemetry and radar support for the mission consisted primarily of stations of the Eastern Test Range augmented by Department of Defense and NASA stations. The coverage provided by the stations is shown in table 7.3-I for telemetry, and table 7.3-II for C-band radar.

One day prior to launch, the Antigua Island radar site was shut down because of a hydraulics system malfunction. The malfunction was corrected in time to support the second orbital pass. Grand Turk Island supported the launch phase in lieu of Antigua. During the countdown, the Grand Turk Island radar had a relay failure which shut down the transmitter and resulted in a hold at T-3 minutes and a recycle to T-13 minutes after the relay was replaced. On the basis of the network checkout tests, the Pretoria, South Africa, telemetry station was not operational at launch. The first valid orbital determination by GSFC computers was made on the basis of data from Carnarvon, Australia, on the first orbital pass.

During the mission, telemetry coverage was obtained on the first four orbital passes and part of the fifth. Radar transponder tracking was obtained during the first two orbital passes and part of the third. After the transponders stopped operating, many of the network stations skin-tracked the vehicle on a programmed schedule throughout its lifetime of 59 orbital passes. The vehicle reentered over the South Indian Ocean.

The times of acquisition and loss of telemetry reception for each station are given in table 7.3-I. In general, each station reported horizon-to-horizon reception on all three spacecraft links. The last station to report reception of link C was Pretoria during the fourth orbital pass. The last station to report reception of link B was Hawaii in the fourth orbital pass. The last station to report reception of link A was Hawaii in the fifth orbital pass. Link A was last received at 07:38:52 g.e.t.

The times of acquisition and loss of C-band radar reception are presented in table 7.3-II. The last station to report tracking of the C-band transponders was Hawaii during the third orbital pass at 04:31:11 g.e.t.

The following anomalies were noted in the performance of the network:

(1) Several of the tracking stations experienced difficulty in lock-on to the spacecraft transponder due to the IU transponder operating longer than anticipated. Several sites seemed confused as to

UNCLASSIFIED

UNCLASSIFIED

which signal to track, but since the second return (spacecraft transponders) was the stronger signal, it was tracked instead of the IU transponder. See section 9.1.

(2) Eglin Air Force Base, Florida, on the first orbital pass, was requested to skin track rather than interrogate the beacon which was still active. Skin track was not obtained because of the extreme range.

(3) White Sands Missile Range, New Mexico, telemetry station, on the first orbital pass, reported heavy multipath interference on link A (the acquisition link) between 0° and 25° elevation. The signal strength varied also, possibly from spacecraft tumbling. Link A had a fairly constant signal strength during the second orbital pass.

(4) Pretoria telemetry station reported dropouts of 4 seconds and 13 seconds duration on the third orbital pass and late acquisition and a 15-second dropout of link C on the fourth orbital pass. Links A and B were satisfactory.

(5) Pretoria telemetry station, on the first orbital pass, was unable to hold automatic track telemetry due to undetermined equipment problems. In switching to manual track, no dropouts in reception were experienced; however, high noise was observed in some periods of the track.

(6) Grand Turk Island radar station lost contact with the vehicle from 00:06:43 to 00:07:55 g.e.t. because of Bermuda interference on beacon reception.

UNCLASSIFIED

UNCLASSIFIED

7-17

TABLE 7.3-1.- TELEMETRY COVERAGE

[All times are ground elapsed time]

Station	Launch phase and first pass			Second pass			Third pass			Fourth pass			Fifth pass		
	Duration of signal, hr:min:sec	Acquisition	Loss	Duration of signal, hr:min:sec	Acquisition	Loss	Duration of signal, hr:min:sec	Acquisition	Loss	Duration of signal, hr:min:sec	Acquisition	Loss	Duration of signal, hr:min:sec	Acquisition	Loss
Eastern Test Range															
Cape Kennedy Telemetry 2	00:00:00		00:09:37	01:53:27		01:42:10									
Cape Kennedy Telemetry 3	00:00:00		00:09:19	01:56:17		01:42:12									
Grand Bahama Island	00:00:00		00:17:02												
San Salvador Island	00:02:05		00:18:30												
Antigua Island	00:07:00		00:14:28	01:47:41		01:47:31									
Ascension Island	00:11:21		00:28:47	01:45:48		02:01:16									
Pretoria, South Africa	00:31:18		00:59:19	02:16:05		02:15:35		03:40:44		03:47:13					
Manned Space Flight Network															
Bermuda	00:51:21		00:11:46												
Canberra, Australia	00:01:47		01:00:00												
Guaymas, Mexico	01:20:49		01:55:55	03:02:11		03:19:28									
Department of Defense Range Stations															
Wallops	01:16:25		01:23:51					04:21:47		04:51:57			04:57:47		04:58:52
California	01:28:32		01:53:47	02:59:02		03:06:23									
Corpus Christi, Texas	01:51:55		01:59:09	03:05:30		03:11:24									
Edlin Air Force Base, Fla.	01:53:19		01:41:25												

^a A and B links^a A and B links only^b C link^b A link only

UNCLASSIFIED

UNCLASSIFIED

TABLE 7.3-17.- C-BAND RADAR COVERAGE

[All times are ground elapsed time]

Station	Launch phase and first pass		Second pass		Third pass	
	Duration of signal, hr:min:sec		Duration of signal, hr:min:sec		Duration of signal, hr:min:sec	
	Acquisition	Loss	Acquisition	Loss	Acquisition	Loss
Eastern Test Range						
Cape Kennedy	00:00:00	00:09:16				
Patrick Air Force Base, Fla.	00:00:16	00:07:45	01:36:15	01:41:45		
Grand Bahama Island	00:01:14	00:09:36				
San Salvador Island	00:02:25	00:10:53				
Grand Turk Island	^a 00:03:03	^a 00:11:55	01:38:38	01:44:01		
Antigua Island			01:45:58	01:47:08		
Ascension Island	00:21:10	00:27:32	01:55:13	02:01:00		
Pretoria, South Africa	00:32:25	00:39:47	02:06:01	02:13:10		
Manned Space Flight Network						
Bermuda	00:06:28	00:11:43				
Carnarvon, Australia	00:54:19	00:59:46				
Department of Defense Range Stations						
Hawaii	01:17:29	01:21:29	02:53:57	02:56:29	04:25:23	04:31:11
California	01:26:33	01:33:27				
White Sands Missile Range, N. Mex.	01:31:35	01:36:23	03:05:23	03:08:35		

^aGrand Turk Island lost contact from 00:06:43 to 00:07:55

UNCLASSIFIED

UNCLASSIFIED

7-19

7.4 Data Coverage and Availability

Data support, general.- All data requested by the Apollo Spacecraft Program Office, Test Evaluation Branch, MSC-Houston, for the evaluation of launch vehicle and spacecraft performance are listed in table 7.4-I.

Responsibility for acquisition and delivery of these data was divided between the Kennedy Space Center (KSC) and the Goddard Space Flight Center, Florida Operations (GSFC-FO). KSC provided launch-phase data and GSFC-FO provided insertion-phase (Antigua) and orbital-phase data. Both Centers delivered all data to the Data Section, Operations Support Branch, MSC-Florida Operations (OSB) for handling and distribution.

Telemetry oscillograph recordings were annotated at OSB prior to distribution to the launch site analysis and reporting team. Real-time telemetry oscillograph recordings were made available to the team within hours after lift-off.

Launch data support.- Delivery of quick-look data required by the analysis and reporting team was satisfactory. Magnetic tapes from Telemetry Building 2 (Tel 2), Telemetry Building 3 (Tel 3), Mission Control Center (MCC), and Hangar S were all received within a time envelope of 1 to 4 hours (table 7.4-I). Real-time oscillograph records from Tel 2 were received within 1 hour after lift-off. Quick-look processed data plots (SC-4020 plots) of commutated and continuous channels were received 24 hours after lift-off. Telemetry signal strength records were received between 5 and 6 calendar days after lift-off. Delivery of engineering sequential film is late at this writing and thus precludes a complete evaluation of photographic coverage at this time.

Insertion and orbital data support.- A 24-hour delay was experienced in obtaining insertion phase telemetry tapes from Antigua. The delay was attributed to breakdown of the Air Force aircraft scheduled to transport data from Antigua to Patrick Air Force Base. The majority of orbital tapes provided by GSFC-FO were generally provided within the time frames specified.

Orbital phase tapes from Hawaii, Bermuda, Corpus Christi, and Eglin were received at GSFC, Greenbelt, Maryland. Copies were forwarded directly to MSC-Houston and arrived at T+14 calendar days. At the present time, the tape from Pretoria has not arrived at GSFC. The delay was caused by breakdown of successive Air Force aircraft enroute from Pretoria to Washington, D. C.

UNCLASSIFIED

UNCLASSIFIED

Photographic coverage.- Photographic coverage, including the quantity of instrumentation committed and data obtained during the launch-phase, is shown in table 7.4-I. The total requirements for engineering sequential camera coverage and usage are shown in table 7.4-II. Locations of the engineering sequential cameras are shown in figures 7.4-1 and 7.4-2.

An evaluation of all films received indicates that, of the six tracking camera films available for review, the quality was generally good with respect to exposure, focus, and tracking, except for one film. Film quality with respect to other camera and film defects was good with the following exceptions: One film appeared very grainy, and two films provided no usable timing image. Five of the films were from the long focal-length tracking cameras and provided very good coverage from approximately 20 seconds after lift-off to approximately 32 seconds after LES jettison (T+160.2 sec). The Patrick IGOR camera tracked the entire space vehicle to staging and then followed the S-I stage. Cocoa Beach and Melbourne Beach ROTI cameras tracked the entire space vehicle through S-I staging and then the S-IV stage and the BP-15 spacecraft through LES jettison. The Vero Beach ROTI tracking camera lost track of the spacecraft at LES jettison but did provide good coverage of the spacecraft prior to and following tower separation. The Cocoa Beach, Melbourne Beach, and Vero Beach films did provide sufficient data to determine tumbling rates and approximate trajectory of the jettisoned LES. The Grand Bahama Island IGOR camera provided no usable data on this mission.

The other film available for review provided a close-up view of the spacecraft at lift-off and for approximately 35 seconds of early flight.

MSC-Houston data reduction.- Spacecraft telemetry data were processed at MSC-Houston by the Computation and Analysis Division (CAD), with support from Instrumentation and Electrical Systems Division (IESD). The tape copy used for launch-phase data reduction (T-10 sec to approximately T+400 sec) was from the Mission Control Center (MCC) telemetry station, Cape Kennedy, Fla., and was received in Houston at T+23 hours. The tape copy used for reduction of insertion-phase data (T+400 sec through insertion) was from Antigua Island telemetry station and was received in Houston at approximately T+72 hours. The first package of engineering analysis plots from these data tapes was provided to the evaluation team at T+6 calendar days. The package contained time-history plots and tabulations of accelerations, strain gages, electrical functions, temperatures, heat flux, conical surface pressure coefficients, root-mean-square (RMS) plots of low-frequency accelerations, fluctuating pressures, and radial vibrations. Conical surface pressure coefficients were determined by using the measured conical surface pressures and the

UNCLASSIFIED

UNCLASSIFIED

7-21

dynamic pressure based on the measured atmospheric density at the time of launch. A second package of engineering analysis plots was made available within T+9 calendar days and contained one-third octave-band time histories; power spectral densities (PSD); and one-third octave-band spectral analyses of fluctuating pressures, radial vibrations, strain gages, and accelerations.

The RMS, PSD, and one-third octave-band analysis plots were produced using the MCC tape. Reduction of vibration data was accomplished by both analog and digital methods. The PSD plots were produced on the digital computer and both RMS, and one-third octave-band analysis plots were produced using analog equipment.

Lift-off (T-0) was established as 11:22:43.26 a.m. e.s.t. as established by launch vehicle umbilical disconnect (17:22:43.26 G.m.t.). Event times were presented on the plots. The event times indicated were the best information available at the time of preparation of the plots. Prelaunch R and Z (Range and Zero) calibration values, which were recorded for the continuous and high-level commutator parameters, were within 2 percent of the original values. No corrections were made as a result of R and Z calibration changes because the change to the data would not have been significant. The R and Z calibrations recorded for the low-level commutator were not precise measurements; consequently, they could not be used for data reduction.

The number and type of parameters processed for BP-15 spacecraft are compared with parameters processed for BP-13 spacecraft in table 7.4-III.

All processed pressure measurements were biased to read ambient pressure at launch. The accelerations were biased to read 1g on the X-axis and zero-g on the Y- and Z-axes.

The data were processed and presented in accordance with requirements established jointly by the Apollo Spacecraft Program Office and the analysis and reporting team subsystem analysts prior to the flight.

Acceleration and strain-gage time-history data were processed and presented in two different formats. An edit routine to determine changes of 3 percent, or greater, of telemetry full scale was superimposed on a basic sample rate of one point every 0.1 second. A second method utilized the same edit routine after a 21-point running average¹ had been performed.

Data recorded by the high-level commutators, except for RCS parameters, were processed using an edit routine to determine transients

UNCLASSIFIED

UNCLASSIFIED

greater than 2 percent. The data produced from the transient detection routine were superimposed on a basic sampling rate of one every $\frac{1}{2}$ second. These data were plotted and printed.

The RCS temperatures were processed with a 5-point running average¹ and every point plotted. Every commutated data point was tabulated without performing a running average.

Every data point recorded by the low-level commutator was processed, plotted, and printed. A 5-point running average was performed on the calorimeter and body temperature data, but no edit routine was performed.

An approximate 3-second drop-out in the data occurred on all receiving station tapes just prior to and during launch-vehicle staging because of flame attenuation from the S-I stage retrorockets. The same drop-out occurred on the BP-13 spacecraft flight.

MSC-Houston data processing anomalies.-

a. The MCC tape, used for primary data reduction at Houston, did not carry the 5-step VCO calibration required for data processing at Houston. As a result, it was necessary to utilize the ground station band-edge calibrations recorded on the MCC tape. The adequacy of this procedure was verified by comparing R and Z calibrations recorded on the Hangar S tape with R and Z calibration information recorded on the MCC tape. The values of these R and Z calibration data were well within system accuracies, and no bias was present.

b. The Hangar S tape was not used for data reduction at Houston because the time information recorded on the tape was direct-recorded as part of a composite. This procedure rendered the extraction of time information recorded on the tape incompatible with existing ground-station equipment since this equipment requires that time information be recorded separately as a frequency modulated subcarrier.

c. The tape from Tel 2 was not used because the tape contained a dropout of approximately 5 to 8 seconds at approximately T+130 seconds which was not apparent in any of the other telemetry tapes.

¹ A running average is accomplished by averaging 21 consecutive points and printing this value versus the time corresponding to the middle or eleventh point. The number one data point is dropped, a new or 22nd included, and a new average is produced and printed out versus the new midpoint. This is continued until all the data points have been included in an average.

UNCLASSIFIED

UNCLASSIFIED

7-23

d. The 100-kc reference frequency on the tape copy from Tel 3 used at Houston was approximately 1.7 kc high.

Marshall Space Flight Center data.- Three spacecraft measurements were transmitted through the launch-vehicle telemetry system on a single side-band link. Data from the three measurements were processed at Marshall Space Flight Center (MSFC) and forwarded to MSC-Houston. The measurements are the following:

	<u>Spacecraft measurement</u>	<u>Launch- vehicle measurement</u>	<u>Launch- vehicle telemetry channel</u>
Adapter radial vibration no. 5	AA0089D	E373-900	S3-13-E01
Adapter radial vibration no. 6	AA0090D	E374-900	S3-14
Service module acoustic	SA2760Y	L69-900	S3-12

Launch-vehicle data essential to the analysis of spacecraft performance were processed at MSFC and forwarded to MSC-Houston. Launch-vehicle parameters processed for MSC-Houston are listed in tables 7.4-IV and 7.4-V.

All MSFC processed data were furnished in formats and engineering units compatible to MSC analyses.

UNCLASSIFIED

UNCLASSIFIED

TABLE 7.4-I. - DATA AVAILABILITY

Data type	Presentation	Requested delivery (a)	Date/time received (a)
Telemetry data from magnetic tapes			
Telemetry Building 2	$\frac{1}{2}$ -in. magnetic tape	T+4 H	T+1 H
Telemetry Building 3	$\frac{1}{2}$ -in. magnetic tape	T+4 H	T+9 H
Mission Control Center	$\frac{1}{2}$ -in. magnetic tape	T+4 H	T+3 H
Hangar S	$\frac{1}{2}$ -in. magnetic tape	T+1 H	T+8 H
Hangar D	$\frac{1}{2}$ -in. magnetic tape	T+2 CD	Did not acquire
Grand Bahama Island	$\frac{1}{2}$ -in. magnetic tape	T+2 CD	T+1 CD
Antigua	$\frac{1}{2}$ -in. magnetic tape	T+12 H	T+2 CD
Ascension	$\frac{1}{2}$ -in. magnetic tape	T+2 CD	T+4 CD
Eglin	$\frac{1}{2}$ -in. magnetic tape	T+2 CD	T+4 CD
Pretoria	$\frac{1}{2}$ -in. magnetic tape	T+2 CD	(b)
San Salvador	$\frac{1}{2}$ -in. magnetic tape	T+2 CD	T+1 CD
Hawaii	1-in. magnetic tape	T+2 CD	T+14 CD
Bermuda	1-in. magnetic tape	T+2 CD	T+14 CD
California	1-in. magnetic tape	T+2 CD	T+14 CD
Guaymas	1-in. magnetic tape	T+2 CD	T+14 CD
Postlaunch instrumentation message	Report (TWX)	T+1 CD	T+1 CD
Data on telemetry receiving station performance			
Signal strength	RECO roll	T+2 CD	T+(5 to 6)CD
Telemetry data sheets (station logs)	Sheet	T+2 CD	T+5 CD (partial)
Data from oscillograph			
Telemetry Building 2	Real-time oscillograph roll	T+1 H	T+1 H
Telemetry Building 3	Playback copy	T+8 H	T+18 H

^aKey:

CD - Calendar Day

WD - Working Day

H - Hours

^bData requested but not received during the postlaunch reporting period.

UNCLASSIFIED

UNCLASSIFIED

7-25

TABLE 7.4-I.- DATA AVAILABILITY - Continued

Data type	Presentation	Requested delivery (a)	Date/time received (a)
Hangar S	Real-time oscillograph	T+2 H	T+3 H
Hangar D	Special real-time oscillograph	T+12 H	T+3 CD
Reduced telemetry data			
Commutated channels	SC 4020 plots-film	T+5 H	T+1 CD
Commutated channels	SC 4020 plots - roll copy	T+5 H	T+1 CD
Commutated channels	SC 4020 plots - book	T+10 H	T+1 CD
Continuous channels	SC 4020 plots - film	T+2 CD	T+1 CD
Continuous channels	SC 4020 plots - book	T+2 CD	T+1.5 CD
Launch-vehicle data			
All launch vehicle measurements	SC 4020 plots - book	T+2 CD	T+1 CD
All launch vehicle measurements	Calibration curves - books	T-0	T-3 CD
SA-7 measurement program	Book	T-14 CD	T-14 CD
SA-7 ground and environmental measurement program	Book	T-14 CD	T-14 CD
Flash reports from ground and environmental measurement program	Page	As available (not to exceed T+4 CD)	(b)
Antigua	SC 4020 plots - book	T+3 CD	T+3 CD
Antigua	SC 4020 plots - book	T+4 CD	T+4 CD
Ground and environmental measurements	SC 4020 plots	T+4 CD	T+3 CD

^aKey:

CD - Calendar Day

WD - Working Day

H - Hours

^bData requested but not received during the postlaunch reporting period.

UNCLASSIFIED

UNCLASSIFIED

TABLE 7.4-I.- DATA AVAILABILITY - Continued

Data type	Presentation	Requested delivery (a)	Date/time received (a)
Radar and metric data			
Quick-look IP transformation (positive velocity acceleration)	Magnetic tape	T+6 H	T+1 CD
Quick-look IP transformation (positive velocity acceleration)	IBM printout	T+6 H	T+1 CD
Quick-look IP transformation (positive velocity acceleration)	Magnetic tape	T+3 CD	T+1 CD
Quick-look IP transformation (positive velocity acceleration)	IBM printout	T+3 CD	T+1 CD
Best estimate of trajectory	IBM printout	T+3 CD	(b)
Aerodynamic parameters containing dynamic pressure, Mach number, Reynold's number/foot	IBM printout	T+3 CD	(b)
Aerodynamic parameters containing dynamic pressure, Mach number, Reynold's number/foot	Magnetic tape	T+3 CD	(b)
Final attitude data (yaw, pitch, roll)	IBM printout	T+3 CD	T+6 CD
Final reduced flight test data (coordinate system 1)	Magnetic tape	T+3 WD	T+7 CD
Final reduced flight test data (coordinate system 1)	IBM printout	T+3 CD	T+4 CD
Final reduced flight test data (coordinate system 2)	Magnetic tape	T+3 WD	(b)
Final reduced flight test data (coordinate system 2)	IBM printout	T+3 CD	(b)
Final reduced flight test data (coordinate system 3)	Magnetic tape	T+3 WD	T+12 CD

^aKey:

CD - Calendar Day

WD - Working Day

H - Hours

^bData requested but not received during the postlaunch reporting period.

UNCLASSIFIED

TABLE 7.4-I.- DATA AVAILABILITY - Continued

Data type	Presentation	Requested delivery (a)	Date/time received (a)
Final reduced flight test data (coordinate system 3)	IBM printout	T+3 CD	T+6 CD
Final reduced flight test data (coordinate system 4)	Magnetic tape	T+3 WD	(b)
Final reduced flight test data (coordinate system 4)	IBM printout	T+3 CD	(b)
Position, velocity and special trajectory parameters (orbital)	IBM printout	T+15 CD	(b)
Position, velocity and special trajectory parameters (orbital)	Magnetic tape	T+15 CD	(b)
Preliminary estimate of data coverage	Sheet	T+2 H	T+5 H
Plotting board charts (stations 1 and LCC 37)	Sheet	T+1 H	T+2.5 H
Plotting board charts (downrange stations)	Sheet	T+2 CD	T+7 CD
Orbital flight parameters	TTY message	T+4 H	T+3 H
Radar beacon log (uprange ETR sites)	Sheet (log format)	T+1 CD	T+4.5 H
Radar beacon log (downrange)	Sheet (log format)	T+4 CD	T+5 CD
Radar event record (uprange)	Strip chart	T+1 CD	T+3 CD
Radar event record (DOD sites)	Strip chart	T+6 CD	(b)
Radar event record (NASA sites)	Strip chart	T+6 CD	(b)
Radar function record (includes signal strength ETR sites)	Strip chart	T+1 CD	T+6 CD

^aKey:

CD - Calendar Day

WD - Working Day

H - Hours

^bData requested but not received during the postlaunch reporting period.

UNCLASSIFIED

TABLE 7.4-I.- DATA AVAILABILITY - Continued

Data type		Presentation	Requested delivery (a)	Date/time received (a)	
Radar function record (includes signal strength DOD sites)		Strip chart	T+6 CD	(b)	
Radar operations log (data sheet - ETR)		Sheets	T+1 CD	T+11 CD	
Radar operations log (data sheet - DOD)		Sheets	T+6 CD	(b)	
Radar operations log (data sheet - NASA)		Sheets	T+6 CD	(b)	
Final special trajectory parameters (inertial-flight path, heading, geo-centric lat., etc.)		IBM printout	T+3 CD	(b)	
Final special trajectory parameters (inertial-flight path, heading, geo-centric lat., etc.)		Tape	T+3 WD	(b)	
Sequential events derived from optics		Sheet	T+1 CD	T+8 CD	
Final analysis of radar support		AFETR Report	T+27 CD	(b)	
PRD 2400					
Page	Item no.	Data type	Presentation	Requested delivery (a)	Date/time received (a)
Engineering sequential film data					
220.2	1	35 mm from T-5 sec to loss of vehicle (LOV)	4 cameras positioned to provide 360° coverage of entire vehicle	T+5 CD	T+8 CD (partial)
202.2	2	35 mm reduction print from T-5 sec to LCV	4 cameras positioned to provide 360° coverage of spacecraft	T+5 CD	T+8 CD (partial)
220.2	3	35 mm from T-5 sec to LOV	4 cameras positioned to provide 360° coverage of first stage	T+5 CD	T+8 CD (partial)
220.5	2	16 mm from T-20 min to LOV (B and W)	2 cameras positioned 90° apart to be used to study wind effects	T+5 CD	T+6 CD
220.5	3	35 mm from T-5 sec to LOV	4 cameras positioned to provide data for use in analyzing vehicle position to LO	T+5 CD	T+8 CD (partial)

^aKey:

CD - Calendar Day

WD - Working Day

H - Hours

^bData requested but not received during the postlaunch reporting period.

UNCLASSIFIED

UNCLASSIFIED

7-29

TABLE 7.4-I.- DATA AVAILABILITY - Continued

PRD 2400		Data type	Presentation	Requested delivery (a)	Date/time received (a)
Page	Item no.				
220.6	2	35 mm from T-5 sec to T+30 sec	1 camera to show vehicle motion for first 15 feet of flight	T+5 CD	T+8 CD
220.8	1	35 mm from T-5 sec to LOV	2 cameras in tandem showing entire vehicle and launcher	T+5 CD	T+8 CD
220.8	2	35 mm from T-5 sec to LOV	2 cameras in tandem showing entire vehicle and launcher	T+5 CD	T+8 CD
220.8	3	35 mm from t-5 sec to LOV	2 cameras in tandem showing entire vehicle and launcher	T+5 CD	(b)
220.9	2	35 mm reduction print from T-5 sec to T+4 min	1 camera alined on range flight azimuth to view falling objects	T+5 CD	T+8 CD
220.13	2	16 mm from T-30 sec to T+5 sec	2 views showing spacecraft umbilical disconnect	T+5	T+12 CD
220.13	3	16 mm from T-5 sec to T+10 sec	3 views of spacecraft during lift-off	T+5	T+12 CD
220.13	4	35 mm from T-5 sec to LOV	2 views showing LES and CM	T+5	(b)
220.13	4	16 mm from T-5 sec to LOV	2 views showing LES and CM	T+5	(b)
220.10	1	70 mm from acquisition to LOV	Copies from Vero Beach, Melbourne Beach	T+1 CD	T+1 CD
220.10	1	35 mm from acquisition to LOV	Copies from Vero Beach, Melbourne Beach, Grand Bahama Island, Cocoa Beach, and Patrick AFB	T+5 CD	T+1 CD
220.10	1	16 mm from acquisition to LOV	Copy from Cocoa Beach	T+5 CD	T+8 CD

^aKey:

CD - Calendar Day

WD - Working Day

H - Hours

^bData requested but not received during the postlaunch reporting period.

UNCLASSIFIED

UNCLASSIFIED

TABLE 7.4-II.- ENGINEERING SEQUENTIAL CAMERA DATA

Program Requirements Document 2400 (ref. 8)		Sequential film coverage item no. (a)	Camera		
Page	Item		Type	Location (b)	Presentation
220.2	1	1.2-53 1.2-54 1.2-55 1.2-56 ^c	Fixed	Launch Complex 37B	Base of launch pedestal centered in bottom of frame to study entire space vehicle motion and structural surveillance during ignition and lift-off
220.2	2	1.2-61 1.2-62 1.2-63 1.2-64 ^c	Fixed	Launch Complex 37B	Camera elevated to frame spacecraft and LES in bottom center of frame for motion study and structural surveillance during early flight
220.2	3	1.2-57 1.2-58 1.2-59 1.2-60 ^c	Fixed	Launch Complex 37B	Launch pedestal centered in bottom of frame for structural surveillance of the launch vehicle during ignition and lift-off
220.5	2		Fixed	Launch Complex 37B	Two cameras positioned 90° apart to study wind effects
220.5	3	1.2-40 1.2-41 ^c 1.2-42 1.2-43	Fixed	Launch Complex 37B (50-foot tower)	Bottom of S-IV stage centered in bottom of frame for structural surveillance and motion study of S-IV stage during lift-off
220.6	2	1.2-35	Fixed	Unbilical Tower 37B (118-foot level)	Lower edge of the S-IV stage checker board pattern in bottom of frame to study vertical displacement of vehicle during first 15 feet of flight

^aData listed by item no. in Operations Directive 2400 (ref. 9)^bSee figures 7.4-1 and 7.4-2^cCameras did not operate

UNCLASSIFIED

UNCLASSIFIED

7-31

TABLE 7.4-II. - ENGINEERING SEQUENTIAL CAMERA DATA - Continued

Program Requirements Document 2400 (ref. 8)		Sequential film coverage item no. (a)	Camera		Presentation
Page	Item		Type	Location (b)	
220.8	1	1.2-76	Tracking	Cape Kennedy	Entire vehicle centered in frame for flight and structural surveillance
220.8	1	1.2-79	Tracking	Cape Kennedy	Track launch vehicle until entire space vehicle is in frame
220.8	2	1.2-75	Tracking	Cape Kennedy	Entire vehicle centered in frame for flight and structural surveillance
220.8	2	1.2-77 1.2-78	Tracking	Cape Kennedy	Track launch vehicle until entire space vehicle is in frame
220.8	3	1.2-74	Tracking	Cape Kennedy	Command module and LES centered in frame for structural surveillance of escape tower during launch and early flight
220.9	1		Tracking	Cape Kennedy Area	Airborne photographic coverage of the launch sequence from specially configured aircraft
220.9	2	1.2-82	Tracking	Cape Kennedy	Camera aligned on range flight azimuth with vehicle centered for structural surveillance and to view objects if separated from vehicle
220.10	1	1.2-86 ^c	Tracking (ROTI)	Vero Beach	Track from first acquisition to loss of vehicle for flight and structural surveillance.

^aData listed by item no. in Operations Directive 2400 (ref. 9)^bSee figures 7.4-1 and 7.4-2^cTiming on film not useable

UNCLASSIFIED

UNCLASSIFIED

TABLE 7.4-II. - ENGINEERING SEQUENTIAL CAMERA DATA - Concluded

Program Requirements Document 2400 (ref. 8)		Sequential film coverage item no. (a)	Camera		
Page	Item		Type	Location (b)	Presentation
220.10	1	1.2-87	Tracking (ROTI)	Meibourne Beach	Track S-IV stage for surveillance and to record flame pattern after ignition; vehicle to be positioned in left side of frame to allow coverage of escape tower jettisoning
220.10	1	1.2-88	Tracking (ROTI)	Cocoa Beach	Track from first acquisition to loss of vehicle for structural and flight surveillance during early flight
220.10	1	1.2-85	Tracking (IGOR)	Patrick Air Force Base	Track space vehicle from first acquisition to separation of S-I and S-IV stage, then track S-I stage to loss of vehicle
220.10	1	3.2-1 ^c	Tracking (IGOR)	Grand Bahama Island	Track from first acquisition to loss of vehicle for flight and structural surveillance and coverage of escape tower jettisoning.
220.11	1	(Support ship).2-1	Tracking	Support ship approximately 5 miles off shore north of flight line	Track to keep space vehicle centered for structural and flight surveillance from a downrange aspect angle
220.11	1	(Support ship).2-1	Tracking	Support ship approximately 5 miles off shore south of flight line	Track to keep space vehicle centered for structural and flight surveillance from a downrange aspect angle
220.13	2	1.2-31	Fixed	Umbilical tower of Launch Complex 37B (208-foot level, NW)	Umbilical connection of Arm 4 centered in right half of frame for detail study of umbilical head release
220.13	3	1.2-69 1.2-70	Fixed	Launch Complex 37B (50-foot tower)	Bottom of service module centered in bottom of frame for structural surveillance of spacecraft during ignition and lift-off

^aData listed by item no. in Operations Directive 2400 (ref. 9)^bSee figures 7.4-1 and 7.4-2^cFilm not useable

UNCLASSIFIED

UNCLASSIFIED

7-33

TABLE 7.4-III. - COMPARISON OF INSTRUMENTATION MEASUREMENTS
USED ON BP-13 AND BP-15 SPACECRAFT

Measurement	BP-13 spacecraft		BP-15 spacecraft	
	Total measurements		Total measurements	
	Continuous	Commutated	Continuous	Commutated
Acceleration	7		7	
Current		1		1
Pressure	15	10	13	11
Heat rate		20		20
Strain	6		6	
Temperature		34		52
Vibration (spacecraft TM)	4		6	
Voltage		10		10
Totals	32	75	32	94

UNCLASSIFIED

UNCLASSIFIED

TABLE 7.4-IV.- LAUNCH-VEHICLE DATA PROCESSED
FOR MSC-HOUSTON AT MSFC

[Data processed at MSFC were required between 7 and 12 calendar days after launch; dates of receipt are listed in table 7.4-V]

Measurement	Launch-vehicle measurement number	Launch-vehicle telemetry channel
Q-ball		
Angle of attack (pitch, coarse)	D133-900	P1-B1-17
Angle of attack (pitch, fine)	D134-900	P1-B1-18
Angle of sideslip (yaw, coarse)	D135-900	F6-X-19-08
Angle of sideslip (yaw, fine)	D136-900	P1-B1-20
Dynamic pressure (coarse)	D137-900	F6-X-19-09
Dynamic pressure (fine)	D138-900	F6-X-19-10
Attitude gyro		
Roll (coarse)	H24-802	F6-X-B12-08
Roll (fine)	H40-802	F5-17M-03
Yaw (coarse)	H25-802	F6-X-B12-09
Yaw (fine)	H41-802	F5-14M-02
Pitch (coarse)	H26-802	F6-X-B12-10
Pitch (fine)	H42-802	F6-14M-02
Rate gyro		
Pitch	F42-802	F6-08
Yaw	F43-802	F6-05
Roll	F44-802	F6-04
Accelerometers		
Apollo mating ring, longitudinal	E210-801	S3-05003
Apollo mating ring, tangential	E211-801	S3-05002
Apollo mating ring, perpendicular	E212-801	S3-05001

UNCLASSIFIED

UNCLASSIFIED

7-35

TABLE 7.4-V.- MSFC DATA AVAILABILITY

Data	Presentation	Calendar day received
Adapter radial vibration no. 5 } Adapter radial vibration no. 6 } Service module acoustic	Magnetic tape in FM mode RMS and PSD 4020 plots (digital)	T+4
Service module acoustic	Analog plots of sound pressure level and $\frac{1}{3}$ octave bandwidths	T+15
Q-ball	IBM compatible tape 4020 plots and tabulations (preliminary) 4020 plots and tabulations (final)	T+7 T+4 T+13
Attitudes and rates	IBM compatible tape Tabulations (preliminary) Tabulations and time history plots (final)	T+7 T+7 T+13
Accelerometers	RMS and PSD 4020 plots (digital)	T+4

UNCLASSIFIED

UNCLASSIFIED

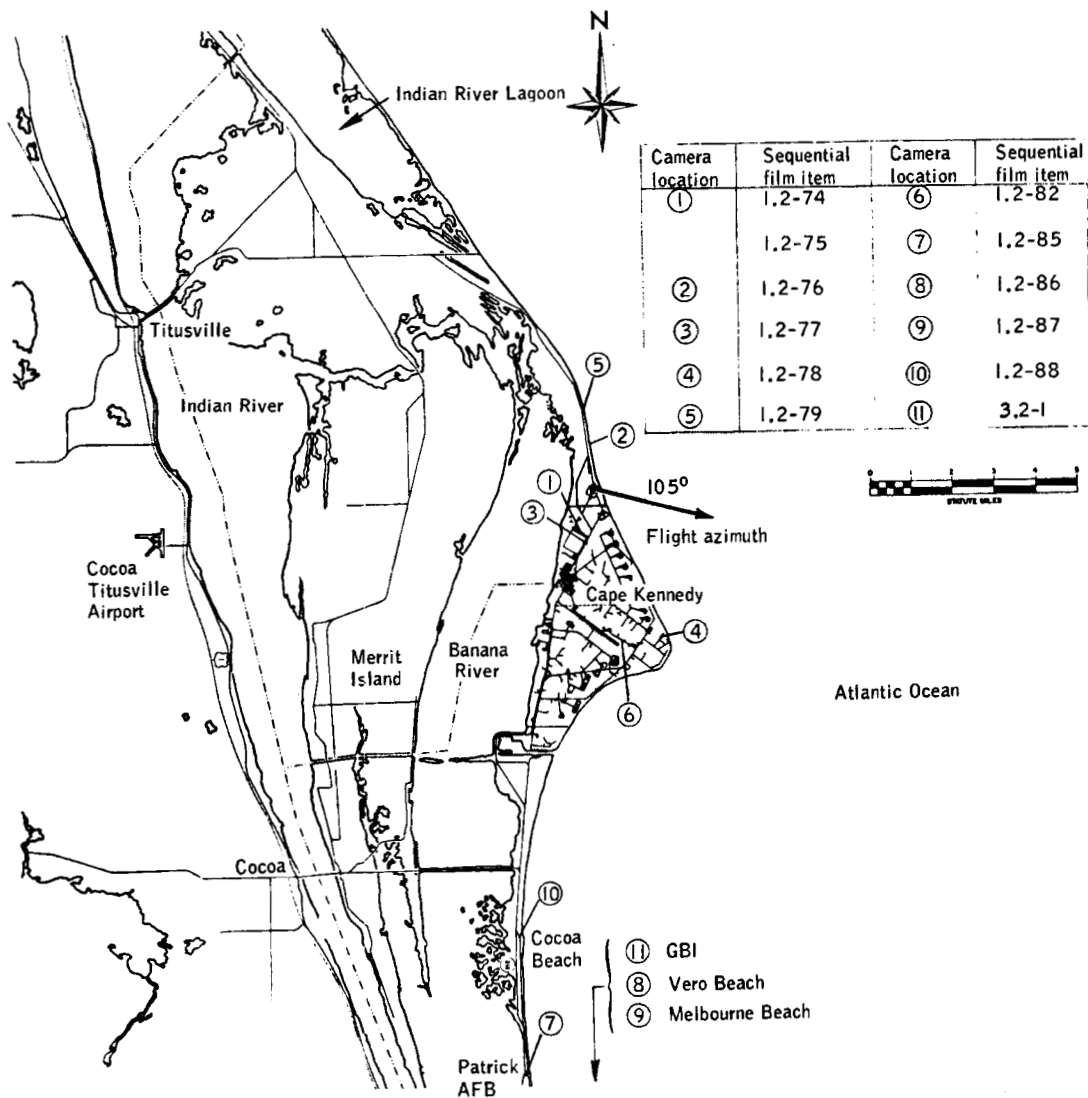


Figure 7.4-1.- Engineering sequential tracking camera locations for Apollo mission A-102.

UNCLASSIFIED

UNCLASSIFIED

7-37

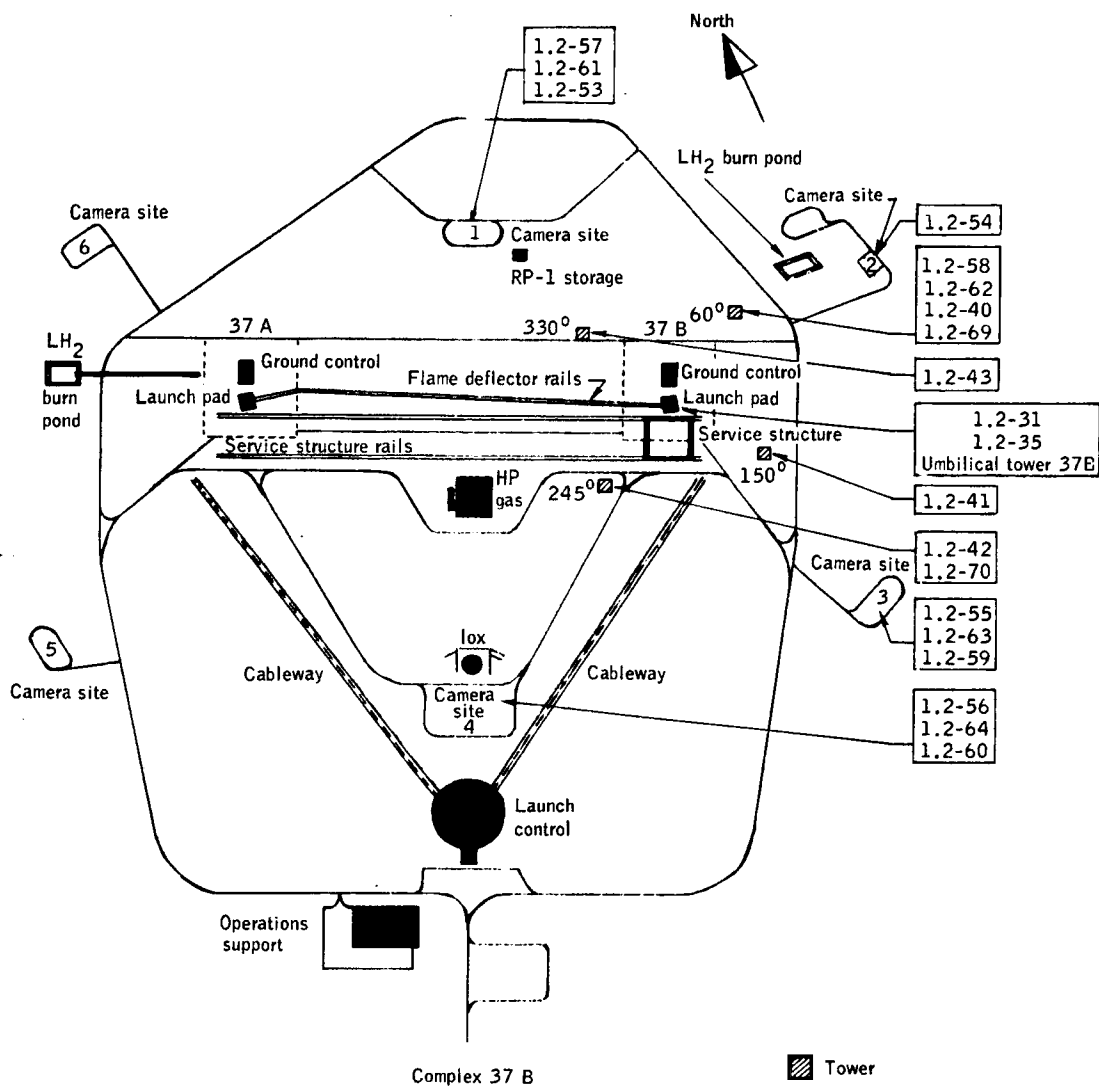


Figure 7.4-2.- Engineering sequential fixed camera locations for Apollo mission A-102.

UNCLASSIFIED

UNCLASSIFIED**7.5 Telemetry Tape Selection and Verification**

Prior to the Apollo mission A-102, a procedure was established to assure that the best of the launch-site telemetry tapes would be selected for processing the launch-phase telemetry data. Telemetry tapes from four launch-site ground stations were obtained for the selection process. They were from the Hangar S station, Telemetry Building no. 2 (Tel 2), Telemetry Building no. 3 (Tel 3), and the Mission Control Center (MCC).

As soon as possible after loss of signal, copies of the Hangar S tape were made at the Hangar S playback station, tape copies of the Tel 2 and Tel 3 tapes were made at the Tel 2 station and taken at once to the Hangar S playback station, and the original MCC tape was taken to the Hangar S playback station. Three oscillographs of selected sub-carriers were made from each of these tapes with the identical format, galvanometer deflection, galvanometer frequency response, and discriminator low-pass output filters. The IRIG standard filters and galvanometers were used. The format for the three oscillograph recordings was as follows:

No. 1	No. 2	No. 3
A-6	B-10	C-6
A-10	B-11	C-7
A-11	B-12	C-8
A-12	B-14	C-10
A-13	B-16	C-11
A-14		C-12
A-15		C-14
A-16		C-16

The oscillographs made from the Hangar S tape copies were compared with the near real-time oscillographs made from the Hangar S original tape to verify these tape copies.

The oscillographs made from the Hangar S, Tel 2, and Tel 3 tape copies and from the MCC original tape were examined by a committee consisting of representatives from MSC-Florida Operations and MSC-Houston for overall signal quality, dropouts, noise content, and possible spikes of the type exhibited in the BP-13 data (ref. 10). The committee judged the Hangar S and Tel 3 tape copies and the MCC original tape to be adequate for the data reduction process.

UNCLASSIFIED

UNCLASSIFIED

7-39

The original MCC tape was selected from these three for data processing for this mission. The MCC tape covered a maximum time of reception after lift-off, and the 100-pps timing signal on a separate track was, at once, compatible with the processing equipment at MSC-Houston. The Tel 2 tape was the least preferred because of a 5-second dropout which occurred approximately 20 seconds before staging. The committee's final judgment of the four tapes in order of preference was (1) Hangar S, (2) MCC, (3) Tel 3, and (4) Tel 2.

UNCLASSIFIED

UNCLASSIFIED

8-1

8.0 APPENDIX B

UNCLASSIFIED

UNCLASSIFIED

TABLE 8.1.1.- MEASUREMENT LIST FOR BOILERPLATE 15 SPACECRAFT

Measurement Identification	Measurement description	Telemetry link, channel, and segment	Frequency response	Measurement range	Location (a)
Acceleration					
LA0011A	Tower acceleration, Y-axis	B-7	30 cps	-2 to 2g	X _L 380 Y0 Z6
LA0012A	Tower acceleration, Z-axis	B-8	30 cps	-2 to 2g	X _L 380 Y6 Z0
CA0001A	Spacecraft acceleration, X-axis, high	C-8	30 cps	-2 to 10g	X _C 78 Y0 Z21
CA0005A	Spacecraft acceleration, Y-axis	C-6	25 cps	-0.5 to 0.5g	X _C 78 Y0 Z21
CA0007A	Spacecraft acceleration, Z-axis	B-6	25 cps	-0.5 to 0.5g	X _C 78 Y0 Z21
SA0003A	Spacecraft acceleration, Z-axis, SM	C-7	30 cps	-0.5 to 0.5g	X _A 866 Y0 Z73
SA0004A	Spacecraft acceleration, Y-axis, SM	A-6	25 cps	-0.5 to 0.5g	X _A 866 Y0 Z73
Quad A reaction control subsystem vibrations					
SA00091D	Clockwise nozzle, X-axis	B-18	1,050 cps	-200 to 200g	X _S 294 191°
SA00092D	Clockwise nozzle, Z-axis	B-15	450 cps	-200 to 200g	X _S 294 191°
		Radial vibration			
CA00021D	Radial vibration 1, CM	A-16	600 cps	-50 to 50g	X _C 114 Y40.4 Z37.3
SA00086D	Radial vibration 2, SM	C-18	1,050 cps	-50 to 50g	X _A 965.2 Y42.8 Z-58
SA00087D	Radial vibration 3, SM	C-17	800 cps	-50 to 50g	X _C 953 Y-53.9 Z47.7
SA00088D	Radial vibration 4, SM	B-17	800 cps	-50 to 50g	X _A 940.4 Y68.3 Z22.8
AA00089D	Radial vibration 5, adapter		50 to 3 kc	-50 to 50g	X _A 777.7 Y0 Z72
		Launch vehicle telemetry, S3-13			
AA00090D	Radial vibration 6, adapter	Launch vehicle telemetry, S4-13	50 to 3 kc	-50 to 50g	X _A 777.7 Y-15.5 Z-71

^aSee figure 4.1.2 for X-axis locations and figure 4.1.3 for Y- and Z-axis locations.

UNCLASSIFIED

TABLE 8.1-1.- MEASUREMENT LIST FOR BOILERPLATE 15 SPACECRAFT - Continued

Measurement Identification	Measurement description	Telemetry link, channel, and segment	Frequency response (b)	Measurement range	Location (a)
Strain					
SA2120S	Strain 1, SM	C-16	600 cps	-500 to 500 min./in.	X _A 940.4 62.25°
SA2121S	Strain 2, SM	B-16	600 cps	-500 to 500 min./in.	X _A 940.4 77.25°
AA0195S	Strain 1, adapter	A-9	60 cps	-500 to 500 min./in.	X _A 736 Y76 Z0
AA0196S	Strain 2, adapter	A-10	80 cps	-500 to 500 min./in.	X _A 736 Y0 Z-76
AA0197S	Strain 3, adapter	B-10	80 cps	-500 to 500 min./in.	X _A 736 Y-76 Z0
AA0198S	Strain 4, adapter	C-10	80 cps	-500 to 500 min./in.	X _A 736 Y0 Z76
Static pressure					
CA0071P	Conical surface pressure 1	A-E-66	10 s/s	0 to 15 psia	X _C 76 557°
CA0072P	Conical surface pressure 2	A-E-67	10 s/s	0 to 15 psia	X _C 76 87°
CA0073P	Conical surface pressure 3	A-E-68	10 s/s	0 to 15 psia	X _C 36 357°
CA0074P	Conical surface pressure 4	A-E-69	10 s/s	0 to 15 psia	X _C 36 93°
CA0075P	Conical surface pressure 5	A-E-70	10 s/s	0 to 15 psia	X _C 29 180°
CA0076P	Conical surface pressure 6	A-E-71	10 s/s	0 to 15 psia	X _C 27 357°
CA0077P	Conical surface pressure 7	A-E-72	10 s/s	0 to 15 psia	X _C 27 87°
CA0078P	Conical surface pressure 8	A-E-73	10 s/s	0 to 15 psia	X _C 20 557°
CA0079P	Conical surface pressure 9	A-E-74	10 s/s	0 to 15 psia	X _C 20 180°

^aSee figure 4.1-2 for X-axis locations and figure 4.1-3 for Y- and Z-axis locations.

^bSampling rate is in samples per second (s/s).

UNCLASSIFIED

TABLE 8.1-1. - MEASUREMENT LIST FOR BOILERPLATE 15 SPACECRAFT - Continued

Measurement Identification	Measurement description	Telemetry link, channel, and segment	Frequency response (b)	Measurement range	Location (a)
Fluctuating pressure					
SA0162P	Fluctuating pressure 3	A-15	300 cps	0 to 15 psia	X _A 1000 329.25°
SA0163P	Fluctuating pressure 4	C-14	300 cps	0 to 15 psia	X _A 959 24.1°
SA0164P	Fluctuating pressure 5	A-14	300 cps	0 to 15 psia	X _A 959 58.9°
SA0165P	Fluctuating pressure 6	B-14	300 cps	0 to 15 psia	X _A 973 277.5°
SA0166P	Fluctuating pressure 7	C-13	220 cps	0 to 15 psia	X _A 959 215.3°
SA0167P	Fluctuating pressure 8	C-15	300 cps	0 to 15 psia	X _A 958 147.9°
SA0168P	Fluctuating pressure 9	B-12	160 cps	0 to 15 psia	X _A 958 187.25°
SA0169P	Fluctuating pressure 10	A-11	110 cps	0 to 15 psia	X _A 919 58.9°
SA0170P	Fluctuating pressure 11	A-12	160 cps	0 to 15 psia	X _C 893.5 316.6°
SA0171P	Fluctuating pressure 12	A-13	220 cps	0 to 15 psia	X _A 906 277.25°
SA0172P	Fluctuating pressure 13	C-11	110 cps	0 to 15 psia	X _A 881 277.25°
AA0173P	Fluctuating pressure 14	C-12	160 cps	0 to 15 psia	X _A 764 183°
AA0174P	Fluctuating pressure 15	B-11	110 cps	0 to 15 psia	X _A 757 3°
Acoustics					
SA2760Y	Acoustics, SM	Launch vehicle telemetry, S3-12	50 to 3 kc	150 to 170 db	X _S 339 0°
Tower temperature					
LA0600T	Tower temperature 1	B-13-52	1.25 s/s	32 to 302° F	X _L 90 Y12 Z0
LA0601T	Tower temperature 2	B-13-53	1.25 s/s	32 to 302° F	X _L 61 Y22 Z0
LA0602T	Tower temperature 3	B-13-54	1.25 s/s	32 to 302° F	X _L 47 Y0 Z23
LA0603T	Tower temperature 4	B-13-55	1.25 s/s	32 to 302° F	X _L 47 Y24 Z23

^aSee figure 4.1-2 for X-axis locations and figure 4.1-3 for Y- and Z-axis locations.^bSampling rate is in samples per second (s/s).

UNCLASSIFIED

UNCLASSIFIED

8-5

TABLE 8.1-1.- MEASUREMENT LIST FOR BOILERPLATE 15 SPACECRAFT - Continued

Measurement Identification	Measurement description	Telemetry link, channel, and segment	Frequency response (b)	Measurement range	Location (a)
Tower temperature - concluded					
LA0604T	Tower temperature 5	B-13-56	1.25 s/s	32 to 302° F	X _L 47 Y-24 Z-23
LA0605T	Tower temperature 6	B-13-57	1.25 s/s	32 to 302° F	X _L 47 Y-24 Z0
LA0606T	Tower temperature 7	B-13-58	1.25 s/s	32 to 302° F	X _L 47 Y-24 Z23
LA0607T	Tower temperature 8	B-13-59	1.25 s/s	32 to 302° F	X _L 36 Y24 Z0
Quad A reaction control system temperature					
SR5065T	Engine supporting bracket	B-13-70	1.25 s/s	32 to 302° F	X _S 294 187.25°
SR5876T	Throat, +P engine	B-13-77	1.25 s/s	32 to 2,012° F	X _S 303 187.25°
SR5877T	Nozzle, +P engine	B-13-78	1.25 s/s	32 to 2,012° F	X _S 310 187.25°
SR5878T	Throat, counterclockwise engine	B-13-79	1.25 s/s	32 to 2,012° F	X _S 294 185°
SR5879T	Nozzle, counterclockwise engine	B-13-80	1.25 s/s	32 to 2,012° F	X _S 294 180°
SR7121T	Engine flange, +P engine	B-13-74	1.25 s/s	32 to 1,472° F	X _S 301 187°
SR7122T	Engine flange, -P engine	B-13-76	1.25 s/s	32 to 1,472° F	X _S 287 187.4°
SR7123T	Engine flange, counterclockwise engine	B-13-75	1.25 s/s	32 to 1,472° F	X _S 290 185°
SR7125T	Injector head, -P engine	B-13-69	1.25 s/s	32 to 392° F	X _S 289 187.25°
SR7126T	Injector head, +P engine	B-13-67	1.25 s/s	32 to 392° F	X _S 299 187.3°
SR7134T	Injector head, counterclockwise engine	B-13-68	1.25 s/s	32 to 392° F	X _S 294 185°
SR7160T	Quad housing, +P engine	B-13-71	1.25 s/s	32 to 707° F	X _S 300 187.5°
SR7161T	Quad housing, counterclockwise engine	B-13-72	1.25 s/s	32 to 707° F	X _S 292 185°
SR7162T	Quad housing, -P engine	B-13-73	1.25 s/s	32 to 707° F	X _S 288 187°
SR7175T	Nozzle, -P engine	B-13-82	1.25 s/s	32 to 2,012° F	X _S 278 187.25°
SR7183T	Quad housing roof	B-13-81	1.25 s/s	32 to 707° F	X _S 294 187.25°

^a See figure 4.1-2 for X-axis locations and figure 4.1-3 for Y- and Z-axis locations.

^b Sampling rate is in samples per second (s/s).

UNCLASSIFIED

UNCLASSIFIED

TABLE 8.1-1.- MEASUREMENT LIST FOR BOILERPLATE 15 SPACECRAFT - Continued

Measurement Identification	Measurement description	Telemetry link, channel, and segment	Frequency response (b)	Measurement range	Location (a)
		Heat flux			
CA0580R	Heat flux, calorimeter 1	B-13-12	1.25 s/s	0 to 25 Btu/ft ² /sec	X _C 74 3°
CA0581R	Heat flux, calorimeter 2	B-13-13	1.25 s/s	0 to 25 Btu/ft ² /sec	X _C 74 180°
CA0582R	Heat flux, calorimeter 3	B-13-14	1.25 s/s	0 to 25 Btu/ft ² /sec	X _C 74 319°
CA0583R	Heat flux, calorimeter 4	B-13-15	1.25 s/s	0 to 25 Btu/ft ² /sec	X _C 53 180°
CA0584R	Heat flux, calorimeter 5	B-13-16	1.25 s/s	0 to 25 Btu/ft ² /sec	X _C 52 3°
CA0585R	Heat flux, calorimeter 6	B-13-17	1.25 s/s	0 to 25 Btu/ft ² /sec	X _C 52 80°
CA0586R	Heat flux, calorimeter 7	B-13-18	1.25 s/s	0 to 25 Btu/ft ² /sec	X _C 52 85°
CA0587R	Heat flux, calorimeter 8	B-13-19	1.25 s/s	0 to 25 Btu/ft ² /sec	X _C 52 95°
CA0588R	Heat flux, calorimeter 9	B-13-20	1.25 s/s	0 to 25 Btu/ft ² /sec	X _C 52 319°
CA0589R	Heat flux, calorimeter 10	B-13-21	1.25 s/s	0 to 25 Btu/ft ² /sec	X _C 42.65 3°
CA0590R	Heat flux, calorimeter 11	B-13-22	1.25 s/s	0 to 25 Btu/ft ² /sec	X _C 27 180°
CA0591R	Heat flux, calorimeter 12	B-13-23	1.25 s/s	0 to 25 Btu/ft ² /sec	X _C 27 319°
SA0550R	Heat flux, calorimeter 17	B-13-28	1.25 s/s	0 to 5 Btu/ft ² /sec	X _S 338 183°
SA0551R	Heat flux, calorimeter 18	B-13-29	1.25 s/s	0 to 5 Btu/ft ² /sec	X _S 315 187.2°
SA0552R	Heat flux, calorimeter 20	B-13-31	1.25 s/s	0 to 5 Btu/ft ² /sec	X _S 305 177°
SA0553R	Heat flux, calorimeter 13	B-13-24	1.25 s/s	0 to 5 Btu/ft ² /sec	X _S 305 187.2°
SA0554R	Heat flux, calorimeter 14	B-13-25	1.25 s/s	0 to 5 Btu/ft ² /sec	X _S 267 160°
SA0555R	Heat flux, calorimeter 16	B-13-27	1.25 s/s	0 to 5 Btu/ft ² /sec	X _S 267 145°
SA0598R	Heat flux, calorimeter 15	B-13-26	1.25 s/s	0 to 5 Btu/ft ² /sec	X _A 933 183°
AA0594R	Heat flux, calorimeter 19	B-13-30	1.25 s/s	0 to 5 Btu/ft ² /sec	X _A 770 183°

^aSee figure 4.1-2 for X-axis locations and figure 4.1-3 for Y- and X-axis locations.^bSampling rate is in samples per second (s/s).

UNCLASSIFIED

UNCLASSIFIED

8-7

TABLE 8.1-1.- MEASUREMENT LIST FOR BOILERPLATE 15 SPACECRAFT - Continued

Measurement Identification	Measurement description	Telemetry link, channel, and segment	Frequency response (b)	Measurement range	Location (a)
Calorimeter body temperature					
CAO651T	Calorimeter body temperature 1	B-13-32	1.25 s/s	32 to 572° F	X _C 74 3°
CAO752T	Calorimeter body temperature 2	B-13-33	1.25 s/s	32 to 572° F	X _C 74 180°
CAO653T	Calorimeter body temperature 3	B-13-34	1.25 s/s	32 to 572° F	X _C 74 319°
CAO654T	Calorimeter body temperature 4	B-13-35	1.25 s/s	32 to 572° F	X _C 53 180°
CAO655T	Calorimeter body temperature 5	B-13-36	1.25 s/s	32 to 572° F	X _C 52 3°
CAO656T	Calorimeter body temperature 6	B-13-37	1.25 s/s	32 to 572° F	X _C 52 80°
CAO657T	Calorimeter body temperature 7	B-13-38	1.25 s/s	32 to 572° F	X _C 52 85°
CAO658T	Calorimeter body temperature 8	B-13-39	1.25 s/s	32 to 572° F	X _C 52 95°
CAO659T	Calorimeter body temperature 9	B-13-40	1.25 s/s	32 to 572° F	X _C 52 319°
CAO660T	Calorimeter body temperature 10	B-13-41	1.25 s/s	32 to 572° F	X _C 42.65 3°
CAO661T	Calorimeter body temperature 11	B-13-42	1.25 s/s	32 to 572° F	X _C 27 180°
CAO662T	Calorimeter body temperature 12	B-13-43	1.25 s/s	32 to 572° F	X _C 27 319°
SAO563T	Calorimeter body temperature 13	B-13-44	1.25 s/s	32 to 572° F	X _S 05 187.2°
SAO564T	Calorimeter body temperature 14	B-13-45	1.25 s/s	32 to 572° F	X _S 267 160°
SAO669T	Calorimeter body temperature 15	B-13-46	1.25 s/s	32 to 572° F	X _A 933 183°
SAO565T	Calorimeter body temperature 16	B-13-47	1.25 s/s	32 to 572° F	X _S 267 145°
SAO560T	Calorimeter body temperature 17	B-13-48	1.25 s/s	32 to 572° F	X _S 338 183°
SAO561T	Calorimeter body temperature 18	B-13-49	1.25 s/s	32 to 572° F	X _S 515 187.2°
AAO665T	Calorimeter body temperature 19	B-13-50	1.25 s/s	32 to 572° F	X _A 770 183°

^a See figure 4.1-2 for X-axis locations and figure 4.1-3 for Y- and Z-axis locations.^b Sampling rate is in samples per second (s/s).

UNCLASSIFIED

UNCLASSIFIED

TABLE 8.1.1.- MEASUREMENT LIST FOR BOILERPLATE 15 SPACECRAFT - Continued

Measurement Identification	Measurement description	Telemetry link, channel, and segment	Frequency response (b)	Measurement range	Location (a)
Command module and service module interior environment					
CA0610T	Interior temperature, CM	B-13-4	1.25 s/s	32 to 302° F	CM interior
CA0611P	Interior pressure, CM	A-E-88	10 s/s	0 to 15 psia	CM interior
SA0612T	Interior temperature, SM	B-13-5	1.25 s/s	32 to 302° F	SM interior
SA0613P	Interior pressure, SM	A-E-87	10 s/s	0 to 15 psia	SM interior
Instrumentation temperature					
CT0201T	TM RF transmitter A temperature	B-13-6	1.25 s/s	32 to 302° F	TM RF transmitter A
CT0202T	TM RF amplifier A temperature	B-13-7	1.25 s/s	32 to 302° F	TM RF amplifier A
CT0203T	TM RF transmitter B temperature	B-13-8	1.25 s/s	32 to 302° F	TM RF transmitter B
CT0204T	TM RF amplifier B temperature	B-13-9	1.25 s/s	32 to 302° F	TM RF amplifier B
CT0205T	TM RF transmitter C temperature	B-13-10	1.25 s/s	32 to 302° F	TM RF transmitter C
CT0207T	TM RF amplifier C temperature	B-13-11	1.25 s/s	32 to 302° F	TM RF amplifier C
Communications, electrical, and sequential					
CC0001V	d-c voltage, main bus A	A-E-24	10 s/s	22 to 32 v d-c	Power control box
CC0002V	d-c voltage, main bus B	A-E-25	10 s/s	22 to 32 v d-c	Power control box
CC0003V	d-c voltage, logic bus A	A-E-22	10 s/s	0 to 36 v d-c	LES sequencer
CC0004V	d-c voltage, logic bus B	A-E-23	10 s/s	0 to 36 v d-c	LES sequencer
CC0005C	Total d-c current	A-E-26	10 s/s	0 to 50 amps	Power control box
BD0001X	Vehicle lift-off signal	A-9, A-10	N.A.	Step	Signal conditioner box

^a See figure 4.1-2 for X-axis locations and figure 4.1-3 for Y- and Z-axis locations.^b Sampling rate is in samples per second (s/s).

UNCLASSIFIED

TABLE 8.1-1.- MEASUREMENT LIST FOR BOILERPLATE 15 SPACECRAFT - Continued

Measurement Identification	Measurement description	Telemetry link, channel, and segment	Frequency response (b)	Measurement range	Location (a)
Communications, electrical, and sequential - concluded					
LD0033X	Tower jettison motor switch	A-E-29	10 s/s	Step	Tower LES sequencer
LD0034X	Tower jettison motor switch	A-E-29	10 s/s	Step	Tower LES sequencer
CD0039V	Tower jettison and separation, command A	A-E-37	10 s/s	0 to 36 v d-c	LES sequencer
CD0040V	Tower jettison and separation, command B	A-E-38	10 s/s	0 to 36 v d-c	LES sequencer
CD0185V	d-c voltage tower pyro, bus A	A-E-28	10 s/s	0 to 36 v d-c	LES sequencer
CD0186V	d-c voltage tower pyro, bus B	A-E-35	10 s/s	0 to 36 v d-c	LES sequencer
CT0002F	Transponder A trigger	A-E-57	10 s/s	0 to 550 prf	Transponder A
CT0003F	Transponder B trigger	A-E-58	10 s/s	0 to 550 prf	Transponder B
CT0007X	R and Z calibration monitor	A-E-59	10 s/s	Step	Signal conditioner box

Measurement Identification	Measurement description	Telemetry link, channel, and segment	Measurement range	Location
Q-ball data				
D133-900	ΔP angle of attack, Q-ball, coarse pitch	Launch vehicle telemetry	-2,550 to 2,550 kg/m ²	X _L 380
D134-900	ΔP angle of attack, fine pitch	Launch vehicle telemetry	-1,000 to 1,000 kg/m ²	X _L 380
D135-900	ΔP angle of sideslip, Q-ball, coarse yaw	Launch vehicle telemetry	-2,550 to 2,550 kg/m ²	X _L 380
D136-900	ΔP angle of sideslip, Q-ball, fine yaw	Launch vehicle telemetry	-1,000 to 1,000 kg/m ²	X _L 380
D137-900	Q-ball coarse dynamic pressure	Launch vehicle telemetry	0 to 1,538 kg/m ²	X _L 380
D138-900	Q-ball fine dynamic pressure	Launch vehicle telemetry	0 to 308 kg/m ²	X _L 380

^a See figure 4.1-2 for X-axis locations and figure 4.1-3 for Y- and Z-axis locations.^b Sampling rate is in samples per second (s/s).

UNCLASSIFIED

TABLE 8.1.1.- MEASUREMENT LIST FOR BOILERPLATE 15 SPACECRAFT - Concluded

Measurement identification	Measurement description	Telemetry link, channel, and segment	Measurement range	Location (a)
Attitude gyro data				
F42-802	Angular velocity, pitch	Launch vehicle telemetry	-10 to 10 deg/sec	Launch vehicle IU
F43-802	Angular velocity, yaw	Launch vehicle telemetry	-10 to 10 deg/sec	Launch vehicle IU
F44-802	Angular velocity, roll	Launch vehicle telemetry	-10 to 10 deg/sec	Launch vehicle IU
H24-802	Coarse attitude, roll	Launch vehicle telemetry	-15 to 15 deg	Launch vehicle IU
H25-802	Coarse attitude, yaw	Launch vehicle telemetry	-15 to 15 deg	Launch vehicle IU
H26-802	Coarse attitude, pitch	Launch vehicle telemetry	-15 to 15 deg	Launch vehicle IU
H40-802	Fine attitude, roll	Launch vehicle telemetry	-2.5 to 2.5 deg	Launch vehicle IU
H41-802	Fine attitude, yaw	Launch vehicle telemetry	-2.5 to 2.5 deg	Launch vehicle IU
H42-802	Fine attitude, pitch	Launch vehicle telemetry	-2.5 to 2.5 deg	Launch vehicle IU
Equipment cooling subsystem				
CF04-00T	Interior temperature, ECS, CM	GSE only	0 to 150° F	CM interior
CF04-01T	Coldplate inlet temperature, ECS	GSE only	0 to 100° F	Coldplate inlet
CF04-02T	Coldplate outlet temperature, ECS	GSE only	0 to 100° F	Coldplate outlet
CF04-03P	Tank inlet pressure, ECS	GSE only	0 to 50 psid	Coolant tank inlet
CF04-04T	Tank outlet temperature, ECS	GSE only	0 to 100° F	Coolant tank outlet
CF04-05P	Pump outlet pressure, ECS	GSE only	0 to 50 psid	Coolant pump outlet

^aSee figure 4.1-2 for X-axis locations and figure 4.1-3 for Y- and Z-axis locations.

UNCLASSIFIED

UNCLASSIFIED

8-11

TABLE 8.2-I.- OPERATIONAL TEST PROCEDURES FOR APOLLO BP-15
SPACECRAFT AT CONTRACTOR'S MANUFACTURING FACILITY

OTP	Title	Date performed (1964)
P-3022	LES horizontal weight and balance	Mar. 12 and 13
P-3018	Forward heat-shield installation	Apr. 7 to 13
P-8019	Beacon systems check-out	Apr. 23 to 24
P-1040	LES check-out	May 14 to 18
P-9019	GSE integrated check-out	Apr. 21 to 24
P-3036	CM vertical weight and balance	Apr. 20 to 22
P-3035	CM horizontal weight and balance	Apr. 22 and 23
P-5000	ECS fill and check-out	May 7 to May 22
P-10002	Test configuration checklist	Apr. 23 to May 19
P-1008	Electrical power systems check-out	Apr. 27 to 30
P-8169	Telemetry and instrumentation check-out	Apr. 30 to May 5
P-8169	(Recycle)	May 8 to 14
P-1094 } P-1095 }	Battery servicing	Apr. 29 to May 28
P-3015	Adapter and SM stack and aline	May 11 to 13
P-3071	CM stack and aline	May 13
P-3013	LES stack and aline	May 14 and 15
P-8077	Omnibeacon system check-out	Apr. 23 and 24
P-0003	Integrated systems test	May 18 to 25
P-5000	ECS drain and purge	May 26
P-3014	Demate LES	May 27 and 28
P-3072	Demate CM	May 28
P-3015	Demate SM	May 29

UNCLASSIFIED

UNCLASSIFIED

TABLE 8.2-II. - OPERATIONAL TEST PROCEDURES FOR APOLLO BP-15
SPACECRAFT AT FLORIDA OPERATIONS

OTP	Title	Date performed (1964)
C-0004	Electrical interface checks	August 7
C-0005	Integrated systems check-out with launch-vehicle simulator	July 9
C-0006	Spacecraft-launch-vehicle overall test no. 1 (plugs in)	Aug. 19
C-0007	Spacecraft-launch-vehicle countdown	Sept. 17 and 18
C-0009	Spacecraft-launch-vehicle RFI test	Aug. 24
C-0021	Spacecraft-launch-vehicle overall test no. 2 with ordnance in and plugs out using swing arms	Aug. 29
C-0028	Spacecraft-launch-vehicle simulated flight test	Sept. 3
C-0031	Launch-vehicle sequencer malfunction - spacecraft monitor test	Aug. 12
C-0033	Spacecraft-launch-vehicle countdown demonstration	Sept. 14 and 15
C-1012	Battery charge, discharge, all batteries	Sept. 16
C-3044	LES total weight and center-of-gravity determination	May 21
C-3045	Buildup and assembly of LES	July 1 to Aug. 3
C-3063	Spacecraft off-loading, transportation to Hangar AF, and preparation for receiving inspection	June 8 to 15
C-3065	Transportation of spacecraft to launch complex and mating of spacecraft to launch vehicle	June 26

UNCLASSIFIED

UNCLASSIFIED

8-13

TABLE 8.2-II.- OPERATIONAL TEST PROCEDURE FOR APOLLO BP-15

SPACECRAFT AT FLORIDA OPERATIONS - Continued

OTP	Title	Date performed (1964)
C-3069	Mate CM and SM assembly to insert- adapter assembly	June 25
C-3071	Mate CM to SM	July 8
C-3075	Transportation of LES to launch complex and mating of LES to CM	Aug. 4
C-3075A	Transportation of LES to launch complex and mating of LES to CM (recycle)	Aug. 18
C-3080	Fit check of spacecraft adapter and instrument unit	June 9
C-3081	Air-conditioning barrier installation	June 25
C-3084	Receiving inspection check list	June 15
C-4058	Pyrotechnic receiving and inspection, handling, and preinstallation check-out procedure	{ July 9 Aug. 7 Aug. 26 Sept. 11
C-4065	Launch-escape motor receiving and pre- installation inspection, storage, and handling, including grain inspection	July 24, 25, and 30
C-4066	Pitch-control motor receiving and preinstallation inspection, storage, and handling	June 15
C-4067	Jettison motor receiving and pre- installation inspection, storage, and handling	{ June 12 June 15
C-5024	ECS service	{ Aug. 26 July 7

UNCLASSIFIED

UNCLASSIFIED

TABLE 8.2-II.- OPERATIONAL TEST PROCEDURE FOR APOLLO BP-15

SPACECRAFT AT FLORIDA OPERATIONS - Concluded

OTP	Title	Date performed (1964)
C-8112	Instrument system PIA procedures	Continuing
C-8114A	Antenna (VSWR, test)	June 29
C-8115	RF systems PIA procedure	Continuing
C-8131	Telemetry systems test	July 1 and 2
C-8132	Power and sequential PIA procedure (tower sequencer)	{ July 23 Aug. 10, 21, 30, and 31 Sept. 2, and 10
C-9002	Functional verification of A14-001 launch-escape tower substitute unit	June 9
C-9036	Water-glycol unit check-out	June 23
C-9037	Ground equipment verification and GSE integrated umbilical check-out	June 15
C-10001A	Pad checklist	(a)

^aPerformed in support of all launch-vehicle-spacecraft integrated tests.

UNCLASSIFIED

9.0 APPENDIX C

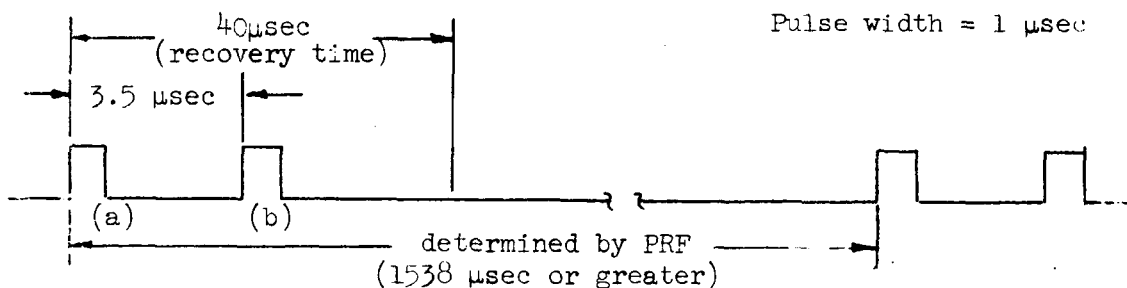
9.1 C-Band Beacon Anomaly

Seven tracking network radar stations reported seeing two beacons during the BP-15 spacecraft's first orbital pass over their stations. Antigua Island and Ascension Island reported detecting the two beacons on the spacecraft's second orbital pass. This two-beacon response was not reported on previous Saturn launches; consequently, the report was unexpected and resulted in some operator confusion during tracking operations.

In all cases, the stations detecting the two beacons tracked on the beacon "... farthest out in range." However, if the operator had elected to track the "closest" beacon, tracking errors of 500 yards would have been introduced on the first two orbital passes.

The instrument unit (IU) beacon transponder was connected to the short-life battery bus (length of operation - approximately 40 minutes) on previous Saturn launches, with the result that the transponder went inoperative prior to the first orbital pass over Ascension Island. On SA-7, the IU beacon was connected to the long-life battery bus which resulted in a probable operation of approximately 110 minutes.

For tracking purposes, the BP-15/SA-7 space vehicle utilized two C-band beacon transponders: one in the IU, and the other in the spacecraft operating on adjacent frequencies (less than 1 mc difference). Two separate redundant beacons operating on the same spacecraft frequency were installed within the command module. The beacons were interrogated by ground-tracking radars utilizing a double pulse interrogation system as shown in the following diagram.



UNCLASSIFIED

Pulse (a) triggers the IU beacon which returns response pulse (A) as shown below. Pulses (a) and (b) trigger the spacecraft transponder which returns response pulse (B). Although the IU and spacecraft transponders operate at slightly different frequencies, both are within the ground radar bandwidth. The 3.5- μ sec delay appears to the operator as two targets 500 yards apart.

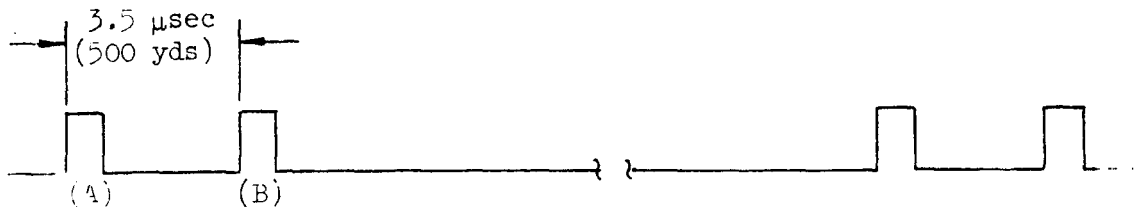


Table 9.1-I is a summary of selected radar reports, with Ascension Island being the last station to see the two beacons at 1:17:56 e.s.t. Subtracting the lift-off time of 11:22:43 e.s.t. from the Ascension time shows that the beacon became inoperable sometime after 115 minutes after lift-off. This time compares favorably with the MSFC preliminary estimate for operation of approximately 110 minutes.

The transponder trigger rate was telemetered to ground stations and is shown in figure 9.1-1. Also shown are the radar pulse repetition frequency (PRF) rates during the periods of beacon interrogation. Correlation of these data indicate proper operation of the transponder.

No additional investigation of this anomaly is planned.

UNCLASSIFIED

UNCLASSIFIED

9-3

TABLE 9.1-I.- SUMMARY OF SELECTED RADAR REPORTS ON ORBITAL PASSES 1 AND 2

Station	Orbital pass	Time, e.s.t.	Message
Ascension Island	1	11:43:53	Two beacon returns were seen separated by approximately 500 yards. Operator chose to track beacon farthest out in range.
Pretoria, South Africa	1	11:55:03	Had two beacons; radar tracked beacon farthest out in range.
Carnarvon, Australia	1	12:17:02	Radar beacon signal weak for easy acquisition of signal. Beacon frequency shifting, and beacon count-down observed.
Hawaii	1	12:40:12	Two beacon replies seen until after point of closest contact.
California	1	12:47:40	Two C-band beacon pulses were received; second pulse was tracked.
White Sands Missile Range, New Mexico	1	Unknown observed two beacon returns at various times. Tracked second beacon, which was proper, as it was very solid return at all times
Cape Kennedy, Fla.	1	12:59:00	Acquired track initially with IU beacon and switched to spacecraft beacon shortly thereafter.
Grand Turk Island	1	1:01:21	Believed to be on lobe.
Antigua Island	2	1:08:31	Beacon track, good beacon, saw both beacons
Ascension Island	2	1:17:56	Beacon strong; same two pulses as seen on orbital pass 1.

UNCLASSIFIED

UNCLASSIFIED

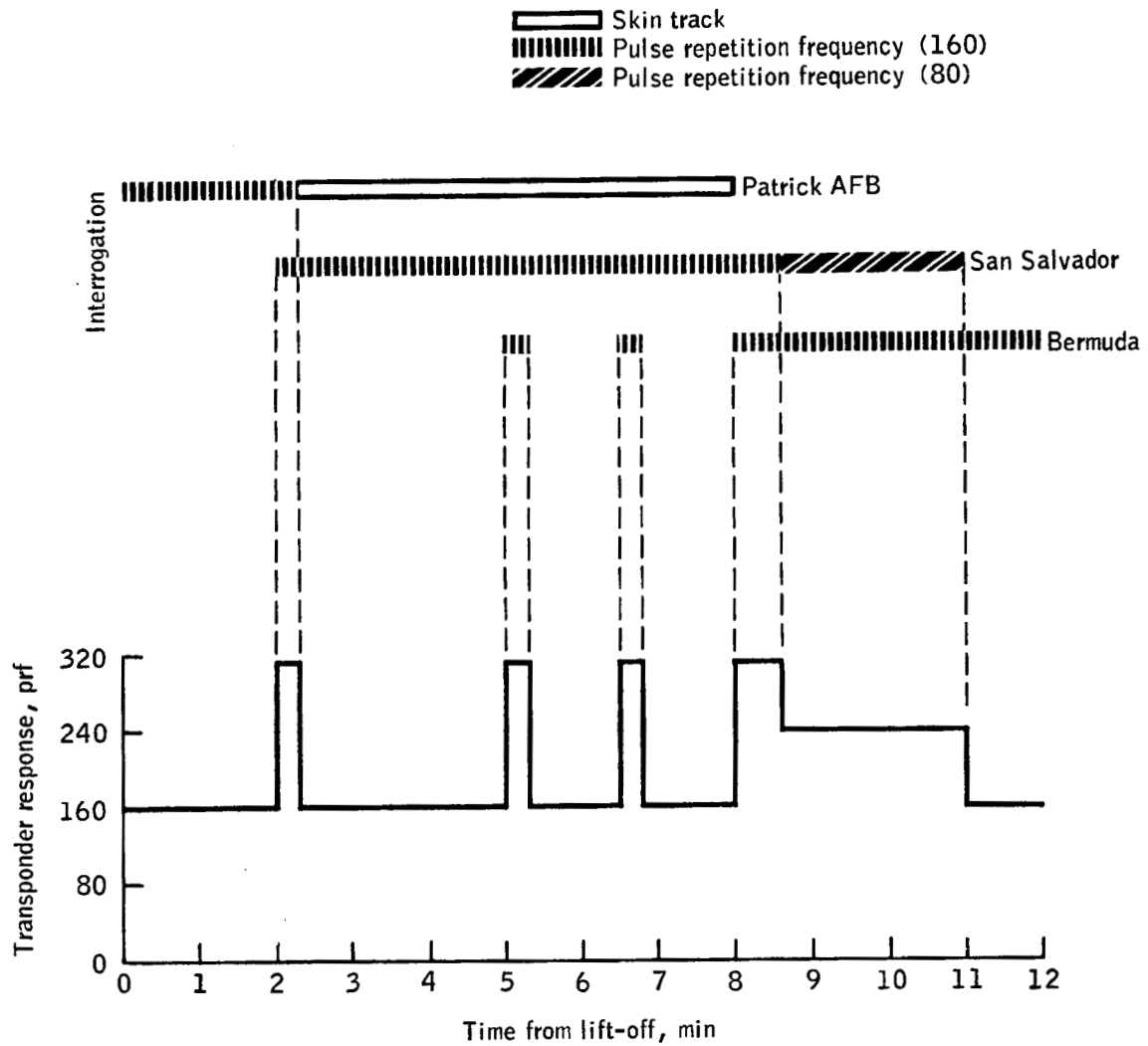


Figure 9.1-1.- BP-15 spacecraft transponder interrogation and response.

UNCLASSIFIED

UNCLASSIFIED

9-5

9.2 Loss of Temperature Measurement SR5877T

Temperature data from thermocouple SR5877T failed to indicate any change during the BP-15 spacecraft mission. The thermocouple was located 1 inch from the rim of the nozzle on the positive pitch engine on the instrumented RCS quad (figs. 4.8-7 to 4.8-9). The temperature measurement indicated an output reading of approximately 4 percent of full scale, equivalent to 10^4 ° F, and remained constant during countdown and flight. This value could be possible during countdown but did not agree with the expected environment indicated by other related thermocouple measurements on the RCS quad during flight.

Data from the thermocouple was highly desirable because the temperature of this particular area was predicted to exceed all other temperature measurements on the RCS quad. Also, temperature data from this area could have been used in the investigation of the loss of data from calorimeter no. 13 located immediately below this nozzle (fig. 4.11-2).

The instrumented RCS quad was installed on the service module on the launch pad on June 29, 1964. A telemetry test was performed on July 2, 1964, during which all thermocouples were thermally excited and tested using a heat gun. All the RCS instrumentation functioned satisfactorily at the time. The same measurement was electrically calibrated 2 minutes before launch and did not indicate any anomaly at the time.

Analysis of flight data did not indicate any solution to this anomaly. The results of additional studies will be reported when available.

UNCLASSIFIED

UNCLASSIFIED**9.3 Loss of Heat Flux Data from
Calorimeter 13 (SA0553R)**

Heat flux data from calorimeter 13 (SA0553R) was questionable and had to be disregarded. The calorimeter was located on the SM under the nozzle of the positive pitch engine of the instrumented RCS quad (fig. 4.11-2). The calorimeter gave normal response when thermally excited by a heat gun during the simulated flight test at T-15 days and again responded normally during electrical calibration at approximately T-2 minutes. The calorimeter did respond to excitation at lift-off. It failed, however, to respond at the main heat pulse during ascent, whereas the body temperature measurement SA0563T located inside the same calorimeter increased to a level above that of the other calorimeter body temperatures. This indicated that an unmeasured heat flux was present in this particular area of the service module. The flight data did not give any information with respect to the time or the cause of the failure.

The data from this calorimeter were highly desirable because this area was predicted to have the highest heating rate on the service module. The same type of calorimeter in the same location on the BP-13 spacecraft also failed. Two other calorimeters failed to produce satisfactory data on the BP-13 spacecraft flight, but performed satisfactorily on the BP-15 spacecraft flight.

Calorimeters of two different ranges were used in both flights. The 0 to 25 Btu/ft²/sec calorimeters located on the command module performed satisfactorily in both flights. The 0 to 5 Btu/ft²/sec calorimeters, located on the SM, differed from the calorimeter located on the CM in size. The diaphragm of the CM calorimeter was 3.5 mils thick with 0.150 inch unsupported diameter and that of the SM calorimeter was 2.5 mils thick with 0.250 inch unsupported diameter (fig. 9.3-1).

As a result of the failures during the BP-13 spacecraft flight, MSC-IESD performed additional environmental tests on the smaller range calorimeter prior to the BP-15 spacecraft flight. The test levels under which the calorimeter specimens were subjected were based on the BP-13 spacecraft launch environment. The time duration during acoustic noise test, however, exceeded the launch environment. None of the environmental test conditions were imposed simultaneously. The following are the environmental conditions to which the calorimeter was subjected:

UNCLASSIFIED

~~CONFIDENTIAL~~

9-7

a. Humidity - 100 percent at 90° F to 150° F for 18 hours

b. Vibration

(1) Parallel to the diaphragm

0.32-inch D.A.D.	10 to 60 cps
100g peak-to-peak	60 to 1,000 cps
120g peak-to-peak	1,000 to 2,020 cps
100g peak-to-peak	300 cps for 15 seconds

(2) Perpendicular to the diaphragm

0.32-inch D.A.D.	10 to 60 cps
120g peak-to-peak	60 to 2,020 cps
120g peak-to-peak	300 cps for 15 seconds

Vibration cycle time in each direction was approximately 5 minutes and 15 seconds

c. Acoustic noise levels

Frequency	Level	Time
60 to 2,400 cps	152 db	15 seconds
60 to 2,400 cps	159 db	30 seconds
60 to 4,900 cps	166 db	5 minutes

6 db/octave roll-off on high side

d. Thermal shock was accomplished by alternately heating to full output of sensor then cooling with CO₂ spray.

The calorimeters passed all tests and a malfunction could not be duplicated in the laboratory.

The acoustic noise level tests were performed at Space and Information Systems Division of North American Aviation, Inc. See reference 11 for the test description and results.

~~CONFIDENTIAL~~

UNCLASSIFIED

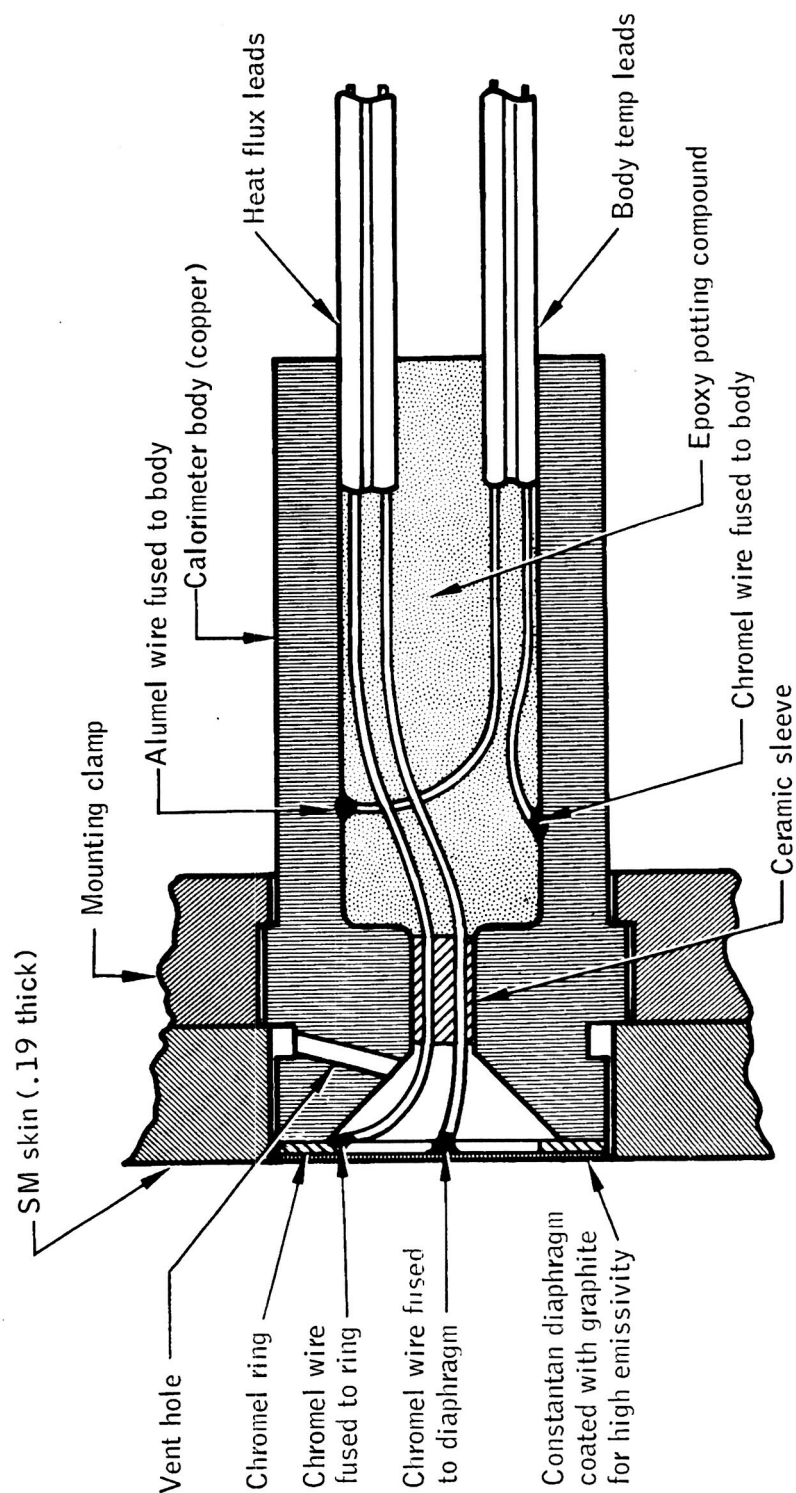


Figure 9.3-1.- BP-15 spacecraft calorimeter.

UNCLASSIFIED

UNCLASSIFIED

10-1

10.0 REFERENCES

1. Staff of NASA Manned Spacecraft Center: Postlaunch Report for Apollo Mission A-101 (BP-13). MSC-R-A-64-2, June 18, 1964.
2. Staff of NASA Manned Spacecraft Center: Postlaunch Memorandum Report for Apollo Pad Abort I. Nov. 13, 1963.
3. Staff of NASA Manned Spacecraft Center: Postlaunch Report for Apollo Mission (BP-12). MSC-R-A-74-1, May 1964.
4. Anon.: Apollo Launch Heating (Proposed MSC Working Paper).
5. Anon.: Data Report for Apollo Model (H-L) Wind Tunnel Test (JPL 21-102), North American Aviation, Inc., SID Report 62-628.
6. Anon.: An Investigation of Aerodynamic Noise Measured on a 0.055-Scale Apollo Saturn Vehicle in the NASA Ames 14-foot Transonic and 9 x 7-foot Supersonic Wind Tunnels. SID 63-1480 (NAS9-150), North American Aviation Inc., Dec. 31, 1963.
7. Staff of Saturn Flight Evaluation Working Group: Results of the Seventh Saturn I Launch Vehicle Test Flight. NASA George C. Marshall Space Flight Center.
8. Anon.: Saturn I. Program Requirements Document 2400, Patrick Air Force Base, Fla., 1963.
9. Anon.: Saturn Launch (Test Code B). Operations Directive No. 2400. Air Force Missile Test Center, Nov. 1, 1963 (supersedes OD 2400, Sept. 19, 1961).
10. Staff of NASA Manned Spacecraft Center: Apollo Postlaunch Report for Apollo Mission A-101 (BP-13), Supplement A. MSC-R-A-64-2A, 1964.
11. Staff of Apollo Instrumentation Test and Checkout Unit: Acoustical Tests on Hy-Cal Calorimeters (NASA type 2.2.1.1.2, 0 to 5 Btu/ft²-sec). SID 64-1632 (contract NAS9-150), North American Aviation, Inc., Sept. 1, 1964.

UNCLASSIFIED